

RADC-TER-64-25, Vol. I



RADAR REFLECTIVITY MEASUREMENTS SYMPOSIUM

TECHNICAL DOCUMENTARY REPORT NO. RADC-TER-64-25, Vol. II

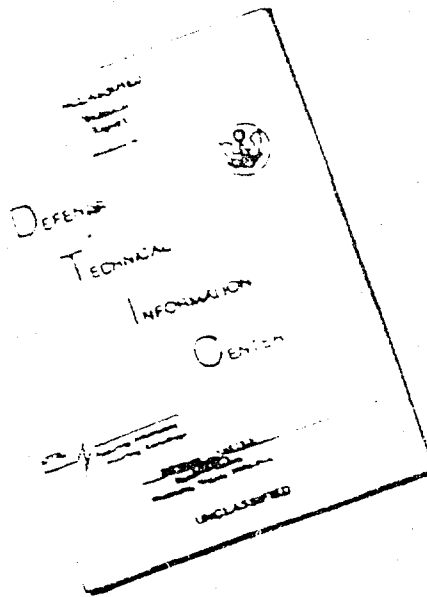
April 1964

Space Surveillance and Instrumentation Branch
Air Development Center
Research and Technology Division
Air Force Systems Command
Randolph Air Force Base, New York

Prescribed by
NATIONAL TECHNICAL
INFORMATION SERVICE

DDC
RECEIVED
JUN 22 1964

DISCLAIMER NOTICE



THIS DOCUMENT IS BEST
QUALITY AVAILABLE. THE COPY
FURNISHED TO DTIC CONTAINED
A SIGNIFICANT NUMBER OF
PAGES WHICH DO NOT
REPRODUCE LEGIBLY.

REPRODUCED FROM
BEST AVAILABLE COPY

TABLE OF CONTENTS (Vol II)

<i>Contents</i>	<i>Page</i>
SECTION V - CALIBRATION AND RANGE INTERCALIBRATION; MEASUREMENT PROCEDURES AND MEASUREMENTS DATA STANDARDS	
Radar Cross-Section Data Generation and Recording in The Cornell Aeronautical Laboratory Ranges	1
Robert V. Gallagher	
Analytical Investigation of Near-Zone/Far-Zone Criteria	5
Lee R. Hendrick	
Some Factors Affecting The Accuracy of Ground-Plane Measurements	20
J. C. Huber, Jr.	
G. M. Hazlip	
Radar Reflectivity Measurement Data Format Standards	33
Stephen L. Johnston	
Radar Measurement Standardizations Needed for Simulation Studies	39
C. Krichbaum	
A New Minimum Range Criterion for Measurement of Radar Cross Sections	50
Leon Peters, Jr.	
Experience With Calibration Targets and Techniques at RCA - ERL	62
R. Sigler	
SECTION VI - MEASUREMENT CORRELATION AND APPLICATION	
Comparison of Radar Cross-Section Signatures	67
D. R. Brown	
A. L. Maffett	
Use of Radar Cross Section Data in Military Systems Analysis	81
H. A. Ecker	
Target Recognition and Discrimination	93
R. F. Goodrich	
O. Ruehr	
Z. Akcasu	
G. Rabson	
Sub-nanosecond Pulse Methods of Radar Cross Section Measurement	119
Robert R. Hively	
Contour Charts for Radar Cross-Section Analyses	129
Daniel Levine	
Geometry and Instrumentation Considerations for Dynamic Reflectivity Measurements	153
E. G. Meyer	
C. L. Mohre	

A Multi-band, Polarization Diversity System for Dynamic Radar Cross- Section Studies	166
I. D. Olin	
F. D. Queen	
A New Method of Correlation of Down-Range Radar Measurements with Static Radar Cross Section Measurements	177
N. E. Pedersen	
H. I. Halsey	
J. F. Torrey	
J. B. Clemente	
Instrumentation of A Tracking Radar for Direct Recording of Radar Cross Section	187
Donald C. Watson	
SECTION VII - RANGE DESCRIPTION	
The University of California Image-Plane Reflectivity Range	197
D. J. Angelakos	
F. D. Clapp	
Avionics Laboratory Radar Cross Section Measurements Facility	201
W. F. Bahret	
Radar Cross Section Measuring Equipment and Range	203
P. Blacksmith	
R. Mack	
The Hughes Back Scatter Measurement Range	208
R. E. Boucher	
Don E. Ludwig	
Range Facilities for Measuring Radar Cross Sections of Low Density Supersonic Plasma Streams	218
Alan I. Carswell	
The AVCO RAD Vertical Range	223
Joseph F. Clougherty	
The Radar Reflectivity Measurement Facility at Electronic Space Structures Corporation	229
Albert Cohen	
Adam P. Smolski	
Aeronutronic Microwave Reflectivity Facility	233
Harold G. Collins	
Millimetre Wave Short Pulse Radars for Indoor Echoing Area Measurements	240
L. A. Cram	

<i>Contents</i>	<i>Page</i>
The Lincoln Laboratory Model Backscatter Range	244
P. C. Fritsch	
D. F. Sedivac	
A. J. Yakutis	
Lockheed Missiles and Space Company Scattering Range Capabilities	250
N. J. Gamara	
Experimental Reflectivity Facilities	252
Robert J. Garbacz	
Scattering Range - The Boeing Company Aerospace Division	266
W. P. Hansen, Jr.	
RCA Dynamic Backscatter Testing Range	270
M. H. Hellman	
J. M. Jarema	
Outdoor Pulsed Radar Reflectivity Range	274
Robert E. Honer	
Wm. D. Fortner	
Cross-Section Range Radars at Cornell Aeronautical Laboratory	286
John E. Hopkins	
An Indoor Radar Scattering Range	295
E. F. Knott	
Static Radar Reflectivity Measurement Facilities at Radiation Incorporated	299
J. E. Landfried	
W. L. Williamson	
A Radar Backscatter Range for Measurement of Large Models	303
Wesley G. Louie	
Charles W. Matthis, Jr.	
An Ultra-High Frequency Reflection Measuring System	306
Siegfried Mikuteit	
Radar Echoing Area Ranges at Royal Aircraft Establishment	314
J. G. W. Miller	
J. Edwards	
Radar Target Scatter (RATSCAT) Site	321
Donald Montana	
Investigation to Design A Method for the Analysis of Radar Cross-Section Measurement Data	330
M. L. Parish	

*Contents**Page*

An Anechoic Chamber for Measurement of Backscatter Amplitude and Phase at Multiple Polarizations	334
R. W. Roop	
S. M. Sherman	
The Scale Ground Plane Range	341
R. A. Ross	
U.S. Naval Missile Center Radar Reflectivity Measurement Facilities and Techniques	354
John K. Rozendal	
Conduction Corporation's Radar Cross Section Range	359
A. W. Wren, Jr.	
Description and Operation Characteristics of a Short-Pulse, Oblique Radar Cross Section Range	363
Malcolm Yaffee	

SECTION V

**CALIBRATION AND RANGE INTERCALIBRATION; MEASUREMENT
PROCEDURES AND MEASUREMENTS DATA STANDARDS**

Panel Chairman: S.L. Johnston

RADAR CROSS-SECTION DATA
GENERATION AND RECORDING IN THE
CORNELL AERONAUTICAL LABORATORY RANGES

Robert V. Gallagher
Cornell Aeronautical Laboratory, Inc.
Buffalo, New York 14221

ABSTRACT

The data recording and handling techniques used with the four Cornell Aeronautical Laboratory radar cross section ranges are discussed and associated equipment is described.

INTRODUCTION

The CAL radar cross-section ranges include four different installations. One pulsed and one CW range operate at K_a band (35 Gc), another CW range is used for X-band (9.2 Gc) investigations, and the fourth range employs a very high resolution FM/CW radar at X-band. Each range uses a different method of measuring radar cross section, and there are some differences between the various data forms. These are discussed below.

K_a Pulse Range

The data acquisition system currently in use on the CAL K_a pulse cross-section range records signal level in terms of radar receiver AGC voltage versus azimuth aspect angle. Analog and digital data are recorded simultaneously. The analog data are recorded on M-H (Minneapolis-Honeywell) and S/A (Scientific Atlanta) recorders and the digital data punched into paper tape by a Tally punch. Data may be punched in $1/4^\circ$ or 1° increments.

The data acquisition cycle is initiated by a microswitch closure on the model drive turntable as the model comes into 180° azimuth aspect angle (tail towards radar antennas). This switch closure starts the Tally punch, marks the charts with first punch position, and starts a data point counter.

The digital tape, which is subsequently processed by the IBM 704 computer, is verified on a Friden Flexowriter. This insures against misspunches, missing digits and poor hole registration. As the data are being verified a new tape is punched simultaneously. The new tape is given appropriate coding compatible with the 704 program and the runs are organized into data sets. This is necessary when more than one roll angle is involved, as it is desirable to take vertical and horizontal polarizations without disturbing the model. The edited and coded tapes are then spooled and delivered to the IBM 704 group for processing.

Fanfold tape has been found to be convenient to handle for the editing and coding process and spools quite well.

The Friden Flexowriter provides a print-out which is filed by run number and kept at the range site. This proves quite useful in resolving questions arising during the 704 processing operation.

Programs have been written for the IBM 704 EDP which permit target signal level to be presented in the following manner:

1. Radar cross section in db referenced to a square meter.
2. Radar cross section in db referenced to a square wavelength.
3. Radar cross section expressed in square meters.
4. Square root of radar cross section, expressed in meters.

(NOTE: When cross section is expressed in meters it is an artificial operation to allow conservation of computer volume in subsequent calculations.)

Processed data are available as a tabulator print-out, IBM punched cards and on magnetic tape.

The azimuth Angle Marker, a synchro device slaved to the turntable, provides pulses ($1/4^\circ$ or 1° increments) to initiate the digitalization of the radar receiver AGC voltage. The conversion from analog to binary coded decimal form is performed in an Epsco digital voltmeter. The BCD data are transferred from the digital voltmeter to the Tally punch via solid state circuitry.

The AGC voltage is recorded in analog form on Minneapolis-Honeywell and Scientific Atlanta recorders. The M-H recorder has a frequency response of one cycle per second. The AGC input to the recorder is adjusted to give full scale coverage for a given set of operating conditions.

The chart is driven in synchronism with the turntable. Three hundred and sixty degrees of azimuth rotation provide a chart 24 inches in length.

The Scientific Atlanta recorder produces a chart 120 inches long for 360° of azimuth rotation and has a frequency response of 4 cps. This provides a better presentation of the fine lobe structure than is available in the more compact Minneapolis-Honeywell record.

Calibration on this range is performed against a corner reflector with two precision attenuators located in the waveguide input to the mixer. Normal calibration increments are 5 db. A 3/4 inch metal sphere reference level is recorded with each calibration. The radar cross section of this sphere is about 6-1/2 db above a square wavelength at 35 Gc. A separate calibration is made for each antenna polarization.

K-CW Range

The K-CW radar cross-section range data are obtained from the output of a logarithmic I-F amplifier which is peak detected, amplified, and fed to a Minneapolis-Honeywell recorder. Target signal is presented versus angle of azimuth rotation. The output of the peak detector is also fed to a Systron digital voltmeter which converts the data to binary coded decimal form. The conversion cycle is initiated in the same manner as on the K_a pulse range. As the logic circuits of this unit are switched by magnetic relays, the system is limited to recording data in one degree increments.

This range is calibrated through an internal calibrating loop with two precision attenuators and appropriate isolation from the transmitter. All runs made on this range are referenced to a 7/16 inch sphere which is approximately 1/2 db above a square wavelength at 35 Gc.

X-CW Range

Radar cross-section data are measured in the X-CW range by using a calibrated, servo-driven microwave attenuator to maintain constant the rectified output voltage of an X-band superheterodyne receiver as the target rotates in azimuth. The attenuation required to do this is inversely proportional to the radar cross section of the target, and the ratio between two cross-section values in decibels may be observed directly from the corresponding difference in attenuator readings. This process has been mechanized by coupling a logarithmic potentiometer to the attenuator shaft and recording the analog signal from the potentiometer on a Minneapolis-Honeywell recorder which produces a record of relative radar cross section in decibels, plotted as a function of azimuth angle of the model.

The logarithmic potentiometer output is also fed to an Epsco digital voltmeter which is coupled by a solid state circuitry to a Tally paper-tape punch. The data are punched out in binary coded decimal form. The conversion cycle is initiated in the same manner as on the K_a pulse range. The X-CW range has the capability of producing a data point for each quarter degree of azimuth angle of model rotation as well as in one degree increments.

The calibration curve of the attenuator is verified periodically by checking against the relative radar cross section from each of a set of spheres of various sizes. All runs on this range are referenced

to the radar cross section of a 1-3/8 inch sphere, which is 3/4 db above a square wavelength at the operating frequency of 9.2 Gc.

FM-CW Range

The fourth range, which uses a high resolution X-band FM-CW radar, presents its basic data as an amplitude versus frequency spectrum with a frequency increment (equal to the cyclic repetition frequency) of 123 cps corresponding linearly to a radar range increment of 1-1/2 inches. A rotating turntable is provided, as for each of the other ranges. Data may be taken either at successive 1° azimuth angles, or, with the turntable clamped into position, at an arbitrarily chosen series of stationary attitudes. Each data set corresponds to a group of points at sequential range intervals, so the data field is much more complex than it is for the simpler K_a -CW, K_a -pulse, and X-CW ranges.

Two choices are available for data readout. One of these is by a bank of 16 filters, each tuned to a separate harmonic of the recurrence frequency and each filter corresponding to a different range interval. Each filter output voltage is proportional to signal amplitude and thus to square root of cross section in its own range interval. The rectified output voltages are fed sequentially through a logarithmic amplifier to a digital and to an analog recorder. The analog recorder is a conventional Sanborn unit and is allowed to run at constant paper speed. The digital recorder consists of a Nonlinear Systems, Inc. digital voltmeter and a Tally punch, and yields punched tape records in binary coded decimal form, for 16 different range intervals. This entire sequence is repeated once every degree of turntable rotation.

The other choice available for data readout is by oscillographic presentation of the radar output signal spectrum, which is done on a commercial panoramic spectrum analyzer. The unit used currently offers a choice of linear ordinate, representing signal amplitude, or logarithmic ordinate scaled in decibels. A photograph of the screen is taken to provide a permanent record. In order to accommodate rapid data rates, a framing-type 16 mm camera has been used with good success. Relative cross-section values may be read at successive range increments, which appear in this record as individual spectral lines.

ANALYTICAL INVESTIGATION OF NEAR-ZONE/FAR-ZONE CRITERIA

Lee R. Hendrick, Assistant Physicist
Cornell Aeronautical Laboratory, Inc.
Buffalo, New York

ABSTRACT

An analytical investigation of the effects of reduction of antenna-to-target distance is performed using simplified targets composed of point scatterers. Also, the effects of restricting the antenna beamwidth are studied.

I. INTRODUCTION

Recent emphasis upon the measurement of small radar cross sections for physically large bodies has required the close scrutiny of the criteria upon which design of measurement facilities is based, in order that they may provide both accurate and economical radar-cross-section data.

One of the more important criteria in facility design is that governing the minimum allowable separation between antenna and target. This separation should be made as small as is consistent with allowable distortion of the measured angular scattering pattern, to maximize the desired back-scattered signal relative to unwanted scattering. Previous investigators of the minimum target range criterion have usually recommended minimum ranges in excess of L^2/λ , where L is the maximum target dimension and λ is the operating wavelength. For large targets at short wavelengths the criterion frequently demands an impracticably large antenna-to-target spacing. This paper will show that in many cases the presently accepted criterion may be relaxed. The investigation reported here has shown that (1) the criterion chosen should be intimately related to the nature of the cross-section data desired, (2) for the data most frequently sought, the minimum range can usually be made less than L^2/λ , (3) the ratio of allowable percentage reduction from L^2/λ increases as the target size increases, and (4) that maintenance of an adequate beamwidth is important.

II. PERTURBATIONS IN CROSS-SECTION MEASUREMENT

The distances between the transmitting antenna, the target, and the receiving antenna which must be maintained in order to achieve accurate measurements have been the subject of much speculation, a great deal of guess work and some analytical investigation. Criteria which have been developed for assessing the behavior of antennas have commonly been taken over bodily. As a consequence, it has become common to use a small multiple of L^2/λ (where L is the maximum target length and λ is the operating wavelength), as the least value for the

allowable separation distance between either antenna and the target.* In a useful addition to the literature of radar cross-section measurement, W. P. Melling notes that, if one writes the criterion as $R \geq \rho(L^2/\lambda)$, the parameter ρ is related to the accuracy required for a particular measurement, and that for certain accuracy standards it might be necessary to accept a value of ρ as large as 10.

The choice of separation distance is not commonly of serious import when dealing with targets which are only a few wavelengths long. It becomes a much more serious matter when attempting to measure objects many wavelengths in extent, as for instance typical ballistic missiles at frequencies above 3000 Mc (wavelengths less than 10 cm). The extremely rapid growth of required separation with L/λ may be easily seen from the alternate form $R = (L/\lambda)^2 \lambda$. It is evident that a target 10 wavelengths long will have a near zone limit of 100 wavelengths (for $\rho = 1$), and a target 100 wavelengths long will have a limit of 10,000 wavelengths. The 100-wavelength separation represents 10 m at 10 cm wavelength, and is relatively easy to achieve and to instrument on a laboratory scale. The 100-wavelength target demands a separation of 1 km which is much more difficult to achieve without encountering limitations produced by background, model mounting, etc. For targets significantly longer than 100 wavelengths, achievement of L^2/λ separation for earth-bound laboratories becomes exceedingly difficult. Recognition of this difficulty, coupled with interest in measuring large objects in the UHF-to-microwave wavelength range, suggested that a critical look at the range separation criteria which we employ was needed.

The effect of choice of antenna-to-target distance upon the properties of the resulting cross-section measurement may best be understood by separating the concepts of scattering measurements into four separate functions as follows:

1. Establishment of illumination field in the test region.
2. Production of surface current and polarization distribution upon target by illumination field.

*Some investigators have used the maximum target dimension transverse to the radar beam axis, instead of maximum target length, as the value L to be inserted in the L^2/λ criterion. This choice obviously decreases the near zone limit for slender targets near nose-on incidence. The limit varies with the angular range over which data are needed, and the "transverse dimension" criterion ignores the effect of radial field gradient which may be serious for small values of L^2/λ .

3. Reradiation from target by virtue of surface current and induced polarization distribution.
4. Sampling of reradiated field by receiving antenna.

The measurement conditions, if they are to produce valid cross section information, should duplicate the real-life situation in which the target is a very great distance from the radar antenna. In this situation, the illumination field at the target will typically be a transverse electromagnetic wave with the ratio of electric to magnetic field equal to the intrinsic impedance of free space, with essentially uniform field distribution over a volume with lateral dimensions at least as great as the maximum target dimension, and with negligible variation of field amplitude along a radial coordinate drawn from radar to target. Under this illumination, and dependent upon the relative target orientation, a distribution of surface current and polarization develops on the target. The relation between these surface fields and the field reradiated by the target is uniquely defined. For the real-life case, the electromagnetic field at a great distance from the radiating target is found to vary inversely with distance from target to observer, and is characterized by a range-independent complex amplitude coefficient.

Most attempts to make radar cross-section measurements rely upon the assumed uniformity of the illumination field and the independence of the complex-amplitude scattering coefficient upon range. The reliance is necessary in order to relate measurements over a certain set of aspect angles to real-life behavior over the same aspect angle range. A reduction in distance between transmitting antenna and target, as would apply under laboratory measurement conditions, will cause the true illuminating field to deviate from the plane wave approximation. The deviation occurs both in the shape of equiphasic surfaces and the field amplitude vs distance from transmitting antenna.

In a similar fashion, the field reradiated by the target is no longer expressible as the product of inverse distance and a range-independent factor when the distance from radiating target to observer is too small. Aspect-angle dependence departs from the distant field approximate value, and observations reported as a function of angle will not truly represent the far-field radiation pattern.

Finally, in either the near- or far-field radiation zones of the target, sampling of the radiated field must be effected by a field probe or antenna of dimensions small enough to permit "point sampling" of the field--an excessively large probe will provide an "average" measurement and obscure the spatial variations of radiated field.

From general consideration of the radiation process, one may gain additional insight into the perturbations induced by inadequate target range. The amplitude and phase of the radiation pattern for any given direction may be specified by an integral with complex integrand, taken over the surface of the body. The magnitude of this integral is approximately equal to the complex sum of field contributions from a very few "scattering centers" on the body. The contribution from each scattering center is proportional to its cophasal area: the area in its vicinity over which the elemental field contributions of successive surface areal elements are substantially in phase (usually within about 45 electrical degrees). *2

For an antenna with maximum dimension L , and with the same maximum dimension for its cophasal area, the criterion L^2/λ allows contributions from the extreme edge of the aperture to be $\pi/4$ electrical radians out of phase with those from the center of the aperture as seen by an observer on the normal to the cophasal area. At much greater distances, the edge contributions are in phase with the central one for the same observer. A slender target of length L may have more than one effective scattering center, but the cophasal area of each will have a greatest dimension much smaller than L except near broadside aspect. Therefore the contribution of each scatterer will not be degraded by near-zone phase variation, although the relative phase and amplitude of the fields scattered from the various scattering centers may be affected by reduction of the measurement distance below L^2/λ . As target aspect is varied, the phase and amplitude of the several scattering contributions also vary and produce the familiar interference pattern which we recognize as angle-dependent radar cross section. The following three effects of measuring at a distance much less than L^2/λ are observed.

1. Phase perturbations caused by too small a measurement distance will cause angular displacement of radar cross-section nulls and maxima of this pattern, but will not alter its main features or the magnitude of the maxima.
2. Relative amplitude perturbations caused by insufficient measurement distance will change the depth of interference nulls but will have a much less pronounced effect upon adjacent maxima.
3. The spacing of successive interference nulls will be altered slightly. For real target bodies the calculation of the surface and reradiated fields is generally too complex to be worth attempting. It is possible, however, to employ simplified models made up of point scatterers which possess many features of real targets with small cophasal scattering areas. It is less difficult to explore the scattering properties of these simplified models as a function of antenna-to-target distance. This approach has been followed in the present work.

*The cophasal area concept is due to R. E. Kell.

antenna beam pattern is assumed to introduce an additional amplitude weighting factor g into the scattered field from each element, where g is defined by Eq. (1).

$$g = \frac{\sin(\alpha\pi y/W)}{(\alpha\pi y/W)} \quad (1)$$

where

y = distance off axis

W = distance of half-power point off axis

$\alpha = 0.433$

The beam pattern factor g is an approximation to the classical form and is based upon the assumption of proportionality between lateral displacement of target element and corresponding antenna beam angle displacement.

The analytic form used in computation is shown in Eq. (2).

IV. DISCUSSION OF RESULTS

Since the principal interest of this investigation is to determine the effect of range upon measured radar cross sections at near nose-on aspect (where small values of cross section occur) the data will be examined in the forward 60° cone. The cross-section distribution at the greatest range calculated is taken as representing the true far-field cross section. For the short model this range is $5L^2/\lambda$; for the larger models, it is $2L^2/\lambda$.

The results are grouped according to the antenna beam width used in the calculation. The wide-beam case, in which antenna beamwidth does not affect the observed cross section, is treated first. The radar cross section computed with lateral beam dimension matched to target length is next discussed, for the five model configurations. The effect of varying antenna beamwidth, for a specific model configuration, is next described. Finally, the calculated results have been used, together with judgement as to reasonably allowable errors, to construct a criterion for the minimum allowable range.

A. Wide-Beam Results

When the wide antenna beam is used, varying the antenna-to-target spacing produced effects such as those shown in Fig. 2.

III. POINT SCATTERER MODEL CALCULATIONS

The angular distribution of the monostatic radar cross section was computed for five different simplified scattering models. The basic model in each case consisted of three scatterers with negligibly small dimensions, arranged in a triangular configuration, as shown in Fig. 1. The two elementary scatterers on the base were chosen to have equal radar cross section, and the third scatterer at the nose of the model has a radar cross section four times that of each of the others. Thus, when the fields from the two small scatterers are in phase agreement, the sum of their joint field plus that from the large scatterer can vary from zero to a maximum of twice that from the large scatterer alone. This choice of scatterers permits the most extreme interference effects to be examined.

The ratio of base to length is approximately 0.3 for each model. For the first short model, the length L is chosen to be 3λ , which produces a local cross-section maximum at zero degrees aspect. The second short model has a length of $3\frac{1}{4}\lambda$ which produces a nose-on null. The first medium-length model has $L = 10\lambda$ with a maximum at zero degree aspect, and the second medium length model has $L = 10\frac{1}{4}\lambda$ and a null at nose-on aspect. For the long model, L is 50λ , which produces a nose-on maximum.

The calculations were made for the monostatic case. The separate fields of each elementary scatterer were computed and the results summed with proper regard for phase. It was assumed that the scatterers did not mutually interact. In each case, calculations were made with two choices of antenna beam width at the target station. First, a very wide beam was used; second, the beam width was restricted so that the distance between the half-power points at the target was equal to the maximum model dimension L ("matched beam"). The wide beam is a less likely configuration for practical testing than the matched beam, although the latter produces additional modification of the measured radar cross section. For the short model an intermediate antenna beam width was also used. The distance between the half-power points of this beam is twice the maximum model dimension. This beam width is more realistic than the narrower matched beam for the short target-to-antenna distances which are used with a small model.

The calculation procedure employed the radar equation to define the scattered power density from each target element separately and took the square root of this power density to obtain scattered electromagnetic field contributions from the individual target elements. The distance of each element from the common receiving and transmitting antenna was used to compute a phase retardation factor $e^{j2\pi r/\lambda}$ for that element. The

$$\sigma = \left(\frac{\sin \left(\frac{0.433 \pi l \sin \theta}{W_{1/2}} \right)}{\left(\frac{0.433 \pi l \sin \theta}{W_{1/2}} \right)} \right)^2 \sqrt{\sigma_1} \left\{ \frac{\cos \frac{4\pi}{\lambda} \left(l^2 + R^2 - 2lR \cos \theta \right)^{\frac{1}{2}} + i \sin \frac{4\pi}{\lambda} \left(l^2 + R^2 - 2lR \cos \theta \right)^{\frac{1}{2}}}{\left(\frac{l^2}{R^2} + 1 + \frac{2lR \cos \theta}{R} \right)} \right\}$$

(2)

$$+ \left(\frac{\sin \left(\frac{0.433 \pi l' \sin(\theta - \phi)}{W_{1/2}} \right)}{\left(\frac{0.433 \pi l' \sin(\theta - \phi)}{W_{1/2}} \right)} \right)^2 \sqrt{\sigma_2} \left\{ \frac{\cos \frac{4\pi}{\lambda} \left(l'^2 + R^2 + 2l'R \cos(\theta - \phi) \right)^{\frac{1}{2}} + i \sin \frac{4\pi}{\lambda} \left(l'^2 + R^2 + 2l'R \cos(\theta - \phi) \right)^{\frac{1}{2}}}{\left(\frac{l'^2}{R^2} + 1 + \frac{2l'R \cos(\theta - \phi)}{R} \right)} \right\}$$

=

$$+ \left(\frac{\sin \left(\frac{0.433 \pi l' \sin(\theta + \phi)}{W_{1/2}} \right)}{\left(\frac{0.433 \pi l' \sin(\theta + \phi)}{W_{1/2}} \right)} \right)^2 \sqrt{\sigma_3} \left\{ \frac{\cos \frac{4\pi}{\lambda} \left(l'^2 + R^2 + 2l'R \cos(\theta + \phi) \right)^{\frac{1}{2}} + i \sin \frac{4\pi}{\lambda} \left(l'^2 + R^2 + 2l'R \cos(\theta + \phi) \right)^{\frac{1}{2}}}{\left(\frac{l'^2}{R^2} + 1 + \frac{2l'R \cos(\theta + \phi)}{R} \right)} \right\}$$

WHERE σ = CROSS SECTION OF COMPOSITE MODEL

l & ϕ = SPECIFICATION PARAMETERS FOR MODEL

$W_{1/2}$ = HALF POWER BEAM WIDTH

θ = ANGLE BETWEEN MODEL AXIS AND LINE OF SIGHT TO RADAR ANTENNA

l = $L/2$

$\sigma_1, \sigma_2, \sigma_3$ = CROSS SECTION OF POINT SCATTERING CENTERS

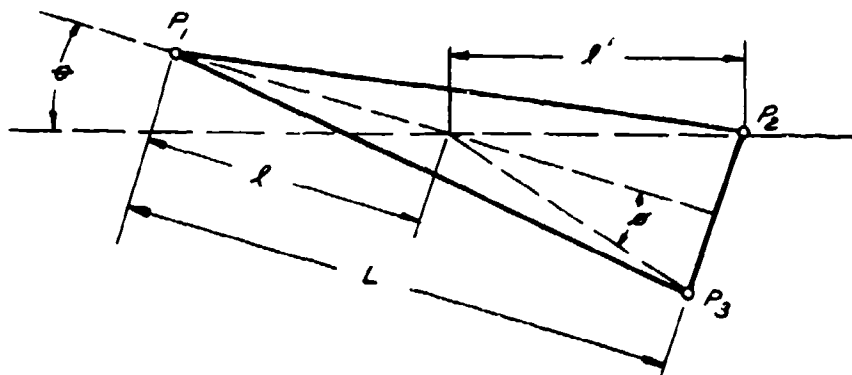


Figure 1 BASIC MODEL CONFIGURATION

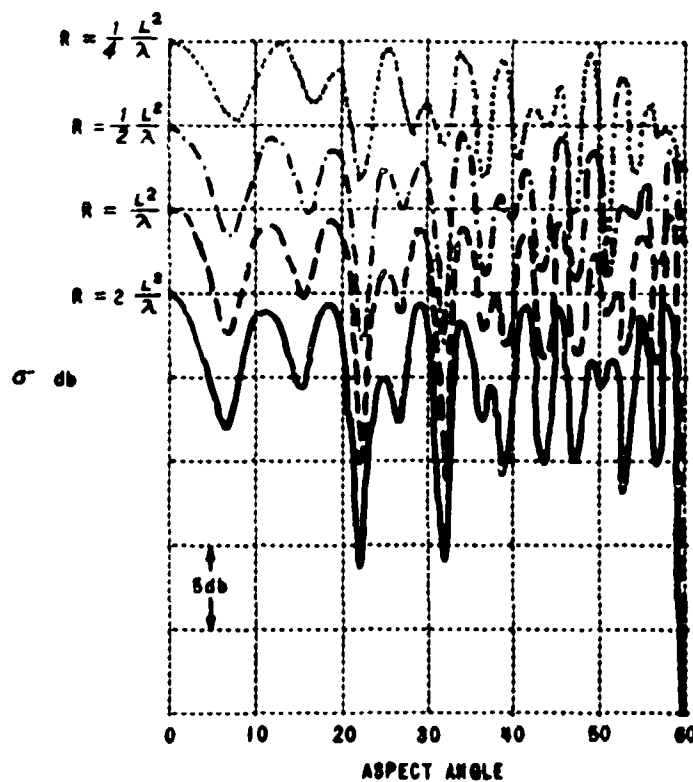


Figure 2 CALCULATED RADAR CROSS SECTION FOR MEDIUM MODEL ($10\lambda \times 3\lambda$) WIDE BEAM

(PLOTS ARE SEPARATED BY 5 db ALONG ORDINATE AXIS FOR CLARITY. 0° ASPECT ANGLE VALUES ARE THE SAME.)

The cross-section distributions of the medium model at $R = 2L^2/\lambda$, L^2/λ , $\frac{1}{2}L^2/\lambda$, and $\frac{1}{4}L^2/\lambda$ are plotted with a 5 db separation for clarity. Subsequent patterns are superposed for more precise comparison of the near zone vs far zone characteristics of cross-section distribution.

The cross-section distribution for the short model begins to show the effects of range reduction at $R = L^2/\lambda$ with very bad degradation at $R = \frac{1}{2}L^2/\lambda$ as seen in Fig. 3. The effects are even more pronounced for the $\frac{3}{4}\lambda$ model which shows the broad nose-on null raised 18 db when the range is reduced to L^2/λ .

For the medium length model the angular spacing of maxima is not seriously disturbed down to $R = \frac{1}{2}L^2/\lambda$ as shown in Fig. 4. The very deep nulls are lost but the mean values of the maxima are fairly well preserved. The nose-on cross section for the $10/4\lambda$ model rises by $7\frac{1}{2}$ db when the range is shortened from $2L^2/\lambda$ to $\frac{1}{2}L^2/\lambda$. The remainder of the cross-section distribution is changed in the same fashion as the model with nose-on maximum. When R is reduced from $2L^2/\lambda$ to $\frac{1}{4}L^2/\lambda$ for the 50λ target the locations of the maxima are shifted but their values are changed by less than 2 db and their angular density is virtually unchanged. These effects are within the specified measurement error of most systems. However, there is a noticeable filling in of deep nulls. Further reduction of R to $\frac{1}{8}L^2/\lambda$ produces more severe pattern shift and null degradation but the mean values of the maxima are not seriously altered.

B. Matched-Beam Results

When the $\frac{3}{4}\lambda$ model is illuminated by the matched-to-target beam the effects of range reduction are seen in Fig. 5. There is a loss in null depth and a 5-db loss in the maxima near

$\theta = 60^\circ$ in comparison to wide-beam illumination but the smaller angular density of maxima for the short model makes these effects much more pronounced than for the longer models. Because of the severity of beam restriction for this model, data were computed for a beam twice the width of the "matched" beam. As seen in Fig. 6 the cross-section distribution for this beam is much closer to the wide beam case than to the matched beam one.

Figure 7 illustrates the effect of going from $R = 2L^2/\lambda$ to $R = \frac{1}{2}L^2/\lambda$ for the medium length model, when the beam is "matched-to-target." The frequency of maxima remains the same while there is some loss of null depth with little change in the mean value of the maxima. Also, there is a noticeable loss in the magnitude of the maxima in both cases as the aspect angle increases, the loss being approximately 5 db at

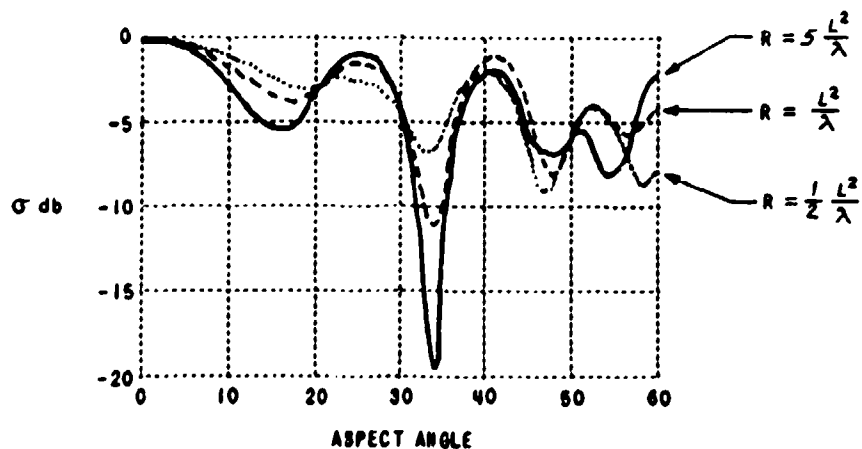


Figure 3 CALCULATED RADAR CROSS SECTION FOR SHORT MODEL ($3\lambda \times 1\lambda$) WIDE BEAM

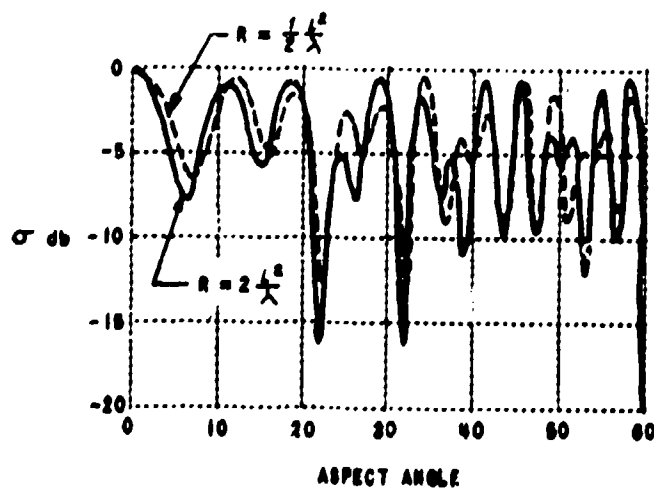


Figure 4 CALCULATED RADAR CROSS SECTION FOR MEDIUM MODEL ($10\lambda \times 3\lambda$) WIDE BEAM

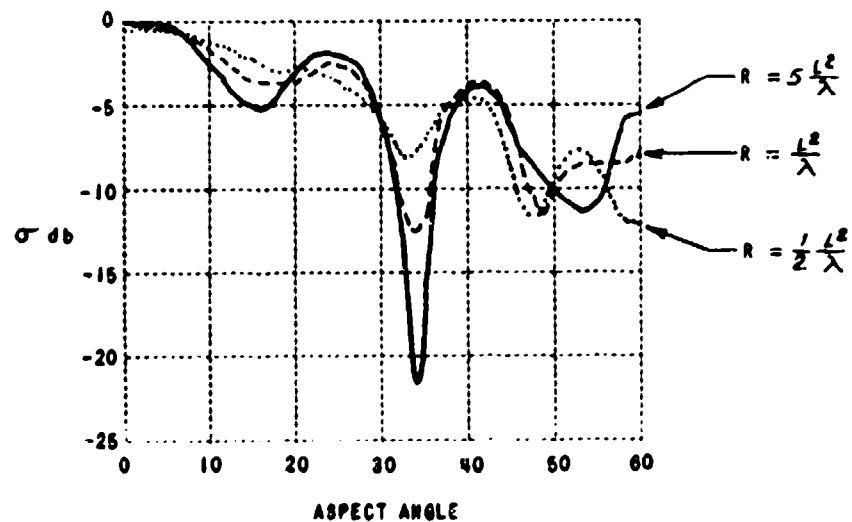


Figure 5 CALCULATED RADAR CROSS SECTION FOR SHORT MODEL ($3\lambda \times 1\lambda$) MATCHED BEAM

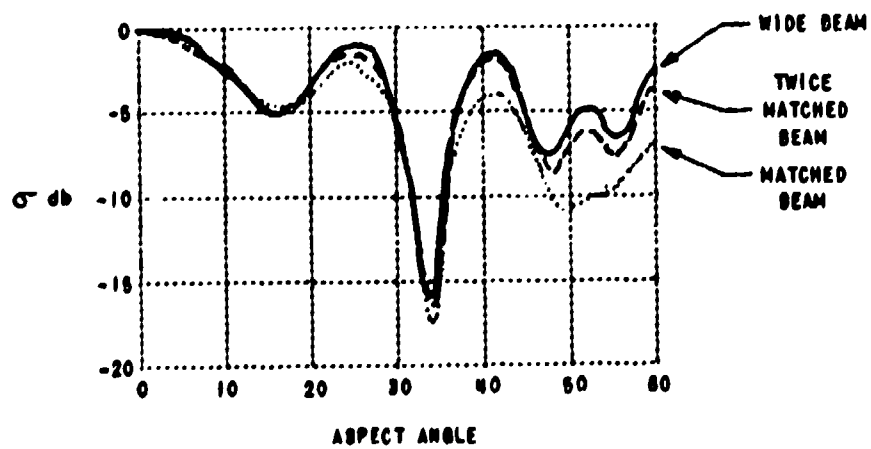


Figure 6 CALCULATED RADAR CROSS SECTION FOR SHORT MODEL ($3\lambda \times 1\lambda$) $R = 2 \frac{L^2}{\lambda}$

$\theta = 60^\circ$ when compared to the wide beam case of Fig. 3. The medium-length model with nose-on null shows similar effects of range reduction.

Range reduction for the 50λ model when the beam is "matched-to-target" produces the usual loss in null depth while the maxima remain nearly the same with a small angular shift.

C. Effect of Beam Width

As seen from the comparison of cross-section distribution of a wide antenna beam to the cross-section distribution of a "matched" antenna beam, the effects of beam width are often more pronounced than the effects of reducing the antenna-to-target distance. As an example of the severity of beam narrowing on the cross section, Fig. 8 shows the return from the medium model at $R = \frac{1}{2} L^2/\lambda$ with four beam widths. The four antenna patterns are wide beam, twice the width of the "matched" beam, the "matched" beam, and half the width of the "matched" beam. There is little difference between the results of the wide beam and the double "matched" width. At $\theta = 60^\circ$ there is a 5-db loss in the maxima for the "matched" beam. The half "matched" beam width produced serious degradation of the cross-section distribution.

D. Suggested Criterion for Minimum Range

A tentative criterion for antenna-to-target separation can be drawn from the above results. One must be mindful of the limited and idealized target configuration on which it is based. The requirement applied to the 10λ and 50λ cases is a reasonably accurate reproduction of maxima, as discussed earlier. For the short (3λ) model, this basis would be misleading because deep nulls can persist over a large angular range, and accuracy of null reproduction is used instead. The resulting minimum allowable ranges for various target sizes are as follows:

L/λ	R
3	$\frac{1}{4} \frac{L^2}{\lambda}$
10	$\frac{1}{2} \frac{L^2}{\lambda}$
50	$\frac{1}{4} \frac{L^2}{\lambda}$

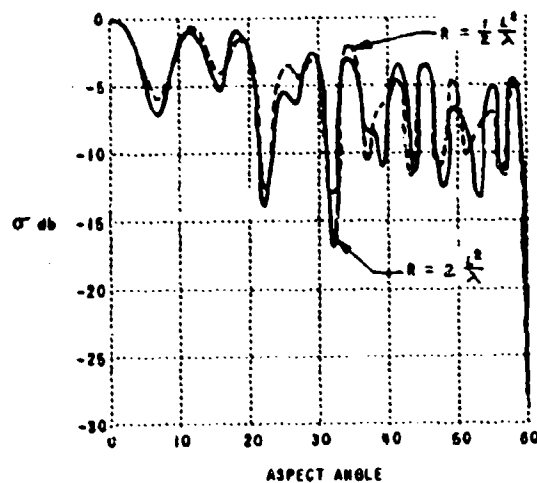


Figure 7 CALCULATED RADAR CROSS SECTION FOR MEDIUM MODEL ($10\lambda \times 3\lambda$) MATCHED BEAM

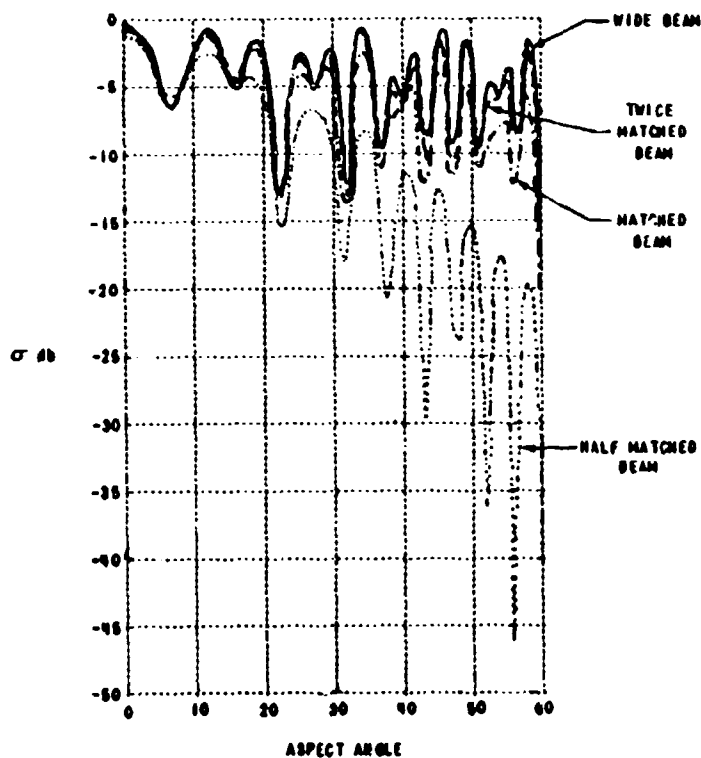


Figure 8 CALCULATED RADAR CROSS SECTION FOR MEDIUM MODEL ($10\lambda \times 3\lambda$) $R = \frac{1}{2} \lambda$

The relations between L/λ and the minimum allowable range, for the values tabulated above, appear as plotted points in Fig. 9. Any attempt to fit a curve to these points should be done with caution, since the numerical values the points represent are obtained from dissimilar criteria. The need for increasing the ratio of minimum range to L^2/λ as target size is reduced is clearly shown, however, and Fig. 9 may be used for coarse estimation of an allowable minimum range.

V. SUMMARY

The necessity of specifying the type of error allowable in making radar cross-section measurements is noted, together with the futility of requiring all measured data to fall within a specified error band.

It has been demonstrated that, for a long target characterized by a few scattering regions with small maximum dimension of cophased area, error in measured radar cross section incurred by testing at range less than L^2/λ may be negligible, and that for targets 50 wavelengths long measurements may be made for most system purposes at $1/4 L^2/\lambda$. It has further been shown that the error produced by using too narrow an antenna beam may be much more serious than that of using too short a range. Finally, the need for relatively larger ranges in testing short targets has been pointed out.

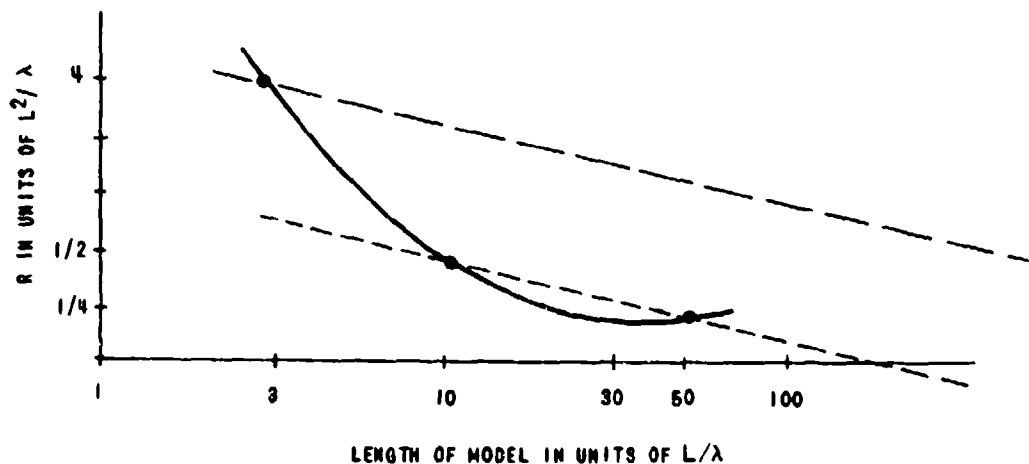


Figure 9 MINIMUM RANGE VS MAXIMUM TARGET DIMENSION

BIBLIOGRAPHY

1. W. P. Melling, "An Analysis of Radar Cross Section Measurement Techniques," CAL Report No. UB-1088-P-104, September 18, 1959.

2. L. Hendrick and R. E. Kell, "Re-examination of Minimum Range Criteria for Radar Cross Section Measurements," CAL Report No. GM-1580-G-101, August 3, 1962.

SOME FACTORS AFFECTING THE ACCURACY OF GROUND-PLANE MEASUREMENTS

J. C. Huber, Jr., Group Leader
G. M. Hazlip, Lead Engineer
Antenna and Microwave Laboratory
Goodyear Aerospace Corporation

ABSTRACT

Three factors affecting the accuracy of ground-plane cross-section measurements are: (1) the fields at the target and at the receive antenna, (2) the effect of the target on the background, and (3) the correct use of a sphere as a reference, including the minimization of sphere-ground interaction. These factors are considered analytically. Data on background changes due to target taken on a quasi-doppler range are presented. Errors due to these causes are found to be significant fractions of a decibel.

INTRODUCTION

The determination of measurement accuracy for a ground-plane radar cross-section test range is quite complex. Power and frequency stability, equipment accuracy, target support reflections, target stability, transmitter to receiver coupling, and the accuracy of the standard are only a few of the factors that must be considered. In addition, there are several other factors that may be more subtle, but their effect on accuracy can be significant. Three such factors are:

1. R-F field amplitude and phase deviations at both the target and the receiver antenna
2. The effect of the target on the background return
3. Accurate use of a reference sphere and the associated problem of coupling between the sphere (or target) and the ground or other objects in the range

When the r-f field at the target and the receiver antenna is computed, small radiators (or scatterers) and a perfect ground plane are generally assumed. The resultant field can be shown to have a sinusoidal amplitude distribution and an elliptical phase front. The foci of the ellipse are the antenna (or scatterer) producing the field and the image of the antenna (or scatterer). The constant phase contour may, in general, be approximated by a spherical wave front emanating from a point on the ground below the radiator. Thus, the viewing aspect angle of the target is determined (approximately) by the target azimuth and the inclined line from the approximate phase center to the target.

For ground that has a reflection coefficient with a phase other than

180 deg, the same conditions as above hold. However, if the amplitude of the ground reflection coefficient is not unity, or if the radiators have finite apertures, a considerably more complex situation exists. These cases are best handled by using the standard far-field criteria for the radiators and their images.

The analysis of fields generally does not consider the effect of background on the field at the receive antenna. This assumption is based on the fact that the background return is either very small or is nulled out by a cancellation network.

When placed in the field, the target will change the illumination of the background. Unless the procedure permits measurement of both the target level and the background level, an error in the target measurement can result. Figure 1 shows the amplitude of this error as a function of the ratio of target return to background return. Of particular importance is the background return that exists with the target in place rather than that existing prior to the measurement.

Measurements have been made in the field of the change in background level that resulted from the introduction of a smooth cone-shaped target. The change produced in a 25-db absorber wall behind the target was appreciable, and a noticeable error would exist even for the extrapolated conditions of a 50-db wall.

In addition to the error caused by the target illuminating the background, an error due to interaction is also possible. The target (or reference sphere) radiates into the ground, and this energy can re-radiate to the receive antenna and the target. Computations for a sphere show that, even for this simple case, coupling errors of 0.5 to 1 db are possible.

Additional errors can occur in the use of a sphere as a reference target because of the use of incorrect bistatic angles. The large forward scatter of a sphere is also significant in terms of the error due to change in background level.

The fact that these several contributors to errors are present in some or many range configurations does not imply that precise measurements are impossible. Methods exist to measure and minimize these errors.

FIELDS AT TARGETS AND RECEIVER, AND SOME COMMENTS ON THEIR EFFECTS

The standard computation for the field at the target in a ground range assumes that the ground has a reflection coefficient Γ_r of -1.^{1-4, a} The resultant field amplitude is then:

^aSuperior numbers in the text refer to items in the List of References.

$$\sin \frac{2\pi Xh}{r\lambda} \times F(\theta), \quad (1)$$

where

h = transmit antenna height,

X = target height,

r = range,

λ = wavelength, and

$F(\theta)$ = pattern of transmit antenna (assumed to be broad-beamed in comparison to angle of reflection to ground)

The associated assumptions are that the ground is flat and that no stray reflections perturb the field.

A more exact computation using only the latter two assumptions can be made. The vector addition of the fields for an isotropic transmitter is given by:

$$P = \left(A_1 e^{j\theta_1} + A_2 e^{j\theta_2} \right)^2, \quad (2)$$

where

P = power at a point, p , in the target aperture,

A_1 = amplitude of the direct ray (see Figure 2),

θ_1 = phase of the direct ray,

A_2 = amplitude of the reflected ray (see Figure 2), and

θ_2 = phase of the reflected ray.

Let the amplitude, A_1 be the transmitter power, A_0 , and

$$\theta = \frac{2\pi l_1}{\lambda} \quad (3)$$

where

l_1 = distance from transmitter to point p ;

and

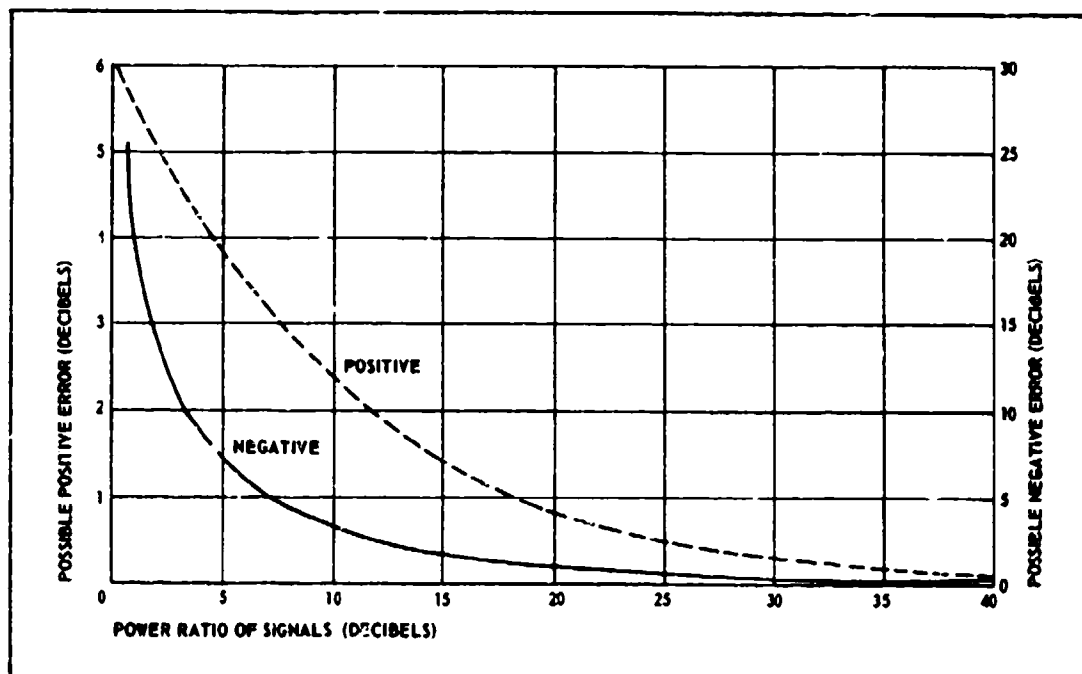


Figure 1 - Possible Errors due to Smaller Unwanted Signal

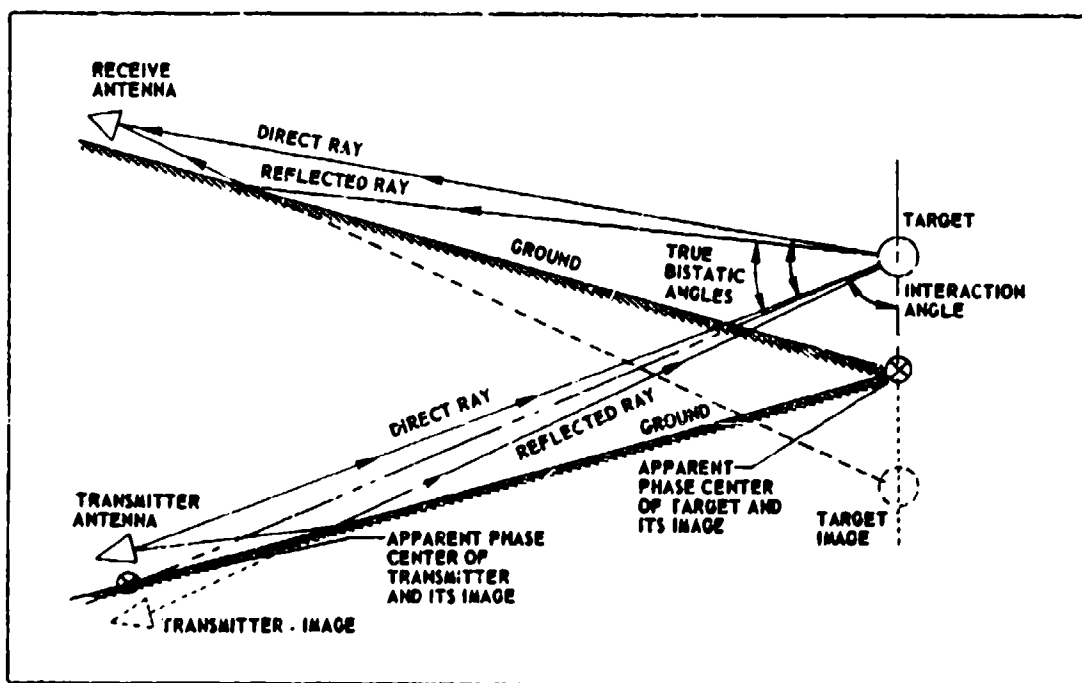


Figure 2 - Range Geometry

$$A_2 = |\Gamma| A_0 \frac{l_1}{l_2}, \quad (4)$$

where

Γ = reflection coefficient of ground and

l_2 = distance traveled by reflected ray; and

$$\theta_2 = \frac{2\pi l_2}{\lambda} + \phi, \quad (5)$$

where ϕ = phase of Γ . In the far field, the effect of the finite transmitter aperture can be accounted for by multiplying p by $F(\theta)$. In the near field, however, a more exact expression is given by

$$P = \left(\sum A_{1i} e^{j\theta_{1i}} + A_{2i} e^{j\theta_{2i}} \right)^2, \quad (6)$$

where points i lie along an assumed flat transmit aperture with amplitude illumination and phase illumination:

$A_{1i} = A_1$ (amplitude illumination at point i), and

$\theta_{1i} = \theta_1$ + phase at point i .

Considering first the case of an isotropic radiation (or approximately the far-field condition with a broad beam-width radiator), the amplitude and phase at a point, p , at the target are given by

$$|P| = (A_1 \cos \theta_1 + A_2 \cos \theta_2)^2 + (A_1 \sin \theta_1 + A_2 \sin \theta_2)^2, \quad (7)$$

and

$$\angle P = \tan^{-1} \left(\frac{A_2 \sin \theta_2}{A_2 \cos \theta_2} \right). \quad (8)$$

If the ground has a reflection coefficient, Γ , the amplitude of which is unity (i. e., $A_1 = A_2 = A_0$), the expressions for amplitude and phase are

$$|P| = 2A_0^2 [1 + \cos (\theta_1 - \theta_2)] \quad (9)$$

and

$$\angle P = \tan^{-1} \left(\tan \frac{\theta_1 + \theta_2}{2} \right) = \frac{\theta_1 + \theta_2}{2} . \quad (10)$$

However,

$$\frac{\theta_1 + \theta_2}{2} = \frac{1}{2} \left(\frac{2\pi \ell_1}{\lambda} \right) + \left(\frac{2\pi \ell_2}{\lambda} \right) + \phi ,$$

where ϕ = phase of Γ , so that a constant phase front is defined by

$$\angle P = \text{constant} , \quad (11)$$

and

$$\ell_1 + \ell_2 = \text{constant} . \quad (12)$$

The latter is the criterion for an ellipse, the foci of which are the transmitter antenna and an image of this antenna. This elliptical phase front can usually be approximated by a spherical phase front emanating from the ground immediately below the transmitter. It is, therefore, evident that in a ground-plane range, the target must be inclined to preserve the correct viewing aspect angle.

For the case of $|\Gamma| \neq 1$, the relationships are not so tractable. The amplitude expression becomes the familiar:

$$|P| = A_1^2 + A_2^2 + A_1 A_2 \cos (\theta_1 - \theta_2) . \quad (13)$$

However, the phase expression does not simplify. Consideration of the vector addition shows that the constant phase surface is approximately elliptical at the peaks of the amplitude pattern but departs rather widely from this surface at the nulls in the pattern.

The reflected radiation from the target follows the same criteria as those for radiation from the transmitter. In general, the phase and amplitude of the scattering aperture are unknown, so that recourse must be made to the approximate or estimated scattering pattern of the target. If the pattern has amplitude variations so that the direct and reflected ray are significantly different, problems in the measurement are evident.

As an approximation, the target may be considered to be small, so that the fields at a point in the receive antenna are

$$A_1 e^{j\theta_1} + A_2 e^{j\theta_2} , \quad (14)$$

where the previous definitions hold, except A_1 and A_2 are multiplied by variations in the scattered pattern.

The power of the field at the receive antenna changes from that for an isotropic scatterer, namely

$$P = 2A_0^2 [1 + \cos(\theta_1 - \theta_2)], \quad (15)$$

to

$$P = A_1^2 + A_2^2 + 2A_1A_2 \cos(\theta_1 - \theta_2). \quad (16)$$

The measured cross section, σ , compared to that of a reference can be in considerable error. From this, it is concluded that the scattered pattern must be broad compared to the angular difference in radiated direction of the direct and reflected rays. This will generally be the case if the far-field condition for the system of the target and its image is satisfied, although the target size should also be considered.

An interesting case is that of a small target. The field produced across the receive aperture is given by Equations 9 and 10. Measurement errors will occur for a finite aperture unless the range is long and the aperture small compared to the sinusoidal amplitude variation. However, if an isotropic receive antenna located at the same height as the transmit antenna is used, these errors are minimal. Thus, the far-field criteria do not apply to very small targets measured with very small antennas.

EFFECT OF TARGET ON FIELD

The errors produced by background are appreciable unless the background return is some very small fraction of the target return. The background of interest is that which exists when the target is being measured and is not usually the level produced by nulling with a cancellation circuit.

The measurement of change of the background level in most systems is not easily accomplished. The change is not readily calculated because of ambiguities in the phase addition between the cancelling network and the background.

One method of measuring background is the quasi-doppler method, in which the target is moved with respect to the background. While this technique has definite limitations (i. e., target motion will change the target-background interaction), it has been found that the level change in the background can be established.

Measurements of target effects on background were made on a 70-ft ground range at 360 megacycles. The background in the target area consisted of a 12- by 12-ft vertically mounted 25-db absorber wall behind the

target. This absorber wall was used to shield the support. Recorded return of the target support was approximately 25 to 30 db below a standard reference sphere.

A target was used in two aspect angles having an optical blockage of 8.2×10^{-4} sq m nose-on and 2.6×10^{-3} sq m broadside. Using the quasi-doppler technique to establish the background level, the changes in background level are indicated in Figure 3.

If it is assumed that, for the case with smaller optical blocking, the ratio of target return to background without the target was 20 db, the ratio return with the target would be yielding, from Figure 1, a potential error of +2.7 to -4 db.

Extrapolating the results to a 50-db wall, the change in background would be on the order of 0.95 db for the monostatic case. Starting with the same 20-db ratio as in the above paragraph, the ratio would degrade to 19.05 db, and the potential error would be between +0.93 and -1 db.

STANDARDS AND INTERACTION

Two standards that have been used extensively are the flat plate and the conducting spheres. The flat-plate cross section is easily calculated using standard equations; however, alignment is critical, and stability in an outdoor range can be a problem. On the other hand, the sphere has negligible alignment and stability problems, although the radar cross section is not always simple to compute.

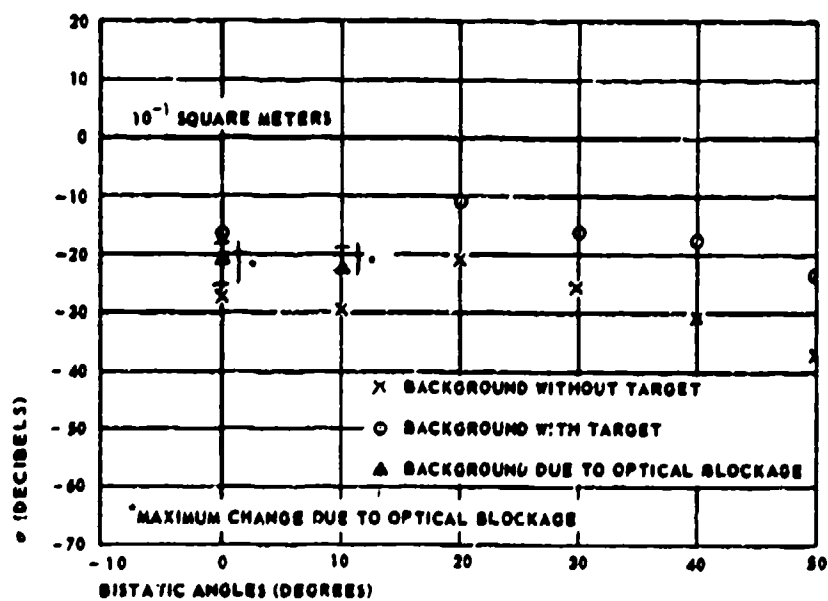
The major problem in the use of a sphere (or any standard) in a ground-plane range is the fact that the bistatic return must be known and used. This requirement arises from the fact that the sphere is not a true isotropic reflector of cross section πr^2 . Hence, the bistatic angle between the direct and the reflected rays, and the angle between transmit and receive antennas (assume they are not the same), influence the received power and the calibration of the range. The bistatic return for spheres in the resonant region is given in Figures 4, 5, and 6. The return is given in decibels relative to πr^2 versus Kr , where

$$K = \frac{2\pi}{\lambda}, \quad (17)$$

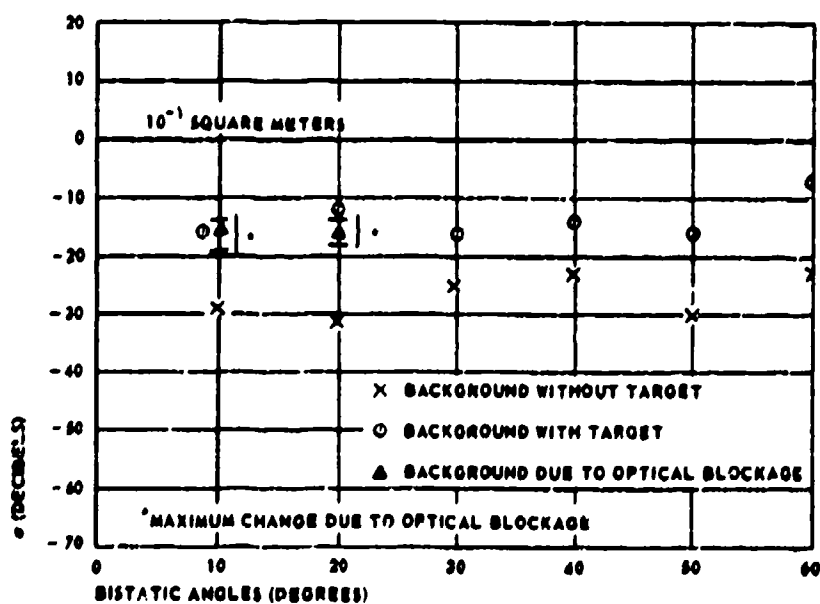
and r = radius of sphere. The curves described above are E-plane only.

Two bistatic angles are of interest. One is formed by the line between the approximate phase center of the transmit antenna system (i. e., including image) and the sphere and of the direct ray to the receive antenna. The other is formed by the line from the transmit antenna system and the ray from the sphere, which reflects to the receive antenna.

These angles, the curves, and the second expression in Equation 8 can be used in establishing the calibration in this case. For a ground



A. NOSE-ON CONDITION



B. BROADSIDE CONDITION

Figure 3 - Effects of Target on Background

with $|\Gamma| \approx 1$, A_1 and A_2 are the values determined from curves for the bistatic angles of interest.

While both a sphere and a flat plate exhibit sensitivities to bistatic angle, the sphere has one characteristic that is a source of error: the scatter at ~ 90 -deg bistatic angle. Since this scatter is appreciable, significant energy is reflected into the ground. This energy is reflected, strikes the sphere, and is re-radiated.

A computation of the ratio of directly scattered energy to this interaction signal can be made if the sphere is at least $4r^2/\lambda$ above the ground (i. e., the image of the sphere is in the far field).

The radar cross section of the sphere is given by

$$\pi r^2 \Delta, \quad (18)$$

where

r = radius and

Δ = correction factor computed from curves.

The directly scattered power per steradian divided by incident power per unit area is then

$$\frac{\pi r^2}{4\pi} \Delta_1. \quad (19)$$

Δ_1 is determined at the bistatic angle between the transmit and receive antennas.

The same ratio for power interacting with the ground or other flat objects is:

$$\left(\frac{\pi r^2}{4\pi} \Delta_2 \right) \left(\frac{\pi r^2}{4\pi R^2} \Delta_3 \right). \quad (20)$$

where

$R/2$ = height of sphere above ground,

Δ_2 = correction factor for bistatic angle between incident field and vertical, and

Δ_3 = correction-factor bistatic angle between vertical and ray to receive antenna.

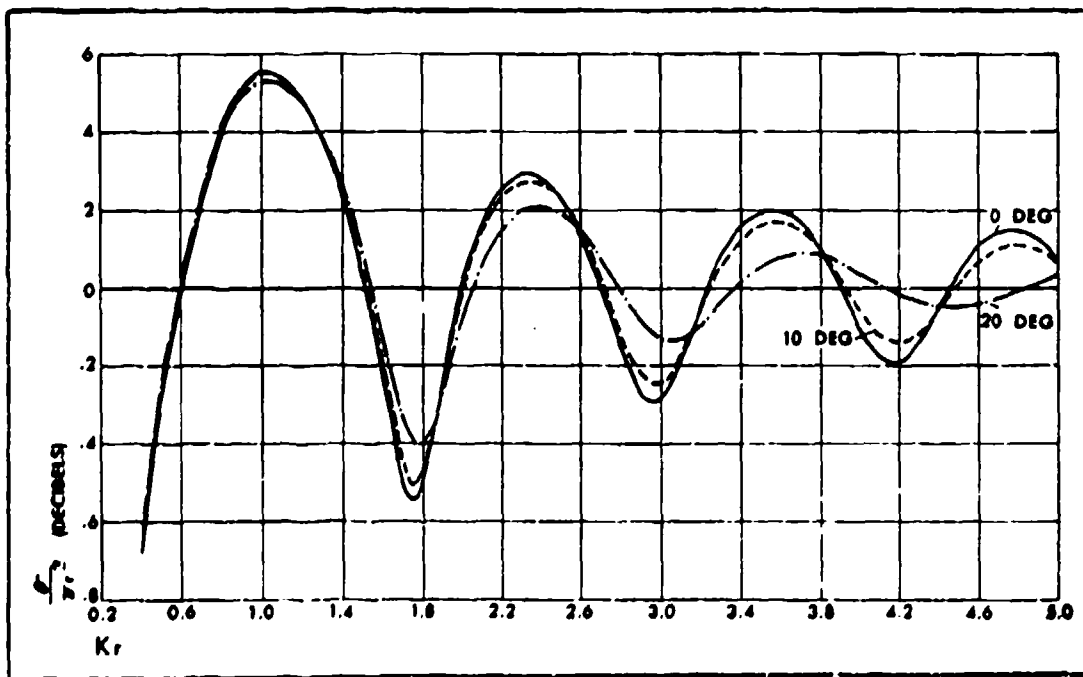


Figure 4 - Sphere Return at 0-, 10-, and 20-Deg Bistatic Angles

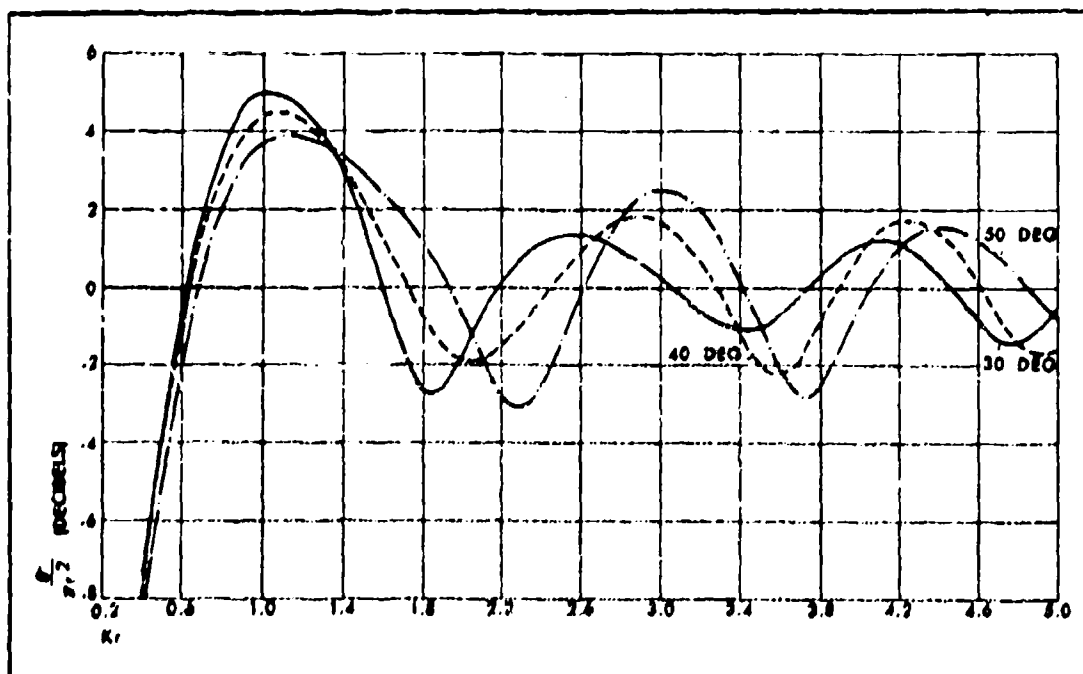


Figure 5 - Sphere Return at 30-, 40-, and 50-Deg Bistatic Angles

The ratio of directly scattered energy (S_1) to interaction energy (S_2) is then:

$$\frac{S_1}{S_2} = \frac{4R^2 \Delta_1}{r^2 \Delta_2 \Delta_3} \quad (21)$$

The worst-case conditions yield a ratio:

$$\frac{S_1}{S_2} = \frac{4R^2}{33.1r^2} \quad (22)$$

at $Ka = 1.75$.

For the case of $Ka = 10$ and R just large enough for the sphere to be on the far field, $S_1/S_2 = 647$, or 28.1 db

From Figure 1, an error of +0.4 or -0.6 may occur for this condition. Since the target can be expected to have interaction, an error is expected unless means are provided to minimize interaction for both reference and target.

In addition to the above considerations, there are other well-recognized factors affecting the use of a sphere. These factors are surface accuracy of the sphere and the effect of the target mount.

CONCLUSIONS

In view of the above considerations, certain procedures must be included in the design and checkout of a cross-section range. After a field probe of the target aperture (without target) has been completed, a preliminary rotational scattering pattern should be recorded to the assumed pattern used in the range design.

The background return should also be measured, since the accuracy of the preliminary pattern and the data is strongly dependent on changes of background. If the background return is high, either it must be proportionately reduced or a measurement procedure used that permits separation of the target and background signals.

A check on the coupling between the target and ground should be made by vertical motion of the target. A similar test with the reference sphere should be made and the coupling reduced through judicious use of absorbers or reflectors. And, finally, considerable care must be exercised in the calibration procedure that employs a reference sphere.

The ultimate objective is to keep measurement accuracy commensurate with the dimensional accuracy of the target and with the intended use of the desired data.

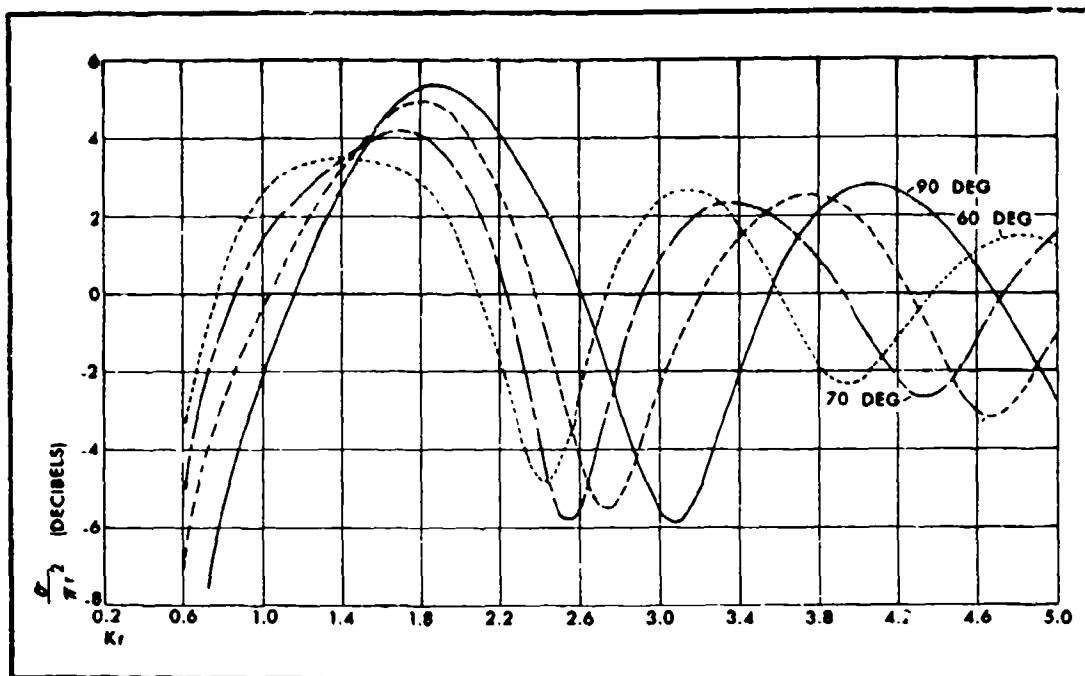


Figure 6 - Sphere Return at 60-, 70-, 80-, and 90-Deg Bistatic Angles

LIST OF REFERENCES

1. Bachman, C. G.; King, H. E.; and Hansen, R. C.: "Techniques for Measurements of Reduced Radar Cross Sections," The Microwave Journal, February 1963; 6:61-67.
2. Bachman, C. G.; King, H. E.; and Hansen, R. C.: "Techniques for Measurements of Reduced Radar Cross Sections, Part II," The Microwave Journal, March 1963; 6:95-101.
3. Bachman, C. G.; King, H. E.; and Hansen, R. C.: "Techniques for Measurements of Reduced Radar Cross Sections, Part III," The Microwave Journal, April 1963; 6:80-86.
4. Willcox, P. J.: Very Small Radar Cross-Section Measurements at UHF. Akron, Ohio, Goodyear Aerospace Corporation. December 1963.

ACKNOWLEDGMENTS

Contributing technical aid and advice were: G. H. Welch, B. M. Bowman, D. L. Brown, F. E. Fischer, and A. E. Marble, Jr.

RADAR REFLECTIVITY MEASUREMENT DATA FORMAT STANDARDS

Stephen L. Johnston
Chief, Radiation Systems Branch
Advanced Systems Laboratory
U. S. Army Missile Command
Redstone Arsenal, Alabama

ABSTRACT

Results of a survey of radar reflectivity measurement data format standards made with invitees of the forthcoming Radar Reflectivity Measurement Symposium are presented. From the results it was concluded that while certain data types are more prevalent than others, at present there are no universally used standards of radar reflectivity measurement data format. Advantages of standards are discussed along with considerations for possible standards.

INTRODUCTION

Current interest in radar cross section of missiles, aircraft, and satellites has caused the installation of a number of radar cross-section ranges in the United States. This interest, in fact, has motivated Lincoln Laboratory to host this symposium on radar reflectivity measurement. The existence of these many ranges is also evident from the number of papers describing ranges presented at this symposium.

During the planning for this symposium, discussion with steering committee members indicated interest in measurement data standards. The writer had previously had experience with a number of ranges in this regard. It was therefore decided to conduct a survey among symposium invitees and determine the situation in greater depth. Study of results and comments could then provide a basis for possible recommendations on this matter. It is recognized that a survey can be a popularity poll, however it was felt that replies would indicate current technical practice based upon engineering and economic considerations rather than popular opinion.

SURVEY

The questionnaire in figure 1 was sent to the 75 organizations that were invited to participate in this symposium. These organizations include both data measurers and data users in Government and industry. The 44 replies received reflected the interest in this topic. While most of the major organizations replied, it is regretted that several prominent groups did not. The majority of the respondents (57%) were from industry as expected, followed by Government (27%) and non-profit organizations (16%). Useful information from organizations currently active in radar cross section measurement/use was received from 37% of the respondents. Approximately the same percentages of useful replies were from those who either use only or both use and measure (32%) as from those who either measure only or both measure and use (84%). Admittedly the term "use" was

somewhat vague in the survey, thus implications regarding users are somewhat uncertain. There were 68% who indicated that they are both measurers and users, 18% who are measurers only, and 16% who are users only. It is unfortunate that most of the replies from users only were very general and lacking in details. Data type and format furnished by a measurer are primarily determined by user requirements. The lack of very definitive replies from users only thus constitutes a deficiency in this survey. Data from those who are both users and measurers somewhat offsets this however. It is also recognized that data type and format are also influenced by the type of measurement facility, the type of object measured, the number of measurements made by a facility and the use which is made of the data. Conclusions therefore are not susceptible to universal application.

Analog data recording is more widely used by the measurers and measurers/users than digital; 66% vs 31%. Nearly all (97%) measurers who take digital data also take analog data. While some of the measurers employ measurement techniques that are not readily susceptible to digitizing, it is clear that digital data is currently not being taken in as many cases as it could be if it were required by the user.

Equal percentages of the measurements are made indoors as outdoors (44%), while 12% of the measurers report dual capability. The majority of measurements are made statically - 66% indicated static only, 19% dynamic only, 15% both, 81% static only or static and dynamic and 34% dynamic only or dynamic and static. Again, the term dynamic was not completely defined, thus not all dynamic measurements indicated are made while the object is in actual flight.

Scale measurements are made by more respondents (37%) than full scale (26%). A dual capability was reported by 37% thus 74% reported either scale only or scale & full scale to 53% for either full scale only or both.

Rectangular coordinates for analog data are extremely popular (96%) for measurements not recorded on film or displayed on an oscilloscope. Only 1% indicated no rectangular coordinate capability, while 18% had no polar coordinate capability. Dual capability was indicated by 27%.

Emission use was not clearly indicated by a number of measurers although CW (69%) seems to predominate over pulse (38%). High resolution measurements were reported by 22%. Phase measurements are made by 13% of the respondents. Many of the respondents have several facilities or facilities with multiple capabilities.

The types of polarization used were not generally indicated by the respondents. Use of different polarizations, e.g., HH or HV either simultaneously, or sequentially would generally result in more recordings, thus conclusions of the survey should not be adversely affected.

The sparse use of digital data recording was further confused by the types of digital data employed - equal percentages (25% of the digitizers) use paper tape, magnetic tape and punched cards. The remainder of the digitizers are now planning to install digitizing devices. No two organizations using digital data appear to use the same data format.

Rectangular chart heights in use vary from 3 inches to 10 inches. The latter is more popular (44%) although 26% of the measurers gave no data, thus the complete picture is unknown. Maximum vertical scale coverage (presumably system dynamic range) varies from 40 db to about 80 db. The most extensively used value cannot be concluded from the replies. Vertical scale factors vary from about one to ten db per inch. Again there is no most prevalent value since the number of no data detailed replies exceeded the apparently most prevalent value. Practically all measurers record in db, usually DBS (decibels with respect to one square meter). Only two indicated use of σ/λ^2 basis. Data linearity was frequently not mentioned.

Aspect angle scale factors vary from 0.5 to 36 degrees per inch. Most measurers can use any of a number of aspect angle scale factors. It is recognized that chart scale factors used are determined by the type measuring system, its dynamic range, measuring frequency, the object, portion of the object measured and usage of the data taken.

SUMMARY OF RESULTS FROM THE SURVEY

1. Most of the measurers have an analog data presentation capability but only 1/3 have a digital capability.
2. The analog capability is divided among a number of recorder paper sizes. The number of scale factors used is large.
3. Most of the measurers have recorders with rectangular coordinates. Rectangular coordinates are more popular than polar coordinates.
4. The limited digital capability is equally divided between paper tape, cards and magnetic tape. (Most facilities can readily convert cards to magnetic tape or vice versa, therefore paper tape is in the minority).

CONCLUSIONS FROM SURVEY

1. The large number of analog recorder paper sizes, coordinate systems, and scale factors in use presently make rapid interchange and comparison of data difficult, causing confusion and requiring extra work in use of data.
2. There is no universally used coordinate system, axis system, direction of rotation, standard reference, or unit of measurement. Confusion exists in this area.
3. Many of the measurers do not now have digital data facilities, indicating an absence of requirements by using personnel. Possibly lack of volume of measurements, application of data, difficulty of digitizing data, or lack of appreciation of usefulness of digital data may be factors in this.

4. Even though a very limited digital data capability exists, no two organizations appear to use the same digital recording medium, or data format. Interchange of digital data therefore requires extensive conversion of medium and format before it can be used by a second organization.

RECOMMENDATIONS

1. A preferred standard for analog recording should be established, covering paper size, coordinate system and scale factor(s). Considerations for a possible standard are discussed in Appendix I.

2. A preferred standard should be established for measurement coordinate system, axis system, direction of rotation, standard reference and unit of measurement. Considerations for a possible standard are discussed in Appendix II.

3. A preferred standard for digital recording should be established for recording medium and data format. Considerations for a possible standard are discussed in Appendix III.

APPENDIX I - PROPOSED ANALOG RECORDING STANDARD CONSIDERATIONS

1. Use of decibels (DRSM) plotted on a linear scale will facilitate application of correction factors, etc, and ready relative comparison of values at different angles, comparison of values for different frequencies, polarizations, bodies, etc. Conversion to square wavelength references is easily accomplished.

2. Separate standards are probably required for static and dynamic measurements. Static measurements should be in the form of DRSM vs aspect angle for various pitch and/or roll angles for each polarization used, while dynamic measurements will probably be in the form of DBCM vs time from some specified reference.

3. While both rectangular and polar coordinates are useful, the rectangular form can more easily be expanded or contracted in recording, by scale change and is therefore somewhat superior.

4. The analog format will have to be different for "special" ranges such as high resolution, swept frequency, etc. Even so, a minimum number of standards is preferred.

5. It is preferable that the measuring system incorporate appropriate linearizing circuitry so that the graph can be read directly in db without necessity for an overlay or special scale. Zero DRSM should correspond to an integral value say -20, -30, etc. as appropriate. The zero DBCM value should be clearly marked in the notes space on the chart.

6. The number of ordinate and abscissa scale factors should be minimized but the value used should be clearly marked in the notes space on the chart.

APPENDIX II - CONSIDERATIONS FOR MEASUREMENT SYSTEM COORDINATE STANDARDS

1. The measurement system coordinate should be standardized to include axis system, direction of rotation, standard reference value and unit of measurement.

2. The document IRIG STD 102-61 "Coordinate System and Data Format For Antenna Patterns" is a good starting point in the preparation of such a standard.

APPENDIX III - PROPOSED DIGITAL RECORDING STANDARD CONSIDERATIONS

1. Paper tape has only limited usage as compared to magnetic tape or punched cards in the automatic data processing field.

2. Data which is to be processed by digital computers generally is most efficiently used if on magnetic tape. Magnetic tape is much more compact than either paper tape or punched cards. Magnetic tape can be readily converted to punched cards or vice versa.

3. The data format should be standardized in detail in order to eliminate the necessity for computer reprogramming, data conversion, etc.

4. Data should be in DBSM vs aspect angle. Both quantities should be sufficiently quantized to faithfully preserve data. This is extremely important for angular data. Quanta of 0.1 degree will generally be adequate.

5. The digital data should require no further conversion to obtain DBSM and angle in degrees.

SYMPOSIUM
OF
RADAR REFLECTIVITY MEASUREMENT

ORGANIZATION _____ CONTACT INDIVIDUAL _____

ARE YOU A DATA MEASURER OR USER? _____ TELEPHONE NUMBER: _____

RANGE TYPE:

INDOOR/OUTDOOR _____ STATIC/DYNAMIC _____

FULL SCALE/MODEL SCALE _____ AIRCRAFT/MISSILES/OTHER _____
(specify)

DATA TYPE: CW/PULSE HIGH RESOLUTION/PHASE, ETC. _____

I. Analog Data

Usual Coordinate System _____

Data Resolution _____

Usual Recorded Quantities e.g. σ -DBSM, Aspect Angle 0° - 360° _____

Make & Model of Recorder: _____

Please attach sample unclassified graph

II. Digital Data

Usual Coordinate System _____

Usual Recorded Quantities _____

Type of Recording: Paper Tape, Punched Cards _____ Magnetic Tape _____

Make and Model of Recorder _____. Please describe digital data
format in detail below, including data sequence, units, number system (binary,
decimal, BCD, etc. and whether fixed or floating point) magnetic tape density
(characters per inch) _____

REMARKS: _____

RADAR MEASUREMENT STANDARDIZATIONS NEEDED FOR SIMULATION STUDIES

**C. Krichbaum
Battelle Memorial Institute**

ABSTRACT

The purpose of this paper is to show some inadequacies of past and present radar-range measurements for use in simulation studies and to show some changes needed to meet the requirements of users of radar-range data in simulation studies. The scope of some of these programs is defined in terms of types of calculations, required inputs, and desired outputs. Factors shown to affect the types of data needed include effects of asymmetries, polarization effects, and the need for complete scattering matrix measurement. The effect of measurement error upon choice of measurement parameters for symmetric targets is discussed.

SIMULATION STUDY

A radar cross section simulation program is a program which attempts to synthesize radar signatures which would be observed by a defensive radar during a hypothesized missile flight. Information necessary for such a calculation includes a history of the relative spatial positions and attitudes of the target and radar site and sufficient static cross section data to completely describe the scattering properties of the target over all ranges of angular variables which might occur during simulated flight. In general, either telemetry data from an actual missile flight or calculated data from a computer six degree of freedom trajectory code is necessary to supply sufficient trajectory information. This trajectory data is then combined with the scattering data, usually by computer calculation, to obtain the calculated signatures. This discussion is limited to some of the problems encountered when attempting to obtain suitable scattering data from static radar range measurements for use in a simulation calculation.

SCATTERING MATRIX FORMULATION

In general, a radar signature calculation must account for:

- (1) radar frequency
- (2) aspect angle
- (3) polarization angle (if linear polarization is assumed)
- (4) target roll angle
- (5) transmitting and receiving antenna polarizations
- (6) possible dielectric coating of target

The aspect angle and polarization angle are defined in Figure 1.

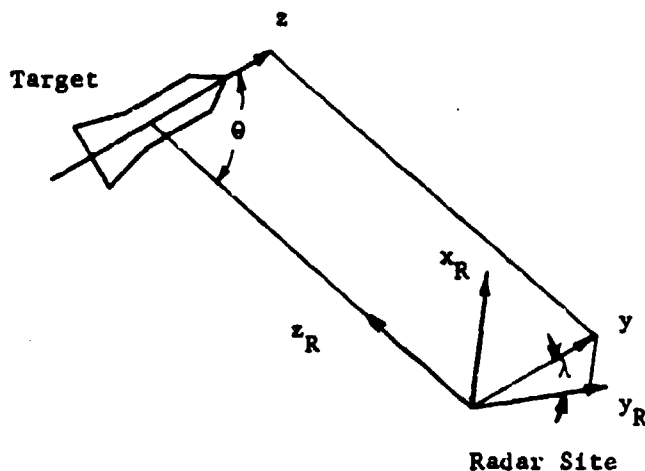


Figure 1

θ = Aspect angle

λ = Polarization angle

z = Target roll axis

z_R = Axis along the radar line of sight

y_R = Axis in a horizontal plane

x_R = Axis which, with y_R and z_R , forms an orthogonal right-handed set

y = The projection of the z axis into the $x_R y_R$ plane

There are two basic methods of considering the effects of aspect and polarization angles. One method is to measure the cross section of the target at all possible combinations of aspect and polarization angles which might be observed during simulated flight. This necessitates measuring cross section vs. aspect angle for a large number of linear polarizations, and storing the data on magnetic tape. If the target is rotationally symmetric, a second method, that of using a set of scattering matrix parameters vs. aspect angle for the target, results in a savings both in amount of data required to describe the scattering properties of the target and in machine time required to calculate the signatures. For targets possessing this symmetry, three measured quantities corresponding to each aspect angle permit calculation of the cross section for any polarization angle and for any combination of linear and circular transmitting and receiving antenna polarizations.

In the past, successful utilization of the scattering matrix to synthesize signatures for configurations of practical interest has been thwarted by a lack of polarization diversity in the available static scattering data.

In general, the scattering matrix solution for cross section is a linear combination of measured parameters with coefficients which are functions of the polarization angle. Because of its form, the solution can contain a cumulative error greater than the individual errors in the various measured parameters. The measured parameters of interest for symmetric configurations will likely be either:

Amplitude Measurements

- (1) amplitude - horizontal polarization
- (2) amplitude - vertical polarization
- (3) amplitude - 45° linear polarization

or

Amplitude With Phase Measurements

- (1) amplitude - horizontal polarization
- (2) amplitude - vertical polarization
- (3) relative phase - between horizontal and vertical returns

This amount of data can easily be held in core memory during computer calculations for the entire trajectory.

The choice of which set of parameters to measure depends upon the measurement capabilities of the radar range involved. If both amplitude and phase measurement capabilities are available, the choice depends upon the relative precision to which these parameters can be measured. This question is discussed in the next section.

If the target does not possess cylindrical symmetry, i.e., sufficient asymmetries exist such that the scattering data is significantly roll-angle dependent, the number of parameters needed to describe the target scattering matrix are five. Up to seven measurements are required to determine these five parameters which are functions of two variables, aspect and roll angles¹. The large number of data points involved requires tape storage and utilization of the static data for the nonsymmetric target.

EFFECT OF MEASUREMENT ERROR UPON CALCULATION OF CROSS SECTION HISTORIES USING STATIC DATA

The radar cross section of a symmetric target may be calculated for arbitrary aspect and polarization angles using either (1) data from

3 static amplitude measurements or (2) data from amplitude and phase measurement for horizontal and vertical polarizations. The expression used to calculate cross sections for linear polarization using static measurements of both amplitude and phase is:

$$\sigma_H = \sigma_{VV} \sin^4 \lambda + \sigma_{HH} \cos^4 \lambda + \sqrt{\sigma_{HH} \sigma_{VV}} \frac{\sin^2 2\lambda}{2} \cos \varphi \quad (1)$$

where:

σ_H = expected radar cross section observed at aspect angle θ and polarization angle λ by a radar using horizontal linear polarization

σ_{HH} = static radar cross section of the target measured at aspect angle θ with the target body axis in the horizontal plane and using linear horizontal polarization

σ_{VV} = static radar cross section of the target measured at aspect angle θ with the target body axis in the horizontal plane and using linear vertical polarization

λ = polarization angle - that angle between the projection of the target axis into a plane at the radar site perpendicular to the radar line-of-sight, and a local horizontal perpendicular to the radar line of sight.

Also,

$$\varphi = \varphi_{11} - \varphi_{22} \quad (2)$$

where

φ_{11} is the phase of σ_{VV}

φ_{22} is the phase of σ_{HH}

Assume that λ is known exactly. The expression showing an incremental change in σ_H is:

$$\begin{aligned} \sigma_H + \Delta\sigma_H &= (\sigma_{VV} + \Delta\sigma_{VV}) \sin^4 \lambda + (\sigma_{HH} + \Delta\sigma_{HH}) \cos^4 \lambda + \\ &+ \sqrt{(\sigma_{HH} + \Delta\sigma_{HH})(\sigma_{VV} + \Delta\sigma_{VV})} \frac{\sin^2 2\lambda}{2} (\cos \varphi + \Delta \cos \varphi) \end{aligned} \quad (3)$$

Substituting (3) into (1),

$$\Delta\sigma_H = \Delta\sigma_{VV} \sin^4 \lambda + \Delta\sigma_{HH} \cos^4 \lambda +$$

$$\begin{aligned}
& + (\sqrt{(\sigma_{HH} + \Delta\sigma_{HH})(\sigma_{VV} + \Delta\sigma_{VV})} - \sqrt{\sigma_{HH} \sigma_{VV}}) \frac{\sin^2 2\lambda}{2} \cos \varphi + \\
& + \sqrt{(\sigma_{HH} + \Delta\sigma_{HH})(\sigma_{VV} + \Delta\sigma_{VV})} \frac{\sin^2 2\lambda}{2} \Delta \cos \varphi
\end{aligned} \quad (4)$$

Assuming σ_{VV} and σ_{HH} are approximately of equal magnitude, σ , and assuming increments in each are positive and approximately $\Delta\sigma$, (4) becomes:

$$\begin{aligned}
\Delta\sigma_H \sim & (\sin^4 \lambda + \cos^4 \lambda + \frac{\sin^2 2\lambda}{2} \cos \varphi + \frac{\sin^2 2\lambda}{2} \Delta \cos \varphi) \Delta\sigma + \\
& + \sigma \frac{\sin^2 2\lambda}{2} \Delta \cos \varphi
\end{aligned} \quad (5)$$

This expression is maximized for positive increments in $\cos \varphi$ except at $\varphi = 0$ where only negative increments are possible. Assuming such values for $\Delta \cos \varphi$ are taken and using trigonometric substitutions, (5) becomes:

$$\begin{aligned}
\frac{\Delta\sigma_H \max}{\sigma} \sim & \left[1 + (\cos \varphi + \Delta \cos \varphi - 1) \frac{\sin^2 2\lambda}{2} \right] \frac{\Delta\sigma}{\sigma} + \\
& + \frac{\sin^2 2\lambda}{2} \Delta \cos \varphi
\end{aligned} \quad (6)$$

An alternate expression for σ_H using amplitude measurements only is²:

$$\sigma_H = \sigma_{45} \sin^2 2\lambda + [\sigma_{HH} \cos^2 \lambda - \sigma_{VV} \sin^2 \lambda] \cos 2\lambda \quad (7)$$

where

σ_{45} = static amplitude measured at 45° linear polarization

$$\begin{aligned}
\Delta\sigma_H = & \sin^2 2\lambda \Delta\sigma_{45} + \cos^2 \lambda \cos 2\lambda \Delta\sigma_{HH} - \\
& - \sin^2 \lambda \cos 2\lambda \Delta\sigma_{VV}
\end{aligned} \quad (8)$$

or

$$\begin{aligned}
\Delta\sigma_H = & \sin^2 2\lambda \Delta\sigma_{45} + (\cos^4 \lambda - \cos^2 \lambda \sin^2 \lambda) \Delta\sigma_{HH} + \\
& + (\sin^4 \lambda - \cos^2 \lambda \sin^2 \lambda) \Delta\sigma_{VV}
\end{aligned} \quad (9)$$

Using similar approximations as were used to obtain (5),

$$\left. \begin{aligned} \frac{\Delta\sigma_H}{\sigma} &= \cos^2 2\lambda \frac{\Delta\sigma}{\sigma} + \sin^2 2\lambda \frac{\Delta\sigma_{45}}{\sigma} \\ \Delta\sigma_{45} &= \Delta\sigma \end{aligned} \right| \quad \frac{\Delta\sigma}{\sigma} \quad (10)$$

Since we are assuming symmetry, knowledge of $\cos \varphi$ and σ_{45} is apparently equivalent. The expression relating these two quantities is:

$$\sigma_{45} = \frac{1}{4} [\sigma_{HH} + \sigma_{VV} + 2 \sqrt{\sigma_{HH} \sigma_{VV}} \cos \varphi] \quad (11)$$

or

$$\cos \varphi = \frac{4\sigma_{45} - \sigma_{HH} - \sigma_{VV}}{2 \sqrt{\sigma_{HH} \sigma_{VV}}} \quad (12)$$

It is not necessary to evaluate $\cos \varphi$ explicitly when calculating cross sections using σ_{HH} , σ_{VV} , and σ_{45} . It seems straightforward to use (6) and (10) to compare the accuracy of the two methods for calculating σ_H . Assuming the measurement error is the same for measurement of σ_{HH} , σ_{VV} , and σ_{45} , the maximum error in the calculated σ_H using amplitude measurements is identically the measurement error (assuming θ and λ are known very accurately). The error in σ_H using σ_{HH} , and σ_{VV} , and φ can be either less than $\Delta\sigma$ or greater than $\Delta\sigma$. Figures 2 and 3 are plots of Equations (6) and (10) for polarizations angles of 30° or 60° and a number of different values of φ . An individual phase measurement error of 5° was assumed for Figure 2 and an error of 10° was chosen for Figure 3. The signs of these errors were chosen to produce a positive maximum error in $\cos \varphi$ corresponding to a total error in φ of 10° and 20° , respectively, for the two cases. If σ_{45} can be measured to the same accuracy as σ_{VV} or σ_{HH} , similar accuracies are obtained by the two methods for an amplitude measurement capability of 1 db. or less if errors in φ can be limited to 10° . However, if φ can be determined to only 20° or more, the use of the three amplitudes measurements appears to result in more accurate calculations. This generalization also seems to hold if a calculation of cross section histories for an observing radar transmitting and receiving opposite senses of circular polarization is desired. A comparison of maximum possible error in calculating circularly-polarized cross sections using only amplitude measurements and using amplitude plus relative phase measurements is shown in Figures 4 and 5.

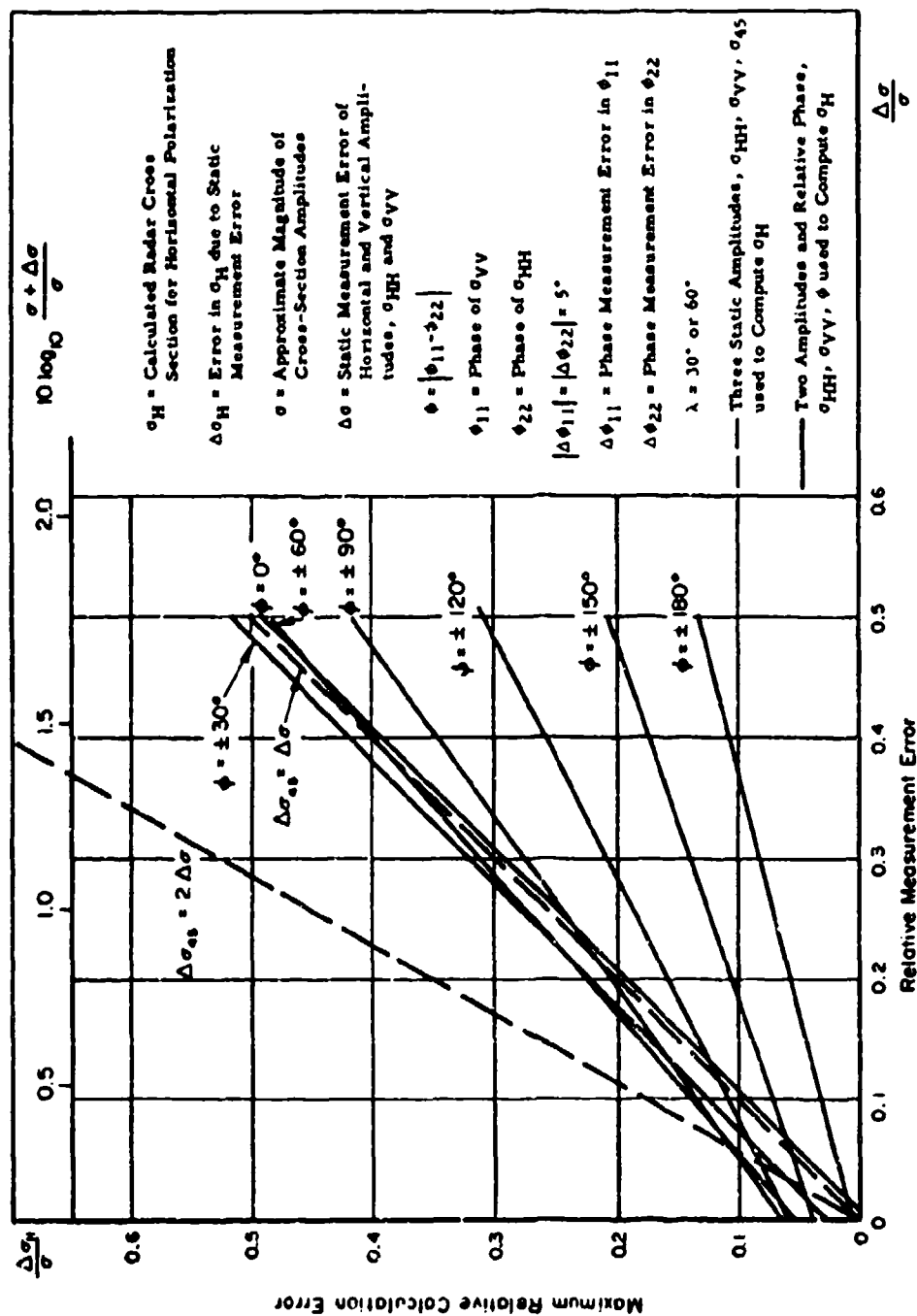


FIGURE 2. MAXIMUM RELATIVE CALCULATION ERROR VERSUS RELATIVE MEASUREMENT ERROR FOR LINEAR POLARIZATION AND 5° PHASE MEASUREMENT ERROR

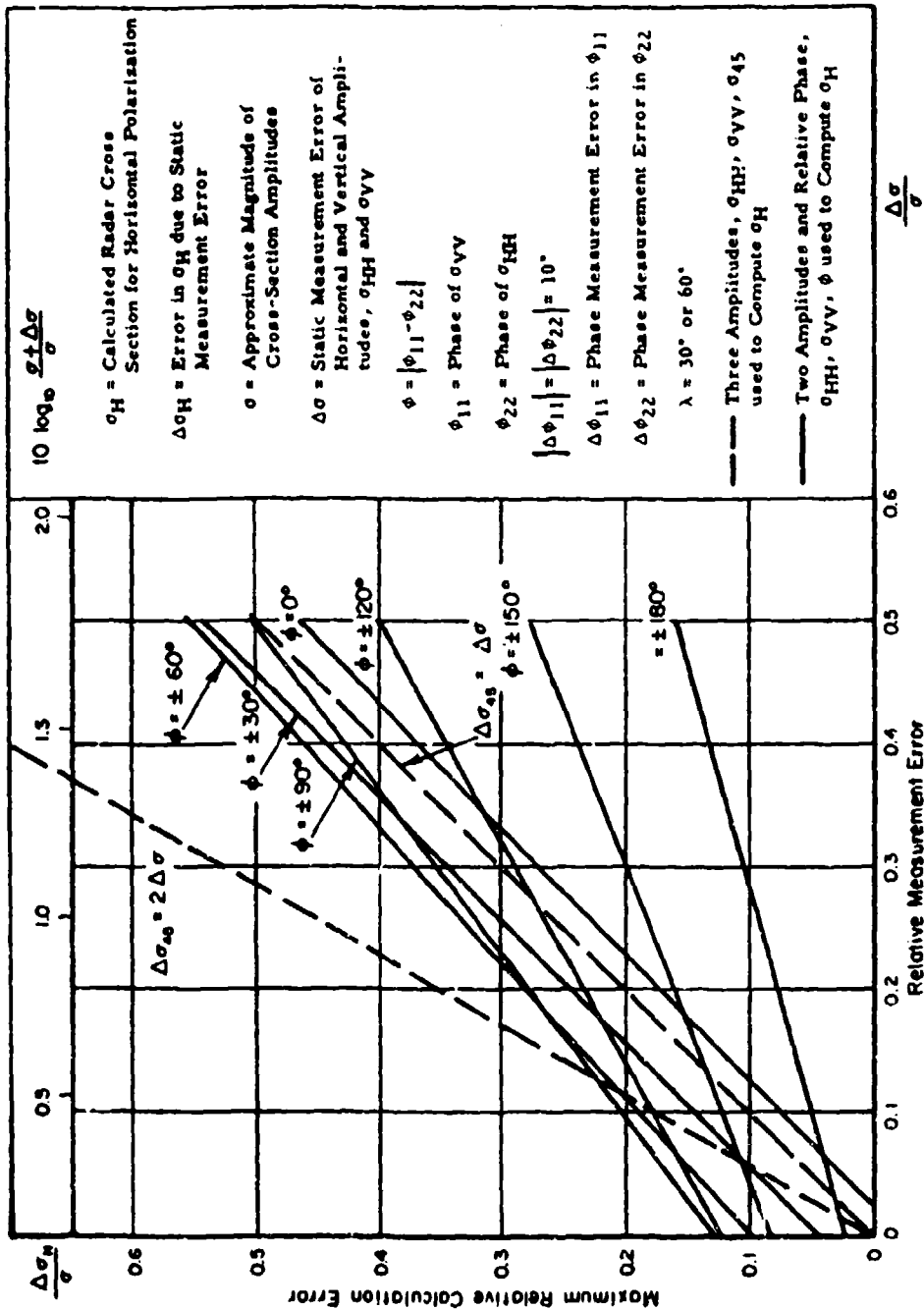


FIGURE 3. MAXIMUM RELATIVE CALCULATION ERROR VERSUS RELATIVE MEASUREMENT ERROR FOR LINEAR POLARIZATION AND 10° PHASE MEASUREMENT ERROR

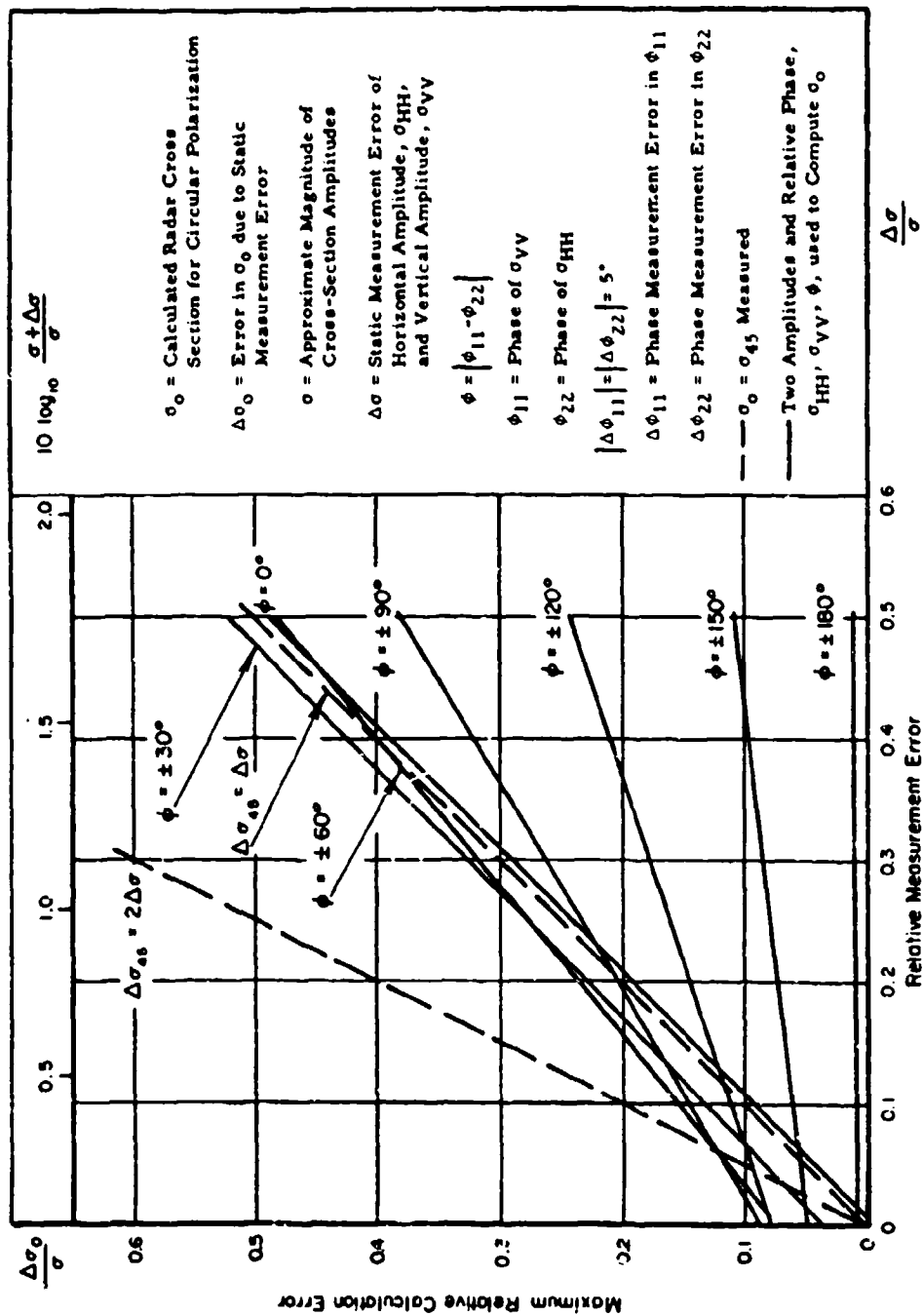


FIGURE 4. MAXIMUM RELATIVE CALCULATION ERROR VERSUS RELATIVE MEASUREMENT ERROR FOR CIRCULAR POLARIZATION AND 5° PHASE MEASUREMENT ERROR

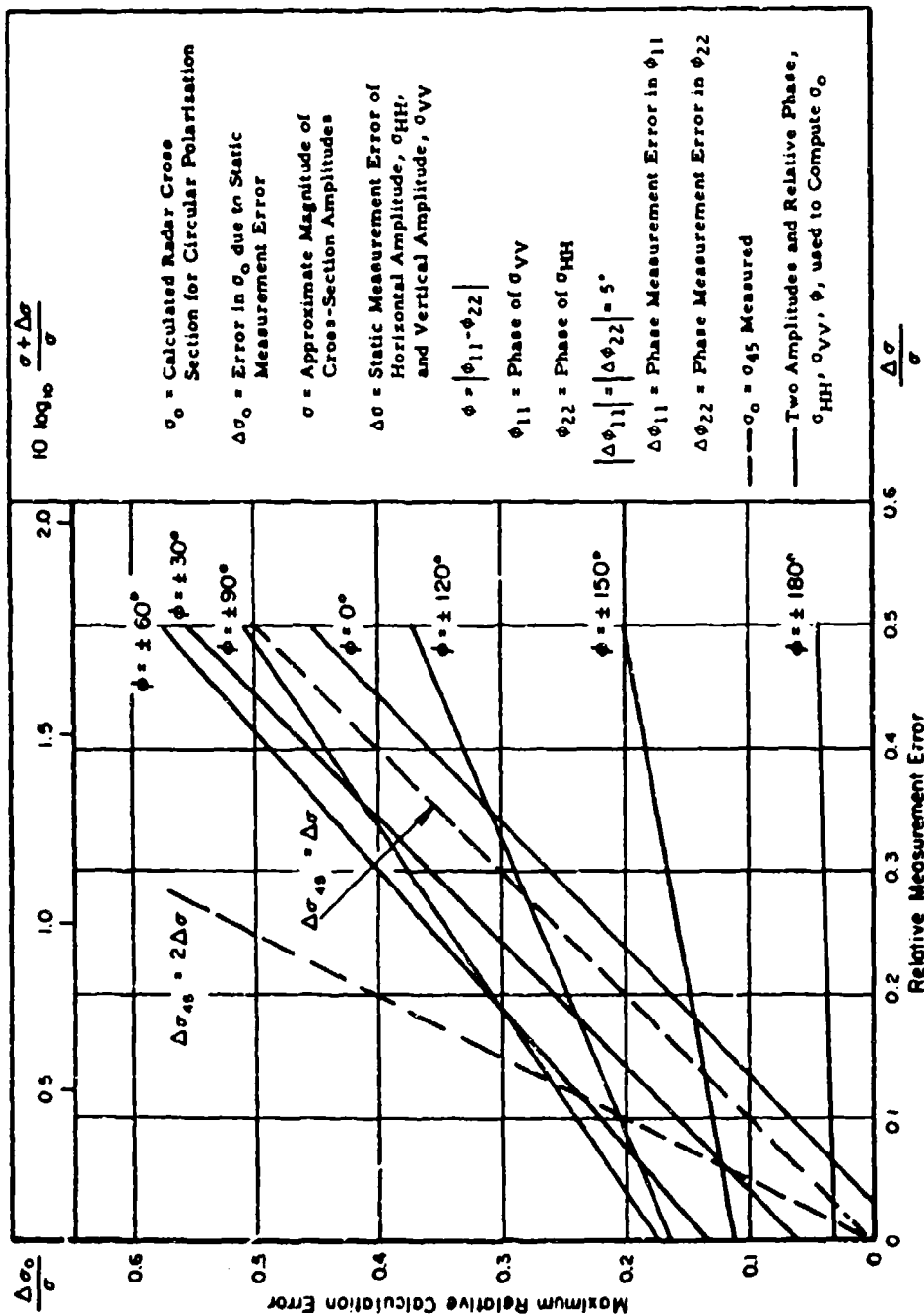


FIGURE 5. MAXIMUM RELATIVE CALCULATION ERROR VERSUS RELATIVE MEASUREMENT ERROR FOR CIRCULAR POLARIZATION AND 10° PHASE MEASUREMENT ERROR

SOME RECOMMENDED STANDARDIZATIONS

From the viewpoint of a user of radar range data for signature synthesis, the following practices are suggested.

1. Operational or test flight targets should be measured on a full scale range.
2. Targets should have dielectric coatings which match as well as possible those coatings which would be present during free-space flight.
3. Measurements on operational vehicles should be made over a wide range of frequencies. Measurements on flight test vehicles should be made at the frequencies of observing radars.
4. Sufficient data should be obtained to compute the scattering matrix.
5. A sufficient number of different polarizations should be used to permit a consistency check of the scattering data. For example, if a symmetric target is involved and amplitudes only are measured at horizontal, vertical, and 45° linear polarizations, a trivial calculation can be made to generate patterns for 30° and 60° linear polarization. If measured data at 30° and 60° were also available, the data user would have a good check on the reliability of the measured data. If horizontal and vertical amplitudes and phases are measured, an extra measurement at 45° would permit this consistency check.
6. Targets with cylindrical symmetry should be measured at several roll angles to check the validity of the symmetry assumption.
7. The measured data should be available to the user by means of magnetic tape or data cards in addition to the conventional analog plots.

BIBLIOGRAPHY

1. "Effects of Type of Polarization on Echo Characteristics", E. M. Kennaugh, The Ohio State University Research Foundation, Report 389-4.
2. "Memorandum on the Scattering Cross Section of Figures of Revolution With Application to Targets Above the Surface of the Earth (U)", R. J. Garbacz and S. Pitts, The Ohio State University Research Foundation, Report 925-4, Secret.

A NEW MINIMUM RANGE CRITERION FOR MEASUREMENT OF RADAR CROSS SECTIONS*

Leon Peters, Jr.
Associate Supervisor
Antenna Laboratory
Department of Electrical Engineering
The Ohio State University
Columbus 10, Ohio

ABSTRACT

This paper considers from a different point of view the assumption that the minimum range is $2D^2/\lambda$ where D is the dimension of the target. In order to obtain a proper phase distribution over the target this assumes the radar range antenna to be a point source. Most treatments of a radar antenna which is not a point source involve the calculations of field of the radar antenna at any target point P and this involves an integration over the surface of the radar antenna. This has led to many minimum range criteria, the most common of which is $2(D+d)^2/\lambda$ where d is the radar antenna dimension.

This entire approach is erroneous even though it is true that the fields at the point P obtained by this integration are correct. The assumption that this causes an increase in the minimum range neglects the cancellation that occurs at P of the energy radiated by different parts of the antenna.

A new picture is developed from the point of view of geometrical optics. The antenna with a uniform phase distribution is approached as a limiting case of a point source radiator. This point source is located so that the minimum range criterion is reduced. A new effective minimum range is given based on this geometrical optics limit.

This new approach is supported by Fresnel zone computations of the phase of a uniform aperture distribution.

It should be noted that the amplitude requirement is distinct from the above discussion and needs to be considered separately.

*The work reported in this paper was supported in part by Contract AF 19(604)-7270 between The Ohio State University Research Foundation and Air Force Cambridge Research Laboratories.

INTRODUCTION

In measuring either antenna patterns or radar cross sections, it is usually desired that the object under test, either an antenna or a scatterer, be illuminated by a plane wave. Often the criterion is that the phase of the incident wave deviate by no more than $\pi/8$ radians or $22\frac{1}{2}^\circ$ at the extremity of the object under test, hereafter referred to as the target.

The illuminating antenna is often assumed to be a point source and then the minimum range criterion is the usual

$$R_{\min} = \frac{2D^2}{\lambda} \quad (1)$$

where D is the target dimension.

However if the illuminating antenna is not a point source then the above minimum range criterion must be modified. It is often assumed that every point on the target must be illuminated by every point on the illuminating antenna. This concept leads to an increased minimum range. The most common criterion is that

$$R_{\min} = \frac{2(D+d)^2}{\lambda} \quad (2)$$

where d is the antenna dimension.

This concept has been recognized to be erroneous by several authors^{1, 2, 3} in discussing the case when the target is another antenna. Richmond² suggests that Eq. (1) be used where D is now the dimension of the larger antenna, in the case of an antenna range. Rhodes¹ notes several interesting points concerning minimum range. First, he determines the phase distribution of several antennas at the range given by Eq. (1) and shows that a better phase distribution at the target is obtained from a planar aperture with uniform phase distribution than for a point source, provided the dimension of the target is less than that of the source. He then concludes that the same minimum range criterion of Eq. (1) may be used. Rhodes also shows the amplitude distribution for this case is adequate, i.e., field at target is down only 0.9 db. There has been no established requirement on the amplitude distribution over the target since it is nearly always assumed that the phase is the most critical parameter. Once the proper phase distribution is obtained, however, the amplitude distribution becomes quite important. This has been clearly established in the design of antennas since the pattern of an antenna with a uniform phase distribution may be modified by controlling the amplitude distribution.

The usual change in amplitude distribution involves at least a 10 db taper or change. It is suggested here that a 3 db deviation be considered as the amplitude criterion for minimum range. This should introduce little error in the maximum values but could increase nulls significantly.

In the case of a point source illuminating a uniform line scatterer, Rhodes shows that the minimum range must be doubled in order that the radar pattern correspond to the antenna pattern. This takes into account the fact that the radar signal must travel from the source to the target and back.

Kay³ also has examined the minimum range criterion and concludes that the use of Eq. (2) is not justified. He states several concepts that are in general agreement with those developed in this report. First, he concludes that the minimum range may be reduced by increasing the size of an illuminating antenna which has a uniform amplitude and phase distribution. Second, he concludes that if the illuminating antenna is larger than antenna under test, its far field pattern may be measured at any range short of physical contact. It is noted that interactions, which he does not treat, must be negligible. This is not quite adequate because of deterioration of the amplitude pattern.

This discussion has made use of an illuminating antenna. Obviously, the source and receiver may be interchanged without affecting the pattern. However the antenna or scatterer whose pattern is to be measured must be smaller than the antenna which has previously been referred to as the illuminating antenna. This nomenclature is to be used in the remainder of this paper for convenience.

The reduction of the minimum range criterion is of great importance for the measurement of the radar cross section of large bodies whose radar cross section is very small. The power received from a signal reflected by a radar target is inversely proportional to the 4th power of the range and thus, for such low cross section studies, it is essential that the range be reduced as much as possible without disturbing the far field conditions.

In the present paper, a physical argument is presented that leads to a different form of minimum range criterion and an example is given which demonstrates its validity. However it is emphasized that this proposed criterion is still in the form of a hypothesis and needs further study.

PHYSICAL REASONING FOR MINIMUM RANGE CRITERION

The use of Eq. (1) as a minimum range criterion as developed for the point source is valid. The development of Eq. (2) as a criterion for minimum range is not valid since it ignores the constraints on the direction of energy flow. These constraints are used successfully in geometrical or ray optics for many cases provided the aperture distribution is continuous. However, it is hypothesized that ray optics will yield the phase distribution with sufficient accuracy even when the aperture distribution is not continuous. It is assumed in this paper that the application of ray optics will yield the required minimum range criterion.

TARGET SMALLER THAN ILLUMINATING ANTENNA

Kay³ has given the minimum range criterion that adequate far field patterns can be obtained provided only that the target lies between the optical boundaries shown in Fig. 1 and the aperture distribution of the illuminating antenna is uniform. Kay also assumes a large

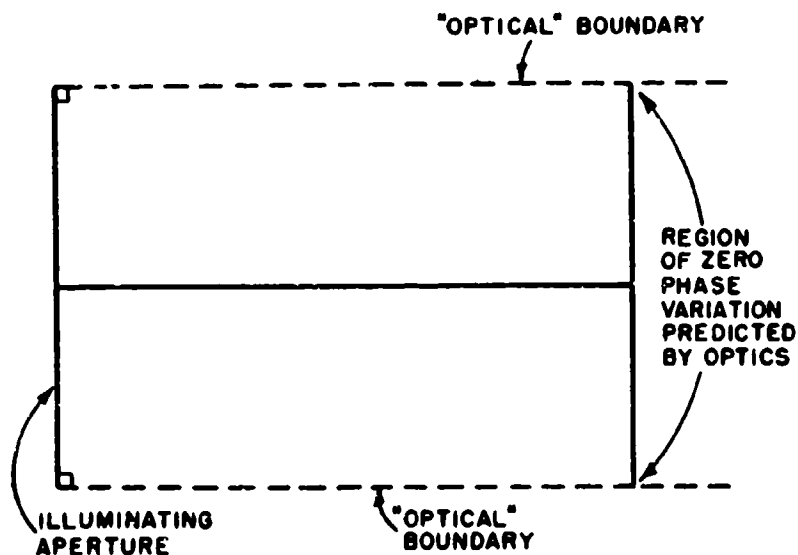


Fig. 1. Region Between Optical Boundaries

illuminating antenna. It is our present purpose to test this criterion using an antenna that is only 3.14λ on a side. If this yields adequate results, then it should be an adequate model for larger antennas which more nearly satisfy the assumptions made by Kay. Available phase patterns computed by Green⁴ are used to check this criterion for this specific case. Others should be considered in the future. Green computed the amplitude and phase patterns of a four inch square aperture with a uniform amplitude and phase distribution in the Fresnel zone for $\lambda = 1.23"$. Computations were made at ranges of 4, 8, 12, 24, 36, and 48 inches in planes parallel to the aperture. The results of these computations are shown in Fig. 2. The maximum deviation of phase in these planes is of interest. The use of geometrical optics predicts the phase deviation in the region between the "optical" boundaries illustrated in Fig. 1 to be zero. The phase calculated by Green shows that the phase at the "optical" boundary is 40° with respect to the phase at the center at the range of 12". This is the greatest phase variation in the region between these "optical" boundaries for ranges treated by Green. At all other ranges that were treated it is considerably less as may be noted in Fig. 2. If this region is reduced to three fourths its extent, the phase variation is everywhere less than $22\frac{1}{2}^\circ$ in this specific case. However the original choice of allowable phase variation of $22\frac{1}{2}^\circ$ is rather arbitrary. Thus these computations of phase tend to support the original hypothesis, i. e., the phase variation may be considered to be negligible in the region between the optical boundaries.

TARGETS LARGER THAN THE ILLUMINATING ANTENNA

Now consider the case of a target larger than the illuminating antenna. A modification of the antenna must be considered if the minimum range is to be reduced. The modification proposed is illustrated in Fig. 3. Now the illuminating antenna is defocussed or the phase variation in its aperture is no longer uniform. It is hypothesized that the minimum range given by Eq. (1) is valid provided it is measured from the apparent point source, i. e., $R_{\min} = R'_{\min} - R_p$. If an amplitude taper is introduced, and the defocussing is sufficient then geometrical optics may be used and the hypothesis is indeed valid.

If the feed is displaced in the opposite direction as illustrated in Fig. 4 then the minimum range would be increased. This is easily avoided and hence is not discussed further.

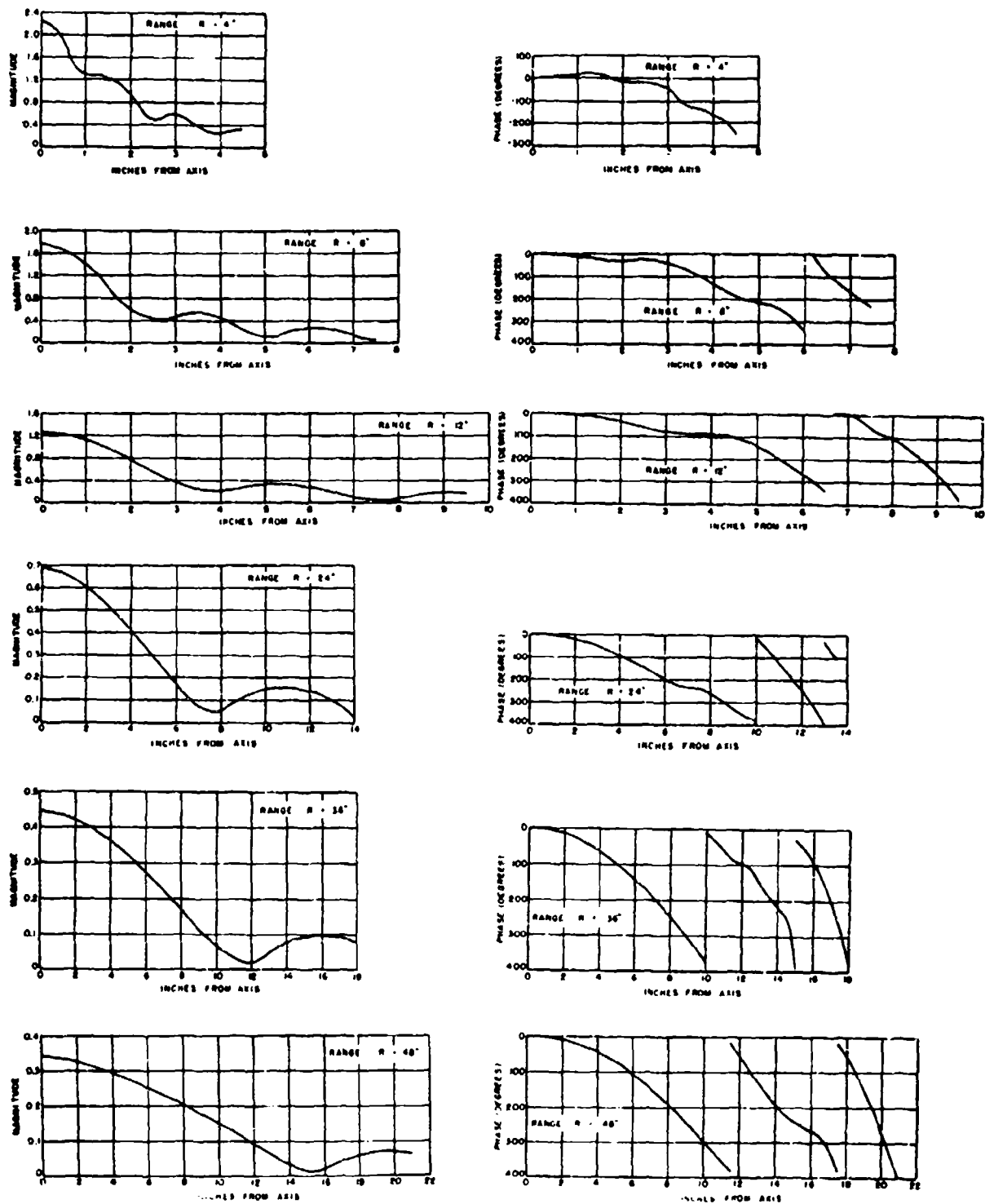


Fig. 2. Fresnel Patterns of a 4" Square Aperture

As another example, the 4" illuminating antenna with a uniform amplitude and phase distribution is considered. However it is taken as the limiting case of Fig. 3 whose point source is removed from the aperture until it approximates the uniform phase condition over the aperture shown in Fig. 5. The fields of this point source in the aperture may be represented by a quadratic phase distribution. The axial far fields computed from this aperture may be obtained approximately either from geometrical optics or by integration of the aperture fields. The two methods yield approximately the same fields provided the maximum phase deviation at the edge of the aperture is approximately $\pi/4$ radians as is shown in the appendix. This quadratic phase distribution would yield essentially the same far field pattern as would the uniform phase distribution. In this case

$$R_p = \frac{d^2}{\lambda}$$

and

$$R_{min} = \frac{2D^2}{\lambda} - \frac{d^2}{\lambda} \quad (3)$$

Consider again the curves of Fig. 2 for the 4" aperture at a wavelength of 1.23". The various minimum ranges are applied to this case for the specific minimum ranges of 4, 8, 12, 24, 36 and 48 inches. The target dimension that yields these minimum ranges, the relative phase ϕ_e and the relative field ΔE at the edge of the target are given in the following table for each of the minimum range criteria.

Minimum Range	$R_{min} = \frac{2D^2}{\lambda}$			$R_{min} = \frac{2D^2}{\lambda} - \frac{d^2}{\lambda}$			$R_{min} = \frac{2(D+d)^2}{\lambda}$	
R_{min} inches	D inches	ϕ_e degrees	ΔE db	D inches	ϕ_e degrees	ΔE db	D inches	ϕ_e degree
4	1.59	15	4.0	2.14	22	4.2	-	-
8	2.25	15	2.3	2.66	21	3.6	-	-
12	2.76	15	2.0	3.1	20	2.4	-	-
24	3.9	18	1.0	4.2	23	1.2	-	-
36	4.8	20	0.6	5.0	22	0.8	0.8	0
48	5.5	20	0.7	5.72	20	0.7	1.5	4°

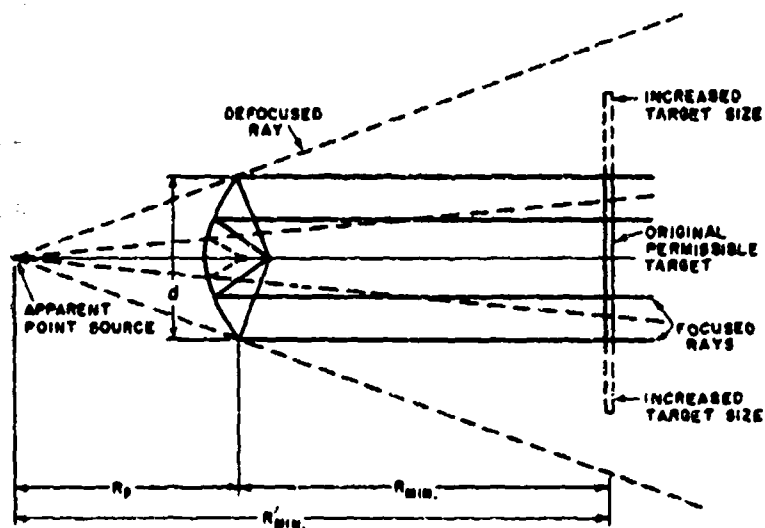


Fig. 3. Defocused Antenna

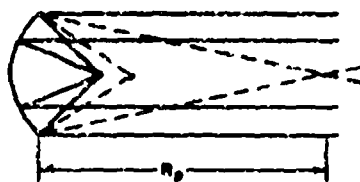


Fig. 4. Defocused Antenna

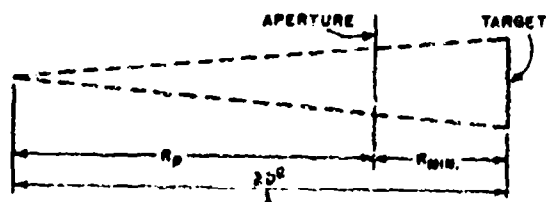


Fig. 5. Illustration of New Minimum Range Criterion

It is apparent that the criterion of Eq. (2) is not valid, that the phase criterion of Eq. (1) may be used with absolute assurance and that Eq. (3) yields an adequate R_{\min} at close ranges. Also Eq. (1) and Eq. (3) yield essentially the same values for larger targets or larger minimum ranges. The close agreement of the relative phase to the value of $22\frac{1}{2}^\circ$ for the criterion of Eq. (3) must at this point be considered coincidental and additional evidence is needed to substantiate this criterion for this particular case. The analysis leading to its development is obviously not rigorous, but is used more as a guide to obtain a much needed new minimum range criterion.

AMPLITUDE VARIATION OVER THE TARGET

Only the phase variation over the target has been discussed. Of equal importance is the amplitude variation. Usually it can be measured in any specific case with relative ease and thus little attention is usually devoted to it. Figure 2 shows the amplitude variation is severe in the region between the optical boundaries for the smaller ranges and it should be considered in any measurement.

Kouyoumjian⁵ has successfully measured the radar cross sections of small bodies in the vicinity of a large horn antenna. He probed the field of this antenna and noted axial as well as transverse variations in the amplitude. The target location was then selected so that the amplitude variations over the target were minimized. It is important to note that there are axial variations that need to be considered at small ranges.

Hansen and Bailen⁶ have computed the axial and transverse amplitude patterns, for a number of amplitude distributions and show similar axial variations for near zone fields of the uniform aperture distribution. These axial variations extend to a range of

$$R \approx 0.1 \left(\frac{2D^2}{\lambda} \right)$$

The variations for the horn are due to energy reflected from the edges of the horn as has been shown by Russo.⁷ and thus the horn can not in general be considered to be a point source. Similarly any practical antenna can yield unexpected amplitude variations in the Fresnel zone from such sources as edge diffraction, aperture blocking, and direct feed radiation. The only safe method of assuring a proper

amplitude distribution for any practical antenna consists of probing the field of that antenna.

INTERACTION EFFECTS

A limitation on the minimum range criterion is the multiple reflections between the illuminating antenna and the target. Interactions should provide no problems for radar targets of low cross section since the energy incident on such a target is either absorbed or scattered in a direction away from the illuminating antenna.

Kay³ describes a technique for recognizing the presence of significant interaction for antenna pattern measurements. This technique consists of repeating the measurement after increasing the range by $\lambda/4$ and noting changes in the pattern. This same technique may be used in radar cross section measurements.

CONCLUSION

A group of antenna patterns in the Fresnel zone have been used to check the various minimum range criteria. If the phase over the target is to vary by no more than $22\frac{1}{2}^\circ$, it is seen that the $2D^2/\lambda$ criterion is a safe one. The new criterion for the antenna with uniform phase distribution of $2D^2/\lambda - d^2/\lambda$ yields a phase variation that is quite close to the $22\frac{1}{2}^\circ$ design value. The requirement that the illuminating antenna be larger than the target nearly satisfies the $22\frac{1}{2}^\circ$ design value and should often prove to be useful.

However amplitude variations appear to place a more severe restriction on this minimum range criterion for shorter ranges. It is suggested that amplitude variations over the target be less than 3 db provided null depths are not of great importance. Otherwise this value should be further restricted.

The safest method of satisfying this amplitude requirement consists of probing the field in both axial and transverse directions. This is particularly true for any reduced range since the field variations at closer ranges may be due to phenomena usually not considered such as diffraction by edges, aperture blocking, and direct feed radiation.

BIBLIOGRAPHY

1. Rhodes, D.R., "On the Minimum Range for Radiation Patterns," Report 475-10, 1 June 1954, Antenna Laboratory, The Ohio State University Research Foundation; prepared under Contract AF 18(600)-19 with Wright Air Development Center.
2. Richmond, J.H., unpublished notes.
3. Kay, A.F., "Far Field Data at Close Ranges," Technical Research Group, Contract AF 19(604)-1126 with Air Force Cambridge Research Center.
4. Green, R.B., "Flare Spot Determination by Use of Photo Conductive Panels," Report 777-14, 31 May 1959, Antenna Laboratory, The Ohio State University Research Foundation; prepared under Contract AF 33(616)-5341 with Wright Air Development Center.
5. Kouyoumjian, R.G., "On the Calculation of the Echo Areas of Perfectly Conducting Objects by the Variational Method," Report 444-13, 15 November 1953, Antenna Laboratory, The Ohio State University Research Foundation; prepared under Contract DA 36-039 ac5506 with U.S. Army Signal Corps Engineering Laboratories, Fort Monmouth, New Jersey.
6. Hansen, R.C. and Bailen, L.L., "A New Method for Near Field Analysis," Toronto Symposium on Electromagnetic Theory, sponsored by Institute of Radio Engineers, Professional Group on Antennas and Propagation, December, 1959.
7. Russo, P., "Complete Radiation Pattern of a Horn Antenna Computed by Diffraction Theory," Report to be published.
8. Silver, S., Microwave Antenna Theory and Design, McGraw Hill Book Co., Inc., 1949, p.12.

ACKNOWLEDGEMENT

The interest and suggestions of Professors R.G. Kouyoumjian and J.H. Richmond are gratefully acknowledged.

APPENDIX - COMPARISON OF APERTURE AND GEOMETRICAL OPTICS FIELDS

The aperture distribution of Fig. 3 is obtained by considering it to be a point source a distance R_p from the aperture. Applying the principle of stationary phase yields an on axis field proportional to⁸

$$\left| \int_{-\infty}^{\infty} e^{-j \frac{\pi}{2} \xi^2} d\xi \right| = \sqrt{2} . \quad (4)$$

If this aperture is now restricted to d where $R_p = d^2/\lambda$, then the phase at the edge of the aperture is $\pi/4$ and the expression becomes

$$\left| \int_{-1/\sqrt{2}}^{1/\sqrt{2}} e^{-j \frac{\pi}{2} \xi^2} d\xi \right| \approx 1.3 . \quad (5)$$

Increasing the limits slightly yields

$$\left| \int_{-0.8}^{0.8} e^{-j \frac{\pi}{2} \xi^2} d\xi \right| \approx 1.4 . \quad (6)$$

Thus the on axis field obtained from the geometrical optics method becomes approximately equal to that obtained by integrating the fields over the aperture. Increasing R_p would reduce the phase variation over the aperture and as a consequence Eq. (5) becomes smaller for a fixed aperture size. However Eq. (4) remains unchanged. Thus geometrical optics fails. If geometrical optics is to be used to find a modified criterion then its use is restricted to the above value, i.e., larger values of R_p should not be allowed. Hence the value $R_p = d^2/\lambda$ is used for the distance of the apparent source from the aperture.

EXPERIENCE WITH CALIBRATION TARGETS AND TECHNIQUES AT RCA - ERL

R. Sigler
Electromagnetic Research Laboratory
RCA Missile and Surface Radar Division
Moorestown, New Jersey

The following is a summary of calibration references and procedures tested and utilized by the ERL for radar measurement purposes. Several reference target configurations are briefly described. The advantages and disadvantages of spheres as primary standards are presented.

* * * *

History

The ERL, operates, as a part of DAMP, the Downrange Antimissile Measurement Program under Project Defender (sponsored by the Advanced Research Projects Agency and administered by the Army Missile Command) an outdoor full-scale range for radar backscatter measurements. Initial evaluations of this range were performed in 1960, with problems common to most measurements, the determination of absolute microwave energy levels. C-band radiation permitted the use of several reflectors of practical sizes, including spheres, corner reflectors, flat plates, cylinders and dielectric lenses. All of these configurations entail careful mounting consideration either because of their low backscatter cross sections relative to any supporting structure, or because their backscatter patterns required support structures capable of holding close angular positions while exposed to the effects of solar radiation and wind.

The spherical reflector was selected as an initial reference. Thin-walled aluminum spheres of six and twelve inch diameters were light enough for support by helium filled weather balloons, and could be tethered over a reasonable area during calm air. A C-band wavelength of 2 inches places the 12 inch sphere circumference at $12 \pi / 2 = 18.85$ wavelengths, which is far enough from the resonance region to establish a reference within 1/2 db without correction. A series of spheres is one way of establishing a calibration curve for the microwave receiving and recording equipment. Aluminum spheres were available up to about five feet in diameter. Small spheres are available in the form of bronze or steel ball bearings. The larger spheres required support more easily obtained from dirigible shaped, gas-filled balloons, with fins for wind alignment and added lift. Tests made, using the above methods, found them satisfactory for experimental purposes but too susceptible to wind conditions for scheduled operations. The relatively small backscatter cross sections of the conducting spheres prevent placing them near the supporting balloons, which have sufficient backscatter to defeat an absolute calibration. Tether and support lines can cause excessive variations in backscattered energy when segments of the lines become normal to the microwave radiation. Initial evaluations of the

ERL range employed a tracking radar capable of following target drift and measuring target ranges, but more specialized backscatter measurement systems, without tracking capability, are likely to find the balloon support method impracticable.

Fixed Amplitude References

Calibration of the ERL outdoor range was originally accomplished by supporting the aluminum reference spheres atop styrofoam columns, with each column measured as part of the site background. One attempt at acceleration of operations was the construction of a separate tower for supporting a sphere, or other suitable reference reflector. The C-band measurements employed pulsed energy, and therefore permitted the advantages of range-gating for exclusion of undesired backscatter. The reference tower could have been displaced in range, but due to the possibility of interference of the reference or target with the microwave beam pattern, the tower was displaced in azimuth only. No gate repositioning or range correction of cross section was necessary, and an angular displacement to a low power area of the antenna pattern provided isolation between the reference and the target.

Absolute level calibration, with the reference tower, precluded the use of hygroscopic materials, or those susceptible to rapid weathering. The tower was therefore constructed for low cross section, with metal elements tilted to position the backscatter lobe pattern for minimum energy at the antenna. In order to provide time stability, a reflector with greater backscatter and smaller size than an equivalent sphere was desired. The corner reflector is one configuration with these characteristics. Two corner reflector shapes were considered. The first is equivalent to three adjacent surfaces of a cube, and the second shape is obtained by cutting-off each of these faces along a diagonal. Backscatter equations for each of the above are derived from the useful projected flat-plate areas, and show the first shape to have a gain of approximately nine times the second, for the same cube size. The first would therefore appear to be the logical solution, until the backscatter energy level is examined with respect to alignment of the reflector axis-of-concentricity with the incident energy. The projected flat-plate area decreases for off-axis illumination, with immediate effect on the backscatter level. Some advantage is gained from the second shape which does not use all of each reflecting surface when concentrically aligned. Misalignment in the order of a few degrees causes a small decrease in the total projected flat-plate area, but some additional reflecting surface area becomes effective. The backscatter level rolls off gradually for small angles of misalignment, and at C-band frequencies a cube size of less than two feet can provide backscatter equivalent to a hundred square meters. Mounting the reflector with one edge tilted 45° from the horizontal permits equivalent backscatter for horizontal and vertical energy. Preliminary measurements on this reflector did not indicate that polarization had an appreciable effect on backscatter, but precise orthogonality of the cube surfaces is necessary for maximum effectiveness in the on-axis position.

Another reflector with relatively large backscatter is the Luneberg Lens. It has some of the advantage of the corner reflector and also some of the alignment

advantage of the sphere, in that reflected level is similar to the normal to the flat plate but can be stable over several degrees of misalignment. Inflatable mylar spheres with a metal film on one surface of the mylar were tried. These had inherent limitations in sphericity because of construction techniques and because of warping from non-uniform support pressures and temperatures. Size was also a function of pressure differential, which precluded stable calibration.

Reflector Mounting

Experience with the previously described tower indicated that absolute level measurements of reference reflectors for the ERL range could better be made with the reference mounted in place of the target. No antenna repositioning was involved, and no periodic evaluation of the reference tower background or reflector necessary. Background evaluation of the target mount is a part of normal operation. Measurements of several spheres on the target mount, using styrofoam columns and steel shafts for the larger spheres, were compared against the normalized curve for spherical reflectors. Results indicated that the use of a steel shaft did not destroy the value of a reference sphere, provided the shaft exterior to the sphere was included in background measurements, and also that the target support structure enclosed the exterior part of the shaft. The above measurements were made for a sphere diameter of twelve wavelengths and a support shaft diameter less than one wavelength.

Step Calibration Reflectors

The sphere is ideal when reflector alignment is a consideration, however the need for reflected energy calibrations at more than one level requires the use of several spheres with a subsequent increase in calibration time. The rotating cylinder can serve as an absolute calibration, and with suitably low background and multipath levels, also provide repeatable steps in energy levels from the lobe pattern. Alignment is an important relationship only with respect to the cylinder axis and incident energy polarization axis. Lobe patterns for the cylinder are then employed as a function of cylinder dimensions versus wavelength and polarization.

A description of a further refinement of the step-calibration reflector technique is included in reference 1. The Witch of Agnesi characteristics would be used to generate an interference pattern containing amplitude steps of the desired magnitude.

Suggested Standard

The reference targets mentioned above all are subject to wavelength for absolute calibration, and are therefore dependent on the accurate determination of frequency. Backscatter equations are available for the basic shapes so that frequency corrections can be computed, and considerable data has been accumulated from measurements to support the corrections.^{2, 3} The sphere has the advantage of only one measurement being needed to determine backscatter as a function of frequency and polarization. It has a reasonably portable size for microwave frequencies and, for example, at C-band, has lost most of the effects of resonance with a diameter of two feet. Alignment of the sphere is not a

problem as with other shapes. This characteristic also makes the sphere a useful tool for evaluation of background level and phase angle. A sphere mounted one-fourth wavelength off a rotating support axis, provides a relatively simple recording of the unknown background modulated by a target of fixed backscatter and controlled phase angle.

Materials

A practical consideration which should accompany the selection of a reference reflector is the mounting provisions. The use of styrofoam columns with contoured surfaces has been satisfactory in most experimental measurements performed at the ERL for spheres, cylinders and cones. At best these are not very durable, however, and have been replaced by metal shafts where possible to permit continuous daily use without too-frequent checks against other primary references. Aluminum or lighter metal is advisable for hollow spheres of one-meter diameter or larger. Conductive coatings on non-metallic bases have been tried but, except for bonded metallic plating, can be affected by abrasion and impact from continuous handling. Ductile metal spinings have been used for hollow spheres but these also require careful handling since they do not spring back to shape after impact. An ideal material would appear to be one with (low) temperature coefficient, density and creep, (high) elasticity and tensile strength, good machinability, and either (good) conductivity and corrosion resistance or good bonding characteristics with a plating of that nature. With all these, the reflector still requires added provision for a mounting socket or shaft, and some type of reinforcement under the adjacent surfaces. Operations at the ERL have suggested a truncated conical socket within the reflector, with a standardized angle and a set of standard cone diameters. An alignment key, or pins similar to aircraft type snap fasteners, should be accepted by the socket, to twist-lock any reflector at the same relative angle. Spring loading of the twist-lock action can be used to hold the conical junction tight, thereby allowing a cone angle large enough to avoid freezing of the joint. Target dimensions and mounting socket size should be permanently indicated on the surfaces. Suitable plugs can provide protection to the sockets and also establish surface continuity during other mounting methods.

Step Calibration Attenuators

A series of reference targets is one method of establishing step calibration of equipment. Speed of operation has dictated the use of vane-type precision waveguide attenuators at C-band and equivalent precision stepping attenuators at longer wavelengths. These attenuators, when mounted in series, can cover any required range and may also be used to check one-another for relative levels. They can be used in conjunction with absolute reference reflectors to calibrate receiving equipment, or they can be used to provide relative power calibration only. The latter method has been used at the ERL, with independent absolute level calibration against a reference reflector on the cross-section range. Step calibration procedure involves a delay line which holds a portion of the transmitted pulse power. It is long enough to permit feeding energy through the step attenuators and into the receiving system well after the decay of transients caused by the transmitter.

REFERENCES

1. Special Apertures for Calibration of Sidelobe Levels. RCA MASRD, Antenna Research Group Report, May 22, 1962.
2. Monostatic and Bistatic Measurement of Scattering Shapes and Synthesis of Scattering Shapes. Ohio State University Antenna Lab. Report AFCRL193 (ASTIA No. 255839) Unclassified.
3. A Theoretical Method for the Calculation of the Radar Cross Sections of Aircraft and Missiles. The University of Michigan Radiation Lab. Report 2591-1-H (ASTIA No. 227695) Unclassified.

SECTION VI

MEASUREMENT CORRELATION AND APPLICATION

Panel Chairman: C.G. Bachman

COMPARISON OF RADAR CROSS SECTION SIGNATURES

D. R. Brown and A. L. Maffett
Conductron Corporation
Ann Arbor, Michigan

ABSTRACT

Effective comparisons of radar cross section signatures are usually made in terms of some signature attribute to be agreed upon in advance or dictated by the system of which the signatures form a part. We develop here a technique, particularly applicable to graphical data, for constructing redistributed functions for the data on the basis of which comparisons can be more easily and directly made. The redistributed functions can also be conveniently applied to obtain from a signature almost any attribute of an "average" nature. These results are used to compare static and dynamic radar cross section signatures.

1. INTRODUCTION

A requirement to compare two or more functions over a given region of a common variable may be quite difficult to fulfill, particularly if the functions intertwine. The tendency is then to seek attributes, or characteristics, of the functions from which comparative information can be drawn. Such attributes may include, for example, the maximum value of a function in a specified domain, or the median or an average. Unfortunately, it is often true that two different attributes of several functions do not obey the same comparative relation. In such cases in order to make judicious choices of attributes to compare, recourse must be had to the particular theory or system in which the functions appear. This fact is particularly true for the radar cross section (RCS) functions with which we will be most concerned here.

Our purpose in the discussion to follow is to achieve an alleviation of the above difficulties by describing a procedure which yields an effective means of comparing, in particular, RCS functions. The procedure, detailed in Section 2.2, reorders the ordinates of a given function, producing a new monotonic "redistributed" function. The usefulness of redistributed functions as comparison devices lies in the fact that they leave invariant most attributes of an "average" nature definable for the original function. We confine ourselves to the particular and very important problem of comparing measured RCS data for variations in the body being measured, said variations to include those of a geometric and/or material nature. Such comparisons are discussed in Section 3.1 for static situations and in Section 3.2 for dynamic situations.

2. REDISTRIBUTED FUNCTIONS

2.1 Introductory Remarks In this section we develop the theory of redistributed functions. This theory is useful when applied to functions presented only in graphical form, and thus we will usually assume the functions with which we are dealing to be of this type.

The fundamental idea is as follows: given a well behaved function $\phi(x)$ defined on an interval $[a, b]$, we construct a monotonic function $R\phi(x)$ by reordering or redistributing the ordinates of $\phi(x)$. We do this in such a way that many of the characteristics of $\phi(x)$ are the same as those for $R\phi(x)$. Specifically, if $G(t)$ is a continuous function, then

$$\int_a^b G(\phi(x)) dx = \int_a^b G(R\phi(x)) dx$$

This statement (made more precise later) constitutes the Fundamental Theorem of redistributed functions.

The compelling property of the redistributed function $R\phi(x)$ is that it is monotonic. This fact renders it more amenable to analysis than the "original" function $\phi(x)$.

As a preliminary example of the applications of the equation above, let $G(t) = t$. Then we have

$$\int_a^b \phi(x) dx = \int_a^b R\phi(x) dx$$

That is, the arithmetic averages of $\phi(x)$ and $R\phi(x)$ are identical.

2.2 Definition of the Redistributed Function Suppose $\phi(x)$ is continuous and of bounded variation* on the interval $[a, b]$. Then consider the class of all functions $R\phi_n(x)$ obtained in the following way:

1. Let $y_k = \phi(a + \frac{k}{n}(b-a))$, $k = 0, 1, \dots, n$

*Any function $\phi(x)$ which is presented to us only in graphical form is obviously of bounded variation.

2. Reorder the set $\{y_0, y_1, \dots, y_n\}$ to obtain:

$$\{y_{j_1}, y_{j_2}, \dots, y_{j_n}\} \text{ where } y_{j_l} \leq y_{j_{l+1}} \quad l = 0, 1, \dots, n-1$$

3. Define $R\varphi_n(x) = y_{j_l} + (n \frac{x-a}{b-a} - l) (y_{j_{l+1}} - y_{j_l})$ if

$$a + \frac{l}{n} (b-a) \leq x \leq a + \frac{l+1}{n} (b-a)$$

The notation in item (3) is complicated, but what we have done is simply to construct a function $R\varphi_n(x)$ by connecting successively, with straight line segments, the points $(a + \frac{l}{n} (b-a), y_{j_l})$, $l = 0, 1, \dots, n$.

The redistributed function for $\varphi(x)$ is defined to be the limiting function obtained as $n \rightarrow \infty$: that is for each $x \in [a, b]$,

$$R\varphi(x) = \lim_{n \rightarrow \infty} R\varphi_n(x).$$

Where we are dealing with continuous functions $\varphi(x)$ presented in graphical form, the sequence $\{R\varphi_n(x)\}$ always converges uniformly, so that $R\varphi_n(x)$ for an appropriately large n is an arbitrarily good approximation to $R\varphi(x)$ for every x in $[a, b]$. Thus in practice we construct $R\varphi(x)$ by constructing $R\varphi_n(x)$ with n large enough to ensure whatever accuracy is required. Note that if $\varphi(x)$ is a measured RGS signature, then $R\varphi(x)$ can be constructed by machine methods directly from a digital recording of $\varphi(x)$.

2.3 Equivalence of the Redistributed Function and the Quantile Function

If k is a number between 0 and 1, then the k th quantile of a function $\varphi(x)$ on an interval $[a, b]$ is defined to be that value φ_k which has the property that $\varphi(x) \leq \varphi_k$ over the fraction k of the interval $[a, b]$. That is, suppose that $\varphi(x) \leq \varphi_k$ on the intervals $[x_1, x'_1]$, $[x_2, x'_2]$, ... whose lengths are L_1, L_2, \dots respectively. Then

$$k = \frac{1}{b-a} (L_1 + L_2 + \dots).$$

Clearly φ_0 is the minimum value of $\varphi(x)$ on $[a, b]$, and φ_1 is the maximum value. The median of $\varphi(x)$ on $[a, b]$ is defined to be $\varphi_{.5}$.

Now the quantiles φ_k generate in a natural way a function on the interval $[0, 1]$. Thus we define

$$Q\varphi(k) = \varphi_k, \quad 0 \leq k \leq 1. \quad (2.3-1)$$

We will refer to $Q\varphi(k)$ as the quantile function for $\varphi(x)$ on $[a, b]$.

We observe at once that the redistributed function $R\varphi(x)$ and the quantile function $Q\varphi(x)$ for $\varphi(x)$ are related by

$$R\varphi(x) = Q\varphi\left(\frac{x-a}{b-a}\right), \quad a \leq x \leq b \quad (2.3-2)$$

This fact is most easily demonstrated graphically. In Figure (2.3-a) we present a function $\varphi(x)$ and show the ordinates $y_k = \varphi(a + k/n(b-a))$ for $n = 40$. In Figure (2.3-b) we have rearranged the 40 ordinates in ascending order. The resulting graph thus represents the approximation $R\varphi_{40}(x)$ to $R\varphi(x)$ except that we have not drawn in the connecting line segments. Next we draw the horizontal line $y = \varphi_k$ at an arbitrary level. Then clearly

$$k = \frac{L_1 + L_2}{b-a}$$

in this case. But $L_1 + L_2$ is approximately $\frac{b-a}{n}$ times the number of ordinates y_j which satisfy $y_j \leq \varphi_k$. Thus, if this number is N_k , we have

$$k = \frac{N_k}{n}.$$

Now referring to Figure (2.3-b) we see that $\frac{b-a}{n} N_k$ is also an approximation to the length L . In each case the accuracy of the approximation can be improved to any degree by choosing an appropriately large value of n . Thus we conclude that $L = L_1 + L_2$. That is $R\varphi(a+L) = R\varphi(a+L_1+L_2) = R\varphi(a+k(b-a)) = \varphi_k = Q\varphi(k)$. Then let $x = a + k(b-a)$, so that $k = \frac{x-a}{b-a}$, and thus

$$R\varphi(x) = Q\varphi\left(\frac{x-a}{b-a}\right) \quad \text{Q. E. D.}$$

It is evident then that the redistributed function and the quantile function are essentially equivalent.

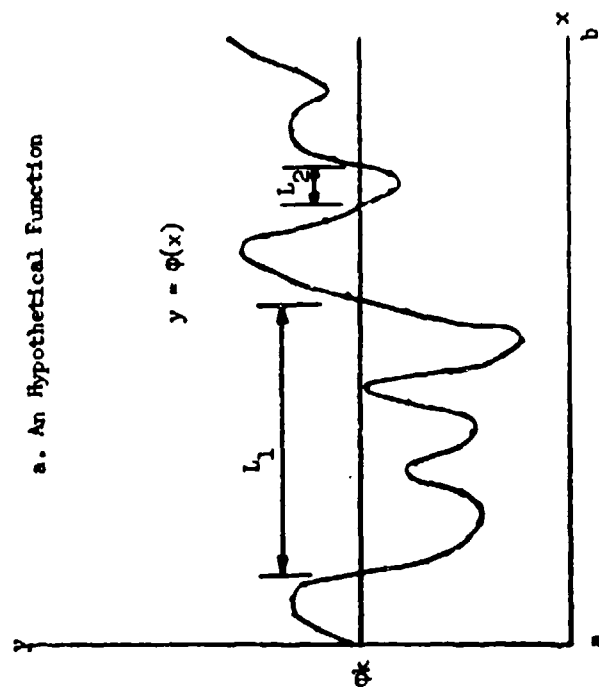
We remark here in passing the following point of interest. It can be shown that the inverse of the quantile function $Q\varphi(k)$ defined in Equation (2.3-1) can be interpreted as the cumulative distribution function which characterizes the distribution of ordinates of $\varphi(x)$ on the interval $[a, b]$.

2.4. The Fundamental Theorem Suppose, as in Section 2.2, that $\varphi(x)$ is continuous and of bounded variation on $[a, b]$ and that $R\varphi(x)$ is its associated redistributed function. Suppose further that $G(t)$ is any continuous function defined on the range of $\varphi(x)$ (hence also on the range of $R\varphi(x)$). Then

$$\int_a^b G(\varphi(x)) dx = \int_a^b G(R\varphi(x)) dx \quad (2.4-1)$$

Proof: Referring to the notation of Section 2.2

$$\int_a^b G(\varphi(x)) dx = \lim_{n \rightarrow \infty} \frac{1}{n} \sum_{k=1}^n G(y_k) \quad (2.4-2)$$



b. The 40-point Approximation to the Redistributed Function

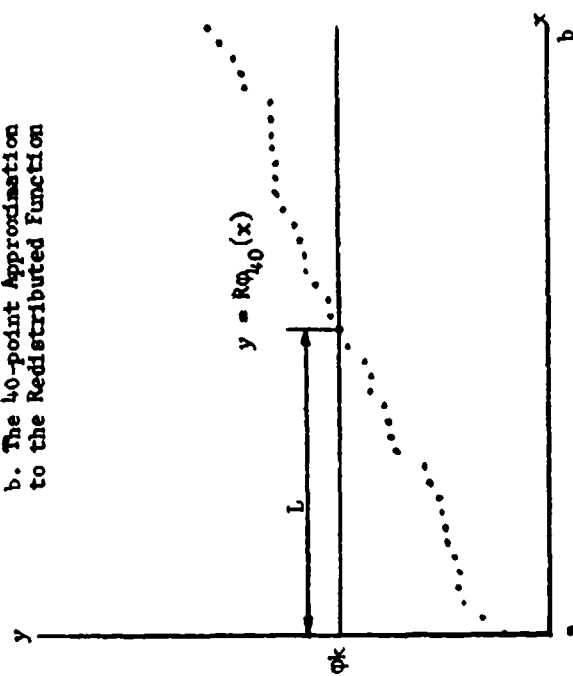


Figure 2.3

We rearrange the terms in the sum:

$$\int_a^b G(\varphi(x)) dx = \lim_{n \rightarrow \infty} \frac{1}{n} \sum_{l=1}^n G(y_{j_l}) \quad (2.4-3)$$

But

$$\int_a^b G(R\varphi(x)) dx = \lim_{n \rightarrow \infty} \frac{1}{n} \sum_{l=1}^n G(y_{j_l}) \quad (2.4-4)$$

as can be seen from the definition of $R\varphi(x)$. Thus the theorem is proved.

2.5 Implications of the Fundamental Theorem; Characterization of a Function by Means of its Redistributed Function If G is a monotonic function on the range of $\varphi(x)$, so that its inverse function G^{-1} exists, then we define a generalized average $A_G\{\varphi(x)\}$ of $\varphi(x)$ with respect to G on the interval (a, b) to be

$$A_G\{\varphi(x)\} = G^{-1} \left(\frac{1}{b-a} \int_a^b G(\varphi(x)) dx \right). \quad (2.5-1)$$

We can immediately apply the Fundamental Theorem, obtaining:

$$A_G\{\varphi(x)\} = G^{-1} \left(\frac{1}{b-a} \int_a^b G(R\varphi(x)) dx \right) = A_G\{R\varphi(x)\}; \quad (2.5-2)$$

that is, every generalized average of $\varphi(x)$ of the form (2.5-1) is identical to the generalized average of $R\varphi(x)$. This, along with the fact that $\varphi(x)$ and $R\varphi(x)$ have identical quantiles, is precisely the extent to which $R\varphi(x)$ characterizes $\varphi(x)$. For example, we pointed out in our Introductory Remarks to this section that the arithmetic averages of $\varphi(x)$ and $R\varphi(x)$ are identical; G is the identity function here.

Two other familiar special examples of G are (a) the logarithm (geometric average), and (b) the inversion (harmonic average):

$$(a) A_{\log \varphi} \{\varphi(x)\} = \exp \left(\frac{1}{b-a} \int_a^b \log(\varphi(x)) dx \right);$$

$$(b) A_{\varphi^{-1}} \{\varphi(x)\} = \left(\frac{1}{b-a} \int_a^b (\varphi(x))^{-1} dx \right)^{-1}$$

2.6 Comparison of Functions Suppose that $\varphi(x)$ and $\psi(x)$ are two functions of bounded variation on $[a, b]$. Suppose that their corresponding redistributed functions are $R\varphi(x)$ and $R\psi(x)$. Then we have the following theorem: If $R\varphi(x) < R\psi(x)$ for all x on $[a, b]$, then every quantile of $\varphi(x)$ and every generalized average of $\varphi(x)$ of the form (2.5-1) is less than the corresponding quantile or generalized average of $\psi(x)$. That is $\varphi_k < \psi_k$, $0 \leq k \leq 1$ and $A_G\{\varphi(x)\} < A_G\{\psi(x)\}$ for every monotonic G .

The proof for the quantiles is obvious in view of the relation from Section 2.3 between the quantile function and the redistributed function. The proof for the averages is covered in two cases:

(a) Suppose $G(t)$ is monotonic increasing on the ranges of $\varphi(x)$ and $\psi(x)$; that is, $G(t_2) > G(t_1)$ if and only if $t_2 > t_1$. Write (2.5-2) in the form

$$G(A_G(\varphi(x))) = \frac{1}{b-a} \int_a^b G(R\varphi(x)) dx; \quad (2.6-1)$$

similarly

$$G(A_G(\psi(x))) = \frac{1}{b-a} \int_a^b G(R\psi(x)) dx \quad (2.6-2)$$

Subtracting these we obtain

$$G(A_G(\psi(x))) - G(A_G(\varphi(x))) = \frac{1}{b-a} \int_a^b [G(R\psi(x)) - G(R\varphi(x))] dx \quad (2.6-3)$$

But our hypothesis is that $R\varphi(x) < R\psi(x)$ on $[a, b]$, so $G(R\varphi(x)) < G(R\psi(x))$ on $[a, b]$; hence the integrand is positive on $[a, b]$, and thus $G(A_G(\psi(x))) > G(A_G(\varphi(x)))$ which implies $A_G(\psi(x)) > A_G(\varphi(x))$.

(b) If $G(t)$ is monotonic decreasing on the ranges of φ and ψ the same inequality is obtained. The proof is identical to the one above except for a "double reverse" in the intermediate inequalities: the integrand in (2.6-3) is negative on $[a, b]$; hence $G(A_G(\psi(x))) < G(A_G(\varphi(x)))$ but $G(t_2) > G(t_1)$ if and only if $t_1 > t_2$, so as before $A_G(\psi(x)) > A_G(\varphi(x))$.
Q. E. D.

2.7 Further Implications of the Fundamental Theorem; Characteristics of Functions Described by Arbitrary Distributions The idea of a redistributed function presented in Section 2.2 may be extended in such a way as to yield a constructive method of studying the characteristics of some given function in terms of whatever variable is appropriate to the situation of interest. In particular, we have in mind for later application the development of a procedure applicable to the study of static and dynamic radar cross section (RCS) signatures. Therefore, we shape our development below in such a way that we are easily able to treat this special topic of interest in a later section.

In addition, we shape our development so as to be able to draw on the wealth of ideas available from function theoretical considerations. The basic notation goes as follows: From Section 2.5 we express the characteristic A_G of the RCS $\sigma(x)$ as

$$A_G(\sigma(x)) = G^{-1} \left(\int_a^b G(\sigma(x)) \frac{dx}{b-a} \right), \quad (2.7-1)$$

where x is some variable (such as time or angle) in terms of which the RCS σ is measured or calculated. The distribution assumed for x is uniform or constant ($= \frac{1}{b-a}$), over the interval $[a, b]$. Now redistribute $\sigma(x)$ so as to obtain the redistributed function $R\sigma(x)$ over the interval $[a, b]$. Normalize this redistributed function (with an appropriate variable change) to the interval $[0, 1]$ and write the resulting quantile function as $Q\sigma(x)$. The fundamental theorem of Section 2.2 then allows us to write the characteristic A_G in terms of the quantile function as

$$A_G(\sigma(x)) = G^{-1} \left(\int_a^b G(\sigma(x)) \frac{dx}{b-a} \right) = G^{-1} \left(\int_0^1 G(Q\sigma(k)) dk \right)$$

Writing the inverse of $Q\sigma(k)$ as $Q\sigma^{-1}(\sigma)$, we note that

$$dk = \frac{d}{d\sigma} Q\sigma^{-1}(\sigma) d\sigma = p(\sigma) d\sigma$$

which implies that $Q\sigma^{-1}(\sigma)$ is a cumulative distribution function characterizing the distribution of cross section values and $p(\sigma)$ is the corresponding density function*. We can now write:

$$A_G(\sigma(x)) = A_G(\sigma, p) = G^{-1} \left(\int_{\sigma_0}^{\sigma_1} G(\sigma) p(\sigma) d\sigma \right) \quad (2.7-2)$$

where $[\sigma_0, \sigma_1]$ is the range of $\sigma(x)$ on $[a, b]$.

Now suppose that θ is aspect angle and t is time and that we are given a compound function for cross section $\sigma(\theta(t))$. Suppose that we wish to compute generalized averages for σ over the time interval $[t_1, t_2]$:

$$A_G(\sigma(\theta(t))) = G^{-1} \left(\int_{t_1}^{t_2} G(\sigma(\theta(t))) \frac{dt}{t_2 - t_1} \right) \quad (2.7-3)$$

Now if $R\theta(t)$ is the redistributed function for $\theta(t)$ on $[t_1, t_2]$, then we can invert as before and write

$$\frac{dt}{t_2 - t_1} = \frac{1}{t_2 - t_1} \frac{d}{d\theta} R\theta^{-1}(\theta) d\theta = q(\theta) d\theta, \text{ so}$$

$$A_G(\sigma(\theta(t))) = G^{-1} \left(\int_{\theta_1}^{\theta_2} G(\sigma(\theta)) q(\theta) d\theta \right) \quad (2.7-4)$$

where $[\theta_1, \theta_2]$ is the range of $\theta(t)$ on $[t_1, t_2]$ and $q(\theta)$ is the density function for $\theta(t)$ on $[t_1, t_2]$.

At this point it is an easy matter to introduce the classical averages which may be used to describe a function σ in various systems. We omit below the limits of integration as well as the arguments of both σ and p since these are matters of detail depending upon particular situations.

* The reader will note that $\int_{\sigma_1}^{\sigma_2} p(\sigma) d\sigma = 1$.

However, we remember that in all cases the appropriate redistributed function can be constructed (and that on this account the usually troublesome problems of multiplicities often encountered in the inversion of many functions are avoided). In the review that follows we rely heavily upon Hardy, Littlewood, and Polya, Inequalities, Cambridge University Press, 1959.

The same remarks made in Section 2.5 hold under the more general circumstances of this discussion: that is, if G is the identity, the logarithmic function, or an inversion, the resulting averages are, respectively, the arithmetic, the geometric, and the harmonic. More generally, we may define the averages resulting from the r^{th} power function $G_r(\sigma) \equiv \sigma^r$ as

$$A_{G_r}(\sigma, p) = \left(\int \sigma^r p \, d\sigma \right)^{1/r} \quad (2.7-5)$$

which covers the whole domain of the function σ . This is demonstrated by the following four statements which review and summarize the chief properties of the averages $A_{G_r}(\sigma, p)$:

- (a) If 0 and ∞ are regarded as reciprocals, then $A_{G_r}(\sigma, p) = A_{G_r^{-1}}(\sigma^{-1}, p)^{-1}$
- (b) If $A_{G_1}(\sigma, p)$ is finite, then $A_{\log \sigma}(\sigma, p) < A_{G_1}(\sigma, p)$, unless σ is identically a constant. Or, more generally, if $A_G(\sigma, p)$, where $r > 0$, is finite, then $A_{\log \sigma}(\sigma, p) < A_G(\sigma, p)$, unless σ is identically a constant.
- (c) If $A_{G_r}(\sigma, p)$ is finite for some $r > 0$, then $A_{G_r}(\sigma, p) \rightarrow A_{\log \sigma}(\sigma, p)$ when $r \rightarrow +\infty$.
- (d) If $0 < r < s$ and $A_{G_s}(\sigma, p)$ is finite, then $A_{G_r}(\sigma, p) < A_{G_s}(\sigma, p)$ provided σ is not identically constant. Moreover, if $A_{G_r}(\sigma, p)$ is finite for every r , then $A_{G_r}(\sigma, p) \rightarrow \max \sigma$ when $r \rightarrow \infty$. And $A_{G_r}(\sigma, p) \rightarrow \min \sigma$ when $r \rightarrow -\infty$.

We see that a set of averages which includes the well-known ones can be defined to cover the entire domain of the function σ , from its minimum to its maximum values. Therefore, a choice of any particular one to serve as a measure of central tendency or as a representation of σ must perforce be somewhat arbitrary - unless some system parameter governs this choice.

Such a governing parameter might arise from the use to which σ is to be put; or, it might arise from the manner in which σ is recorded. We discuss these matters further in the following section where we seek to obtain characteristics which enable us to compare static to dynamic RCS data.

3. COMPARISON OF RADAR CROSS SECTION SIGNATURES

3.1 Comparison of Static Radar Cross Section Signatures. The problem to which we here address our attention is the following: Suppose we wish to compare the effectiveness of various treatments of a radar target aimed at reducing its radar cross section (these treatments might be shape modifications or application of radar absorbing material). What criteria can we use in making such comparisons? For example, suppose that a radar target has a radar cross section signature $\sigma(\theta)$. Suppose that two radar cross section reducing treatments A and B yield signatures $\sigma_A(\theta)$ and $\sigma_B(\theta)$ for the target, and suppose that $\theta_1 \leq \theta \leq \theta_2$ is the range of aspect angles over which we are interested in reducing the cross section. Now if we say $\sigma_A(\theta) < \sigma_B(\theta)$ for all θ on the interval $\theta_1 \leq \theta \leq \theta_2$, then it is obviously meaningful to say that treatment A is more effective than treatment B in reducing the cross section on this interval. However, it is more common for $\sigma_A(\theta)$ and $\sigma_B(\theta)$ to intertwine in a more or less complicated way, and in this case it may be not at all obvious which treatment is really more effective. In fact we must agree upon what we mean by "more effective" before we can make any decision.

The typical way of handling such a situation is to choose some single number characteristic of each function $\sigma_A(\theta)$ and $\sigma_B(\theta)$ and agree to call treatment A more effective than treatment B if the chosen characteristic of σ_A is less than that of σ_B . Typically the chosen characteristic is the maximum value of cross section on the interval or the median value or some kind of average value. Unfortunately there is no consensus among radar cross section specialists as to which of these characteristics is most appropriate as a comparison standard. Thus one person recommends the use of treatment A because the median value of σ_A is less than that of σ_B ; but another says that treatment B is really better since the geometric average of σ_B is less than that of σ_A . On the other hand, even if the median value and the geometric average and the maximum value and the arithmetic average of σ_A were all less than those for σ_B , there is still the possibility that there is some reasonable characteristic of σ_A which is greater than that for σ_B ; and thus at least a shadow of doubt is cast upon the decision about which treatment is best.

Fortunately, the theory of redistributed functions allows us in many cases to circumvent entirely the question of which characteristic to choose for comparison purposes. Thus, suppose that $R\sigma_A(\theta)$ and $R\sigma_B(\theta)$ are the redistributed functions for $\sigma_A(\theta)$ and $\sigma_B(\theta)$ on $[\theta_1, \theta_2]$ and suppose that $R\sigma_A(\theta) \leq R\sigma_B(\theta)$ for all θ in the interval $[\theta_1, \theta_2]$. This situation occurs in many cases even though the functions $\sigma_A(\theta)$ and $\sigma_B(\theta)$ intertwine. Now the Comparison Theorem (Section 2-6) tells us that every quantile and every generalized average of $\sigma_A(\theta)$ is less than the corresponding quantile or generalized average of $\sigma_B(\theta)$. Thus, treatment A is certainly more effective in reducing the radar cross section over the interval $[\theta_1, \theta_2]$. By comparing the redistributed functions we have compared all the quantiles and generalized averages simultaneously.

Now we must consider the cases in which the redistributed functions (as well as the "original" functions) intertwine. In these cases the decision as to which treatment is more effective is necessarily somewhat subjective and may depend on considerations specific to a particular use for the target. However, with or without external factors, a study of the redistributed functions will usually indicate a choice. Let us consider some hypothetical cases.

(1) Suppose the redistributed functions look qualitatively like those depicted in Figure 3.1-a. Note that $R\sigma_A(\theta)$ is less than $R\sigma_B(\theta)$ except for the lower radar cross section (RCS) values. Typically the lower values of an RCS signature involve background noise, so we tend to discount their accuracy. Thus, the indication is that treatment A is more effective.

(2) (See Figure 3.1-b) In this case the choice must depend on external considerations. The higher values of $\sigma_B(\theta)$ dominate those of $\sigma_A(\theta)$, but the general level of RCS is lower for σ_B .

(3) (See Figure 3.1-c) In this case the redistributed functions indicate that there is little to choose between treatments A and B. It should be pointed out that this fact might be not at all obvious from a comparison of the signatures $\sigma_A(\theta)$ and $\sigma_B(\theta)$.

In summary, we have shown how a comparison of the redistributed functions leads in some cases to positive determination of relative effectiveness, whereas in the cases where a positive determination is not possible the redistributed functions remain a powerful tool for comparison.

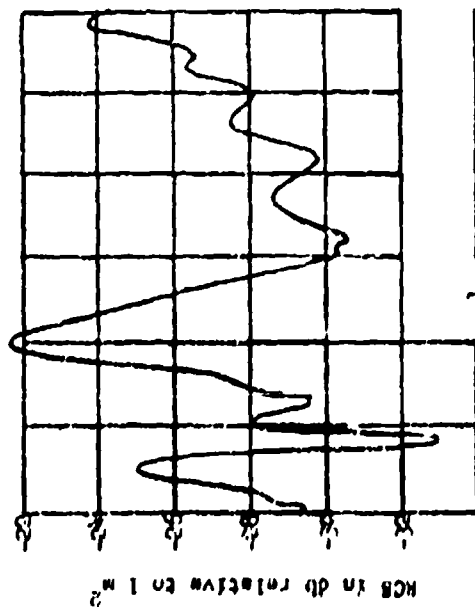
3.2 Comparison of Characteristics of Static and Dynamic RCS Signatures.

There are at least two very good reasons to compare statically and dynamically measured RCS data. The first stems from a desire to predict characteristics of one from the other, usually the unknown characteristics of a dynamic situation from known characteristics of a static situation. A prediction of this sort will always require information about the distribution of aspect angle pertaining to the dynamic situation. A second reason may stem from a desire to compare measured data from static and dynamic experiments; again a knowledge of aspect angle distribution is required of the dynamic situation. This requirement is necessary of course because of the manner in which RCS is usually recorded - as a function of aspect angle in the static case - as a function of time in the dynamic case.

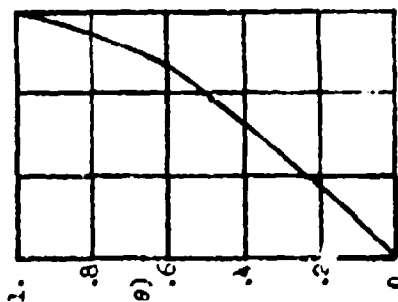
The need to turn to the characteristics discussed earlier for a means of comparison of data is clear. The reason is essentially the same as the one given in previous discussion covering comparison of RCS for altered bodies even though the curves from each situation were presented as functions of the same variable, possible overlapping and intertwining would preclude quantitative comparisons.

Figure 3.2

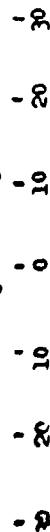
a. A Measured RCS Signature $\sigma(\theta)$



b. A Cumulative Distribution Function $F(\theta)$ For Aspect Angle



Azimuth Angle in Degrees



c. The Quantile Functions for the Static Case (---) and for the Dynamic Distribution $F(\theta)$ (—)

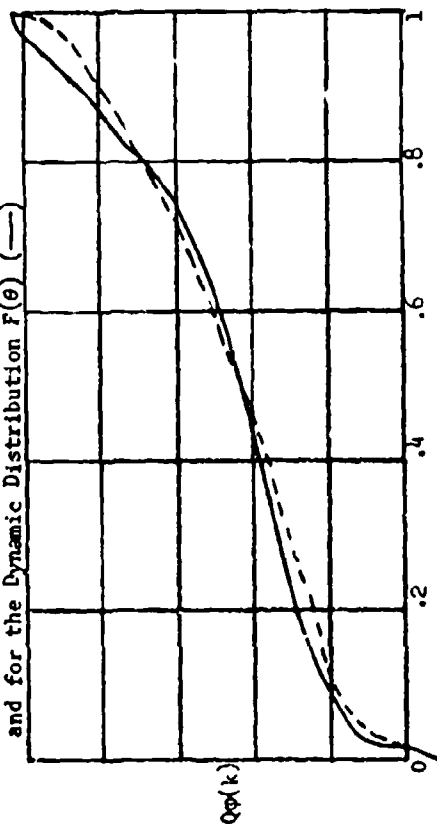
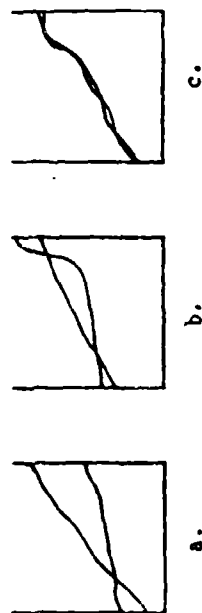


Figure 3.1 Some Hypothetical Comparisons of Redistributed Functions



Let us proceed then to a discussion of how the theory of redistributed functions can be applied for the purpose of making the above-mentioned comparisons. Suppose that a particular radar target has a static cross section signature $\sigma^s(\theta)$. Suppose that this target is observed in a dynamic situation (for example in flight), and that the aspect angle (between the observers line of sight and the nose-on axis) is $\theta(t)$. For the purposes of this discussion we now postulate that if $\sigma^d(t)$ is the observed cross section in the dynamic situation, then $\sigma^d(t) = \sigma^s(\theta(t))$. To specify the problem further, let us suppose that we are interested in the dynamic cross section during a time interval $t_1 \leq t \leq t_2$ during which the aspect angle varies over the range $\theta_1 \leq \theta \leq \theta_2$.

We can compute the various generalized averages and quantiles for $\sigma^d(t)$ on $[t_1, t_2]$ exactly as we computed them in the static case for $\sigma^s(\theta)$ on $[\theta_1, \theta_2]$. For example the generalized averages are of the form

$$A_G(\sigma^d(t)) = G^{-1} \left(\frac{1}{t_2 - t_1} \int_{t_1}^{t_2} G(\sigma^d(t)) dt \right) \quad (3.2-1)$$

We can thus proceed to make comparisons of cross section signatures just as we did in the static case.

It happens, however, that we can apply the theory of redistributed functions to improve this procedure. Referring to Section 2.7 we can rewrite (3.2-1) as an integral over θ :

$$\begin{aligned} A_G(\sigma^d(t)) &= G^{-1} \left(\frac{1}{t_2 - t_1} \int_{t_1}^{t_2} G(\sigma^d(t)) dt \right) \\ &= G^{-1} \left(\int_{\theta_1}^{\theta_2} G(\sigma^s(\theta)) p(\theta) d\theta \right) \end{aligned} \quad (3.2-2)$$

where $p(\theta)$ in this case is the density function for aspect angle in the particular dynamic situation. Thus a generalized average for a dynamic signature is reduced to an integral of the static signature with a weight function.

The advantage of (3.2-2) is that we can predict the generalized averages for a dynamic situation if we know (or can estimate) only the distribution (as given by $p(\theta)$) of aspect angles during $[t_1, t_2]$. We do not have to know $\theta(t)$ explicitly.

As might be expected, we can also construct the redistributed function $R\sigma^d(t)$ knowing only $p(\theta)$ and $\sigma^s(\theta)$. We will not develop the theory, but the procedure, except for one alteration, is identical to that presented in Section 2.2 for constructing the redistributed function assuming a uniform distribution of the variable of integration. First we make the

following notation changes to correspond to the present discussion: replace $\varphi(x)$ by $\sigma(x)$ and $[a, b]$ by $[\theta_1, \theta_2]$. Then we need only redefine y_k (compare with item 1 of Section 2.2):

$$y_k = (\theta_2 - \theta_1) p \left(\theta_1 + \frac{k}{n} (\theta_2 - \theta_1) \right) \sigma \left(\theta_1 + \frac{k}{n} (\theta_2 - \theta_1) \right)$$

Hereafter we proceed exactly as before in Section 2.2. The resulting redistributed function is defined on the interval $[\theta_1, \theta_2]$. It only remains to map this interval linearly (by a change of variable of the form $\theta = \alpha t + \beta$) to the interval $[t_1, t_2]$. Thus finally we obtain $R\sigma^d(t)$ and are in a position to apply all the comparison techniques discussed in Section 3.1.

As an illustrative example we present in Figure 3.2 a measured static cross section $\sigma(\theta)$ on the interval $-30^\circ \leq \theta \leq 30^\circ$, a cumulative distribution function $F(\theta)$ characterizing a particular distribution of aspect angle, and two quantile functions for $\sigma(\theta)$, one the static quantile function, and the other the quantile function for the weight function $p(\theta) = \frac{d}{d\theta} F(\theta)$. The cross section $\sigma(\theta)$ was measured from a ballistic missile. The distribution function $F(\theta)$ was calculated assuming the missile to be in flight, precessing at an angle of 15° about an axis which subtends an angle of 15° with the observers' line of sight. The conclusion which we draw in this particular case is that the predicted distribution of cross section values for the dynamic situation (i.e., for the assumed angular weighting) is essentially the same as the static distribution of cross section values over the same angular interval.

4. SUMMARY

We have developed in the sections above a technique particularly applicable to graphical radar cross section data for constructing redistributed functions for such data. We have shown that redistributed functions are useful to obtain from a radar cross section signature almost any attribute of an "average" nature; and we have shown that this property of redistributed functions renders them extremely useful as tools with which to make comparisons of radar cross section signatures.

USE OF RADAR CROSS SECTION DATA IN MILITARY SYSTEMS ANALYSIS

H. A. Ecker
Systems Engineering Group
Research and Technology Division
Wright-Patterson Air Force Base, Ohio

INTRODUCTION

The Research and Technology Division of the Air Force Systems Command has established a Systems Engineering Group at Wright-Patterson Air Force Base, Ohio. Within this Systems Engineering Group, the Synthesis and Analysis Division has a mission to perform in-house analyses of existing and proposed Air Force systems and syntheses of new systems to meet specific requirements. The Synthesis and Analysis Division uses radar-reflectivity measurement data on various target and clutter sources to accomplish penetration and defense analyses and studies of airborne detection of ground targets. Therefore, this paper is presented from the point of view of a customer who requires radar-reflectivity measurement data to perform his work.

Three main areas are discussed in this paper. The first concerns the way in which radar-cross-section measurement data are being used to perform military systems analyses. The second area covers a discussion of the shortcomings in radar reflectivity data that have limited our studies in the past. Finally, the type and form of radar cross section data that will be required in the future are discussed.

PENETRATION AND DEFENSE ANALYSES

Penetration analyses and defense analyses are really the same. The penetration problem amounts to finding the survival probability of friendly penetrators in a hostile defense environment. In the defense problem, the viewpoint of the analyst has changed; however, the problem is the same - that of finding the probability of survival of penetrators in a defense environment.

In penetration and defense studies, a mathematical model must be derived for each type of encounter that a penetrator may have with an element of the defense environment. These individual models are integrated into a complete penetration or defense model, which considers the tactics and philosophies of the defense and the offense.

The basic building block, however, is the model that represents the one-on-one encounter between a single penetrator and a single defensive weapon. All factors that affect the ability of an offensive weapon to survive an encounter with the individual defensive weapon must be considered in the model. Obviously, any defensive weapon that relies on radar for guidance and control will be greatly affected by the radar cross section of the penetrating vehicle.

Only a few years ago, many penetration and defense analyses considered the cross section of the penetrating vehicle to be a constant regardless of aspect angle. Typically in these studies, the nose-on cross section of the aircraft was used. There was some justification for using a single value of radar cross section, because in most instances complete radar-cross-section measurement data on the vehicles being considered were not available. Frequently, the results of theoretical calculations were used to determine several possible values of radar cross section to represent a range of values to be considered in the penetration model.

The availability of complete cross-section patterns and the use of computers have made it possible to develop more accurate and meaningful models of one-on-one engagements between a penetrator and a defensive weapon. This paper will describe the basic model used by the Synthesis and Analysis Division for utilizing radar-cross-section data and calculating the effect of radar cross section on survival probability.

Reflectivity data are usually obtained in one of the following two forms:

1. Median radar-cross-section values given at 10° increments in both angles of a normal spherical coordinate system as illustrated in Figure 1.
2. Median values at every 10° increment in azimuth from 0° to 180° for roll planes from -90° to $+90^\circ$ with respect to horizontal. This coordinate system is shown in Figure 2.

Since the data given in the latter form can be converted to normal spherical coordinates by a simple coordinate transformation, the model will be discussed with relation to spherical coordinates only.

In all the individual encounter models involving systems with radar, the basic starting point is a 19 by 19 array of median radar-cross-section values at 10° increments in elevation angle (θ) and azimuth angle (ϕ). Since the aircraft is symmetrical about a plane containing its longitudinal center line and yaw axis, θ and ϕ need only vary from 0° to 180° to completely define the reflectivity of the aircraft.

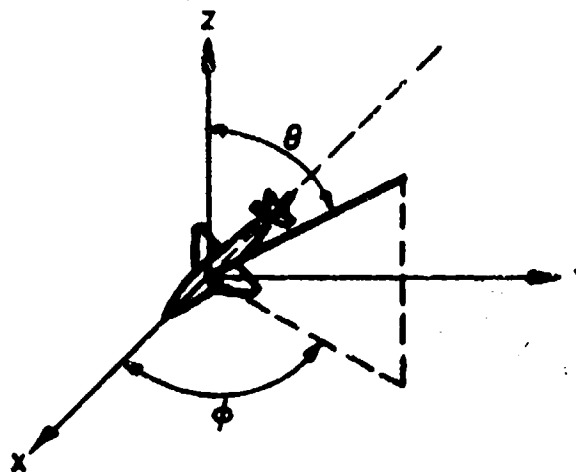


Figure 1. Spherical Coordinates

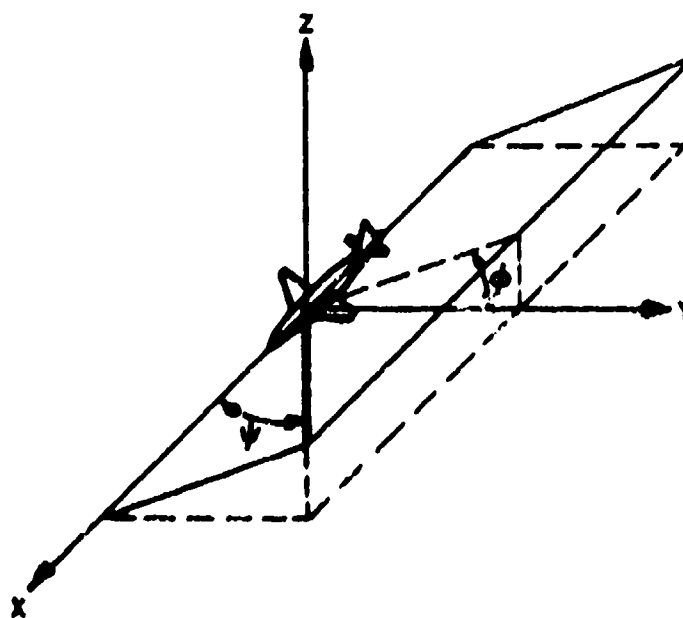


Figure 2. Roll Plane Coordinates

For ease of computation, the one-on-one encounter mathematical models have been programmed for the IBM 7094 digital computer. The array of radar-cross-section data is easily stored as a two-dimensional, subscripted array. A flight path for the penetrating vehicle is simulated to determine the geometric relationships between the penetrator and the radar of the defense weapon as a function of time. These relationships allow computations as function of time and penetrator position, the aspect angles with which the radar views the penetrating vehicle. The essence of this part of the model may be stated as a simulation of the flight of a penetrator in the vicinity of the defense weapon with calculation of the radar-viewing aspect angles at each simulated time increment.

Since the radar cross section data are present in the model only at discrete 10° intervals in azimuth and elevation angles in the coordinate system about the aircraft, interpolation must be performed in two dimensions to obtain the radar-cross-section value at each calculated point along the flight path. Linear interpolation has been used in all our past studies. Curve fitting to a higher degree polynomial would be possible if additional complexity were warranted. This increase in complexity has not been necessary in our past work.

The signal-to-noise ratio in the radar receiver is continually calculated as a function of the range and aspect angles. This calculation is made with the following standard radar equation:

$$S/N = \frac{G^2 \lambda^2 P \sigma (0,0)}{(4\pi)^3 R^4 L kT \Delta f NF} \quad (1)$$

where

- P = transmitted power
- R = the slant range
- σ = radar cross section
- L = losses as a function of range
- G = gain of radar antenna
- λ = wavelength of radar signal
- $kT \Delta f NF$ = average noise in receiver

At each time increment, the average signal-to-noise ratio is compared to the required threshold signal-to-noise ratios for detection and tracking of the particular radar being considered. Two thresholds are used: one for initial detection and, the second, a higher threshold, for adequate tracking. The detection threshold is obtained by calculating the average signal-to-noise ratio required in a receiver to obtain a 50-percent probability of detection. The radar detection problem is assumed to be that as explained by Marcum and Swerling in References 1 and 2. When the calculated average signal-to-noise ratio exceeds this threshold, detection is assumed. This calculation is admittedly a simplification of the detection problem;

however, since median cross-section values are used, this reasonably indicates when detection is possible. The tracking threshold signal-to-noise ratios are obtained primarily from empirical relationships based on radar design.

The effectiveness of various electronic-countermeasures techniques are also considered. If a jammer is simulated on the penetrating aircraft, the jamming-to-signal ratio at the radar receiver can be calculated as a function of time and position of the penetrator. The model is designed to handle constant-power or repeater-type jammers.

This basic model, using the radar cross section pattern of the penetrator, is used in connection with models that simulate:

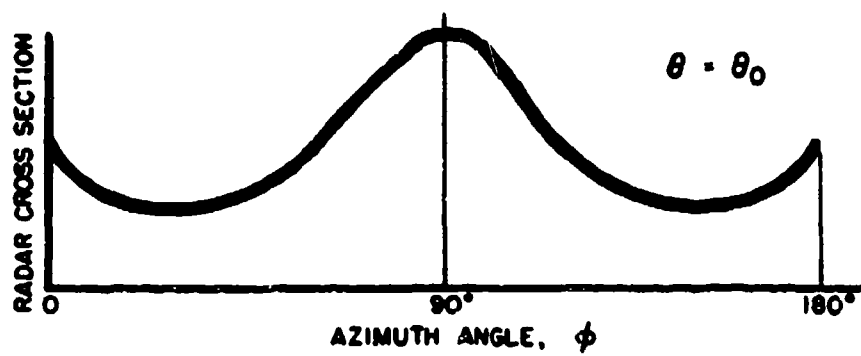
1. Surface-to-air missile systems,
2. Interceptors with air-to-air missiles,
3. Anti-aircraft guns.

The details of the individual defensive weapon models may be found in the Synthesis and Analysis Division Technical Reports, "(U) Analytical and Specific Simulation Models for Determining Penetration Effectiveness of Manned Aircraft,"³ November 1963, SECRET Report, and "(U) An Approach to the Study of Satellite Vulnerability,"⁴ May 1962, SECRET Report. Each of these defensive weapon simulations is designed to indicate:

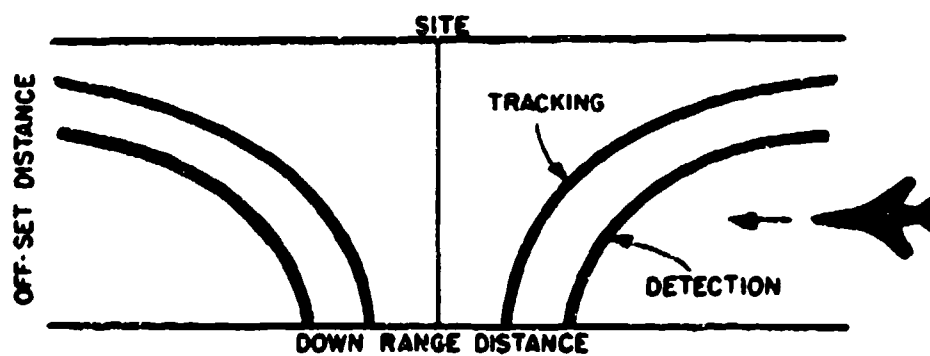
1. Detection and tracking ranges of the penetrator,
2. Number of shots attempted against the penetrator,
3. Probability of survival of the penetrator.

These three measures of the effectiveness of a penetrator to survive an encounter with a defensive weapon are usually plotted as functions of offset distance of the penetrator with respect to the defensive weapon, and for a given speed and altitude of the penetrator. If a radar cross section pattern is considered to have the general form as shown in Figure 2a for each plane of constant elevation angle θ , Figures 3b, 3c, and 3d indicate typical results from the defensive weapon simulations. For a given offset distance, probability of survival is determined by the number of shots possible and the single-shot probability of kill. An average probability of survival is calculated for an encounter with each defensive weapon by the following equations:

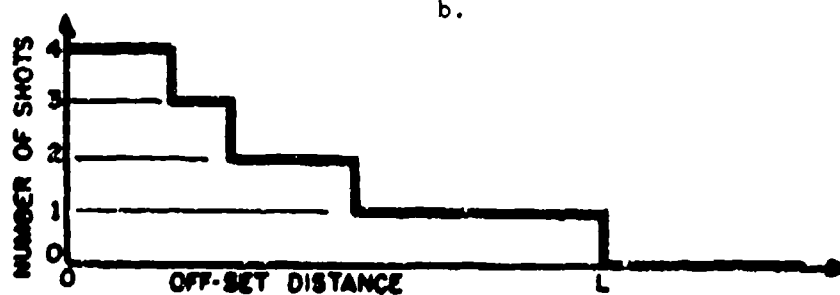
$$\overline{P}_G = \frac{1}{L} \int_0^L P_G(x) dx \quad (2)$$



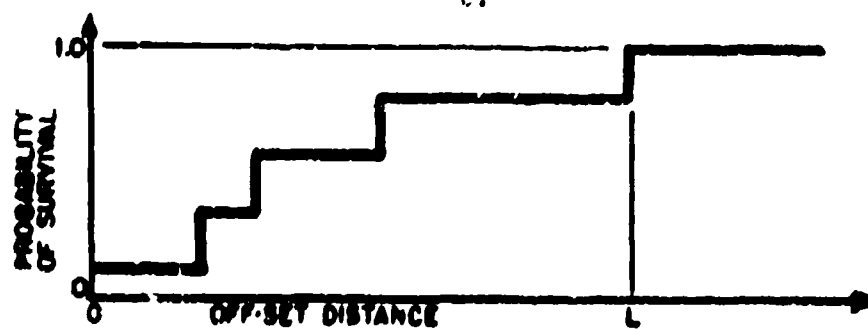
a.



b.



c.



d.

Figure 3. Typical Penetration Analysis Results

where

L = total offset coverage of the weapon
 $p_S(x)$ = probability of survival function
x = offset distance

For the purposes of determining where emphasis should be placed for reducing the radar reflectivity of a penetrating aircraft, the penetration problem has been worked in reverse. That is, a requirement is set so that a weapon can get only a specified number of shots at a penetrating vehicle. The required radar-cross-section pattern is then determined for this vehicle as a function of aspect angles to limit the defensive weapon to this capability. This pattern is compared with the actual reflectivity pattern of a vehicle to determine where reduction is necessary.

A number of criteria could be chosen to establish radar cross section requirements. The cross section requirement could be such that no shots are possible. However, this requirement usually leads to unrealistic values for radar cross section. The number of shots is a more definite criterion than survival probability since survival probability is a function of warhead yield, miss distance, and the vulnerability of the aircraft. Because of the emphasis on reduced radar cross section in recent years, some new system designs consider low radar cross section as well as the other performance characteristics, which have dominated the picture in the past.

AIRBORNE DETECTION OF GROUND TARGETS

The problem of airborne detection of ground target is one of determining the ratio of the signal reflected from the target to the signal reflected from the surrounding clutter. This ratio may be calculated by considering two adjacent resolution cells; one that contains a target and the other only clutter. Figure 4 illustrates this situation. The signals received from the two cells are:

$$S = \frac{K \sigma_{T+C}(\theta, \phi)}{R^4} \quad (3)$$

$$C = \frac{K \sigma_C(\theta, \phi)}{R^4} \quad (4)$$

where the subscripts T+C and C apply to the target-plus-clutter cell and clutter cell, respectively; and K is a constant to account for the radar performance and losses. Since both cells are essentially at the same range, the signal-to-clutter ratio is simply the ratio of the radar reflectivity of the cell with the target to the radar reflectivity of the cell without the target:

$$S/C = \frac{\sigma_{T+C}(\theta, \phi)}{\sigma_C(\theta, \phi)} \quad (5)$$

This resulting number can be interpreted as an average signal-to-clutter ratio, which is a function only of the resolution cell size, the type target and background, and the angle with which they are viewed. Statistical analysis is required to determine the probability of detecting the given ground target since both the target-plus-clutter echo and clutter echo vary randomly in amplitude and phase. For a given threshold in the radar receiver, the probability of detection and the probability of false alarm can be calculated through standard techniques if the probability distribution functions are known for the clutter echo and the target-plus-clutter echo. Quite often the clutter return is assumed to be Rayleigh-distributed; however, depending on the nature of the clutter producing sources, this assumption may prove to be incorrect. Also, quite often the target and clutter returns together are assumed to be a Gaussian process combined with a fixed signal return, or simply a Gaussian distribution with other than zero mean.

The statistical problem of determining the false alarm and probability of detection is illustrated in Figure 5. If the probability density functions and average reflectivities of the clutter and target-plus-clutter are known, the probabilities can be calculated by integration of the respective density functions:

$$P_D = \int_{S_T}^{\infty} p_{T+C}(x) dx \quad (6)$$

$$P_{FA} = \int_{S_T}^{\infty} p_C(x) dx \quad (7)$$

where

P_D = probability of detection

P_{FA} = probability of false alarm

$p_{T+C}(x)$ = probability density function of target-plus-clutter echo

$p_C(x)$ = probability density function of clutter echo

S_T = threshold level

Note that the return from the clutter and from the target must be sufficiently above the noise level, so that detection in noise is not the problem.

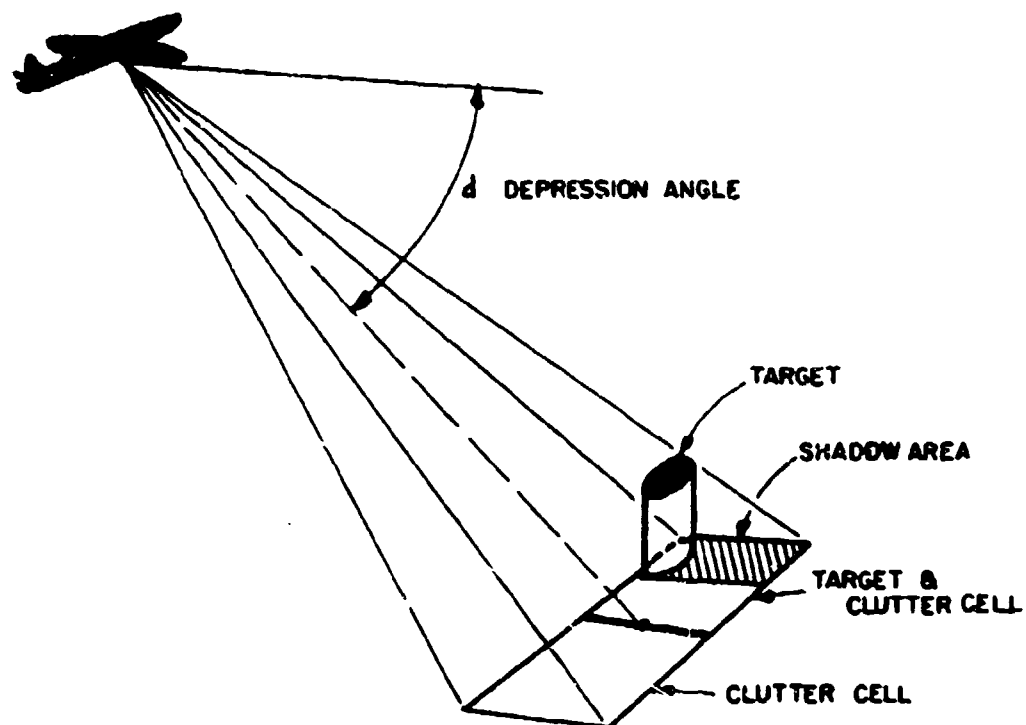


Figure 4. Radar Return Geometry for Detection Requirements

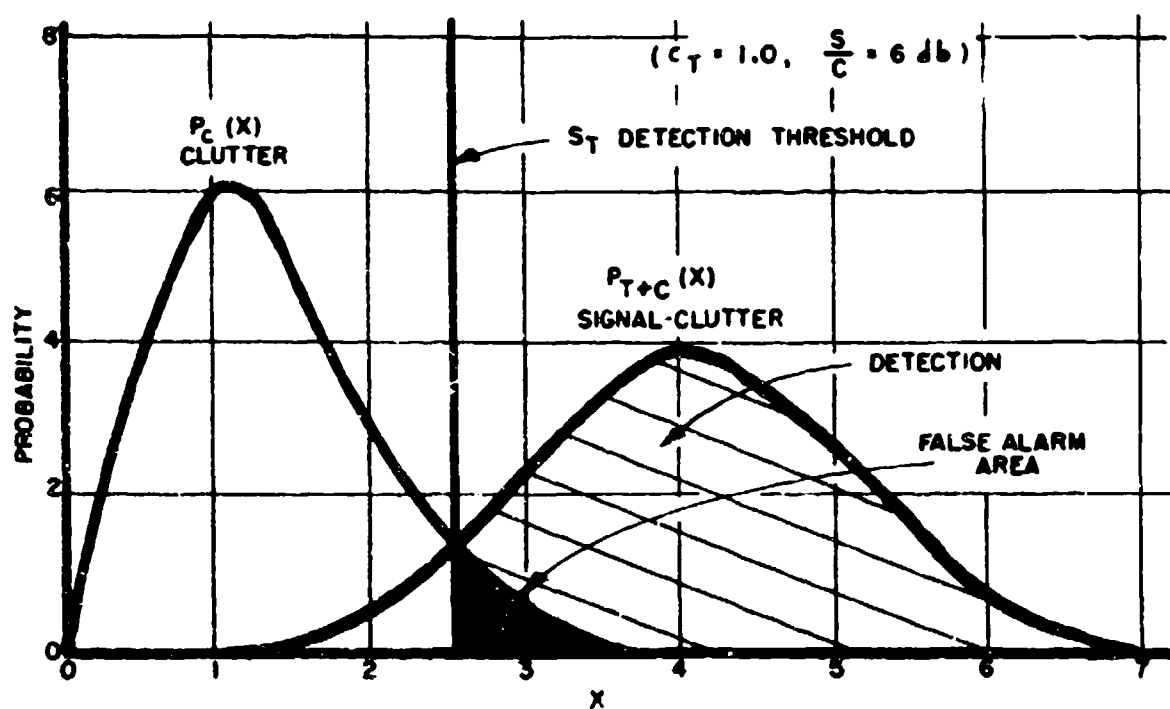


Figure 5. Statistical Detection for Fixed Detection Threshold

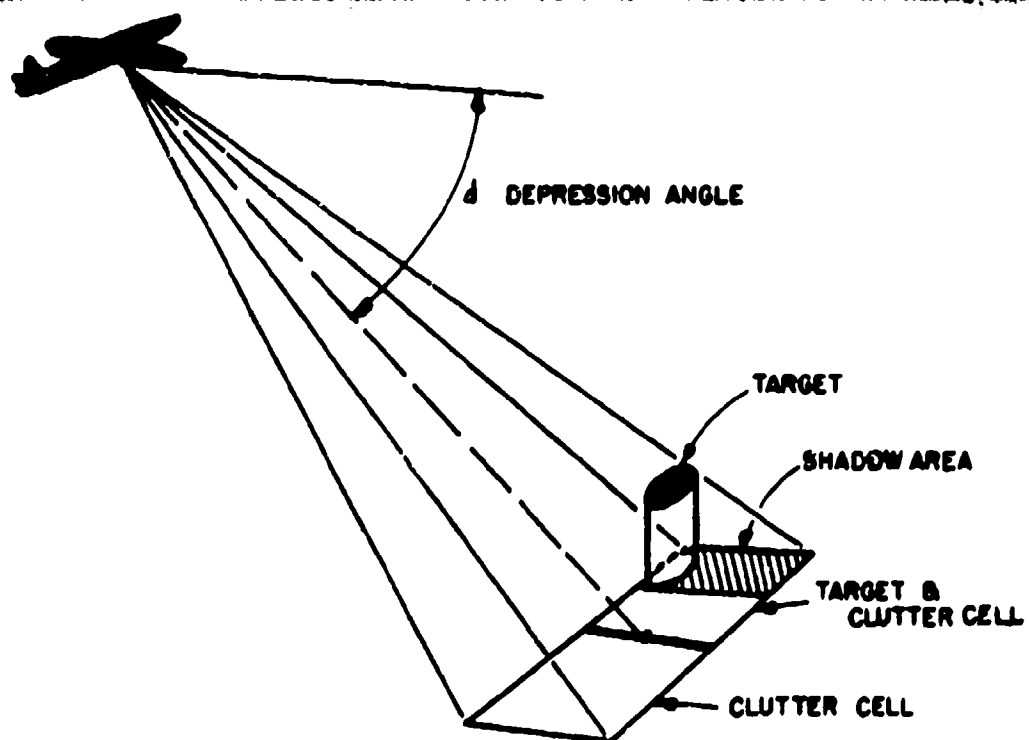


Figure 4. Radar Return Geometry for Detection Requirements

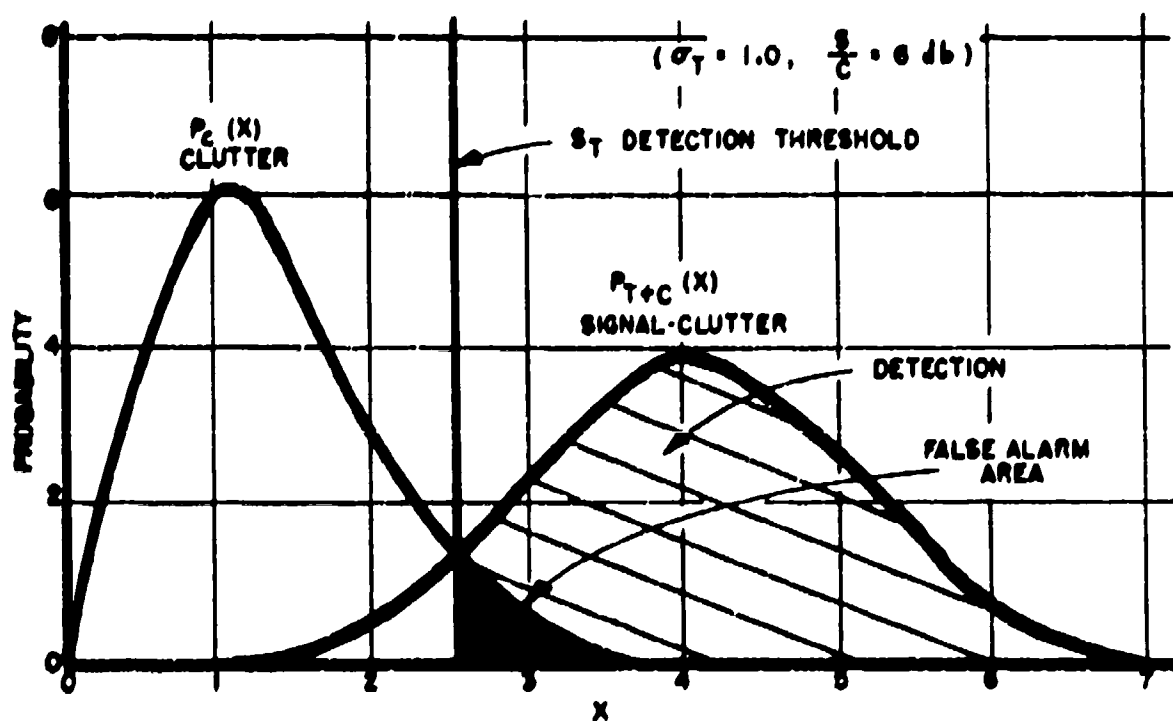


Figure 5. Statistical Detection for Fixed Detection Threshold

Again, for ease of calculation, digital programs were developed for performing these calculations that simulate aircraft, target, and background conditions. These models are presented in Counter-insurgency Study, Volume IV - "Sensors."⁶ In that report, a variety of aircraft, altitude, and speed combinations are presented for typical tactical targets and backgrounds. Numerical integration is performed on the digital computer to calculate the detection and false alarm probabilities from the two probability density functions.

INADEQUACY OF RADAR-REFLECTIVITY MEASUREMENT DATA

The most serious inadequacy of radar reflectivity data is that data are not available on all of the targets and the background clutter sources that must be considered in our systems analyses and syntheses. The effectiveness of two different aircraft performing penetration missions cannot be compared if the complete radar-cross-section pattern is not known for both aircraft. Likewise, estimating the detection capability of the airborne radar is extremely difficult if the cross section of a target on the ground and the clutter surrounding the target are not known.

In most instances, when radar reflectivity measurement data are available, only a restricted frequency range has been considered. The very least consideration of the frequency dependence of the reflectivity data should be with respect to measurements in the upper frequency bands where specular reflection can be assumed, and in the lower frequency region where the target dimensions are comparable to the wavelength.

Although much experimentation has been done using the various radar polarizations, there is still a lack of data indicating the effect of polarization of the radar signal on the reflectivities of ground targets and clutter sources. It may seem trite to say that complete reflectivity patterns over all aspect angles are required for both target and clutter series; however, especially in the case of ground targets, we have been able to find reflectivity data only for very restricted viewing angles of the target. Many clutter sources may possibly be considered to have radar reflectivity, which does not depend on viewing angle. There are also many clutter sources that have a strong angular dependence and few data are available on these sources.

As an example of lack of reflectivity data, I refer to a situation that recently occurred in one of our studies. In a tactical or counterinsurgency type operation, personnel are a primary target. To determine the ability of airborne radars to detect a man on the ground, one must know a man's radar cross section as a function of viewing aspect angles, polarization, frequency, and position of the man. We were able to find only very limited data on the radar reflectivity of a man and these data were not from recent measurements.

FUTURE RADAR-REFLECTIVITY DATA REQUIREMENTS

Obviously, our first requirement is to have complete radar-reflectivity patterns on the targets and backgrounds necessary to perform a military systems analysis. These data should be at least given at two frequencies that represent the two types of radar reflectivity possible. Also, the effects of the polarization of the radar signal should be indicated.

Beyond the point of having the data available, there are several factors, which if included in the measurement program, could greatly increase the utility of the reflectivity data. If actual data patterns were provided rather than just median values, our ability to handle the detection and tracking problem would be greatly increased. The entire detection and tracking problem could be simulated using a pulse-by-pulse simulation of the radar signal and the aircraft motion and vibration. With present computer technology, this simulation would probably be too detailed to include in the over-all penetration or defense model. However, such a detailed radar simulation would provide extremely accurate signal-to-noise threshold levels to be included in the over-all penetration model.

It appears that the problem of detecting targets that are surrounded by clutter will be with us for many years to come. For this reason, we wish to investigate in more detail the statistics of the clutter signal and the statistics of the radar return that include both clutter and target. Much measurement work is necessary to provide the data for such a statistical analysis. As radar technology advances and resolution becomes better, targets that were formerly considered point targets must now be considered as extended targets. Clutter sources that were considered to be many randomly oriented point scatterers must now be investigated from a different point of view. For the purposes of our analyses, we would like to see data on targets and clutter measured with radars with extremely small resolution cells.

SUMMARY

Much progress has been made toward effective use of radar reflectivity data in military systems analyses. There is still insufficient data in many areas; however, steps are being taken to remedy this situation.

The consideration of radar reflectivity in the initial design of weapons systems is the primary area where increased emphasis is necessary. Designing low radar reflectivity into a system would be easier and more effective than modifying the system at some later date after production.

REFERENCES

1. Marcum, J. I., A Statistical Theory of Target Detection by Pulsed Radar, RM-754, (ASTIA No. AD 101287), RAND Corporation Santa Monica, California, 1 December 1947, Reissued 25 April 1952.
2. Swerling, P., Probability of Detection for Fluctuating Targets, RM-1217, RAND Corporation, Santa Monica, California, 17 March 1954.
3. Vukmir, Vladimir, Sudheimer, Richard H., Lum, Gwon H., Mosteller, Capt. Lawson P. Jr., Ecker, Harry A., Bell, Raymond J., Libby, Travis L., (Unclassified Title) Analytical Methods and Specific Simulation Models for Determining Penetration Effectiveness of Manned Aircraft, RTD-TDR-63-4254, Synthesis and Analysis Division, Directorate of Systems Dynamic Analysis, Research and Technology Division, Wright-Patterson AFB, Ohio, November 1963. (SECRET Report)
4. Vukmir, Vladimir, Shover, Capt Donald R., Ecker, 1/Lt Harry A., Egan, David F., Frick, Roy K., (Unclassified Title) An Approach to the Study of Satellite Vulnerability, ASD-TDR-62-340, Synthesis and Analysis Division, Directorate of Systems Dynamic Analysis, Aeronautical Systems Division, Wright-Patterson AFB, Ohio, May 1962. (SECRET Report)
5. Hayes, R. D., Walsh, J. R. Jr., Eagle, D. F., Ecker, H. A., Long, M. W., Rivers, J. G. B., Stuckey, C. W., (Unclassified Title) Study of Polarization Characteristics of Radar Targets, Final Report, Project A-235, Engineering Experiment Station of Georgia Institute of Technology, Atlanta, Georgia, October 1958. (SECRET Report)
6. Ecker, H. A., Egan, D. F., Fawcett, C. D., Martin, E. H., Wetzel, P. D., (Unclassified Title) Counterinsurgency Study, Vol IV "Sensors," ASD-TDR-63-292, Synthesis and Analysis Division, Directorate of Systems Dynamic Analysis, Aeronautical Systems Division, Wright-Patterson AFB, Ohio, May 1963. (SECRET Report)

TARGET RECOGNITION AND DISCRIMINATION

R. F. Goodrich, O. Ruehr, Z. Akcasu, G. Rabson
Radiation Laboratory, The University of Michigan

ABSTRACT

We approach the problem of target recognition and discrimination from the viewpoint that since we can make a previous determination of the response of various classes of targets as a function of frequency we can devise frequency filters which will accept only those which are characteristic of the target we look for. In other words, for a given radar look we attempt to filter out all but the signal characteristic of the target we are attempting to find during that look.

The type of filter we consider is one which we have parameterized so as to vary from an inverse filter to a matched filter. The inverse filter is best for range discrimination; the matched filter is best for noise suppression. Hence, we have gone to a "mixed" filter leaving the specific choice of the parameter to the requirements of the system.

This recognition scheme depends critically on the prior classification and characterization of the "interesting" targets. Briefly, this requires an analysis of the return from various targets as a function of frequency, the choosing of the parts of the returns which are best able to characterize the targets with respect to one another and to the background clutter, and an evaluation of these choices in terms of a discrimination criterion.

The above classification scheme is much simplified if a "uniform" method of comparing target signatures is devised. We do this making use of a theorem of Wiener's on the representation of a given function by means of the translates of another function.

The research reported in this paper was supported by the U. S. Army Electronics Research and Development Laboratory, Fort Monmouth, New Jersey, under Contract DA 36-039 SC-90733

INTRODUCTION

In order to discriminate between targets we propose to make use of the property that sufficiently 'different' targets scatter differently as a function of frequency. Given an emitted pulse having a frequency spectrum $F(\omega)$ a given target will produce a return $F(\omega) = T \circ f(\omega)$ which is modulated as a function of frequency in a way which is characteristic for that target. Here, T is the operator which takes the emitted frequency spectrum into the received frequency spectrum. The operator T is then a method of describing the target, in fact, T is of the form

$$T \circ f(\omega) = t(\omega) f(\omega) , \quad (1)$$

where $t(\omega)$ is the target return from a monochromatic signal of unit amplitude.

To elaborate, we suppose an experiment in which a group of targets designated by the indices $\{\alpha\}$ is irradiated by a pulse $f(t)$. The return as a function of time will be of the form

$$\tilde{R}(t) = \sum_{\alpha} A_{\alpha} \tilde{S}_{\alpha}(t - \tau_{\alpha}) + \tilde{\epsilon}(t) \quad (2)$$

where A_{α} is an amplitude factor depending upon the target range, etc., τ_{α} is the time delay due to the range, and $\tilde{S}_{\alpha}(t)$ is the transform of

$$S_{\alpha}(\omega) = t_{\alpha}(\omega) f(\omega) , \quad (3)$$

and $\tilde{\epsilon}$ is the noise.

On taking the Fourier transform with respect to time of both sides of (2) we find

$$R(\omega) = \sum_{\alpha} A_{\alpha} e^{i\omega\tau_{\alpha}} S_{\alpha}(\omega) + \epsilon(\omega) . \quad (4)$$

The information we would like to get from our experiment is whether or not a given target, say the β 'th, is present; how many are present and, if present, what are their ranges. In terms of equation (4) we would like to know how many A_{β} 's are above a certain threshold value and what are the values of the τ_{β} to within some resolution requirement. We propose to extract this information making use of filters constructed using our prior knowledge of the frequency signatures, $S_{\beta}(\omega)$, of the various targets of interest.

We now present a very simplified case. Suppose there are targets of only one kind and there is no noise. The return as a function of time will be of the form

$$\tilde{R}(t) = \sum_k A_k \tilde{S}(t - \tau_k) \quad (5)$$

where the summation is over the identical targets. On transforming

$$R(\omega) = \sum_k A_k S(\omega) e^{i\omega\tau_k} \quad (6)$$

If we have prior knowledge of the signature $S(\omega)$ we can form

$$\frac{R(\omega)}{S(\omega)} = \sum_k A_k e^{i\omega\tau_k} \quad (7)$$

If the inverse Fourier transform of (7) can be defined in some sense we obtain

$$\int \frac{R(\omega)}{S(\omega)} e^{-i\omega t} d\omega = \sum_k A_k \delta(t - \tau_k) \quad (8)$$

The result (8) then will give just the information we sought. This scheme we refer to as inverse filtering.

The above example of the inverse filter is so simplified that the objections to it are immediate. Since we use this example only to orient our approach we need not be too concerned over the objections. However, a critique of the inverse filter scheme will lead to the design criteria for an effective implementation of our filter method. We now present a discussion of these objections and their resolution.

First we remark that in the above we have assumed an infinite bandwidth in the inverse filtering operation. On limiting ourselves to a bandwidth $\Delta\omega$ we would get, rather than the δ -function of (8), distributions of the form

$$\frac{\sin \left[\frac{\Delta\omega}{2} (t - \tau) \right]}{\frac{\Delta\omega}{2} (t - \tau)} \quad (9)$$

This is then an essential restriction on the resolution obtainable with the inverse filter using a finite bandwidth.

Second, if there are other targets and noise present in the received signal, the ratio $R(\omega)/S(\omega)$ diverges at the zeros of $S(\omega)$. This difficulty can be circumvented by a further restriction on the effective bandwidth by adopting the convention that we set

$$\frac{R(\omega)}{S(\omega)} = 0, \quad (10)$$

for those values of ω such that

$$|S(\omega)| < \epsilon \quad (11)$$

where ϵ is a positive number which is to be determined from the system requirements. The set of frequencies defined by (11) are removed from the effective bandwidth.

Finally we come to the most important limitation on the inverse filter; in the presence of noise or other targets the inverse filter tends to detect spurious peaks. Because of this and because a matched filter is best in the presence of these unwanted signals we propose a compromise between the two which we refer to as a 'mixed' filter.

THE MIXED FILTER

We parameterize a filter so that it varies continuously from the inverse to the matched filter as a function of the parameter.

Although there are arbitrarily many ways of effecting the parameterization we have chosen one because it gives a simple representation of the filter and also the specific form of the parameterization is not important for our purposes.

We start with the return $r(t)$ in the time domain:

$$r(t) = \sum_{\alpha, \beta} a_{\alpha\beta} s_{\alpha}(t - t_{\alpha\beta}) + n(t) \quad (12)$$

where the index α indicates the type of targets, and β distinguishes between the targets of the same type. Furthermore, $t_{\alpha\beta}$ is the time required for the signal to return from the β 'th target of type α , and $a_{\alpha\beta}$ are constants depending on relative distances. The function $s_{\alpha}(t)$ characterizes the return signal from a target of type α , and $n(t)$ is the noise (white, gaussian).

Finite Fourier transform of $r(t)$ gives:

$$R(\omega) = \int_{-T}^{+T} r(t) e^{-i\omega t} dt = \sum_{\alpha, \beta} a_{\alpha\beta} e^{-i\omega t_{\alpha\beta}} \int_{-(T-t_{\alpha\beta})}^{T-t_{\alpha\beta}} s_{\alpha}(u) e^{-i\omega u} du + \epsilon(\omega), \quad (13)$$

where

$$\epsilon(\omega) \equiv \int_{-T}^{+T} e^{-i\omega t} n(t) dt. \quad (14)$$

Assuming that the integration time $2T$ is large compared to $t_{\alpha\beta}$, and defining

$$S_{\alpha}(\omega) \equiv \int_{-T}^{+T} s_{\alpha}(u) e^{-i\omega u} du \quad (15)$$

one obtains $R(\omega)$ as follows:

$$R(\omega) = \sum_{\alpha, \beta} a_{\alpha\beta} e^{-i\omega t_{\alpha\beta}} S_{\alpha}(\omega) + \epsilon(\omega). \quad (16)$$

Note that $R(-\omega) = R^*(\omega)$, $S_{\alpha}(-\omega) = S_{\alpha}^*(\omega)$ and $\epsilon(-\omega) = \epsilon^*(\omega)$. If we process $R(\omega)$ with the 'mixed' filter using the filter function

$$X_m(\omega) \equiv \frac{S_{\alpha}^*(\omega)}{m^2 + |S_{\alpha}(\omega)|^2} \quad (17)$$

we obtain a function $D_{\alpha_0}(t)$ as follows:

$$D_{\alpha_0}(t) = \frac{1}{A_{\alpha_0, m}} \int_{-\Omega}^{+\Omega} R(\omega) X_m(\omega) e^{i\omega t} d\omega \quad (18)$$

where $A_{\alpha_0, m}$ is the normalization factor defined by

$$A_{\alpha_0, m} \equiv \int_{-\Omega}^{+\Omega} \frac{|S_{\alpha_0}(\omega)|^2}{m^2 + |S_{\alpha_0}(\omega)|^2} d\omega, \quad (19)$$

where Ω is a constant frequency determining the range of integration.

The explicit form of $D_{\alpha_0}(t)$ is obtained by substituting $R(\omega)$ from (16) into (18):

$$D_{\alpha_0}(t) = \frac{1}{A_{\alpha_0, m}} \sum_{\alpha, \beta} a_{\alpha\beta} \int_{-\Omega}^{+\Omega} \frac{S_{\alpha}(\omega) S_{\alpha_0}^*(\omega) e^{-i\omega(t-t_{\alpha\beta})}}{m^2 + |S_{\alpha_0}(\omega)|^2} d\omega$$

$$+ \frac{1}{A_{\alpha_0, m}} \int_{-T}^{+T} n(u) du \int_{-\Omega}^{+\Omega} \frac{S_{\alpha_0}^*(\omega) e^{i\omega(t-u)}}{m^2 + |S_{\alpha_0}(\omega)|^2} d\omega \quad (20)$$

Obviously, $D_{\alpha_0}(t)$ is a real quantity. The 'matched' filter limit is obtained by letting $m \rightarrow \infty$:

$$D_{\alpha_0}(t) = \frac{1}{A_{\alpha_0}} \sum_{\alpha, \beta} a_{\alpha\beta} \int_{-\Omega}^{+\Omega} S_{\alpha}(\omega) S_{\alpha_0}^*(\omega) e^{i\omega(t-t_{\alpha\beta})} d\omega$$

$$+ \frac{1}{A_{\alpha_0}} \int_{-T}^{+T} n(u) du \int_{-\Omega}^{+\Omega} S_{\alpha_0}^*(\omega) e^{i\omega(t-u)} d\omega, \quad (21)$$

where

$$A_{\alpha_0} \equiv \lim_{m \rightarrow \infty} m^2 A_{\alpha_0, m} = \int_{-\Omega}^{+\Omega} |S_{\alpha_0}(\omega)|^2 d\omega \quad (22)$$

The expected value of $D_{\alpha_0}(t)$ is the first term on the right-hand side of (20), because the mean value $\overline{n(u)}$ of the noise is zero. Let $\overline{D_{\alpha_0}}(t)$ denote the expected (or mean) value of $D_{\alpha_0}(t)$. One can express $\overline{D_{\alpha_0}}(t)$ as follows:

$$\begin{aligned} \overline{D_{\alpha_0}}(t) = & \sum_{\beta} a_{\alpha_0 \beta} \int_{-\Omega}^{+\Omega} \frac{|S_{\alpha_0}(\omega)|^2 e^{i\omega(t-t_{\alpha_0 \beta})}}{A_{\alpha_0, m} [m^2 + |S_{\alpha_0}(\omega)|^2]} d\omega \\ & + \sum_{\alpha \neq \alpha_0} a_{\alpha \beta} \int_{-\Omega}^{+\Omega} \frac{S_{\alpha_0}^*(\omega) S_{\alpha}(\omega) e^{i\omega(t-t_{\alpha \beta})}}{A_{\alpha_0, m} [m^2 + |S_{\alpha_0}(\omega)|^2]} d\omega . \end{aligned} \quad (23)$$

Before beginning to discuss the various aspects of this expression, it seems to be in order to consider the variance of $D_{\alpha_0}(t)$.

Noise-to-Signal Ratio: We define the noise-to-signal ratio ρ_{α_0} as

$$\rho_{\alpha_0} \equiv \left[\overline{[D_{\alpha_0}(t) - \overline{D_{\alpha_0}}(t)]^2} \right]^{1/2} . \quad (24)$$

Using (20), one obtains

$$\rho_{\alpha_0}^2 = 2 \pi \left(\frac{\sigma}{A_{\alpha_0, m}} \right)^2 \int_{-\Omega}^{+\Omega} \frac{|S_{\alpha_0}(\omega)|^2}{[m^2 + |S_{\alpha_0}(\omega)|^2]^2} d\omega . \quad (25)$$

In obtaining (25), we have used the fact that the noise is white, viz., $n(u)n(u') = \sigma^2 \delta(u-u')$, and the approximation

$$\int_{-T}^{+T} e^{-i(\omega+\omega')t} dt = 2 \pi \delta(\omega+\omega') .$$

It is noted that (ρ_{α_0}/σ) , where σ is the effective value of the noise, depends on the type of the target as well as on m . The variation of (ρ_{α_0}/σ) with m is of interest. Qualitatively, this variation is expected to be as shown in Fig. 1.

For $m=0$, one has

$$\left(\frac{\rho_{\alpha_0}(0)}{\sigma} \right)^2 = \frac{\pi}{2 \Omega^2} \int_{-\Omega}^{+\Omega} \frac{d\omega}{|S_{\alpha_0}(\omega)|^2} , \quad (26)$$

which corresponds to the 'inverse' filter. When $m \rightarrow \infty$, the 'matched' filter limit is obtained:

$$\left[\frac{\rho_{\alpha_0}(\omega)}{\sigma} \right]^2 = \frac{2\pi}{\int_{-\Omega}^{+\Omega} |S_{\alpha_0}(\omega)|^2 d\omega} \quad (27)$$

The fact that the above value of the noise-to-signal ratio represents the smallest possible value is proven in the theory of matched filters.

Pulse Width: We now turn to the first term in (23), and investigate the quantity

$$d_{\alpha_0} \beta(t) \equiv \frac{1}{A_{\alpha_0} m} \int_{-\Omega}^{+\Omega} \frac{|S_{\alpha_0}(\omega)|^2 e^{i\omega(t-t_{\alpha_0}\beta)}}{m^2 + |S_{\alpha_0}(\omega)|^2} d\omega,$$

which is a typical term in the summation of β . It represents a peaked function at $t=t_{\alpha_0}\beta$ with a height 1. The half-width $W(m)$ of this peak is defined by

$$\int_{-\Omega}^{+\Omega} \frac{|S_{\alpha_0}(\omega)|^2}{m^2 + |S_{\alpha_0}(\omega)|^2} e^{i\omega W(m)/2} d\omega = \frac{A_{\alpha_0} m}{2} \quad (28)$$

The dependence of $W(m)$ on m is also of interest. Fig. 2 depicts the predicted qualitative variation of $W(m)$ with m . The minimum value of the width is obtained from (26) as the root of

$$\sin(W_{\min}\Omega/2) = (\Omega W_{\min}/4) \quad (29)$$

which is approximately given by

$$W_{\min} \approx \frac{2\sqrt{3}}{\Omega} \quad (30)$$

This is the minimum width attainable by any filter.

The asymptotic value of $W(m)$ as $m \rightarrow \infty$ follows from (28) as the solution of

$$\frac{1}{2} \int_{-\Omega}^{+\Omega} |S_{\alpha_0}(\omega)|^2 d\omega = \int_{-\Omega}^{+\Omega} |S_{\alpha_0}(\omega)|^2 e^{i\omega \frac{W_{\max}}{2}} d\omega, \quad (31)$$

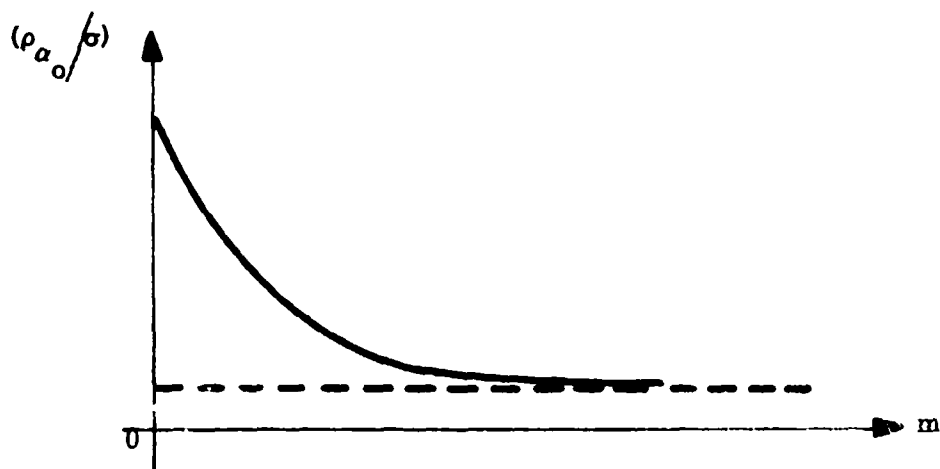


FIG. 1: SIGNAL-TO-NOISE RATIO VS: FILTER PARAMETER

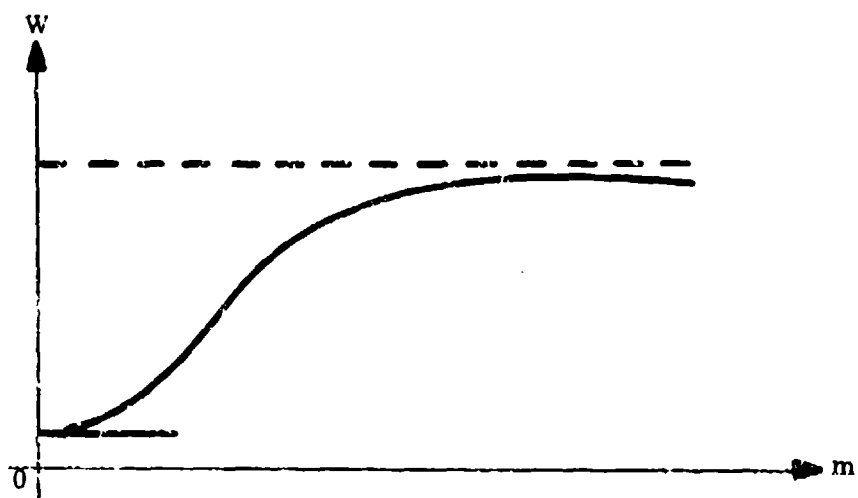


FIGURE 2: RANGE RESOLUTION (PEAK WIDTH VS: FILTER PARAMETER)

which can be approximated by

$$W_{\max}^2 \approx 4 \frac{\int_0^{\Omega} |s_{\alpha_0}(\omega)|^2 d\omega}{\int_0^{\Omega} \omega^2 |s_{\alpha_0}(\omega)|^2 d\omega} \quad (32)$$

Counting the Number of Identical Targets: When there is only one type of target, (23) reduces to

$$\overline{D}(t) = \sum_{\beta} a_{\beta} \int_{-\Omega}^{+\Omega} \frac{|s(\omega)|^2 e^{i\omega(t-t_{\beta})}}{\Lambda_m [m^2 + |s(\omega)|^2]} d\omega \quad (33)$$

where we have dropped the subscript α_0 which is now necessary.

If one is interested primarily in the number of targets, and if the ranges determined by t_{β} do not have to be determined with the maximum possible accuracy, one may choose $m \rightarrow \infty$, viz., 'matched' filter, since it provides the minimum noise-to-signal ratio. The possibility of overlapping peaks can be handled by forming the product of the pulse height and the pulse width. When the two pulses representing two different targets coincide completely, the height of the resultant peak is 2, and the width is just W_{\max} given by (31). Therefore the product

$$\eta = \frac{\text{height} \times \text{width}}{W_{\max}} \quad (34)$$

is also 2. On the other hand, if the two peaks are adjacent and the tip of the resultant curve is obscured by the noise, one would interpret the result as one peak of height 1, but with a width $2W_{\max}$. Thus, again the product η would be 2. It follows that the number of targets corresponding to an observed peak can be predicted from the values of η . If $.5 < \eta < 1.5$ there is one target, and if $1.5 < \eta < 2.5$ there are two targets, etc. This procedure can be applied, of course, to the finite values of m , also. In that case, the η will be normalized to the width $W(m)$ which is obtained by (28) for the chosen value of m . Whether one can increase the accuracy in the determination of t_{β} , and thus of the range, by choosing a smaller m , will depend on the relative shape of the curves giving the m -dependence of the pulse width and the noise-to-signal ratio. Therefore, it is desirable first to plot these curves, for a few target types, by computing (25) and (28) numerically.

Distinguishing Between Two Different Types of Targets:

Suppose that there are two different targets at the same distance. Then, (23) gives

$$\bar{D}_{\alpha_1}(t) = 1 + \int_{-\Omega}^{+\Omega} \frac{s_{\alpha_1}^*(\omega) s_{\alpha_2}(\omega)}{A_{\alpha_1, m} [m^2 + |s_{\alpha_1}(\omega)|^2]} d\omega, \quad (35)$$

where we denoted the targets by α_1 and α_2 . If one processes the same return by the mixed filter corresponding to the target α_2 , one obtains

$$\bar{D}_{\alpha_2}(t) = 1 + \int_{-\Omega}^{+\Omega} \frac{s_{\alpha_2}^*(\omega) s_{\alpha_1}(\omega)}{A_{\alpha_2, m} [m^2 + |s_{\alpha_2}(\omega)|^2]} d\omega. \quad (36)$$

On the other hand, if the return is processed by the filter corresponding to a third filter α_3 , the outcome will be

$$\bar{D}_{\alpha_3}(t) = \int_{-\Omega}^{+\Omega} \frac{[s_{\alpha_2}(\omega) + s_{\alpha_1}(\omega)] s_{\alpha_3}^*(\omega)}{A_{\alpha_3, m} [m^2 + |s_{\alpha_3}(\omega)|^2]} d\omega. \quad (37)$$

In the case of a matched filter, (35) takes the following form:

$$D_{\alpha_1}(t) = 1 + \frac{\int_{-\Omega}^{+\Omega} s_{\alpha_1}^*(\omega) s_{\alpha_2}(\omega) d\omega}{\int_{-\Omega}^{+\Omega} |s_{\alpha_1}(\omega)|^2 d\omega}.$$

Similar expressions are obtained for (36) and (37) when $m \rightarrow \omega$.

The foregoing formulas indicate that the different targets can be identified by using a matched filter if the following inequality is satisfied for all target pairs:

$$\int_{-\Omega}^{+\Omega} s_{\alpha_j}(\omega) s_{\alpha_i}^*(\omega) d\omega \ll \int_{-\Omega}^{+\Omega} |s_{\alpha_i}(\omega)|^2 d\omega. \quad (38)$$

The procedure to be followed is to process the return with the matched filters corresponding to the various targets, one at a time. The targets which are present in the return will be identified by a peak of a height greater than or equal to 1 if the left-hand side of (38) is positive. Those that are not present in the return will not give rise to a peak of any appreciable magnitude if (38) holds. Since the effective value of the noise at the output of the matched filter is given by (27) as

$$\left[\frac{\sigma^2}{\int_{-\Omega}^{+\Omega} |S_{\alpha_1}(\omega)|^2 d\omega} \right]^{1/2}$$

one finds that the false peaks corresponding to the missing targets will be buried in the noise if

$$\int_{-\Omega}^{+\Omega} S_{\alpha_j}(\omega) S_{\alpha_1}^*(\omega) d\omega \leq \sigma \left[\int_{-\Omega}^{+\Omega} |S_{\alpha_1}(\omega)|^2 d\omega \right]^{1/2}. \quad (39)$$

COMPUTER EXPERIMENTS

In order to demonstrate the filter scheme we have devised a means of experimenting using a digital computer.

Each target consists of a linear array of six point reflectors spaced .06 meters apart at an angle of 30° to the wave front. These targets were simply intended as an example to test the method.

Let: θ = aspect; d = spacing; n = number of point reflectors, and c = velocity of light. For any pulse $T(t)$ the response (except for noise) will be

$$R(t) = K \sum_{\alpha=0}^{n-1} T(t + 2\alpha \frac{d \sin \theta}{c}) ,$$

where $t=0$ when the pulse returns from the first point and K is a constant.

The Fourier transform is

$$R^*(\omega) = \int_{-\infty}^{\infty} R(t) e^{-i\omega t} dt = K T^*(\omega) \sum_{\alpha=0}^{n-1} e^{2i\omega d \frac{\sin \theta}{c} \alpha} .$$

We call the factor

$$\sum_{\alpha=0}^{n-1} e^{2i\omega d \frac{\sin \theta}{c} \alpha} ,$$

the unit response and denote it by $I^*(\omega)$. It depends only on the target and not on the transmitted pulse.

We have, upon summing the geometric series

$$I^*(\omega) = \sum_{\alpha=0}^{n-1} e^{2i\omega d \frac{\sin \theta}{c} \alpha} = \frac{e^{\frac{2i\omega d \sin \theta}{c} n} - 1}{e^{\frac{2i\omega d \sin \theta}{c}} - 1} ,$$

and this may be put in the form

$$I^*(\omega) = \frac{\sin \frac{\omega d \sin \theta}{c}}{\sin \frac{\omega d \sin \theta}{c}} e^{\frac{i\omega d \sin \theta}{c} (n-1)}$$

$|I^*(\omega)|$ is a periodic function of ω , ($2\pi \times$ frequency), with period $2\pi c/d \sin \theta$ and $I^*(\omega)$ has a period of $\pi c/d \sin \theta$. In terms of frequency the period of $I^*(\omega)$ is $5 \cdot 10^8$ cps. Fig. 3 is a graph of the function $|I^*(\omega)|$ as ω varies from $\pi c/2d \sin \theta$ to $3\pi c/2d \sin \theta$ (or equivalently from 250 - 750 Mc) for $n=6$, $\theta=30^\circ$, and $d=0.6$ meters.

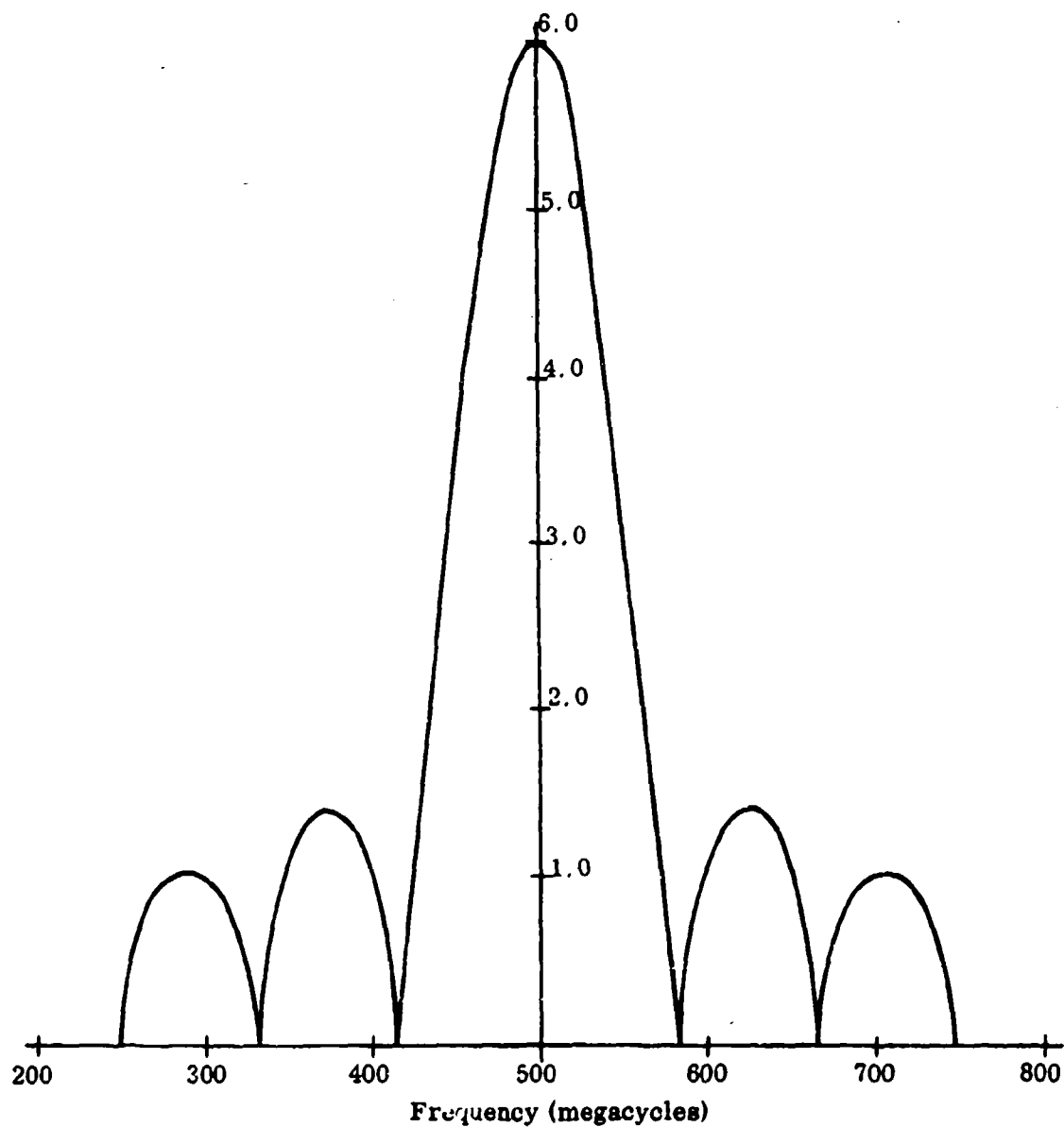


FIGURE 3: UNIT RESPONSE ($I^*(\omega)$) OF A 6-REFLECTOR ARRAY

We consider a rectangular pulse of length $2T$ seconds. The Fourier transform of the pulse is

$$T^*(\omega) = \int_{-T}^T (\sin \phi t) e^{-i\omega t} dt \approx i \frac{\sin(\omega - \phi)T}{(\omega - \phi)},$$

where ϕ is the nominal frequency. For the experiment described here the nominal frequency should be irrelevant; however, if aspect is included as a variable, the choice of nominal frequency will be important.

Fig. 4 illustrates $|T^*(\omega)|$ as a function of $(\omega - \phi)$ and a pulse of 10.4 meters ($T = 1 \times 10^{-8}$ sec). Fig. 5 illustrates $|T^*(\omega)|$ for a pulse of 104 meters ($T = 1.73 \times 10^{-7}$ sec).

The Fourier transform of the return is proportional to the product of the Fourier transforms of the pulse and the unit impulse response. We have chosen our units so that the constant of proportionality is 5×10^8 . The returns for pulses of 10.4 and 104 meters at nominal frequency of 500 Mc are illustrated in Figs. 6 and 7.

We assume that the noise is Gaussian and independent at different frequencies, that the mean is zero and that the standard deviation, σ , is independent of frequency. The average power of the noise is σ^2 and the average power of the signal for one period of $|T^*(\omega)|$ is given by

$$P = \frac{K^2}{\pi} \int_{\pi/2}^{3\pi/2} \left| \frac{\sin(n\omega d \sin \theta/c)}{\sin(\omega d \sin \theta/c)} \cdot \frac{\sin(\omega - \phi)T}{\omega - \phi} \right|^2 d(\omega d \sin \theta/c).$$

For convenience, K was set equal to $2c/d \sin \theta$ or 5×10^8 . At the present time the computer accepts a signal-to-noise ratio, R and computes σ from the relation $\sigma^2 = P/R$.

This is unsatisfactory for two reasons. The computer's estimate of the value of P is very inaccurate at present, and, since the value of P depends so much on the size of the region of integration, it is felt that R as we have defined it does not have much physical significance. However, the signal-to-noise ratio, R , is used only to determine σ . It is σ which is used in the subsequent computations. The value of σ is the average power of the noise and can be interpreted by comparing it with the signal given in Figs. 6 and 7.

In the original design signal-to-noise ratio was used as the independent parameter, but it seems now that it would be better to use σ .

In interpreting the value of σ it should be remembered that we are processing only one pulse. Since the value of σ may be reduced by a factor of $1/\sqrt{n}$ by taking averages over n pulses, the value of σ given here would correspond to a value \sqrt{n} times as great when there are n pulses. For example, a value of 10 for σ in our examples would correspond to $\sigma = 100$ if we are processing 100 pulses.

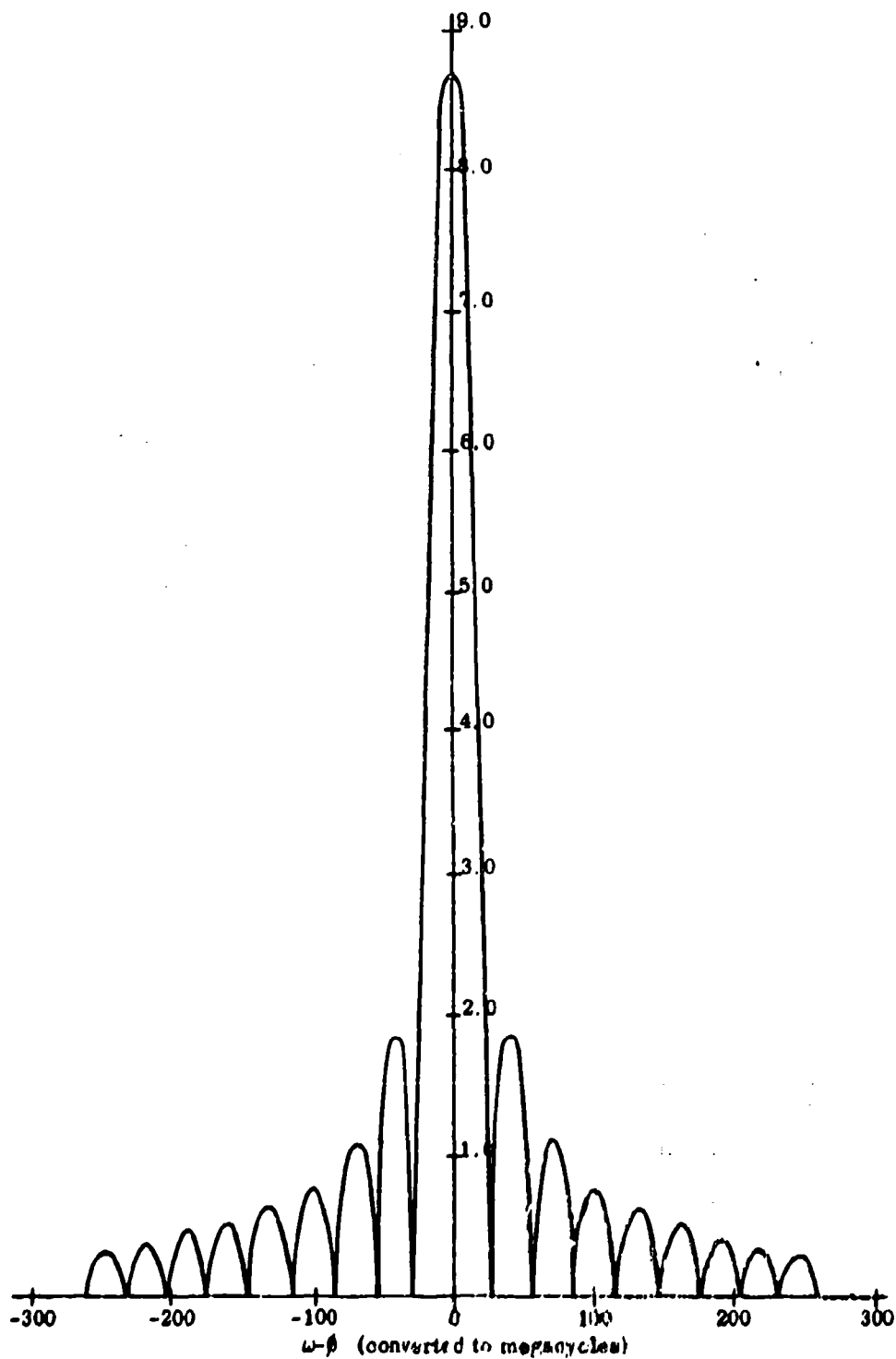


FIGURE 4: AMPLITUDE SPECTRUM OF A 10.4 METER PULSE

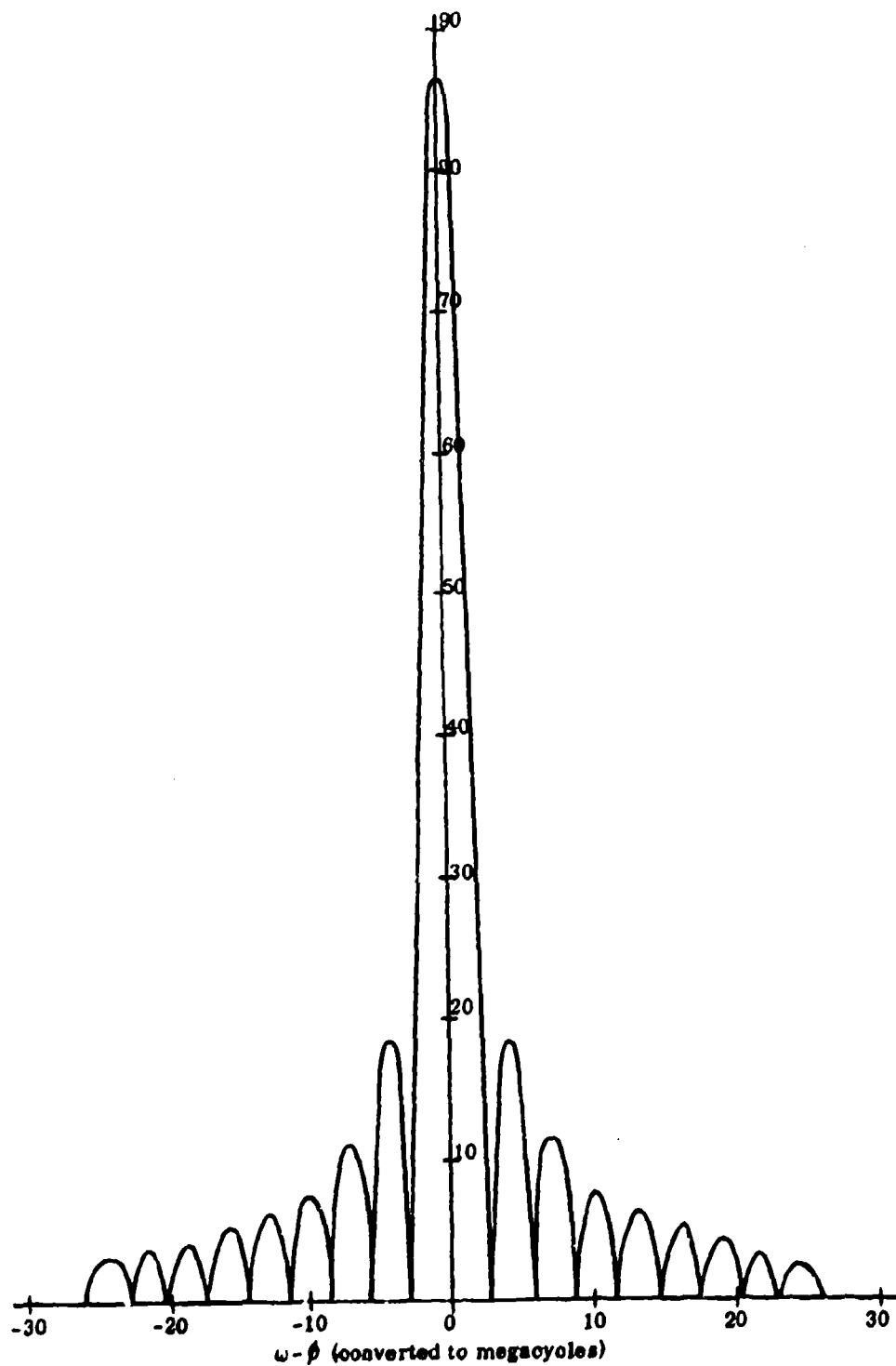
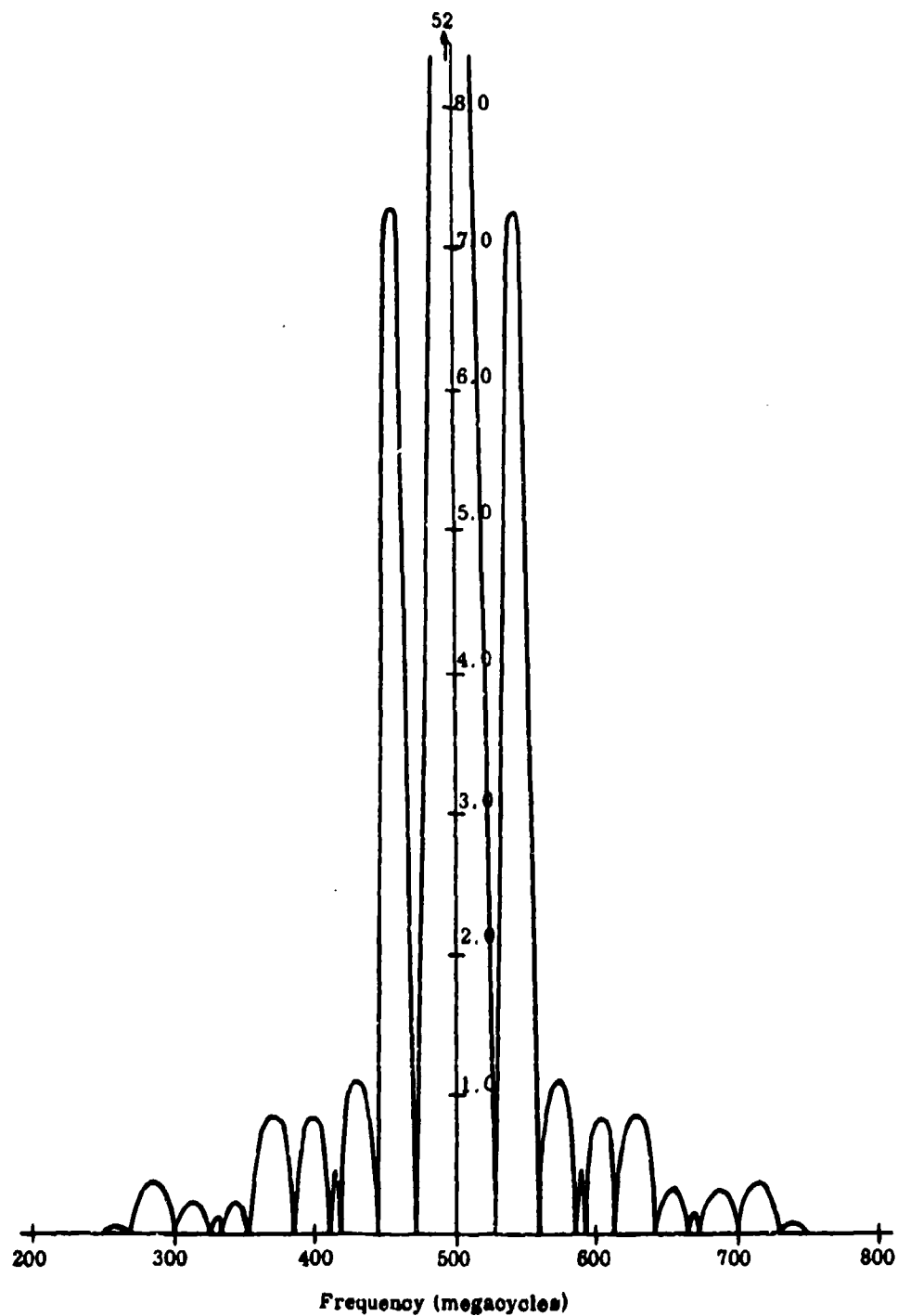


FIGURE 5: AMPLITUDE SPECTRUM OF A 104 METER PULSE



**FIGURE 6: AMPLITUDE SPECTRUM OF REFLECTION FROM TARGET
USING 10.4 METER SQUARE PULSE**

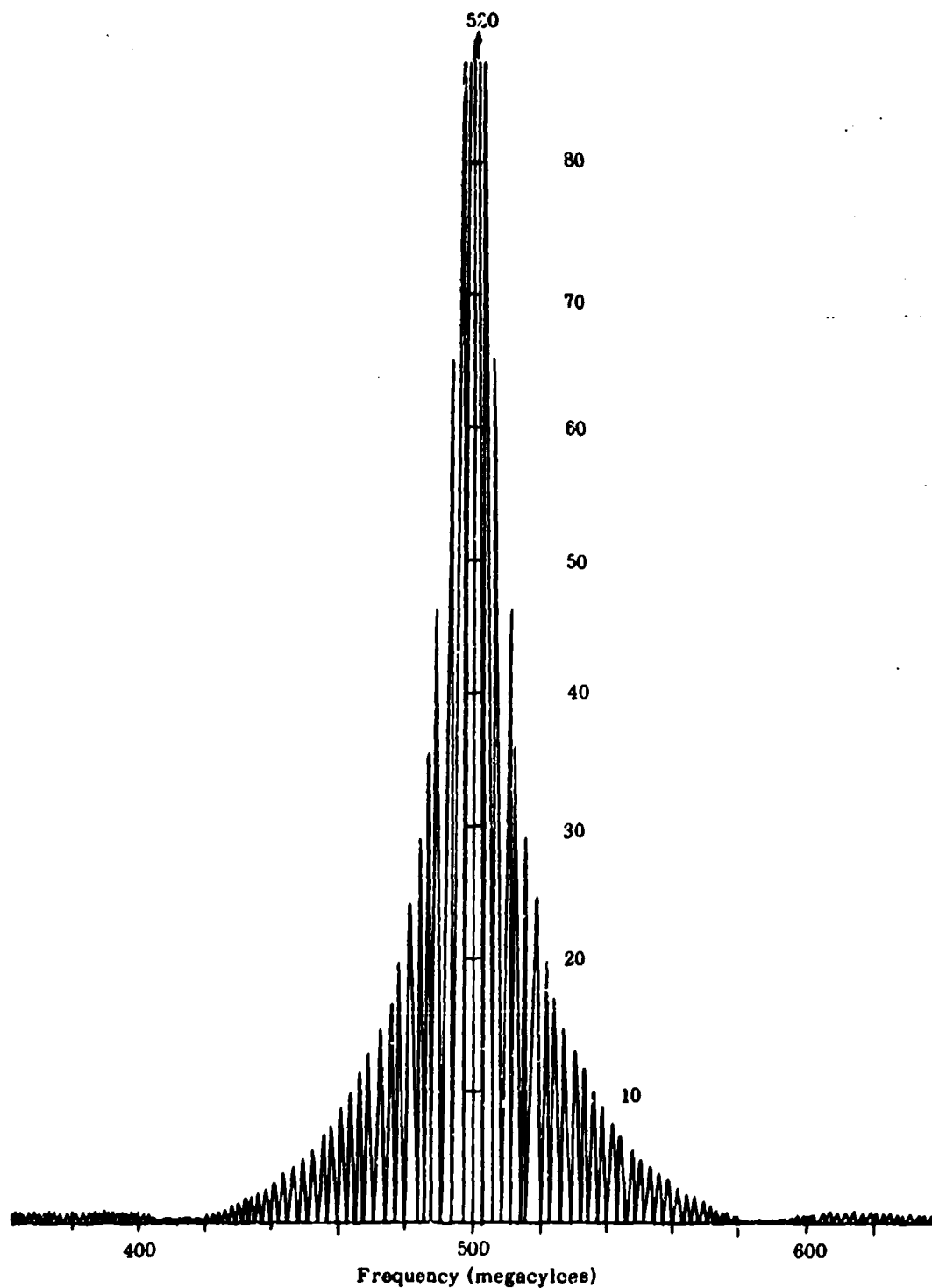


FIGURE 7: AMPLITUDE SPECTRUM OF REFLECTION FROM TARGET
USING 104 METER SQUARE PULSE

The bandwidth that the receiver must be capable of processing is not at the present time an independent parameter; however, it is easily determined from the values of m , σ , and Figs. 6 and 7. The return is considered only when the characteristic return (given in 6 and 7) is above $m\sigma$. Consequently, the bandwidth may be estimated by laying a horizontal line at a height of $m\sigma$ across the curve and noting the difference of the corresponding abscissae. We note that as the value of m decreases (holding everything else fixed) the bandwidth increases and we should expect improved resolution. However, as more noise is now processed we might expect to pay a price in spurious identifications.

Although the receiver must be capable of processing frequencies through the bandwidth the resolution is determined, not by the bandwidth itself, but by the "effective bandwidth". That is, the sum of the lengths of the frequency intervals on which the return is greater than $m\sigma$. This will be roughly equal to half the bandwidth in general.

By means of these computer experiments we have determined the effect of the mixed-filter parameter on the range resolution. This is shown in Fig. 8. We note that in the limit of the inverse filter the resolution approaches zero while in the limit of the matched filter the resolution approaches the physical pulse length.

The above experiments on the resolution as a function of the filter parameter were performed at a sensibly zero noise level. If there is noise present, however, we find spurious peaks for the inverse or near inverse filter. To demonstrate this we reproduce the results of three runs all at a signal-to-noise ratio of 10 and for the filter parameter values of 2, 5, and 25. There are two of the array targets present; one inclined at 30° , the other at 25° . The range of the 25° target is 1503 and that of the 30° is 1500. We use the filter designed to detect the 30° target.

For the filter parameter $m=2$ we note two spurious peaks at ranges of 1495 and 1504. In the other cases, $m=5$ and $m=25$, there are no spurious peaks. Moreover, the noise background in the $m=25$ case is very low.

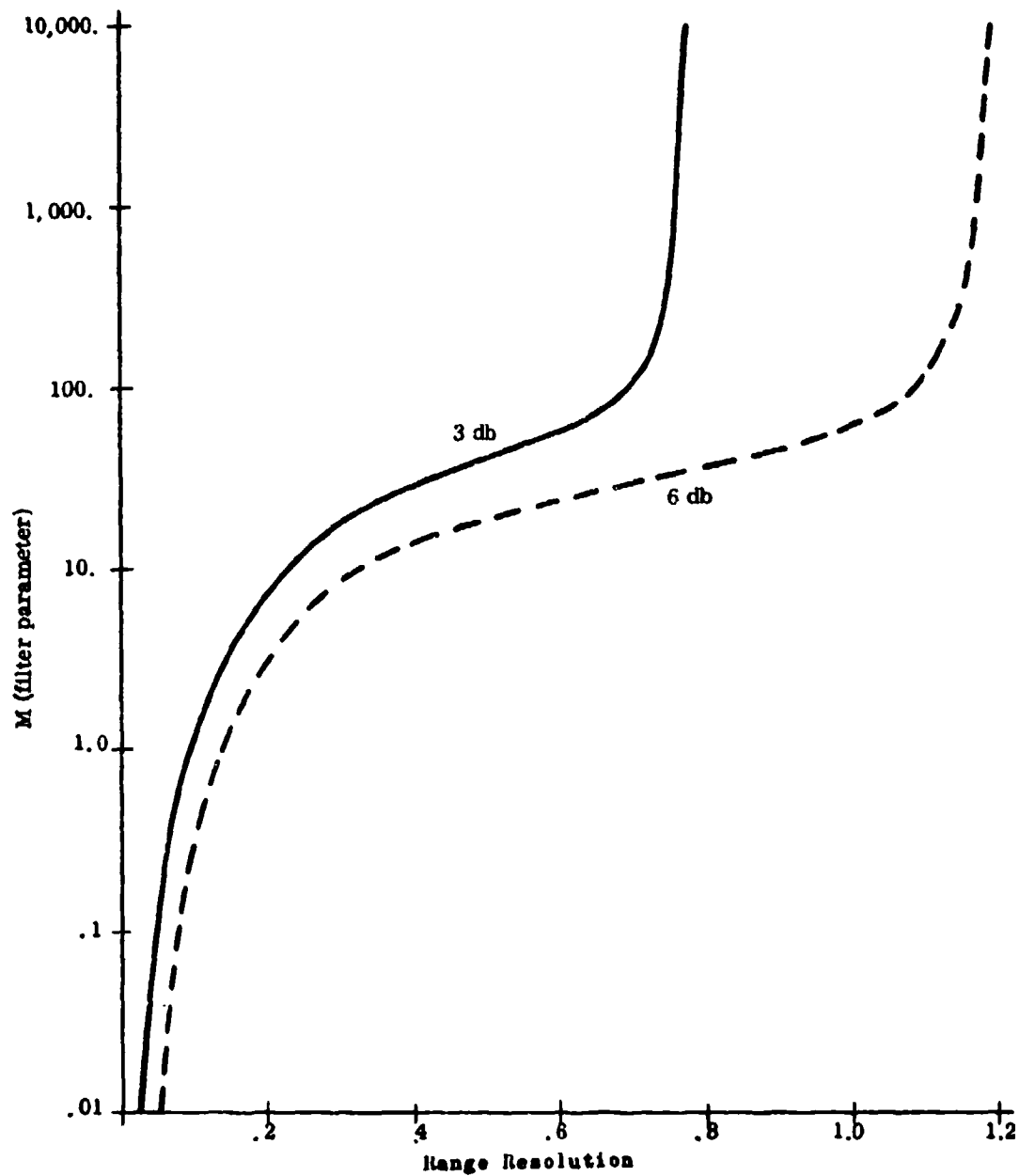


FIGURE 8: RANGE RESOLUTION (PEAK WIDTH/INCIDENT PULSE LENGTH)

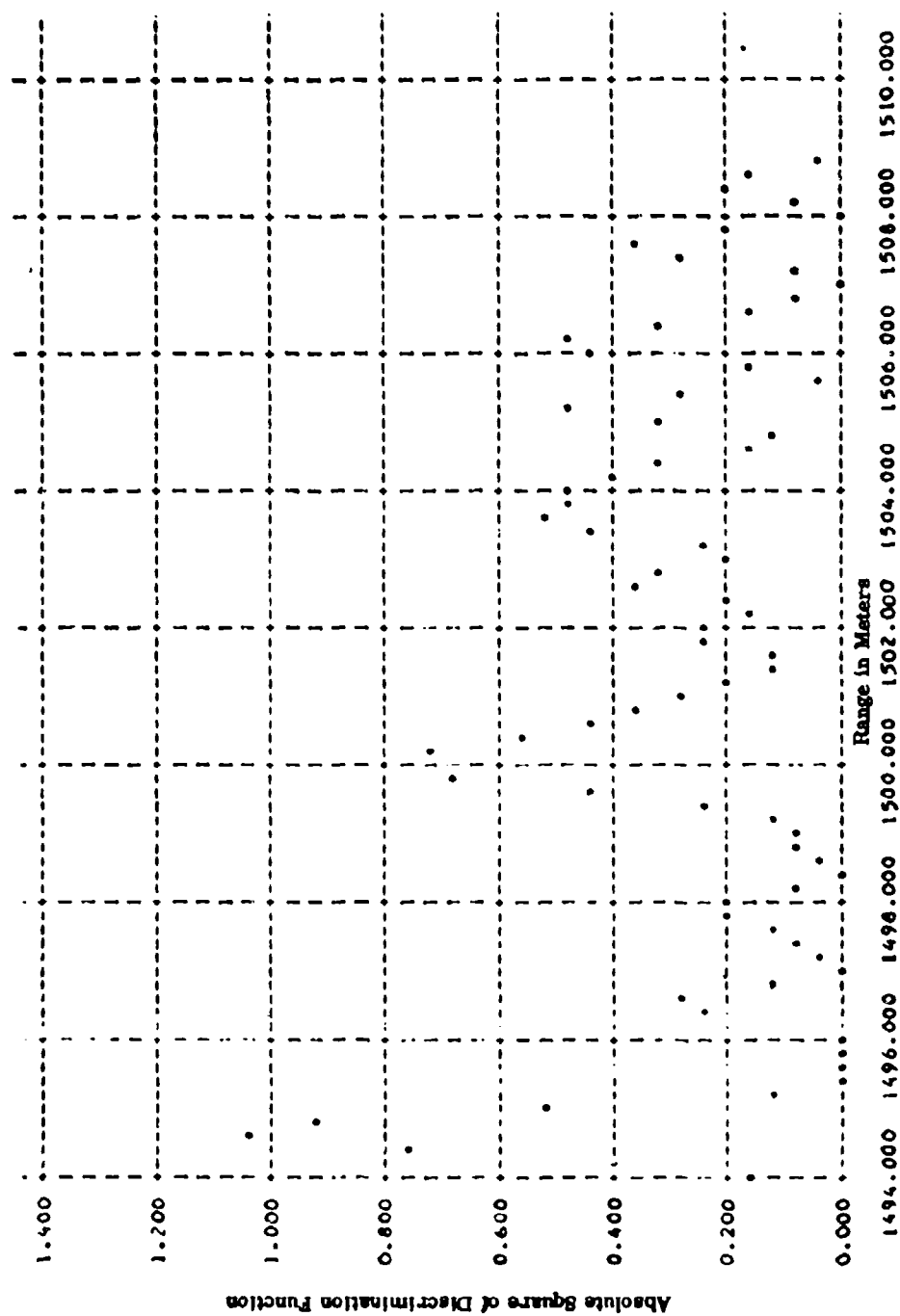


FIGURE 9. GRAPH OF DISCRIMINATION FUNCTION FOR $m = 2$.

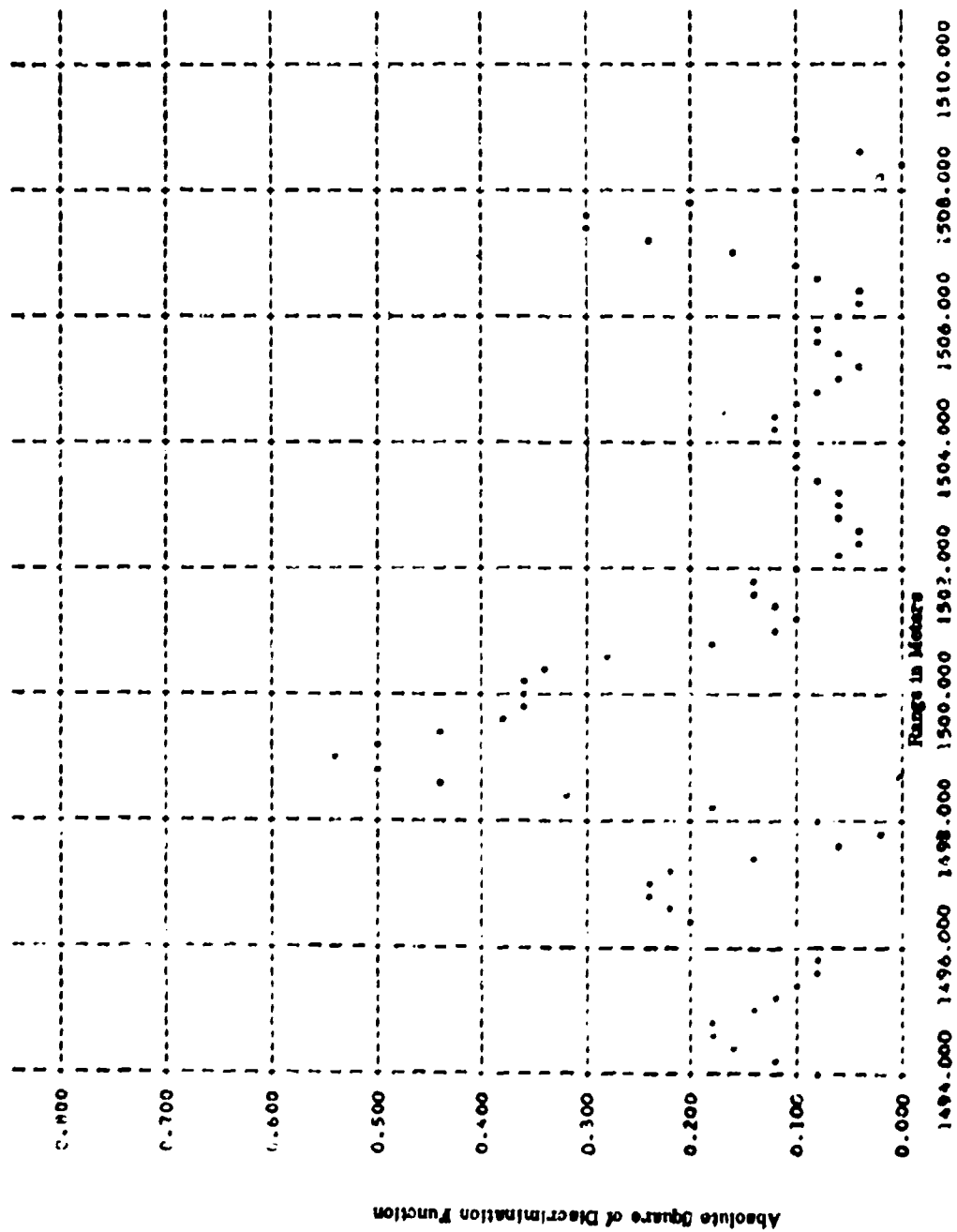


FIGURE 10. GRAPH OF DISCRIMINATION FUNCTION FOR \mathbf{R}^2 5.

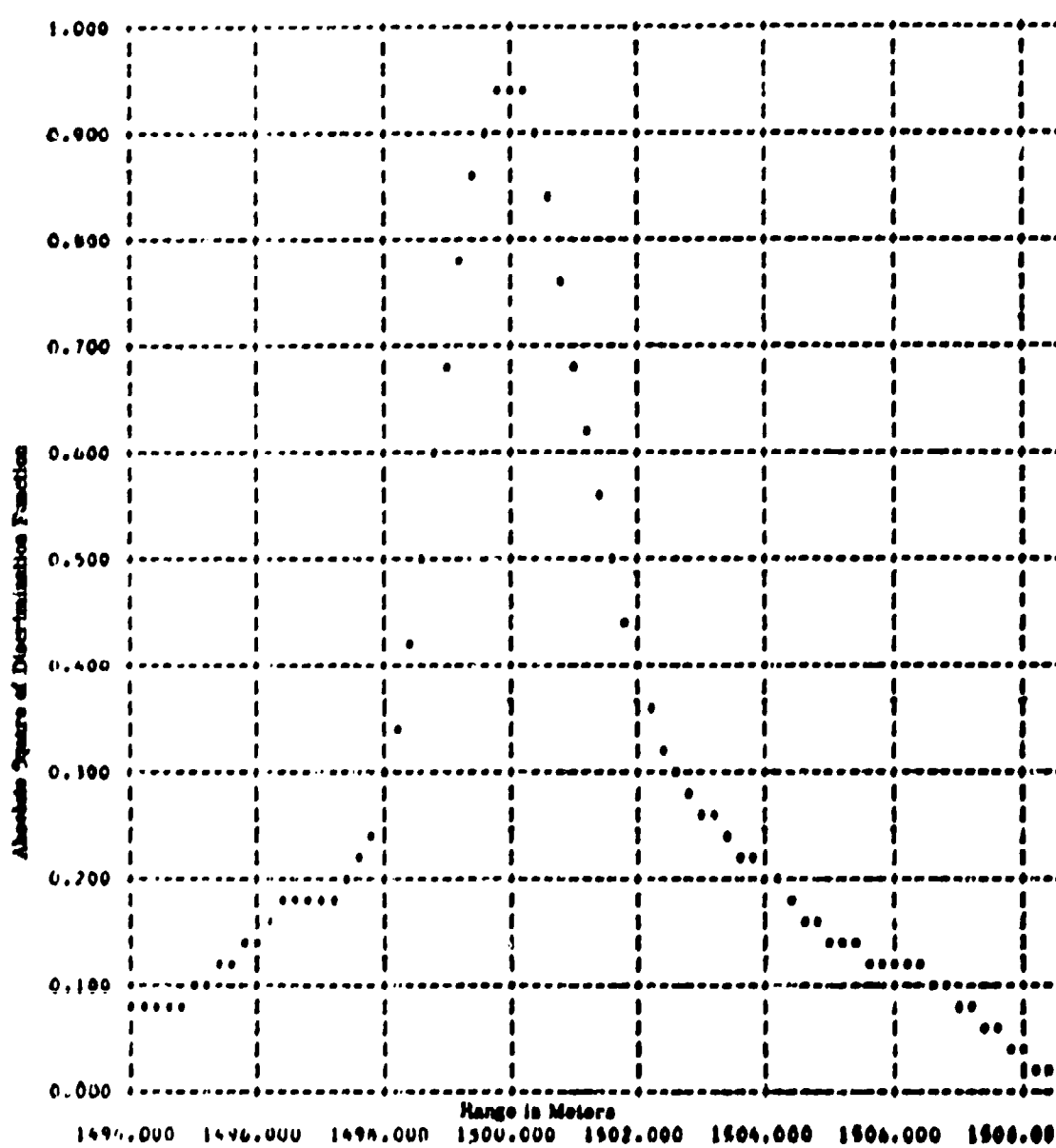


FIGURE 11: GRAPH OF DISCRIMINATION FUNCTION FOR $m = 25$

TARGET CLASSIFICATION

The most difficult part of this target recognition scheme is the construction of filters which, in fact, do make it possible to discriminate between different targets. The problem is to find the frequency signatures of the targets of interest which both represent a sufficiently strong return to be detectable and are so different, one from another, that discrimination is possible. If we denote the filter operation by F_α where α designates the α th type target, then we wish to construct the filter operation so that if S_α represents the frequency spectrum of the return from a target of the β th type we would have the filter have the properties

$$F_\alpha \cdot S_\alpha > M \quad (40-a)$$

$$F_\alpha \cdot S_\beta < \eta \quad (40-b)$$

where M and η are positive numbers which must ultimately be determined from the system requirements.

We note that in general the filter will not be constructed from the total signature $S_\alpha(\omega)$ since for $\alpha \neq \beta$ there may be sufficient overlap in $S_\alpha(\omega)$ and $S_\beta(\omega)$ that the inequality (40-a) will not be satisfied. Rather we decompose $S_\alpha(\omega)$

$$S_\alpha(\omega) = \sum_{i=1}^N C_i S_{\alpha}^i(\omega) \quad (41)$$

choose a subset $\{i_n\}$ and form

$$S_{\alpha}^f(\omega) = \sum_{n=1}^M C_{i_n} S_{\alpha}^{i_n}(\omega) \quad (42)$$

in order to satisfy (40).

The method of decomposition in (41) is in a sense arbitrary. We have devised two general methods for effecting the decomposition. The first stems from the way in which the frequency signature of a given target is computed. If the target is complex we decompose it into simpler constituents, compute the signature for each of these, and combine the signatures of the constituents into that of the whole target. Now in the decomposition of the various targets we would discriminate between we can choose those constituents of each which best satisfy the inequalities (40).

A second approach we have taken is to make use of a theorem of N. Wiener which states that certain functions may be represented by a series of translates of a given function; that is, a signature $S_\alpha(\omega)$ may be represented in terms of a function $S(\omega)$ by

$$S_{\alpha}(\omega) = \sum_k A_k^{\alpha} S(\omega + \omega_k^{\alpha}) .$$

If we now determine the set of translations ω_k^{α} for all the targets of interest, we have a set $\{\omega_k\}$ which can be used for all α and the targets may be characterized by the 'vectors'

$$(A_k^{\alpha}) \equiv \vec{A}^{\alpha} .$$

From the various \vec{A}^{α} we then need to choose the nearly orthogonal components to construct the filters for the various targets.

In principle the representation and classification scheme using translates is established. We would wish to go further and find a constructive method of realizing the representations. This is a main area of our research effort.

SUB-NANOSECOND PULSE METHODS OF RADAR CROSS SECTION MEASUREMENT

Robert R. Hively, Vice President
Micronetics Incorporated

ABSTRACT

A description of the history of development, and the present and projected uses of sub-nanosecond pulses in radar cross section measurements is presented. Of particular interest is the use of sub-nanosecond pulses as a diagnostic tool for radar cross section reduction and for exact measurement of creeping waves.

HISTORY

Early in 1959, the search for a sub-nanosecond pulsed source led to the investigation of many modulation techniques. These included direct pulsing of an oscillator tube, ferrite switching of a CW signal, gating the grid and/or helix of a traveling wave tube, and diode switching of a CW signal. It soon became obvious that direct pulsing of the oscillator and ferrite switching of CW would not produce sub-nanosecond pulses, and they were discarded.

The interest then turned to switching with traveling wave tubes. Beck and Mandeville of Bell Telephone Laboratories¹ had achieved pulses of a few nanoseconds' duration by sweeping the helix voltage of a TWT through its synchronous value, while a CW signal was applied to the input of the TWT. During the short time interval when the helix voltage was at or near its synchronous value, the tube would amplify, thus forming a short r.f. pulse at its output. These results were not difficult to repeat in the laboratory, but did not produce pulses of less than six nanoseconds' duration.

The search then concentrated on diode switching of CW. Valuable advice and references were obtained from Robert Garver of Diamond Ordnance Fuze Laboratories². Switching of a CW signal with germanium diodes provided acceptable rise and decay times, but the on-off ratio was not adequate to perform scattering measurements since a substantial CW signal was always present at the transmitting antenna even when the diode was switched off. Several exotic crystal switch combinations were tried in an attempt to improve on the on-off ratio, but diode burnout resulted. A brief study of the literature on diode burnout revealed that the Sylvania Company tests diodes for burnout by subjecting them to a very short transient (about 2 nanoseconds duration) to simulate the spike leakage through a TR tube³.

In May 1959, it was decided to investigate the TR tube spike leakage as a source of short pulses, and immediate success was achieved. Figure 1 shows a 1959 photograph of the TR tube spike leakage at X-band as viewed on a traveling wave tube oscilloscope⁴. The sine wave is a timing signal with a wavelength of 3 nanoseconds. Figure 2 shows a 1963 photograph of the spike from the same type of TR tube, as viewed on a sampling oscilloscope⁵. The sweep speed of the oscilloscope is 2 nanoseconds per centimeter, and the pulse duration is 0.7 nanosecond at the half power points. The peak power is 100 watts and the pulse repetition rate is 1000 pulses per second.

A program of classified radar cross section measurements was funded from June 1959 through September 1961 by the Advanced Research Projects Agency through the Rome Air Development Center⁶. The formal reports resulting from this funding are listed as References 7 through 12 in the Bibliography. During the course of this funding, many improvements were made in the transmitter and receiver, and the equipment that evolved is shown in the block diagram of Figure 3.

Another technique for generating sub-nanosecond pulses appeared in the literature in 1961. Pulfer and Whitford¹³ discovered that a very short video pulse fed into the r.f. input of a TWT produced short r.f. pulses at the output of the TWT. This technique was easy to reproduce in the laboratory, and produced pulses as short as 0.4 nanosecond duration at repetition rates up to 10^5 pulses per second. Of even more interest was the fact that these pulses could easily be produced in several frequency bands. When the video pulse was fed into an L-band (1-2 Gc.) TWT, a 0.4 nanosecond pulse was produced. This pulse is physically shorter than one r.f. cycle at the TWT center frequency. Micronetics' personnel have successfully generated sub-nanosecond pulses at L, S, C, X and K_u -bands and have successfully amplified X-band pulses to more than 1/2 megawatt of peak power.

RADAR CROSS SECTION MEASUREMENTS

Reduction of Radar Cross Section

When a radar pulse is physically much shorter than the target it is illuminating, each scattering point or scatter-center on the target furnishes a discrete echo which is separated in range from the other echoes. Consider the composite photograph shown in Figure 4. The oscilloscope display is the short pulse radar echo from the model aircraft superimposed above it with "nose-on" radar illumination of the model. The sweep of the scope is from left to right at



Figure 1. Sub-Nanosecond
Pulse Viewed on TWT Scope
in 1959

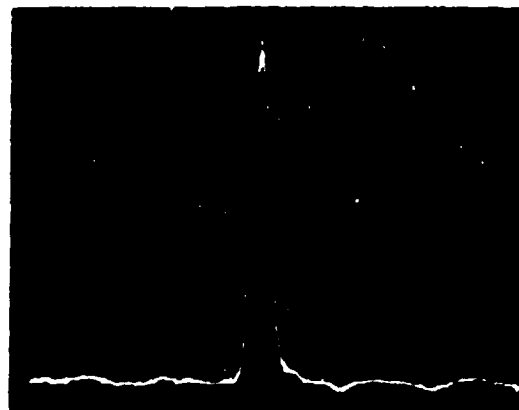


Figure 2. Sub-Nanosecond
Pulse Viewed on Sampling
Scope in December 1963

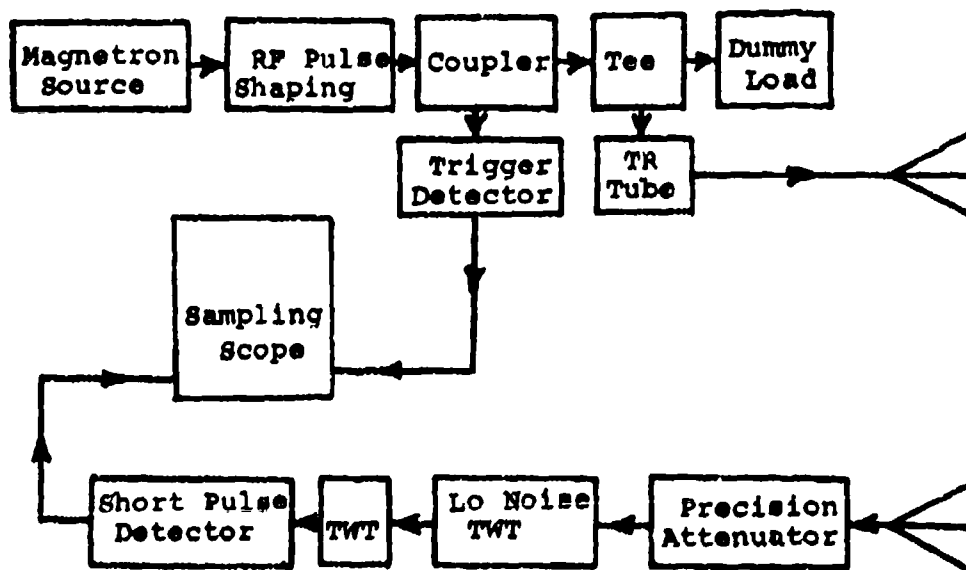


Figure 3. Block Diagram of Micronetics'
Sub-Nanosecond Scattering Radar

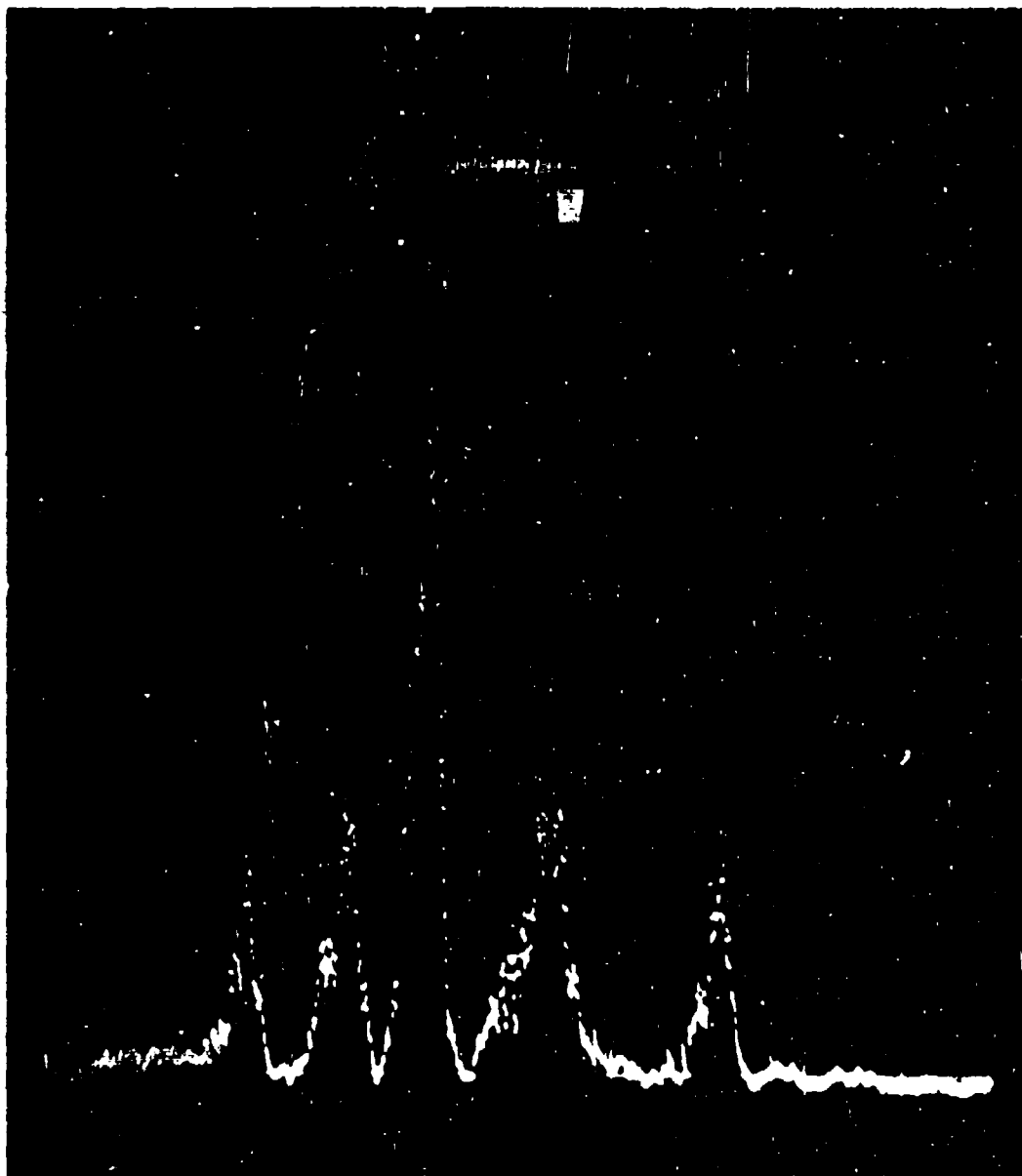


Figure 4. Composite Photograph Showing Fiberglass
Aircraft above the Radar Display of Its
Short Pulse Signature

2 nanoseconds per centimeter. The model is a 6-foot-long scale model of an F-102 fighter aircraft. The skin of the model is fiberglass and, therefore, the dominant contributors to the radar cross section are metal structures inside the aircraft. Reading from left to right on the display, the first pulse is from a battery inside the radome, the second and third pulses are from structural cross braces inside the fuselage, the fourth pulse is from the main landing gear struts, and the fifth pulse is from a control cable mechanism inside the fuselage. It is obvious that by shaping these individual scatterers to eliminate specular returns, or by covering each with radar absorber, the overall radar cross section can be drastically reduced. Micronetics has utilized this technique on several contracts to reduce radar cross section and, in each case, the results have been extremely gratifying. The technique used consists of measuring a conventional radar cross section pattern and then repeating this with a short pulse pattern to show the amplitudes and locations of all scatterers. A study of the conventional pattern and the tactical use of the model determines what pattern characteristics need to be minimized or modified. A study of the short pulse pattern determines what portions of the model must be treated to reduce or modify the radar cross section. After modifications are made to the model, a conventional pattern is then re-run to show that the desired results have been achieved.

Flare Spot Determination

The determination of flare spots can sometimes be made by comparing a conventional radar cross section pattern to the physical shape of a model. In many cases, this technique has been successful because the source of the flare spot was obvious; i.e., a flat wing or tail surface on an aircraft or missile model. In other cases where the flare spot is caused by a more complex scattering center or combination of scattering centers, the evaluation is tedious and time-consuming and the results are subject to conjecture.

Consider again the data shown in Figure 4. The unusual characteristic of this model is that its skin is fiberglass and is essentially transparent to radar, so the radar echoes are from internal structures. An intuitive approach to flare spot reduction is not possible since the scattering centers are not visible to the human eye. They are, however, visible to the short pulse radar and can be measured precisely in both location and magnitude.

Background Noise

The background clutter from the Micronetics' scattering range is below 10^{-7} square meters when using pulses

up to 250 nanoseconds duration. Since the background clutter is a direct function of the pulse duration¹⁴, another 25 db reduction in background is achieved by using pulses of 0.7 nanosecond duration. There is still the problem of the echo from the model support, but for sub-nanosecond pulses, even this echo can be resolved separately and thus ignored in many cases. Consider the sketch shown in Figure 5. The relative amplitudes of echoes are not drawn to scale, but measurements similar to this have been made at Micronetics. A cylindrical styrofoam column provides a radar echo at each air-styrofoam interface and even though they may be of greater magnitude than the model echo, they can be measured independently. To confirm the results, the model can be shifted slightly on its mount and the positions of the styrofoam echoes will remain constant.

Anechoic Chamber Evaluation

Sub-nanosecond radar pulses have been used as a diagnostic tool to reduce the background scattering in the Micronetics indoor range. With the three inch range resolution capability of these short pulses, it is possible to determine the source and magnitude of any reflections within the chamber. The short pulses can also be used to evaluate individual pieces of absorber in order to choose those with the lowest cross section for critical placement.

PROJECTED SHORT PULSE MEASUREMENTS

Creeping Waves

The measurement of creeping waves that have traversed around the rear of a sphere or other scattering body is a tedious and time-consuming task, and requires a great deal of analysis of data since it can be measured only by its effect on specular and traveling waves using conventional radar cross section techniques. Even with sub-nanosecond pulse techniques at X-band, it has not been possible to measure creeping waves at Micronetics. However, the magnitude of the creeping wave increases exponentially with increasing wavelength and the use of sub-nanosecond pulses at L-band should make independent observation and measurement of creeping waves possible. An attempt was made on the week of December 28, 1963, to obtain measurement of a creeping wave in time for inclusion in this paper, but the peak power transmitted was less than one watt and another stage of TWT amplification was not available. It is anticipated that data will be taken in time to discuss it at the symposium in April.

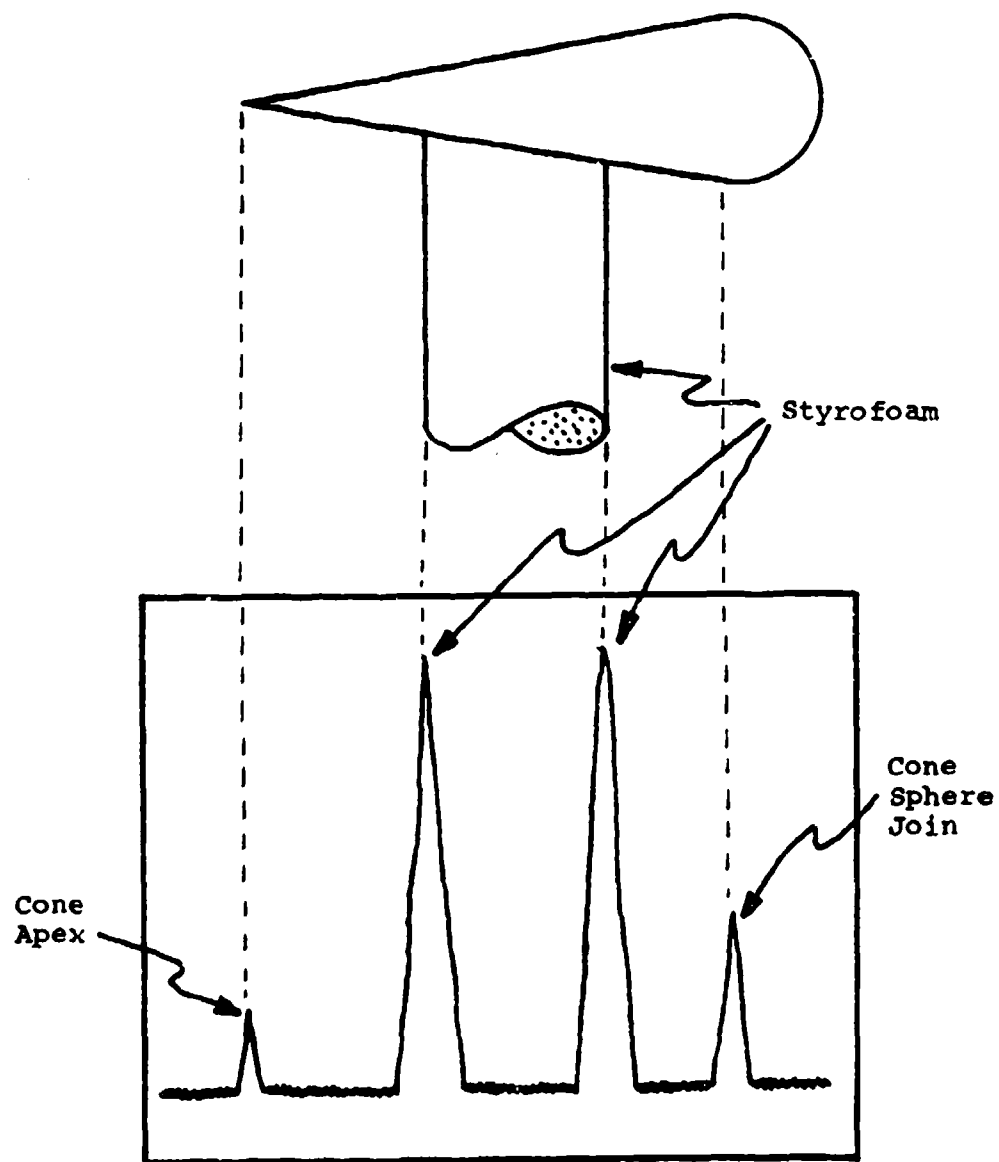


Figure 5. Exaggerated Sketch to Illustrate How Sub-Nanosecond Pulses Can Measure a Low Cross Section Model in the Presence of a High Cross Section Mount

Plasma Diagnostics

Much can be learned about the basic physics of a plasma by probing with short radar pulses. Some measurements have been reported by H. J. Schmitt of Harvard University¹⁵ using the afterglow of a coaxial discharge tube as the plasma medium.

If short radar pulses are transmitted transversely through a plasma column in a large chamber, accurate scattering measurements could be obtained by range gating the noise from surrounding scatterers out of the display. In addition, it should be possible to measure the depth of penetration for each radar frequency, and the amount of dispersion in a pulse transmitted through the plasma could be related to the ion concentration in the plasma.

Propagation Studies

The use of sub-nanosecond radar pulses enables a detail study of multipath propagation effects over long one-way transmission paths. Multiple paths whose total path length difference is as little as six inches can be resolved simultaneously and the effects of atmospheric dispersion can be measured and analyzed.

CONCLUSIONS

Sub-nanosecond radar pulses have proven to be an extremely useful diagnostic tool in the measurement, analysis, modification, and reduction of radar cross section. This usefulness is due to the ability to resolve separate scatterers on a single target and to ignore background clutter. It is anticipated that even more interesting results will be obtained in the near future in studies of creeping waves and in plasma diagnostics.

BIBLIOGRAPHY

1. A. C. Beck and G. D. Mandeville, "Microwave Traveling-Wave Tube Millimicrosecond Pulse Generators", IRE Transactions on Microwave Theory and Techniques, Vol. MTT-3, p 48, December 1955.
2. R. V. Garver, E. G. Spencer and M. A. Harper, "Microwave Semiconductor Switching Techniques", IRE Transactions on Microwave Theory and Techniques, Vol. MTT-6, p 378, October 1958.
3. Sylvania Microwave Newsletter, Sylvania Electric Products, Inc., Vol. 1, No. 1, Copyright 1956.
4. Traveling Wave Tube Oscilloscope Model 2236, Mfg. by Edgerton, Germeshausen & Grier, Incorporated, Boston, Mass.
5. Sampling Oscilloscope Model 661, Mfg. by Tektronix, Incorporated, Beaverton, Oregon.
6. The "Short Pulse Signature Study" contract was awarded to Convair Division of General Dynamics in San Diego, California, in June, 1959, and was completed in September 1961. The funding was from the Advanced Research Projects Agency of the Department of Defense and was administered through the Rome Air Development Center under Contract No. AF 30(602)-2069. The next six references are major reports resulting from the "Short Pulse Signature Study".
7. Robert R. Hively, "Technical Note on Millimicrosecond Pulse Generation", Convair Report No. MW-129 to Rome Air Development Center, 13 August 1959 (Unclassified).
8. Robert R. Hively, "Technical Note on Preliminary Operation of the Short Pulse Backscatter Range", Convair Report No. MW-134, 15 September 1959 (Secret).
9. Robert R. Hively, "Semi-Annual Report on Short Pulse Signature Studies", Convair Report No. ZN-449, RADC Report No. RADC-TN-60-33, 31 December 1959 (Secret).
10. Robert R. Hively, Warren T. Fey, William R. Bradford, "Final Report on First Year of Short Pulse Signature Studies", Convair Report No. ZN-474, RADC Report No. RADC-TR-60-217, DDC No. AD 321 609, 12 June 1960 (Secret).
11. Robert R. Hively, Warren T. Fey, William R. Bradford, "Semi-Annual Report on Short Pulse Signature Study", Convair Report No. ZN-508, RADC Report No. RADC-TN-61-22, DDC No. AD 321 430, 31 December 1960 (Secret).

12. Robert R. Hively, Warren T. Fey, William R. Bradford, Thomas J. Barrett, "Final Report on Second Year of Short Pulse Signature Studies", Convair Report No. ZN-526, RADC Report No. RADC-TR-61-154, DDC No. AD 325 187, September 1961 (Secret).

13. J. K. Pulfer and B. G. Whitford, "A Simple Method of Generating Nanosecond Pulses at X-Band", Proceeding of IRE, Vol. XLIX, No. 1, May 1961, p 968.

14. A. J. Simmons, "Theoretical Estimate of Background Back-Scattering Cross Section of the Lincoln Laboratory Antenna Range", TRG Report 221-1, p 5, 28 February 1962.

15. H. J. Schmitt, "Plasma Diagnostics with Short Electromagnetic Pulses", Harvard University, Sandia Corporation Report No. SCR-692, July 1963.

CONTOUR CHARTS FOR RADAR CROSS-SECTION ANALYSES

Daniel Levine, Ph. D.
Lockheed Missiles and Space Co., Sunnyvale, California

SUMMARY

Contour charts of radar cross section provide a useful form of data reduction for the set of pattern cuts required to measure the return at all angles in space. The best configuration of the coordinate grid on which the data are plotted depends upon symmetries in the shape of the test model. Several equal-area cartographic projections are described, and illustrations are given of the type of body for which each projection is best suited. In addition, a new projection based on the geometry of stabilized vehicles above the spherical earth is presented, which is especially pertinent for satellite measurements.

INTRODUCTION

Experimental values of radar cross section generally are plotted in a set of curves taken along great circle cuts through the model under test. This form of data presentation is difficult to interpret in terms of spatial (three-dimensional) variation of reflectance. A contour map drawn on a curvilinear coordinate system has proven to be a preferable means of presenting the data for many reflective bodies.

CONTOUR MAPS FOR JACKS *

The jack drawn in Fig. 1 has a rather complicated variation in its back-scattering pattern, as illustrated by a typical great circle cut, Fig. 2. The angular variation of the cross section has so much structure that it is impossible to visualize the spatial distribution of the lobes. Contour charts were prepared from a complete set of patterns, with cuts spaced at 10-degree intervals of tilt.

The coordinate system employed in preparation of the contours appears in Fig. 3, where the coordinate axes are aligned with the legs of the jack. The locus of angles in the first quadrant that are measured during a great circle cut is illustrated in Fig. 4. By means of a routine coordinate transformation, the pattern angles are converted to the coordinate angles (θ, ϕ). The consistency of the data in each great circle cut is verified by the presence of a local maximum when the measurement is within one of the coordinate planes. The angle at which this occurs is a function of the orientation of the great circle plane, as plotted in Fig. 5.

With the conversion of the pattern angles to the coordinate system of

* This section is adapted from Ref. 1.

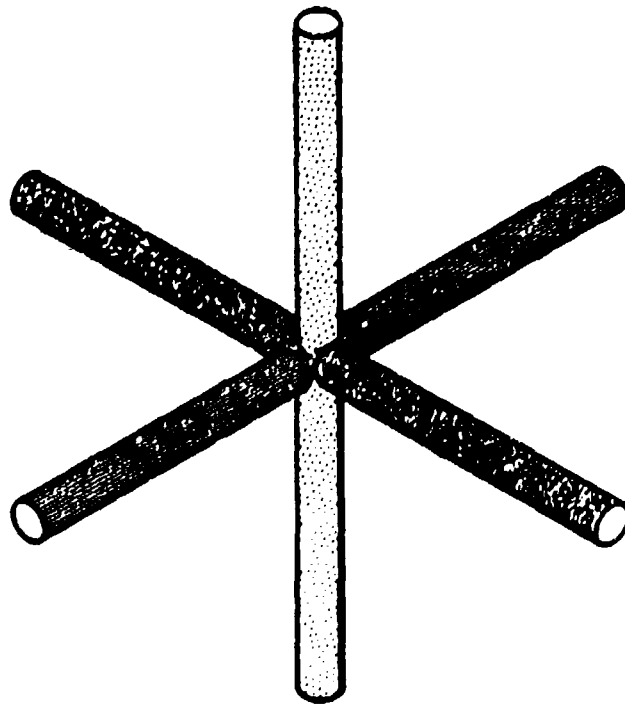


Figure 1. 5λ Jack.

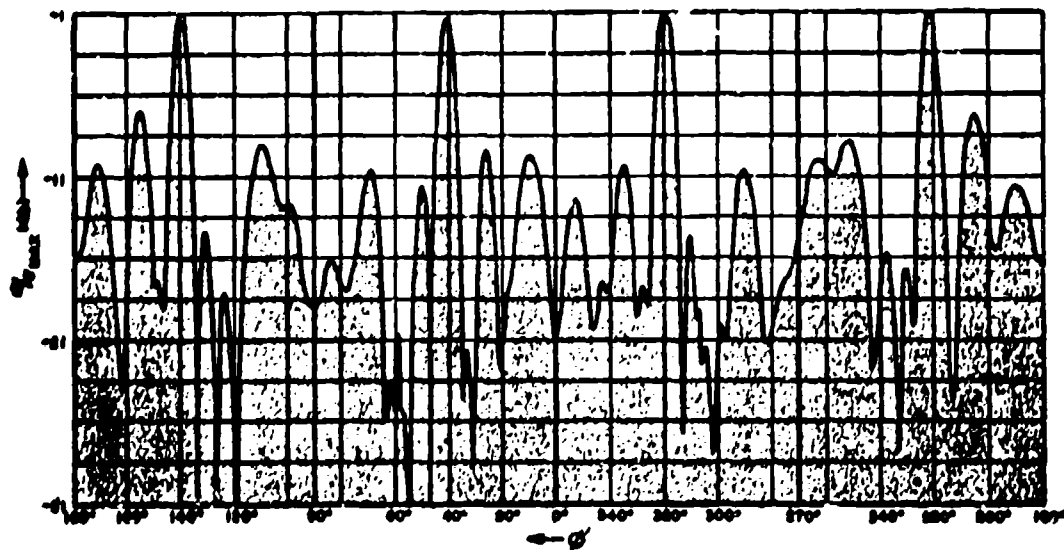


Figure 2. Typical Pattern Obtained for 5λ Jack.

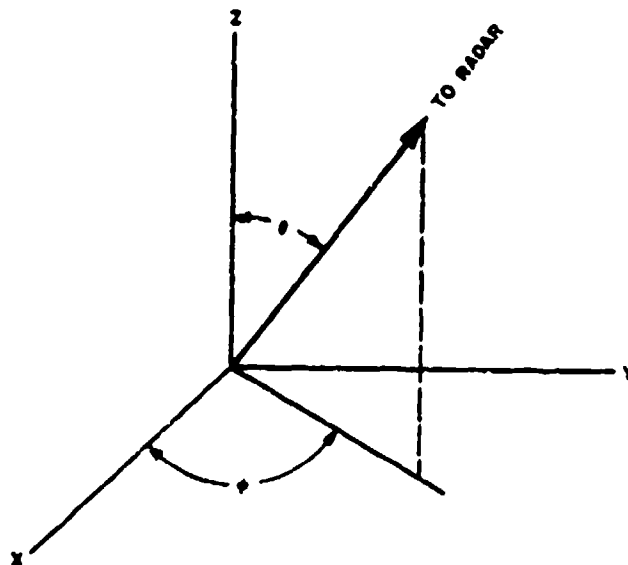


Figure 3. Spherical Coordinate System.

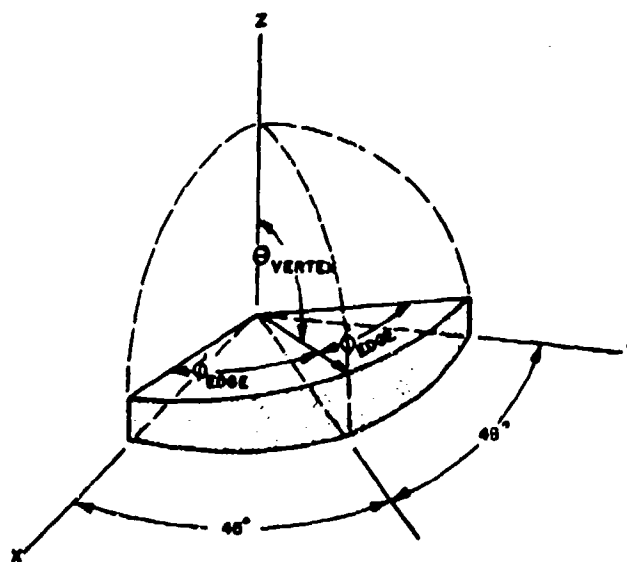


Figure 4. Geometric Relations for Great-Circle Cut.

Fig. 3, we are in a position to construct a contour chart. Three criteria are suggested for evaluating grid systems for plotting backscattering contours:

1. The coordinate system should be simple to construct, with curvilinear coordinates in the form of lines, circles, or other simple shapes.
2. The colatitude and azimuth of points within the grid should be readily associated with the geometry of the reflector.
3. The area within an arbitrary boundary should be proportional to the solid angle subtended by the corresponding boundary in space. (Projections that satisfy this condition are termed equal area.)

Three projections meet these conditions and are suitable for plotting the return of the jack within at least one octant. Since the backscattering from the jack is similar in each octant, the single octant is satisfactory for a representation through all space. The first projection is the Lambert azimuthal grid, which was used by Kennaugh in 1953.² The curves of constant colatitude are concentric circles, and the curves of constant azimuth are radial straight lines, as illustrated in Fig. 6. The colatitude represents the angle measured from one leg of the jack, and the azimuthal angle is measured in the plane of the other two legs. The equal-area property is achieved in this projection by spacing the colatitude circles more closely with increasing distance from the pole. *

Collignon's projection, Fig. 7, represents both the colatitude and the azimuthal circles as straight lines,** so that interpolation is precise and point plotting is rapid. Also, for objects that show symmetry about the 45-degree plane in ϕ , such as the jack, the contours can be drawn up for one-half of the pattern and then readily reflected in the 45-degree line to complete the representation throughout the octant.

The same data are plotted again in Fig. 8 on the Mercator sinusoidal projection, which has parallel, equally spaced colatitude lines and represents the circles of constant azimuth by sine curves. The sinusoidal shape of the curves of constant azimuth provides the equal-area property. Both interpolation and reflection through the 45-degree azimuth are somewhat more difficult than with Collignon's projection, but the uniform spacing of the angular intervals along the polar axis facilitates transfer of data from pattern cuts that are run at constant ϕ angles.

A fourth projection, the Lambert cylindrical equal-area grid, is recommended in Ref. 9, pp. 22-24. Since the cylindrical projection represents the pole by means of an extended horizontal line, it violates the second of the properties initially specified: it is difficult to associate points on a projection with the corresponding angles in space about the reflector. Since the projection has no particularly attractive features of its own, it is not

* References 3 through 8 are listed for their pertinence to the cartographic aspects of this paper.

** The equal-area characteristic is obtained by spacing the colatitude lines more closely with increasing distance from the equator.

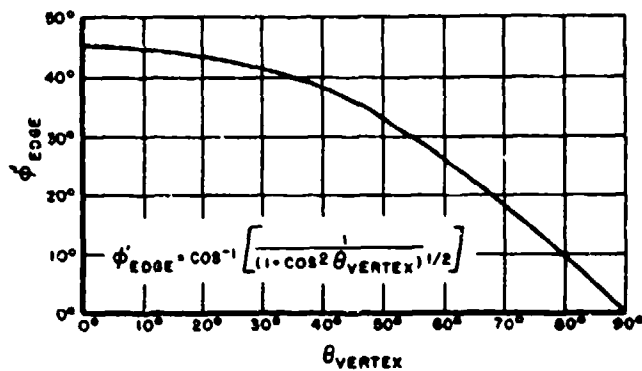


Figure 5. Angle of Coordinate Plane for Great Circle Cut.

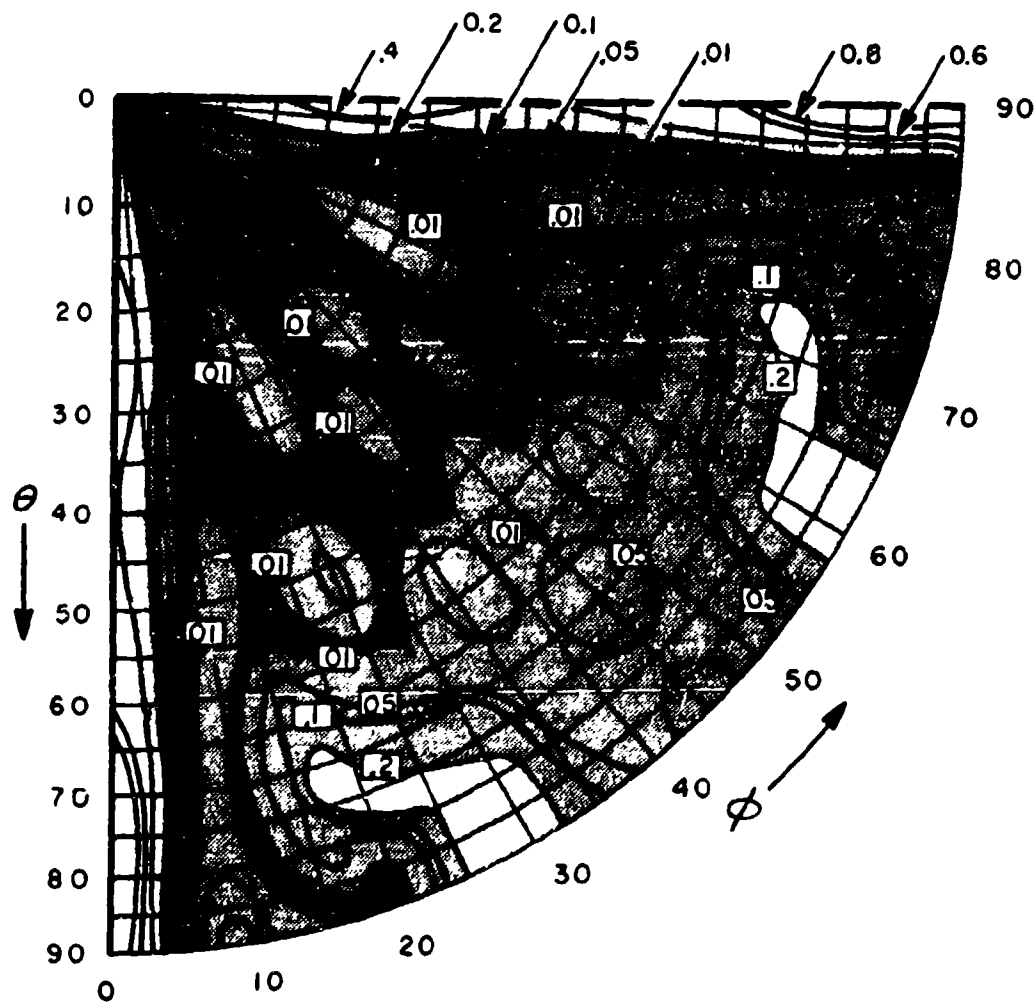


Figure 6. 5λ Jack Return on Lambert Azimuthal Projection.

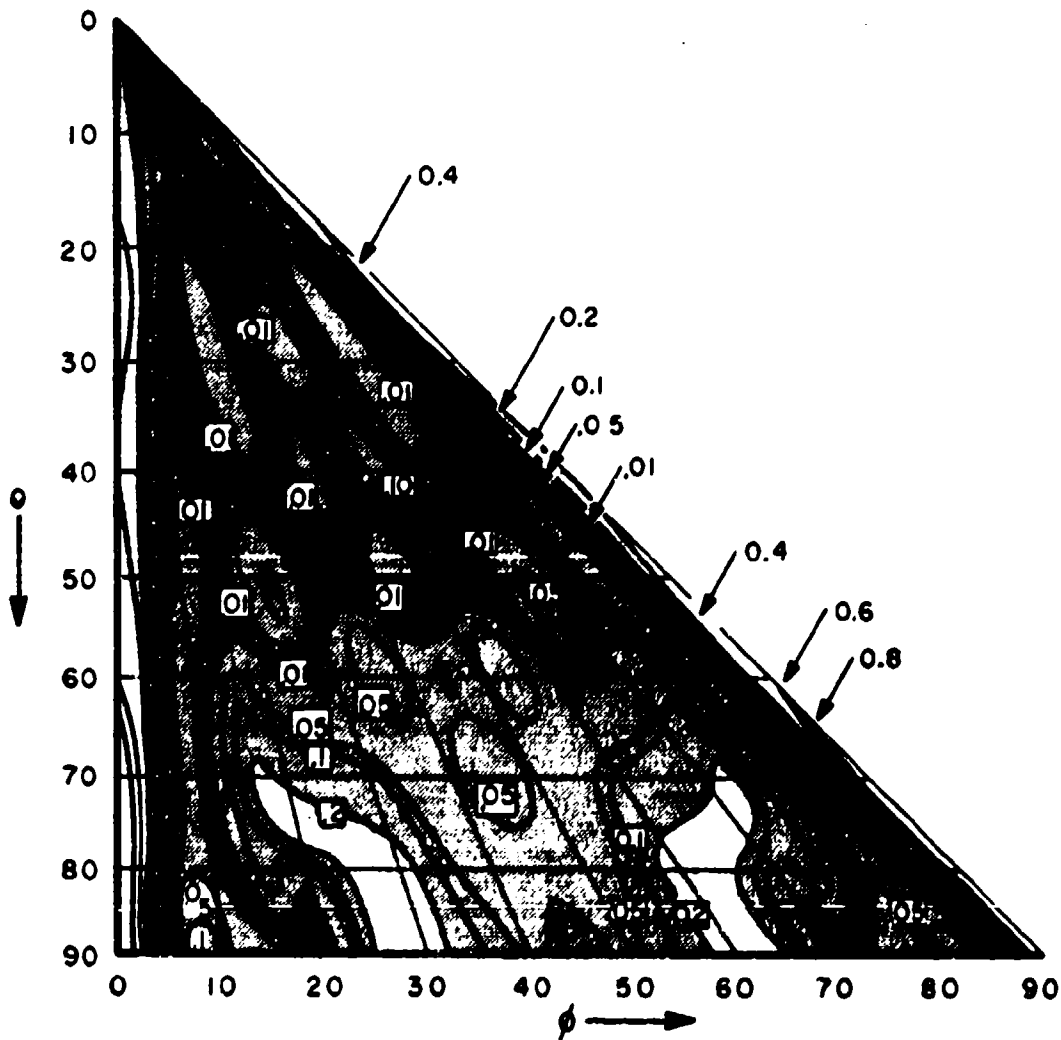


Figure 7. 5λ Jack Return on Collignon's Projection.

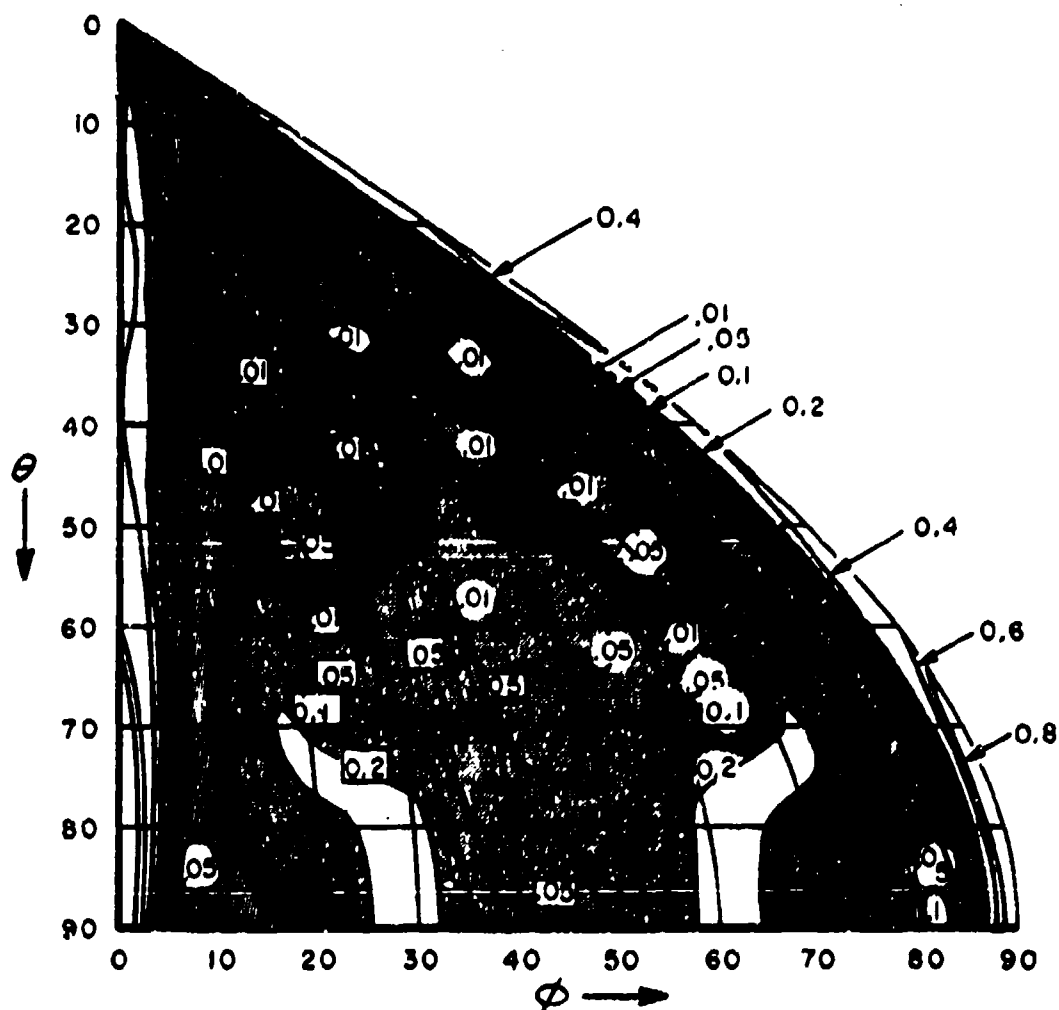


Figure 8. 5λ Jack Return on Mercator Sinusoidal Projection.

worthy of further consideration.*

To this point, no use has been made of the third property of the projections described above -- that the area within an arbitrary boundary be proportional to the solid angle subtended by the corresponding boundary in space. As a consequence of this quality, the probability of observing any level of backscattering may be determined with a high degree of precision merely by running a planimeter over a contour. This procedure has been used to measure the area within the contours for the jack. The resulting curve, Fig. 9, gives the probability that the reflecting area exceeds σ for random orientation of the jack, where σ is expressed along the abscissa relative to its maximum value. The curve shows that the jack provides a high level of return over only a very small solid angle in space. It is virtually impossible to grasp the spatial distribution of the backscattering return in this manner by viewing the raw data in the form of the patterns measured on the radar range.

FINITE CONE

The simplest way to plot and to observe the roll symmetry of bodies of revolution is on a chart that projects the circles of constant colatitude as straight parallel lines -- a requirement that excludes the Lambert azimuthal grid. The finite right circular cone is an interesting example of a body of revolution. The measured pattern for the backscattering from a 30-degree cone, Fig. 10, having a diameter-to-wavelength ratio of 3.34, is given in Fig. 11. There is a peak at the apex ($\theta = 0$ degrees), at the angle normal to the generating element ($\theta = 60$ degrees), and also at the base ($\theta = 180$ degrees). Examination of this pattern does not provide a good indication of the spatial extent of the lobes.

The contour chart of Fig. 12 shows clearly the very limited solid angle occupied by the lobes at the apex and the base, where each contour level is separated by 9 db in this plot. The lobe at 60 degrees is quite extensive, occupying a rather sizeable solid angle. Measurement of the area furnishes the cumulative probability that is given in Fig. 13. There is a very low probability that the return from the cone will be within 10 db of the peak when it is viewed at a random orientation. On one-half of the random sightings, the backscattering level is less than 31 db below the peak.

MANUAL CONSTRUCTION

When the great circle cuts are taken in planes of constant ϕ about a model, the routine for preparing a contour chart in color is quite straight-

* If the return at the pole of the coordinate system varies with polarization, then the reflectivity at the pole does not have a unique value. The cylindrical equal-area projection permits showing this effect in great detail, while its representation would be lost on the first three grids. For this type of body, a compromise based on the Eckert principle is recommended. (Eckert represented the pole by a straight line half the length of the equator. See Ref. 4, pp. 183-187, especially Fig. 51; also, Ref. 5, p. 10 ff.)

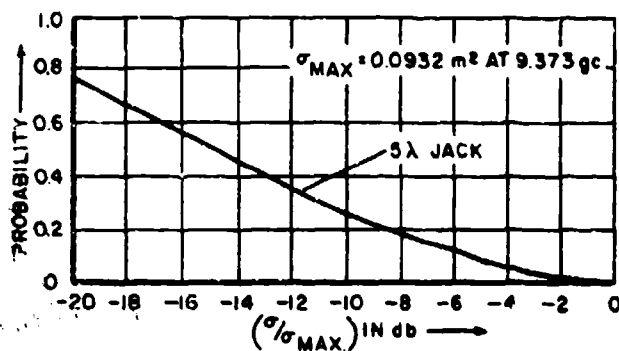


Figure 9. Cumulative Distribution for 5λ Jack.

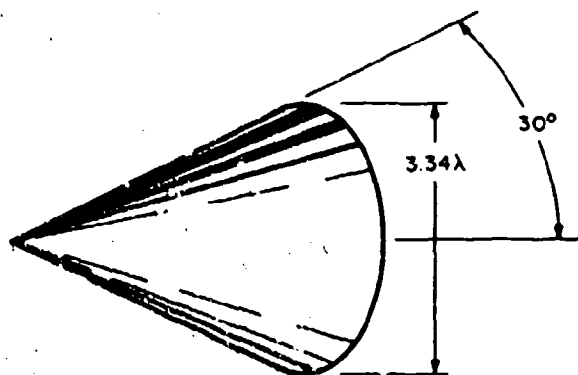


Figure 10. 30-Degree Half-Angle Cone.

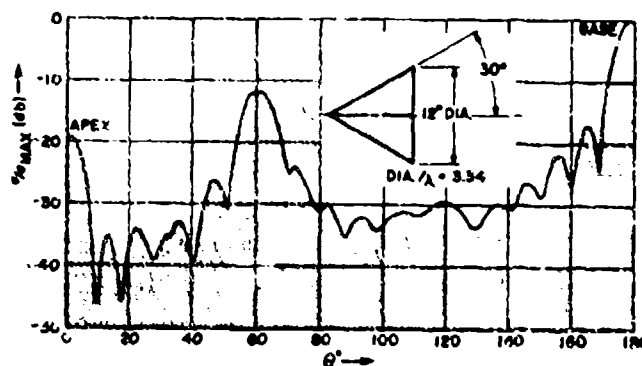


Figure 11. Pattern Obtained for Cone With Vertical Polarization.

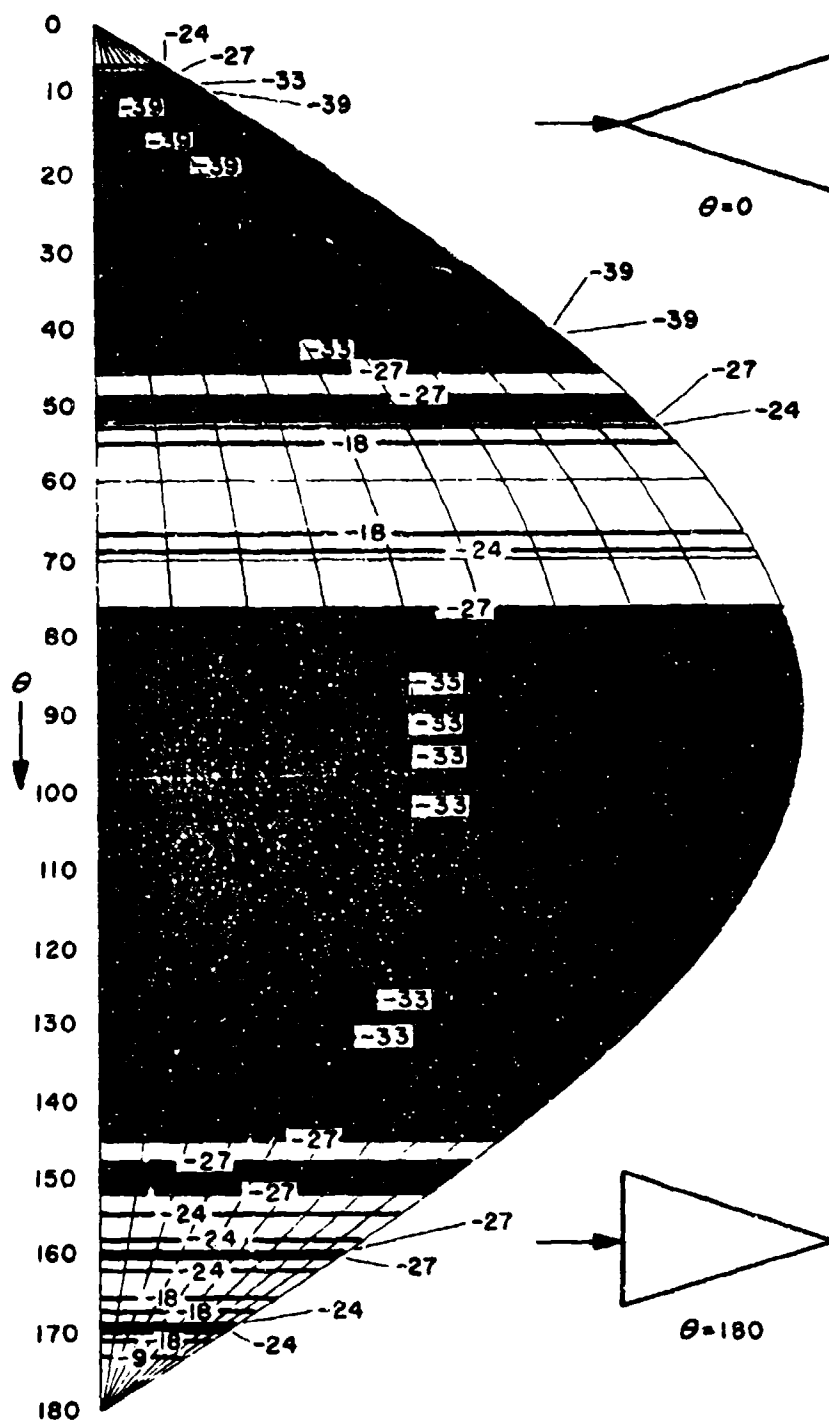


Figure 12. Cone Return on Mercator Sinusoidal Projection.

forward. The steps are as follows:*

1. The greatest maximum and the lowest minimum of interest throughout the complete set of patterns are noted, and a decision made as to the number of intermediate contour steps, as well as their separation. The spacing between contour levels need not be uniform, especially at the lower levels, where there may be very deep, but narrow, nulls.
2. A horizontal line is run across each of the pattern cuts at the level of the greatest maximum, even though this particular value may not appear on all patterns of the set. This line is the level 0 db, and additional parallel lines are placed below it at the other contour levels, as illustrated in Fig. 14.
3. Vertical lines are dropped from each intersection of the pattern with one of the contour levels. The color associated with each contour interval is run along the ordinate in the spaces between adjacent horizontal lines. In Fig. 14 the colors are represented by pencil number** along the abscissa, and both the name and the number associated with each contour interval are listed to the right of the diagram.*
4. The abscissa is placed adjacent to the central meridian of a Mercator equal-area grid that has the same scale for its polar angle, as in Fig. 15, which shows only a portion of the base grid. Each colored line segment is transferred vertically to the sinusoidal curve of constant ϕ at which the cut was made. For any of the other grids described in this paper the transfer of colors is a more tedious process, since the polar angle scales do not match.
5. The final step is to connect regions of the same color on adjacent ϕ curves, thereby completing the contour plot.

PROJECTIONS FOR STABILIZED SATELLITES

When a satellite rotates about the earth, it remains in its orbital plane, which intersects the stationary earth in a great circle, as shown in Fig. 16 for the case of a polar orbit. A ground radar site, shown here on the equator, observes only the lower side of a horizontally stabilized vehicle, and only the forward region of one that is vertically stabilized in a nose-down attitude. It is obvious, therefore, that not all angles of observation are possible, let alone equally likely in a probabilistic sense. The locus of angles that is traversed as a function of the distance of nearest approach, designated as d , appears in Fig. 17. This graph is taken from a paper by Bredall,¹⁰ who used the cylindrical equidistant projection recommended in IRIG standards for antenna patterns.⁹ Contours can be placed on this chart, but the best that can be said in its favor is that the grid is easy to construct; there is no ready association of points within the grid to the geometry of the reflector, and there is

* Computer programs have been developed for plotting contours automatically, as in Fig. 18 of Ref. 1. For surfaces of revolution that have only a few lobes, however, it is more efficient to plot by hand.

** Turquoise Prismacolor Pencils, Eagle Pencil Co., are in current use.

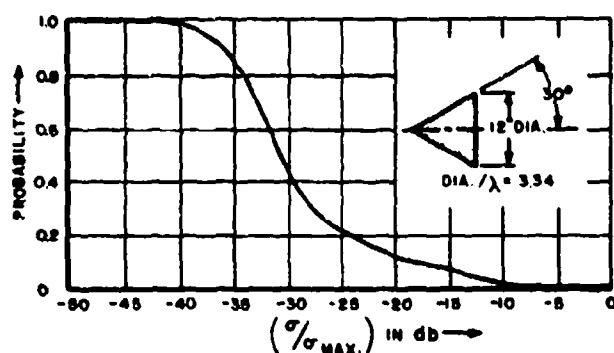


Fig. 13. Cumulative Distribution for Cone

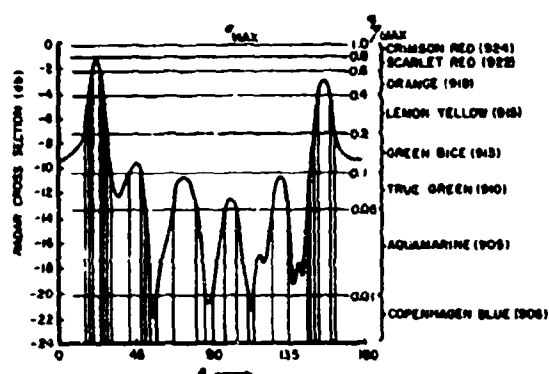


Fig. 14. Initial Steps in Manual Construction of Contour Chart

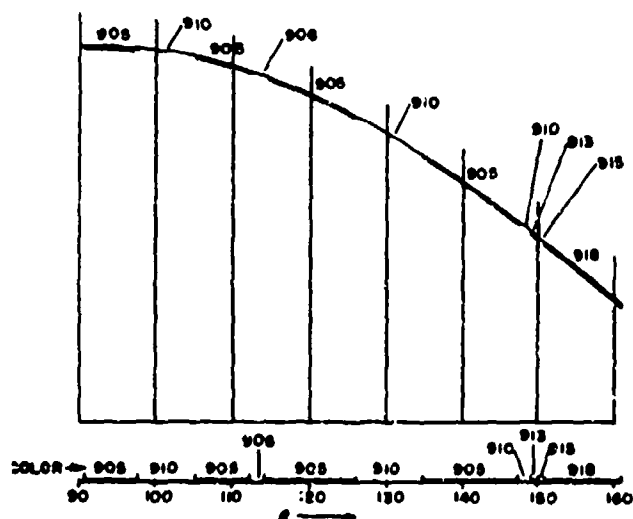


Fig. 15. Data Transfer to Mercator Sinusoidal Grid

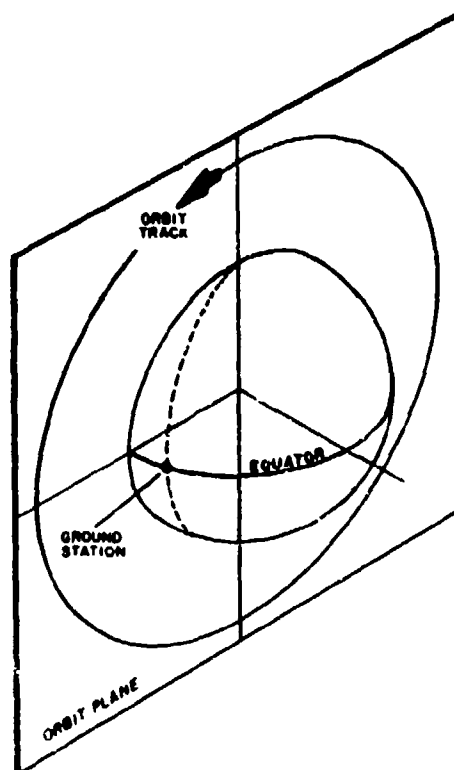


Figure 16. Satellite in Polar Orbit.

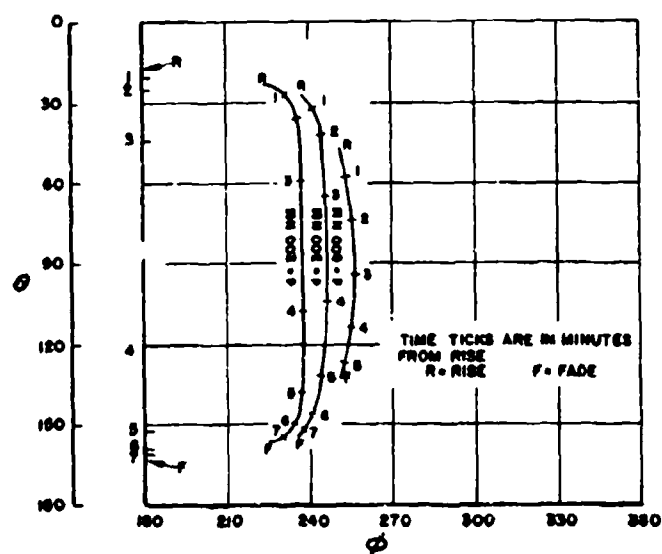


Fig. 17. Family of Aspect Traces Derived from SATRAK
(From Bredall¹⁰)

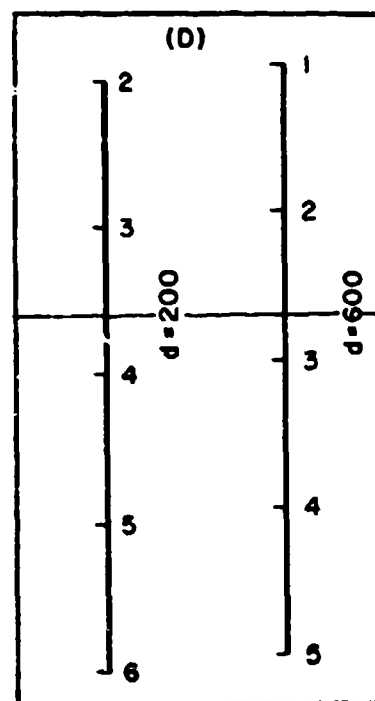
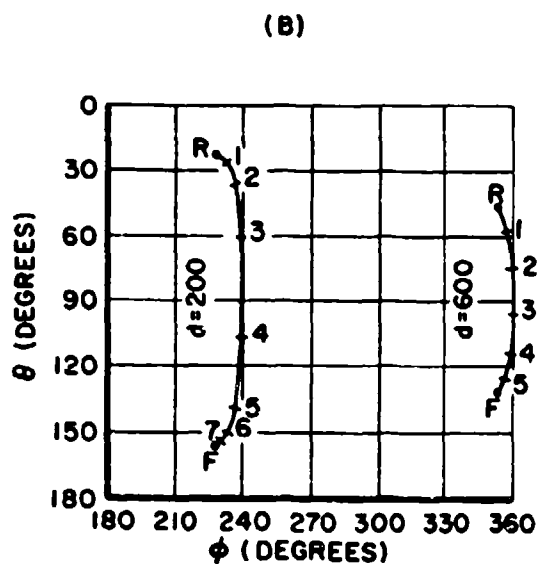
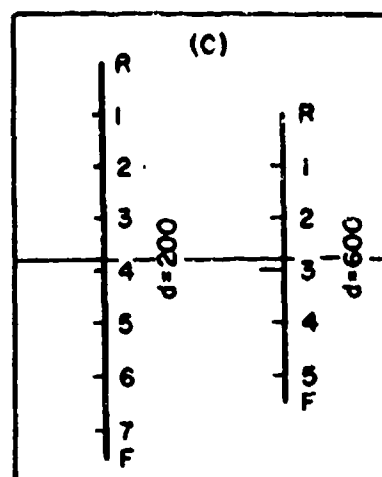
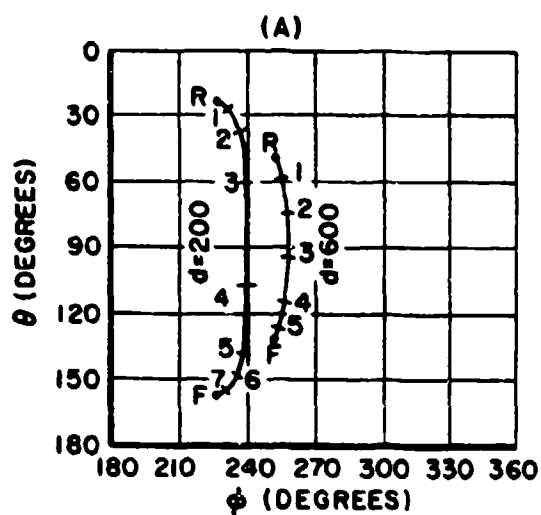


Figure 18. Development of Equal-Area Projection for Stabilized Satellites
 (a) Locus of Angles on Cylindrical Equidistant Projection.
 (b) Linear Scale for Distance of Nearest Approach.
 (c) Linearized Locus of Angles. (d) Equal Scales in x and y .

no relation to the probability of observing a given level of return.

The first conceptual step in deriving a suitable projection is to stretch the horizontal scale of Fig. 17 (repeated in Fig. 18a) in a nonlinear fashion so that the x value where it crosses the axis is proportional to the distance of nearest approach to the ground station, as in Fig. 18b. The second step is to straighten each of the curved loci, so that a great-circle orbital path plots as a straight line. The third step is to stretch the linear scale so that equal time intervals occupy equal y intervals (Fig. 18c). The fourth step is to make the equivalent distance in y equal to the distance scale in x , by taking the satellite velocity into account (Fig. 18d).

The sequence of steps listed above provides a basis for appreciating the novel properties of the projection for satellite coordinates that is shown in Fig. 19 for a horizontally stabilized body at an altitude of 125 nautical miles. The derivation of the equations for θ and ϕ in terms of x and y is not dependent on this listing, but follows from a parallel set of characteristics. Because of the utility of the resulting grid in data reduction for aerospace vehicles, the properties employed in its derivation are given in full:

1. The locus of angles for a satellite in a circular orbit above a stationary earth is a vertical line.
2. Time (and distance along the suborbital track) are linear in y .
3. The distance of nearest approach, measured along the surface of the earth, is linear in x .
4. The x and y distance scales are equal.

The data for the cone are plotted on this base grid in Fig. 20 for the case that the cone axis is oriented along the flight path. The time variation of the cross section for any orbital pass may be read off directly by following a vertical line positioned by means of the distance scale which is 1 inch to 50 nautical miles in the original chart. The time history is read from top to bottom if the cone is traveling apex first, and it is read from the bottom up if the cone is traveling base-first along its orbit. This is illustrated in Fig. 21 for passes at $d = 0$ (overhead) and at $d = 375$ nautical miles. As d increases, the angular scale spreads so that peaks become broader, and adjacent maxima are separated by longer periods of time.

If the satellite is traveling in a vertical orientation, the coordinate grid appears as in Fig. 22. (Figure 22 is illustrative rather than precise, although it is believed that exact computation would result in very little change in the appearance of the grid.) The same cone data are plotted on this grid in Fig. 23. Fig. 24 shows the time variation of return for the first half of an overhead pass and one that is 175 nautical miles to the side. When d exceeds 370 nautical miles, there is essentially no variation in return as the cone travels through the zone of radar coverage represented on Fig. 23.

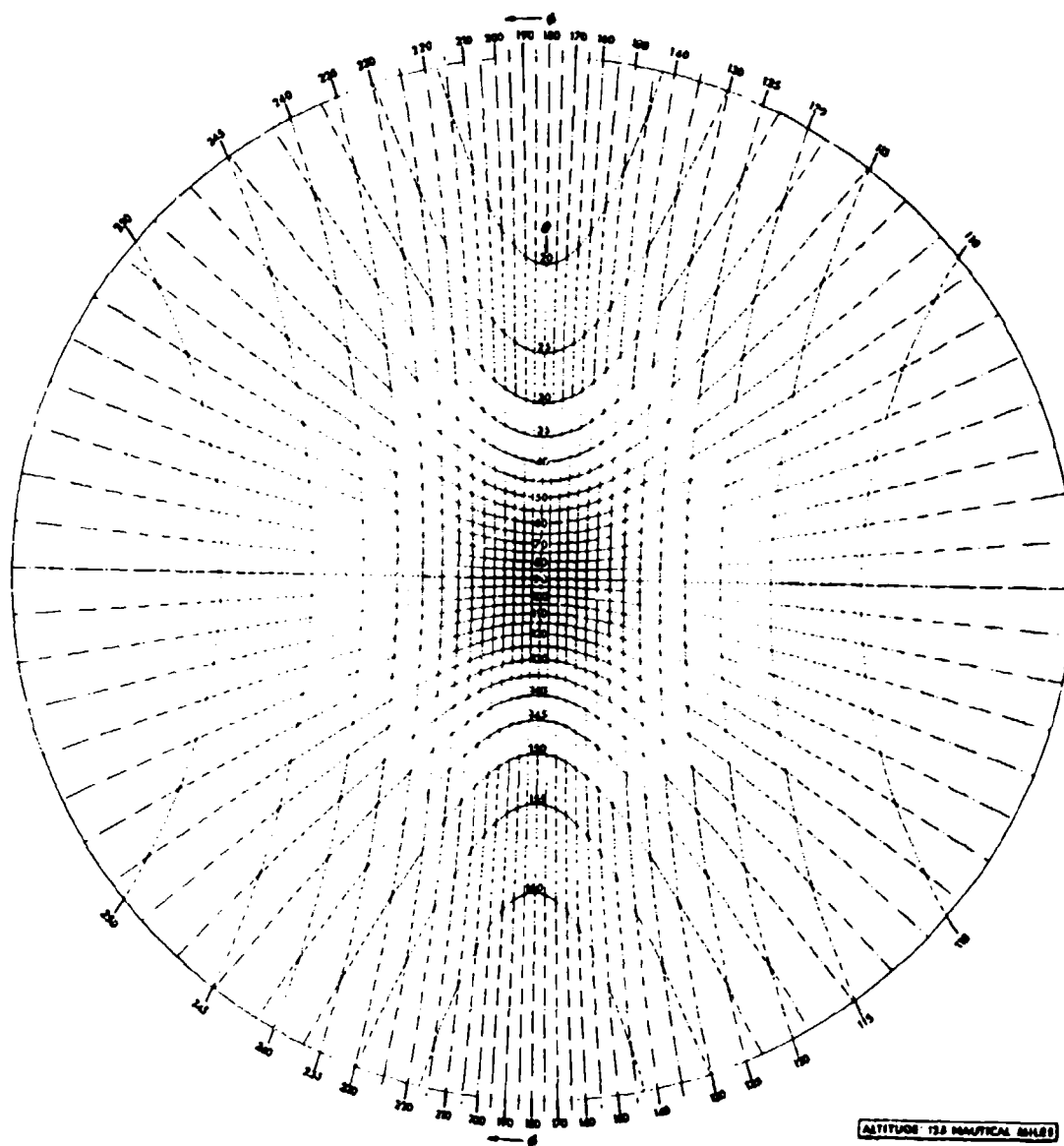


Figure 19. Coordinate Grid for Horizontally Stabilized Satellite (125-NM Altitude).

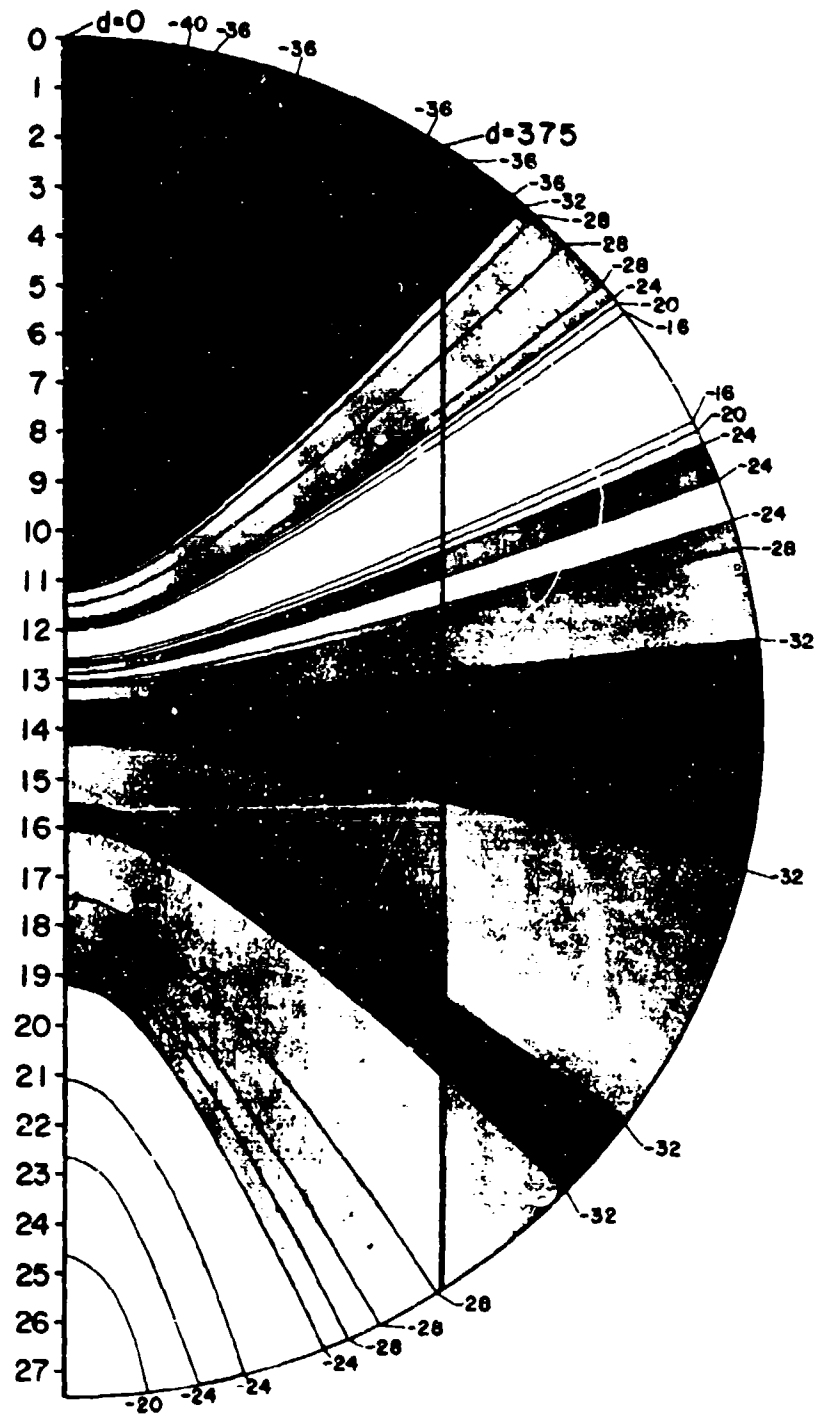


Figure 20. Contour Plot for Horizontally Stabilized Cone.

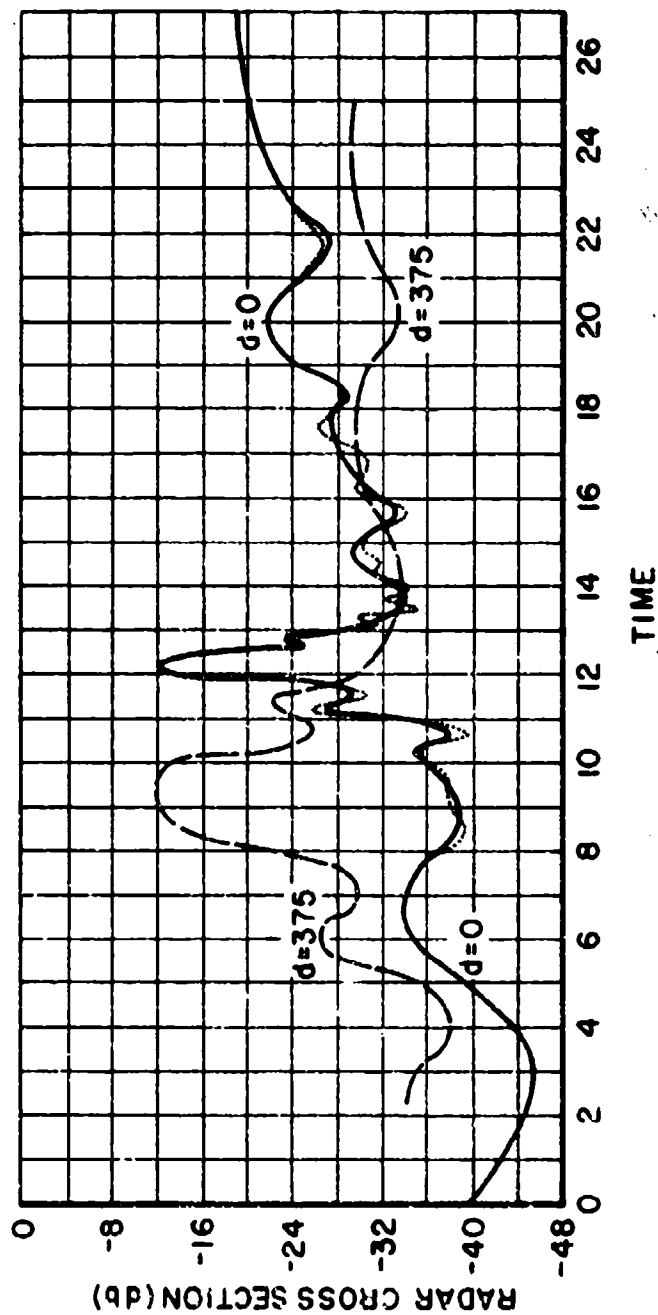


Figure 21. Backscattering From a Horizontal Code as Function of Time.

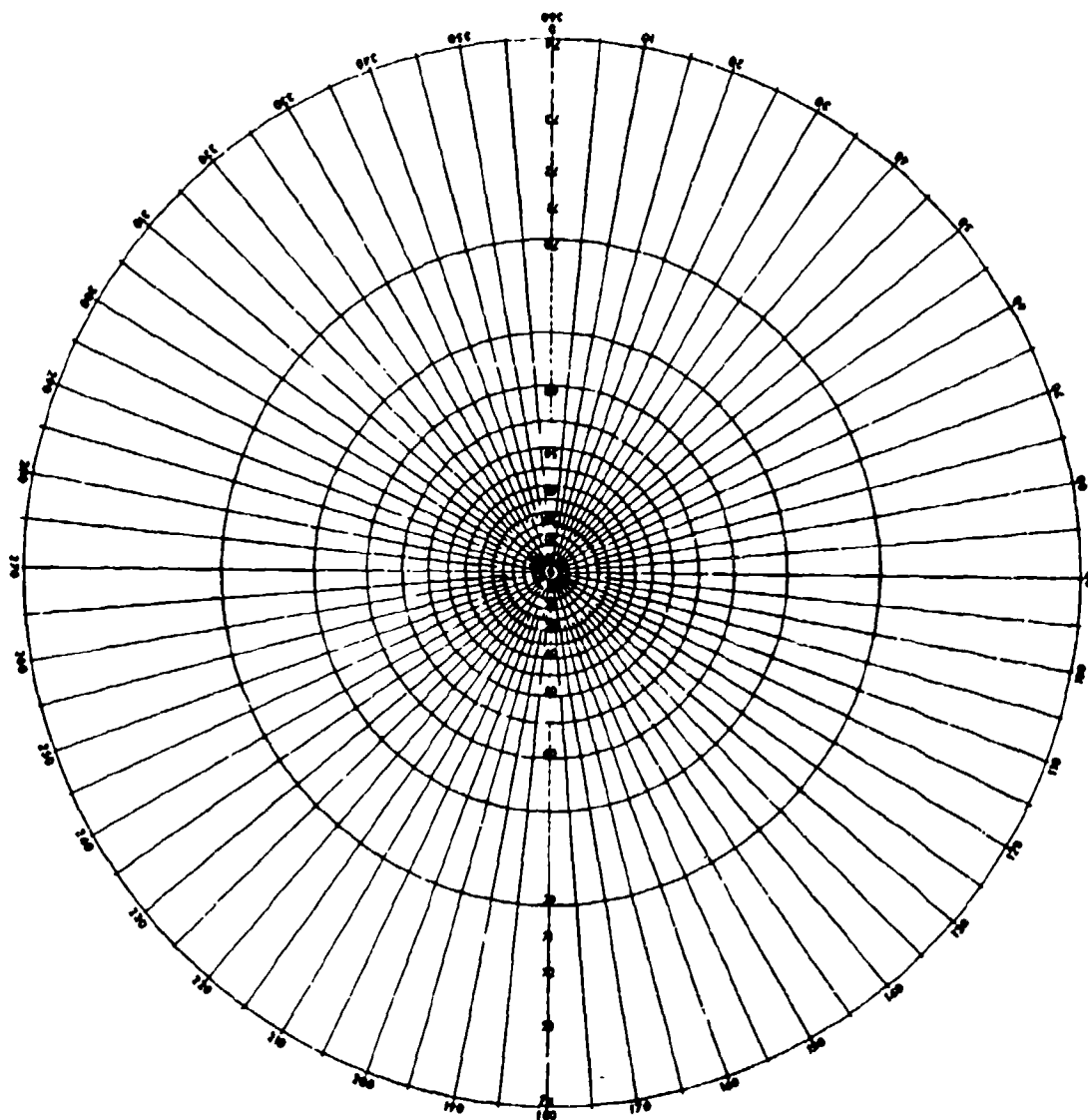


Figure 22. Coordinate Grid for Vertically Stabilized Satellite.

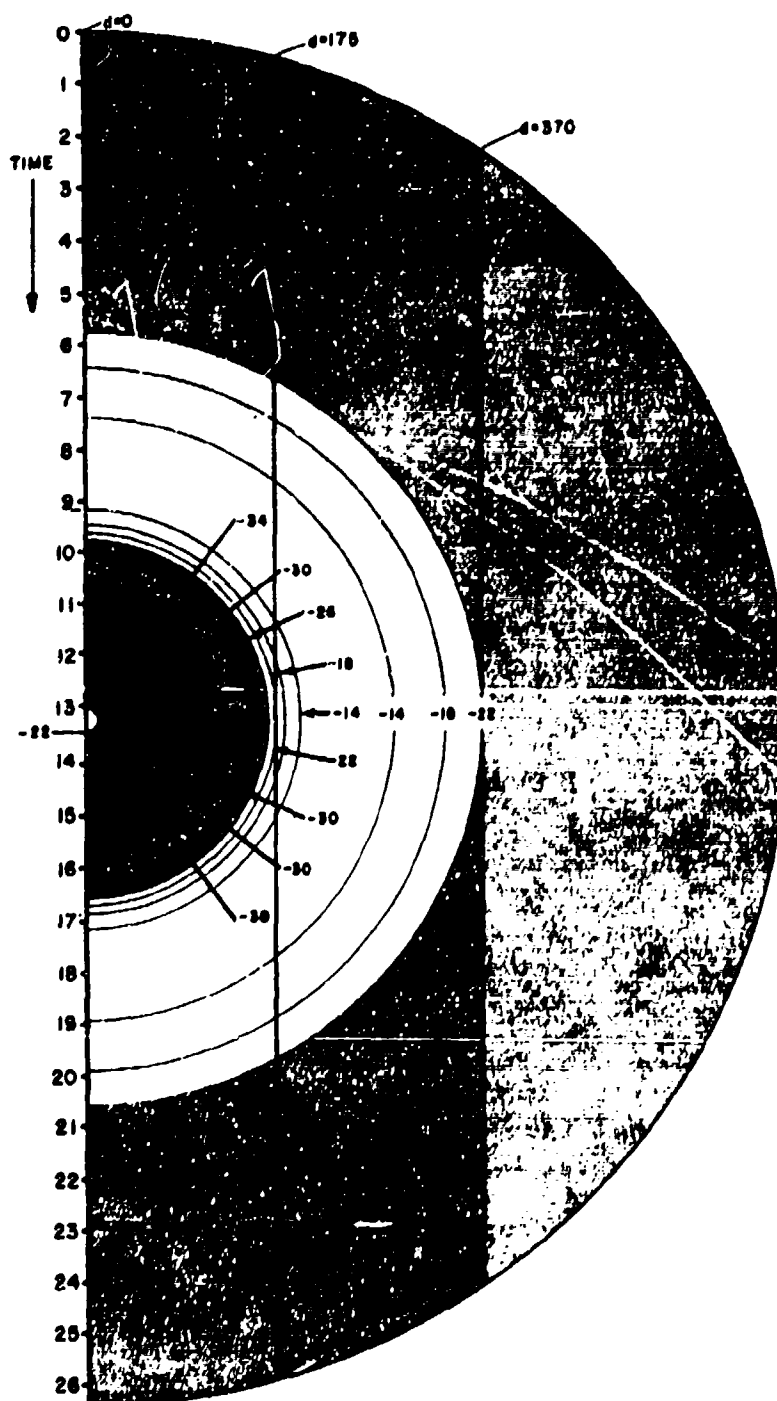


Figure 23. Contour Plot for Vertically Stabilized Cone.

The new projections also possess an equal-area property that is of great importance in data reduction. The nature of the equal-area characteristics follows from the considerations below:

1. The satellite is equally likely to cross the abscissa between x and $x + dx$, whatever the value of x may be.
2. The satellite spends equal time between y and $y + dy$, no matter what value is given to y .
3. As a consequence, equal time is spent in any element of area $dx dy$ for a sufficiently large number of passes.
4. Since equal areas on the chart are occupied for equal periods of time by the satellite, the projection has an equal-area property.
5. Measurement of the total area within each contour level provides a value for the total time that the backscattering lies within the bounds of the interval, when the observations extend over a large number of orbital passes.

Cumulative distributions for the horizontally and vertically stabilized cones are given in Fig. 25, which shows the probability of exceeding the level of the abscissa when within the bounding circle of the chart. The bounding circle, it may be mentioned, has been placed arbitrarily at an elevation about 4 degrees above the horizon. If the radar equipment of interest has a coverage cone that lies higher above the horizon, which is usually the case, then a different (smaller) bounding circle should be employed in evaluating the cumulative distributions.

LIMITATIONS OF SATELLITE COORDINATE PROJECTIONS

The grid of Fig. 22 for a vertically stabilized body is simple to plot, for it consists of circles and straight lines to close approximation. The complex coordinate grid in Fig. 19, however, is best generated by an automatic plotter. The straight lines favored in the classical grids are replaced in Fig. 19 by straight-line flight paths so that the contours provide values that are readily related to physically meaningful measurements. The resulting non-linear variation of one or both coordinates in these projections makes interpolation a tedious process, and requires data processing of contours in a computer for their practical utilization, unless the body has roll symmetry and a small number of lobes in its longitudinal backscatter pattern.

The requirement that the orbit be circular may be relaxed slightly, so that the projections may be used for orbits that are slightly elliptical. For nearly circular orbits there is only a small altitude change within the limited coverage cone of a ground station, and the mean altitude over the station may be used in preparing a chart.

Earth rotation is small during a satellite pass over the coverage cone of a ground station, and only small error is introduced into the chart by assuming that the earth is stationary.

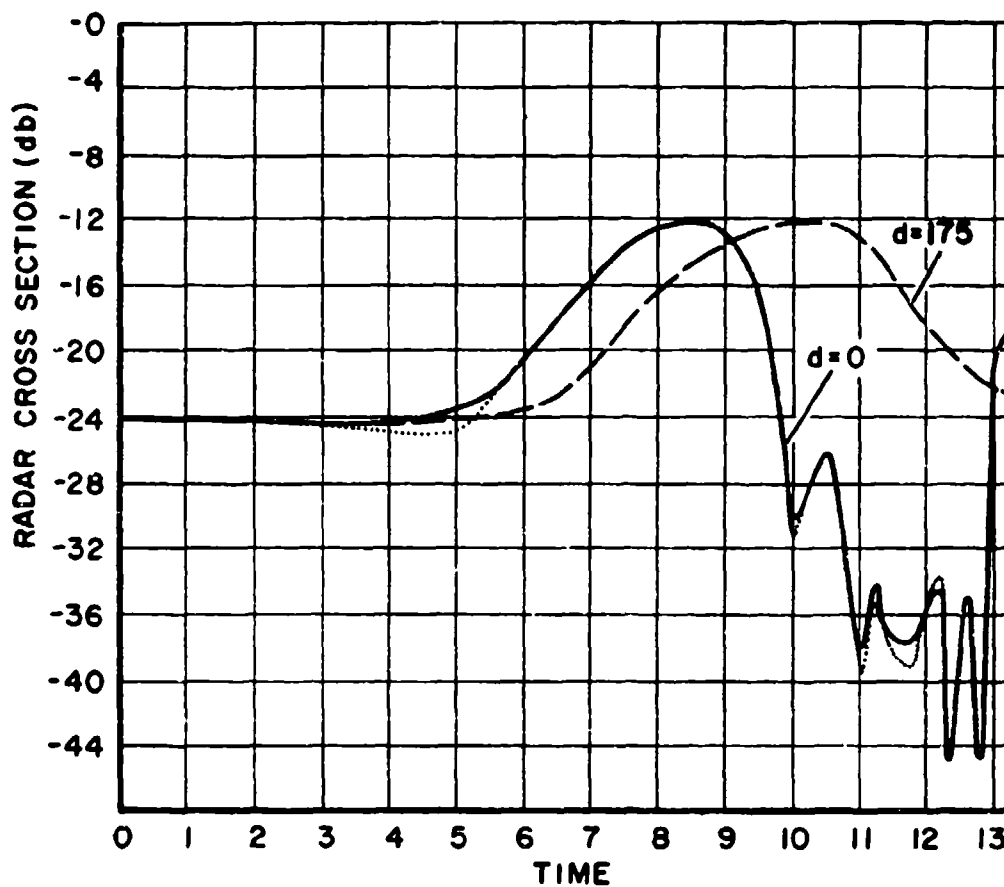


Figure 24. Backscattering From Vertical Cone as Function of Time.

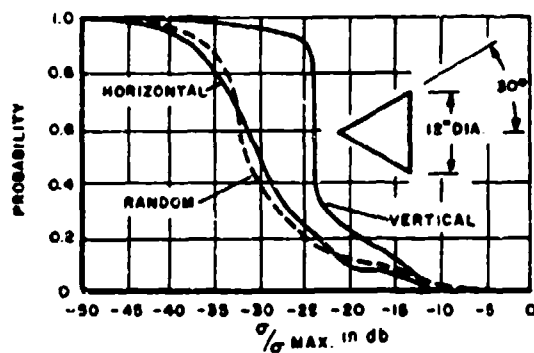


Figure 25. Cumulative Distributions for Stabilized Cone.

The purely geometric derivation of the satellite projections makes no allowance for atmospheric bending of the radar beam. The angular deviation becomes significant for low elevation angles and should be included in any precise treatment when within about 10 degrees of the horizon.

The time variation of the reflectivity read from the contours of either Fig. 20 or Fig. 23 loses small fluctuations that occur within a contour interval. This loss is illustrated in Figs. 21 and 24, where the dotted curves show the complete time variation for an overhead pass, as computed directly from the original pattern, Fig. 11. The contour interval should be small enough to eliminate any significant errors of this type, where the level of what is significant depends upon the application of the analysis. (In practice, a 1-db contour interval would be selected for the cone, but the resulting patterns would be so difficult to reproduce in publication that a 4-db interval was selected in preparing Figs. 20 and 23 for this paper.)

For general location of the radar site and the orbital inclination, it is not true that all distances of nearest approach are equally likely. As an obvious counterexample, when a ground station lies north of the maximum satellite latitude, there can never be an overhead pass. In particular, we consider a ground station at 50° N. latitude that has a coverage circle of 600 nautical miles radius at the satellite altitude, so that it observes any passes above 40 degrees at the radar longitude. Then a satellite in orbit at an inclination of 45 degrees never comes closer than 300 nautical miles, so that the satellite projection does not have an equal-area property for this specific radar site.

Even for a ground station located on the equator, the satellite projection may not have an equal-area character for a specific orbit. Thus, any earth synchronous orbit passes over the same ground track each day. For example, when there are precisely 16 orbits per day, the suborbital tracks are separated by exactly 22.5 degrees at the equator, and the identical suborbital points are retraced every day.

If interest is centered in a small number of radar sites and a small number of orbital parameters, any assumption that the satellite projection has an equal-area property should be carefully tested. For a large number of orbital altitudes and inclinations, or for a large number of radar sites, the equal-area property becomes a powerful tool for determining the cumulative distribution of all radar observations.

REFERENCES

1. D. Levine and W. Welch, "Spatial Coverage of Radar Reflectors," IEEE International Conference and Exhibit on Aerospace Electro-Technology, Phoenix, Arizona, April 19-25, 1964
2. E. M. Kennaugh, "Memorandum on Presentation of Radar Cross-Section Data by Contour Maps," Ohio State University Antenna Lab Report 475-8, Oct. 30, 1953

3. C. H. Deetz and O. S. Adams, "Elements of Map Projection," U. S. Coast and Geodetic Survey Special Publication No. 68, Fifth Edition (Revised 1944), Washington, 1945
4. F. Fiala, "Mathematische Kartographie," VEB Verlag Technik, Berlin, 1957
5. F. W. McBryde and P. D. Thomas, "Equal-Area Projections and World Statistical Maps," U. S. Coast and Geodetic Survey Special Publication No. 245, Washington, 1949
6. R. K. Molluiah, An Introduction to the Mathematics of Map Projections, Cambridge University Press, London, 1931
7. O. S. Adams, "General Theory of Equivalent Projections," U. S. Coast and Geodetic Survey Special Publication No. 236, Washington, 1945
8. O. S. Adams, "Latitude Developments Connected with Geodesy and Cartography," U. S. Coast and Geodetic Survey Special Publication No. 67, Washington, 1949
9. Inter-Range Instrumentation Group, "IRIG Standard Coordinate System and Data Format for Antenna Patterns," IRIG Document No. 102-61, Sept. 1961
10. C. H. Bredall, The SATRAK Simulator, Aerospace Corporation Report TDR-169(3305) TN-3, SSD-TDR-63-63, March 30, 1963

ACKNOWLEDGEMENT

The assistance of numerous associates was most helpful in preparing this paper; in particular, William H. Welch, Richard Falconer, and James L. Hodgson prepared the contour charts; Otis C. Myers, Jr., derived the explicit form of the coordinate transformation for Fig. 19; and Michael H. Seigel performed all necessary computer programming. The author also benefited from numerous stimulating discussions with Thomas B. Friedman and Charles H. Bredall of Aerospace Corporation.

The great-circle cuts for the jack were made by Micronetics, Inc., San Diego, California.

GEOMETRY AND INSTRUMENTATION CONSIDERATIONS FOR DYNAMIC REFLECTIVITY MEASUREMENTS

E. G. Mayer, Section Head
C. L. Mohre, Associate Principal Engineer
Radiation Incorporated
Melbourne, Florida

ABSTRACT

Dynamic reflectivity measurements require precise information about the position and attitude of the airframe relative to the illuminating radar. Four parameters of the airframe (heading, roll, pitch, and altitude) and two parameters derived from a radar tracking the airframe (azimuth and range) will serve to completely define the aspect of the airframe relative to the illuminating radar. Dynamic reflectivity measurements can be made of the airframe using either the tracking radar or radars in other frequency bands slaved to the tracking radar by making measurements of returned signal amplitude in a non-gain controlled receiving channel. The relations between measured parameters and target aspect are derived. Considerations affecting data sampling rates are discussed along with instrumentation and data reduction configurations. The measurement and data reduction techniques and equipment are also applicable to dynamic antenna testing of antennas mounted on an airframe.

GENERAL

Dynamic reflectivity is simply the determination of the reflectivity of a vehicle while the vehicle is in flight. Successful dynamic reflectivity measurements have been performed on both atmospheric and exo-atmospheric vehicles at a number of facilities including the Atlantic Missile Range, Chesapeake Bay Annex, White Sands Missile Range, and Radiation Incorporated. Dynamic reflectivity measurements have become increasingly important in the past few years due to:

1. The need to determine the degree of correlation with static reflectivity measurements.
2. The difficulty of determining the extremely low cross section data representative of present day nose cones.
3. The inability of static measurements to provide dynamic reflectivity effects, such as ion sheaths, that occur during vehicle re-entry.
4. The difficulty of scaling ablative materials, absorber materials, and other measurement parameters.

Dynamic measurements eliminate the need for target supports and their associated errors, permit a wide enough separation of radar and target to ensure essentially plane wave incidence at the target and receiving antenna, and can minimize stray returns from the earth and nearby structures.

The major disadvantages of dynamic measurements are the large number of uncontrollable variables present, the difficulty of correcting the data for propagation effects, and the relatively high cost of these measurements.

By proper instrumentation, the effects of uncontrollable variables can be measured and eliminated from the data. The most difficult effect to remove is that of the propagation medium. However, only in the absolute measurement situation does this become a real problem. For relative measurements, the effect of the propagation medium can normally be neglected by having the vehicle remain in the same general location during the measurements. Propagation medium effects are aggravated in the ballistic case due to variations in the propagation path throughout the vehicle's trajectory.

From the ballistic viewpoint, reflectivity measurements must be made dynamically or corrections for re-entry effects estimated and added to the static values. Reflectivity of a ballistic vehicle is not only a function of attitude, but of the position of the vehicle in its trajectory.

SYSTEM CONSIDERATIONS

The accuracy and the type of reflectivity data required dictates the complexity and configuration of the overall measurement system. For instance, system requirements for aircraft reflectivity measurements differ significantly from the requirements imposed by ballistic vehicle measurements. Instrumentation requirements for absolute measurements are much more stringent than those for relative measurements. Thus, a careful analysis of the instrumentation complex should be made in terms of possible future reflectivity requirements to insure maximum measurement flexibility. A block diagram of a dynamic reflectivity range for aircraft reflectivity measurements is shown in Figure I.

As shown in the diagram, three instrumentation groupings are present, aircraft instrumentation, ground instrumentation, and the data processing complex. Data can either be recorded and time correlated at the aircraft and ground installation or the data from the aircraft can be telemetered to the ground station for recording purposes. The choice of system is primarily a function of the instrumentation available on the aircraft, since modification of the aircraft for measurement purposes is undesirable. Determination of the vehicle aspect with respect to the illuminating radar is one of the primary data problems involved with dynamic reflectivity measurements. Four parameters of the airframe (heading, roll, pitch, and altitude) and two parameters of the airframe - radar geometry (range and azimuth) are required to define this relationship. Development of the defining equations is given in the Appendix I.

Aircraft Instrumentation

There are two major subsystems in the aircraft instrumentation system, an attitude monitor and a recording or telemetry subsystem. The attitude monitor determines the roll, pitch, and heading of the aircraft. Altitude data is normally not required, since this information is supplied by the ground tracking radar. If the data is recorded in the aircraft, the system

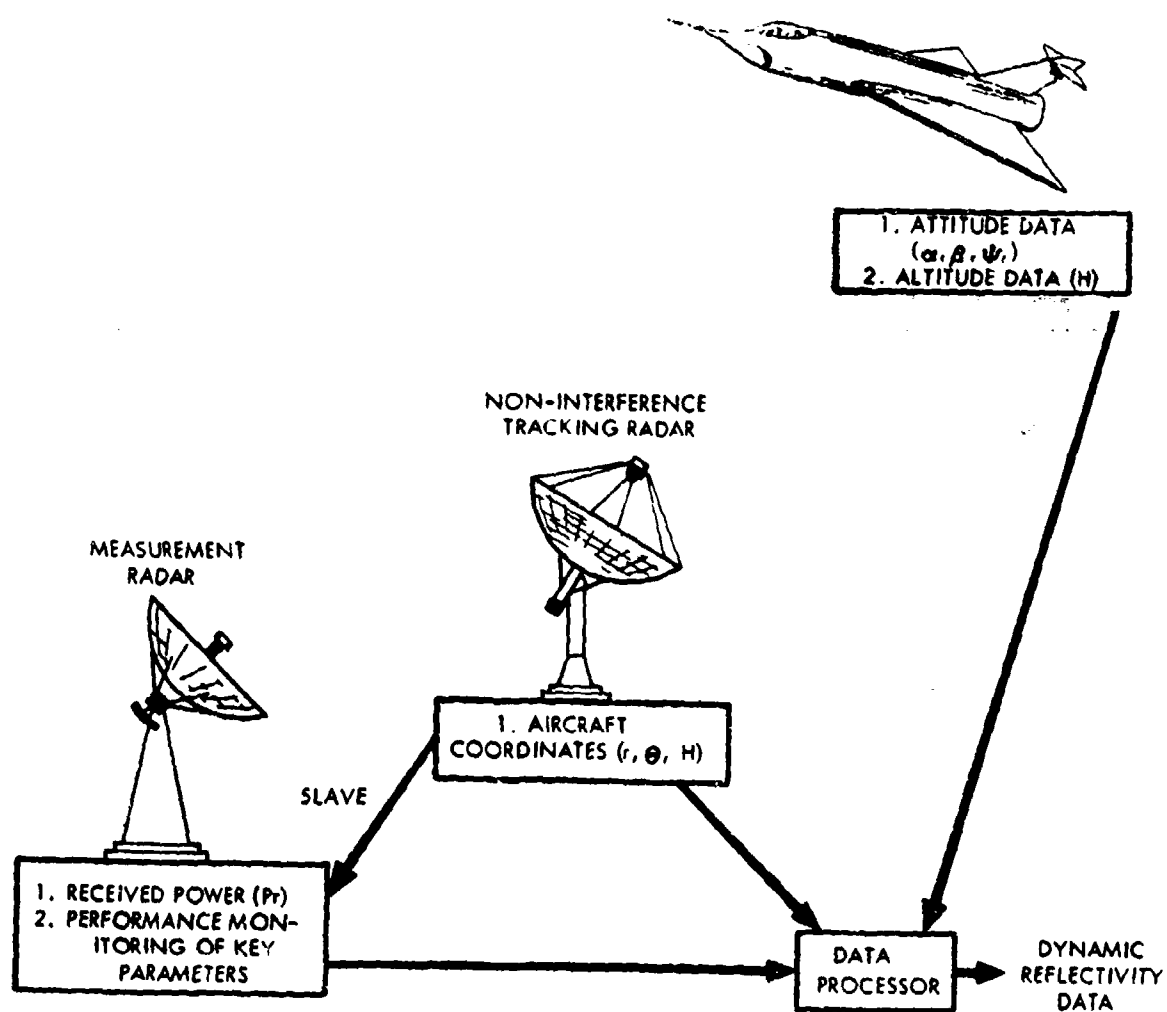


Figure 1. Dynamic Reflectivity Range

would time multiplex the analog signals, convert them to digital pulses, and record them on tape. Digital time information is transmitted to the aircraft via the communication link for time correlation purposes. If the data is telemetered, the analog signals would be the multiplexed, converted to digital signals, and transmitted to the ground station.

Sampling Rates

An aircraft, due to its inertia, cannot change its attitude very rapidly under normal weather conditions. In a full needle turn (15 degrees), for example, the azimuth of the aircraft is only changing at the rate of 3 degrees per second. As another example, an aircraft diving at 600 miles per hour at a 45 degree angle would be changing altitude at a rate slightly in excess of 600 feet per second. Both of these examples are extreme cases and indicate that a sampling rate of a few times a second will be adequate to describe the aircraft attitude as a function of time.

Attitude Monitoring

Two different approaches can be taken to obtain pitch and roll information from the aircraft. The first approach involves deriving this data from the autopilot's gyro stabilized vertical reference. This approach requires that the vertical reference be operational at all times regardless of whether the aircraft is being flown manually or by the auto-pilot. In addition, the connections to the vertical reference would have to be non-interfering with ancillary equipment. The primary advantage of this approach is that a minimum of additional equipment is required. Disadvantages include probable loss of vertical reference during accelerated maneuvers and possible difficulty in establishing the true zero-pitch and zero-roll references.

An alternative approach is to provide either a separate vertical reference or a stable platform. However, most operational vertical references suffer from acceleration errors. Stable platforms, although considerably more expensive, provide accurate attitude information regardless of vehicle maneuvers.

Heading information can be derived from a stable platform or from a gyro stabilized directional compass system. Earth's rate effects and other geophysical phenomena can be compensated for either by the measuring device or by data corrections based on the aircraft's flight path.

Ground Instrumentation

The non-interfering tracking radar provides the aircraft coordinates and positions the measurement radar on the target of interest. The measurement radar is used to accurately determine the reflected power from the target vehicle. By slaving several measurement radars each transmitting at a different frequency, simultaneous reflectivity measurements at different frequencies can be obtained.

The non-interfering tracking radar could also provide the function of the measurement radar. However, the basic requirements imposed upon the two are different. That is, a narrow beamwidth is required for accurate tracking information, while a broad beamwidth is desired to minimize the effect of antenna modulation on the received signal. Also, conical scan tracking systems introduce amplitude modulation on the received signal that would have to be removed from the data.

Measurement Radar Antenna System

There are several considerations that should be observed regarding the antenna system. These include:

1. Tests should be run so the ground antennas are always operating at elevation angles in excess of 10 to 15 degrees to avoid ground bounce and lobe breakup. This will not limit the angles which can be measured on the airborne antenna since the aircraft can be flown with various pitch and roll angles to provide complete angle coverage.
2. The beamwidth of the antenna should be wide enough to insure that antenna pattern modulation will not affect the results. Lobe widths of 50° or greater are desirable.
3. When making multiple frequency measurements, the measurement antennas should be located close enough to the ground tracking system so they are essentially at the same point in terms of the testing distances involved.

Measurement Receiver

Reflectivity data is obtained from the received power level in a dynamic system in identically the same way as in a static configuration. However, there are certain tradeoffs and system considerations that are more important in the development of a dynamic system. These include dynamic range considerations, sampling rates, and performance monitoring.

Dynamic range requirements are more stringent in dynamic measurements, since the received power from the target is continually changing as the fourth power of the range. Dynamic range requirements can be reduced by restricting the range over which target measurements are made.

The required sampling rate is essentially determined by the maximum rate of change of attitude of the aircraft, the size of the aircraft, and the transmit frequency. As stated previously, the maximum rate of change in azimuth of an aircraft is normally on the order of 3 degrees per second. Assuming a medium sized aircraft, on the order of six to eight lobes per degree are generated at S-Band. With a 3 degree per second attitude change, about 125 samples per second would be required to provide 5 data points per lobe. A sampling rate on the order of two hundred samples per second for the received power would yield the fine structure pattern for this situation.

This is about an order of magnitude less than the effective sampling rate of a medium range radar, with a PRF of 1,000 pps, that could be used for these types of measurements. However, in order to obtain the fine structure of the lobe pattern, very accurate attitude sensors would have to be employed.

Performance monitoring of transmitter parameters such as transmit power and frequency is required to insure that if variations in these parameters occur during a test, their effects can be removed from the final data.

DYNAMIC ANTENNA TESTING

Airborne antenna testing can be rapidly and accurately accomplished with only a few modifications on the basic system. One approach would involve mounting transmitters in the aircraft connected to the antennas to be tested. On the ground, receiving antennas are provided which are slaved to the ground tracking radar. Thus, a direct measure of received signal as a function of aircraft attitude can be derived. The antennas could be constructed to provide both vertical and horizontal polarization outputs. With the use of time multiplexing or parallel receiving channels, information could be obtained on both polarizations simultaneously.

APPENDIX I - ASPECT GEOMETRY

Determination of the vehicle aspect with respect to the illuminating radar is one of the primary data problems involved in dynamic reflectivity measurements. The following analysis shows that six parameters are required to define the aspect of the air frame relative to the illuminating radar. In the derivation of the "aspect-radar geometry" an attempt was made to develop the equations such that the effect of attitude changes on the system parameters can be easily visualized.

By common usage the position of a point in space with respect to an aircraft is defined in terms of R , θ and ϕ where

R = slant range

θ = depression angle

ϕ = angle projected on the horizontal plane through the aircraft measured from the nose

Figure 2a illustrates a general situation of an aircraft in level flight being illuminated by a radar. Figure 2b shows this situation projected onto a horizontal plane and serves to define ϕ , heading angle, and radar azimuth angle.

θ and ϕ can be defined for this simple case in terms of the other parameters as follows:

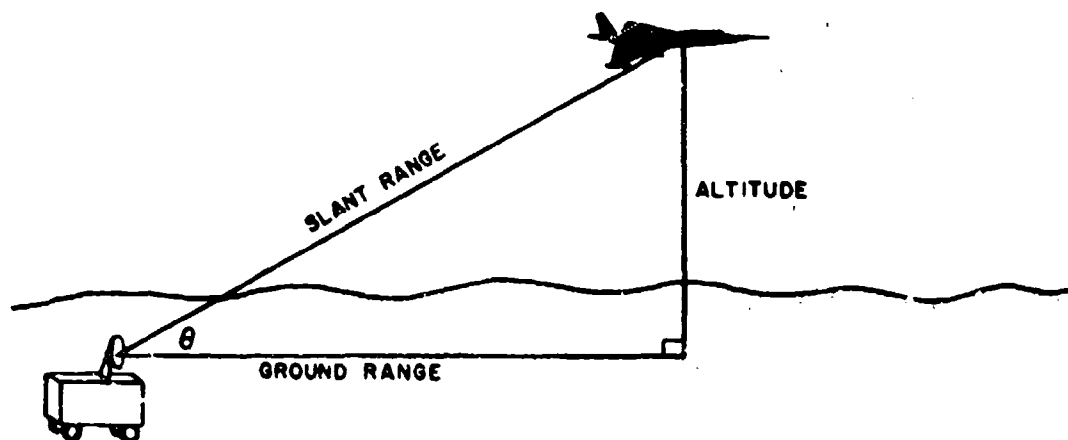


Figure 2a. Aircraft In Level Flight Illuminated By Ground Radar

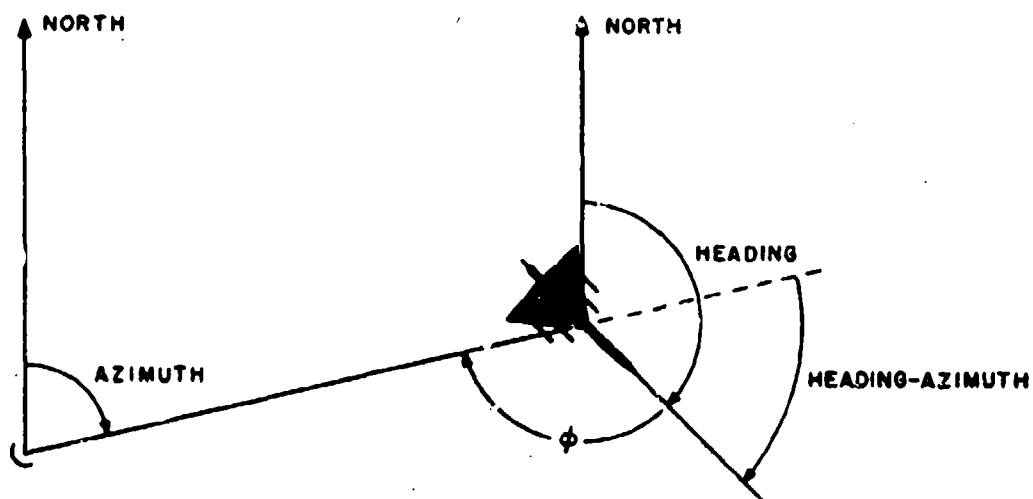


Figure 2b. Projection Of Figure 2a On A Horizontal Plane

$$\phi = 180 - (H - AZ) \quad (1)$$

$$\theta = \sin^{-1} \frac{ALT}{R} \quad (2)$$

where: AZ = radar azimuth angle measured from north
 ALT = altitude of aircraft with respect to the radar
 H = heading angle of aircraft measured from north

For aircraft measurements the distances involved are relatively small in terms of earth dimensions, thus no corrections for earth curvature are required. However, for ballistic measurements earth curvature corrections are required. This development is based on a flat earth condition.

Visualization of the changes in θ and ϕ brought about by pitch and roll angles can be aided by considering the aircraft to be located at the center of a sphere and the radar on the surface of the sphere. Thus, the radius of the sphere is equal to the slant range, R. Figure 3 shows a side view of the sphere with the radar at point A. Changes in aircraft attitude can be considered as changes in the position of the radar with the aircraft remaining stationary. Thus, changes in aircraft heading can be represented as movement of the radar on the heading circle BC. Roll of the aircraft can be represented as movement of the radar on the roll circle DE. Pitch of the aircraft can be represented as movement along the pitch circle which passes through point A. A combination of roll and pitch, as an example, would be represented by movement from A along the roll circle to F, followed by movement along the new pitch circle to point G. The order of the movement is immaterial; the result could have been obtained by proceeding along the pitch circle to point H and then along the new roll circle to point G.

With the addition of roll, pitch, and heading circles to the sphere additional quantities may be defined as follows:

R_R = radius of the roll circle

R_p = radius of the pitch circle

R_H = radius of the heading circle = ground range

S_R = separation of roll circle or the distance from the center of the roll circle of the origin of the sphere.

S_H = separation of the heading circle = altitude

S_p = separation of the pitch circle

These may be defined in terms of R, θ , and ϕ with the aid of Figure 4.

Thus, $S_H = ALT = R \sin \theta \quad (3)$

$R_H = R \cos \theta \quad (4)$

$S_p = R_H \cos (\phi - 90) = R \cos \theta \cos (\phi - 90) \quad (5)$

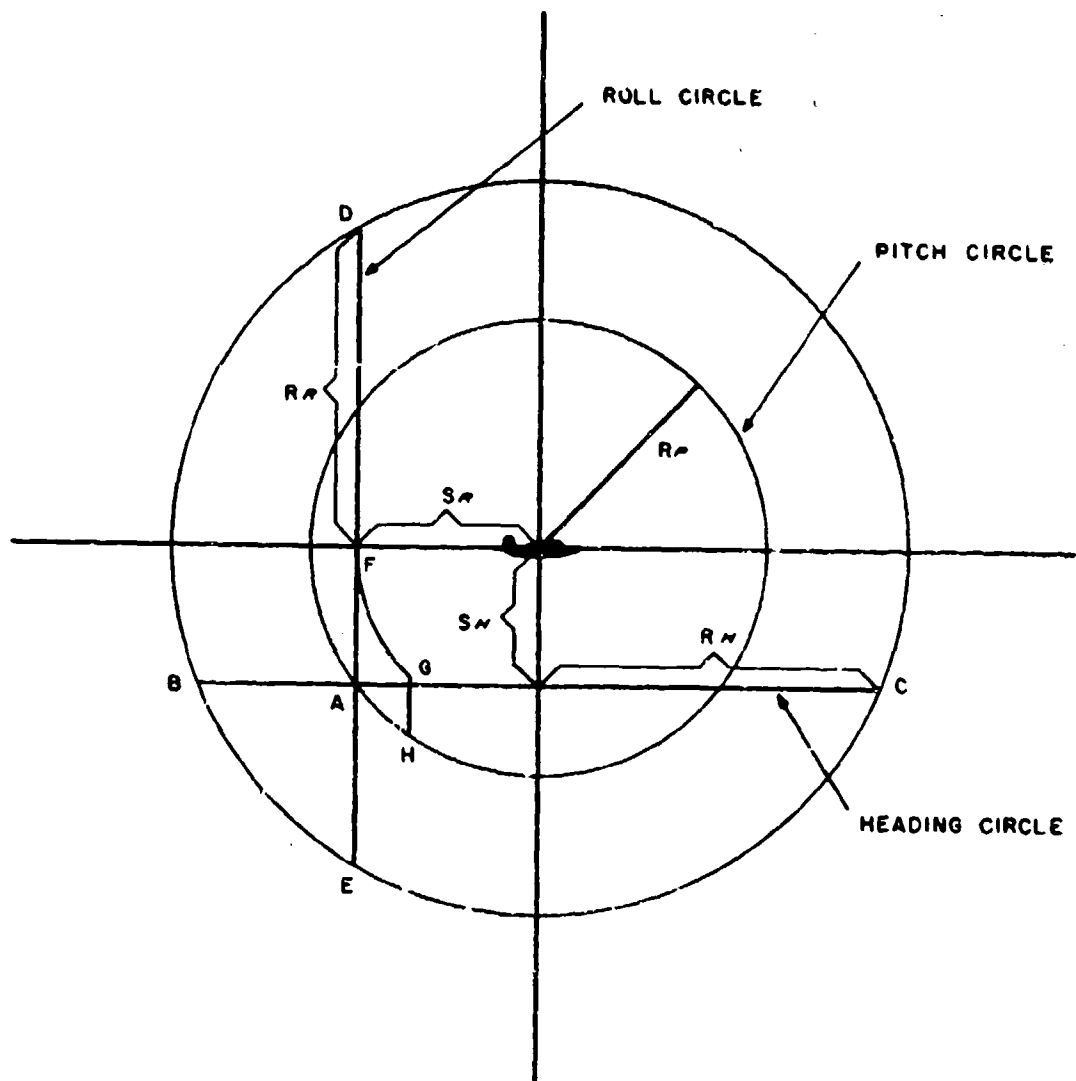


Figure 3. Side View Of A Sphere With The Radar At Point A

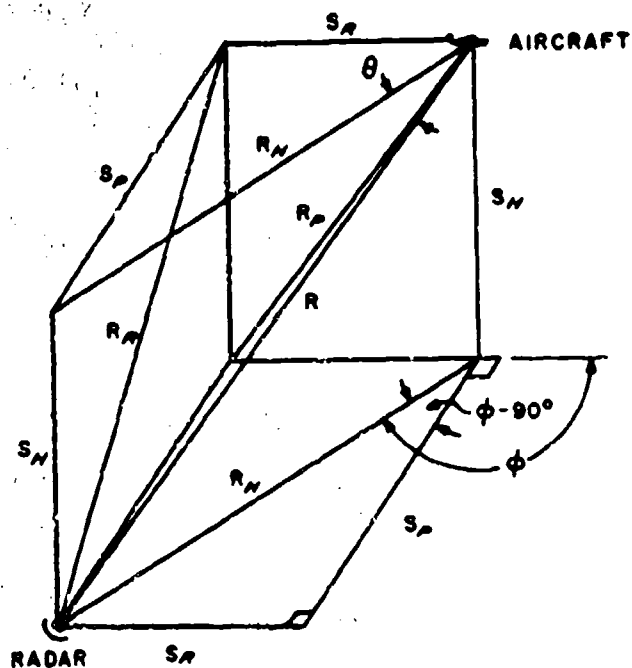


Figure 4. Roll, Pitch, And Heading Quantities In Terms Of R , θ , And ϕ

$$S_R = R_H \sin (\phi - 90) = R \cos \theta \sin (\phi - 90) = R \cos \theta \cos \phi \quad (6)$$

$$R_P^2 = S_P^2 + S_H^2 = (R \sin \theta)^2 + (R \cos \theta \sin \phi)^2 \quad (7)$$

$$\begin{aligned} &= R^2 \left[\sin^2 \theta + \cos^2 \theta \sin^2 \phi \right] \\ &= R^2 \left[1 - \cos^2 \theta \cos^2 \phi \right] \\ R_P^2 &= S_H^2 + S_R^2 = (R \sin \theta)^2 + (R \cos \theta \cos \phi)^2 \quad (8) \\ &= R^2 \left[\sin^2 \theta + \cos^2 \theta \cos^2 \phi \right] \\ &= R^2 \left[1 - \cos^2 \theta \sin^2 \phi \right] \end{aligned}$$

Since θ and ϕ were defined in terms of H, AZ, ALT, and R, all of the quantities are now defined in these terms.

Now consider the introduction of a roll angle. Figure 5a shows a portion of the roll circle with a roll angle α introduced. The roll angle moves the relative position of the radar to new heading and pitch circles with new heading and pitch separations $S_{H'}$ and $S_{P'}$, and a new pitch circle radius $R_{P'}$.

$$S_{H'} = R_R \sin \left[\alpha + \sin^{-1} \frac{S_H}{R_R} \right] \quad (9)$$

$$S_{P'} = R_R \cos \left[\alpha + \sin^{-1} \frac{S_H}{R_R} \right] \quad (10)$$

$$(R_{P'})^2 = (S_{H'})^2 + S_R^2 \quad (11)$$

Now if a pitch angle β is introduced as shown in Figure 5b, the pitch angle moves the relative position of the radar to new heading and roll circles. This results in new heading and roll separations $S_{H''}$ and $S_{R'}$.

$$S_{H''} = R_{P'} \sin \left[\beta + \sin^{-1} \frac{S_{H'}}{R_{P'}} \right] \quad (12)$$

$$S_{R'} = R_{P'} \cos \left[\beta + \sin^{-1} \frac{S_{H'}}{R_{P'}} \right] \quad (13)$$

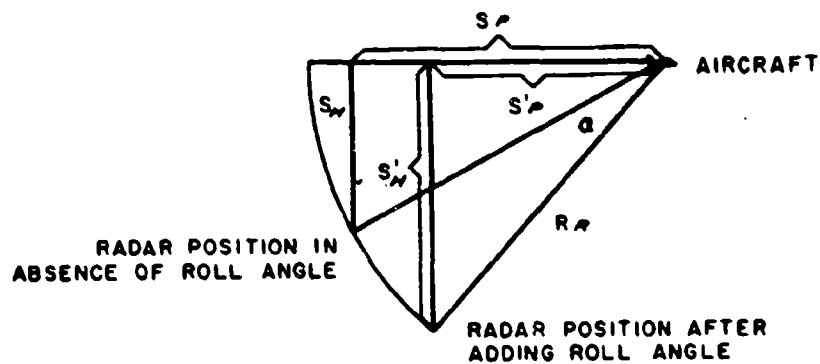


Figure 5a. Portion Of The Roll Circle

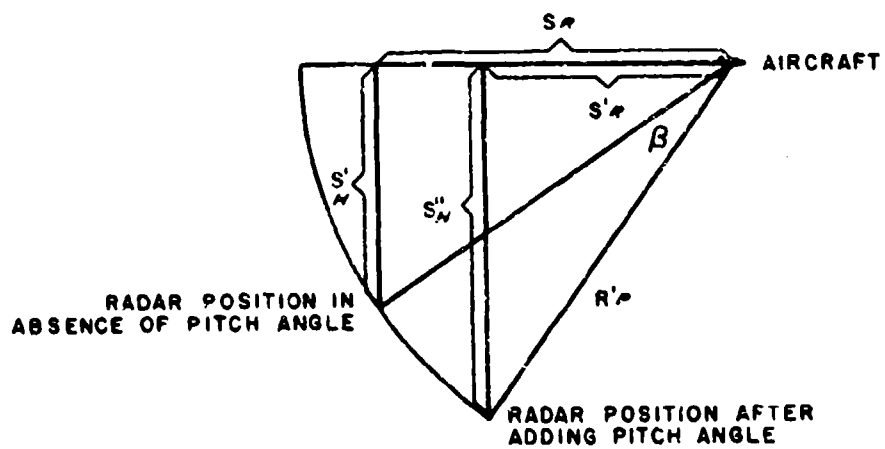


Figure 5b. Portion Of The Pitch Circle

Figure 4b may now be redrawn in terms of the new circles and separations as shown in Figure 6 and the resulting θ'' and ϕ'' determined.

$$\sin \theta'' = \frac{S_H''}{R} \text{ or } \theta'' = \sin^{-1} \frac{S_H''}{R} \quad (14)$$

$$\cos (\phi''-90) = -\sin \phi'' = \frac{S_{P_1}}{\sqrt{(S_{R_1})^2 + (S_{P_1})^2}} \text{ or} \quad (15)$$

$$\phi'' = -\sin^{-1} \frac{S_{P_1}}{\sqrt{(S_{R_1})^2 + (S_{P_1})^2}}$$

Thus, the resulting angles of the radar with respect to the aircraft may be obtained in terms of the basic parameters of R , AZ , ALT , H , α , and β .

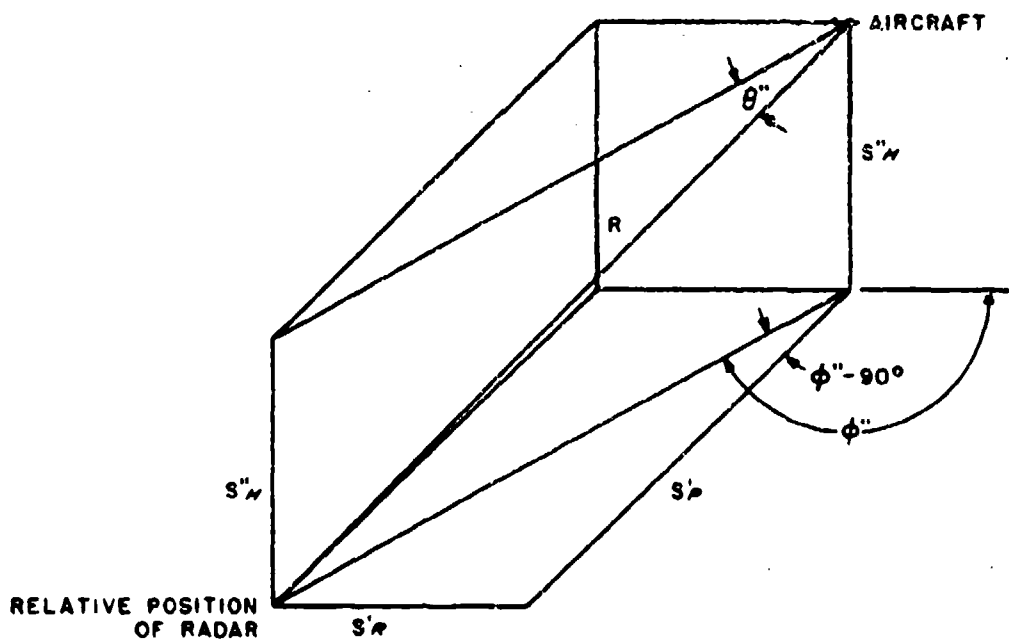


Figure 6. New Separations Showing θ'' And ϕ'' Determined

A MULTI-BAND, POLARIZATION DIVERSITY SYSTEM FOR DYNAMIC RADAR CROSS-SECTION STUDIES

I. D. Olin, F. D. Queen
U. S. Naval Research Laboratory
Washington, D. C. 20390

ABSTRACT A high-power, pulsed-radar system specially designed for cross-section measurements of full-size targets, under dynamic conditions has been completed and placed into operation. The system permits simultaneous measurement and recording at L, S and X-band frequencies on a pulse-to-pulse basis. The system, completely trailer mounted, uses magnetron transmitters pulsed together and an antenna assembly mounted to a single-servo controlled director. Operation at L and S bands may be with either vertical or horizontal polarization. At X-band, transmission may be selected at either vertical, horizontal, right-circular or left-circular polarization, while receiving components of all four simultaneously. The system is currently being employed in studying a variety of target characteristics germane to radar cross-section and target identification.

INTRODUCTION A pulsed radar system designed specifically for cross-section measurements at three frequencies was completed and placed into operation in the fall of 1963. The principal design objectives of the system were: to measure radar cross-section at L, S, and X-bands; provide for some polarization flexibility; record returns on a pulse-to-pulse basis; collect data in a form which could be analyzed rapidly. In addition, the system was required to operate in the range interval of 2000 to 20,000 yards, so that optical tracking was possible.

The complete system is mounted on four trailers. An operations trailer is used for the control equipment, master timing circuitry, and automatic range unit. A data trailer contains the pulse-to-pulse video recorder and amplitude distribution recorder. In addition, the i-f and video sections of the receivers and the amplidyne-drive units for the antenna assembly are also accommodated. The director and antenna assembly are mounted on a 25-ton flat-bed trailer and lowered for transit. An electrically driven hydraulic system is provided to operate the erecting pistons and trailer-leveling pistons. An additional manually operated hydraulic system operates a servicer platform. When erected the overall trailer height is 22 feet. The fourth trailer mounts the optical handstand assembly used for target tracking. Additional trailers for spares, and trailer-mounted equipment, air conditioners and generators, are used as required.

SYSTEM CHARACTERISTICS

Antenna Systems The X-band system utilizes separate identical, circularly symmetric antenna feed-reflector combinations. Each antenna assembly

provides a 3-degree pencil beam. The receiver antenna terminates in the NRL microwave polarimeter¹. It provides simultaneous reception of vertical, horizontal, right and left circularly polarized components of the target-reflected signal². The transmitting antenna terminates in switching equipment designed for remote designation of transmission polarization. Present operation provides selection of vertical, horizontal, right or left circularly polarized transmission.

The L- and S-band antennas consist of a concentric horn assembly illuminating a single parabolic dish. These antennas are duplexed for transmission and reception and two polarization modes are provided, vertical and horizontal. Change-over is accomplished by uncoupling two coaxial feed lines, rotating the feed assembly 90 degrees, and re-connecting two coaxial components inside the rf box. In order to permit simultaneous operation at high power, the primary feed uses separate waveguide horns. To provide L- and S-band beams of the same boresight, the L-band horn was split and the two sections properly phased, with the S-band horn between the two sections. The resulting E- and H-plane secondary pattern widths are: 3.5×3 degrees for the beam at S-band and 7.5×6 degrees for the beam at L-band. Owing to the high aperture blocking, the sidelobe level is -15db at S-band and -13db at L-band. Impedance match is good, the input VSWR being less than 1.1 for both systems.

Transmitters The transmitters are all manual tuned magnetrons, pulsed simultaneously at 500 pulses per second and with pulse durations of 1 microsecond each. Nominal radiated power at all three frequencies is 250 kw. The complete system is presently operated at 9225, 2800, and 1300 megacycles.

Duplexers The system specification required measurements on targets as close as 2000 yards, thus the receivers must be switched to the antenna within about 10 microseconds. Moreover, de-ionization of gas device switch tubes must be sufficiently rapid so that the attenuation remaining at 10 microseconds is negligible. Conventional duplexers, using T-R tubes and exhibiting such short recovery times, were unavailable at L- and S-bands. The solution was to split the magnetron power by means of a hybrid. The power to the isolated arm is then down at least 30db from the generated power. The resulting 500-watt peak pulse excites a conventional T-R tube. With the reduced ionization, so obtained, insertion loss in the T-R tube was unobservable after 8 microseconds. On the other side of the hybrid, one-half the generated power is radiated through the antenna and the other half absorbed in a high-power load. This scheme results in a 6db overall loss; however, with the present maximum range specification of 20,000 yards, this does not prove excessive. At X-band, conventional T-R tubes are used as receiver protectors in all channels.

Receivers A block diagram of the entire system is shown in Figure 1. The system uses six receiver channels, one each for L- and S-band and four for X-band (one for each polarization). Stable vacuum tube oscillators with AFC are used in all channels. To minimize the effect of magnetron-local oscillator frequency variation, a broad i-f response is employed in the i-f system. A bandwidth of 5 megacycles, flat to within 0.5db, is maintained within all receivers.

In order to fulfill the pulse-to-pulse measurement capability, no automatic gain control (AGC) is used in the receivers. Instead, the receivers operate linearly over a 40db dynamic range. A manual gain control is provided in each i-f strip to set the level during system calibration. Since a 10:1 range change is to be accommodated, a given target can be expected to exhibit a 40db change in signal reflectivity due solely to its range. To prevent this change from occupying the linear portion of the receiver characteristic, a unique servo-controlled attenuator circuit is placed in the front end of each receiver. The circuit uses the rotary attenuator in which the attenuation varies as the fourth power of the cosine of the rotary vane angle. By deriving an error voltage between cosine potentiometer, coupled to the rotary attenuator, and a linear potentiometer, coupled to automatic range unit, the servo motor drives the attenuator to make the target appear at a constant range of 20,000 yards. In the X-band receiver, four commercial rotary attenuators are mounted within the receiver box. In the S- and L-band receivers, rotary attenuators were specially designed and fabricated to reduce their length (over a scaled X-band unit). The rotary attenuators are arranged so that the 0-db insertion loss point, which will correspond to the maximum target range, can be set at 5000, 10,000, or 20,000 yards. This will permit observation of smaller targets at closer ranges without needless sacrifice in receiver sensitivity, but still retaining the range compensation feature. Additional attenuators are placed in all channels to provide a fixed 0-db, 10-db, or 20-db insertion loss, depending upon target size.

Detected video from the six i-f channels is connected to the six channel video recorder. Four of the six outputs are selected for presentation on the gray wedge pulse-height analyzer and for recording on a chart recorder. In the present system, L- and S-bands are always included together with two X-band channels, depending upon the transmitted polarization. After the video in the four gray wedge channels is stretched, outputs are provided for a single cathode-ray tube visual display of the return signal levels. This display is the basis on which the target size attenuators are controlled.

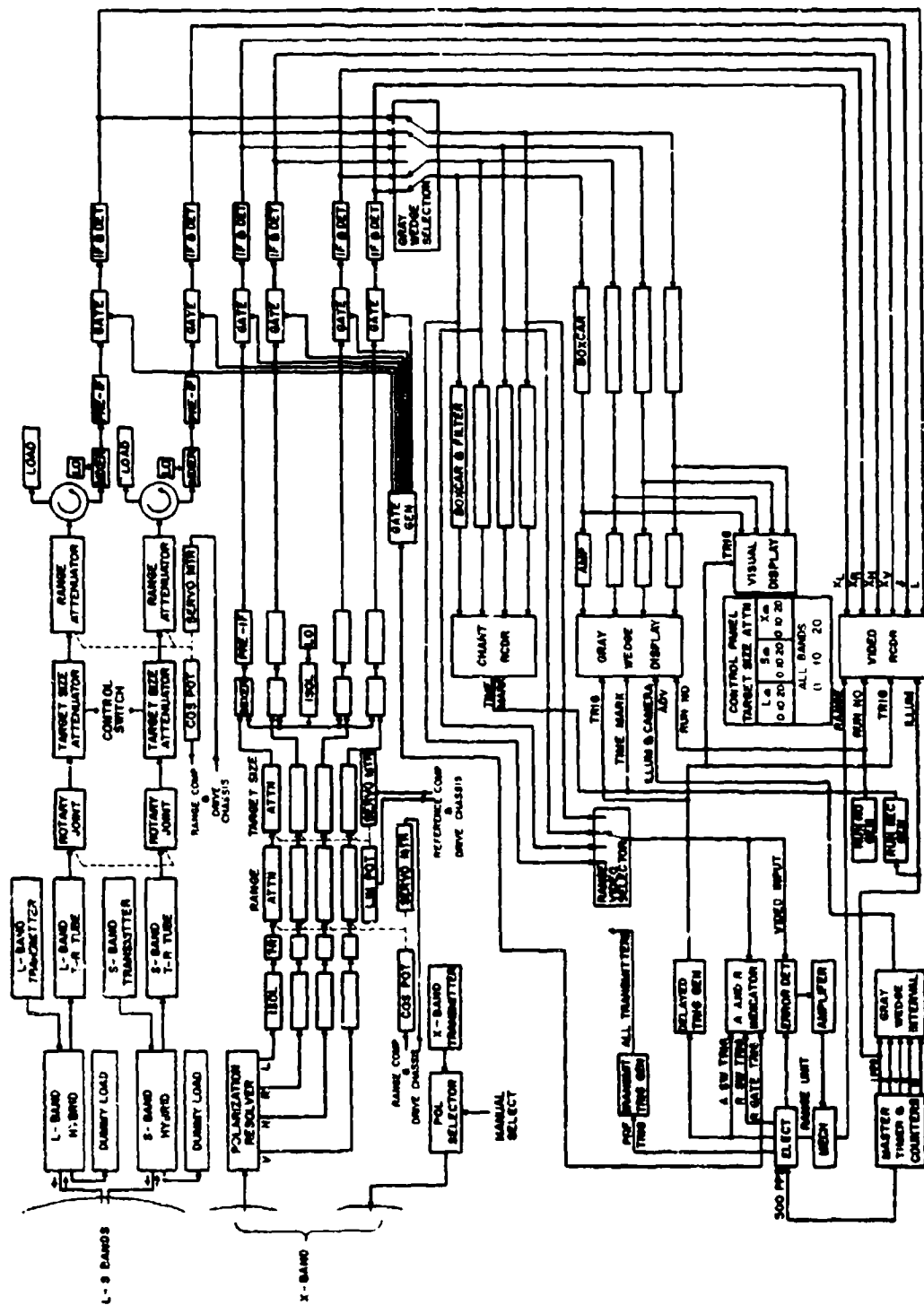


Fig. 1

Data Recording Data is recorded in the form of pulse-to-pulse video, amplitude distribution density plots, and stretched, filtered video on a multichannel chart recorder. Voltage time information from each of the receivers is processed and displayed on a cathode-ray tube. The image consists of a line with a fixed base position and length which vary in accordance with the received signal. One line is written at a constant velocity for each transmitter echo. The starting point of this display is controlled and always occurs at the same time after the transmitter is triggered. An assembly of six tubes is then photographed by a film strip camera. The traces are aligned for time coincidence for channel-to-channel comparison. Additional film space is used to record a data box which is flash illuminated.

The strip camera uses 400 feet of unperforated 35-mm film. The drive system consists of a closed loop servo-controlled capstan and a servo-controlled supply and take-up reels arranged to provide constant film tension. All friction trains are used to prevent any short time speed variations. Film travel may be adjusted from 0.1 to 1.0 inch per second. Figure 2 shows an enlargement of one channel.

The second type of recorded data is the amplitude distribution density of the echo pulses. The present instrument records only four channels, so that not all the available data is processed and recorded in this manner. This instrument, a pulse-height analyzer which uses photographic techniques, has been described previously³. Processed data from the radar is suitably displayed and photographed for a preset interval. The result shows the logarithm of the number of pulses versus the received echo voltage for the duration of the exposure.

The video channels selected for presentation on the gray wedge are also displayed in the form of voltage time plots on the chart recorder. The video is stretched and filtered for this recording. An additional 16-mm boresight camera is used to aid in correlating the data with the target. Timing pulses, synchronized with the amplitude distribution analyzer, are used to mark the film.

SYSTEM OPERATION

Calibration Calibration of the system is accomplished by use of free-flight balloons, fabricated from metalized Mylar. Balloons presently in use are 4 feet in diameter and provide a reasonable calibration at all three frequencies. Performance checks on the system are required prior to calibration. Remotely triggered rf sources and an antenna assembly are used to set receiver sensitivity, provide polarization reference signals for the X-band receiver, and aid in radar collimation.



Fig. 2

171

601305

Target Tracking The director containing the rf boxes and antenna, is rotated by amplidyne and motor drives mounted within the director. The system is presently tied in a servo loop with an optical means for target tracking. Range tracking is accomplished by a conventional unit operating from any of the six receivers used.

Target Aspect Determination The radar range, elevation and azimuth angles are displayed and photographed on the video recorder presentation. A computer program is used to determine the angles of the beam incident on the aircraft. For the program, the longitudinal axis of the aircraft is assumed to coincide with the flight path and the wings assumed parallel to the ground. Boresight films provide an approximate verification of the assumptions.

EXPERIMENTAL DATA

Interim X-Band System Measurements were made in late 1960 with an X-band polarization radar similar to the present system. Video from the four channels was stretched, filtered, and modulated for recording on magnetic tape. The output of the tape recorder was detected and played into a chart recorder for analysis. Data was taken on targets of opportunity, except for extensive tests on dihedral-corner radar navigational buoys supplied by the Coast Guard. Results of these tests are described in references 4 and 5.

Calibration of the radar for this series of tests was accomplished by use of a 6-inch aluminum sphere. A Kytoon was employed to lift the sphere 250 feet above the water at 2000 yards range. To minimize interaction of the Kytoon and sphere, the Kytoon was tethered at an altitude of 500 feet. The arrangement proved very satisfactory during calm weather, and optical tracking of the sphere provided a steady reliable radar calibration.

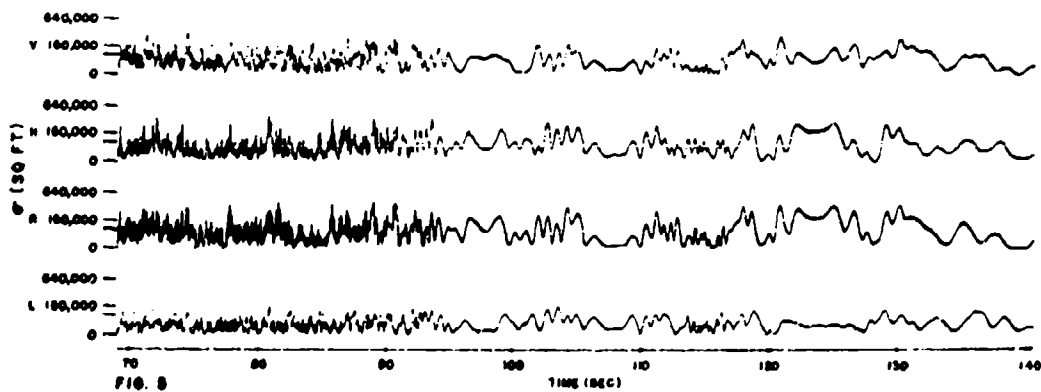
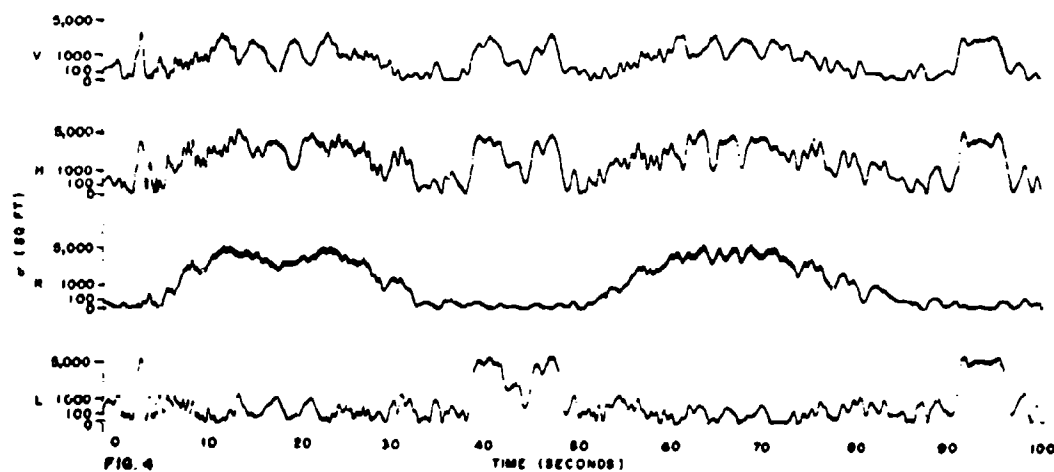
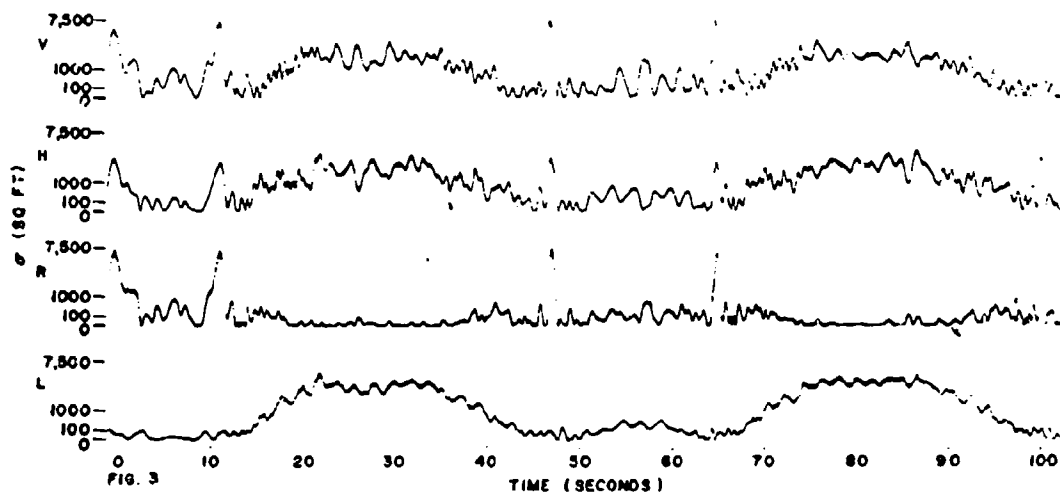
Voltage Time Plots Samples of the data from the radar buoys are shown in Figs. 3 and 4. Each chart is a complete run taken with a single transmitter polarization. The components are from top to bottom in each chart V, H, R, L. The voltage calibration is the same for the four returns on each run, but varies from run to run to make use of the dynamic range of the four-channel recorder. One large division from the bottom corresponds to zero volts on all recordings. For convenience, the calibrated echo area σ in square feet is given for each chart.

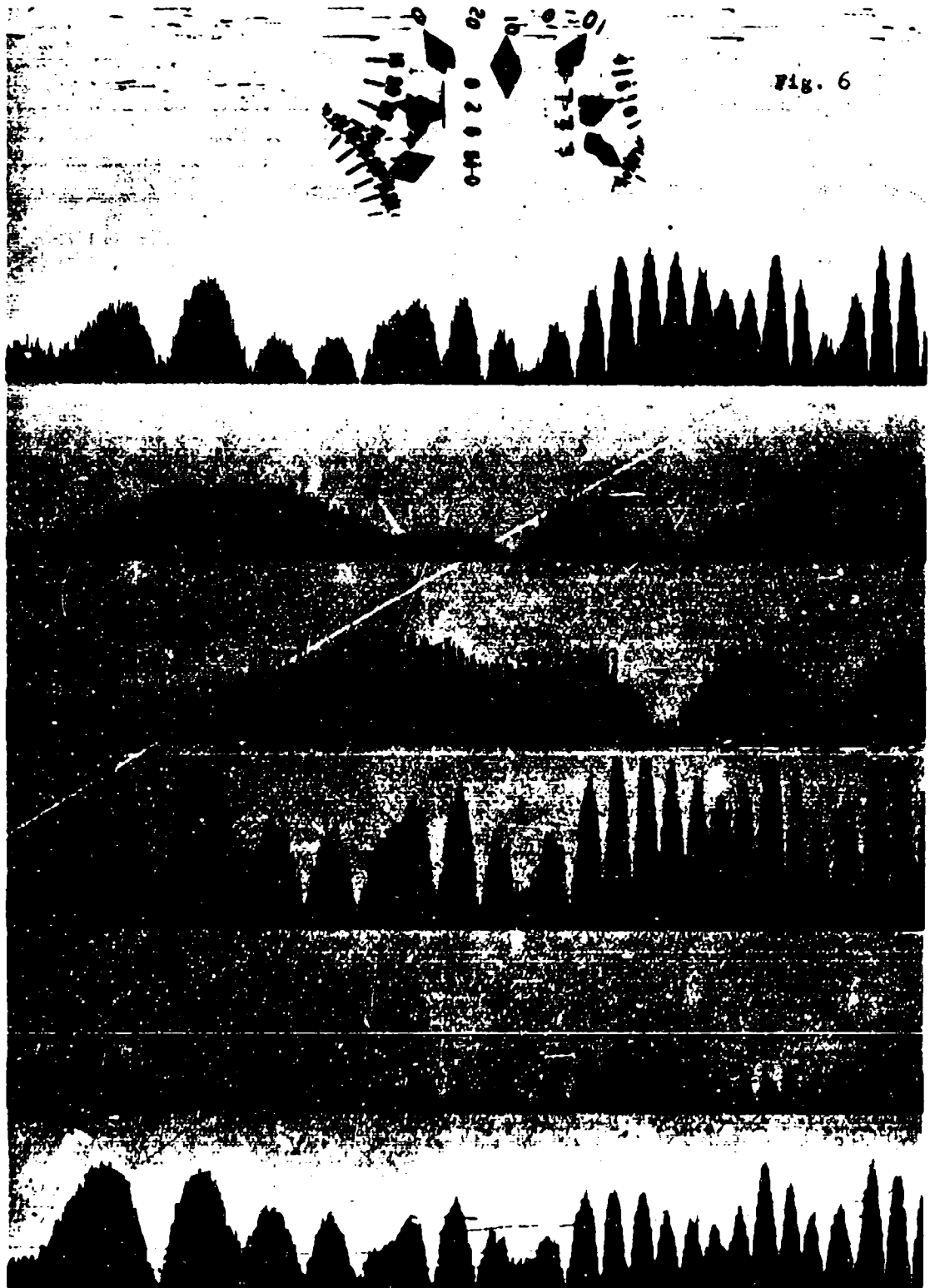
A general property shown by the data is that transmitting either vertical or horizontal polarization results in a return in which no cross-polarized component is generated, whereas transmitting circular polarization results in a return in which the cross-polarized component is present.

Run 47L (Fig. 3) is an example of almost ideal conditions for observation of a buoy and follows patterns made on a model buoy. Since each reflection (bounce) reverses the sense of circular polarization, the broad peaks in the left circular return indicate that a dihedral corner is being observed for most of the run. At this point it is not known which dihedral, that is, the one formed by two vertical plates or one vertical plate and the bottom plate. The opposite sense or right circular return shows sharp peaks at the times the broad peaks decay, indicating a single or triple bounce. The manner in which they occur in time would describe a slow oscillatory motion.

Run 48R (Fig. 4) shows the same oscillatory rotation as shown in 47L. The angle through which the buoy rotates appears to be decreasing; similarly, the angular velocity is decreasing. These conclusions are drawn from the flat plate response in the left circular return which is broad and more closely spaced in time than for run 47L, indicating the buoy stopped turning with the flat plate roughly perpendicular to the radar. Figure 5 is the return from a large tanker (range approximately 16,000 yards). Transmitter polarization is right circular. Since the same sense component (right circular) as transmitted contains significant amplitudes, the double-bounce mechanism, producing two polarization sense reversals, is prominent. Assuming that the ship was in continuous motion, a possible explanation is the large corner formed by the deck and superstructure, which was visible from the observed aspect angle. The power-density spectrum for both circular components in the 80 to 85 second interval contains components to 10 cps.

PRESENT SYSTEM Data recording presently uses 35-mm unperforated photographic film to facilitate pulse-to-pulse analysis and permit a ready comparison between the six receiver output channels. An enlargement of a $\frac{1}{4}$ second interval of this film is shown in Fig. 6. The image tones have been reversed from a normal printing to permit better reproduction. The data box at the top contains radar pointing and range information together with step attenuator positions and a run number identification. In the particular format used, the receiver outputs from top to bottom are: X_L , S_L , X_H , X_V , X_R . Horizontally polarized transmission was used on all bands. The target was a twin engine transport near a broadside aspect. A greater enlargement of a section from one channel, during a different run, is shown in Fig. 2. The particular section chosen illustrates the propeller modulation clearly. The detailed resolution provided by film, coupled with the channel-to-channel pulse alignment, provide a valuable tool in the study of target return. In addition, since data is recorded on relatively short lengths of film, a direct qualitative look at an entire run is readily available.





CONCLUSION The 3-band system described is currently in operation and being employed to examine a variety of aircraft. Each run consists of a straight course flown so that a pre-designated cross-over range is attained. Precision in flying the planned courses is a problem, since small errors in initial sighting of landmarks result in large errors at cross-over and departures from the planned aspect intervals.

In order to improve the accuracy of the courses, a TACAN System is being installed near the radar site. Since the ranges between the aircraft and TACAN are relatively small, close course control is possible.

BIBLIOGRAPHY

1. P. J. Allen and R. D. Tompkins, "An Instantaneous Microwave Polarimeter," IRE Proc. 47:1231, July 1958.
2. P. J. Allen and I. D. Olin, "A Four-Component Polarization Resolver for Microwaves," NRL Memo. Report 1086, April 1960.
3. I. D. Olin and F. D. Queen, Rept. NRL Prog., December 1958, pp. 42-44.
4. I. D. Olin and F. D. Queen, "Measurements using a Polarization Instrumentation Radar on Navigational Buoys," NRL Report 5701, November 1961.
5. I. D. Olin and F. D. Queen, "Measurements using a Polarization Instrumentation Radar on Selected Targets (U)," NRL Report 5755, April 1962.

A NEW METHOD OF CORRELATION OF DOWN-RANGE RADAR MEASUREMENTS WITH STATIC RADAR CROSS SECTION MEASUREMENTS

N. E. Pedersen
H. I. Halsey
J. F. Torrey
J. B. Clemente

Research Directorate
Research and Advanced Development Division
Avco Corporation
Wilmington, Massachusetts

ABSTRACT

Methods have been devised whereby re-entry vehicle dynamics during midcourse and early re-entry are directly correlated with static radar cross section returns of the vehicle. At present, only scale model measurements are used. Strong emphasis is placed on the statistical methods which are employed to obtain useful information. High speed computer techniques are used to provide this information in a short time and in a format which is easily interpreted. The procedures require the knowledge of radar cross section as a function of aspect and polarization angles, the various aerodynamic coefficients and dynamical constants for the vehicle, the statistics of the various thrust mechanisms, and the location and polarization of the radar.

INTRODUCTION

An important problem in the field of electromagnetic scattering has been the time and expense which are required to obtain experimental free space radar cross section data in quantities which are sufficient for the interpretation of actual in-flight data on various re-entry vehicles and satellites. In addition, the format of data readout in present radar cross section measurements facilities leaves much to be desired when it is necessary to correlate static radar cross section measurements with in-flight data. It is the purpose of this paper to describe experimental methods which are being developed in the Research Directorate at Avco/RAD to overcome a number of these difficulties. The general areas of application of the facility are:

1. The study of the overall scattering characteristics of various classes of scatterers, such as cone-spheres, etc., taking polarization effects into account.
2. The prediction of radar cross section signatures of re-entry bodies during midcourse and early re-entry. This includes most probable scattering cross section, scintillation frequency and scintillation amplitude, as well as the standard deviations of these quantities. These parameters are all given as a function of altitude and/or time. Cross polarization effects can also be studied.
3. The study of bistatic (or multistatic) scattering characteristics of various types of scatterers.

Due to the fact that the facility presently operates at 35 kilomegacycles, it is best suited for the measurement of dimensionally scaled targets which are composed of combinations of good conductors and/or non-lossy dielectrics.

The target orientation scheme is arranged in such a way that an axi-symmetric body can be positioned to simulate any combination of aspect angle and polarization angle of the incident electromagnetic field vectors with respect to the target. This is accomplished by rotation of the target about two mutually orthogonal axes. The extra angular degree of freedom, i.e. polarization, allows for the accumulation of data at a rate which is at least an order of magnitude faster than can be accomplished with conventional methods. This greater speed considerably broadens the functional capabilities of the laboratory, especially when the IBM 7094 digital computer at Avco/RAD is included as an integral part of the approach.

APPARATUS

The main geometrical features of the system are shown in Figure 1. The basic system has been in operation since February, 1961. A machined aluminum ring of 3 feet diameter is rotated by means of a servo motor which is mounted below the table. A 5-slip ring assembly is mounted on the rear of the ring which provides control power to the two synchro motors which are attached along a diameter of the ring. Rotations about these two axes are thus independently controllable. The microwave transmitter normally points down the axis of the ring. The axi-symmetric target is mounted at the center of the ring, with its symmetry axis perpendicular to the (monofilament nylon) target suspension lines. It can be easily seen that this geometry makes possible any orientation of the target axis with respect to the incident electric field vector. The receiver aperture can be positioned for any bistatic angle up to 90° by means of a

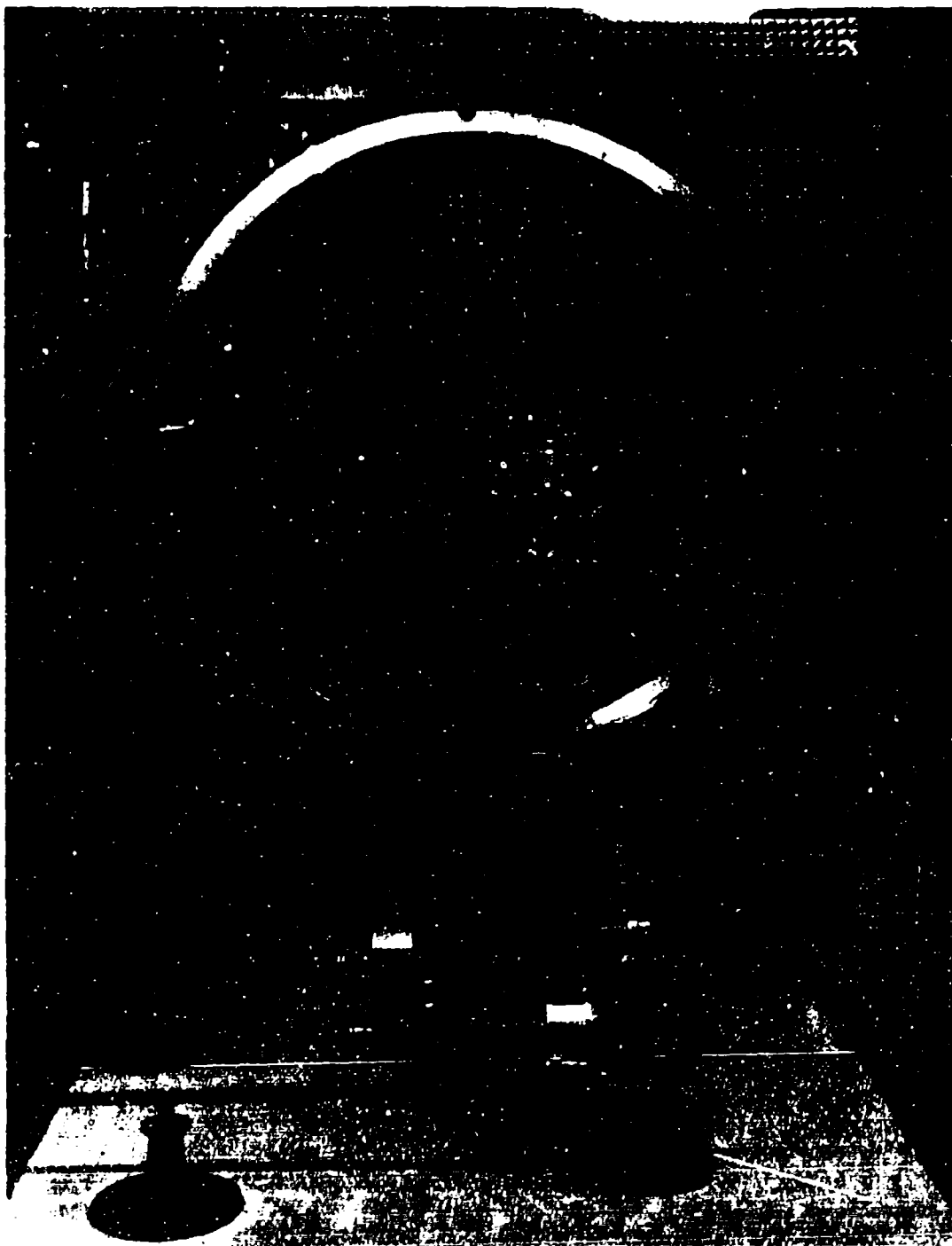


Figure 1

179

601345

rotary joint located below the ring. A similar joint can be used in the transmitter line for cross section measurements at bistatic angles up to nearly 180° , the maximum bistatic angle.

Also shown in Figure 1 is a microwave bridge arrangement which is used to null out the microwave background. In this bridge, a portion of the signal in the transmitter line is adjusted for the proper phase and amplitude, and is combined vectorially with the received background signal to produce a null when no target is present.

Figure 2 is a photograph of the portion of the laboratory which contains the microwave system. The microwave apparatus is mounted on a table which can be positioned at any elevation angle up to 30° . A large window in the laboratory was replaced by a pair of doors which, when opened, provide a large aperture through which the transmitter and receiver horns are directed. This feature of the scattering range affords the convenience of an indoor facility but retains the advantages of an outdoor slant range.

A late model Scientific Atlanta microwave receiver is used. This device has a basic accuracy of ± 0.2 db over a 60 db range. The receiver output can be used to drive either the (60 db) pattern recorder or it can be recorded on tape by means of the 7-channel Ampex tape recorder. This device has a frequency response of DC-10 KC in the FM mode, and can handle the entire dynamic range of signal level from the receiver. The pattern recorder, capable of recording in both rectangular and polar coordinates, has linear, square root, 40 db and 60 db plotting ranges. A radiation distribution printer is also used. This device has a basic accuracy of $\pm \frac{1}{2}$ db and $\pm \frac{3}{4}$ db in the 40 db and 60 db ranges respectively. It will print a matrix of radar cross section as a function of both aspect and polarization. The microwave source is a Litton Industries, type 8TFK2 klystron. This tube, which provides 20 watts of cw power, is operated by a specially designed Litton power supply. The above combination has proved to be exceptionally stable. The microwave background level has been measured to be consistently below -80 db below 1 m^2 . This is equivalent to less than -50 db below 1 m^2 at L-band, for example, which compares favorably with the present state of the art. This background level is determined through the use of calibration spheres, which is the usual method.

EXPERIMENTAL AND COMPUTATIONAL METHODS

It is the purpose of this section to describe methods and procedures which are being used, or can be used, to obtain quantitative predictions of scattering parameters for in-flight re-entry vehicles or satellites.

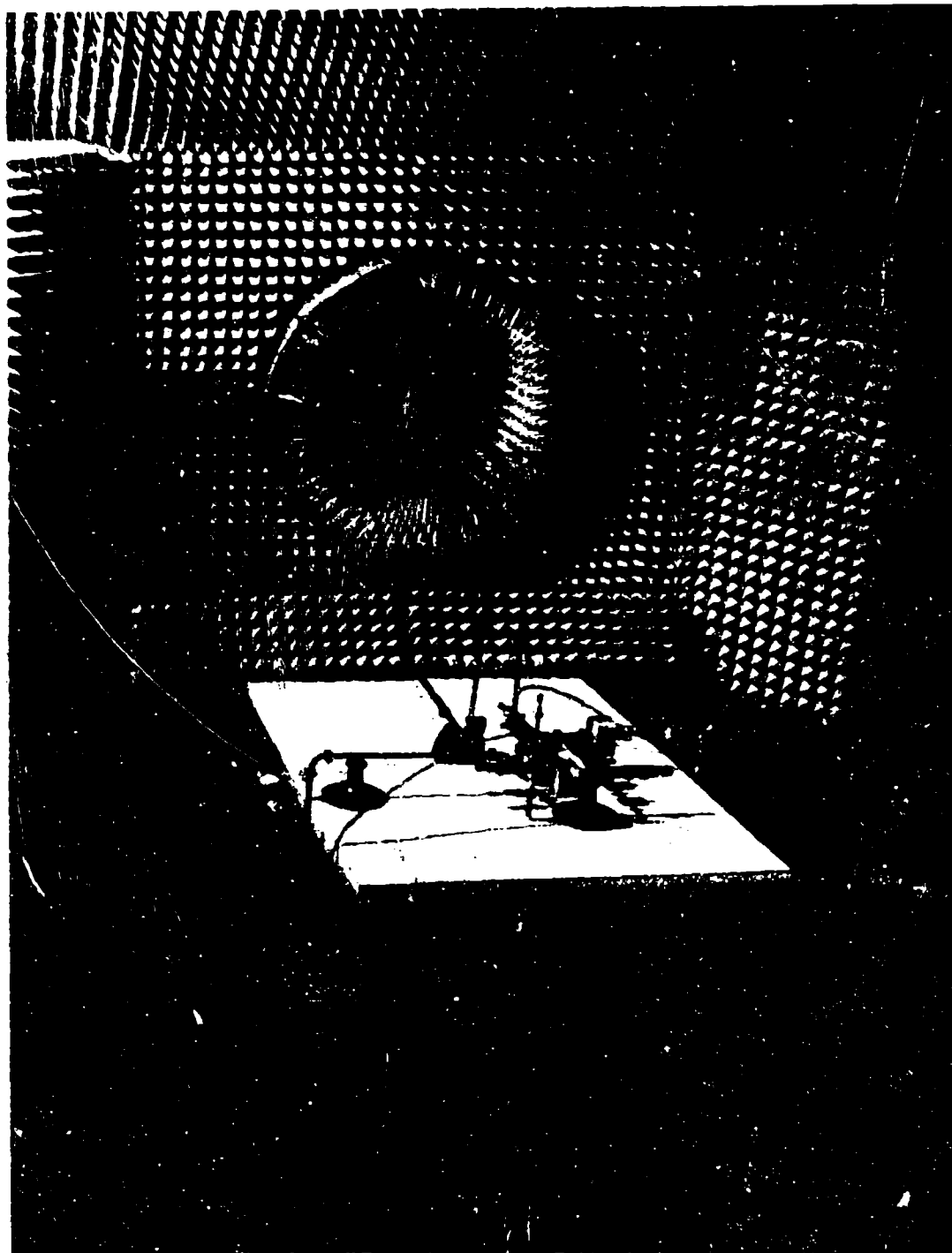


Figure 2

The dynamic radar cross section simulation techniques to be described below were conceived at Avco/RAD in October, 1962, and work was immediately begun to implement these ideas.

Although a great deal of in-flight radar information has been and is being obtained, there is in general insufficient information from static (range) measurements to correlate the measured down-range data with meaningful predictions. It is a purpose of this work to provide such predictions. A second objective is to provide radar cross section information in a form which permits comprehensive analysis of the effectiveness of an overall penetration aids system or a satellite decoy system. The accomplishment of these objectives is dependent upon:

1. A mathematical description of the in-flight vehicle dynamics, which depends upon the various forces (and the time of application) which are applied to the vehicle during the early part of its flight, as well as the various static parameters, such as moments of inertia, mass, static margin, etc.
2. The above forces and times are subject to known statistical variations from flight to flight. A knowledge of these probabilities leads to a well defined statistical distribution of vehicle motions.
3. A complete definition of scattering cross section as a function of aspect and polarization. This data must be available in a form which lends itself to a large number of separate trajectory "runs". The simulated down-range radar cross section information is then directly related to the above statistical probabilities for vehicle dynamics, and leads to well defined statistical probability distributions for the various scattering cross section parameters as a function of altitude or time.

This procedure appears rather formidable. However, the combination of already developed computer calculational techniques and the ability to rapidly measure cross section as a function of aspect and polarization makes it possible to do the job in a straightforward manner, at relatively small cost, and (most important) in a time short enough so that the results are still of value.

Use of the Aerodynamics 6-Degree-of-Freedom Code

The Aerodynamics group at Avco/RAD has developed over the years a computer code (code 967) which predicts, for a re-entry vehicle, its entire angle of attack history as a function of altitude and time. This code has been extremely useful in the development of re-entry vehicles as well as decoys. The inputs to the code are the

various moments of inertia, static margin, and other aerodynamic characteristics of the re-entry vehicle. The initial conditions are the altitude, latitude, and longitude which fix the location of the body in space; the flight path angle and azimuth angle which orient the velocity vector, three Eulerian angles which fix the orientation of the body in space, and three components of the angular velocity vector along the body axis which orient the angular momentum vector.

One of the authors (H. Halsey) has derived the mathematical relationships between the angular outputs from Code #967 (the 6-degree-of-freedom code), and the laboratory coordinates (which are the aspect and polarization angles at which a radar "sees" the target as it proceeds along its trajectory). The position of the radar with respect to the impact point is adjustable; the rotation of the earth is even taken into account. If sufficient RCS data is taken in the laboratory and is stored in the computer memory, it is clear that the output of the modified 6-degree-of-freedom code (# 1410) can be used to generate an RCS vs time or altitude profile for each run. Of course, these cross section profiles are generated as a direct consequence of the initial conditions which are used as inputs to the 6-degree-of-freedom code. Therefore, before too much significance can be given to individual RCS profiles, an understanding must be gained as to the probabilities of occurrence of the sets of initial conditions.*

The initial conditions for the 6-degree-of-freedom code are governed by the thrusts of the booster, spin, pitch and retro-pitch rockets, and the time durations over which these thrusts operate. The statistical fluctuations of the initial conditions for the 6-degree-of-freedom code are obviously the result of the statistical fluctuations of the various thrust parameters. It is very important to recognize that, although the thrust parameters and their statistical fluctuations are completely independent of each other, the initial conditions for the 6-degree-of-freedom code are not independent of each other. For example, an error in timing or thrust of the pitch retro-rocket will finally (after the spin rocket has been fired) result in errors in both pitch and yaw. This obviously involves more than one of the initial conditions. As pointed out above, one or several RCS profiles are of little value unless we know how likely is the occurrence of a given profile. What is really needed is a "most probable" RCS vs altitude (or time) profile, as well as the standard deviation of the RCS as a function of altitude or time. Similarly, the same type of information is needed in the case of scintillation amplitude and

* If the vehicle dynamics are specified (by telemetry, for example), at any point on the trajectory, only one RCS vs altitude profile would be necessary.

frequency,* cross polarization, etc. These quantities must be obtained through appropriate averaging methods. The averaging can best be done with a high speed computer, using standard Monte Carlo methods. However, such methods are useable only if the variables (the initial conditions in our case) are either independent, or if their functional relationship is known. At the moment, neither case applies. Therefore, it is necessary to go back in time to the case where the variables and their statistical fluctuations are truly independent. This is, of course, the time period during which the various forces are being applied. A computer code has been developed at Avco (Code #1570) which calculates all vehicle motions during this time period and provides the initial conditions for the 6-degree-of freedom code as a function of the completely independent set of variables each of whose statistical variations is well known.

The procedure, then, is to first generate a large number of sets of initial conditions by the Monte Carlo method. Each set has a known relative probability. Secondly, a radar cross section profile is generated from each set of initial conditions. Third, since the relative probabilities of occurrence of the various sets of initial conditions is known, the relative probabilities of occurrence of the various RCS vs altitude profiles is also known. These results can then be appropriately weighted and averaged to yield most probable values as well as standard deviations, both as a function of altitude or time. The procedure is outlined schematically in Figure 3. It should be noted that, in this case, the vehicle motions are not programmed. Instead, aspect angle data is taken over 360° for each increment of a few degrees in polarization. The entire matrix of RCS data is then stored in the (random access) memory of the 7094 computer. Linear interpolation provides RCS for any θ , ϕ . This makes possible an entire run every few minutes. The only real way to know if enough runs have been made is to observe the convergence of the averaged results and their standard deviations as more and more runs are made. Obviously, the shapes of the individual RCS vs θ patterns will be a strong factor in determining the rate of convergence. Also, the ranges of fluctuations of the various initial conditions will also be important. For example, if the target were a homogeneous sphere, its RCS profile would be a constant and would be completely independent of the initial conditions and of number of runs made. Conversely, if the vehicle were not spherical but if the initial conditions were precisely defined (only one set allowed), only one RCS profile would result.

* Scintillation amplitude and scintillation frequency would both be averaged to nearly zero in the most probable RCS profile.

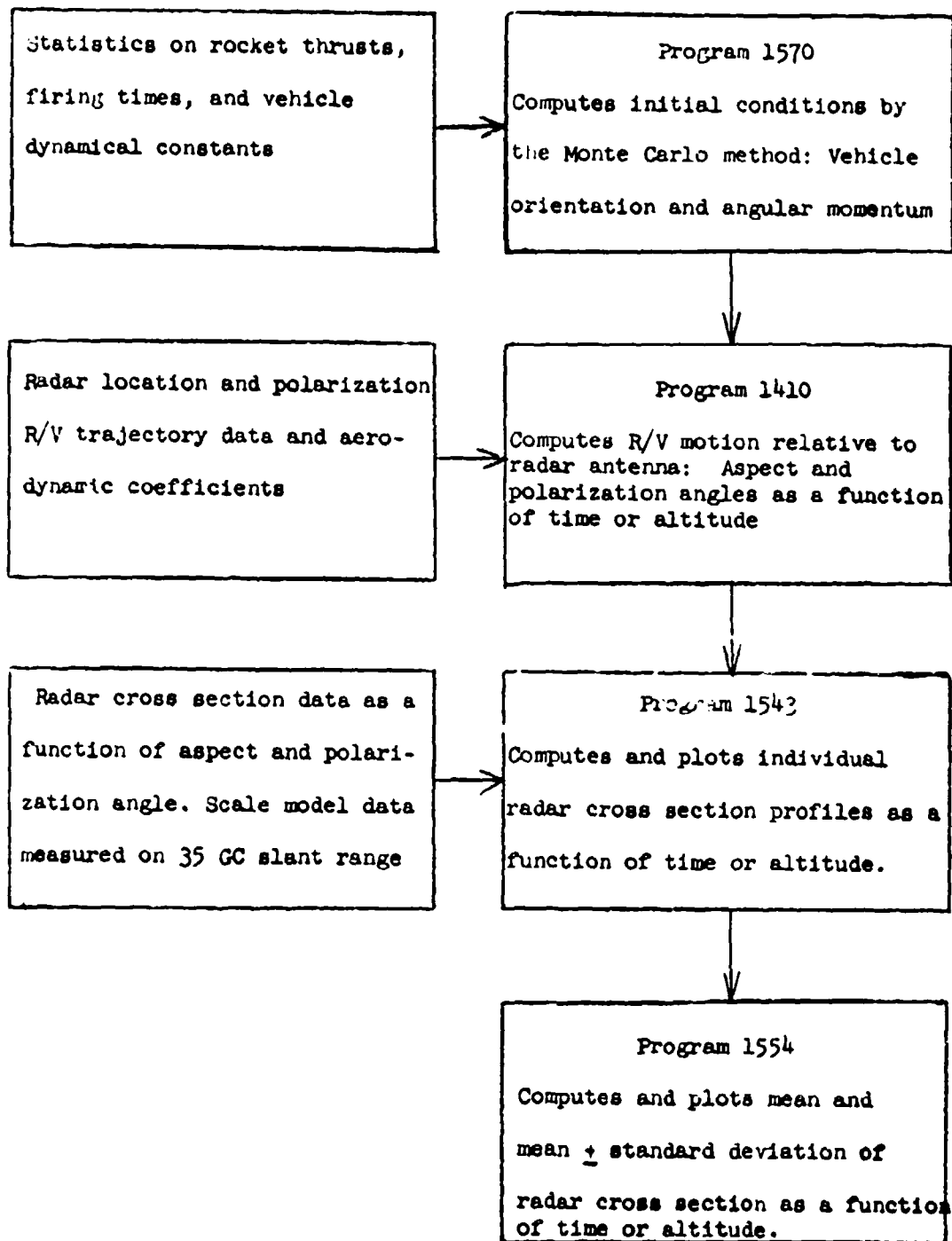


Figure 3

OTHER APPLICATIONS

One immediate application of the methods which were described in the last section is the prediction of RCS signatures of satellites and/or satellite decoys. In cases where frictional drag effects the body dynamics, the identical procedures which have been outlined would be used. When drag can be neglected, the problem is simplified in that a simpler code could be substituted for the 6-degree-of-freedom code. The satellite application can be broadened to include the bistatic case. In this case, we would provide a separate RCS matrix for each of a number of closely spaced bistatic angles (say 5° apart). This would amount to a 3-dimensional RCS matrix. The bistatic angle as well as θ and ϕ would be computed as a function of time, and linear interpolation would be used to predict the bistatic cross section of an orbiting object as a function of time.

In the case of one transmitter and a number of receivers (the multistatic case), the relative phases of the various received signals is of importance. The problem of phase could probably be handled in as complete a manner as the bistatic cross section case. Two receiver apertures would be used. They would be independently adjustable regarding bistatic angle, and an automatic phase comparator would be employed. Both receiver lines would be independently nulled. A three dimensional matrix of relative phase vs time would be provided and put into the computer memory, and trajectories run as described above. The result would be profiles of relative phase vs time.

It should be noted that three dimensional RCS matrices are required in the bistatic or multistatic cases since the bistatic angle(s) itself is a function of time.

DISCUSSION

The methods described above have been developed to the point where meaningful predictions are now being provided for certain vehicles. It is hoped that in the near future these methods will be used to correlate down range radar data on actual vehicle flight. Unfortunately, the re-entry vehicles which are actually flown do not have the same scattering characteristics as do the scale models. This is due to the presence of mechanical discontinuities, non-uniformities in the heat shields, etc. This problem can be dealt with by conducting a series of RCS measurements and an analysis on a scale model. The differences between the production vehicle and the scale model can be then taken into account by perturbation methods applied to the final scale model results. Of course, the effectiveness of such a procedure will be dependent upon how great is the deviation between the re-entry vehicle and its scale model. An alternative approach is to make many pattern measurements on the re-entry vehicle itself.

* INSTRUMENTATION OF A TRACKING RADAR FOR DIRECT RECORDING OF RADAR CROSS SECTION

Donald C. Watson, Senior Aerosystems Engineer
General Dynamics/Fort Worth

ABSTRACT

This paper contains a description of a technique for obtaining a capability of real time, dynamic radar cross section measurement by adding an attachment to a tracking radar. The AN/MPS-9 tracking radar is used as an example to show the adaptability of the attachment. The dynamic measurement instrumentation is shown in block diagram form, and a functional description of each block is presented in terms of signal flow. A procedure for calibration and operation is described for use with the instrumentation to enable direct calibration through the measurement of the backscatter from a sphere. Several of the possible error sources are discussed, and a brief analysis of instrumentation error is presented.

INSTRUMENTATION SCHEME

Dynamic radar cross section measurements can be effected with a tracking radar, if the various parameters in the radar range equation are known or may be measured. Several of the large tracking radars in existence today record the various parameters so that radar cross section may be calculated. However, in some cases, there appears to be added advantages in the use of a direct recording of cross section in decibels above one square meter (dbm^2).

The attachment presented in this paper is basically the receiving system developed and used by General Dynamics/Fort Worth for static radar cross section measurements with the provision added to compensate for target range variation. An accurate measurement is made possible through the use of a reference signal injection technique at the RF level.

System Operation

The measurement system to be discussed is essentially a large servo loop. A reference pulse is injected at the RF level. The system then maintains the reference pulse at the same level as that of the target pulse which is being measured. A variable RF attenuator is used as the sensor to convert signal level to radar cross section in decibels.

An understanding of system operation can be obtained by tracing a received signal through the block diagram shown in Figure 1. The received target signal to be measured travels through a variable RF attenuator and directional coupler which have been added to the basic radar

*Patent rights reserved

values obtained to a numerical ratio and subtracting 1.0 to obtain an error value, the following calculation may be made:

$$\begin{aligned} \text{Maximum error} &= \sqrt{0.24^2 + 0.26^2 + 0.26^2 + 0.26^2} \\ &+ 0.51 \text{ or approximately } 1.8 \text{ db} \end{aligned}$$

Therefore, the system RMS error is less than 1.0 db.

SUMMARY

The radar cross section measurement attachment presented in this paper will provide real time recording of the radar cross section of targets in flight. It is readily adaptable to most existing tracking radars and can be added without degrading the performance of the radar. The range normalization scheme can be used to provide an accurate and convenient means of removing range variations from the returned signal. Through proper system calibration and operation, measurement errors of less than 2.0 db are realizable.

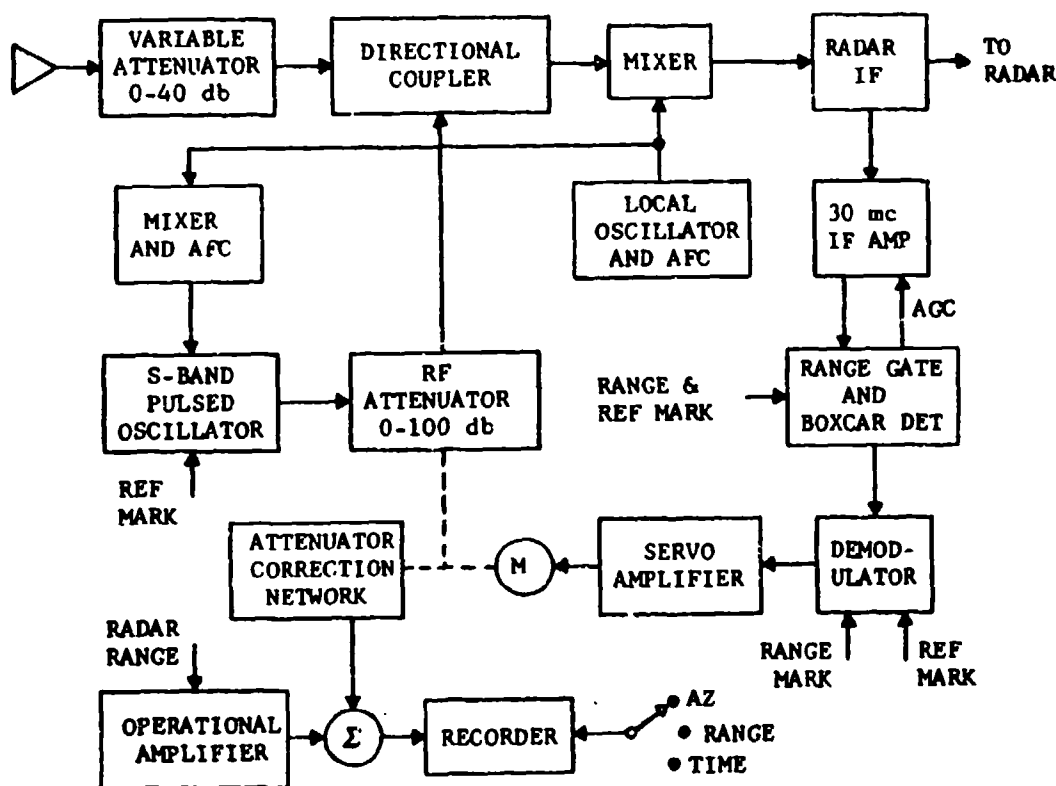


Figure 1. Dynamic Radar Cross Section Measurement Attachment

between the duplexer and the mixer. The RF attenuator allows a scale change to be made when a large cross section target is being measured. The reference pulse is injected just prior to the system trigger signal.

The injected reference pulse and the target pulse are converted to 30-megacycle pulses in the radar mixer. These two pulses are then picked up in the radar IF amplifier and are amplified in the system IF amplifier. The latter amplifier is gated on only during the time that these pulses are present. The gate used for the target signal is the tracking radar range gate. The gate for the reference pulse is obtained by using the radar pretrigger to trigger a gate circuit. The automatic gain control (AGC) is implemented so that it controls the IF amplifier gain as a function of maximum target signal strength. The AGC attempts to hold the amplitude of the target signal out of the IF amplifier at a constant level for insertion into the boxcar detector.

The signal waveform which enters the boxcar detector is composed of two 30-megacycle pulses. On a pulse-to-pulse basis, the first (target) pulse will be very nearly constant, and the following reference pulse will vary with target radar cross section changes. The boxcar detector, also called a recycling peak detector, is used to detect the peak signal level of an incoming pulse and to hold this value as an output until the next pulse is received. When the next pulse is received, the output level is first reduced to zero and is then immediately raised to the new peak signal level. Therefore, the output of the boxcar detector is a string of square pulses. Any difference in level between adjacent pulses is an indication of an error.

During each interpulse period, the demodulator sequentially samples the target signal level and then the reference signal level, each for a 20-microsecond time interval. These values are then stored in capacitors. A chopper and filter convert these values into a 400-cycle per second error signal. This error signal is a function of the difference in the signal level between the target pulse and reference pulse. The servo amplifier then amplifies the error signal to drive the servo motor. The motor in turn positions the RF-reference attenuator as a function of the error signal.

The reference signal is generated in a stable S-band oscillator which is gated on only at the reference time. The frequency of the reference oscillator is controlled by an automatic frequency control (AFC) circuit. The frequency of the reference oscillator is held at the radar transmitter frequency by mixing the radar local oscillator signal and reference oscillator signal and maintaining this difference frequency at 30 megacycles. The pulsed output of the RF reference oscillator is passed through a variable RF attenuator and is then injected as the reference pulse at the directional coupler ahead of the radar mixer. The attenuation produced by use of the variable RF attenuator is controlled by means of shaft positioning. The shaft is driven by the servo motor as explained above. This action closes the servo

loop, and the servo maintains the reference signal at the same level as the target signal by controlling the reference signal level logarithmically.

The RF attenuator is used as the sensor in obtaining a logarithmic function of radar cross section. It converts a linear rotational input to a logarithmic attenuation. The shaft position is a true logarithmic function of the reference signal level if the attenuator is logarithmic. Since the reference signal level is maintained equal to the target signal level, the shaft position may be converted to radar cross section at a given range by calibrating the position against a known value of radar cross section.

A true logarithmic attenuation, by the use of linear shaft rotation, cannot be obtained from commercial RF attenuators; the shaft position must be corrected to obtain a linear output in decibels. This correction is effected by matching the resistance curve of a potentiometer to the attenuation curve of the RF attenuator. Then, when the attenuator and potentiometer are mechanically coupled, the potentiometer resistance at the wiper arm is a true logarithmic function of radar cross section, i.e., it is linear in decibels.

A dc level is placed on the potentiometer, and the wiper arm voltage is recorded for static radar cross section measurements. However, since the target range is changing constantly in dynamic measurements, the range variable must be removed. This action is effected in the range normalization circuitry.

Range Normalization

The removal of range from the output of the measurement system involves normalizing the output so that all data is related to a particular range. In terms of the radar range equation, the signal returned from a target varies inversely as the fourth power of range, or received power decreases by 12 db per octave of increase in target range.

The normalization of the radar cross section of the target may be accomplished at the input of the measurement device by attenuating the incoming signal. If a variable RF attenuator is placed ahead of the mixer and the attenuator is controlled as a function of range, the range variable can be removed. When this method is used, the attenuation must be zero at the chosen maximum measurement range (normalization to maximum range). Then, as target range decreases from the chosen maximum, the attenuation must increase so that the signal strength obtained at the output of the attenuator remains constant for a constant radar cross section target. However, in such a scheme, the receiver must always be operated in an environment of near minimum signal level since the target appears to remain at the chosen maximum range insofar as the amplitude measurement is concerned.

An increased signal level may be used in the receiver at shorter ranges, provided range normalization can be accomplished at the output of the device. This is the approach presented in this paper, and it can be implemented by biasing the output from the servo loop described above by use of a function that varies logarithmically with range to compensate for signal variations which result from changes in target range. However, when this technique is used, the mixer and IF amplifier must be capable of handling a dynamic range of 100 db to allow for signal strength variation which results from range and radar cross section variations. The AGC allows the IF amplifier to handle the large dynamic range. The crystal detector is not linear throughout the full 100 db; however, since it is within the compensating servo loop nonlinearities which exist at the upper and lower end of the range tend to be removed. Nevertheless, the nonlinearities do reduce the system response and should be avoided where possible.

The range compensation scheme is shown in Figure 2. The signal from the sigma potentiometer consists of radar cross section information mixed with range information. All this data is summed, along with a logarithmic bias, to remove the range information. This bias level is controlled by use of the radar tracking range normalization circuitry. A potentiometer shaft is attached to the tracking range servo motor in the radar through the proper gear ratio to allow the use of the full potentiometer range over the radar tracking range. A dc signal, which varies linearly with tracking range, is then obtained from the potentiometer. This linear function is changed to a logarithmic function in the operational amplifier. The necessary output logarithmic function is $40 \log (\text{target range}/\text{minimum range})$. This function is used to convert the range information to the proper form to be summed with the sigma potentiometer output. The operational amplifier input and output functions are shown in Figure 3.

Integration with AN/MPS-9 Tracking Radar

The subject radar cross section measurement system may be attached to the AN/MPS-9 tracking radar without changing any existing circuitry. A variable attenuator and directional coupler must be added between the duplexer and the mixer. The remainder of the attachment involves the use of signals which are present in the radar.

The range gate and system pretrigger are obtained from the AN/MPS-9 synchronizer unit. Range information is available as a shaft position in the range computer unit. The radar local oscillator output must be brought out to the mixer in the attachment. The IF signal must be obtained in the radar IF prior to range gating.

Target azimuth angle information is needed to allow the recorder paper position to vary with target azimuth. If the radar antenna is referenced so that zero degree is north, the target azimuth angle (θ) is defined by use of

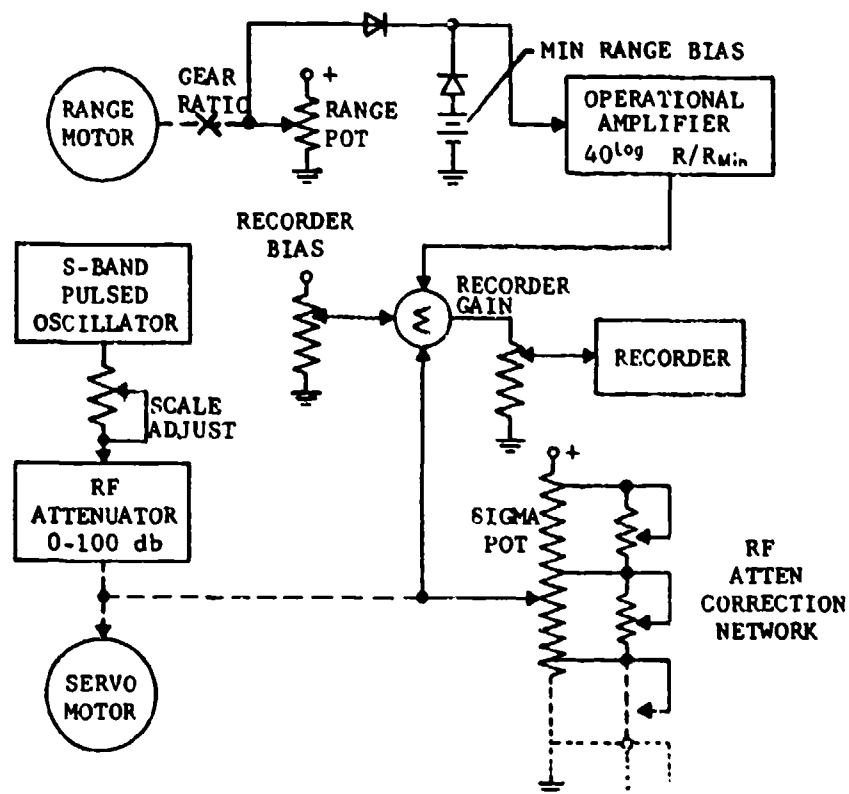


Figure 2. Range Normalization

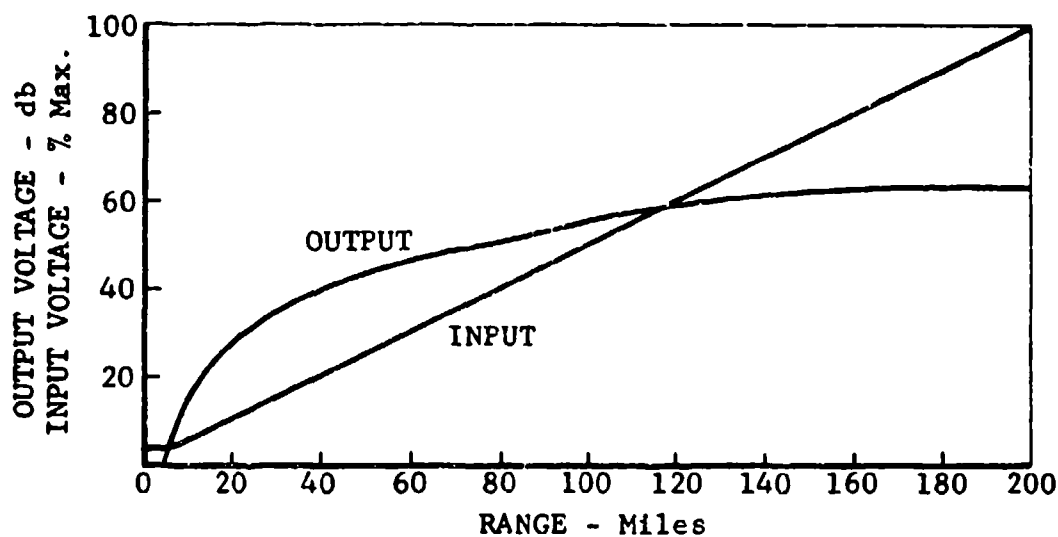


Figure 3. Operational Amplifier Input and Output

$$\theta = \text{antenna angle} + 180 \text{ degrees} - \text{target heading.}$$

This equation may be implemented by obtaining antenna azimuth information from the azimuth synchro. This is used as one input to a differential synchro. The second input to the differential is target heading which is inserted as a shaft position. Target heading may then be inserted manually or automatically (a data link is needed for automatic azimuth positioning). The differential output then is target azimuth angle.

The maximum range at which a specific cross section target may be tracked with the AN/MPS-9 can be calculated by using the radar range equation. This calculation indicates that a one-square meter target may be tracked to approximately 35 miles. Ground return and high side lobe return prevent the use of this radar below approximately 5 miles for cross section measurements. Therefore the AN/MPS-9 radar with the subject attachment will provide a dynamic radar cross section measurement capability of 5 to 35 miles in range on a one-square meter target.

OPERATION PROCEDURE

The radar cross section attachment discussed thus far can be used to measure the radar cross section of a target which is being tracked by the radar, in dbm^2 , provided the device is calibrated against a known standard radar cross section. In order to eliminate unnecessary errors and obtain maximum utility, the following calibration and equipment setup is suggested.

Calibration

A helium-filled, metallic-coated, spherical mylar balloon can be used as the calibration standard. The balloon is put into the air by permitting it to rise on a string to several hundred or possibly to several thousand feet at a range dictated by radar ground clutter. The balloon should be high enough to raise the antenna beam above the ground and far enough in range to avoid the ground clutter. The operation amplifier for range normalization is set for 0 db output, and the recorder gain is adjusted to obtain a 100-dbm^2 plotting scale.

The radar is then allowed to track the balloon. The value of radar cross section obtained from the balloon is plotted on the recorder, and the tracking range is recorded. From the recorded range and the calculated balloon radar cross section, it may be determined what recorder value corresponds to the radar cross section value of the sphere when the range is normalized to one nautical mile. It will be necessary to vary the balloon height through several altitude positions to insure that there is no interference from a ground-reflected wave.

Once the radar has been calibrated in this manner, it is highly advantageous to establish a transfer standard so that the calibration

may be checked periodically without putting the balloon up each time. This calibration is effected by picking a prominent but isolated target (water tower, smoke stack, TV tower, or other convenient, permanent target) in the area at a range of several miles. The radar is directed onto this target immediately after the balloon radar cross section is plotted. By plotting the value of the transfer standard, the radar cross section of this latter standard will be established with respect to the spherical balloon. If the transfer standard and weather conditions do not change, this standard will be available to check the calibration before and after each plot. It should not be necessary to check calibration by use of the spherical balloon more than once or twice a day, provided there are no drastic weather changes.

Operation

Upon establishment of a transfer standard, the attachment is set up to measure radar cross section; however, a plotting scale should be established on the basis of the approximate radar cross section value of the target to be plotted. For example, it may be assumed that a target with an average radar cross section of 100 square meters is to be plotted and that the variation of cross section of the target with azimuth angle will be 50 db. (This variation will cover the range of variation of radar cross section of most aircraft and missiles.) If the AN/MPS-9 radar is used with the attachment set for a minimum plotting range of 4 miles, the radar and attachment should be capable of detecting a -40-dbm^2 target at 4 miles. Therefore, to preserve this sensitivity, the 100-db RF attenuator should be adjusted to 40 db of attenuation for a 20-dbm^2 value at 4 miles. This adjustment allows the attenuator to reach its maximum attenuation of 100 db at the approximate minimum discernible signal (MDS) for the system on a 20-dbm^2 target. The adjustment is made by locking the radar on the secondary standard and adjusting the RF reference oscillator output until the following equation is satisfied:

$$\begin{aligned} \text{Ref. Attn. Value} &= (\text{MDS in dbm}^2 \text{ at range of transfer std.} \\ &\quad - \text{target cross section} + 100 \text{ db}). \end{aligned}$$

The recorder bias should then be adjusted to place 20-dbm^2 at the center of the recording scale. The attachment is then ready to plot a 20-dbm^2 target with maximum utilization of system dynamic range.

If the 20-dbm^2 target is approaching the radar site, it should be detected at approximately 130 miles. However, at this range, if the radar cross section varies below 20-dbm^2 , track will be lost. The attachment has been set up so that the 100-db attenuator will be near its maximum limit of attenuation when radar track is lost. As the target range is decreased from maximum range, the received signal strength will increase at the rate of 12 db per octave of decrease in range. The attenuation provided by the 100-db attenuator will decrease, and the functioning of the attenuator will not involve operation near

the 100-db limit. Consequently, the minimum radar cross section needed to produce a detectable return is also decreased. Over the range of 30 miles to minimum range (4 miles), the target radar cross section may vary by plus or minus 25 db without forcing the 100-db attenuator to either limit. If a target to be plotted has a very large radar cross section, it may be necessary to attenuate the incoming signal in order to be able to plot over a specific range increment without being limited by maximum plotting range. Nothing can be done to shift the lower plotting limit short of increasing the sensitivity of the radar.

INSTRUMENTATION ERROR ANALYSIS

There are several possible sources of error in the combined system of a tracking radar with the subject attachment. These error sources include interference from a ground reflected wave, radar tracking errors, and calibration errors which result from a change in weather conditions. Most of these errors may be detected and avoided through proper system analysis. The errors encountered in the attachment and its calibration device are considered the instrumentation errors and will be present in measurements made with the attachment.

Range Potentiometer Error

If it is assumed that a precision 10-turn potentiometer is used for the range potentiometer, a reasonable expected accuracy is 0.025 per cent linearity with a resolution of 1 part in 10,000. If the potentiometer is adjusted to use the best linearity over a 200-nautical mile range, the maximum linearity error is $(200) (.00025) = 0.05$ miles. The maximum error which results from potentiometer resolution is $\frac{200}{10,000} =$

0.02 mile. If it is assumed that these independent errors are normally distributed and are not exceeded 99 per cent of the time, the maximum potentiometer error may be obtained by use of the equation for the standard error of a sum,

$$\sqrt{0.05^2 + 0.02^2} = 0.054 \text{ mile maximum.}$$

This value may be considered three standard deviations or the maximum error. However, the potentiometer output is the input to an operational amplifier with a transfer function defined by

$$y = 40 \log \frac{R}{R_{\min}}$$

where y is the output, R is the measured range, and R_{\min} is 4 miles, as proposed earlier. Therefore, the maximum error in y resulting from an error in R may be obtained by taking the differential,

$$dy = (40) (4) \frac{(0.434)}{R} dR$$

By using $dR = 0.054$ miles, as obtained above, then

$$dy = \frac{3.74}{R}$$

Therefore, the maximum resultant potentiometer error occurs at the minimum range of 4 miles. This maximum error is 0.935 db and decreases rapidly with range.

Operational Amplifier Error

It is possible to build a dc operational amplifier with the output shown in Figure 3 with an accuracy of 0.5 db without a great deal of difficulty. In order to allow for slight drift and aging, a maximum error of 1.0 db is assumed.

Servo Loop Error

Error in the servo loop, which is used to measure radar cross section and range variation, is attributable primarily to the linearity of the attenuator. Any bias errors in the loop are a result of errors in calibration. Through proper matching of the sigma potentiometer network curve to the RF attenuator curve, it is possible to obtain the 100-db range with an error in linearity of less than 1.0 db.

The servo loop has a response of 120 db per second through the mid-range of the system. It is impossible to determine the maximum rate of change which will be encountered in measurements; however, 120 db per second appears adequate to plot target scintillation without appreciable error.

Calibration Errors

In addition to the electronic instrumentation errors, the other instrumentation errors encountered in calibrating the system consist of errors which result from the use of an imperfect sphere and from variation in the return from the transfer standard. Experience at the General Dynamics/Fort Worth static radar cross section range indicates that this composite error is less than 0.5 db when approximately perfect spheres are used. The sphere proposed for use with this system will not be as perfect a sphere as those used on the static range. However, the average backscatter from the sphere should not vary from that of a perfect sphere by more than 0.5 db, and the average value is used for calibration purposes. In view of the possibility of slight error from interference and transfer of the standard, a maximum calibration error of 1.0 db seems realistic.

System Errors

The instrumentation system maximum error may now be calculated by using the maximum errors determined above. By converting the db

SECTION VII
RANGE DESCRIPTIONS

THE UNIVERSITY OF CALIFORNIA
IMAGE-PLANE REFLECTIVITY RANGE

D. J. Angelakos and F. D. Clapp
Electronics Research Lab., U. of California
Berkeley 4, California

The scheme used in reflectivity measurements at the University of California consists of an image-plane range in conjunction with a magic-tee circuit. The mechanical and electrical characteristics of the range are described.

GENERAL

The reasons for constructing an image-plane range instead of other types were as follows: (1) The projected use of the equipment involved mainly the experimental verification of theoretical results so that the shapes of the scatterers to be measured could be chosen with a symmetry suitable for measurements with this type of apparatus. Of course, this limits the choice of objects by excluding such models of aircraft fuselages for example. (2) The presence of the ground plane provides a field-free region for placement of auxiliary equipment and the operator where their presence will not disturb the experiment. (3) The use of the equipment for near-zone measurements is made possible by permitting the protrusion of field probes through the plane.

The procedure followed in obtaining back-scattering measurements is straightforward and makes use of a simple concept. Referring to the block diagram of Figure 1, the procedure is as follows. Adjustment of the tuner will allow a null to be obtained at the detector with no target on the plane. Placement of the target will now produce an output at the detector proportional to the backscatter from the target. By placing first an object of known cross-section and noting its scattering, the cross-section of the unknown target can be deduced by comparison.

Accurate measurement by this method requires that the depth of the initial null must be considerably below the signals which are to be observed. If it is not, destructive interference results between the desired signal and the residual at the output, being affected by the position of the target. For targets of small scattering, initial nulls of from 90 to 100 db below incident fields are required.

Reflections off of the wall facing the illuminating horn and 15 feet away are reduced by 20 db using absorbing material. The phase effect mentioned in the previous paragraph can be effectively circumvented by pulling the scattering object along the image-plane on the centerline away from the horn while making a graph of the backscattered signal versus distance. With a linear detector this should ideally result in a

curve proportional to $1/R^2$ - in practice the desired curve will have superimposed on it a more or less sinusoidal variation. The magnitude of the sinusoidal variation is generally small for most scatterers so that the required averaging process can easily be performed.

MECHANICAL DESIGN

The image-plane is 12' by 12' designed for use at X. It is constructed of several sheets of honeycomb sandwich side de, each comprising an epoxy-glued aluminum core about one inch thick with thin aluminum skins glued on the core. This construction results in a very strong, but light, surface, and one which can be held quite flat over the entire area. The joints between pieces are made by molding in a piece of 1" by 2" aluminum bar along the edges to be joined and machining a lap joint. The underside of the lap is made a few thousandths of an inch narrower than the top side, so that the latter can be pulled up as tightly as possible. Similarly, the thickness of the top lap is made slightly thinner than the bottom lap so that a series of adjusting screws placed at intervals along the underside will allow the surfaces to be adjusted to a perfectly smooth joint, avoiding any step in the plane which might otherwise occur due to bending or imperfect machining. A detail of the joint is shown in Figure 2.

Two concentric turntables are supported in an appropriate position about two thirds of the distance from the driving end. The outer table (actually a rotating ring) is about 30" in diameter and contains the inner table of about 12" diameter. The two may be driven as a unit, or either independently. The outer ring also has a radial slot 8" long with a drive carriage underneath which can carry an electric field probe. Thus it is possible to rotate an object on the inner table to the correct aspect relative to the transmitting horn, lock it in place, and to rotate the probe to any point outside of it on the surface occupied by the outer ring.

Contact between table rims and the remaining surface is obtained by a specially designed wiping-finger contact. This is shaped to the turntable edge and held in place by a slightly corrugated metal band which acts as a spring to keep tension on the finger stock. The latter has an elevation of only 0.003" above the image-plane surface, causing very small reflections.

The inner table is geared to a selsyn transmitter which conveys angular information to a polar recorder used for recording polar backscatter patterns when required.

In making backscatter measurements of the type described, one of the principal problems is that of placing and removing targets from the ground plane surface without mechanical jarring which may upset the null balance.

To accomplish this, a rotating platform supported by a column secured at both floor and ceiling and completely independent of the image-plane support structure has been built to carry the operator over any portion of the image-plane. The platform is swung away during the time the actual measurements are made.

ELECTRICAL CIRCUIT

The electrical circuit is shown in Figure 3. Presently, the signal source consists of a Dymec type 2650A synchronizer which synchronizes the output of a Varian V58 oscillator to a microwave signal derived from a crystal controlled standard. An HP type 716A power supply is used since it has superior regulation on all voltages and supplies well-filtered d-c to the klystron heater. The klystron is forced air cooled by a blower with a mechanical filter to remove vibration. Stability runs using a frequency counter have indicated a stability of ± 200 cps in the 9330 mc/s output frequency over several hours. Residual hum and FM are extremely low as is amplitude modulation.

The tuner is a specially constructed item with coarse and vernier adjustments in order to obtain the high balance required. Three screws are mounted along the center of the wide side on a waveguide section machined from an aluminum block--these serve as the coarse adjustment. The vernier adjustment is obtained from three screws along the center line of the narrow side of the guide. Spacing between screws in each set is about 240, 480 and 720 electrical degrees at 9330 mc/s. The vernier screws are located midway between the coarse screws to save space.

The magic tee is machined from a solid aluminum block. Matching post and iris give a separation of about 70 db between the E and H arms.

The present detecting system is a homodyne type (a superheterodyne in which the local oscillator (LO) signal is derived by frequency shifting the original signal by means of a rotating phase shifter) somewhat similar to one described by Bell Labs. workers some years ago. The phase shifter is a modified Hewlett-Packard type X-885A provided with high-speed ball bearings and driven by a synchronous motor at about 8250 rpm. This results in a change in frequency of about 275 cps. Figure 3 shows the detecting scheme. The output of the balanced detector is a signal of 275 cps proportional to the desired microwave signal. This is amplified by an HP-415B amplifier which has had the internal filters adapted to the 275 cps frequency.

The detection law is linear so that the 10 db scales on the VSWR meter become 20 db steps. Using 1N23E crystals with a LO current of about 1.0 ma, the noise level of this detector system is about -100 dbm. Lower noise level performance is possible using the new junction detectors specifically designed for low i-f superheterodynes.

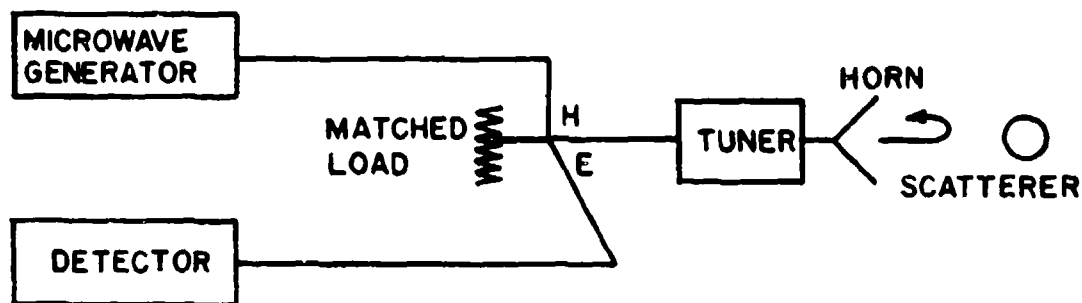


Figure 1. Block diagram of circuit.

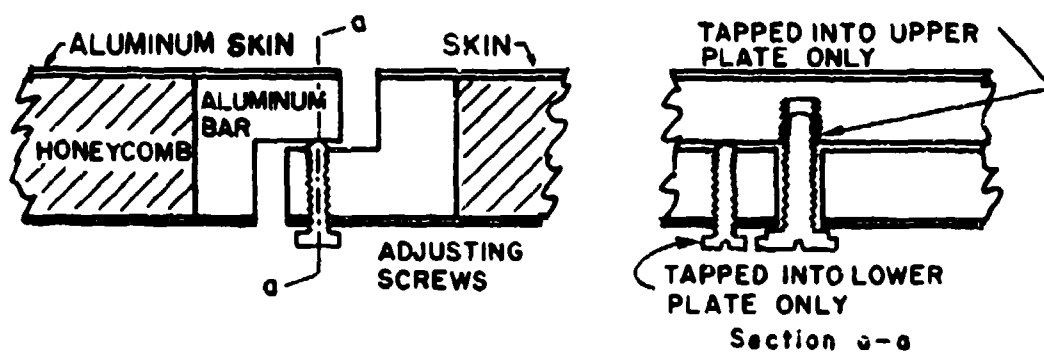


Figure 2. Mechanical detail of image-plane joint.

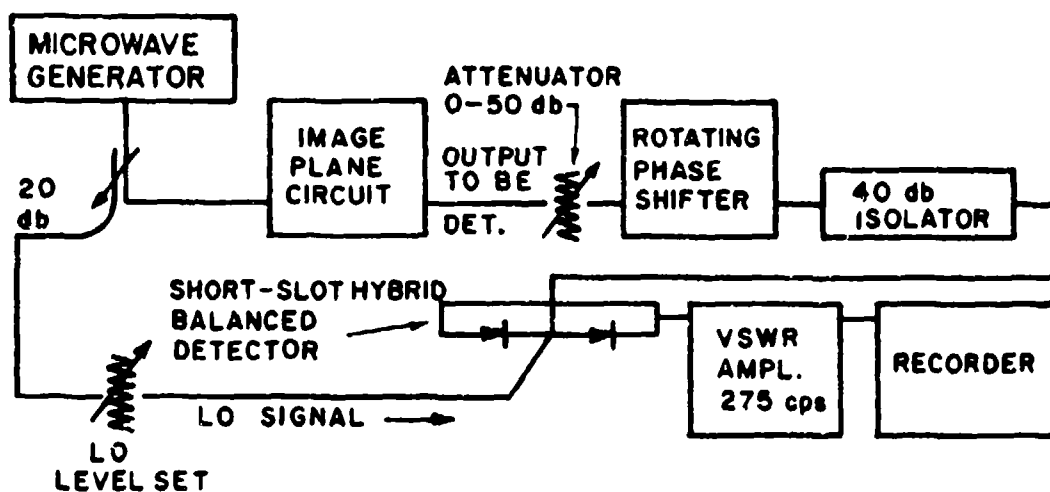


Figure 3. Electrical circuit detail.

AVIONICS LABORATORY RADAR CROSS SECTION
MEASUREMENTS FACILITY

W.F. Bahret, Electronics Physicist
Air Force Avionics Laboratory
Research and Technology Division
Wright-Patterson Air Force Base, Ohio

The facility to be described is physically located in building 821, Area B, Wright-Patterson Air Force Base. This building has an unobstructed floor space which is 100 feet wide and 200 feet long and a parabolic-arched roof whose peak is about 90 feet above the floor. The area used for cross section measurements is bounded by movable panels of radar absorber material and is 65 feet long by 30 feet wide. However, the arrangement is flexible and may be adjusted to suit the needs of any particular target. At the time of this writing the absorber panels on the sides of the chamber are each 8 feet high by 8 feet wide and are tilted 10° back from vertical. The backwall (that viewed directly by the measurements equipment) is 12 feet high x 20 feet wide, and is also tilted 10° from vertical. Work is underway to increase the height of the side panels to 12 feet and the size of the backwall to 20 feet high by 30 feet wide.

Targets are supported either by thin nylon line (8 lb test) or shaped styrofoam columns as appropriate for the size, weight and radar cross section of the body. The strings, if used, are suspended from an overhead bar, 16 feet above the floor, and are tied to a rotatable platform on the floor for rigidity and control of target azimuth.

The bulk of our instrumentation is conventional CW apparatus typified in Figures 1 and 2 of a companion paper.* Currently S band (2600 - 3900 mc), C band (4000 - 5800 mc) and X band (8200 - 11,000 mc) systems are in operation while L band (1120 - 1700 mc) and X_H band (5850 - 8200 mc) are being added. All systems are tunable over the frequency ranges indicated to permit evaluation of such things as radar absorber materials. All have or will have the capability to detect target cross sections of 10^{-3} square wavelengths or less at a range of 25 feet. All have antennas with beamwidths in the order of 10° to 12° in both E and H planes. Transmitted power levels are in the 0.25 to 1.0 watt range. Receiver sensitivity is approximately -85 DBM to -90 DBM over the frequency range.

Because of antenna size, all systems except X band use a single antenna with a hybrid tee junction and tunable load for "nulling" the received signal in the absence of target. The X band system uses separate horns for transmission and reception and a background nulling technique that involves movement of the chamber backwall (see referenced paper.) The C band, X band and the new X_H band systems use "tunnel" antennas which have low sidelobe levels and, for the dual-antenna arrangement, very low cross talk. The "tunnel" section,

*"Comments on Static Radar Reflectivity Measurements Techniques" by W.F. Bahret, published elsewhere in these proceedings.

an absorber-lined extension of the sides of the normal horns, does not influence main lobe amplitude or beamwidth but diminishes side lobe levels by more than an order of magnitude. Figure 3 of the referenced paper presents patterns on an X band horn with and without absorber extensions and demonstrates typical performance. Leakage between the X band tunnel antennas when side by side is down by more than 100 DB below transmitted power.

Our facility also includes a short pulse (10 nanoseconds) X band radar which was obtained from Harry Diamond Fuze Laboratory. This fixed frequency (9325 mc) radar has a pulse repetition rate of 25 kc and a peak output power of approximately 50 watts. The block diagram of the system is shown in Figure 4 of the companion paper. The superheterodyne receiver uses a balanced crystal mixer and an IF amplifier tuned to 450 mc with a bandwidth of 100 mc. A sampling oscilloscope provides a conventional pulse amplitude versus range display. At the time of this writing, target cross sections are determined by a manual read-out technique in which an attenuator in the RF line to the receiver is adjusted to reduce all target signals to a standard height on the oscilloscope. Receiver noise figure, which is not particularly good in this radar (approximately 20 DB), limits minimum measurable target cross sections to $8 \times 10^{-7} \text{ M}^2$ at a range of 15 feet. A parametric amplifier now on order is expected to improve performance by almost two orders of magnitude. The beauty of this pulse system is the automatic elimination of all chamber influence upon the measured echo from a target - a situation which cannot be obtained for low cross section targets with a CW system.

In addition to the improvements mentioned above for this facility, we are obtaining a short pulse system which will operate at 3000 mc and will be capable of automatic recording of target echo. This automatic recording capability is also to be added to our X band system and should reduce the time for recording a target pattern by a factor of 10. The technique to be used for recording, which involves long time integration of received pulses, is expected to improve the sensitivity of the systems such that the echo from a 10^{-7} M^2 target at 25 feet will have a 20 DB signal-to-noise ratio.

It is important to note that the minimum detectable target cross sections mentioned earlier for the CW systems are not necessarily the same as the minimum sizes which can be measured accurately. As pointed out in the referenced paper, the effect of changes of background level due to introduction of a target may be so large that only targets with cross sections several orders of magnitude larger than minimum detectable may be measured with any assurance of accuracy. This effect is a function of the target parameters, so no single number can be specified for "minimum measurable." For the short pulse systems, minimum detectable and minimum measurable are essentially the same.

RADAR CROSS SECTION MEASURING EQUIPMENT AND RANGE

P. Blacksmith and R. Mack
Air Force Cambridge Research Laboratories

Introduction

This report was written to describe in detail the model radar cross section measuring system which has been developed at the Microwave Physics Laboratory of the Air Force Cambridge Research Laboratories, Bedford, Mass., for making dynamic measurements of radar reflection characteristics of targets, such as missile configurations and aircraft.

Site

The system used at the Air Force Cambridge Research Laboratories is located at Ipswich, Mass., and operates on X-band (9302.4 Mcps) and S-band (3100.8 Mcps). It can be used for measuring either monostatic or bistatic cross sections. The site is located on a hill overlooking the ocean and is ideal for measurement work since reflections from extraneous objects are reduced to a minimum. The measurement ramp extends 90 ft from a penthouse in which the transmitting horn and receiving equipment are located. The lower level of the structure contains the frequency generating equipment.

Electronic Equipment

Fig. 1 is a block diagram of the complete system. During bistatic operation the hybrid junction is dispensed with, and separate horns are used for transmitting and receiving. To balance out the equipment for bistatic operation, power is extracted from the transmitter chain through a directional coupler, and fed to the receiving antenna through a precision phase shifter and attenuator.

The basic system consists of three units which generate the proper frequencies. Fig. 1 designates these units as the Transmitter Chain, the Local-Oscillator Chain, and the Adder-Multiplier Chain. A 100 Kcps cw signal is fed from a General Radio Secondary Frequency Standard to the transmitter chain and the adder-multiplier chain.

Multiplication in the transmitter chain by 3^5 or 243 in the multiplier circuits yields a frequency of 24.3 Mcps. This frequency is added to a frequency of 6.4 Mcps (obtained from the adder-multiplier chain) in the adder unit to obtain a resulting frequency of 30.7 Mcps. Proceeding through another adder a frequency of 1.6 Mcps (obtained from the adder-multiplier chain) is added to the 30.7 Mcps to obtain a frequency of 32.3 Mcps. This frequency of 32.3 Mcps

is then fed to a multiplier resulting in an output of 258.4 Mcps. Depending on the band of operation required, this output can be used in the appropriate circuits. Operation in L-band [$4(258.4) = 1033.6$ Mcps] can be obtained through the conventional cavity lighthouse-tube circuits. Operation in S-band [$12(258.4) = 3100.8$ Mcps] is available by feeding the 258.4 Mcps into a 2K47 amplifier-multiplier klystron. Operation in X-band [$3(3100.8) = 9302.4$ Mcps] can be realized by taking the output from the 2K47 and feeding it into a 2K46 amplifier-multiplier klystron. All measurements made with this equipment at the Air Force Cambridge Research Laboratories have been done at X- and S-bands.

The local-oscillator chain is similar in operation and construction to the transmitter chain for the purpose of identification. The major difference between the local-oscillator chain and transmitter chain is that three different frequencies can be obtained in the former chain. The purpose of these frequencies is to maintain a frequency difference of 28.8 Mcps between the transmitter chain and local oscillator chain, regardless of whether L-, S-, or X-band is used. This is done by choosing the proper adder frequency to be fed to the oscillator chain.

The adder-multiplier chain supplies the necessary low frequencies needed in the transmitter and local-oscillator chain.

The klystron-multiplier assembly consists of four klystron multiplier-amplifier tubes (2K47's and 2K46's). These klystrons are immersed in a constant temperature-controlled oil bath. The temperature of the oil is kept at 140° by a thermistor-type temperature-regulating system, a heat exchanger and oil circulating pump. Temperature control of the oil bath was found to be an important factor in maintaining a stable output. A change of a few degrees will cause the output from the klystrons to decrease requiring retuning of the klystrons for maximum output. At present the equipment is operating at X-band (9302.4 Mcps) and S-band (3100.8 Mcps). All the circuits and equipment, therefore, have been tuned to X- and S-band for maximum efficiency at these frequencies.

Antenna System

The antenna consists mainly of the horn, hybrid tee, stub tuners, crystal mixer, and load. Fig. 2 is a block diagram of the X-band antenna system. The horn being used is made of Invar and measures 25.5 inches in length with an E-plane flare of 10° and an H-plane flare of 13° . The measured gain of the horn was found to be 24.5 db.

The hybrid-tee junction is also constructed of Invar. The use of Invar for the whole antenna system is preferable, since this material tends to reduce instability caused by the thermal expansion and contraction.

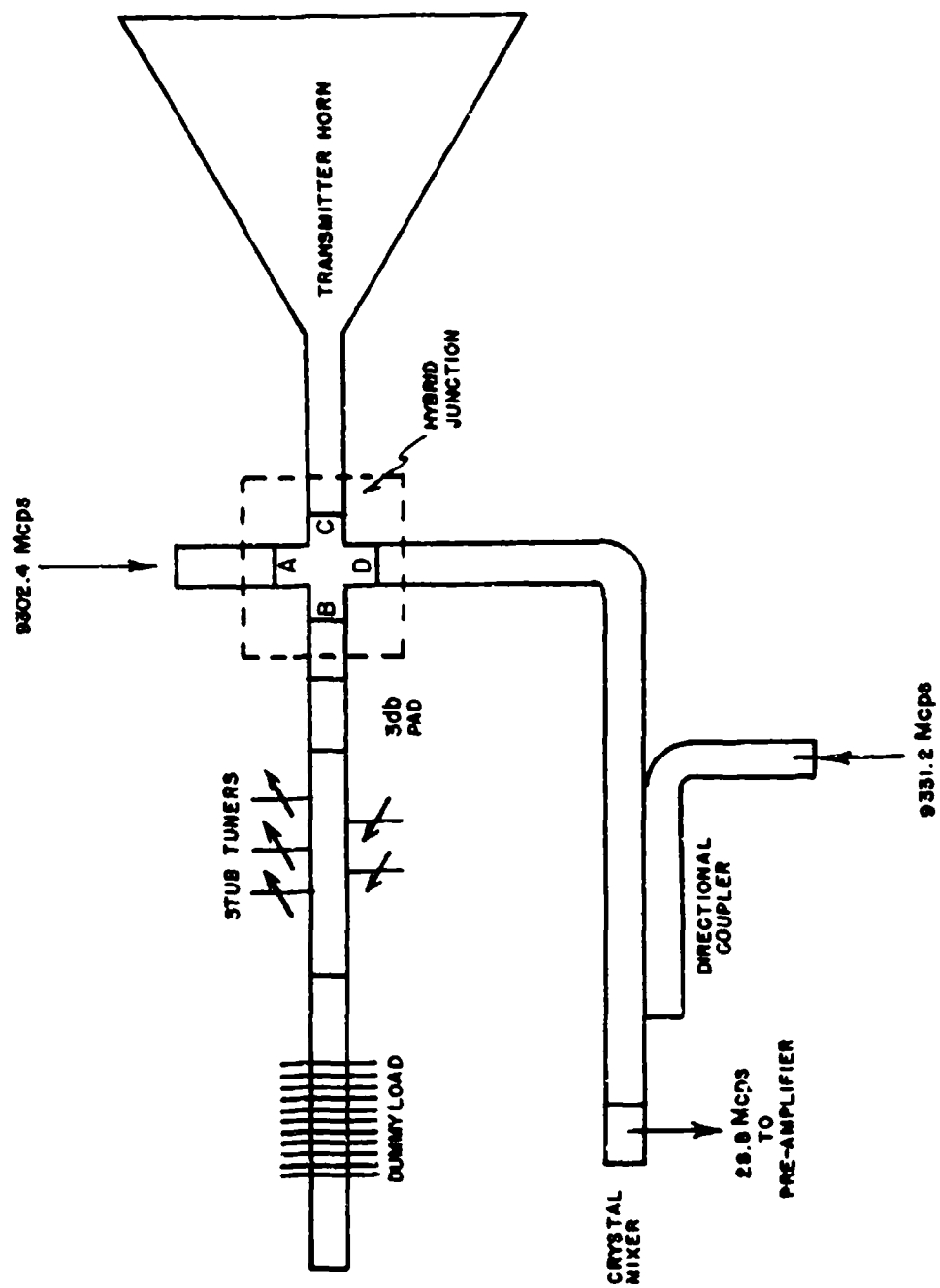


FIG. 2 Block diagram of antenna system.

The stub tuners are precision machined and consist of 1/16 inch polystyrene rods and brass rods. Micrometers are used on the stubs.

The load used in the antenna system is a mixture of sand and graphite. The mixer is a standard commercial tunable X-band crystal mixer. Since the complete antenna system is not constructed of Invar, additional insulation is used over the load, stub tuners, hybrid tee, and crystal mixer to ensure minimum discontinuities due to expansion and contraction.

The transmitter frequency (9302.4 Mcps) is fed into the A arm of the junction through a directional coupler. Arm B contains the matched dummy load and five-stub tuner. This five-stub tuner can be replaced by a three-stub tuner if necessary. The tuner has three metallic posts and two polyrod posts for fine tuning. With the setup, it is possible to balance the equipment down to the noise of the receiver (greater than 90 db from the maximum return).

Receiver and Recorder

The echo or return signal is mixed in Arm D with the local-oscillator signal. The difference (28.8 Mcps) is then fed to a preamplifier which in turn feeds the signal into a piston attenuator. The position of this attenuator is plotted on a graph. The signal is then fed to the receiver which in turn drives the servoamplifier. In the servoamplifier the amplitude of the signal is compared with a fixed reference (set at the receiver), and if a change in amplitude results, the servoamplifier readjusts the piston attenuator until the signal level returns to its prescribed level. Thus, the input to the receiver is maintained at a fixed level, and the received-signal strength is indicated by the amount of attenuation necessary to achieve this condition.

Targets are generally mounted on a polyfoam tapered column so that interaction between mount and target is a minimum.

THE HUGHES BACK SCATTER MEASUREMENT RANGE

R. E. Boucher
Head, Electronic Studies Section
Don E. Ludwig
Head, Circuit Studies Group
Hughes Aircraft Company
Radar Division
Fullerton, California

INTRODUCTION

This paper describes the outdoor, ultra-short pulse, back scatter measurement range which has been constructed at Hughes Ground Systems. An oblique type range layout is used in conjunction with dielectric line test object suspension and positioning. The measurement radar antenna-test object separation (500 feet) is sufficient to permit valid radar cross section measurements of full scale test objects. Excellent short pulse measurement sensitivity has been maintained with this antenna-test object range separation.

Since the majority of the background interference return can be gated out at the radar receiver when performing short pulse back scatter measurements, a low background interference level is obtained which is invariant with environmental conditions. At C-band, the measurement sensitivity is currently a -50 dbsm (decibels below 1 square meter) cross section with a 10 db signal-to-noise ratio. The C-band interference background level is below the return from a -60 dbsm radar cross section target.

Range calibration tests which were performed are described in this paper, and examples are given of the measurement data obtained from several types of test objects.

RANGE GEOMETRY

The range geometry which was used is shown in Figure 1. Test objects were suspended midway between two telephone poles on a dielectric line. These telephone poles are located in the first nulls of the radar antenna's azimuth radiation pattern, and are displaced in range from the test object suspension point by ± 25 feet. A 50-foot range sector is thereby provided which is free from any major reflective obstructions. Test objects are suspended at a height such that the first null of the antenna's elevation radiation pattern intercepts the ground at the same range as the test object suspension point. At this height, approximately 20 feet from the ground, the suspension line connected between the telephone poles makes acute angles of 25 degrees with respect to the horizontal plane. The suspension line thereby assumes a completely oblique geometry with respect to the incident radiation wavefront from the radar antenna.

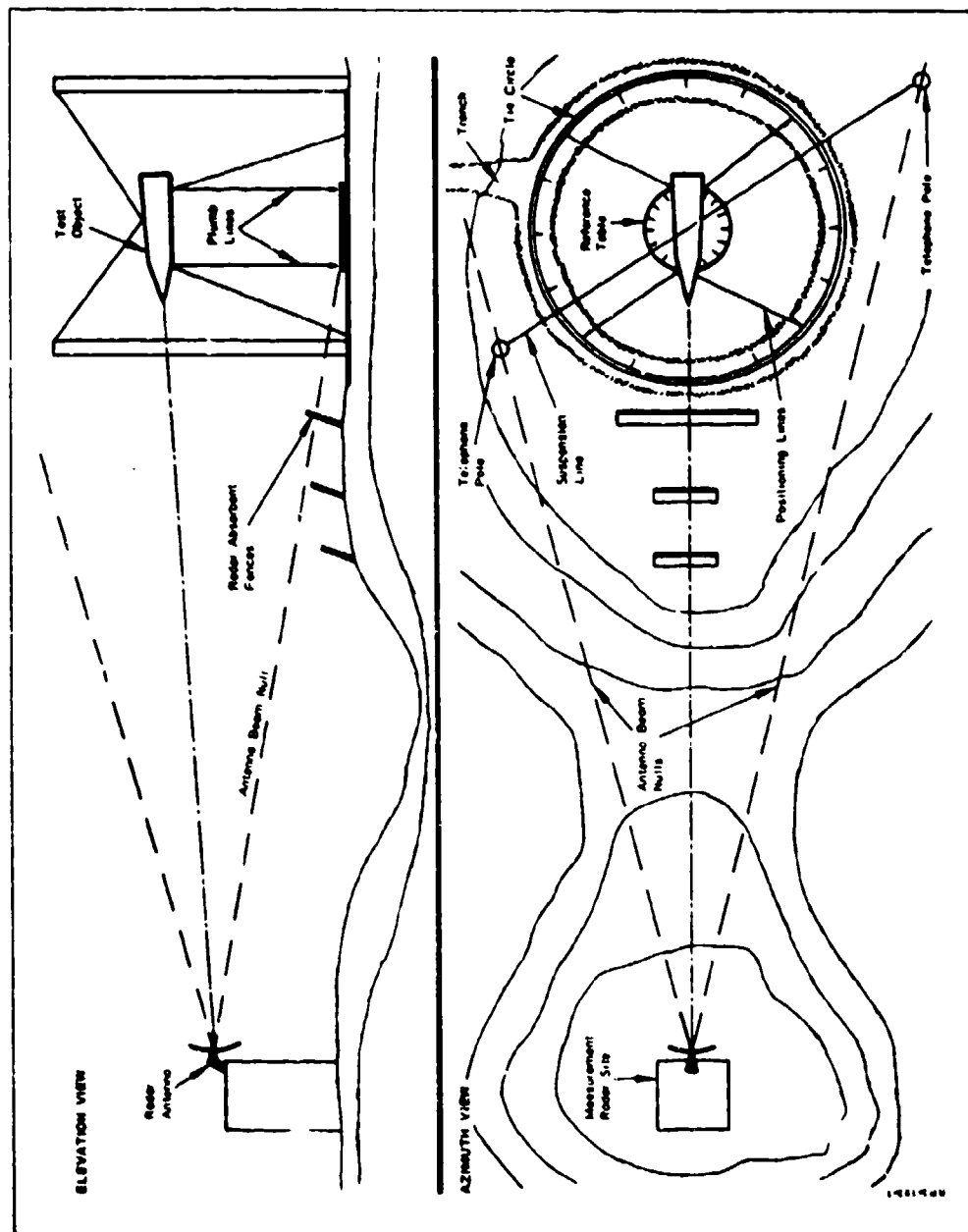


Figure 1. Range Geometry

Test objects are positioned by means of four thin dielectric lines, two attached to the forward portion of the test object and two to the aft portion. These four lines are then fastened to a large tiedown circle which is centered about the test object suspension point. Tie points are located 1 degree apart on the circle. Test object orientation relative to the incident radiation wavefront is determined through use of two plumb lines attached to the test object, one at the forward portion and one at the aft portion, and a 6-foot diameter reference table which is centered about the test object suspension point. This table has been surveyed to lie in a plane parallel to the azimuth plane of the boresighted radar antenna. Positioning and plumb lines are always maintained at oblique angles relative to the incident radiation wavefront when performing cross section measurements.

Microwave-absorbent fences have been placed between the test object suspension area and the radar antenna in order to reduce any interference return reflected from the reference table and tie circle area, as well as to reduce any forward scatter ground reflection interference. Microwave-absorbent material has also been wrapped around the telephone pole closest to the radar antenna in order to eliminate any possible low level reflections between the pole and a test object. These types of interference return cannot be removed by range gating at the radar receiver, since the differential time delay between these returns and the back scatter return from a test object is not sufficient. Proper range geometry and the use of microwave-absorbent fences must therefore be relied upon.

Plans have been made to automate the test object rotation system. The large tie circle will be replaced with a motor-driven rotating tie ring, and a low radar cross section dielectric rotary joint will be used in attaching a test object to the suspension line. The test object will then be free to rotate continuously in an azimuth plane. Pickoff contacts located on the tie ring will be used to provide test object azimuth aspect angle information once a test object has reached rotational equilibrium. Incorporation of this automated rotational system will greatly reduce the measurement times required and, correspondingly, the effects of wind motion. With the present manual rotation system, approximately 3 hours is required to cover a 180-degree azimuth sector in 5-degree increments, whereas approximately 1 minute will be required with the automated system.

DIELECTRIC LINES

After a thorough investigation into the possible types of dielectric and metallic materials available for use as test object suspension lines, polypropylene was selected. This choice was based upon its low dielectric constant ($\epsilon_r \approx 2.25$ at 50 mc/s), elongation (8% when used 20% below its maximum breaking strength), and excellent tensile strength. Three sizes of line are used for test object suspension: 1/8-inch diameter for suspending test objects weighing up to 70 pounds, 3/8-inch diameter for suspending test objects weighing up to 490 pounds, and 1/2-inch diameter for suspending targets weighing up to 900 pounds. Dacron line of 0.03 inch

diameter, is used for test object positioning because of its strength, elongation, and availability. Positioning using these lines is sufficiently stable that only very minor adjustment is required after three or four hours of test object suspension.

A series of back scatter measurements of the Dacron and polypropylene lines was made to determine their radar cross section as a function of orientation. A measurement radar with a range resolution capability of less than 1 foot was used. The measured radar cross sections are shown in Figure 2. All of the lines were measured at a 90-degree angle of incidence (where the angle of incidence is defined as the angle between the dielectric line and the antenna boresight axis) and one of the lines, 1/4-inch diameter polypropylene, was measured as a function of the angle incidence. The range geometry is shown in Figure 3. At the time this data were taken, the measurement radar had a sensitivity threshold of -43 dbsm, which is indicated on the plot. The radar sensitivity threshold has since been increased to -60 dbsm, but additional data have not been taken.

The measured radar cross section at a 90-degree angle of incidence was -6 dbsm for a 3/8-inch diameter polypropylene line, -29 dbsm for a 1/4-inch diameter polypropylene line, and -40 dbsm for a 0.03-inch diameter Dacron line. The radar cross section of the 1/4-inch diameter polypropylene line decreased rapidly as the angle of incidence was decreased, reaching a cross section of -41 dbsm at approximately 87 degrees, where the back scatter return fell below the radar sensitivity threshold and never reappeared over a 45-degree measurement sector. As is evidenced from this measurement data and the range calibration tests which were performed, a suspension and rotation system using dielectric lines will produce a minimum amount of interference back scatter return when a reasonably oblique geometry is maintained.

MEASUREMENT RADAR AND DATA RECORDING SYSTEM

A general block diagram and photograph of the measurement radar and data recording system are shown in Figure 4. The pulse has a range ambiguity level -30 db below its peak value. A photograph of the display for the point source radar return from a calibration sphere is shown in Figure 5 to illustrate the measurement pulse waveform. The recording system will accommodate a 30 db dynamic range of radar return amplitudes. This range of display can be shifted on a relative basis by means of the precision microwave attenuator at the input to the receiver.

A sampling type oscilloscope is used as the primary display for the radar system. Outputs are derived from this prime display for digital data recording, as X-Y analog plots, or as oscilloscope display photographs. Because the video on the prime oscilloscope display has a nonlinear amplitude scale factor, the outputs derived from this display are passed through a log shaper to provide, for recording purposes, an amplitude scale factor which is linear in decibels. Correlation between the actual target scattering points and the radar returns displayed is provided by means of an ultra-stable synchronization trigger derived from the transmitter leakage. The estimated accuracy of correlation by this method is ± 1.5 inches.

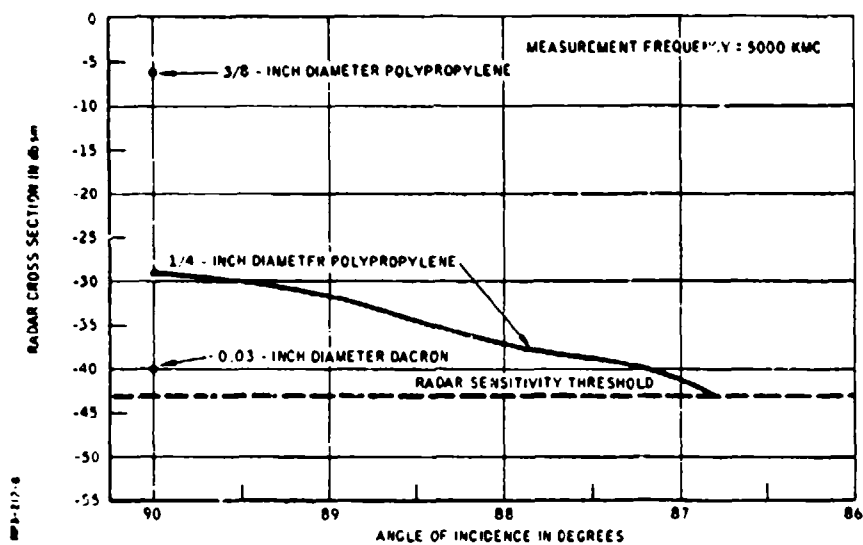


Figure 2. Measured Dielectric Line Radar Cross Sections

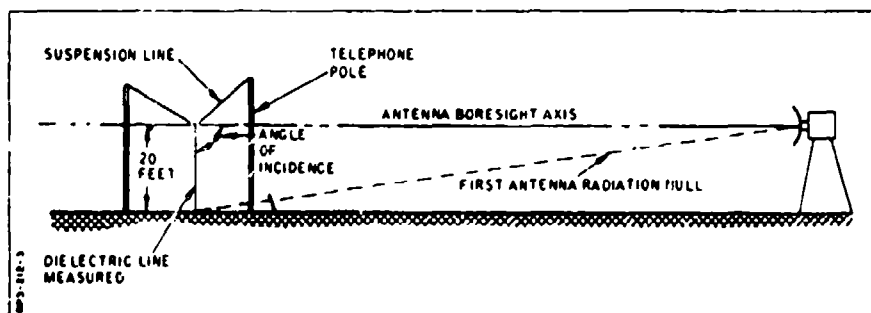


Figure 3. Dielectric Line Measurement Geometry

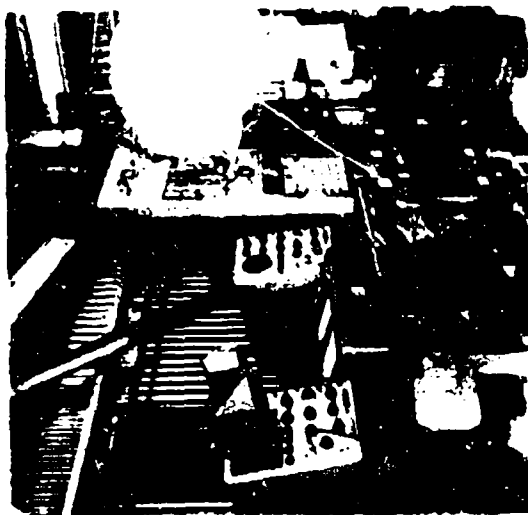
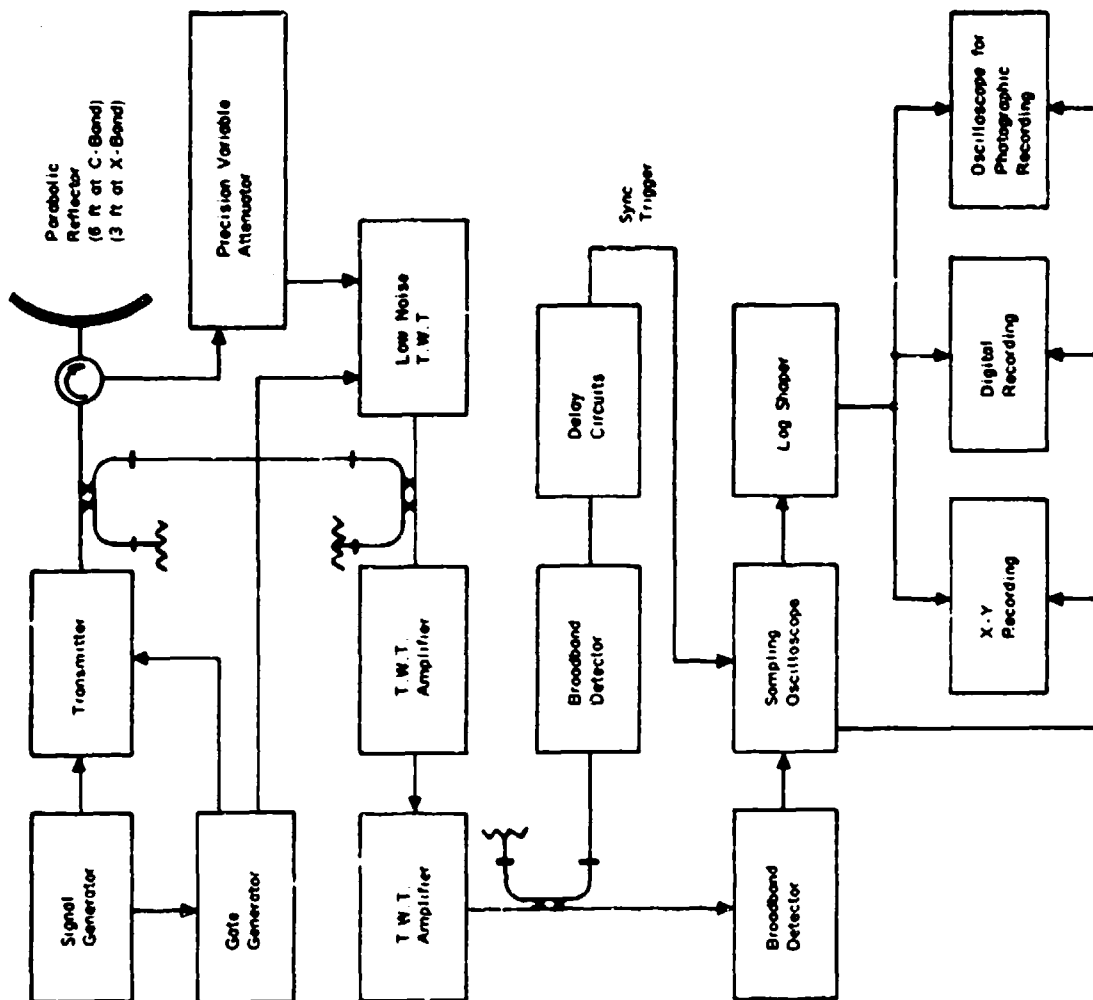


Figure 4. Measurement Radar and Recording System

RANGE CALIBRATION

A series of range calibration tests was performed at C-band using spherical and cylindrical test objects. The back scatter return from each of a family of conductive spheres ranging in diameter from 0.312 inch to 24.00 inches was measured. Good agreement was found between the theoretical radar cross sections and the measured radar cross sections based upon a 9 500-inch diameter reference sphere. The calculated and measured radar cross section values are tabulated below:

Sphere Diameter (Inches)	Calculated Radar Cross Section (Square Meters)	Measured Radar Cross Section (Square Meters)*
24.00	0.293	0.32.
9.500	0.0457	0.0457
3.00	4.1(10 ⁻³)	5.86(10 ⁻³)
1.00	1.2(10 ⁻³)	1.1(10 ⁻³)
0.312	1.2(10 ⁻⁵)	0.44(10 ⁻⁵)

*Estimated accuracy in obtaining the tabled measurement values is ± 1 db.

Based upon the radar return from the smallest sphere (-53 dbsm radar cross section), the interference background from the range was checked with the suspension and positioning lines present. The measured background interference level at C-band was found to be below the return from a target of -60 dbsm radar cross section. At this level the radar receiver noise level became a limitation, and the background interference return was never actually observed. In the near future the radar sensitivity will be increased to a point where the background return can be measured. Display photographs for this interference background test are shown in Figure 6. The same results were obtained regardless of antenna polarization and suspension line diameter (0.5-inch diameter line was the largest tested).

Tests were made to determine whether proper phase and amplitude relationships exist between a given test object and the measurement radar antenna at the 500-foot range separation used. These tests were performed using a series of 5-inch diameter cylinders with lengths varying from 3 to 10 feet. The broadside (specular) radar return from each of the cylinders was measured, and a curve was plotted of this measured radar cross section versus the cylinder lengths squared. This curve was a straight line to within the ± 1 db measurement accuracy, indicating proper phase and amplitude relationships for radar cross section measurement of targets up to 10 feet in length. Targets consisting primarily of conical sections and having overall lengths up to 15 feet have been measured at their specular positions, and good agreement was found to exist between the measured radar cross sections and the predicted values based upon a mean cylinder approximation. These results tend to invalidate the commonly used test object-radar antenna separation criteria, $R = \frac{2(D_1 + D_2)^2}{\lambda}$

where: $\begin{cases} R = \text{Minimum allowable separation distance} \\ D_1 = \text{Test object linear dimension} \\ D_2 = \text{Antenna diameter} \\ \lambda = \text{Wave length} \end{cases}$

when a measurement accuracy of the order of ± 1 db is desired. Based upon this quoted range separation criterion, test objects longer than

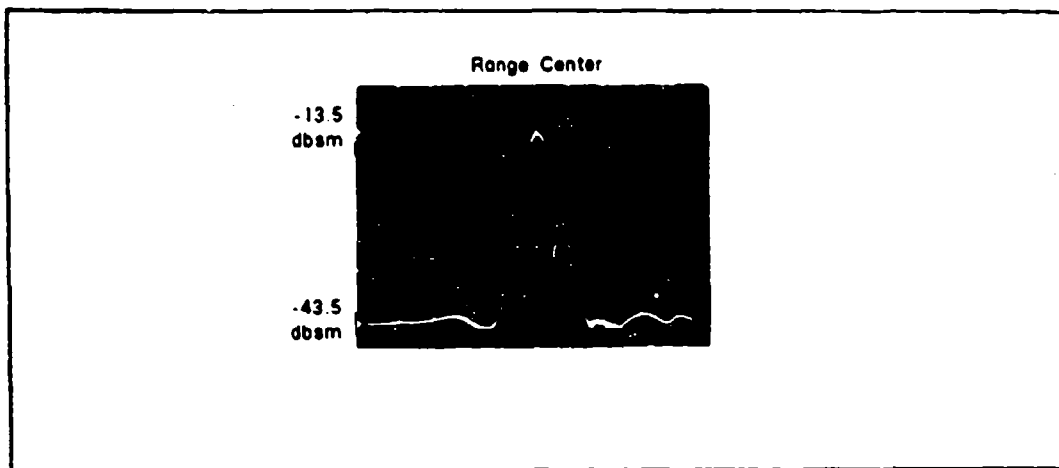


Figure 5. 9.500 Inch Diameter Calibration Sphere Return

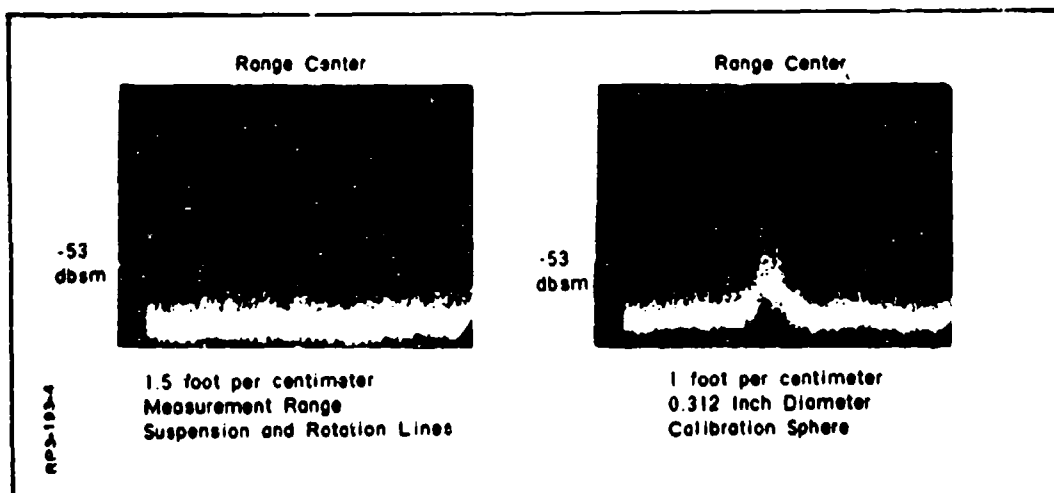


Figure 6. Range Interference Calibration

1 foot in length could not be measured in their specular aspect position at the Hughes facility.

Symmetry tests were also performed as a check on forward scatter, ground-reflected interference. Several test objects were checked for radar return symmetry in the azimuth plane, and a truncated cone target (rotationally symmetrical about its longitudinal axis) was checked for radar return symmetry between the azimuth and elevation planes by recording the return for both vertical and horizontal antenna polarizations. In all cases good correlation was found between the appropriate radar return data, indicating that a minimum amount of ground reflection interference exists as a result of the absorbent fences and geometry used for the range.

MEASUREMENTS PERFORMED

A wide variety of test object types has been measured at the Hughes facility using a C-band measurement radar with a range resolution capability of better than 1 foot. Among the objects which have been measured are spheres, cylinders, flat plates, truncated cones, and cone-spheres. Included in this list of test objects are some bodies which were measured with various radar-absorbent and dielectric coatings. In general, good agreement was found between the measurement data and the predicted major scattering point contributions to the radar return. As might be expected, some unpredictable surface wave and dispersed returns were noted for targets with dielectric coatings, as well as those fabricated from a dielectric material. Surface wave contributions to the radar return from several of the test object geometries were noted. Some short pulse radar return data taken for two of the test objects, a truncated cone and a cone-sphere, are shown in Figures 7 and 8.

Two short pulse radar return signatures from a truncated cone target are shown in Figure 7. An experimental investigation was performed to determine the origin of the extended return noted for a basic truncated cone target. This extended return occurs in time beyond the last geometrical target discontinuity which could produce a radar return. After extensive experimental investigation, it was found that a piece of hairflex microwave-absorbent material placed on the hidden back flat plate surface would greatly reduce the magnitude of this extended return. An explanation for this return, which correlates well with the relative time (range) displacement between the extended return and the target geometry, is as follows: A surface wave is launched across the back flat plate surface from the leading cone-flat plate interface. This wave is then relaunched back toward the radar from the diametrically opposite flat plate-cone interface. Placement of the hairflex on the flat plate surface then has the effect of attenuating this surface wave.

The short pulse return from a full scale cone-sphere target at a nose-on aspect is shown in Figure 8. Three radar returns are noted. The middle return, as noted on the plot, is from a short vertical tie member which was used in suspending the target. The leading return is from the cone tip and corresponds in magnitude to the return from a sphere

with the same radius. The trailing return corresponds in time to the return from a surface wave which completely traverses the rear hemisphere and is reradiated back toward the radar at either the cone-sphere matching surface or is reradiated from the cone tip after traversing the length of the cone. Since no return is initially noted from the cone-sphere matching junction (first-order matching was used), and assuming reciprocity, the second explanation (wherein the surface wave traverses the entire body before re-radiation at the tip) appears the most plausible. When the target's azimuth aspect angle is varied from nose-on, the tip return remains constant over a 70 degree change in aspect angle, whereas tail return rapidly diminishes until it falls below a -50 dbsm level at a 15-degree aspect angle.

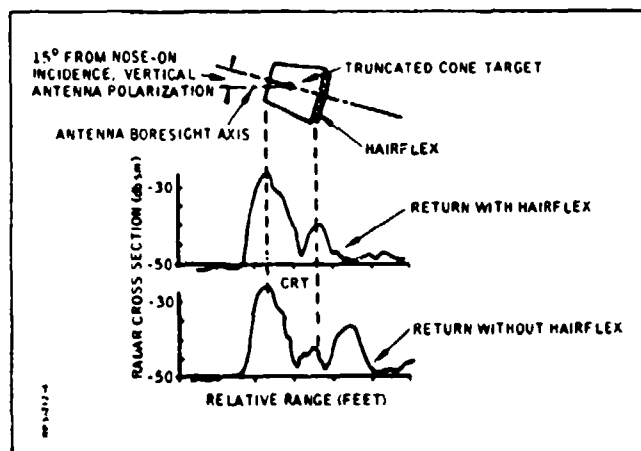


Figure 7. Truncated Cone Extended Return Experiments

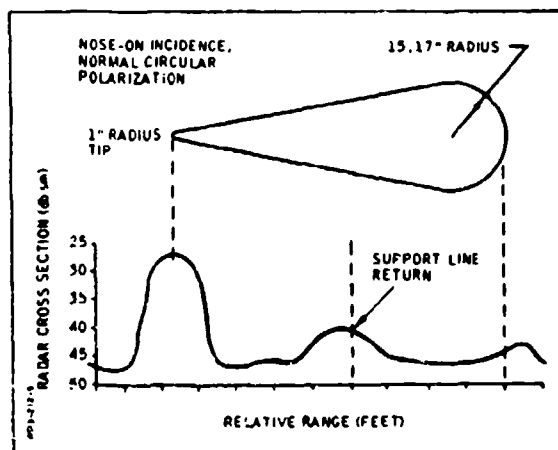


Figure 8. Cone-Sphere Target Return

RANGE FACILITIES FOR MEASURING RADAR CROSS
SECTIONS OF LOW DENSITY SUPERSONIC PLASMA STREAMS

Allan I. Carswell
RCA Victor Research Laboratories
RCA Victor Company, Ltd.
Montreal, Canada

Radar measurements of bodies travelling at very high velocities in the earth's atmosphere are complicated by the plasma sheath and wake which are generated at the hypersonic speed. Since, in many cases, the scattering from the plasma can be predominant in the radar return, it is necessary to understand the scattering characteristics of such a plasma flow-field if any meaningful information concerning the body itself is to be extracted from the information contained in the radar return. To simulate such plasma systems for laboratory type range studies, it is, in general, necessary to develop a facility which will provide an accessible and controllable supersonic plasma flow-field having parameters in the range of interest.

A schematic view of a radio-frequency excited plasma tunnel constructed for this purpose^{1,2} is shown in Fig. 1. The system was designed to provide supersonic, free-jet plasma flow streams with static pressures in the range from about 0.1 to 10 Torr. With the present pumping system (approximately 240 cfm capacity) the lower portion of the pressure range is attained over a limited time interval by using the system as a blow-down tunnel. At test-section pressures above about 0.3 Torr it is possible to run the system continuously, and operation times up to several hours have introduced no major difficulties.

In order to ensure gas purity (and to minimize stray microwave reflections) the entire flow system, with the exception of the large tank, was constructed of pyrex glass. Necessary metal flanges and couplings were kept well removed from the region of the electrical discharge and were left ungrounded to float at the plasma potential. In this way contamination of the plasma stream by contact with metal surfaces was avoided.

In the present system a six-arm "cross" of standard pyrex tubing is used for the test-section to provide a large and easily accessible test region. There are two 4-inch, two 6-inch and two 9-inch diameter arms as shown in Fig. 2. One of the 6-inch diameter arms is connected to a 6-inch diameter flow-pipe leading to the evacuation system. The remaining five arms may be used for a variety of arrangements of nozzle assemblies and diagnostic instrumentation, (e.g. optical and microwave apparatus, probes and obstacles).

The high-frequency rf field used for the plasma generation is capacitively coupled³ to the gas stream with two external cylindrical

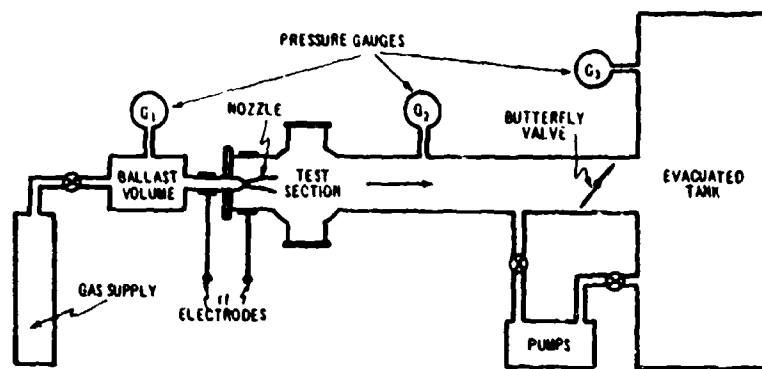


Figure 1. Schematic Diagram of the Plasma Tunnel

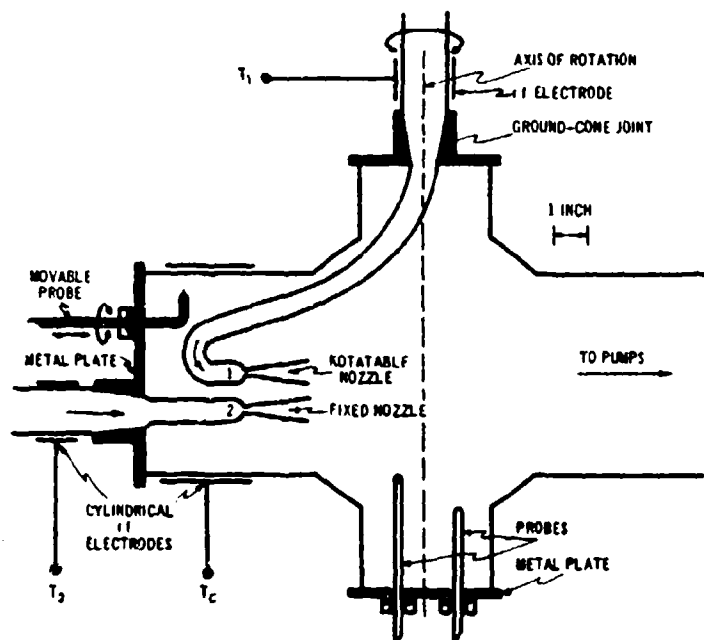


Figure 2. Side View of the Test-Section

electrodes which are both located "upstream" from a protruding nozzle (Fig. 2). The capacitive coupling provides a uniform excitation across the gas stream and allows the size and position of the region of excitation to be easily controlled by the relative positions of the two electrodes. By placing the electrodes as shown in Fig. 2, the electrical discharge is forced to pass through the nozzle and this provides maximum excitation at the throat of the nozzle where the cross-section area is smallest. In addition, since both electrodes are "upstream" from the exit of the protruding nozzle there is no extraneous excitation of the ambient gas in the test section³.

Using this method of rf coupling, a rotatable nozzle assembly has been developed for the apparatus. With this assembly it is possible to rotate the nozzle while the gas is flowing so that the plasma stream can easily be positioned at any desired angle (about the axis of rotation) with respect to the stationary test-section.

In Fig. 2 the arrangement used for many recent back-scattering measurements is illustrated. In this diagram two nozzles are shown. One of these (No. 2) is fixed in position and the other (No. 1) is free to rotate about a vertical axis centred in the test-section. The gas flow can be directed through either nozzle by external valves (not shown) and the rf power can be applied through the appropriate pair of electrodes (T_1 and T_0 , or T_2 and T_0). The rotational motion of the nozzle indicated in Fig. 2 is limited to an angle of approximately 40 degrees but other assemblies have been used which provide up to a full 360 degrees rotation of the nozzle. The ability to rotate the plasma stream within the fixed apparatus has proved to be of great value in the microwave study of the plasma stream properties since the aspect angle dependence of the back-scattering cross section of the jet can be measured very readily with stationary microwave apparatus.

In addition to an unmodulated signal the rf plasma generator can be used to supply a signal which is amplitude modulated at audio frequencies. The present unit can apply one hundred percent amplitude modulation to the carrier signal over a frequency range from about 50c/sec to 4.5Kc/sec. In this way the intensity of ionization in the plasma stream can be modulated at audio frequencies. This feature has proved to be particularly useful for examining the microwave scattering properties of the plasma stream. By modulating the plasma (while using c.w. microwaves) and using detectors tuned to the same frequency, it is possible to measure the microwave scattering from the stream accurately even in the presence of stray scattering from the apparatus (tunnel walls etc.).

Langmuir-type probes can be introduced from the bottom or end of the test-section through vacuum seals in the metal plates as shown in Fig. 2. The O-ring seals permit both translation and rotation of the probes so that any point in the plasma stream can be reached. In this way a simultaneous comparison of the microwave scattering and probe measurements can be made. The two 9-inch diameter ports in the test

section are covered with transparent polystyrene plates and are utilized for microwave reflection and transmission studies of the plasma stream. For the back-scattering (reflection) measurements, layers of microwave absorber are inserted in the test-section as shown in Fig. 3.

Because of the many parameters involved in the description of the partially ionized gas stream it is difficult to state "typical" conditions for the facility but in Table I a summary is given for sample operating conditions for argon gas using a rotatable nozzle such as that shown in Fig. 2.

TABLE I - SAMPLE ARGON PLASMA STREAM PROPERTIES

Discharge supply	1kw at 13.56 mc/sec
Nozzle exit diameter	1.7cm
Mass flow rate	2.5gm/min
Test-section pressure	1.0Torr
Stream velocity	~ Mach 2
Degree of ionization	0.04%
Gas temperature	750°K
Electron temperature	6.5×10^4 °K
Electron density	1.5×10^{13} /cc

In addition to the system described above a two-phase (liquid-vapour) mercury plasma tunnel² of similar design has also been used to provide supersonic plasma jets with properties suitable for the scattering measurements.

Using these flow facilities microwave back-scattering measurements have been carried out at 9.5, 24 and 35Gc. In all cases c.w. signals (with and without audio frequency square wave modulation) have been employed. A single horn transmitter-receiver configuration has been used with directional couplers to sample the transmitted and reflected signals. Measurements have been made with and without dielectric (polystyrene) lenses to "shape" the microwave beam. For some investigations the multiple probe system⁴ developed in our laboratory has been used to supply simultaneous measurements of both the amplitude and phase of the back-scattered return. The design of the plasma tunnel allows for the insertion of metal and dielectric cylinders (and spheres) in place of the plasma stream so that direct calibration and assessment of the microwave system can be affected using scatterers of known radar cross section.

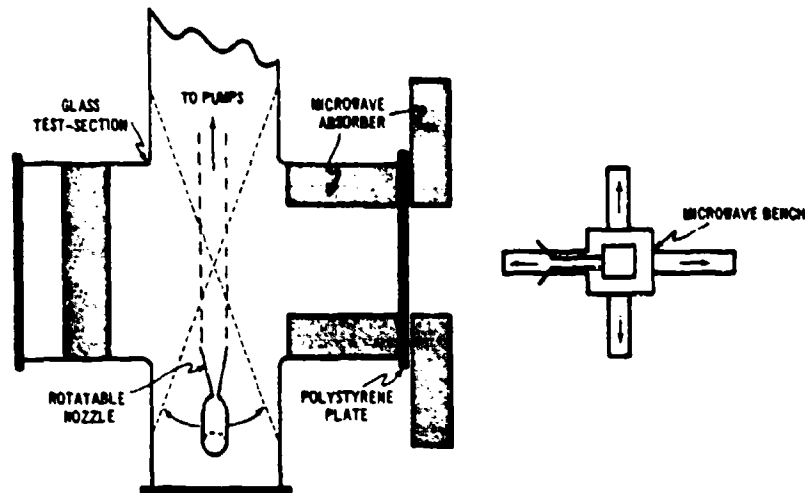


Figure 3. Top View of the Test-Section Showing the Apparatus Arrangement Used for the Microwave Back-Scattering Studies

REFERENCES

1. A.I. Carswell, "Radio-Frequency Excited Plasma Tunnel for Laboratory Studies of Supersonic Plasma Flow-Fields", Rev. Sci. Instr. 34, 1015 (1963).
2. A.I. Carswell, "Microwave Scattering from Supersonic Plasma Flow-Fields", RCA Victor Res. Report 7-801-24, Jan. (1963).
3. A.I. Carswell, "Gas Flow Visualization Using Low Density Plasma Streams", Phys. Fluids 5, 1128 (1962).
4. F.J.F. Osborne, "A Multiple-Probe Microwave System for Plasma Studies", Can. J. Phys. 40, 1620 (1962).

THE AVCO RAD VERTICAL RANGE

Joseph F. Clougherty, Group Leader
Avco RAD
Wilmington, Mass.

ABSTRACT

Presently existing radar cross-section measurement facilities are, for the most part, of the horizontal range type. There are several problems associated with the operation of a horizontal range which are especially bothersome when making low radar cross-section measurements. They are: (1) variation in illumination of the vehicle because of the presence of ground reflections; (2) the possibility of illumination by multiple scattering; (3) the "background" problem, i. e., the level of the return from the target support when the target is not present. In many cases, the radar cross-section of the target support can equal or exceed the return from the target whose radar cross-section is to be measured. The Avco RAD full-scale vertical radar cross-section range which will be described is felt to offer the solution to these problems.

1. DESCRIPTION OF FACILITY (MECHANICAL)

An aerial photograph of the Avco RAD vertical range is shown in figure 1. The facility consists of three 400 foot towers equiangularly spaced on the circumference of a circle of 388 foot radius. The triangular platform from which the target is suspended is supported by means of three steel cables extending from the vertices of the triangle to the tops of the towers. An allowable cable sag of 50 feet is required in order to accommodate the combined weight of the platform and vehicle which can be as great as 4,800 lbs. The weight of the triangular platform is 2,300 lbs. which permits the handling of a vehicle weighing up to 2,500 lbs. The triangular platform is equilateral, being 60 feet on a side. The vehicle whose radar cross-section is to be measured is supported by means of three dacron cords extending from the vertices of the triangle to the rear of the vehicle. The length of these cords is 65 feet, permitting the vehicle to be suspended 50 feet below the level of the platform, 300 feet in the air. These ropes, when under tension, are at an angle of 55.3 degrees with respect to the plane of the incident wavefront. The diameter of the dacron cords is determined by the weight of the vehicle whose radar cross-section is to be measured. Five sixteenths of an inch diameter rope can be used to support a 1,000 pound vehicle with a safety factor of 7. The triangular platform from which the vehicle is suspended is raised and lowered by means of a hydraulic lift located immediately adjacent to the tower shown in the left side of the photograph.

Angular rotation of the vehicle whose radar cross-section is to be measured is accomplished by means of a remotely controlled motorized winch assembly located within the platform structure. When making radar cross-section measurements with experimental vehicles, two small holes, diametrically opposed, are drilled well forward of the center of gravity of the vehicle. A unique type of plastic collet permits "quick-connect" and "quick-disconnect" operation without having to go inside the vehicle.



Figure A-1 AVCO RAD FULL-SCALE RADAR CROSS SECTION RANGE

601365

In this type of suspension system the rope knots are internal to the vehicle. For those vehicles which do not permit the drilling of holes, it is necessary to use a plastic strap around the vehicle. The strap is restrained from slipping from the nose by means of two loops around the strap which are extended to the rear of the vehicle and tied. In either case, the two front ropes extend from the vehicle to two pulleys located at the midpoints of two adjacent sides of the large (60 feet on a side) equilateral triangle. These two ropes then extend parallel to the sides (30 feet in length) of an inner triangle used for mechanical support. The ropes are then joined at the midpoint of the third side of the platform whereupon they are drawn in by means of the motorized winch assembly.

The originally conceived method of obtaining angular information was to mount a pendulum box within the vehicle. Angular information is fed from the rear of the vehicle by means of a cable extending vertically to the platform, along one of the steel cables used to support the platform, down the tower, and finally along the ground to the recorder. Subsequent radar cross-section measurements made at UHF and L-band frequencies both with and without the cable indicate that the presence of the cable has no measurable effect upon the pattern. At C- and X-band frequencies, however, the return from this "messenger" cable is extremely high and a different approach must be used. The presently used method of obtaining data at C- and X-band frequencies is to use the system to obtain an analog plot of aspect angle versus time. Next, the cable is disconnected and a radar cross-section measurement is made as a function of time. Finally the time is eliminated to obtain the plot of radar cross-section versus aspect angle. This method of obtaining the data is tedious and time-consuming. Present plans call for the incorporation of a function generator and a curve follower into the system. The output of the curve follower will be used to drive the servo which in turn drives the x-axis of the recorder.

With regard to the effect of the wind velocity on model stability, calculations show that stability is dependent upon the vehicle weight and shape in addition to the wind velocity. These calculations show that a 500 lb. vehicle will remain stable to within a quarter of a degree when subjected to 15 m.p.h. winds.

2. DESCRIPTION OF FACILITY (ELECTRONIC)

When "looking" vertically at the target with a narrow pulse width radar utilizing a range-gated receiver, it is possible to obtain return from any object located within a hemispherical shell whose width is equal to the range gate and whose effective radius is the distance from the antenna to the target.

Included in this problem is the possibility of ground return from a circular annulus of the same dimensions as the hemispherical shell being picked up on antenna side lobes. This problem has been eliminated by the erection of a circular cylinder of screening of 70 feet radius and 15 feet height. The radius of the cylinder is great enough to prevent improper illumination of the target, e.g., reflection of antenna side-lobe energy from the screen to the target, since the range-gate used is only 50 nanoseconds wide. Also, the fence height is great enough to "mask-out" any ground return from the annulus which might occur during the range gate. There is some return from the screening but it can be separated from the target return in time. Thus, the only return that can occur during the range gate is that from the target plus support cords which make an angle of 55.3° with respect to the plane of the incident wave front.

Background measurements have been made. The vehicle support system was simulated by running three ropes from the vertices of the platform to tie points on the ground so located that the support lines would intersect at a point 50 feet below the level of the platform. Measurements made at UHF, L, and C-band frequencies indicate that the background is better than 60 db below a square meter.

Radar operation is the same at all four frequencies. In order to obtain truly monostatic radar cross-section data only one antenna is used. The output of the transmitter is fed to a horn antenna by way of a four port circulator. The return signal enters the same horn and travels to the receiver arm of the circulator. A horn antenna is used in preference to a paraboloid for two reasons: (1) it is possible to obtain a better broadband VSWR with a horn, thereby minimizing transmission line ringing problems; (2) if a paraboloid were used there would be a great deal of "spillover" illuminating the ground and various objects in the vicinity of the antenna, thereby causing unwanted clutter.

All of the existing systems operate over a 160 db dynamic range, i.e., the minimum detectable signal level is approximately 160 db below the level of the transmitter output. Since the return signal occurs approximately 650 nanoseconds after transmission, it is imperative that a TR tube with extremely rapid recovery time be used both to protect the receiver during the period of transmission and to be "wide-open" during the time of reception of the return signal. This is accomplished at L-band by the use of a solid state self-biasing limiter used in conjunction with a tunnel diode amplifier. At UHF only the tunnel diode amplifier is used. At C- and X-bands TWT pre-amplifiers are used. In addition to their performance as TR tubes, these low noise pre-amplifiers essentially "mask" the conversion losses associated with the various mixers, thereby yielding a low overall system noise figure.

In the original design of the range, primary emphasis was placed on a low background range employing an L-band radar. At the time consideration was given to the possibility of making radar cross-section measurements with a pulse width as narrow as 10 nanoseconds which requires a receiver bandwidth of 100 mc/s. For this reason, it was decided to amplify the return signal at the RF frequency rather than to use the standard superheterodyne technique where the RF signal is converted to a signal in the intermediate frequency range, usually 30 to 60 mc/s. In order to obtain full utilization of this receiver, mixers are incorporated into the UHF, C-, and X-band radars to convert the return signal to the L-band frequencies.

The system capabilities are tabulated below.

A. Mechanical Characteristics

1. Maximum target weight - 2,500 pounds
2. Maximum target length - There is no physical limitation other than satisfying far-field requirements and the pulse width problem.
3. Antenna - target separation - 300 feet.
4. Angular coverage - 120° from nose-on. In order to obtain this coverage, one measurement is made from nose-on to 120° from nose-on. The vehicle is then rotated 180° about its roll-axis and the measurement is repeated.
5. Transmitted polarization - any linear.
6. Received polarization - any linear.
7. Target aspect angle accuracy - 1° with servo system; 2° when using the independent calibration prior to radar cross-section measurement.

B. Electrical Characteristics

1. Frequency - 300 to 500 mc/s (tunable)
 - 1.32 to 1.44 Gc/s (tunable)
 - 5.4 Gc/s (fixed)
 - 9.375 Gc/s (fixed)

2. Transmitter pulse width - 40 nanoseconds.
3. Range gate width - 50 nanoseconds.
4. Pulse repetition frequency - 1,000 pps.
5. Antenna gain - 15 db at UHF.
23 db at L-band.
23 db at C-band.
23 db at X-band.
6. Calibration accuracy - 1 db.
7. Equivalent noise level of the receiver at 300 feet range
 10^{-6} square meters at UHF
 10^{-8} square meters at L-band
 10^{-7} square meters at C-band
 10^{-7} square meters at X-band.
8. Measured value of background (with support ropes)
 10^{-6} square meters at UHF (-60 dbm)
 3×10^{-7} square meters at L-band (-65 dbm)
 3×10^{-7} square meters at C-band (-65 dbm)
 2.5×10^{-7} square meters at X-band (-66 dbm)

THE RADAR REFLECTIVITY MEASUREMENT FACILITY AT ELECTRONIC SPACE STRUCTURES CORPORATION

Albert Cohen, Senior Engineer
Adam P. Smolski, Engineer

Electronic Space Structures Corporation
West Concord, Massachusetts

GENERAL DESCRIPTION

Introduction

The Electronic Space Structures Corporation's antenna and radar reflectivity measurement facility is located on a 20 acre tract of land in West Concord, Massachusetts. The dominating feature of the ESSCO facility is the ground plane range. This range is approximately 2000 feet long, 400 feet wide, and is graded to a true plane. The ground-plane technique essentially eliminates the deleterious effect of random reflections commonly observed in the general antenna test facility¹. For the ground level case, the transmit-receive antennas and targets are located proximate to ground at that height where the direct ray and reflected ray combine to produce the maximum of the interference pattern. With "free-space" conditions thus simulated and terrain problems either eliminated or under direct control, advantageous instrumentation techniques can be applied and excellent measurements can be made.

General Characteristics

The large area of the test site makes it especially attractive for the measurement of full scale targets as well as frequency scaled models. The length of the range is variable with a maximum length of approximately 1800 feet. A 100 nanosecond transmitter pulse width is presently employed in conjunction with a 100 nanosecond variable range gate pulse width. The range of the receiver gate is adjustable from 300 feet to over 2000 feet. Targets and target support columns are fastened to an azimuth rotator which is recessed into the ground so that the turntable top can be at or below the ground plane level. This recessed rotator is another important and desirable feature of this type of range in that minimizing the reflections from the target support column is the only primary concern. Tapered styrofoam columns are used as the target supports and at present reflections from these columns are the limiting component of background return. This is in contrast to attempting to eliminate the reflections from the combination of tower, pedestal, azimuth rotator and target support columns as would be experienced on a so-called "high level" range.

The measuring system is presently monostatic, although bi-static measurements could be readily instrumented. Target positioning and

rotation are remotely controlled from the reflectivity instrumentation console located adjacent to the transmit-receive parabolic antennas. These antennas are housed in a cubicle adjacent to the transmit-receive control room. One side of the cubicle is a metal "roll-up" door which is automatically raised when measurements are in process. Particulars of the overall facility are as follows:

1. Frequency Range -- Typical Band 8.2 - 12.4 gc. The equipment is designed so that only the RF sections of the reflectivity console need be changed if operation at other frequencies is desired.
2. Background Level -- 10^{-5} - 10^{-6} m². At present the background return is limited by target support considerations. Without target supports, the return from the ground plane, over the area comparable to the pulse width, cannot be observed because of power limitations. If and when the return from the ground-plane becomes limiting, special grading or paving techniques over the area comparable to the pulse, in conjunction with narrow pulse widths, can be employed to further reduce the background².
3. Pulse Width -- 100 nanoseconds.
4. Pulse Repetition Frequency -- 24 kc.
5. Power -- 500 m w peak.
6. Polarization -- Linear horizontal, linear vertical, circular for grazing angles of approximately 1° or less.
7. Receiver Sensitivity -- -110 dbm.
8. Receiver Bandwidth -- 10 mc.
9. Dynamic Range -- 60 db.
10. Receiver Range Gate -- variable 300 feet to > 2000 feet.
11. Maximum Target Weight -- 2000 lbs.
12. Target Support -- For light targets a tapered styrofoam column is used. For heavy targets a metal support is used with a specially designed baffle of absorbing material.
13. Azimuth Resolution -- .05° (synchro readout)
14. Data Forms -- Analog rectangular plot and/or data may be recorded on magnetic tape using an FM recording process.

Measurement Technique

The measurement technique adhered to in all reflectivity measurements is outlined below.

1. A standard reference sphere is positioned on a tapered styrofoam column attached to the ground flush-mounted rotator. The transmit-receive antenna is then adjusted to the proper height and the cross section data recorded.

2. The entire 60 db dynamic range is calibrated in 5 db steps.

3. If magnetic tape recordings are required, the recorder is calibrated so that its ± 1.5 vdc input will coincide with the input to the chart recorder with respect to target aspect angle and signal levels.

4. The target is revolved through at least two complete revolutions (720°) in order to demonstrate the data repeatability.

5. The standard reference sphere is again measured as in (1) above as a check on long term stability of the measuring system.

MEASUREMENT PROGRAMS

Range Evaluation

Initially a comprehensive range evaluation program was conducted to determine background levels and also to see if there were any undesirable effects in using a ground plane range for cross section measurements. Upon completion of this program it was evident that the advantages of a ground-plane range as used in measuring conventional antenna parameters were also applicable to radar reflectivity measurements.

1. Sphere Measurements. Spheres varying in size from approximately $.05\text{m}^2$ to $.3\text{m}^2$ were measured. All of the measured values were in excellent agreement with calculated values.

2. Cylinder Measurements. In order to check the effects of the separation distance between the transmit-receive antenna and targets, a series of measurements were conducted using eight inch diameter cylinders. The lengths measured were 5, 10, 15, 20, 25, and 30 feet. The measurements were taken at X-Band at a range of approximately 1800 feet. The results indicated that if a minimum separation of $1.6 D^2/\lambda$ is used, the measured values will have excellent agreement with calculated values. As the separation distance decreases below this limit, the target return decreases. For example, the broadside return of the cylinder target 30 feet in length ($0.2D^2/\lambda$) measured 7.5 db lower than the calculated value.

Typical Measurement Project

The cross section return as a function of aspect angle of various full scale satellite models such as the Tiros, Nimbus, Sputnik,

Lunik, and Vostok II, were measured. The measurements were performed at the X-Band frequency for both vertical and horizontal polarization. The range length was approximately 1800 feet. Target sizes varied from a few feet in diameter (Tiros) to approximately eight feet in diameter and thirty feet long (Vostok II). Target weights averaged about 300 lbs. Analog rectangular and magnetic tape recordings of the target cross section returns as a function of aspect angle were compiled. The dynamic range was 60 db. At various aspect angles where the target configuration was such as to allow approximate calculations, the measured cross section return agreed very closely with the calculated values.

CONCLUDING COMMENT

The experience gained on the Electronic Space Structures Corporation ground-plane reflectivity range reinforces the high performance expectation for this type of facility. Within the range's physical limitations, excellent measurements can be made for full scale as well as model targets. A carefully conducted experimental program is needed to determine the ultimate utility of the ground-plane range technique.

Bibliography

1. "The Lincoln Laboratory Antenna Test Range," by A. Cohen and A. W. Maltese, Microwave Journal, April 1961. Messrs. Cohen and Maltese are now on the staff of ESSCO.
2. "Techniques for Measurement of Reduced Radar Cross Sections," C. G. Backman, H. E. King, R. C. Hansen, Aerospace Corporation, October 1962, Contract No. AF04(695)-69.

AERONUTRONIC MICROWAVE REFLECTIVITY FACILITY

Harold G. Collins, Research and Development Engineer
Aeronutronic Division of Philco Corporation
Newport Beach, California

ABSTRACT

This paper describes an indoor anechoic chamber measurement site and accompanying instrumentation. A microwave system, its measurement accuracy, and results of facility performance are also presented.

INTRODUCTION

In the following discussion, the Aeronutronic Microwave Reflectivity Facility is described which features an integrated instrumentation system and microwave anechoic chamber. Measurement instrumentation presently includes L- and C-bands. Included is the predicted accuracy of the measurement facility.

The facility is concerned primarily with the monostatic type of cross section measurement. Investigations involve measurements of scale models as well as full scale targets. Targets, however, are limited in physical size and weight. Some results of performance are also illustrated.

THE MEASUREMENT SITE

The site for radar cross section measurements is a microwave anechoic chamber, 18 ft. wide x 18 ft. high x 70 ft. long¹ combined with an adjoining operations room. The chamber utilizes the longitudinal baffle concept. The canted surfaces of the overhead, deck and three walls are covered with a lightweight artificial dielectric loaded flexible foam material.² The transmitter end wall is covered with lightweight rigid foam block absorber material.³ The flexible foam exhibits a power reflectivity of about 0.01 percent or -40 db through K_a band, and gradually diminishing to -30 db at L band. The rigid foam absorber functions over a broad frequency range with nominal power reflectivity of 1.0 percent or -20 db. Figure 1 shows an internal view of the chamber looking toward the transmitter end wall, as technicians position a precision calibration sphere atop an electrically rotated styrofoam column. The chamber is designed to exhibit low reflectivity.

The design of the chamber is such as to produce a cylindrical quiet zone about the longitudinal axis of the chamber. Tests conducted in evaluating its performance indicate an overall quiet-zone reflectivity level of nearly -55 db within a three and one-half foot diameter cylindrical zone at 2.6 Kmc. This level was measured using the pattern comparison technique.⁴ The technique is one of several methods of evaluating a microwave anechoic chamber. Quiet-zone reflectivity is defined as the

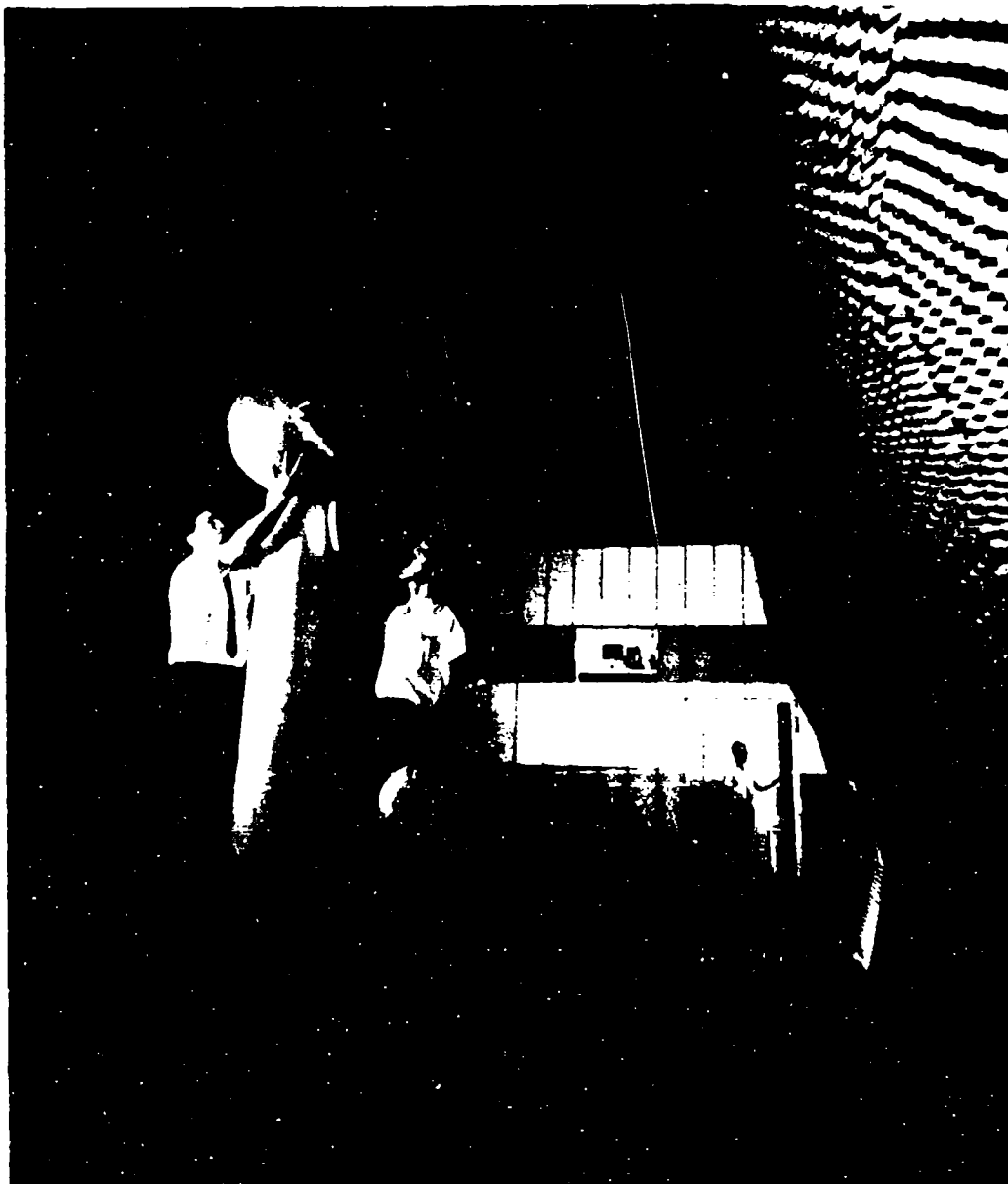


**FIGURE 1. INTERNAL VIEW OF THE ANECHOIC CHAMBER.
TECHNICIANS POSITION A PRECISION CALIBRATION SPHERE
ATOP AN ELECTRICALLY ROTATED STYROFOAM COLUMN.**

ratio of reflected power density to direct transmitted power density in the specified zone under a condition of one way energy propagation between transmitting and receiving antennas.⁵ In addition, the chamber equivalent radar cross section is exceedingly small. The measured value is 0.001 M^2 at a target distance of 50 feet, which is equivalent to 0.00006 M^2 at a target distance of 25 feet. The chamber equivalent radar cross section is defined as the apparent "background" cross section in square meters at a specified target distance. Typical transmitting and receiving antennas are arranged as for the measurement of a target, but no target is in position.⁶ Thus, use of a microwave darkroom for measurement of radar cross section characteristics of a target implies two-way propagation.

MEASUREMENT INSTRUMENTATION

The adjoining operations room houses the instrumentation equipment and provides personnel work areas. The facility is presently instrumented for CW operation at C- and L-bands. Instrumentation at other bands is planned and will be carried out in the future.

The limit of measurement of cross section is determined by the transmitter power output and the detection sensitivity of the device employed as the r-f detector. The detection sensitivity is ultimately limited at the level of the equivalent input noise of the receiving device. A receiver-recorder combination is provided as the r-f detector. Hence, for a given transmitter-receiver combination, the lower limit is determined by the resultant equivalent radar cross section of the receiving system noise.

To achieve the greatest capability from the measurement facility, some means must be incorporated to provide maximum signal isolation between the transmitter and receiver. The transmitter signal as well as an extraneous reflected background signal from the target environment into the receiver must be reduced to below the equivalent input noise of the receiver. There are two conventional wave guide configurations employed for this purpose: (1) the two-antenna wave guide system, (2) the single-antenna wave guide system. Either may be employed in measurement of monostatic radar cross section.

Transmitting and Receiving Equipment

The transmitter output power generally will range from 100 mw to perhaps 10 watts depending on frequency of operation, system losses encountered, minimum cross section requirements, antenna gain, target distance, and error limitations. For C-band operation, the signal source provides 100 mw output power at a frequency of 5.6 Kmc.

The r-f detector is a receiving system which includes a wide range superheterodyne receiver and rectangular coordinate pattern recorder. The receiver operates over a dynamic range of 40 db with linear deviation of less than 1 db, and fulfills all requirements of a receiver in a measurement system over an operating range of 30 Mc - 75 Kmc. The receiver-recorder combination provides a detection sensitivity of -100 dbm at 5.6 Kmc.

ACCURACY OF THE MEASUREMENT FACILITY SYSTEM

Recorder error and receiver non-linearity in combination is shown to be less than 0.25 db over the operating range. This test is performed with precision step attenuators in the receiver i-f. Additional uncertainty is allowed due to errors within the instrumentation equipment. Thus, a value of 0.5 db is taken in addition to the error that arises from measurement of a target in the presence of residual background σ_r .

Figure 2 illustrates the error for levels of cross section with a random noise (incoherent) background σ_n . This indicates the expected accuracy in which the described C-band system can measure target radar cross section with receiving system noise as the residual background.

It is interesting to note the decrease in measurement accuracy of a given target level with increase in residual background level. Figure 3 illustrates the error for levels of cross section σ_t with single frequency coherent residual background σ_r . Hence, if the residual background changes from the initial incoherent to coherent state with a 10 db change in level, then the error for a given target cross section can be expected to lie within the values given in Figures 2 and 3. One can see the desirability of reducing the coherent signal into the receiver noise and maintaining this condition during the measurement period. This shows the necessity for good signal source frequency stability and controlled environment of wave guide circuits in regard to temperature and mechanical stability.

FACILITY PERFORMANCE

The dynamic recorded range of received signal power is calibrated by a target of known radar cross section which provides an absolute reference calibration. Various precision spheres ranging in size up to 24 inches in diameter are used to establish the absolute response of recorded patterns for both horizontal and vertical polarizations. The values of radar cross section are expressed in square meters (M^2). Recorded patterns are scaled linearly in db.

Targets evaluated to date have shown that cross sections can be measured to within the predicted accuracies indicated in Figure 2. For example, a cross section of $0.001 M^2$ can be measured with an uncertainty of less than 1 db. A current program includes effort to produce measurements of $0.0001 M^2$ targets with an accuracy of 1 db. The success of techniques used is demonstrated by the mirror symmetry of the cylinder response pattern shown in Figure 4. The cylinder, 16 inches long by 0.5 inches in diameter, was illuminated by horizontally polarized C-band energy at a range of 25 feet. The response of a 2.02 inch diameter flat plate shown in Figure 5 was measured at a range of 15 feet at C-band.

σ_i	σ_r/σ_i	ERROR DUE TO σ_r	EXPECTED ERROR WITHIN
0.015 M ²	0.0001	0.1 db	0.5 db
0.001 M ²	0.0015	0.2 db	0.7 db
0.00025 M ²	0.006	0.5 db	1.0 db
0.00005 M ²	0.03	1.0 db	1.5 db
0.00002 M ²	0.08	1.5 db	2.0 db

FIGURE 2. OVERALL ERROR OF C-BAND SYSTEM FOR GIVEN LEVELS OF σ_i ,
WITH A RANDOM NOISE RESIDUAL BACKGROUND

σ_i	σ_r/σ_i	ERROR DUE TO σ_r	EXPECTED ERROR WITHIN
0.15 M ²	0.0001	0.1 db	0.5 db
0.005 M ²	0.003	0.5 db	1.0 db
0.0015 M ²	0.01	1.0 db	1.5 db
0.0005 M ²	0.025	1.5 db	2.0 db

FIGURE 3. OVERALL ERROR OF C-BAND SYSTEM FOR GIVEN LEVELS OF σ_i ,
WITH A SINGLE FREQUENCY RESIDUAL BACKGROUND
10 db ABOVE RECEIVER-RECORDER EQUIVALENT INPUT NOISE.

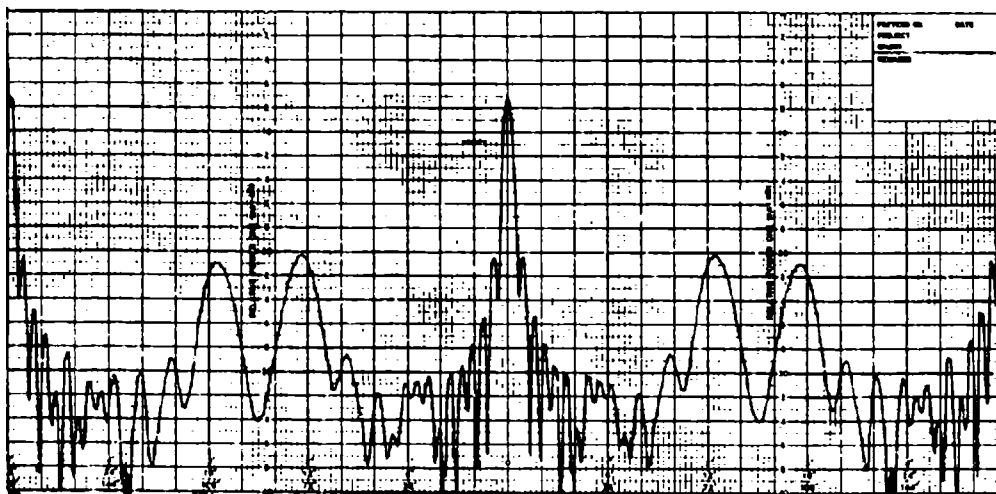


FIGURE 4. RESPONSE PATTERN OF CYLINDER 16 IN. LONG x 0.5 IN. IN DIAMETER. CYLINDER IS HORIZONTALLY MOUNTED AT A DISTANCE OF 25 FEET AND ROTATED THRU ASPECT OF 360°. FREQUENCY - 5650 mc.; POLARIZATION - HORIZONTAL; CALIBRATION STANDARD - 12 IN. SPHERE.

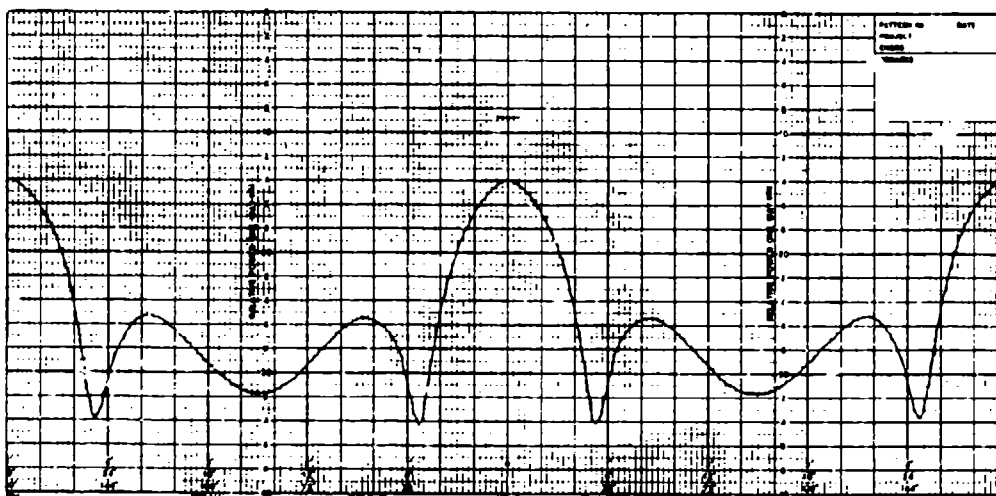


FIGURE 5. RESPONSE PATTERN OF CIRCULAR FLAT PLATE 2.02 IN. IN DIAMETER. DISC IS MEASURED AT A DISTANCE OF 15 FT. AND ROTATED THRU ASPECT OF 360°. FREQUENCY - 5650 mc.; POLAR. - VERTICAL; CALIBRATION STANDARD - 12 IN. SPHERE.

REFERENCES

1. Design No. 300, Emerson & Cuming, Inc., Canton, Massachusetts
2. Preliminary Technical Bulletin 8-2-14, Eccosorb CV, "40 db Down Microwave Absorber", Emerson & Cuming, Inc., Canton Massachusetts.
3. Technical Bulletin 8-2-5, Eccosorb FR, "Rigid Foam Microwave Absorber", Emerson & Cuming, Inc., Canton, Massachusetts.
4. Buckley, E. F., "The Design and Evaluation of Microwave Anechoic Chambers", Emerson & Cuming, Inc., Canton, Massachusetts, 1960. p. 2
5. Ibid., p. 2
6. Ibid., p. 3

MILLIMETRE WAVE SHORT PULSE RADARS FOR INDOOR ECHOING AREA MEASUREMENTS

L. A. Cram
E.M.I. Electronics Ltd.
Hayes, Middx, England

ABSTRACT

A brief description is given of equipment used for measuring radar echoing area by modelling methods. Pulse radars at 8.6 mm. and at 4.3 mm. are used indoors to measure echoes from models up to 10 feet in extent. Nylon strings support the model from a gantry structure by means of which the reflector may be rotated. Bistatic and monostatic measurements are possible. Calibration is against a sphere. Sensitivity is to $1/30$ square wavelengths at 8.6 mm. and 6 square wavelengths at 4.3 mm.

INTRODUCTION

Model radar equipments have been made at wavelengths of 8.6 mm. and 4.3 mm. These are pulse radars and use 25nS R.F. pulses to illuminate a volume of about 10 feet cube at a range of about 45 feet. With the 8.6 mm. equipment a minimum detectable reflecting area of $0.03 \lambda^2$ has been achieved in this volume of 1,000 cu. feet. Reflecting models have included simple geometrical shapes as well as models of aircraft made from metal or metalised wood. Nylon strings are used for model support and facilities are available for varying a model's attitude and for rotating it on a vertical axis. Some data has been obtained on reflections from suspension strings.

The equipment is used indoors and interfering reflections from the building are avoided by the combination of aerial polar diagrams and range gating.

8.6 mm. RADAR SYSTEMS

The radar operates at 35 Gc/s and uses 25nS pulses at 500 p.p.s. Separate lens aeriels are used for transmission and reception so that bistatic measurements are possible. However, the receiver can be used quite adjacent to the transmitter so as to effectively simulate monostatic operation.

TRANSMITTER

A Q-band magnetron type VX 5027 made by E.M.I. is used and delivers 20kW peak power. A Blumlein modulator was originally used with a thyratron but this has now been replaced by a hard valve modulator using two tetrodes in parallel (Type C 1149 by English Electric). This produces an R.F. pulse with $1\frac{1}{2}$ nS rise time, 25nS flat top, and 12nS fall time.

RECEIVER

The receiver uses a superheterodyne circuit with 4,000 Mc/s I.F. frequency. The local oscillator is a klystron (E.M.I. R 9521) and is tuned to 39 Gc/s. The high

Intermediate frequency was chosen to simplify the avoidance of gating pulse transients. Two travelling wave tubes comprise the I.F. amplifier. These are W 9/2 E (9dB noise factor) and W 7/4 G - both by S.T.C. Range gating is applied at the first TWA with a 50nS pulse on its anode. This provides 80dB attenuation outside the gating period and some compensation for R^4 within the gate. Bandwidth is limited to 50 Mc/s by a 3 section post filter in waveguide. The detected output is displayed on a travelling wave oscilloscope for monitoring. It is also fed to a pulse stretching amplifier and feeds both a roll chart recorder and a pulse height analyser with dekatron display. The dekatron display is photographed at intervals to simplify the plotting of echoing area probability curves.

AERIALS

Separate aerials are used for transmission and for reception and these consist of identical lenses illuminated by the main lobe and by part of the first side lobes of the feed horns. This provides a flat pattern with less than $1\frac{1}{2}$ dB change over a region $12^\circ \times 12^\circ$ thus giving less than 3dB change in radar response over a region 9 ft. \times 9 ft. at 45 ft. range. The pattern falls off fairly rapidly at greater angles so that at 12° off axis the return signal is 40dB down. Since the radar horns are mounted about $4\frac{1}{2}$ feet from the floor and are aimed 10° upwards at the target this sharp cut off protects against reflections from the concrete floor or from the roof. Reflections from the gantry which supports the model and from the back walls and most of the roof are prevented by the range gating which provides a working region 12 feet in length along the beam axis in which the sensitivity changes by only 1dB.

CALIBRATION

The output signal level is recorded with a range of only 12dB. For greater excursions than this the experiment is repeated with a different setting of microwave attenuation to permit examination of the troughs or the peaks of the pattern. Repetitions without attenuation change give identical records. The microwave attenuator is of the rotating type and is highly reliable. Consequently, calibration is done with a single sphere of 20 square cms. echoing area which is suspended in the centre of the radar beam and range gate. A number of attenuator settings at 1dB intervals are then used to mark the record with different equivalent echoing areas. A very convenient secondary calibration is also available in the form of a fraction of power bled from the transmitter by a 33dB directional coupler and fed via a 90nS microwave delay line (60 feet of WG 22). This signal then couples through a calibrated attenuator to a microwave switch. The mechanical operation of this switch substitutes the secondary calibration signal for the signal from the aerial to the receiver. This secondary standard is used at intervals throughout an experiment.

MODEL CONTROL

The model is supported on nylon strings from pulleys in the ends of a cruciform. A string from one point of the model passes over the pulley and down to the opposite extremity of the model. The pulleys are motorised and may be operated from the ground to set the model at any attitude without altering its height. The cruciform can be rotated continuously on a vertical axis to rotate the model. Translation of the model in a horizontal plane is also possible because the cruciform is mounted on a railway which is itself mounted on an orthogonal railway in the roof. Provision has been made on the main translational control for smooth acceleration and deceleration so that smooth model motion can be obtained for projected coherent work. All control is done from the ground. In rotational trials, marker signals are provided for the records at 5° intervals. In translational motion, markers are available at 1 ft. intervals.

NYLON STRINGS

H-plane and E-plane reflections from nylon strings of different breaking strains were measured. For the 1mm. diameter 60 lbs. string the E-plane echo was 40 sq. cms. but this was mainly specular and could be reduced 20dB by ensuring that the first normal Fresnel zone did not lie in the string. Stringing with this angular restriction has proved satisfactory for much of the work and permits a fairly rigid mounting with negligible oscillation of the model during rotation. If horizontal polarization is permissible then some 6dB further reduction is achievable while a string of half the breaking strain gives yet another 6dB reduction in reflection.

PERFORMANCE

The radar loop loss is 140dB and provides a detectivity of 1.6 square millimetres at 14 metres range. This is equivalent to $1/30$ square wavelengths. No attempt has been made to improve on this. In rotating a model to plot its radar cross section one rotation takes 150 seconds. The chart recorder usually used has 50 c/s bandwidth and consequently gives data every 3 minutes of arc representing the integration of 10 echo pulses from the 500 p.p.s. radar.

4.3 mm. RADAR SYSTEMS

The 70 Gc/s radar has similar specifications to the 35 Gc/s radar and uses the same modulation and aerial diagram.

The 4 Gc/s I.F. is retained and to provide this the 8 mm. klystron is tuned to 38 Gc/s and is used to drive a harmonic mixer. A loop loss of 114dB is achieved with 1kW radiated from the transmitter and this provides a detectivity of 6 square wavelengths or 10^{-4} sq metres. This detectivity is ample for some purposes but it is proposed to increase the loop loss by 20dB for other applications, by increasing the transmitter power

and by using a 74 Gc/s klystron with direct mixing.

ACKNOWLEDGEMENT

This work was carried out at the E.M.I. Laboratories at Wells, Somerset, under a contract from the Ministry of Aviation and was directed by the Royal Radar Establishment, Malvern.

THE LINCOLN LABORATORY MODEL BACKSCATTER RANGE

P. C. Fritsch, D. F. Sedivec, A. J. Yakutis
M.I.T. Lincoln Laboratory

ABSTRACT

The Lincoln Laboratory Range houses two major equipments in a room a little over 100 feet long, viz., a K_u band C. W. radar and a K_u band short pulse radar. Special emphasis has been given to the development of precise methods of measuring very low values of radar cross section.

The Lincoln Laboratory model backscatter range was set up in 1961 under the aegis of the BMRS (Ballistic Missile Re-entry Systems) program in order to supply that program with valid data on the radar scattering cross section (RCS) of a variety of objects. Its main interests have been in the measurement of low cross section objects and in the development of cross section measuring techniques.

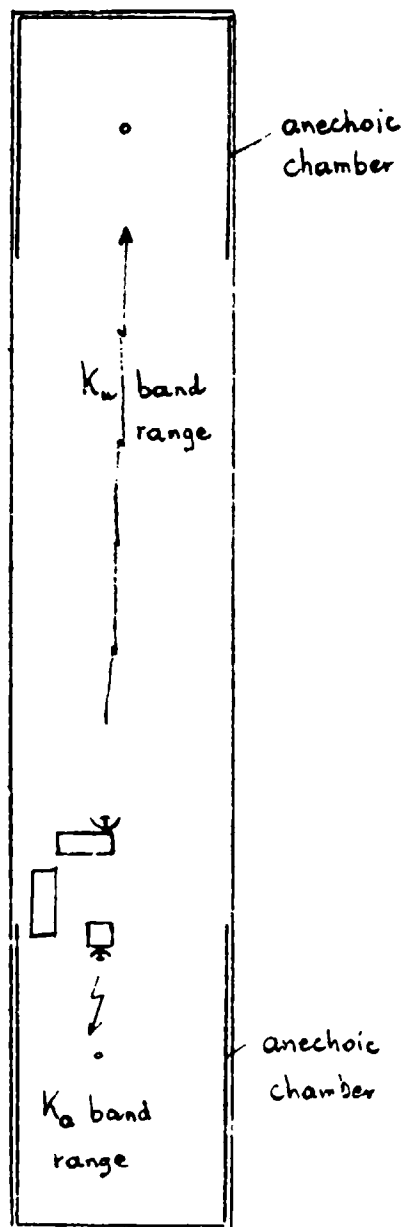
The laboratory operation to date has been a complete success in acquainting us with the complexities of RCS measurement and related problems, such as operation of a specialized machine shop, optical tooling and alignment techniques, and digital computer data processing. Although only a modest effort, (at least in terms of man power) we feel that in addition our range has already made some novel contribution to RCS measurements techniques; many new concepts remain to be explored.

While the RCS range itself constitutes a more or less conventional indoor model facility, the personnel involved have also been called upon to carry out logically related tasks on behalf of the U. S. Air Force. These have included technical consultations for Project RATSCAT (a full scale RCS range), and periodic surveys of RCS facilities in the U. S. and abroad. Sponsorship by Lincoln Laboratory of this Symposium is also a consequence of the experiences with our RCS laboratory.

Despite the attraction of other sites, such as penthouse areas and quiet field stations, it was decided early to locate the RCS laboratory within the main complex of Lincoln Laboratory for easy access from and to the many other laboratory facilities. Located in a high-bay basement area, the laboratory is 113 feet long, by about 20 feet wide and 12 feet high. Anechoic chambers have been constructed at each end (Fig. 1), while work benches, desks, and test equipment are located along the side walls. Operationally, the area is divided into a 35 foot long K_u band C.W. radar range, and a 70 foot long K_u band pulsed radar range.

To date, virtually all measurement work has been carried out by means of the C.W. radar. Operating at a fixed frequency near 35 Gc, this equip-

*Operated with support from the U. S. Air Force.



— 20 FT.

Fig. 1. Floor Plan of Radar Reflectivity Laboratory

ment consists of a 1 watt transmitting tube and a local oscillator. These two sources are offset 30 megacycles above and below the nominal operating frequency, respectively; thus, on mixing, they result in an intermediate frequency, of 60 mc. Both the r.f. and i.f. are derived from and continually compared to a 5 mc crystal controlled oscillator by means of a series of phase-locked multiplier circuits. The 5 mc oscillator and most of the multiplier circuits up to 1000 mc are commercial equipment; a "times 35" crystal multiplier mounted in K_u band waveguide and all other waveguide circuitry were constructed at our laboratory.

The 35.03 Gc signal from the transmitter tube is radiated via a lens-corrected conical horn, and received, after reflection from a target, by a near-by receiving antenna of similar construction. Mixing with the 34.97 Gc local oscillator signal produces a 60 mc i.f., which is divided into two parts. One portion forms the input to a logarithmic amplifier (successive detection type) for amplitude measurement, the other portion is clipped in a limiting amplifier for subsequent processing by a phase detector. Particular attention is drawn to the "balancing branch", by means of which a small portion of the transmitter signal can be withdrawn before it reaches the antenna, modified in amplitude and phase, and injected at the receiver input in parallel with the signal received from the target through the receiving antenna. This device is used to "cancel the background": in the absence of the test target, the radar still receives a certain signal due principally to reflections from the anechoic chamber, the target support, and the rest of the environment. The balancing branch is then used to generate a signal of equal amplitude but opposite phase to cancel the background signal as seen at the receiver input terminals. Since the target is many wavelengths distant, it is easy to see that any frequency drift on the part of the transmitter would make the cancellation a very phase sensitive operation, which is the main reason for phase locking both transmitter and local oscillator. With a two antenna system as described above, we have succeeded in cancelling the background signal to below the noise level of the receiver for fractions of an hour at a time (amounting, in other terms, to virtual isolation between receiver and transmitter in excess of 110 db).

Ordinarily, the targets measured by use of the K_u band radar are placed on a styrofoam column 5 to 10 feet in front of the antennas. Typical targets have been up to 6 inches long and weighing a few pounds. The column stands on a rotator which permits control of the azimuth angle of the target. Both that angle and the corresponding amplitude are recorded using Scientific-Atlanta antenna pattern recorders. More sophisticated support and data recording systems are described elsewhere in this Symposium Record.

The two antennas, being conical horns, are inherently capable of supporting any polarization. Dual-linear and dual-circular polarization transducers, which can be coupled directly to the horns, have been constructed to take advantage of this flexibility.

The primary reason for constructing the second major equipment in the RCS laboratory (the K_u band pulsed radar) was to extend the limitation on

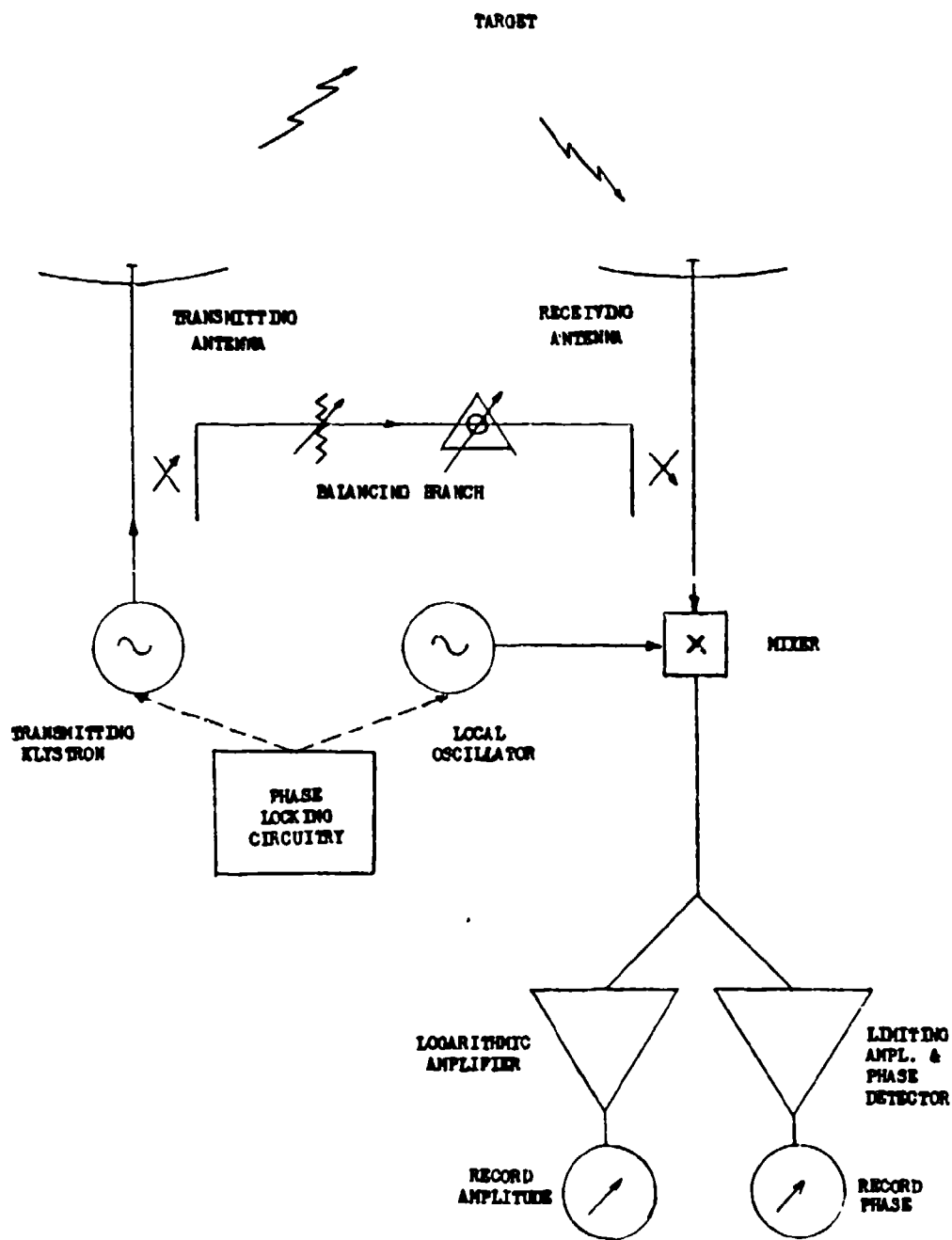


Fig. 2. Schematic of K_a Band C.W. Radar

target sizes imposed by the relatively low sensitivity of the C.W. radar. At a distance of 70 feet, it should be possible to examine 2 foot long targets at K_u band. In order to avoid having to convert the entire laboratory into an anechoic chamber, and also in order to avoid interference from the back wall, it was decided to pulse the transmitter and gate the receiver. Because of the limitations of size, pulses and gates must be quite short, of course: our equipment was therefore designed to radiate pulses as short as 10 nanoseconds. In order to exploit the maximum duty factor permissible, pulse repetition rates of to 50 kc can be obtained.

The basic block diagram is shown in Fig. 3. It can be seen that the transmitter consists of a chain of two grid-pulsed TWT amplifier tubes excited from a C.W. klystron. Tuning the latter can produce any frequency between 14 and 18 Gc. The final amplifier is capable of delivering 1 kw peak pulses into the antenna; a nearby receiving antenna picks up the target reflection, which at present is converted to an i.f. of 30 mc. An experiment has been performed in which the driver klystron was phase locked much in the manner of the K_u radar; by means of a balancing branch, it was then shown, it was possible to perform background cancellation within the region encompassed by the range gate.

A small machine shop supporting the RCS laboratory exclusively contains three pieces of equipment worth mentioning. A Hendey 16 inch lathe with a Mimic hydraulic tracer attachment has been found very useful for the fabrication and reproduction of rotationally symmetrical models; an FC-14 Jones & Lamson 14 inch optical comparator is invaluable for inspecting models and other critical parts; and a MU-6 Micro-Balancing Corporation (Division of Giannini Scientific) balancing machine which, as is pointed out elsewhere, is indispensable for drop-spin measurements.

The entire installation is staffed by two to three professional engineers and a like number of electronic and electro-mechanical technicians. Besides the authors, Mr. F. B. Magurn has made notable contributions to the operation of the laboratory.

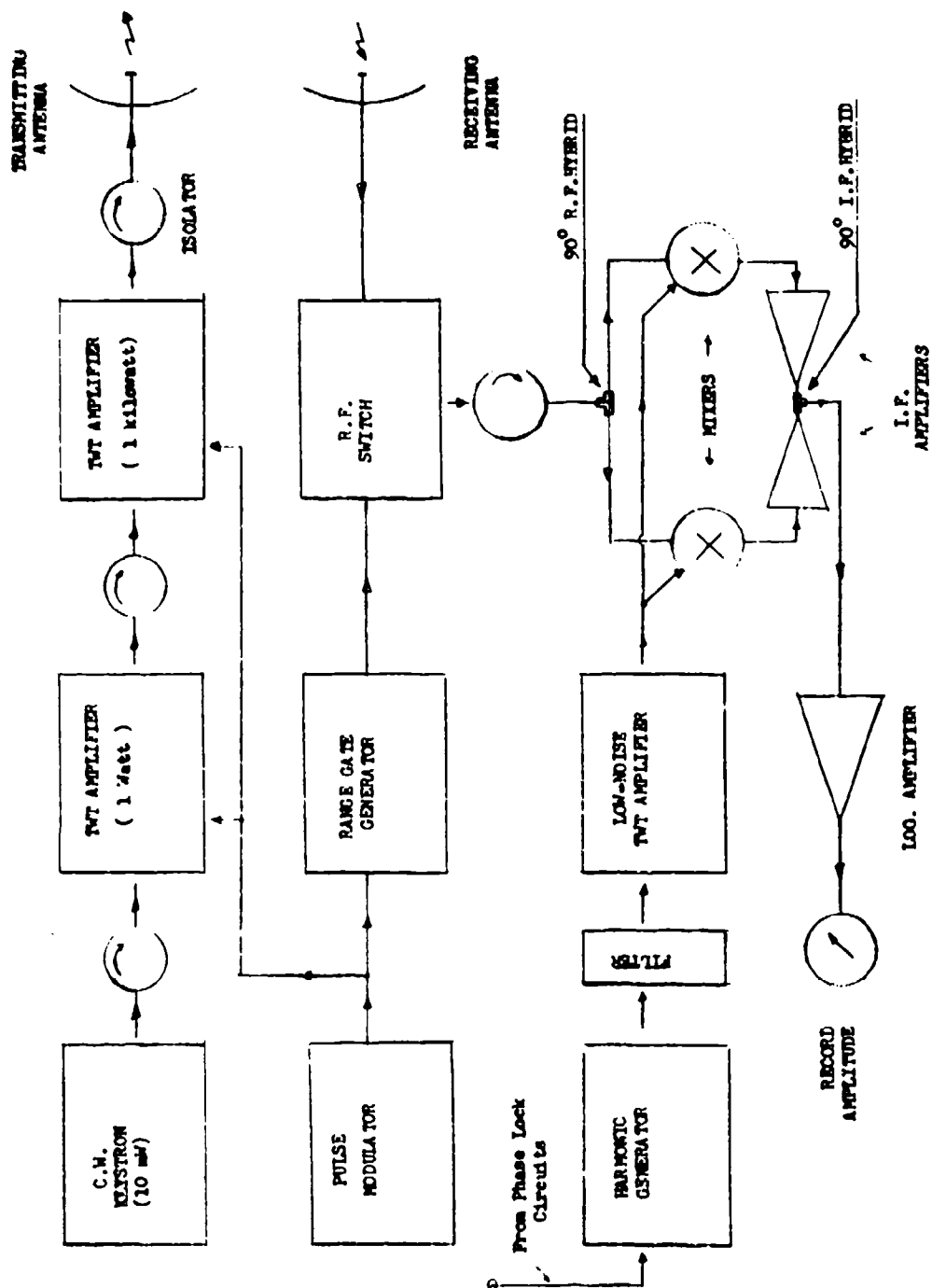


Fig. 3. Schematic of K_u Band Short-Pulse Radar

LOCKHEED MISSILES AND SPACE COMPANY SCATTERING RANGE CAPABILITIES

N. J. Gamara
Electromagnetics Branch
Sunnyvale, California

11 Dec 63

Outdoor Range

Frequency Range (C or Continuous)	Mode of Operation	Transmitter Power	Transmitter Power Stability (db/hr)	Transmitter Sensitivity (dbm)	Receiver Linearity/ Dynamic Range (db)	Receiver Gain Stability (db/hr)	Receiver Gate Rejection (db)	Background Nulling Capability (db below transmitter power)	Antenna Target Separation (meters)	Max. Linear Target Dyn. (meters)	σ Min. Detec- table (m ²)
VHF -band .40 - 1.00	CW	500MW	.50	-100	40.0 ⁺ 5/40	.5	NA	100	38 - 76	4.0	10 ⁻⁵
L-band 1.00 - 1.7	CW	100MW	.50	-100	40.0 ⁺ 5/40	.5	NA	100	38 - 76	2.6	10 ⁻⁵
S-band 3.05	Pulse	12KW P1 sec width at base: .1 usec. PRF:1000	.50	-85	40.0 ⁺ 1/40	.5	70	NA	360	4.0	10 ⁻⁵
C-band 5.45 - 5.85	Pulse	60KW P1 sec width at base: .1 usec. PRF:1000	.50	-85	40.0 ⁺ 1/40	.5	70	NA	360	2.2	10 ⁻⁵
X-band 8.50 - 9.60	Pulse	12KW P1 sec width at base: .1 usec. PRF:1000	.50	-65	40.0 ⁺ 2/40	1.0	40	NA	360	2.2	10 ⁻¹
K-band 23.88	Pulse	10KW P1 sec width at base: .1 usec. PRF:100	.50	-60	40.0 ⁺ 2/40	1.0	40	NA	360	1.1	10 ⁻¹

LOCKHEED MISSILES AND SPACE COMPANY SCATTERING RANGE CAPABILITIES

N. J. Gamara
Electromagnetics Branch
Sunnyvale, California

Frequency Range (Gc Continuous)	Mode of Operation	Transmitter Power	Transmitter Power Stability (db/hr)	Receiver Sensitivity (dbm)	Anechoic Chamber				Antenna Target Separation (meters)	Max. Linear Target Dim. (meters)	σ Min. Detec- table (m ²)
					Receiver Linearity/ Dynamic Range(db)	Receiver Gain/ Stability (db/hr)	Gate Rejection (db)	Background Nulling Capability (db below transmitter power)			
S-band 2.60 - 3.95	CW	100MW	.50	-105	60.0 ⁺ .5/60	.5	NA	110	3 - 16	.8	1x10 ⁻⁷
G-band 3.95 - 5.85	CW	100MW	.50	-100	60.0 ⁺ .5/50	.5	NA	110	3 - 16	.6	1x10 ⁻⁷
J-band 5.85 - 8.20	CW	100MW	.50	-100	60.0 ⁺ .5/60	.5	NA	110	5 - 16	.5	1x10 ⁻⁷
X-band 8.20 - 12.40	CW	100MW	.50	-90	60.0 ⁺ .5/60	.5	NA	110	10.5 - 16	.5	1x10 ⁻⁷
K _u -band 12.40 - 18.00	CW	100MW	.50	-85	60.0 ⁺ .5/60	.5	NA	100	7.0 - 16	.3	1x10 ⁻⁶

EXPERIMENTAL REFLECTIVITY FACILITIES

Robert J. Garbacz
Antenna Laboratory
Department of Electrical Engineering
The Ohio State University
Columbus, Ohio 43210

INTRODUCTION

The Ohio State University Antenna Laboratory has had various radar reflectivity facilities in continuous operation since the end of the Second World War and its staff has been instrumental in developing equipment and techniques for echo study. Today, reflectivity facilities at the Laboratory include two pulse ranges at 24 and 35.1 Gc, amplitude CW ranges in S- and X-band, a CW amplitude and phase range in X-band, and mobile terrain equipment. These facilities are used primarily for experimental verification of theoretical analyses and to provide graduate students in Electrical Engineering, Mathematics, and Physics data for the completion of modern theses and dissertations. Since 1947, 14 thesis, 15 dissertations, and 68 published and oral papers on the subject of radar cross section have been completed by the staff of the Laboratory.

Before describing The Ohio State University facilities in detail, some preliminary discussion is necessary concerning range measuring capability. It is our opinion that to quote some "magic number" for the lowest measurable cross section or background level within a particular accuracy is naive and misleading. So many variables enter into the problem that it is unrealistic to think that their varying effects can be compressed into one number. Such variables as polarization, transmitter and receiver locations, range, target support, size, shape, and location of target, all influence the measurement accuracy and so should be specified. Consequently, the capabilities of The Ohio State University ranges are given here in terms of measurements actually recorded on particular targets. No attempt has been made to extrapolate these results to some optimum minimum cross-section.

Brief descriptions of each range are given and all pertinent specifications are summarized in table form.

ANECHOIC CHAMBER

The Ohio State University Antenna Laboratory has one anechoic chamber in operation at present. This air conditioned chamber is 50 feet long, 20 feet wide, 20 feet high, and has walls and ceiling covered with Goodrich hairflex. In addition three large movable panels, each 6 feet wide, 14 feet high of Goodrich VHP-3 material have been provided for flexible room arrangements. A fourth panel of Emerson and Cuming material is being constructed. The floor is uncovered. Targets are supported by nylon strings whose rotation is synched to strip chart pen recorders. Transits are used for accurate positioning of targets. The target site is approximately at the geometric center of the room, provided a working circle of about 7 feet radius for bistatic arrangements of transmitter and receiver antennas. Bistatic angles to 180° are possible, but only those to 140° have been found practical. In the monostatic configuration a range of about 7 feet is maintained, although this can be increased to about 13 feet if necessary. The microwave system,¹ sketched in block form in Fig. 1, is mounted within a steel tower supporting a 5 inch square horn antenna at a height of 9 feet above the floor. An L. F. E. cavity-stabilized klystron, continuously variable in frequency from 8.5 to 10.0 Gc. and with a maximum output power of 500 MW, is used as the microwave source. In bistatic operation, the receiver horn, and ferrite modulator are mounted compactly on a movable stanchion.

In both the monostatic and bistatic cases as shown in Figs 1 and 2 the echo signal is combined in a hybrid tee with a coherent reference signal such that the amplified and filtered output is proportional to a time-quadrature component of the echo signal; a 90° phase change of the reference yields the other quadrature component, thereby permitting a resolution of the phase as well as the amplitude of the scattered field. In this phase sensitive mode a linear, zero-centering strip chart is the output format; if the amplitude mode is desired, it is a simple matter to short the reference loop and use a logarithmic strip chart output format. A provision has been made using a 90° sidewall coupler to permit simultaneous recording of quadrature patterns but this is not shown on the diagram because instrumentation is incomplete. In addition, an alternative stringing arrangement has been provided for use with the phase-sensitive system which permits a slow motion of the target along the line-of-sight. Such a technique² reduces background problems and allows quite low cross-sections to be measured.³ Provision is also made for a slow, smooth line-of-sight motion of the entire steel tower supporting the microwave transmitter for use in evaluating integrated room performance.

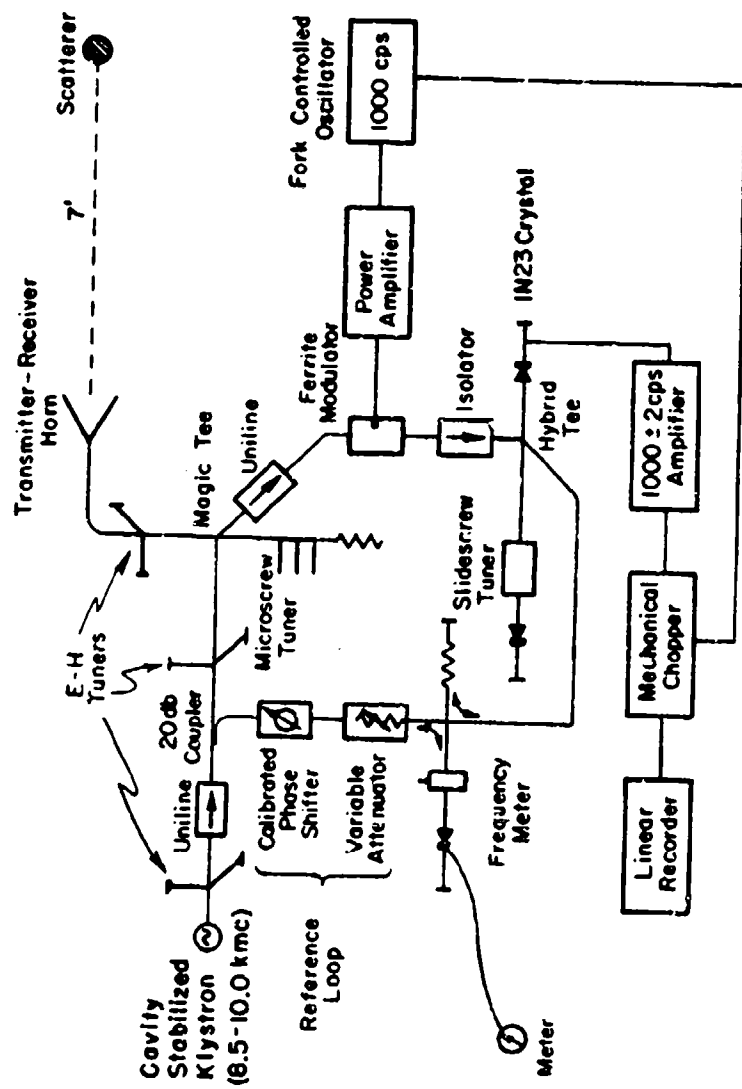


Fig. 1 Schematic diagram of equipment for measuring time-quantum components of a monostatic r field.

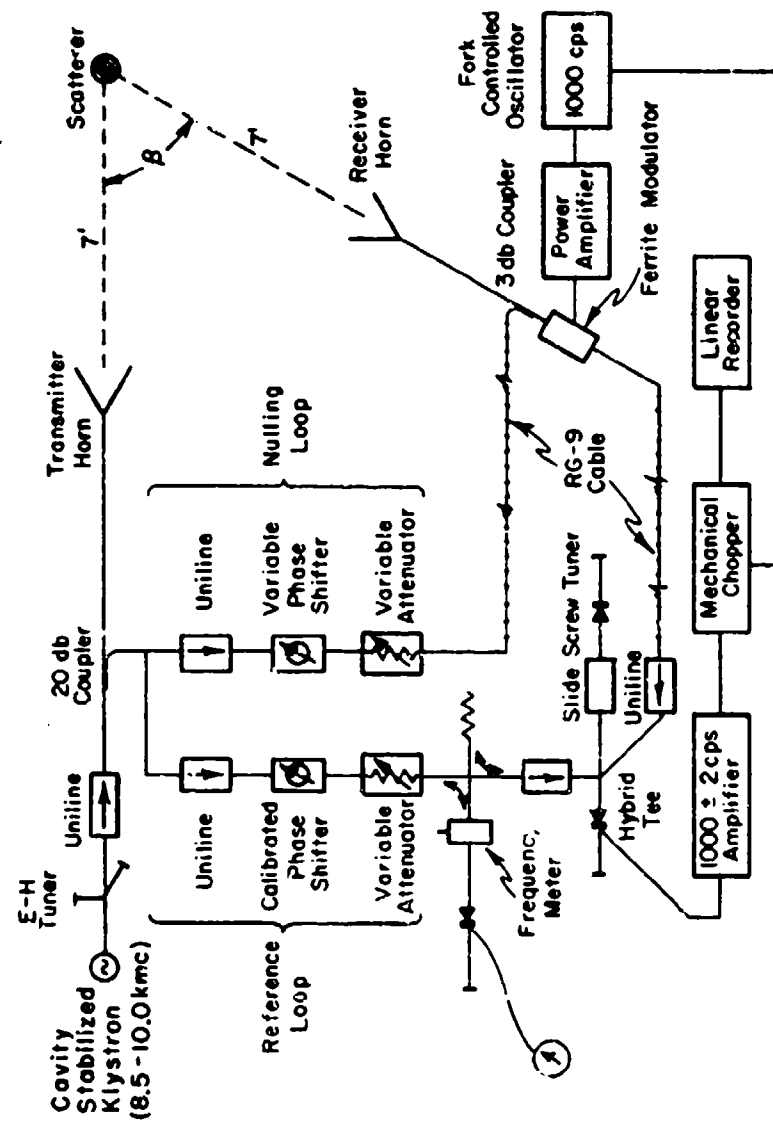


Fig. 2 Schematic diagram of equipment for measuring time-quadrature components of a bistatic scatter field.

Additional points which require comment are as follows.

All polarizations may be transmitted by use of a square horn in tandem with a dielectric plate polarization transformer section. Only linear polarization may be received bistatically.

At a 7 foot range, the amplitude of the wavefront varies less than 1 db within a circular disk 6 inches in diameter. The phase variation at this range over a 4 inch diameter disk is almost exactly that of a point source located at the throat of the transmitter horn, i. e., less than 15° variation over this disk at 10 Kmc.

Typical minimum measurable echo areas: In the amplitude mode metallic spheroid echoes as low as $0.03\lambda^2$ have been measured to within ± 0.5 db at a 3 foot range. This level was about 20 db above the null level.

Employing target motion, echoes of the order $0.01\lambda^2$ have been measured to within ± 1 db on cone-spheres and spheres at a 7 foot range. Data recorded by this method on metallic spheroids check those taken in the amplitude mode to within ± 0.5 db when the echo exceeds $\sim 0.03\lambda^2$.

Employing the phase sensitive system, echoes measured on metallic spheroids check within ± 0.5 db those measured in the amplitude mode when the echo exceeds $0.03\lambda^2$. Phase error is estimated at about $\pm 5^\circ$ under ideal measuring conditions. Echoes as low as $0.003\lambda^2$ have been measured with an estimated error of ± 1 db. Verification at such low levels is difficult.

All the above measurements were taken with horizontal polarization to minimize string return. Return from room reflection was considered satisfactory if the null varied less than 2 db (by beating with a known leak-through signal) when the transmitter tower was moved slowly along the line-of-sight. Such a "stable null" was found necessary for accurate low cross-sections.

K- AND KA-BAND RADAR ECHO RECORDING SYSTEMS^{4,5,6}

Both the K- and KA-band pulsed radar echo recording systems are basically the same. The description which follows applies to both; the transmitting and receiving characteristics for the individual systems are presented in table form.

Both systems make use of the same pedestal and A-frame for supporting and rotating strings and styrofoam columns. An absorbing fence, placed in front of the pedestal as a shield, can be positioned to improve background level. Coupling between the separate receiving and transmitting antennas limits the minimum range of operation.

The receiver input is maintained at a constant level by a servo-controlled resistive card attenuator located between the receiver antenna and the receiver input (see Fig. 3). The linear-logarithmic movement of the attenuator is a measure of the signal strength and is recorded in synchronism with rotation of the target on strip chart. The signal from the gated amplifier is observed on an oscilloscope enabling gating of the correct signal return from the target.

A portion of the transmitted signal is applied to the receiver AFC circuits which control the frequency of the local oscillator to remain in the passband of the IF's.

OUTDOOR CW FACILITIES

A permanent outdoor CW amplitude range is maintained by the Laboratory in X-band. In addition, the sources, antennas, and auxiliary equipment for operation in K-, K_u-, K_a-, S-, and L-bands are available. Only the X-band facility will be described here. The basic working site is 50 feet by 400 feet, with a building at one end of the plot to house the microwave equipment. The terrain is flat in all directions. Targets are supported by nylon strings from an A frame similar to the one used with the pulse ranges. Target rotation is synched to a strip chart pen recorder. At the usual operating range (25 feet to 40 feet) the A frame and pedestal rest on a cement pad. The basic operation is quasimonostatic; bistatic measurements are possible, the range in this case being limited to 50 feet or less. The target site is 9.5 feet above the ground. The antennas are 2 foot parabolic dishes with standard waveguide-dipole feeds. A metal-sheet between the antennas provides ≈ 25 db of isolation. The microwave system sketched in Fig. 4 is the standard null loop configuration. Details of the range are given in Table A.

Background level of the system with 20 pound test strings at 25 feet is approximately $0.08\lambda^2$ for horizontal polarization. Seasonal variations of 3 to 5 db above this figure due to foliage, winds, etc. are common. The amplitude and phase of the incident field vary no more than 1.0 db and 40° respectively over a 1 foot cube centered at the target site. The background levels with

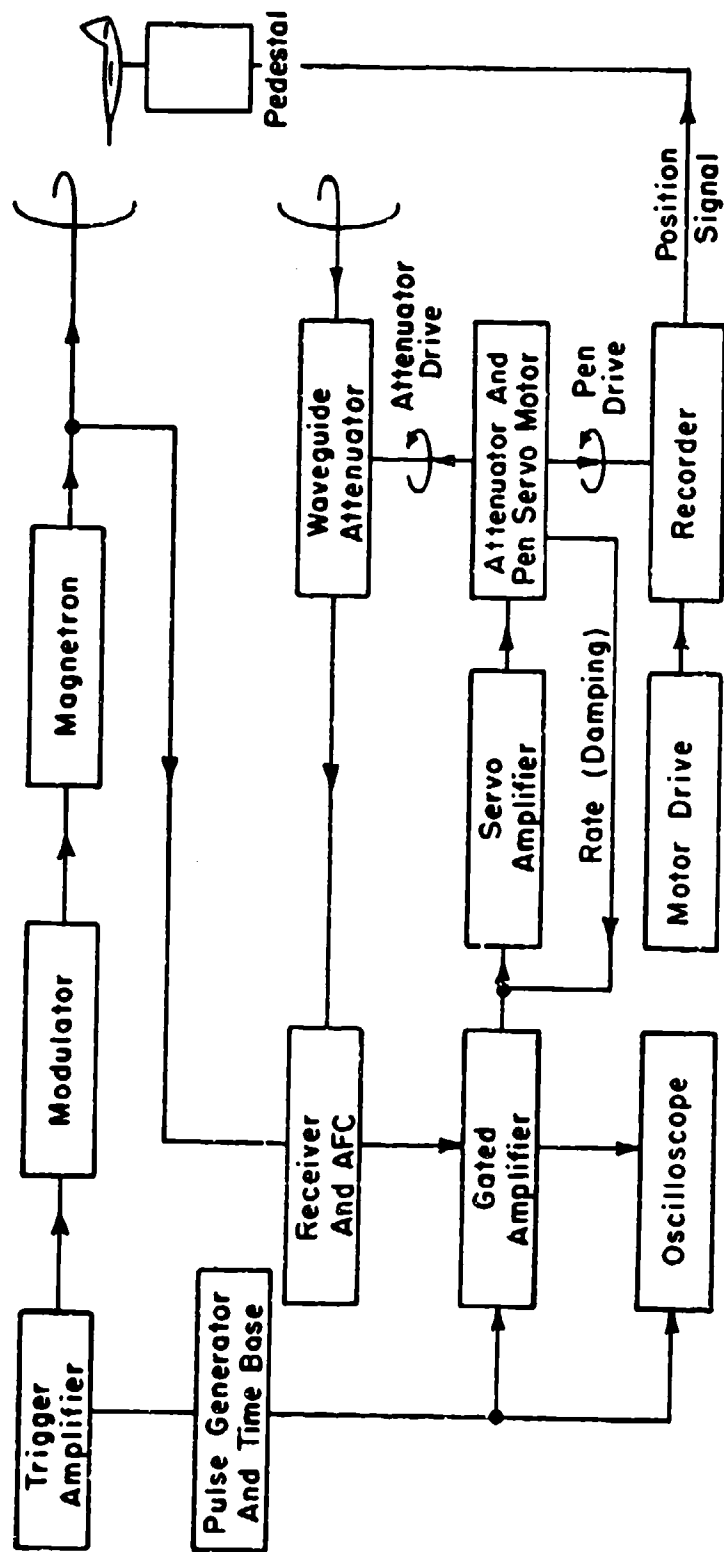


Figure 3. Block Diagram of Pulse Ranges.

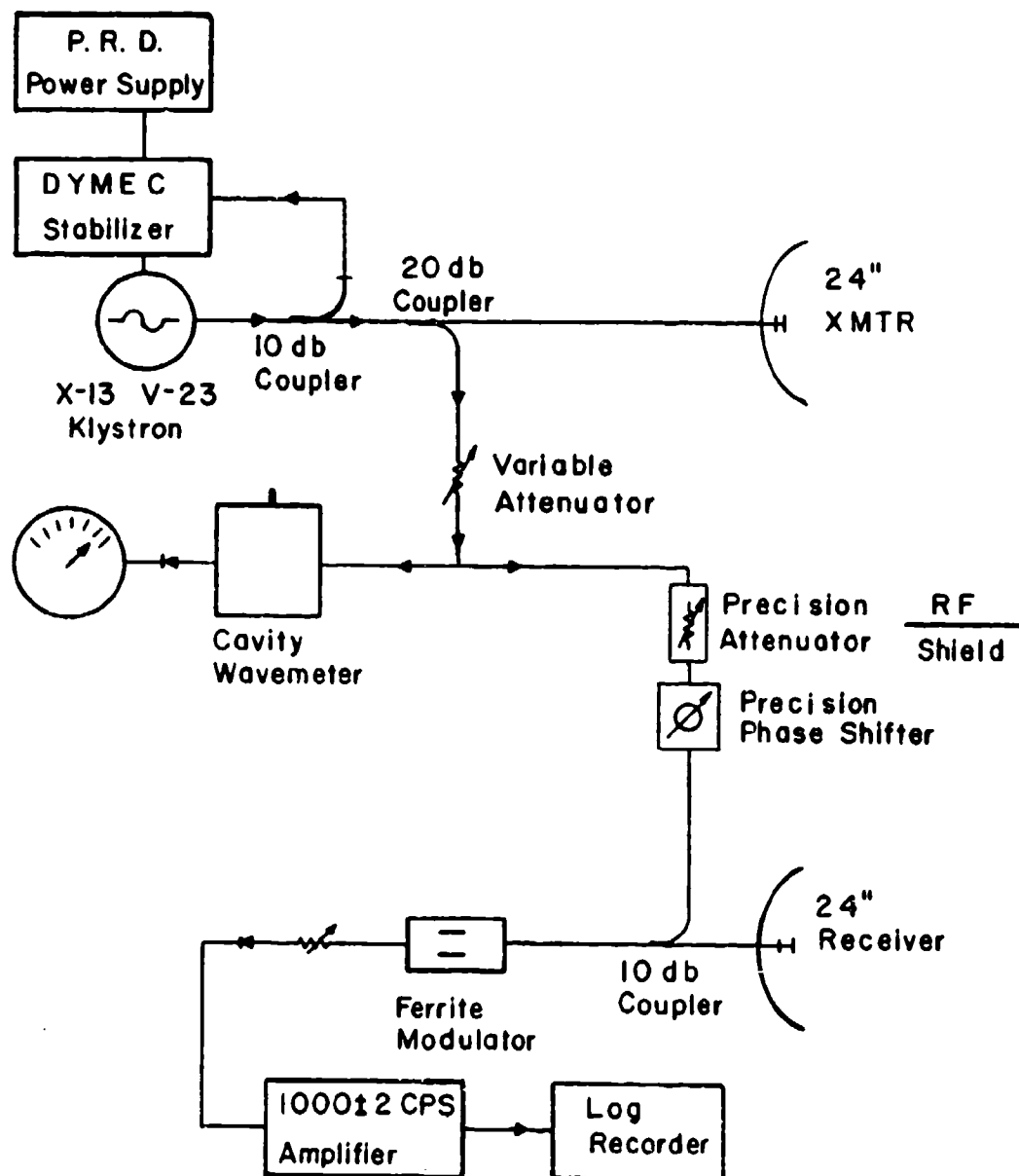


Figure 4. Diagram of X-Band Outdoor CW Range.

horizontal polarization are approximately $0.01\lambda^2$ without motion (rotation) of the target support and $0.08\lambda^2$ when the pedestal and associated strings (20 lb test) are rotated. Thus cross sections of the order of $10\lambda^2$ may be measured with an accuracy of ± 1 db when motion is required.

TABLE A

	K _A -band pulse	K-band pulse
Frequency Gc	34.512 to 35.208	24.00
Stability	-----	-----
Range	250' to 400'	270' to 400'
Polarization	Any linear	Any linear
Orientation	Quasimonostatic	Quasimonostatic
	M.A.	BOMAC
Source	5789	6551
Peak output power	25 KW	40 KW
Pulse width	1/6 μ sec	1/4 μ sec
Pulse repetition rate	1520 cps	3750 cps
Modulation	Pulse	Pulse
Target support	Strings or styrofoam column	Strings or styrofoam column
	A-Frame	A-Frame
Target Motion	0 to 1/3 rev/min	0 to 1/3 rev/min
Max. target dimension	3' at 250'	3' at 250'
Antennas	2' parabolic dishes	3' parabolic dishes
Feed	Waveguide-dipole	Waveguide-dipole
Data	Analog	Analog
Output form	Strip chart-Pen	Strip chart-Pen
Dynamic range	35 db	50 db
Background limit	Target support strings	Target support strings
Target height	9.5'	9.5'

TABLE A (Contd.)

	Anechoic chamber	Outdoor CW
Frequency Gc	8.5 to 10.00	8.50 to 12.40
Stability	5 parts in 10^8 short term	1 part in 10^8 short term
Range	3' to 15'	20' to 400'
Polarization	All	Any linear
Orientation	Monostatic bistatic 0 - 140°	Quasimonostatic bistatic 0 - 120°
Source	L. F. E. Cavity stabilized Varian X-13	Varian X-13 klystron Varian V-23
Avg. output power	250 mw	250 mw - 5 watts
Pulse width	-----	-----
Pulse repetition rate	-----	-----
Modulation	Receive arm, ferrite 500, 750, 1000 c. p. s.	Receive arm, ferrite 500, 750, 1000 c. p. s.
Target support	Strings	A-Frame strings
Target motion	0 to 2 rev/min	0 to 2 rev/min
Max. target dimension	5" at 7'	15" at 40'
Antennas	5" x 5" square horn	2' parabolic dishes
Feed	-----	Waveguide dipole
Data	Analog	Analog
Output form	Strip Chart-Pen	Strip Chart-Pen
Dynamic range	40 db	40 db
Background limit	-----	20 lb test strings, H. P. at $25' \approx 0.8\lambda^2$
Target height	9.0'	9.5'

RADAR SYSTEMS FOR TERRAIN SCATTERING MEASUREMENTS

Two radar reflection measuring facilities for terrain investigations have been developed and currently are being used by this laboratory. The two systems, one monostatic and one bistatic, will be discussed separately in the following paragraphs.

The backscattering radar is a mobile CW Doppler system utilizing a single antenna as shown in Fig. 5. The system operates at frequencies of 10, 15.5, and 35 KMC by interchanging the RF section of the transmitter-receiver. The reference signal is applied to the crystal detector by unbalancing the hybrid tee, introducing a small amount of transmitted power into the receiver arm. Because of the relative velocity of the terrain with respect to the antenna, the terrain return signal of constantly changing phase, beats in the crystal mixer with the fixed-level signal purposely introduced, producing an audio frequency signal. This audio frequency signal is amplified by a narrow band amplifier and integrated electronically to obtain an average reflection coefficient from the terrain. The antenna used in the three frequency bands are high-gain pyramidal horns with dielectric lenses designed to give an optimum pattern at the operating range of 20 feet. The entire radar system is mounted in a truck. The transmitter and receiver are mounted in a specially designed enclosure at the end of a 40 foot boom controlled from the truck. The angle of incidence can be varied from 10° to 80° (90° being normal incidence) and slant range to the terrain is maintained at 20 feet. The Doppler shift in frequency is obtained by driving the truck at a predetermined speed across the terrain so that the Doppler shift in frequency is an audio signal within the pass band of the amplifier. The calibration of the system is accomplished by measuring the return from a standard target such as a corner reflector, rotating on a 4-foot arm at a predetermined speed. The system can be operated using vertical, horizontal, or circular polarization. Echo areas of 55 db below 1 sq. ft. have been measured within an accuracy of ± 1 db.

The bistatic radar is a modulated CW system as shown in Fig. 6. The system operates at a frequency of 10 KMC and transmits and receives either right or left circular polarization. The antennas and data processing equipment are identical to that contained in the backscattering radar. The angle of incidence can be varied from 10° to 80° (90° being normal incidence) and the bistatic angle varied from 10° to 180° (180° being the forward scattering direction). The terrain or surface to be measured is placed in a flat bed railroad car and moved slowly through the beam of the antennas. A continuous measurement of the radar scattering is made allowing an integrated average scattering coefficient to be evaluated. The system is calibrated by the use of a standard sphere. Echo areas of 45 db below 1 sq. ft. have been measured within an accuracy of ± 2 db.

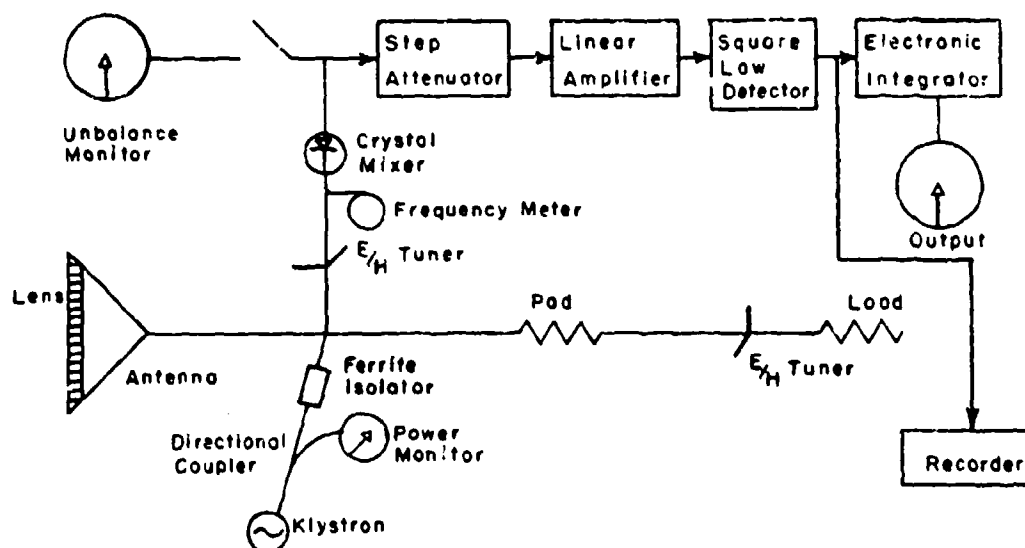


Fig. 5 Block diagram of cw Doppler system.

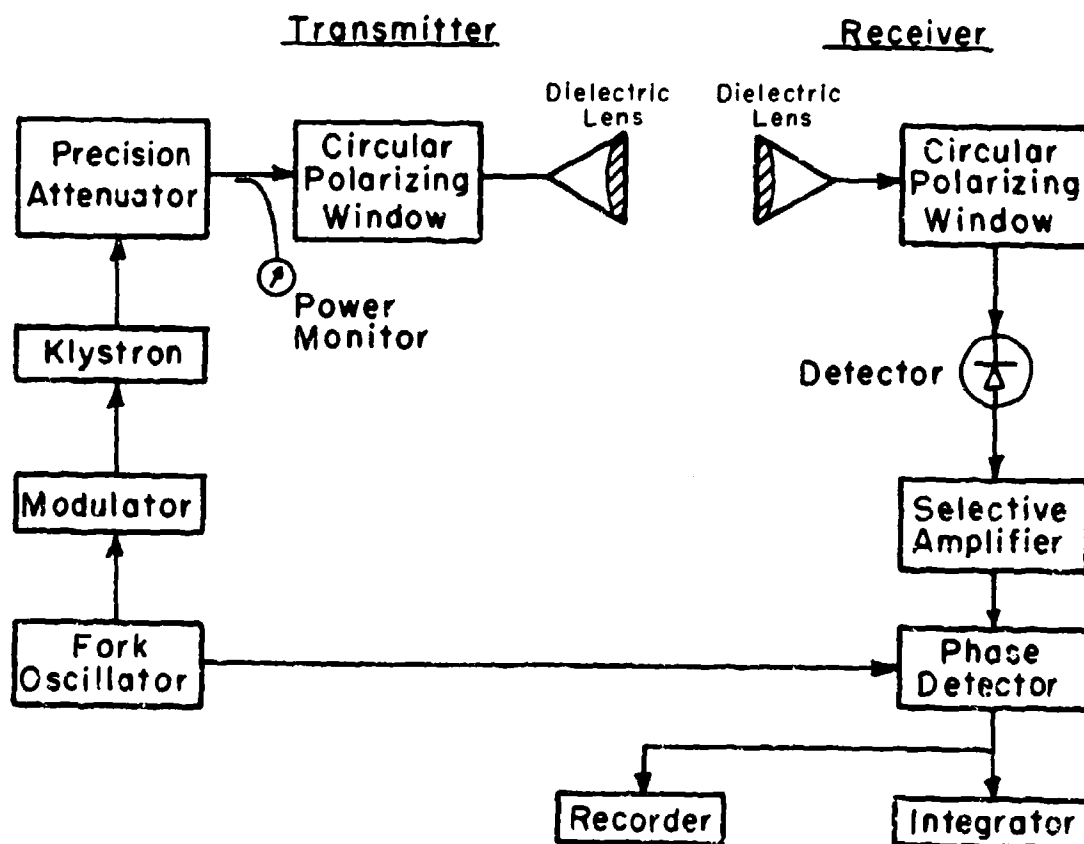


Fig. 6 Block diagram of X-band bistatic radar.

BIBLIOGRAPHY

1. Garbacz, R. J. , and Eberle, J. W. , "The Measurement of Time-Quadrature Components of a Scattered Field," IRE-WESCON Convention Record, Part 1, August 1960.
2. Garbacz, R. J. , "A Memorandum on a Measurement Technique for Low Cross Sections," Report 1223-7, 1 May 1962, Antenna Laboratory, The Ohio State University Research Foundation. AD 276 102
3. Kennaugh, E. M. , and Moffatt, D. L. , "On the Axial Echo Area of the Cone-Sphere Shape," Proc. IRE, Vol. 50, No. 2, February 1962.
4. Final Report, "Modification of a Radar System for Automatic Recording of Back-Scattering Radiation Patterns," Vol. I, Report 406-1, 2 July 1951, Antenna Laboratory, The Ohio State University Research Foundation. ATI 117 688
5. Final Report, "Automatic Recording of Back Scattering Patterns," Vol. II, Report 406-2, 1 May 1952, Antenna Laboratory, The Ohio State University Research Foundation. ATI 161 644
6. Rhodes, D. R. , "An Investigation of Pulsed Radar Systems for Model Measurements," Report 475-6, 1 December 1953, Antenna Laboratory, The Ohio State University Research Foundation. AD 2255

SCATTERING RANGE - THE BOEING COMPANY

AERO-SPACE DIVISION

W. P. HANSEN, JR.

SUMMARY - A description of the scattering range facilities at the Aero-Space Division of The Boeing Company in Seattle is presented. The facility includes image-plane ranges, an indoor range in an anechoic chamber and outdoor ranges. Frequencies of operation are from 1 to 10 gc in various bands. CW operation is used for all facilities. For accurate measurements, maximum model dimensions are limited to between 10 and 20 wavelengths, depending on frequency.

I. INTRODUCTION

The purpose of the scattering facilities is to obtain, by experimental means, information regarding the electromagnetic scattering characteristics of various objects. The particular equipment and range configuration are selected on the basis of the desired information, sensitivity and accuracy required.

Two image-plane ranges are in operation, both at X-band frequencies. One is covered with a liquid dielectric and is used for plasma simulation measurements; the other is a standard image plane. An anechoic chamber is used for indoor measurements at frequencies of 2 to 10 gc. Two outdoor ranges are available. One is located on the roof of a building and operates at X-band frequencies. The other is in the side of a building overlooking a river and operates at frequencies of 1 to 10 gc in several bands. The scattering data is usually displayed with a pattern recorder. If desired, however, the data may also be digitalized and stored on magnetic tape for subsequent computer analysis. Transmitting and receiving equipment used for most of the ranges consists of LPE Ultra Stable Microwave Oscillators and a Scientific-Atlanta Series 402 Wide Range Receiving Unit⁻⁴ (0.03 to 75 gc). Maximum range sensitivities are on the order of 10 square wavelengths.

II. IMAGE PLANES

The image plane, shown in Fig. 1, operates at X-band frequencies and is true monostatic with a half-horn being used as both the transmitting and receiving antenna. Operation is CW with separation between the

received and transmitted signal being accomplished by a magic-tee arrangement; a precision five-stub tuner is used for balancing the tee. A turntable near the center of the image plane is used for rotating the models under test. Measurement of near-field scattered and diffracted waves is accomplished by inserting coaxial-fed probes into the turntable near the model. Coaxial cable connections are also made to the model under test for antenna scattering and current distribution measurements. The surface of the image plane is aluminum and is 8 by 16 feet in size.

A second image plane, shown in Fig. 2, is used for plasma simulation. It is similar to the image plane described above except that it is physically smaller. Plexiglass side walls are used for containing a liquid dielectric in which the model under test is immersed. For plasma simulation, the model is coated with a dielectric of desired shape and with a dielectric constant less than that of the liquid dielectric. The image plane is 30 by 40 inches in size. Present operation is at X-band frequencies. The dielectric used is a solution of titanium dioxide powder and transformer oil. A mixture of 55 percent oil, 40 percent titanium dioxide and 5 percent vaseline (by volume) has produced a liquid with a dielectric constant of 4.3 with a loss tangent of 0.004. This solution is similar to that proposed by Peters¹. In Fig. 2, the plane is covered only with oil. Addition of titanium dioxide yields a non-transparent liquid.

III. ANECHOIC CHAMBER

The anechoic chamber was designed and built by Emerson and Cuming. It is 36 feet wide, 21 feet high, 56 feet long and contains four screen rooms which open into the chamber. Equipment for scattering measurements is located in two of the screen rooms as shown in Fig. 3. Frequencies of operation are from 2 to 10 gc with polyurethane foam towers, 5 to 6 feet in height, being used for model supports.

Two range configurations are in general use. One consists of a tower mounted on a stand 10 feet high and fixed in location near the rear of the room. The antenna system is composed of two 2-foot diameter paraboloidal antennas for use at X-band. A phase cancellation system is used for antenna isolation and cancellation of room reflections. The upper screen room is used as shown in Fig. 3.

¹ T.A. Brackey, L. Peters Jr., W.G. Swarner, and D.T. Thomas, "A Proposed Scattering Range For Simulated Echo Area Measurements of Plasma Coated Objects," Antenna Lab., The Ohio State University Research Foundation, Report 1116-17, 27 January 1962.

The other configuration consists of a lower tower, which is readily movable about the room, and a single-horn antenna system. Frequencies of operation are from 2 to 10 gc. A magic tee arrangement, the same type as described for the image plane, is used for signal separation and cancellation of room reflections. High gain horns with relatively small apertures are used to insure proper amplitude and phase distribution across the model under test. LS, C, and X-band horns are used. The C-band horn is shown in Fig. 3; it has a 13- by 15-inch aperture and is 6 feet long.

IV. OUTDOOR RANGES

Two outdoor ranges are available, one located on the roof of a building and the other located in the side of a building overlooking a river. These ranges are shown in Fig. 4.

In Fig. 4a, the roof range is shown. It is an X-band facility using two 2-foot diameter paraboloidal antennas. A phase cancellation system is used for antenna isolation and cancellation of background reflections. Both string and polyurethane foam tower supports are used. Antenna-to-target distances of up to 240 feet are available.

The other outdoor range is shown in Fig. 4b. It is used primarily at L- and LS-band (1.12 to 1.7 gc and 1.7 to 2.6 gc) and at higher frequencies for large models which cannot be conveniently handled in the anechoic chamber. A stand containing antennas and other equipment is placed at the end of the track behind the tower for measurement of forward scatter. The L-band antenna (6-foot diameter) is shown in the figure. Antenna-to-target distances of up to 175 feet are available.

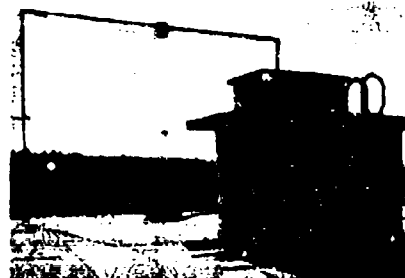
V. DATA READOUT, REDUCTION AND ANALYSIS

The scattering data is usually read out and displayed on rectangular chart paper by means of a pattern recorder. Analysis of the data is then a visual and manual process. Provision, however, is provided for data reduction (analog to digital) and storage on magnetic tape for computer (7094) analysis.

A particular application for which the program was set up was that of comparing signature characteristics from two different objects. Actual body motion is simulated and backscatter measurements are taken as a function of time. The data so obtained from the different bodies are read into the computer where they are cross correlated to obtain a similarity factor.



Fig. 1 - Image Plane.



(a)



Fig. 2 - Image Plane
For Plasma Simulation.



Fig. 3 - Anechoic Chamber.



(b)

Fig. 4 - Outdoor Ranges.

RCA DYNAMIC BACKSCATTER TESTING RANGE*

M. H. Hellman
J. M. Jarema
RCA
Burlington, Mass.

1. Origin and Use of Range

The RCA "Dynamic Testing" range was designed and constructed for use in evaluating the performance of radar systems under dynamic conditions. This is in contradistinction to the usual backscatter range which is designed to measure the cross-section characteristics of targets. Target characteristics are determined indirectly from the radar performance. It is the only range known to have this capability.

Typical of the parameters measured on the range are the angle tracking variations of a pulse type fire control radar and range output signal of an FM-CW type radar when performing against full scale models of satellites. Both the translation and rotation dynamics of the satellite targets are controllable.

2. Range Characteristics

The range configuration is shown in Figure 1 with a typical target. A cable which supports the target is approximately 200 feet long and makes an angle of approximately 30 degrees with the horizontal. The target can be translated up and down this cable by means of a hauling cable and electric motor drive located on the ground near the radar. A motor suspended from the cable can rotate the target while it is stationary in range or as it is being translated along the cable. The system has a translation speed capability up to 16 feet per second and a rotational velocity up to 10 revolutions per minute. Target range can be varied a maximum of 200 feet.

The upper end of the cable is attached to the midpoint of a bridle cable whose ends are anchored to the top of two 150 foot high vertical towers. These towers are 100 feet apart and are 215 feet from the test radar at ground elevation.

Radars to be tested are mounted on a platform which makes an angle of approximately 30 degrees with the horizontal so that the boresight axis of the radar is parallel to the messenger cable. The radar is surrounded by adequate anechoic baffling to minimize side lobe effects. Background noise is sufficiently low so that radar calibration is performed with an .033 square meter cross-section target (sphere).

* The Range is located at RCA, Aerospace Systems Division, Burlington, Massachusetts. It was built with funds supplied under a contract with the USAF Space Systems Division.

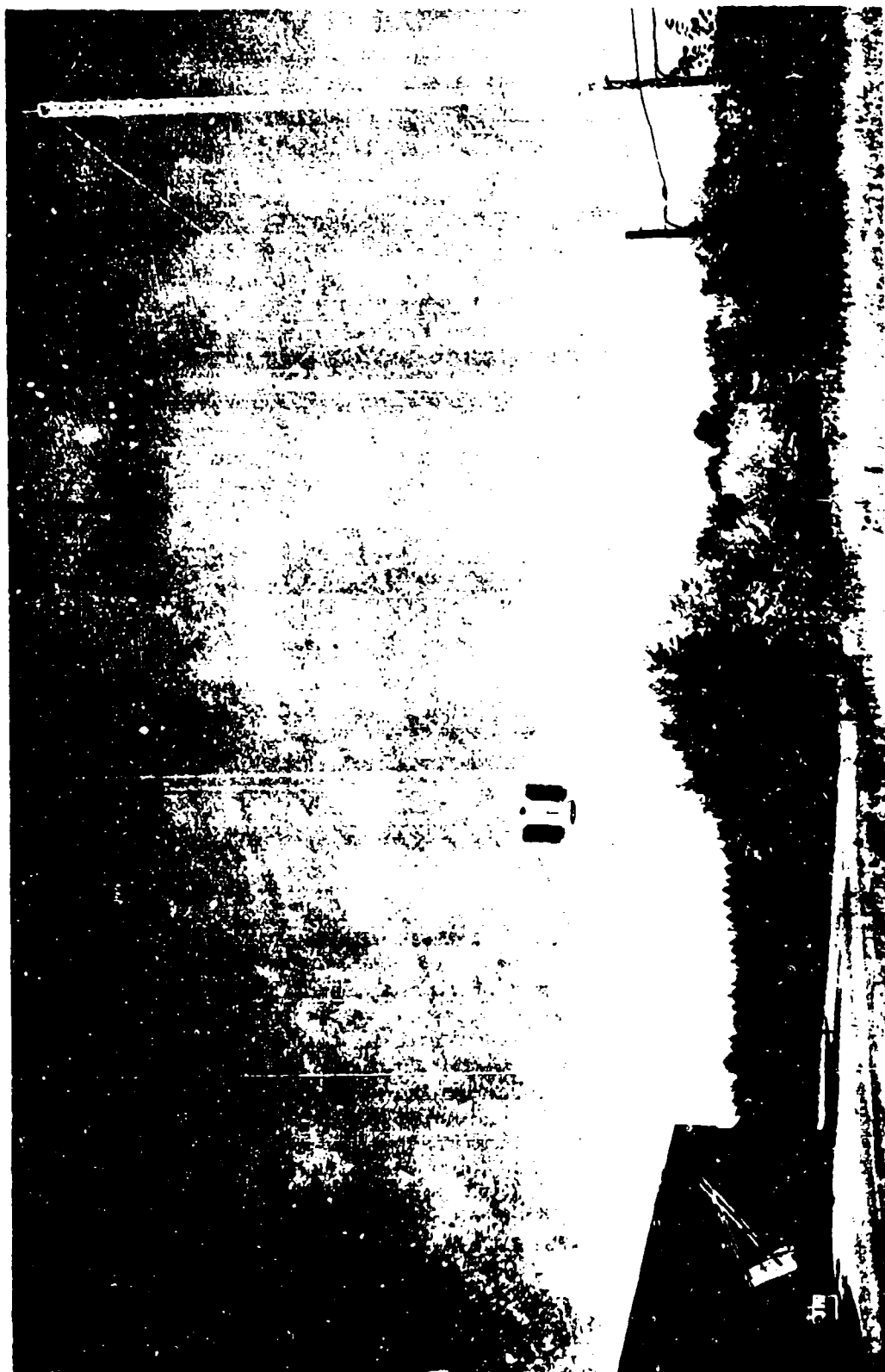


Figure 1. RCA Dynamic Backscatter Range

3. Range Operation

As stated above, the primary purpose of the RCA range is to determine the performance of radar systems designed to operate on space missions. In this environment, the radar would acquire, angle track and measure range to the target. The target may be cooperative or non-cooperative. In particular, if a non-cooperative target is in the near field of the radar the ability of the radar to maintain track when the target is rotating and translating relative to the radar is difficult to predict from theory alone. This is even more exaggerated when targets are physically large. It is the latter situation for which the range is particularly useful.

In order to check predicted radar performance under conditions which closely simulate space operating environment the range was designed for use of full scale model satellites whose dynamics relative to the radar can be simulated over a wide range of conditions.

The radar tracking performance is determined with the aid of a camera mounted on the radar antenna. Range is determined and simultaneously recorded by measuring the length of cable from the target to the radar.

4. Typical Measurements

A typical record of radar performance measured on the range is shown in Figure 2. The target was a 28 inch diameter aluminum sphere suspended by a nylon rope. For this test, the target started from rest at an actual range of 30 feet. It was accelerated rapidly to 15 feet per second at which speed it traveled out to a range of approximately 200 feet where it decelerated to zero velocity. At this range, the target accelerated from rest to a closing velocity of 15 feet per second and came to rest at a range of 30 feet.

The second channel from the top shows the actual target range (coarse range) as measured by a potentiometer geared to the hauling cable. A recording of fine range which has a sensitivity of about 9 to one compared to coarse range is shown on the top recording. This was obtained by using the appropriate gear ratio with the coarse range drive. The radar measured range is recorded on the third channel. In addition to range, the radar azimuth and elevation angles are recorded on the fourth and fifth channels, respectively. It is obvious that large variations in tracking angle and range occur with the target at the shorter ranges. This is so because during this interval the rope-suspended target is accelerating and/or decelerating and its motion is erratic and does not follow the rope suspension point. A motion picture camera attached to the radar antenna and synchronized in time with the pen recordings verify this phenomenon and can be used to account for it.



Figure 2. Typical record of radar performance measured on the RCA range.

OUTDOOR PULSED RADAR REFLECTIVITY RANGE

Robert E. Honer, President
Wm. D. Fortner, Senior Electronics Engineer
Micrometetics Incorporated

INTRODUCTION

There are several types of facilities presently employed in the measurement of radar cross-section. These include both outdoor ranges and anechoic chambers employing a variety of instrumentation such as CW, pulse, and linear ramp (chirp) radars.

Indoor Ranges

The indoor range is severely limited in its application due to the far-field criteria of measuring the target in a relative plane wave region. This poses a very real restriction on both target size and frequencies of measurement.

Outdoor Ranges

Conventional outdoor scattering cross-section ranges have several inherent drawbacks¹, i.e., weather, temperature and humidity variations, a significant specular contribution to the background, and a variety of non-specular paths. Support structures present a particularly perplexing problem for all ranges.

CW Radars

CW systems endeavor to balance out background effects by introducing a signal at the receiver which is equal in amplitude but in counterphase with the background signal. This balance is a function of the stability of the transmitter frequency, the stability of the environment, and the mechanical stability of the components of the radar. Adverse effects result from even the gentlest breezes as well as from the slightest variations of temperature and humidity. Even after the background has been balanced out, skip path effects, multi-path effects, and shadowing can result in a change in background level when the target is placed in the field. These target-induced effects depend on target orientation and vary as the target is rotated when complex models are involved.

Pulsed Radars

Pulsed systems employ time discrimination to minimize background effect. They are not seriously affected by

temperature and humidity variation. The problems of specular and non-specular background contributions, though reduced by range gating, are not entirely solved. The weather problem also remains.

Micronetics' Facility

Micronetics has developed a unique outdoor scattering cross-section range in which these drawbacks have been largely eliminated, or minimized to the point at which they are negligible for most purposes.

Weather

The environmental problem was minimized by locating the facility in San Diego, California. The weather in San Diego is nearly ideal for an outdoor range; the annual rainfall is very light, humidity is low, and the wind is seldom stronger than 2-knot breezes. There is, normally, an absolute calm for at least 10 hours a day; this calm being from 6 in the morning until 12 noon and again extending in the early evening hours after 6 p.m.

Background Minimization

Minimization of the background problem is partially achieved through the use of a stable, accurately calibrated, pulsed radar system with 200 nanosecond range gating. Of equal importance is the geometry of the earth within the confines of the antenna beamwidth as well as other external conditions that can affect measurement accuracy. The use of range gating and radar pulses of 200 nanoseconds or less permits the radar receiver to look only at that section of range in which it is interested, and completely ignore reflections from outside the range gate. The non-specular ground reflection and skip path problem was minimized by shaping and paving the range surface in an inverted "V" shape so that the skip path reflections are diverted away from the path of propagation. The real estate adjacent to the range is controlled to the extent that any significant extraneous reflections are outside the maximum range gate.

Short Pulse Radar

Micronetics has also developed instrumentation for exact measurement of flare spots in both location and magnitude². This technique uses very short pulses and real range resolution. It is referred to throughout the remainder of this paper as the "short pulse" technique. This is in distinction from the "long pulse" (200 nanosecond) technique

referred to above with which the target is immersed in an essentially CW field.

GEOMETRY

Inverted "V" Range

The Micronetics' facility is shown in Figure 1 with a 1000-foot range in front of the radar trailer and a 600-foot range extending out from the 10-foot antenna tower. Each range is paved along its full length with an inverted "V" shape. The 600-foot range is used for measurements at L-band and lower frequencies. The 1000-foot range is used for frequencies above L-band. The paved strip between the inverted "V" ranges provides access for positioning targets and their support structures.

Pads

Slots are cut at 150, 300, 500 and 1000 feet on the 1000-foot range, and at 125 and 600 feet on the 600-foot range. Each slot is provided with a concrete pad for mounting turntables. The edges of the slots are inclined so that if any sidelobe energy from the illuminating antenna does strike them, it is scattered specularly away from both the target and the radar. The turntable, being positioned on the pad within the slot, is below the line-of-sight and out of the radar field-of-view.

Barrier

A metal barrier having an inclined "V" geometry is positioned ahead of the tower and turntable. This barrier, positioned between the 500-foot and 1000-foot stations in Figure 1, enhances the shadowing of the turntable and tower base. The barrier is always well below the antenna beamwidth to prevent diffraction effects and is outside the range gate. The pad positions have been evaluated and for all operational frequency and position combinations, the background level in the absence of any target or model support structure is less than 10^{-7} square meters. In each case, the turntable was positioned on the pad within the appropriate slot, and the barrier was in place.

Bistatic Range

In addition to the monostatic ranges of 600 and 1000 feet, a 300-foot bistatic range is provided at X-band, which permits evaluation of bistatic angles at 2.5, 5, 7.5 and 10 degrees.

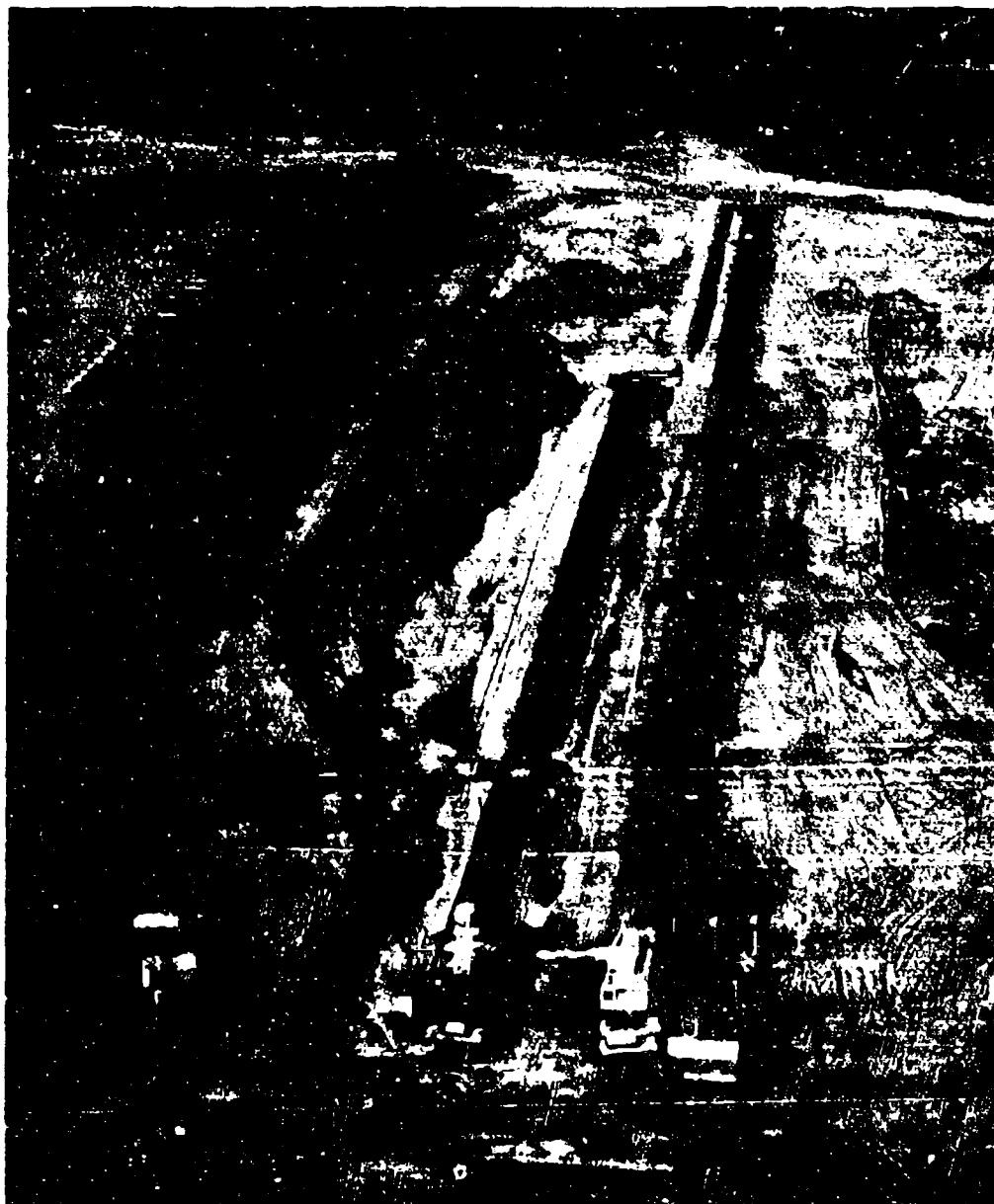


Figure 1. Aerial View of Micronetics
Outdoor Reflectivity Range

LONG PULSE RADARS

The concept of the long pulse radars employed by Micro-netics is depicted in Figure 2.

Transmitter

Pulses having typical amplitudes of 50 KW and durations of 200 nanoseconds are formed by a magnetron driven by a line type or hard tube modulator. These pulses are generated at a prf of 1000 pps. A coupler draws off sample pulses having peak powers between 10^2 and 10^4 watts for transmission.

Receiver

The receiver consists of a low noise front end, tunable bandpass filter, medium power traveling wave tube post-amplifier, diode gating element, and bolometer detector cascaded in that order. The low noise front end provides an optimum signal-to-noise ratio and some preamplification. The bandpass filter limits the receiver's noise bandwidth to the information bandwidth of the transmitted pulse. The medium power TWT amplifies the signal pulses to a level adequate for video detection. A high degree of rejection of out-of-gate signals is provided by the limiting characteristic of the traveling wave tubes in conjunction with the 80 db on-off ratio of the p.i.n. diode r.f. gating element.

Range Gating

A sample of the transmitted pulse is used to feed a variable delay line for triggering a gate pulse generator. The gate pulse generator drives the p.i.n. diode r.f. switch mentioned above. Range is proportional to the delay in the trigger-gate network and is adjusted via the variable delay line.

Signal Detection

The return signal from the target passes through the p.i.n. diode r.f. switch to a bolometer detector. The bolometer detector, which has a square law characteristic and acts as an average power detector and integrator, drives a standard antenna pattern recorder.

Recording

The antenna pattern recorder records data on a rectangular chart. This instrument records signal level on a decibel scale as a function of target aspect. It has an r.f. dynamic range of 40 db and a response time of 40 db per second. The recorder chart drive is synchronized, via an

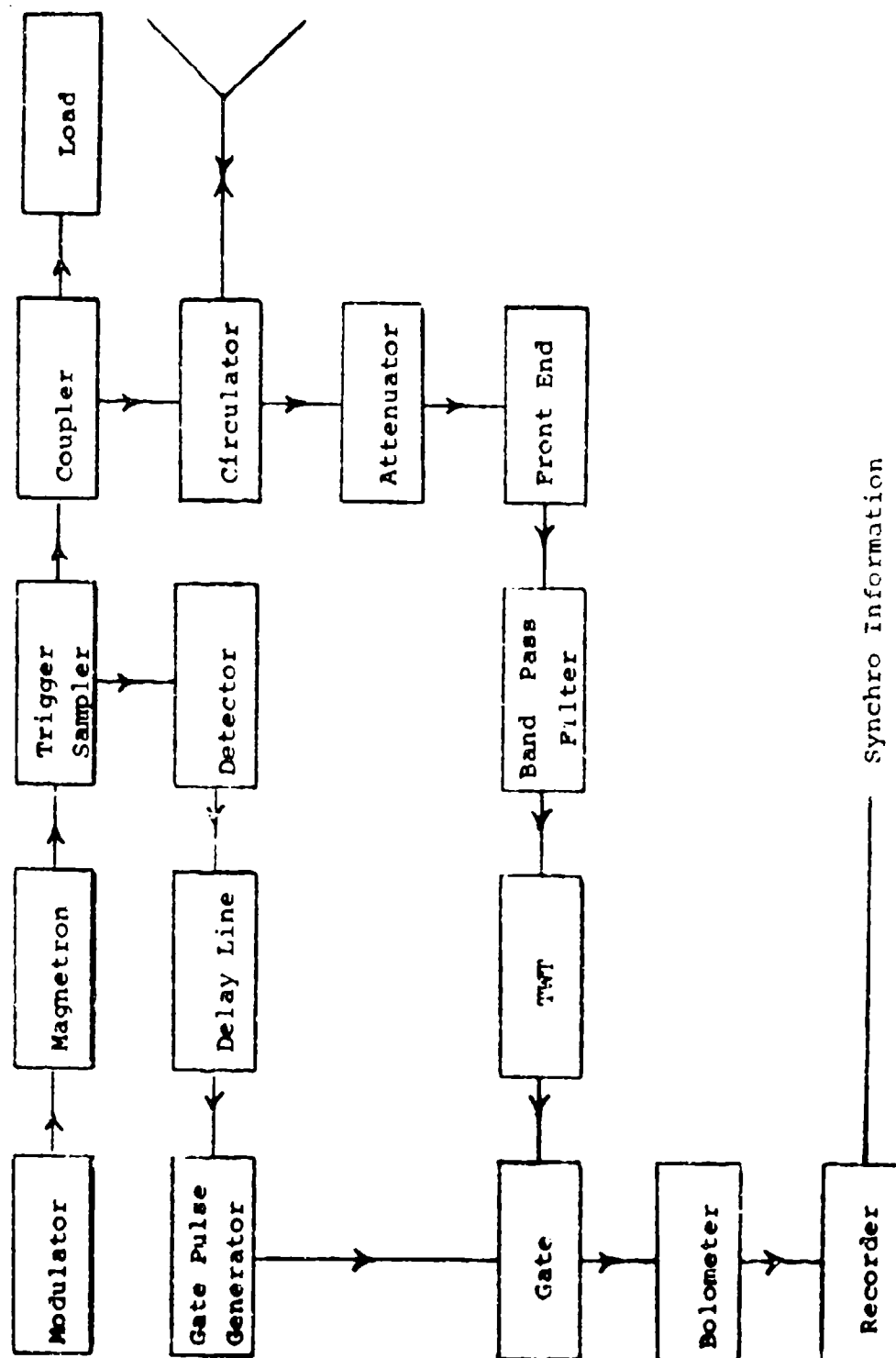


Figure 2. Functional Diagram, Long Pulse Radar

electromechanical servo loop, with the turntable used to rotate targets so that radar cross-section versus target aspect is recorded automatically.

LONG PULSE CAPABILITIES

The present capabilities of the Micronetics radar reflectivity range are detailed as follows:

R.F.Frequencies: L, C, X, K_u , and K_a bands

Modulation: 200 nanosecond pulses at all frequencies
10 nanosecond pulses at X-band
1 nanosecond pulses at X, L, and K_u bands

Polarizations: Linear (any orientation) at all frequencies; circular at C and X bands

Sensitivities: L-band = 10^{-5} m^2 at 600 feet
C-band = 10^{-5} m^2 at 500 feet
X-band = 10^{-5} m^2 at 500 feet
 K_u -band = 10^{-5} m^2 at 500 feet
 K_a -band = 10^{-4} m^2 at 1000 feet

Background: Below 10^{-7} at all frequencies*

Geometry: Monostatic at all frequencies; bistatic at X-band to 10 degrees

Data Recording: Rectangular chart recording, strip chart recording, or oscilloscope photographs

Range Length: 1000 feet maximum

Model Handling: Great circle cuts on models up to 2500 pounds. Conic cuts on lighter models. Crane and fork lift used for hoisting.

Model Supports: Shaped styrofoam columns or nylon cord suspension*

* Background levels of less than 10^{-7} square meters are achieved in the absence of any model support. Therefore, the major contribution to background, in all cases, is the model support. The level of this contribution depends on the particular model support being used and on the frequency. Cases are discussed in the section on model supports.

SHORT PULSE RADAR

Two methods are used for generating short pulses:

1. Spike leakage from a T.R. tube.
2. Direct amplification of the high frequency components of a video pulse by a traveling wave tube.

The spike leakage technique is described briefly in the following paragraphs. A functional block diagram of the Micronetics' X-band short pulse mechanization is shown in Figure 3.

Transmitter

The basic X-band pulses are formed by a magnetron driven by a hard tube modulator. The resulting r.f. pulses at this point have a duration of 100 nanoseconds. These pulses are then fed through an r.f. pulse shaping network and finally to a T.R. tube. The spike leakage from the T.R. tube then becomes the source of the nanosecond pulses and the balance of the r.f. power is absorbed in a dummy load.

"Range Gating"

A sample of the transmitted pulse is used to feed a variable delay line for triggering the display device in the receiver.

Receiver

The backscattered signal is fed from the receiving antenna, through a precision variable attenuator, through two stages of traveling wave amplifiers, to a short pulse video detector, and finally to a sampling oscilloscope.

Recording

The short pulse train which is backscattered from the target and amplified by the receiver is displayed on a sampling oscilloscope.

Data is either tabulated or photographed depending on the quantity and intended use. A photograph or table entry is made for each aspect angle of interest.

TARGET MOUNTS

As noted in the section which describes Micronetics' Long Pulse Capabilities, the background level contributed by the

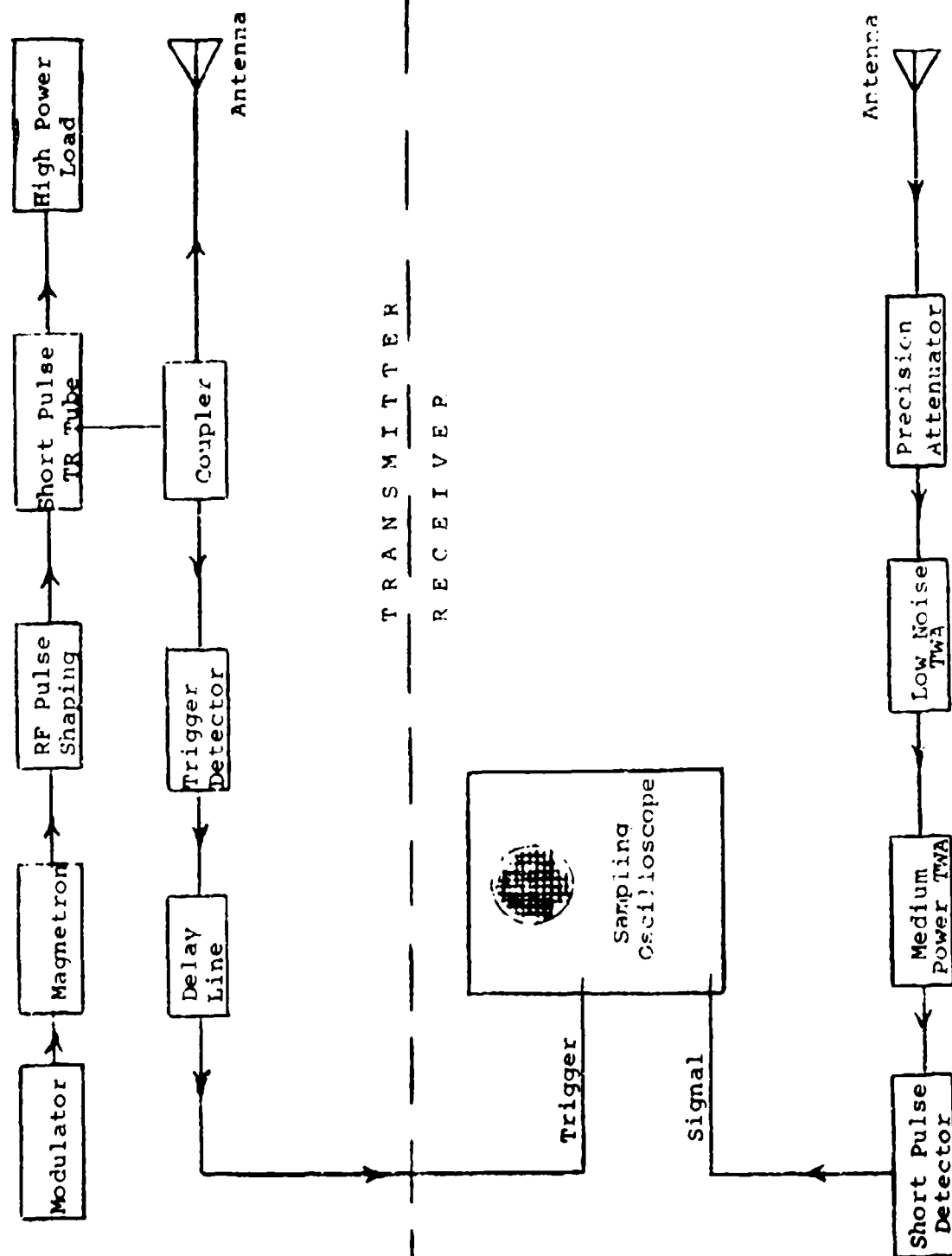


Figure 3. Functional Diagram, Short Pulse Radar

range in the absence of any model support is less than 10^{-7} square meters. The only significant undesirable signal originates from the model mount. The subnanosecond pulses used on the range for radar cross-section reduction studies were utilized to study model mounts. Figure 4 shows an example of the short pulse measurement of the echo from a cylindrical styrofoam column.

Shaped Foam Columns³

Columns were then shaped by different techniques to eliminate the long specular surface of the right circular cylinder. Figure 5 shows three column configurations, all of which exhibit cross-sections of less than 10^{-4} square meters at X-band. In general, the number and depth of circumferential grooves should be varied with frequency, i.e., more and shallower grooves at higher frequencies.

For very small models, small tapered columns have shown cross-sections of less than 10^{-5} square meters.

Styrofoam shapes with wavelength sensitive characteristics are now being investigated. It is hoped that the cross-section of large columns can be reduced by 20 db using this technique.

Nylon Cord Suspension

A nylon cord suspension system has recently been installed and is under evaluation. This system consists of a pair of telephone poles positioned within the first null of the illuminating antenna. The two poles are inclined 20 degrees away from the radar and are positioned at slightly different ranges from the radar. The target is suspended from the poles and attached to a turntable via a system of nylon strings. Care has been taken to insure that no part of this system is perpendicular to the radar line-of-sight.

At this writing, the string suspension system has been evaluated at 9.37 Gc. The background contribution due to this target support structure is less than -60 dbm at 9.37 Gc.

FLARE SPOT MEASUREMENT TECHNIQUE

The short pulse radar described above is a powerful tool for measuring both position and amplitude of flare spots. The spike leakage from the T.R. tube provides a pulse having a nominal one nanosecond duration. This pulse is triangular in shape. A target having a length greater than a few inches is larger than the spatial extent of the r.f. pulse. Scattering

centers displaced along the line-of-sight by three or more inches are resolvable by this system. This topic is pursued at greater length in two papers by Robert R. Hively, "Nanosecond Pulse Scattering Systems" to be presented in Session III and "Nanosecond Pulse Methods of RCS Measurement" to be presented in Session VI.

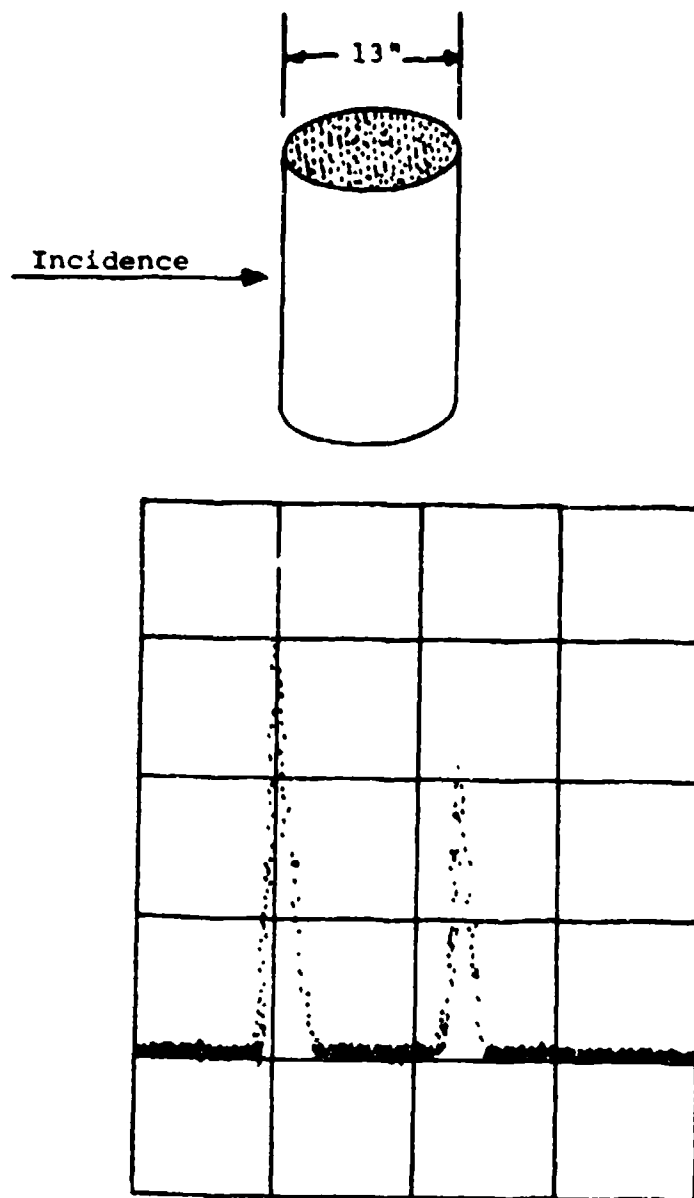


Figure 4. Echoes from a Styrofoam Cylinder

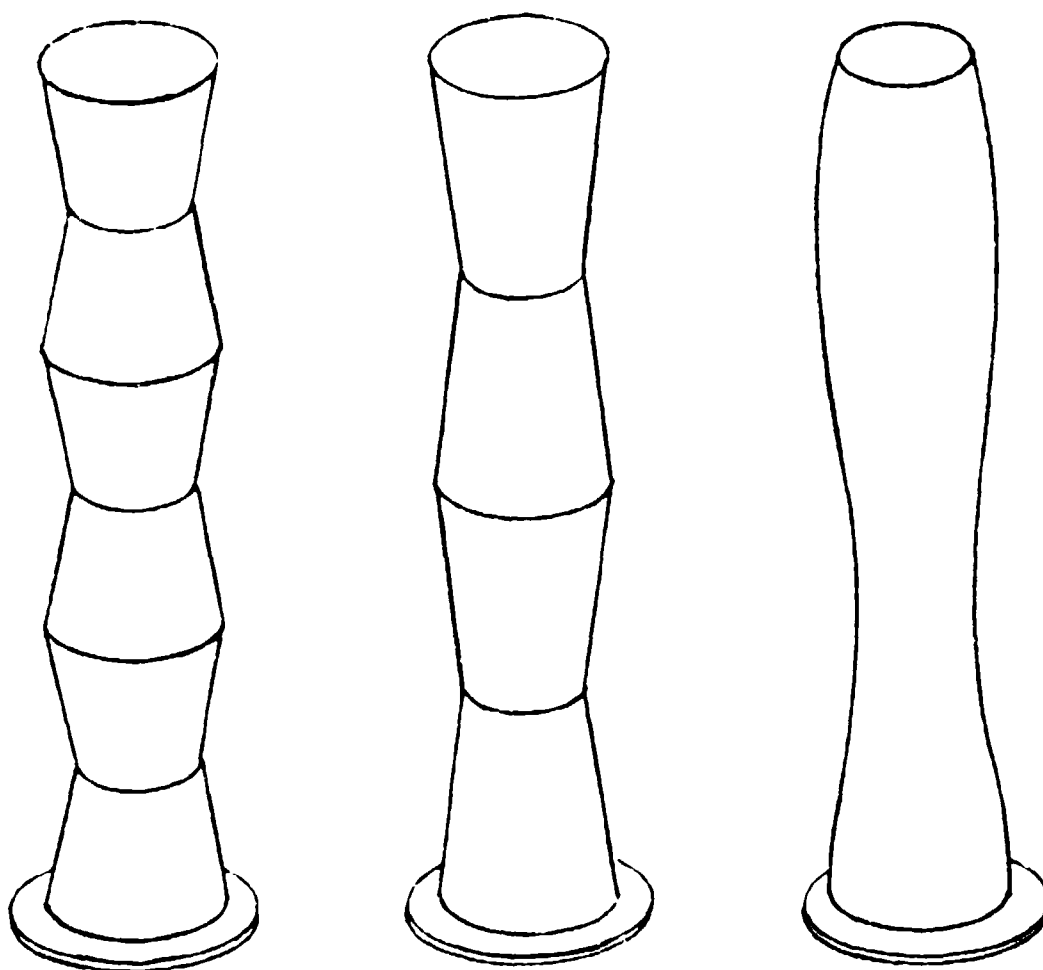


Figure 5. Shaped Styrofoam Columns

BIBLIOGRAPHY

1. C. G. Bachman, H. E. King, R. C. Hansen, "Techniques for Measurement of Reduced Radar Cross Sections", Parts I, II and III, The Microwave Journal, Vol VI, No. 2, 3 and 4, February, March and April 1963.
2. R. Honer, R. Hively, "High Resolution Backscatter Techniques", Microwaves, April 1963
3. W. R. Bradford, "Radar Cross-Section of a Corrugated Metallic Pipe", Submitted to PTGAP, August 1963.

CROSS-SECTION RANGE RADARS AT CORNELL AERONAUTICAL LABORATORY

John E. Hopkins
Cornell Aeronautical Laboratory, Inc.
Buffalo, New York 14221

INTRODUCTION

There are four separate radars used for radar cross-section measurement in the current Cornell Aeronautical Laboratory range program. These are conveniently distinguished by frequency and type, as in the following list:

1. K_a -band pulsed radar
2. K_a -band CW radar
3. X-band CW radar
4. X-band FM/CW high resolution radar

The principal features and capabilities of each of these radars will be described in this paper.

K_a -BAND PULSED RADAR

A functional block diagram for the K_a -band pulsed radar system is shown in Figure 1. This radar operates in a quasi-monostatic mode with a bistatic angle of approximately 1° . Distances of 100 feet and 165 feet are available for target to antenna separation. Measurements can be made using linear polarization (vertical or horizontal, parallel or crossed) or circular polarization.

The operating frequency is adjustable between the limits of 34.2 Gc and 35.5 Gc. The pulse length is 50×10^{-9} sec. and the prf is 2000 pps. Range gate width is normally 30×10^{-9} sec. although a smaller gate has been used at a slight sacrifice in sensitivity.

In this system, a master timer determines the pulse recurrence frequency of the modulator which, in turn, causes the magnetron to generate an equispaced series of rf pulses for illumination of the target. The scattered energy captured by the receiving antenna passes through a K_a -band mixer to produce an S-band IF signal. The IF signal is amplified by two travelling wave tubes and then range gated. Control signal for the range gate is derived from the transmitter modulator.

The output of the range gate goes to a second detector. The resulting video is amplified and then stretched in a box-car circuit. The amplified output of the box-car circuit is used as a feedback AGC voltage which is applied to the IF section of the receiver. The AGC

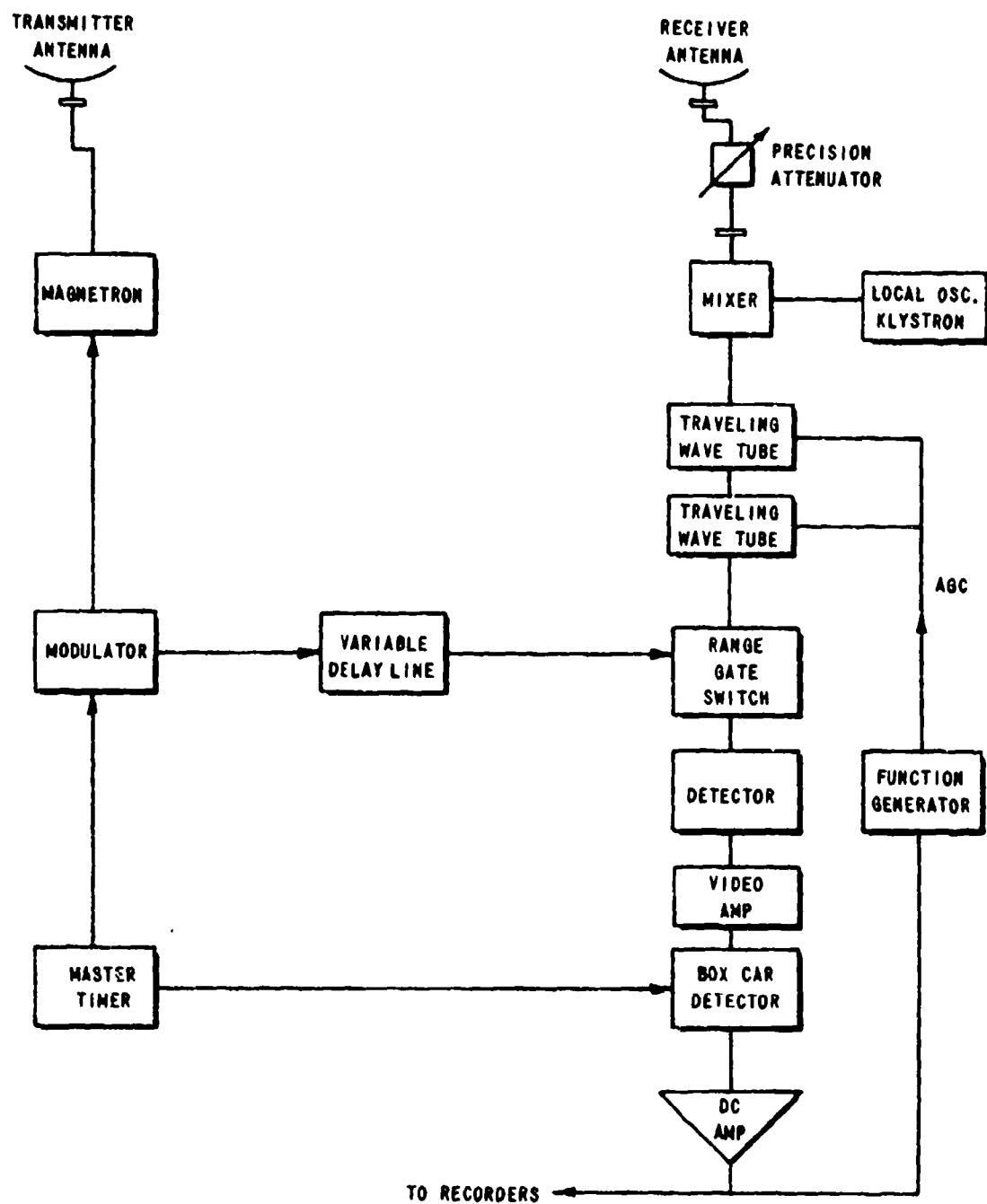


Figure 1 FUNCTIONAL DIAGRAM - K_a BAND PULSED RADAR

voltage is nearly proportional to the logarithm of the received power, and these are the basic output data which are recorded to represent target cross section.

Calibration of this range is normally accomplished using a standard sphere for an absolute reference. The precision attenuator in the receiver antenna line is varied incrementally while observing return from a bright target (e. g., corner reflector) in order to obtain relative calibration and to determine the dynamic range over which the AGC voltage will be essentially logarithmic.

The practical measurement sensitivity of this range is limited by the transmitter power and receiver sensitivity to approximately 45 db below λ^2 at the 165 foot target distance. The room background is at least 55 db below λ^2 .

K_a -BAND CW RADAR

A functional block diagram for the K_a -band CW radar system is shown in Figure 2.

This radar is normally operated in the quasi-monostatic mode with a bistatic angle of approximately 3.5° and an antenna-to-target distance of 6 feet. Measurements can be made using linear polarization (horizontal or vertical, parallel or crossed) and circular polarization. The operating frequency is adjustable between the limits of 33.5 Gc and 36.0 Gc.

As shown in Figure 2, a small amount of transmitter power is mixed directly with the received signal in order that, by proper adjustment of amplitude and phase of the injected signal, residual background return can be canceled. Another path between the transmitter and receiver contains precision variable attenuators which can be used to obtain a relative calibration of the system when the waveguide switch is properly positioned. Absolute calibration may be accomplished using a series of spheres although one single sphere together with the precision attenuators generally suffices.

The local oscillator for this system is a klystron which is modulated linearly in frequency over a range somewhat greater than the bandwidth of the logarithmic amplifier which follows the mixer. The center frequency of the mixer output is approximately 30 mc. The logarithmic amplifier output is applied to a peak detector whose output is then proportional to the logarithm of power received as a result of target backscatter, hence proportional to target cross section.

Data readout is in the form of an analog strip chart and/or punched digital paper tape. The recorders are synchronized with target aspect angle. The maximum sensitivity of this range, which is limited by darkroom background, is approximately 35 db below λ^2 .

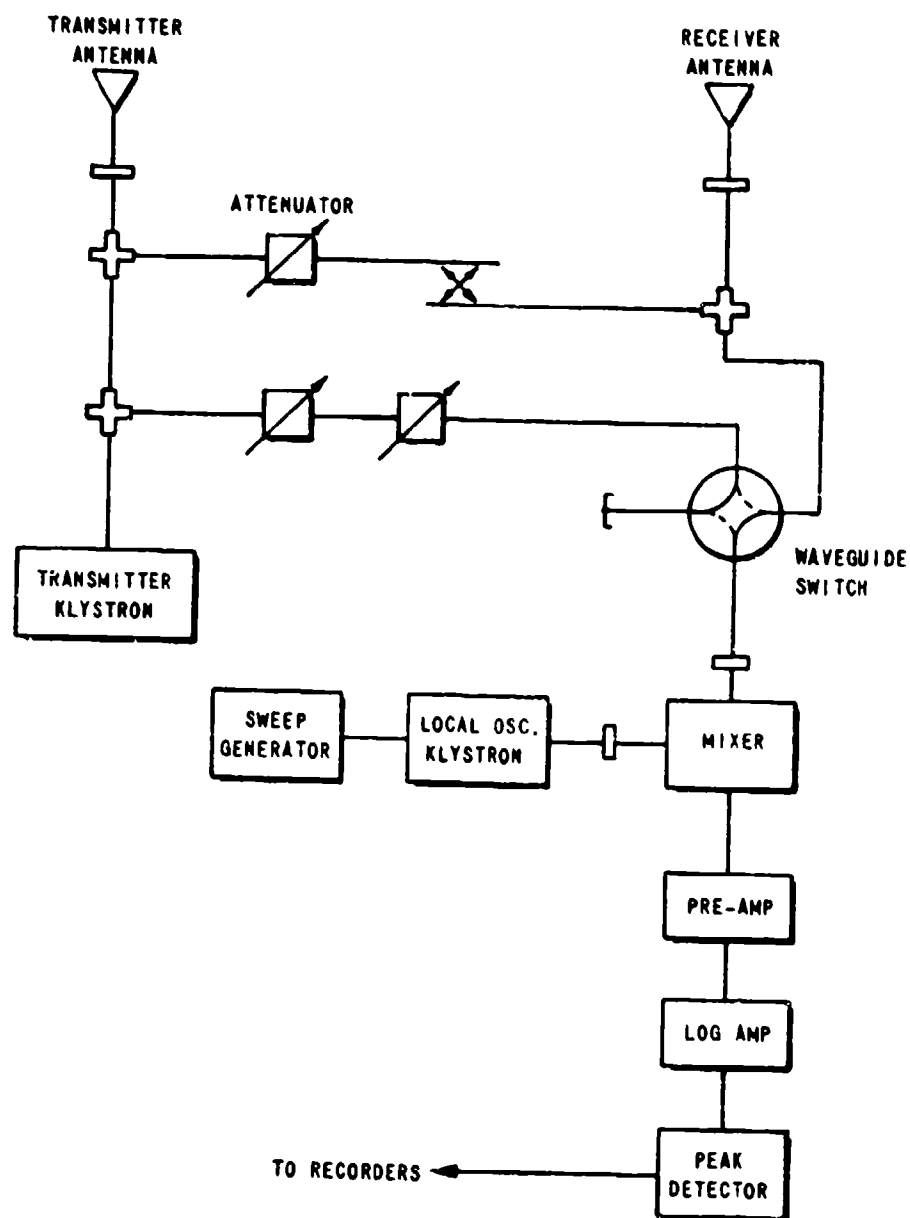


Figure 2 FUNCTIONAL DIAGRAM - K_a BAND CW RADAR

X-BAND CW RADAR

A simplified functional diagram of the X-band CW radar is shown in Figure 3. The usual mode of operation employs separate transmitting and receiving antennas in a quasi-monostatic configuration which has a bistatic angle of approximately 5° . Monostatic operation with a magic Tee is possible; this mode of operation is infrequently used because the system remains balanced for longer time intervals in the quasi-monostatic mode.

Commonly used antenna-to-target distances are 8.5 feet, 13.5 feet and 18.5 feet. Polarization can be either linear (vertical or horizontal, parallel or crossed) or circular. The operational frequency is fixed at 9.2 Gc.

As shown in Figure 1, a directional coupler transfers a small percentage of the power from the transmitter into the receiver through an adjustable attenuator and a phase shifter. By proper adjustment of the amplitude and the phase of this energy in the absence of a target, the room background signal can be essentially canceled.

Signal reflected from a target into the receiver antenna first passes through a servo-controlled attenuator and then is combined with energy from a local oscillator to yield a 30 mc IF signal. This signal is amplified, rectified, and compared to a fixed d. c. reference voltage. The servo controlled attenuator maintains the output of the d. c. comparator very close to zero.

Coupled to the servo driven attenuator is a compensated nonlinear potentiometer. Its output voltage is directly proportional to the logarithm of the attenuation. Thus the output of this potentiometer when properly calibrated furnishes a measure of target cross section directly in decibels.

A complete calibration for this range is accomplished by recording potentiometer reading for each of a series of graded spheres of known cross section. The full calibration procedure is unnecessary except as an occasional check; stability of this equipment is such that a one point check with a single sphere normally suffices.

The target aspect angle is determined by a remotely controlled turntable. Data readout is synchronized with the latter so that the resulting data records present radar cross section as a function of aspect angle. Data are recorded both on analog strip chart and on punched digital paper tape. In the latter instance, sampling at either each degree or at each quarter degree may be chosen by the operator.

The maximum sensitivity for this range is limited by the minimum background interference. In the present configuration, background is approximately 25 to 30 db below λ^2 . Target backscatter 10 db below λ^2 can be observed with about 1.0 db maximum error.

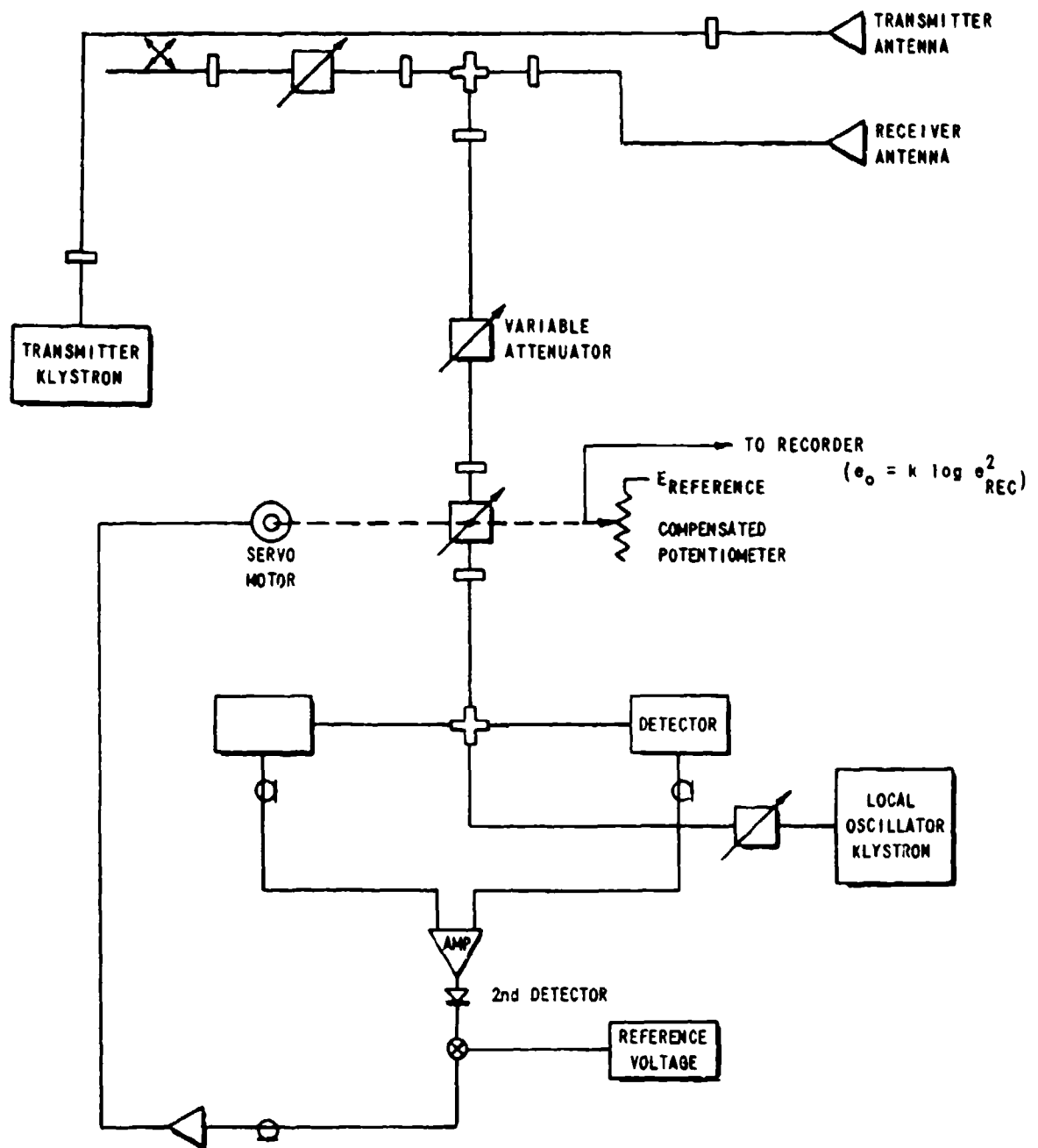


Figure 3 FUNCTIONAL DIAGRAM - X-BAND CW RADAR

X-BAND FM/CW HIGH RESOLUTION RADAR

The X-band FM/CW high resolution radar is designed to provide the capability of measuring the radar cross section of separate scatterers on complex targets with a resolution equal to a small fraction of the target's length. A functional block diagram of the equipment is shown in Figure 4.

This system operates quasi-monostatically with a bistatic angle of approximately 3° . Linear polarization, either horizontal or vertical, is used. The center frequency is 10 Gc, and the swept bandwidth is usually adjusted to be 3500 Mc/sec.

The target is illuminated by rf energy from the transmitter which is modulated linearly in frequency. The modulation is repeated cyclically. A portion of the transmitted energy is fed directly through a fixed delay line to the mixer. This energy comprises a local oscillator signal which is combined with the received signal. The product contains a low-frequency component with frequency proportional to range of the target. Although in principle this low audio beat frequency could be used as the target signal, phase modulation is used to impose an additional constant frequency shift which translates the target signal from the audio frequency region to approximately 465 Kc/sec, and thus minimizes a noise problem otherwise inherent in the low frequency operation. The desired low frequency signal, which is recovered by means of a synchronous detector, consists of a set of harmonics of the sweep recurrence frequency with spectral distribution maximizing at a frequency corresponding to target range and frequency sweep rate. Inspection of the spectral distribution then permits determining the relative separation in range of several scatterers by the positions of their corresponding spectral maxima.

If the amplitude of the low frequency beat note were constant during each sweep, the spectrum for a point target would have undesirably large range sidelobes. To suppress these unwanted sidelobes, the amplitude is modulated during the sweep by an approximation to Taylor weighting. Experimental evidence demonstrates that this weighting process reduces the range sidelobe magnitude to below -30 db relative to the central response maximum.

The basic data of scattering amplitude (square root of radar cross-section) versus range lie in the amplitudes of the individual recurrence rate harmonics which appear in the low frequency waveform. Two techniques are used to obtain the data. In one technique, the radar signal is connected to conventional panoramic spectrum analyzer and photographic records are made of the spectrum analyzer screen. In the second technique, a special 16-channel filter bank is used to separate the amplitudes of the individual harmonics. The a-c signal in each filter is rectified separately, then each rectified signal is sampled in turn to scan the radar output in range. The sequentially sampled signal is recorded both in digital and analog form.

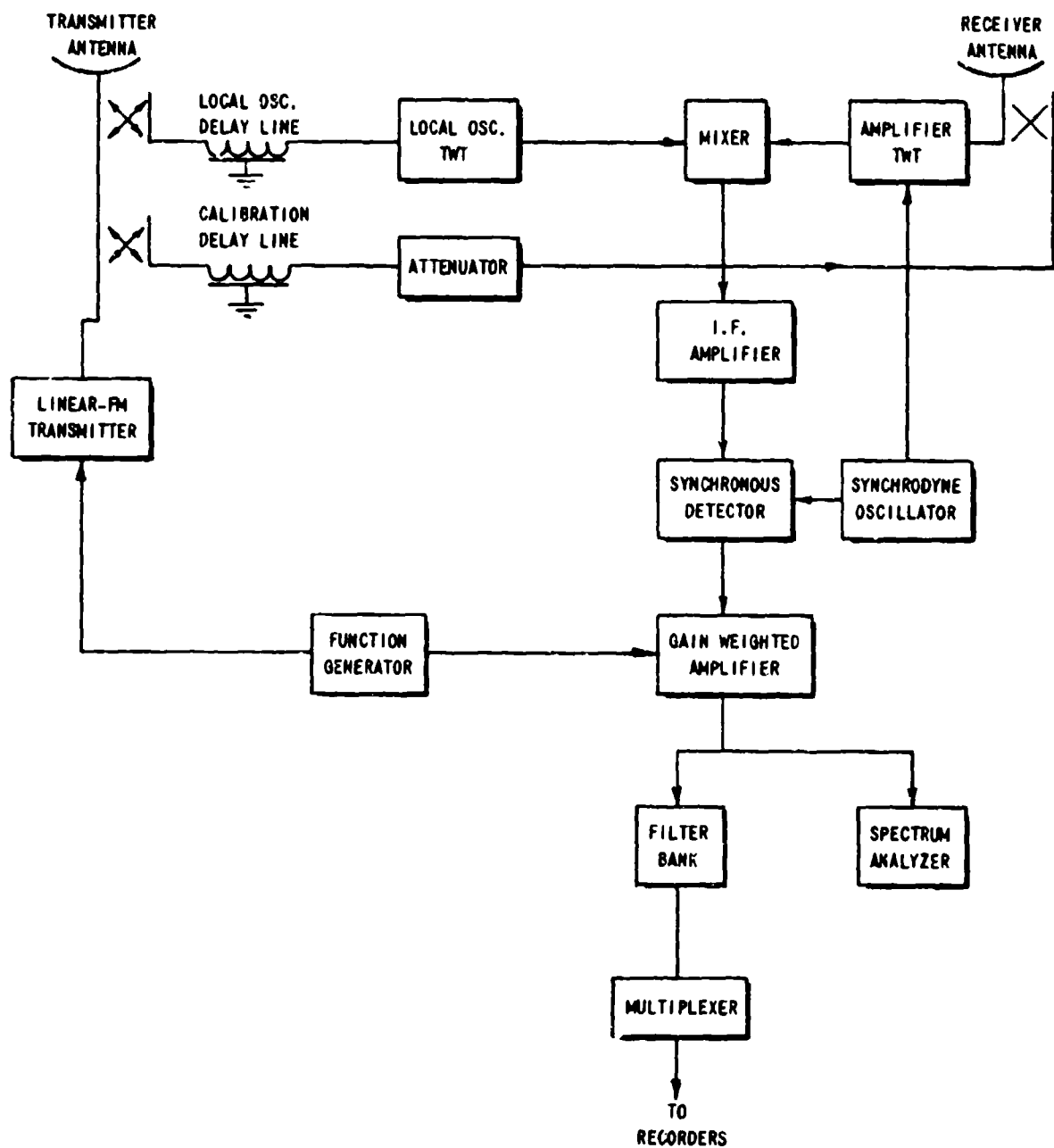


Figure 4 FUNCTIONAL DIAGRAM - X-BAND FM/CW RADAR

The FM/CW high resolution radar is usually calibrated with a standard target -- either a small flat plate at normal incidence, or a small corner reflector.

The measured resolution of this radar (at 3 db points) is approximately three inches. The present sensitivity lies between 35 and 40 db below a square wavelength, with room background at least 55 db below a square wavelength.

AN INDOOR RADAR SCATTERING RANGE

E. F. Knott

Radiation Laboratory, The University of Michigan

The Radiation Laboratory operates an anechoic chamber located in Building 2602 at the Willow Run Airport near Ypsilanti, Michigan. The chamber is part of a room 28' wide, 15' high and 148' long; the chamber itself occupies 105' of the length, the remaining 43' forming a work and test bench area. The two parts of the room are separated by a pair of 8' x 8' sliding panels which can be brought near each other to form an aperture through which the antenna may be directed.

The walls of the room and the sliding panels are covered with a layer of 2-inch thick hairflex absorber manufactured by B. F. Goodrich. Most of the rear wall is covered with VHP-18, another Goodrich product, and a layer of hairflex covers the concrete floor. The equivalent room cross section at 25' is -18 dbm^2 at S-band and -31 dbm^2 at X-band. At this range typical sensitivity for a 10 db S/N ratio is of the order of 10^{-5} at X-band and 10^{-4} m^2 at S-band. Figures are not available for other frequencies.

A steel track made of pipe extends some 30' into the room and a carriage bearing the pedestal turntable can be positioned anywhere along the track. A shield which hides the carriage and turntable is clamped to the track just forward (on the antenna side) of the carriage and is covered with VHP-18 and VHP-8. A rocking mechanism is affixed to the carriage making it possible to cause the carriage to oscillate a few wavelengths along the track. This operation is performed electro-mechanically and is given the name 'rocking'. All portions of the track except near the carriage are shielded with hairflex. Styrofoam columns are generally used for model support, but for certain low cross section shapes a nylon cord or cotton thread suspension has been found to be advantageous.

The microwave circuitry is exclusively a balanced bridge CW system employing a hybrid tee. The waveguide items are mounted on rolling equipment stands, one each for L-, S- and X-bands, and are mounted such that any linear polarization can be selected. With the exception of L-band, where a paraboloidal dish is used, all the radiating elements are pyramidal horns with gains in excess of 24 db. The receiver, recorder, and turntable are standard items manufactured by Scientific-Atlanta.

Phase locked klystrons and crystal excited multiplier chains are used as microwave sources from L- through S-band. At X-band, an LFE cavity-stabilized source, 8.5 Gc to 10.0 Gc, is used as well as phase locked klystrons, and beyond X-band klystrons are used. Much of the work done at The University of Michigan is at X-band and the LFE oscillator, which is continuously variable

in frequency, is one of the important sources.

The operation of the Radiation Laboratory chamber is a flexible one for several reasons. Firstly, because each band has its own equipment stand, large changes in frequency (say from S- to X-band) can be made rapidly by merely wheeling one stand into position and wheeling the other out of the way. Secondly, because of the design of the polarization equipment, any desired polarization may be selected and set up in a matter of seconds. Thirdly, by virtue of the track and carriage design, any range from 3' to 30' can be set up in a few minutes; ranges exceeding 30' are possible but require more time. Finally, because of the versatility of the X-band LFE source, detailed investigations can be made to study the behavior of radar cross sections as a function of frequency.

Frequency scanning is a useful diagnostic tool that can be used to study bodies whose scattering arises from two or more effective sources. From a plot of cross section versus frequency one can deduce not only the electrical separation of the scattering centers but their relative amplitudes as well. In most cases, the model is specified in terms of d/λ , where d is some characteristic dimension of the body. Either d or λ may be varied, but for fixed frequency, one must vary d , and this is accomplished by the use of a series of similar models, each different from the other by a scaling factor. There is a possibility that imperfect machining or imperfect scaling will cause inaccuracies in the σ vs d/λ plot. In addition, fabrication costs can run very high for several models, especially if they have complex shapes. When these considerations are compared with frequency scanning, the utility of the latter becomes apparent.

In the radar cross section measurements field, the point has been reached where the cross sections to be determined are of the order of the interference effects of the room and even the support mechanism can mask the true cross section one seeks to measure.

The Radiation Laboratory has devised a scheme to separate and account for these effects in the event they cannot be further decreased or suppressed. The method makes use of model 'rocking' as described above. The rocking motion causes the signal from the model and pedestal to change phase with respect to the stationary background signal, producing a periodic variation in the received power which is recorded. Although the background effect may be removed by noting the extremes of this variation, the result still contains a pedestal contribution of some unknown phase and amplitude. This effect can be separated from the desired model return by causing a model-to-pedestal phase variation which would yield the same kind of information derived from a model-to-background variation. However, the two phase variations cannot be performed independently and some care is required to extract the desired information.

The phase between the model and pedestal is varied by placing the model on the pedestal in different positions, but always such that the model is viewed from the same aspect. If the positions are separated by small enough intervals, at least one position will correspond to a phase of zero and another will correspond to 180° . The model and pedestal are rocked for each position and this permits the separation of the cross sections due to model, pedestal, and room contribution. This scheme is described in detail in a Radiation Laboratory report¹ and has been used to separate a model cross section as low as $3.1 \times 10^{-6} \text{ m}^2$ from a room contribution of $1.5 \times 10^{-6} \text{ m}^2$ and a pedestal return of $1.7 \times 10^{-6} \text{ m}^2$. The method is customarily used for fixed azimuth, and coupling effects between pedestal and model are neglected.

In applying the method, it is helpful to relate the effective cross sections by the phase angles α , ϕ and θ as shown in Figure 1, where ϕ and θ are varied as described above. The cross sections are real, as required by definition, but they lie in the complex plane by virtue of the phase relations. Both α , ϕ and θ are constant for a given frequency but ϕ and θ vary with pedestal distance.

$$\sigma = \text{Re} \left[\sqrt{\sigma_r} e^{j\alpha} + \sqrt{\sigma_p} e^{j(\alpha+\phi)} + \sqrt{\sigma_m} e^{j(\alpha+\phi+\theta)} \right]^2.$$

One may now analyze the effect of $\sqrt{\sigma_m}$ and $\sqrt{\sigma_p}$ being perfectly in or out of phase; when model and pedestal are rocked together there obtain four equations in terms of only three unknowns. (The redundancy is helpful in establishing the relative value of the unknowns since it is not known at the beginning which is the largest or smallest.) The four measured values are:

- σ_1 : the maximum signal which occurs when $\theta=0^\circ$ and $\phi=0^\circ$
- σ_3 : the maximum signal which occurs when $\theta=180^\circ$ and $\phi=0^\circ$ (or 180°)
- σ_2 : the minimum signal which occurs when $\theta=0^\circ$ and $\phi=180^\circ$
- σ_4 : the minimum signal which occurs when $\theta=180^\circ$ and $\phi=180^\circ$ (or 0°).

It can be seen that $\sigma_1 > \sigma_3 > \sigma_4$ and $\sigma_1 > \sigma_2$.

The roots of the four equations are extracted but since this is accompanied by plus and minus sign options, one must consider the effect of the relative values of $\sqrt{\sigma_m}$, $\sqrt{\sigma_p}$, and $\sqrt{\sigma_r}$. It can be shown that these fall into six cases and the four equations must be solved for each case. Because of the redundancy each unknown may be expressed in terms of one pair of the measured quantities while a check of this value is given in terms of the other pair. The solutions for the six cases may be listed as indicated in Table I and the correct case must be separated from the other five. This is done by first inspecting the solutions

for $\sqrt{\sigma_r}$ and it will be found that four of the cases may be eliminated immediately since the alternate solutions within a given case will agree for only one pair of cases. The correct case of the remaining pair may be isolated by repeating the measurements at another frequency, preferably several. Usually the pedestal effects vary more slowly with frequency than the model cross section and the correct case may be isolated. Other ways to effect the isolation are to repeat the measurements at a different range (this changes $\sqrt{\sigma_r}$ but not $\sqrt{\sigma_m}$ or $\sqrt{\sigma_p}$) or to measure the pedestal itself.

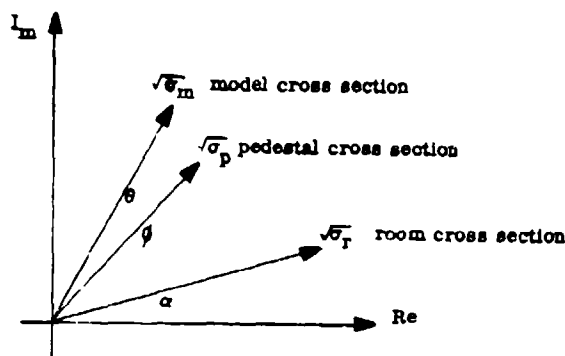


Figure 1

TABLE 1- SOLUTIONS FOR THE SIX POSSIBLE CASES

Case	$2 \sqrt{\sigma_r}$	$2 \sqrt{\sigma_p}$	$2 \sqrt{\sigma_m}$
a	$\sigma_1 - \sigma_3$	$\sigma_2 + \sigma_3$	$\sigma_1 - \sigma_2$
a	$\sigma_2 - \sigma_4$	$\sigma_1 + \sigma_4$	$\sigma_3 - \sigma_4$
b	$\sigma_1 - \sigma_3$	$\sigma_1 - \sigma_2$	$\sigma_2 + \sigma_3$
b	$\sigma_2 - \sigma_4$	$\sigma_3 - \sigma_4$	$\sigma_1 + \sigma_4$
c	$\sigma_1 + \sigma_3$	$\sigma_2 - \sigma_3$	$\sigma_1 - \sigma_2$
c	$\sigma_2 + \sigma_4$	$\sigma_1 - \sigma_4$	$\sigma_4 - \sigma_3$
d	$\sigma_1 + \sigma_3$	$\sigma_1 - \sigma_2$	$\sigma_2 - \sigma_3$
d	$\sigma_2 + \sigma_4$	$\sigma_4 - \sigma_3$	$\sigma_1 - \sigma_4$
e	$\sigma_1 - \sigma_3$	$\sigma_2 + \sigma_3$	$\sigma_1 - \sigma_2$
e	$\sigma_2 + \sigma_4$	$\sigma_1 - \sigma_4$	$\sigma_3 + \sigma_4$
f	$\sigma_1 - \sigma_3$	$\sigma_1 - \sigma_2$	$\sigma_2 + \sigma_3$
f	$\sigma_2 + \sigma_4$	$\sigma_3 + \sigma_4$	$\sigma_1 - \sigma_4$

REFERENCES

- 1 Hiatt, R. E., E. F. Knott and T. B. A. Senior, "A Study of VHF Absorbers and Anechoic Rooms," The University of Michigan Radiation Laboratory Report 5391-1-F (February 1963).

STATIC RADAR REFLECTIVITY MEASUREMENT FACILITIES AT RADIATION INCORPORATED

J. E. Landfried and W. L. Williamson
Radiation Incorporated, Melbourne, Florida

ABSTRACT

The static radar reflectivity measurement facilities at Radiation Incorporated are described with details of system parameters, range layout, and target support techniques. The facility provides measurement capabilities for (1) frequency coverage from 0.3 to 24 kmc with selectable polarizations (2) a wide range of target sizes and weights (3) operating ranges up to 2000 feet for monostatic and bistatic measurements (4) and simultaneous operation at several frequencies on separate ranges. The systems have been designed to meet a wide variety of measurement requirements.

INTRODUCTION

The static radar reflectivity measurement facilities at Radiation Incorporated have been in almost continuous operation for the past ten years. The facility was originally established to provide scale model measurements of aircraft. It has since been expanded to include full scale measurements on a wide variety of current targets of interest, including re-entry vehicles and penetration aids. Available systems provide frequency coverage in all bands from UHF to K-band with a system being completed to provide continuous coverage from 300 to 1000 mc. Ranges up to 2000 feet are available for both monostatic and bistatic measurements.

The site consists of 165 acres of cleared, level ground which may be used with essentially no restrictions. Two buildings with 13,000 feet of floor space provides adequate office, laboratory and storage space. The facility and personnel are cleared to handle and store classified materials, and 24 hour guard service is maintained.

SYSTEMS

Present systems cover frequencies from UHF to 24 kmc. The Ku band, X-band, C-band and UHF pulse systems are tunable and the others are fixed frequency systems. Many of these systems can be modified for operation at other frequencies by acquiring signal sources and other RF components where required. The UHF pulse system was designed for continuous tuning from 300 to 1000 mc, but will be capable of operation at somewhat lower frequencies. Table I describes the characteristics of the systems.

TABLE I CHARACTERISTICS OF REFLECTIVITY MEASUREMENT SYSTEMS

Band	Frequency (mc)	Range (R)	Background Level (dbm)	Peak Power	Pulse Width (usec)	Receiver Sensitivity (dbm)	System Sensitivity (dbm)	Antenna Polarization
K	24,000	450-2,000	-35 to -45	10 kw	0.25	-95	-50	Linear- Circular
K	16,000 to 17,000	450-2,000	-35 to -45	60 kw	0.25	-90	-60	Linear
X	8,500 to 9,600	350-2,000	-40 to -55	50 kw	0.25	-90	-65	Linear- Circular
C	5,400 to 5,800	500-1,000	-40 to -55	175 kw	0.25	-90	-60	Linear
S	3,000 3,300	500	-40 to -50	20 kw 175 kw	0.20	-90	-60	Linear
L	1,200 1,450	450	-40 to -45	1 kw	0.10	-90	-50	Linear
L	1,335	500-1,000	-50 to -60	10 kw	0.10	-85	-60	Linear
UHF	550	35-100	-40 to -50	10 w	CW	-105	-50	Linear
UHF	550	500-1,000	-40 to -45	1 kw	0.10	-90	-45	Linear
UHF*	300 to 1,000	500-1,000	-50 to -60	250 w	0.05	-90	-60	Linear

* Operational Soon

The systems are range-gated pulse systems with the exception of one UHF CW system. All measurements are performed on outdoor ranges. The systems from S- to K-bands use magnetrons for sources and develop an error signal from the AGC loop to drive the pen recorder. The L-band systems use cavity oscillators as sources and the 1335 mc system has a linear RF attenuator connected to the pen-drive servo. The 300 - 1000 mc system uses continuously tunable TWT amplifiers as sources and has a linear IF attenuator connected to the pen-drive servo. The systems provide a rectangular chart output, with digital output on punched paper tape to be implemented soon.

The systems are of conventional design except for the UHF pulse system which features 300 - 1000 mc continuous tuning and auto-calibration. (A separate paper is presented on the dual-channel technique being utilized in this system.) This system is compatible with modification for phase measurements.

Separate transmit-receive antennas are used in all systems except the UHF systems to increase transmitter-receiver isolation. The polarizations of the antennas are independently selectable, thus permitting crossed or other combinations of transmit-receive polarizations. The inherent bistatic angle is negligible (on the order of 1 degree) at the higher

frequencies. It is anticipated that cross-mode or other duplexers will be employed at UHF, rather than separate antennas, if separate transmit-receive polarization are required. Circular polarization is available at X- and K-bands and can be made available on any of the other systems.

OPERATION

Table I describes the ranges typically used at the various frequencies. While the 2000 foot range is the longest of the six ranges presently cleared and in use, up to 2800 feet can be made available. Range roads are provided for bistatic operation at all frequencies up to 90 degrees at a range of 2000 feet. Bistatic measurements have been made up to 140 degrees bistatic angle at shorter ranges. The range layout further affords simultaneous operations of different ranges as well as permitting measurements and range preparation concurrently.

Free space techniques, ground level (sometimes called ground plane) techniques, and a combination of these are used to provide a plane wave front over the target aperture. Microwave absorber fences are employed to eliminate ground reflections completely in some cases and to control a portion of the ground reflections in other cases. As opposed to the method of minimizing the effects of reflections by limiting their magnitude, the ground-level technique is a method for controlling reflections and utilizing them to obtain a sufficiently uniform field over the target aperture. Detailed field probes are taken during range preparation to document field conditions over the target aperture. The antennas are mounted at various heights up to fifteen feet and the target height is normally held from 15 to 20 feet to facilitate mounting. The small tilt angle of the beam can in most cases be compensated for by adjusting the axis of target rotation.

Table I lists the background levels normally obtainable with the various systems. Background level is, of course, dependent on target size and weight. The values listed in the table are maintained nominal values with the lower background levels pertaining to the smaller targets.

Styrofoam columns tailored for the specific target are normally used for target support during measurements. Cylindrical columns about 18 inches in diameter have been used to support targets of 400 pounds. Load tests indicate that weights of at least 500 pounds can be supported. Dual column support has been used on large models (15 to 20 feet) and models weighing in excess of 400 pounds with some degradation in background levels. Column shaping and cancellation techniques are used to maintain optimum target signal to background signal separation. The columns are tapered according to target weight to preclude normal incidence illumination of the column. The background contribution of Styrofoam generally decreases with frequency. At L-band and lower frequencies, background contribution of Styrofoam columns is quite low. As bonding or adhesion techniques are devised to allow fabrication of larger size

Styrofoam columns (or if larger logs become available), this support technique should be applicable for supporting much heavier weights at the lower frequencies.

Suspension techniques using a mobile crane have been used on larger targets weighing up to 4000 pounds. Results obtained indicate that the particular technique used is limited to targets with responses on the order of 0.1 square meter or larger. A suspension technique has been devised and proposed which should show substantial improvement over the mobile crane in the areas of background level and aspect accuracy. The proposed technique provides an approach for large, heavy targets (in order of 40 feet in dimension). The limitation of suspension techniques for measurements of low radar cross section is anticipated to be the inherent return of the sling which is dependent on target shape and weight. The support fixture, excluding sling, is expected to provide background levels on order of 50 db using cancellation techniques.

The data is recorded on rectangular charts with a linear dynamic range of 50 db or greater. Chart coordinates corresponding to azimuth aspect are varied according to the complexity of response to facilitate data reduction and analysis. The recorded data is often reduced to median or average values or presented in probability distribution plots. Computer facilities are available for the more complex data reduction. Plans have been made to implement concurrent digital outputs on the systems. Data will be multiplexed on punched paper tape in incremental values on the order of 0.1 db and 0.1 degree.

SUMMARY

The systems in operation at Radiation are designed for handling a wide range of targets including full scale re-entry and orbital vehicles, RV penetration aids, scale model RVs and OV's, scale model airframes, and various other targets. The systems cover frequencies from UHF and below to 24 kmc with capabilities for simultaneous operation and for bistatic operation. As previously indicated, changes can be made in many areas to meet specific requirements not currently satisfied.

A RADAR BACKSCATTER RANGE FOR MEASUREMENT OF LARGE MODELS

Wesley G. Louie, Research Engineer
and
Charles W. Matthis, Jr., Research Engineer
The Boeing Company, Airplane Division-Wichita Branch

An outdoor, monostatic, continuous wave, oblique type radar cross section range is utilized by the Airplane Division of The Boeing Company at Wichita, Kansas, for the measurement of large scaled aircraft models.

RANGE DESCRIPTION

The range, located on a portion of an eleven acre microwave facility, consists of a mobile transmitter-receiver-recorder station housed in a trailer and a fixed radar absorber covered platform for target mounting. The mobile trailer can be positioned along a roadway to obtain separation distances up to 800 feet between transmitter and target. A series of equipments including several ultra-stable signal sources and parabolic antennas of from one to ten foot diameters are available to obtain reflection measurements from 300 to 40,000 megacycles. The transmitting and receiving antennas can be independently adjusted in azimuth and elevation for focusing on the target. The separate transmitting and receiving antennas result in measurements which are made at a bistatic angle of one-sixth of one degree to six degrees depending on the selection of antennas and the antenna-target spacing for the particular measurement. This small bistatic angle can normally be neglected in establishing the monostatic return of a model.

A 20 foot high fixed platform, positioned diagonally with the trailer roadway, is utilized for mounting the components for model target positioning. The model to be measured is placed on top of a circular symmetrical 12 foot high foam tower or a foam and fiberglass tower which is mounted on an azimuth over elevation turntable. Towers are available for supporting models up to 500 pounds. The towers can be tilted in elevation to obtain proper alignment depending on antenna-target separation and rotated in azimuth through 360 degrees. For aircraft models, roll angles can be obtained by placing the model on the tower at the desired angle.

RANGE CAPABILITY

The minimum radar cross section that can be measured consistently is in the order of -30 dbm^2 for a target-antenna separation of 300 feet. The minimum radar cross section measurements achievable are dependent upon wind, the radar absorber material used on the tower structure, and also upon the effectiveness of the background

cancellation system. Weather conditions also govern operating time; an average utilization factor of about 0.5 has been experienced during the three years the range has been in operation.

RANGE EQUIPMENT

Signal Sources

Ultra-stable signal sources are used that have a frequency stability of 1 part in 10^8 or better for each of the principal radar bands of interest (S, X and K_a). Lower and intermediate frequencies are obtained from low power klystron oscillator signal generators having frequency stabilities in the order of 1 part in 10^4 or better.

Amplifiers

Several TWT amplifiers, covering a frequency range of 2.0 to 11.0 Gc, are employed when required. The power output of these tubes ranges from 3 to 15 watts.

Antennas

Four sets of two parabolic dish antennas are used to cover the frequency range of 0.2 to 40 Gc.

Receiver-Recorder-Control Console

Scientific-Atlanta receiving-recording equipment is employed with a model positioner and control console. The receiver provides a dynamic range of up to 60 db over a frequency range of 0.3 to 75 Gc. Sensitivity varies from -90 dbm at 0.3 Gc to -70 dbm at 65 Gc. A precision attenuator permits insertion of up to 41 db I.F. attenuation in 1.0 db increments. A rectangular type recorder with selectable linear, logarithmic, or square root pen response is used to plot the received instantaneous radar cross section.

Average Field Voltage Integrator

A specially designed average field voltage integrator and recorder is employed to eliminate the task of manually reducing instantaneous radar cross section data obtained from the conventional pen function amplifier and recorder to average values of radar cross section.

The dynamic range of this equipment is 40 db over the previously quoted frequency range. Averaging is available in increments of 2, 5, or 10 degrees of target aspect.

MEASUREMENT METHODS

A significant factor contributing to error in the radar cross section measurement is the proximity of target reflected signal to the background signal which is composed of reflected return from surrounding objects including the foam support column and the microwave absorber used to shield the platform and turntable. To reduce the static background signal to a minimum, a portion of the transmitted signal is coupled to the receiving circuits and adjusted in amplitude and phase to cancel the stable background return. This cancellation is accomplished immediately before the model is placed on the tower for measurement and the remaining background signal is recorded before and after each measurement.

Normally, several measurements are taken of a particular target configuration at identical frequencies and target attitudes and these plots averaged together to achieve as high a degree of accuracy as possible. This procedure minimizes the errors introduced in the measurements by any changes in background noise level, phasing, and wind conditions.

AN ULTRA-HIGH FREQUENCY REFLECTION MEASURING SYSTEM

Siegfried Mikuteit
Research Associate
Antenna Laboratory
Department of Electrical Engineering
The Ohio State University
Columbus, Ohio 43212

ABSTRACT

For the study of echo-area control a CW radar facility operating at a frequency of 422 Mc with a variable range from 30 to 103 feet and the capability to vary the polarization of the transmitting and receiving antennas continuously through 90 degrees has been constructed and calibrated. The system has a linear dynamic range of 50 db with accurate calibration possible over a range of 80 db if necessary. Presently the minimum measurable cross section of a target supported on a steel tower at a range of 48 feet is one square wavelength with an accuracy of one db. With further mechanical stabilization of the transmitting and receiving antennas it would be possible to measure radar cross sections approximately 20 db below one square wavelength. The null depth is about 75 db below a direct connection. Closed system stability evaluated over an 8-hour period is $\pm 1/2$ db. The frequency stability is ± 1 kc, resulting in a sufficiently small phase error in the nulling circuit so as not to affect the null depth significantly. Measurements with flat plates and a hybrid T-bar slot antenna agree with theoretical values to within the system accuracy.

DESCRIPTION OF UHF ECHO- AREA MEASURING SYSTEM

This paper describes the construction, calibration, and operation of a CW reflection measuring system used for automatic recording of backscattering radiation patterns of unified systems at a radiated frequency of 422 Mc. The ultimate use of the system to be described is to investigate the feasibility of using antenna^{1,2} techniques.

The research reported in this paper was sponsored in part under Contract AF 33(657)-10386 between The Ohio State University Research Foundation and Research Technology Division, Wright-Patterson Air Force Base, Ohio.

(antennafier is a term used to describe the combination of an antenna and an amplifier into a single unit), as developed at this laboratory, to control the echo area of body-antenna systems.

A block diagram of the system is shown in Fig. 1.

Transmitter

The signal source for the radar system is a crystal-controlled 144 Mc transmitter by Tecraft (model TR 20/144) operating with an input power between 5.0 and 7.0 watts. For CW operation the modulator output transformer is disconnected, but the modulation capability is retained through a jumper connection. The transmitter is operated with a Tecraft PTR-2 power supply. By the addition of a tripler amplifier the output power has been increased to 10 watts at 420 Mc.

Receiver

The accuracy of the echo-area recordings is principally determined by the calibration of the receiver AGC voltage against the RF signal power delivered to the receiver. The Collins 51S-1 laboratory receiver has proven to be very stable and also possesses very good AGC characteristics. Excellent logarithmic response is obtained over a 50 db range, which is normally adequate for a CW system. However, if need be, it is possible to obtain a dynamic range in excess of 80 db with calibration.

Converter

The energy scattered by the target and collected by the receiving antenna passes through a directional coupler to a Tapetone Model 100A converter which has an input frequency of 422 Mc and a bandwidth of 1.5 Mc. The intermediate-frequency is 22 Mc. The gain of the converter is 20 db with a noise figure of 8 db. The local oscillator is crystal controlled at a frequency of 44.4440 Mc. A crystal oven is used to insure maximum frequency stability. During initial tests, it was noted that the crystal oven provided good average (long-time) frequency control. There was, however, always a considerable amount of frequency hunting caused by the oven heating cycle. The recording of echo-area pattern requires a high order of stability during the process of measurement therefore the temperature sensing switch was inactivated by inserting a series resistor in the heater circuit. With this arrangement the current is limited and the oven

temperature stays below the maximum temperature of 85°C where normally the oven heating is interrupted.

ANTENNA SYSTEM AND RADAR RANGE

The transmitting as well as the receiving antenna is a 15-element Yagi array with a boom length of 11 feet. The measured gain of these antennas at 420 Mc is 17 db with respect to an isotropic source. The antennas and the target are mounted on towers as shown in Fig. 2. The antennas are connected to the tower through mounting brackets which provide for continuous changes in linear polarization through 90 degrees. It is possible to aim the beam in the vertical plane from 5 degrees below the horizontal plane to 45 degrees above it. The target was mounted slightly higher than the radar transmitting and receiving antenna to reduce background signal from the structures behind the target tower. The radar range can be varied from 30 feet to 103 feet.

AUTOMATIC RECORDING SYSTEM

The recording system consists of a Speedomax Tyne G recorder, the target selsyn generator and the recorder selsyn motor. The target is rotated at a rate of one revolution per 90 seconds. For automatic recording of reflection patterns as a function of target aspect, the recorder selsyn motor is connected to the recorder through a shaft which drives the recording paper at a speed of 12 inches per minute, thus providing an aspect coverage of 20 degrees per inch of paper.

SIGNAL ANALYSIS

The stability problem that arises because of frequency changes has been substantially reduced by inserting in the nulling circuit an amount of transmission line such that the length of the nulling circuit is equal to the free-space distance between antennas plus the lengths of transmission line from the antennas to the nulling circuit connections. With the present arrangement of the antenna system it is possible to achieve isolation between antennas in excess of 80 db for over an hour.

Since it must be assumed that there is some drift in the transmitter frequency, it becomes necessary to get an estimate of the phase lag at the receiver, caused by the signal reflected back from the target tower with respect to the signal through the nulling loop. This was found to

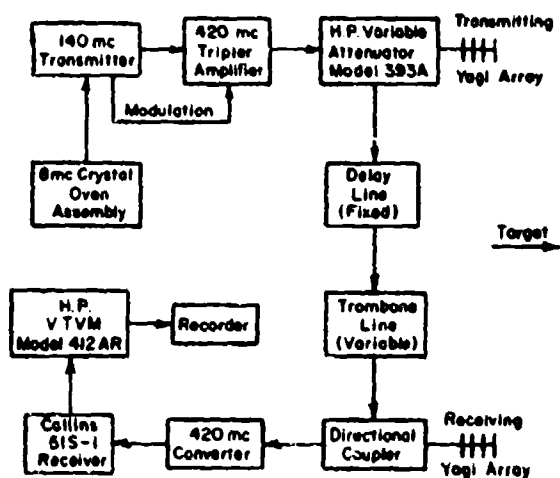


Fig. 1. Block Diagram of 420 Mc Reflection Measuring Installation

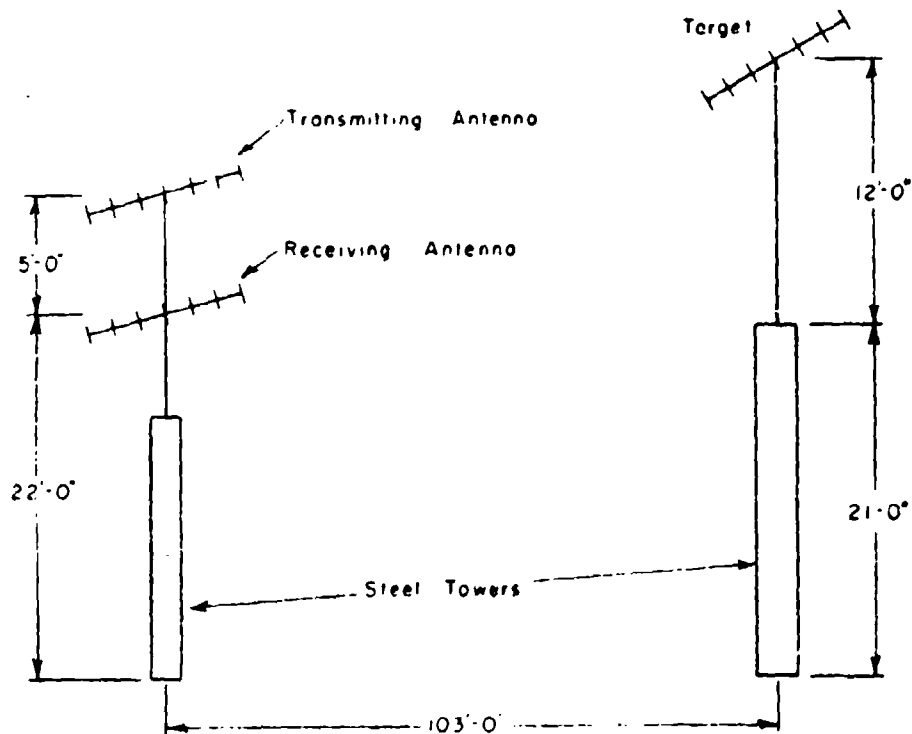


Fig. 2. Radar Range and Associated Dimensions

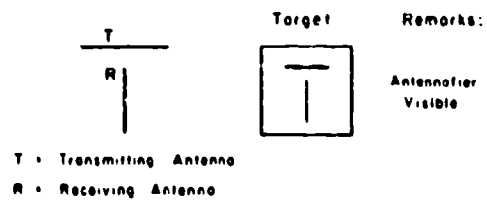
be 7.55×10^{-5} deg/cycle/sec. and since the maximum frequency drift measured over an 8-hour period does not exceed 1 kc the system is quite insensitive to small frequency changes.

The electrical stability of the radar observed with the transmitter output connected to the receiver input through a suitable attenuator indicated 0.5 db variation which corresponds to an amplitude stability of better than 5% relative to the initial amplitude, observed over an 8-hour period. When the antennas are connected to the radar system, such long-term stability cannot be obtained because of the relative motion of the antennas induced by the wind. Another factor influencing the stability of the null is a change in temperature. This causes the transmission lines to the antennas to change in electrical length, which results in a substantial phase change affecting the null. With perfect weather conditions the depth of the null has been measured to be 95 db below a direct connection. The calibration and measurements are usually made with a null depth of approximately 75 db.

CALIBRATION AND MEASUREMENTS

Calibration of this system is most readily achieved by using targets whose echo areas are known and which can therefore be used as standards. The echo areas for square flat plates of different sizes have been calculated and measured by Kouyoumjian and Lentzer.³ Using their results, several flat plates were built to provide calibration over the desired dynamic range of reflection levels. Comparative measurements on an X-band range at The Ohio State University using a scaled flat plate shows close agreement between patterns.

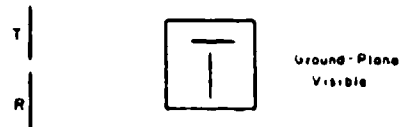
One target structure that has been tested consists of two T-bar compensated slot antennas mounted orthogonally in a ground plane. With the antennas connected to the input and output ports of a hybrid parametric amplifier, the echo-areas for three different cases of transmitting and receiving antenna polarization were considered as illustrated in Fig. 3. Because of the bilateral nature of the hybrid amplifier, the signal received by either antenna is amplified and radiated from the other, with the orthogonal polarization. Antenna orthogonality permits discrimination between the antenna scattering and the ground-plane scattering. Figure 4 shows the echo pattern of the T-bar slot antenna alone, using the polarization properties to suppress the flat-plate echo. The pattern is considered reliable only near the broadside region ($\pm 45^\circ$) because the suppression



Case 1



Case 2



Case 3

Fig. 3. Polarization Arrangement for Pattern Measurement With the Hybrid T-Bar Slot Antennafier

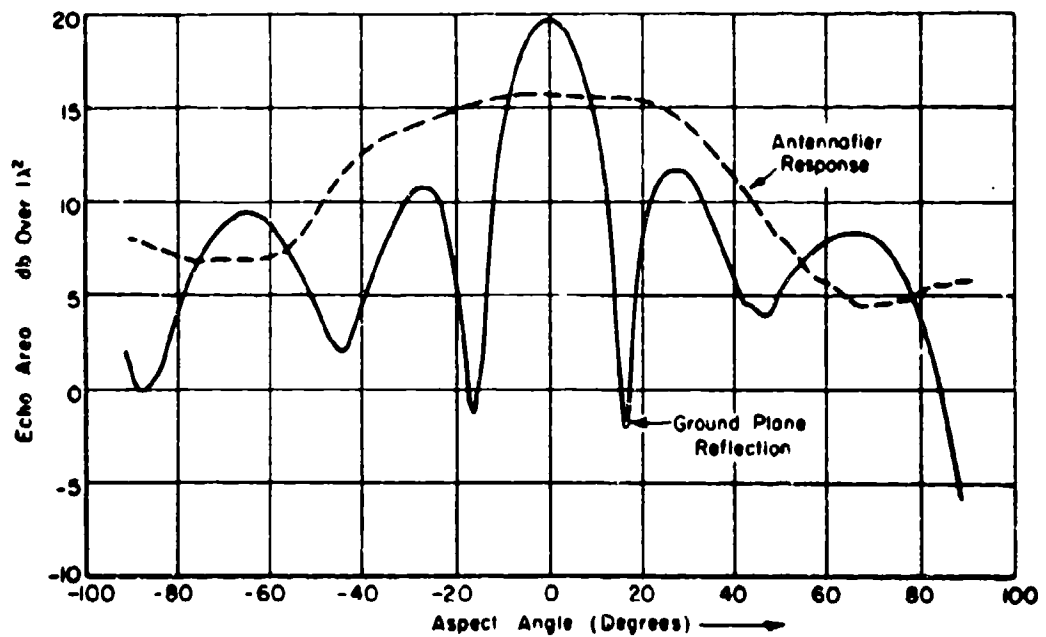


Fig. 4. Echo Area of the Hybrid T-Bar Slot Antennafier and the 4-Foot Ground Plane

of the flat-plate echo becomes poor near the edge-on aspects. Shown in the same figure is the echo pattern of the ground plane alone, taken with the antenna inoperative but located in the ground plane. Figure 5 shows the combination pattern of the ground plane with the operating hybrid T-bar slot antennafier. The main lobe of the ground plane pattern is virtually unaffected by the presence of the antennafier, while the nulls are filled in and the first sidelobes are considerably enhanced.

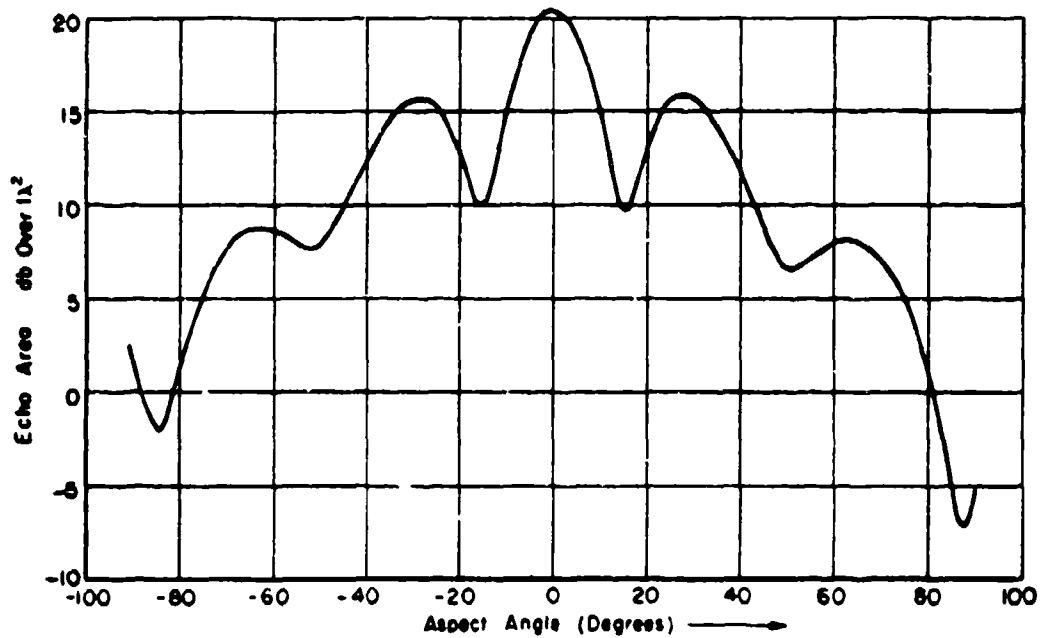


Fig. 5. Echo Area of the Combined Ground Plane and Hybrid T-Bar Slot Antennafier

RESULTS AND CONCLUSION

The two most difficult problems of operating the reflection measuring system are the random component of background power, and drift in the null of the system. Either effect results in received power which consequently adds to the desired signal according to the relative phases of the two.

Since the prime objective is to measure changes in echo area, a number of measurements were made with flat plates; these measurements show agreement with calculated values to within less than one db. No measurable effects on the pattern due to reflections from the ground were observed.

In general the stability problems associated with the transmitting and receiving antennas because of wind indicate that a good solution would be to use parabolic dishes securely mounted against the wall. This would also solve the problem of null stability, since at the present time mechanical instability in the Yagi antennas is the first cause of null fluctuation. With increased mechanical stability it is expected that a null in the order of 100 db below a direct connection could be obtained. It would then be possible to measure echo areas approximately 20 db below one square wavelength.

REFERENCES

1. Copeland, J.R. and Robertson, W.J., "Antennaversers and Antennafiers", Report 903-24, 15 December 1961, Antenna Laboratory, The Ohio State University Research Foundation; prepared under Contract AF33(616)-6211, Aeronautical Systems Division, Air Force Systems Command, United States Air Force, Wright-Patterson Air Force Base, Ohio.
2. Copeland, J.R., Robertson, W.J., Green, R.B., and Mikuteit, S., "Antennafiers for Echo Area Control", Report 903-30, 15 December 1962, Antenna Laboratory, The Ohio State University Research Foundation; prepared under Contract AF 33(616)-6211, Aeronautical Systems Division, Air Force Systems Command, United States Air Force, Wright-Patterson Air Force Base, Ohio.
3. Quarterly Progress Report, "Echo Properties of Various Objects," Report 444-9, 17 November 1952, Antenna Laboratory, The Ohio State University Research Foundation; prepared under Contract DA 36-039-sc-5506, Signal Corps Supply Agency, Laboratory Procurement Office, Fort Monmouth, New Jersey. AD 13 784.

RADAR ECHOING AREA RANGES AT ROYAL AIRCRAFT ESTABLISHMENT

J. G. W. Miller, B. Sc., and J. Edwards, B. Sc.

SUMMARY

This paper describes the layout and limitations of two outdoor radar model ranges in use at the Royal Aircraft Establishment, Farnborough, England. These work at frequencies in S- and X-bands. Both are capable of measuring very small radar echoes (10^{-4} square metres at S-band and 10^{-5} metres at X-band), and can accommodate models up to 300 lbs in weight and 10 ft in length. Echoes can be measured to within about $\pm 1/2$ db, and aspects to within $\pm 1^\circ$.

INTRODUCTION

Two measurement systems will be described. These are outdoor S- and X-band ranges designed and built at R. A. E. Farnborough in early 1958. Both systems are able to measure very small radar cross sections, of the order of 10^{-4} and 10^{-5} square metres at S- and X-bands respectively. The smallest objects measured on the X-band range have had cross sections equivalent to that of a $1/8$ in diameter ball bearing. At the other end of the scale the largest echoes measured have been several hundreds of square metres arising from a parabolic antenna viewed along its axis.

The upper limit to the physical size of model which can be measured depends on the linear beamwidth at the target, considerations of the Rayleigh criterion, and the weight carrying capacity of the suspension mechanism. In practice models are restricted to having a maximum dimension, normal to the beam, of 3 ft and a weight not more than 300 lbs.

A similar range of radar cross sections can be accommodated on the S-band equipment. Since the suspension system used here is the same as that used at X-band the weight limitations are identical. However the maximum target dimension normal to the radar beam can be increased to 7 ft.

As the above conditions are the only physical limitations imposed on the systems, the shape of the target is immaterial, and models varying from simple geometric shapes, such as spheres, cones, etc., to more complicated structures, such as finned missiles, radar antennae, birds, etc., have been successfully measured.

There is also a separate receiver system on X-band which allows bistatic measurements to be made. This facility enables results to be obtained for bistatic angles up to about 120° . A recent series of measurements has been made on models of certain civil aircraft in connection with the development of an instrument landing system.

It should be mentioned that both radars are trailer mounted and therefore mobile. This mobility allows them to be moved to other sites where they have been used to measure large echoes from targets on the ground: - for example vehicles, jet-flames, full size missiles and the principal sources of echo from aircraft.

There are two main advantages of the outdoor systems to be described. These are (1) the background echo can be kept small (equivalent to 10^{-6} and 5×10^{-5} square metres at X-band and S-bands respectively), and (2) the Rayleigh criterion for a plane wave front can be satisfied with reasonably large models. The primary disadvantage of outdoor systems is that accurate measurements depend on reasonable weather conditions.

In addition to these equipments it may be noted that there are facilities at R. A. E. for measuring S- and X-band echoes from full scale aircraft in flight. There are also facilities for monostatic and bistatic measurements by optical simulation. Since these equipments do not form a part of the subject of this paper they will not be described.

MEASURING EQUIPMENT

Model Suspension System

For those models with small radar echoes, where it is necessary to minimize the background echo, a suspension system for the model is used. This consists of a main terylene cord stretching between two towers 400 ft apart. The model is hung 6 ft below the main cord at a height of about 50 ft above the ground. The reason for suspending the model so far below the main cord is that at X-band the chief source of background echo, namely that from the knot on the main cord, is then outside the radar beam. This knot echo can reach a value as much as 5×10^{-5} square metres, when large models, requiring thicker suspension cords, are being measured.

The length of the main cord makes an angle of about 45° with the direction of the radar beam. This ensures that the reflections from the cord are directed away from the radar receiver.

X-band Radar

The radar system itself is straightforward. It consists of a unit producing a $1/20 \mu$ sec pulse at a p. r. f. of 1000 pulses/sec., peak power of 10 KW, and at a wavelength of 3.2 cms. Adequate sensitivity has been obtained by working at a range of 150 ft. The main difficulty encountered on this range was in avoiding excessive direct breakthrough from transmitter to receiver (for the receiver recovery time). This was largely overcome by using separate transmitting and receiving antennae, suitably decoupled and employing a short range gate in the receiving system. In addition, when extremely small targets have been measured (below 10^{-5} square metres), provision has been made to feed back a proportion of

the transmitted power to the receiver dish to cancel the direct breakthrough signal. This facility is occasionally used and improves the situation by some 6 db.

Both transmitting and receiving antennae are 3 ft diameter paraboloids giving beams 2° wide at the half power points resulting in beams about 6 ft wide at the target. The primary feeds are arranged to keep the sidelobes to a minimum. The polarizations of transmitter and receiver are independently variable. When plane polarized they are continuously variable from horizontal to vertical, and when circularly polarized either the same or opposite hands can be selected.

The received signal, after amplification to a suitable level, is detected and fed into a box-car detector and squarer. This produces long pulses of amplitude proportional to echoing area. The output of this circuit is integrated (with a time constant of $1/25$ second), and fed via a logarithmic D. C. amplifier to a pen recorder.

S-band Radar

This is a C. W. frequency modulated radar operating at a wavelength of about 10 cms and radiating $1\frac{1}{2}$ watts. The frequency deviation is 300 Mc/s, or 10 per cent which results in measured echoes being averaged over this band. Separate 3 ft diameter transmitting and receiving antennae are used which give 6° beams at the half power points with either horizontal or vertical plane polarization. The working range from radar to target is normally 300 ft but is sometimes twice this figure when very large models are measured, in order to keep within the Rayleigh criterion.

The system has a theoretical range resolution to 2 ft. This can be achieved in practice only when the adjacent sources of echo are of comparable magnitude. The range gate can be adjusted so that the echo from various portions along the length of a target can be individually investigated.

The echoing area is recorded as a function of aspect angle as in the X-band radar. In addition, there is a direct record of the ranges of the individual sources.

EXPERIMENTAL PROCEDURE

Since the models are hung at a height of 50 ft above the ground the radar antennae in both cases must look up at an angle of 20° to the horizontal to ensure that the model lies in the centre of the beam.

The model is allowed to rotate slowly under the action of the torsion in its supporting cord. With the recorder running continuously the echoing area polar diagram is traced directly onto the paper. It is clear that only $\pm 140^\circ$ of aspect will be seen for one complete revolution of the model. However, the method is quick and continuous. Depending on the detail and accuracies required, a complete polar diagram drawn on standard graph paper takes from $1/2$ hour to 1 hour to produce.

To obtain a 360° polar diagram the model has to be rehung. To investigate one particular aspect the model must be hung such that this aspect makes an angle of 20° with the horizontal.

A recent addition to the equipment has been a large boom, some 56 ft long, pivoted at its centre. This is sited immediately under the model. Strings running from the model to the extremities of this boom form a 30° equilateral triangle with the boom as base. As the boom is rotated in a horizontal plane there is sufficient torque in the strings to cause the model to follow closely the motion of the beam. This arrangement enables very low rates of rotation to be achieved with models which would normally tend to turn stably into the wind under the normal free method of turning.

Aspect angles are estimated from the symmetry of the polar diagram about an axis of symmetry in the target and the known angular positions of recognized lobes, e.g. broadside flashes.

Calibration is achieved by comparison with a standard sphere $3\frac{3}{4}$ in. in diameter at X-band, and a 1 ft diameter sphere at S-band.

It may be noted that when the X-band system was first constructed its operation was checked by measuring a series of spheres which varied in size from a standard $3\frac{3}{4}$ in diameter sphere down to a $1/3$ in diameter ball bearing. Good agreement with the theoretical curve was observed (see Fig. 1).

ERRORS

Because of the simplicity and speed of operation of the systems a penalty is paid in terms of measurement accuracy. A thorough investigation of the limitations of the X-band system has been carried out and is summarized here. Parts of this investigation are directly applicable to the S-band system; for example, those concerning the hoisting arrangements.

Angular Errors

There are two fundamental sources of inaccuracy in the equipments which introduce errors into estimates of aspect angle. The first, which can be attributed to the accuracy with which the target axis is set at 20° to the horizontal, contributes an error which varies with aspect in a complicated manner. A very rough estimate of the average error encountered from this source over a range of aspects from 0° to $\pm 90^\circ$ is $\pm 0.3^\circ$.

The second source of error is purely experimental arising from random causes. Its average value for the X-band system is approximately $\pm 0.6^\circ$. Unlike the former error it is independent of aspect angle. It depends mainly on the prevailing weather conditions at the time of measurement; in particular wind which must be less than about 4 knots. The error will therefore be similar in size on the S-band system.

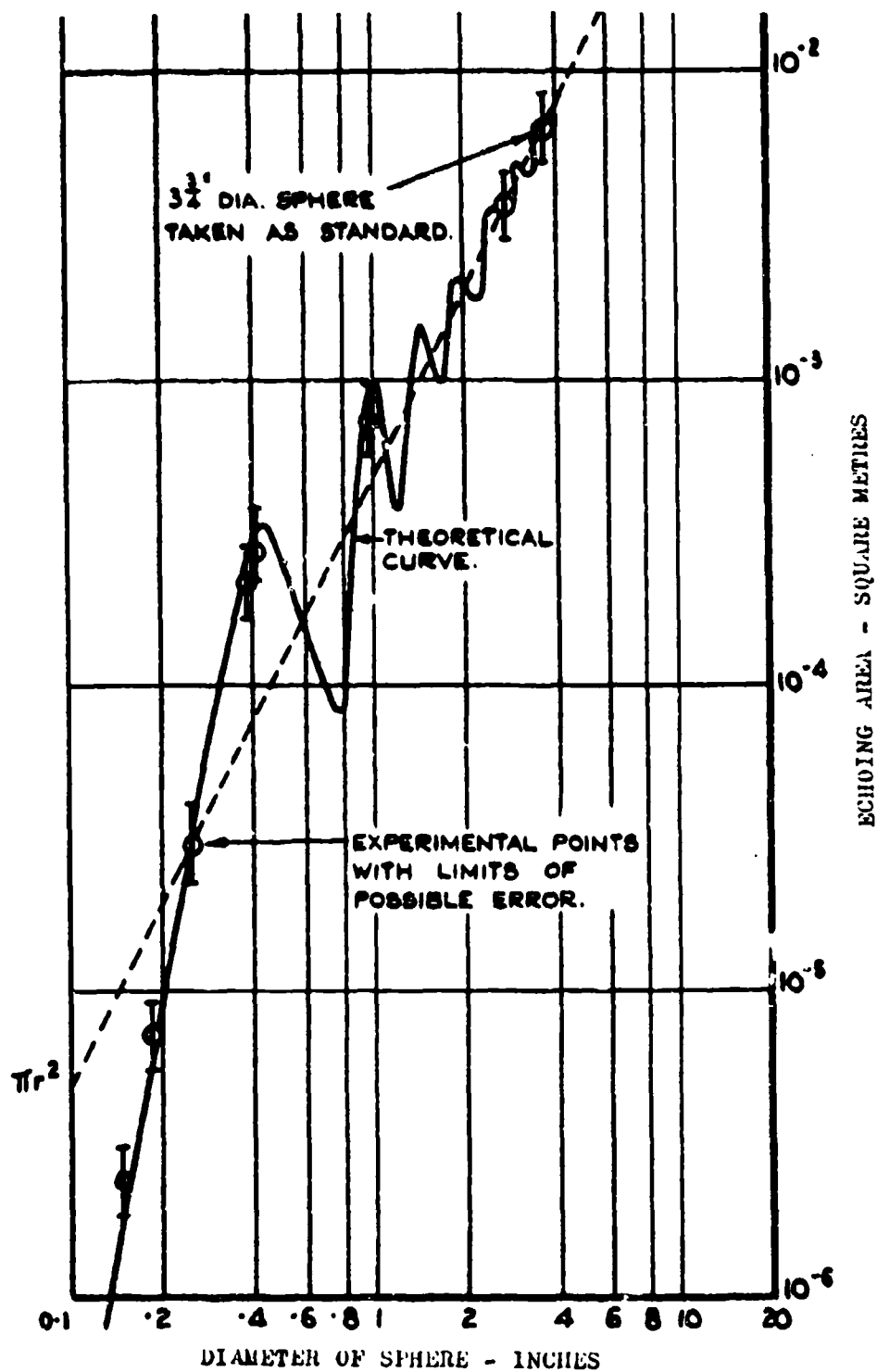


FIG. 1. CALIBRATION OF EQUIPMENT USING SMALL SPHERES
($\lambda = 3.2$ cms)

Thus aspect angles can be determined to an accuracy within $\pm 1^\circ$.

Magnitude Errors

Echoing area magnitudes depend for their accuracy of measurement primarily on the speed with which the target rotates relative to the time constant of the equipment. The extent to which the angular velocity remains constant is unimportant provided it is very low (less than 16 seconds/revolution). An experimental estimate of the size of this error shows that the vast majority of readings are accurate to ± 2 db, while 75 per cent of readings are accurate to about $\pm 1/2$ db.

Polarization Effects

The above errors assume that polarization effects are neglected. If the target axis of symmetry does not lie in the plane of polarization of the radar the polarization seen by the target will rotate through 90° as the target rotates through 180° about a vertical axis. Since polarization effects are normally neglected an error of about 8 per cent (less than 0.4 db) is introduced into the experimental values of echo magnitudes at 90° aspect. At greater aspects the error is larger, and vice versa.

CONCLUSIONS

The radars described allow echoing areas to be measured with $\pm 1/2$ db down to values below 10^{-5} square metres at X-band, and 10^{-4} square metres at S-band. The upper limits of measurement can be extended to some hundreds of square metres by inserting microwave attenuation. The accuracy with which target aspect can be measured is about $\pm 1^\circ$.

In addition to their use on a fixed range the radars, being mobile, can be employed to investigate the detailed echoing structure of targets on the ground.

As an example of a typical polar diagram obtained on the X-band radar, Fig. 2, is attached. The target was 20" long and consisted of two equal 8° apex-angle right-circular cones joined base to base.

ACKNOWLEDGEMENTS

The S-band F. M. radar was designed and built by the Plessey Co. Ltd to an R. A. E. specification. The principle of using elevated models was first suggested by Mr. T. W. G. Dawson and the basic design of the X-band radar was due to Mr. I. M. Hunter, both of R. A. E.

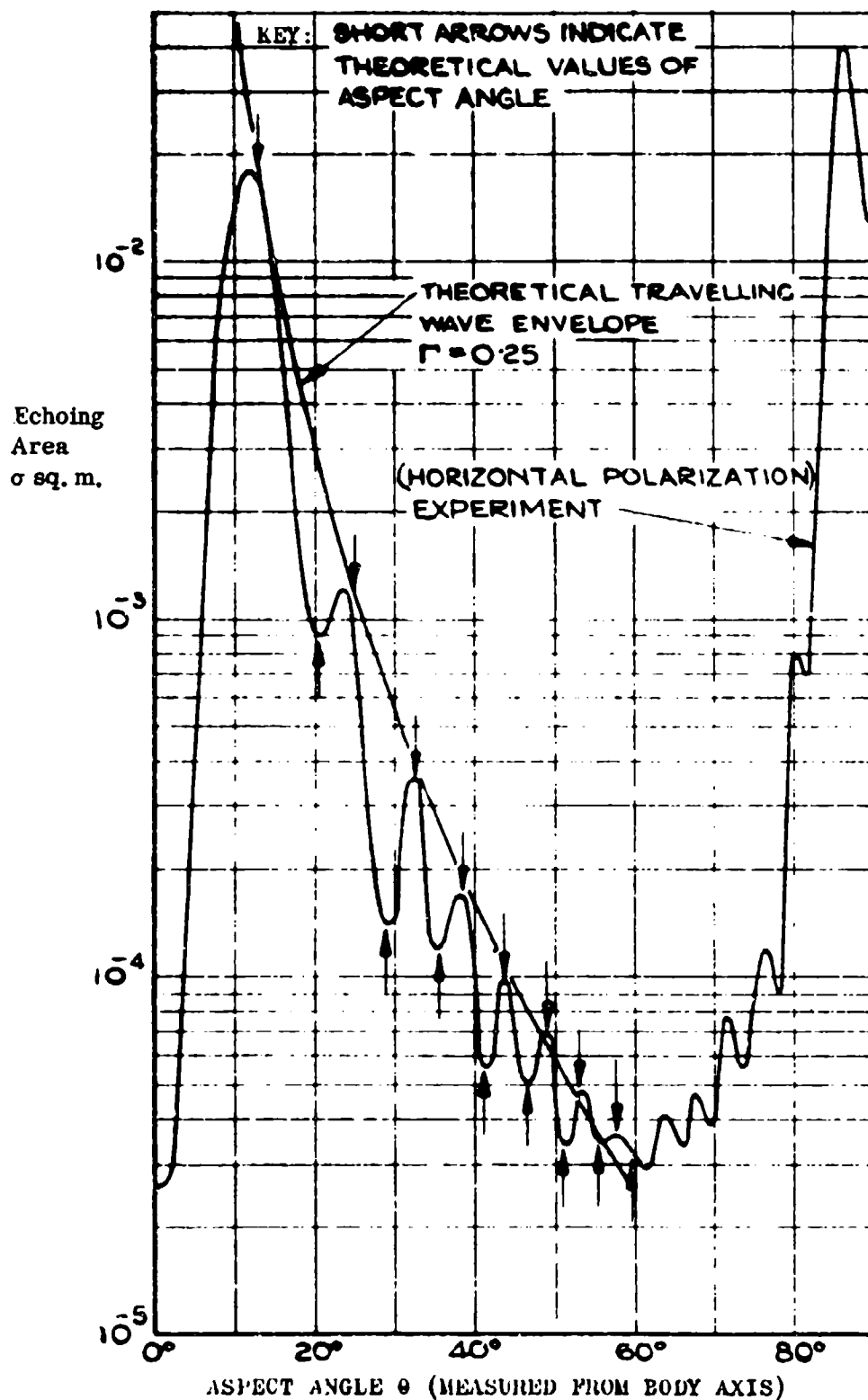


FIG. 2, ECHOING AREA OF A DOUBLE-ENDED CONE

RADAR TARGET SCATTER (RATSCAT) SITE

Donald Montana, Program Manager
Rome Air Development Center
Griffiss Air Force Base, New York

ABSTRACT

This report describes the design and operation of a Radar Target Scatter Site (RAT SCAT) radar cross-section measurement range presently being implemented at Holloman Air Force Base, New Mexico. Briefly described are RAT SCAT site characteristics and capabilities, including a description of a ground plane range, the frequency coverage, data recording, calibration and target size. Measurement rate is treated only briefly. The initial capability is compared with the advanced capability build-up in terms of target size, minimum cross section, and measurement accuracy.

INTRODUCTION

This report is provided to acquaint potential users with the existence and capabilities of the Radar Target Scatter Site located at Alkali Flats, Holloman Air Force Base, New Mexico. The RAT SCAT Site is being developed under the direction of the Rome Air Development Center, Griffiss Air Force Base, New York. The prime contractor is General Dynamics/Fort Worth, a division of the General Dynamics Corporation.

Operation of the site will meet a current and future need for making static radar cross-section measurements of advanced full-scale re-entry vehicle designs and of certain other selected targets. The site will represent an appreciable extension of the state of the art of radar cross-section measurement. The contract, AF30(602)-2831, was let on 1 July 1962. The initial site capability was operational on 1 April 1963; it will build up to full operation by 1 March 1964.

The RAT SCAT Site is a pulsed radar, range-gated, ground plane range. Target rotators are installed at ranges of 500, 1200, and 2500 feet from the radar building. Other distances are available through use of a mobile van. Frequency coverage is continuous between 0.1 and 12 kilomegacycles at 1 kilowatt peak power. Spot high power coverage is provided between 1 and 12 kilomegacycles at 100 kilowatts peak power. Receiver sensitivity is -94 dbm and the linear dynamic range of the receiver is 50 db. The receiver is preceded by a variable attenuator of 50 db in 10 db steps extending the measurement range to 100 db. Bistatic as well as monostatic measurements are available. Target weights up to 8000 pounds and target lengths up to 12 feet can be accommodated. Target lengths up to 28 feet may be handled but may involve a compromise in performance.

MISSION OF THE RAT SCAT SITE

The purpose of the RAT SCAT Site is to measure the static radar cross section of re-entry vehicles and other aerospace craft. The use of the

facility will be available to all DOD and National Agencies. It is anticipated that these measurements can be used to establish the magnitude and characteristics of vehicle radar cross section which can be used to determine probability of detection, recognition, and interception. Data gathered could provide a means for developing small radar cross-section targets. The site will also be used to establish and validate aerospace vehicle design criteria. Theoretical vehicle design results will be checked and the data produced will be used to evaluate various theories, criteria, and techniques. A standard for future design criteria will result from the analysis of test results and the comparison of such results with theoretical calculations. The development of advanced measuring techniques will improve range capability.

LOCATION AND ACCESS

The RAT SCAT Site is located on the "Alkali Flats" area west of Holloman AFB, New Mexico. The location of the site is shown in Figure 1. Railway access to the site is provided by a spurline of the Southern Pacific Railroad located at the main base of Holloman AFB. This spurline connects with a branch line of the Southern Pacific Railroad from El Paso, Texas, that passes through Alamogordo. Commercial air access is provided by the Alamogordo Municipal Airport located approximately three miles southwest of Alamogordo south of US Highway 70. Daily service is provided by Continental Airlines. In addition, a military air facility is located at Holloman AFB. A graded runway is located on the Alkali Flats near the site, but no control facilities are available. Security and proprietary safeguards at the site are provided on a 24-hour, 7-day-a-week basis. These are supplied in the form of secure building construction and a guard during working and nonworking hours. Fire protection is provided in the form of fireproof building construction and fire extinguishers (chemical, CO₂, and water), located at strategic points conforming to FIA regulations.

CAPABILITIES

The operation of the RAT SCAT Site is controlled from the Operations Building shown in Figure 2. In addition, there is a 40 x 40 x 15 ft warehouse for storing targets. A discussion of the fundamentals of operation, frequency coverage, data recording, calibration, and target size follows.

Fundamentals of Operation

Ground plane range operation is based on the addition of the ground-reflected wave and the direct wave from an antenna as shown in Figure 3. Interaction between the two waves causes the original radiation pattern of the source to be broken up into a vertical lobe structure. The result of combining the direct wave and reflected wave at the target depends on the relative intensity and

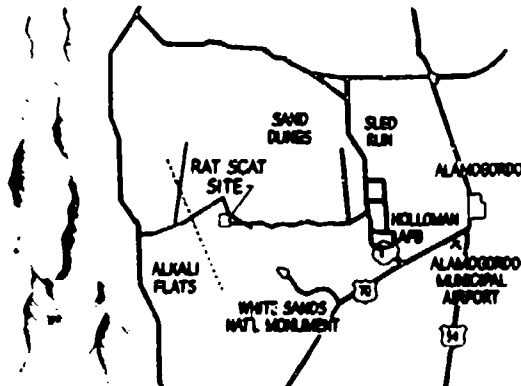
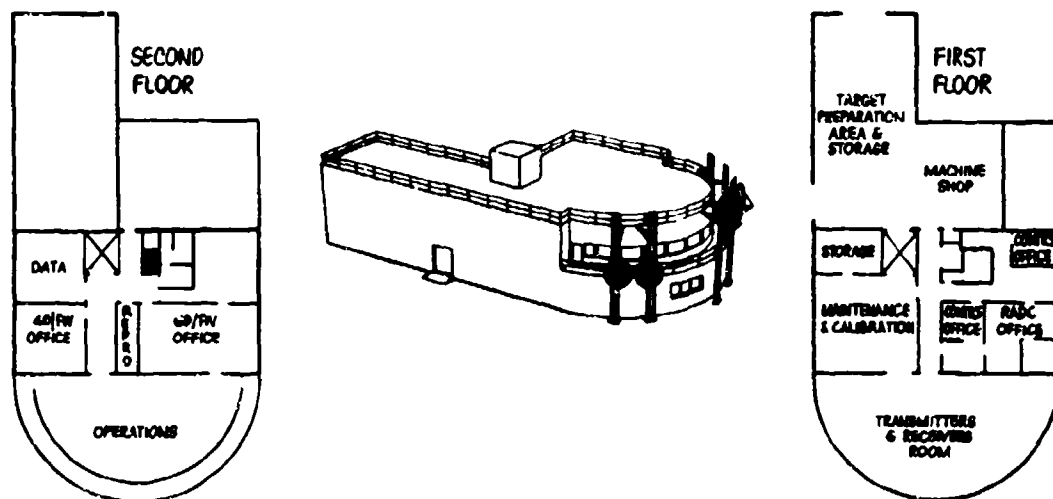
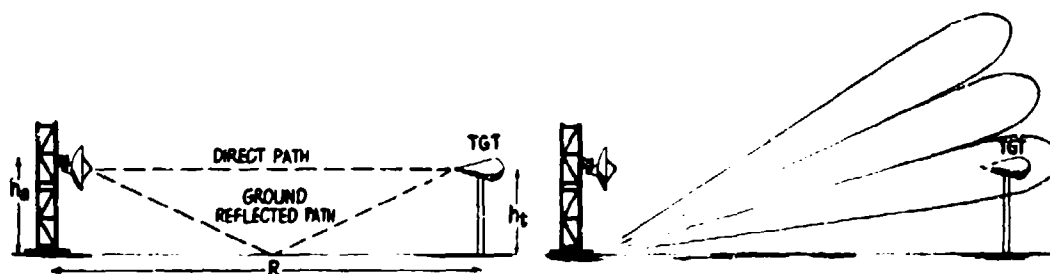


Figure 1. RAT SCAT Site Location



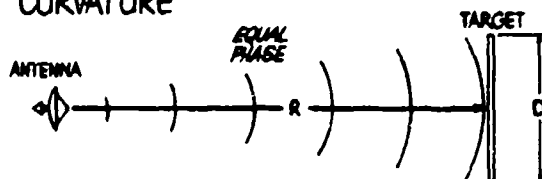
- Machine shop for making target supports
- Reproduction room for turning out reports quickly
- Maintenance room for repairing & calibrating all equipment
- Room large enough to do ven maintenance
- Operations room is separate from transmitter & receiver room
- Office space for GD/FW, RADC & contractor personnel
- Freight elevators to service both floors & roof

Figure 2. Operations Building



- Constructive and destructive interference between direct path and ground reflected energy produce a lobe structure in the radiation pattern of the source - The target is located in the first lobe when $h_a h_t = \lambda R/4$

PHASE FRONT CURVATURE



- The range requirement due to phase front curvature is $R = \frac{kD^2}{\lambda}$ where k is a function of the allowable error.

Figure 3. Ground Plane Radar Range

phase of the two waves. In turn, relative phase and intensity depend on the difference in length between the two paths and upon the change of phase and intensity introduced by the process of reflection. On a ground plane radar cross section range, the antenna and model are located at the proper positions in space so that the direct wave and the ground-reflected wave add at the target to produce a maximum lobe. For a perfectly conducting plane earth and point source, the relationship between antenna height, target height, range length, and frequency is expressed by the equation $h_a h_t = \lambda R/4$, where h_a is antenna height, h_t is target height, R is the range between the antenna and target, and λ is the wavelength. Tests set up in accordance with this equation yield low background levels.

The range R , used in the preceding equation, is also constrained by the allowable error due to phase front curvature at the target. Errors due to phase front curvature are not peculiar to a ground plane range but are primarily a function of the distance between the target and the transmitter/receiver. If the phase front incident on a target is curved as shown in Figure 3, the returns from scatterers located on various portions of the target will not be in the proper phase relationship. The required range is $R = kD^2/\lambda$ where D is the maximum dimension of the target perpendicular to the beam. The nature of the target and the tolerable error determine the value of k to be used. A value of 1 is suitable for many situations.

Frequency Coverage

The RAT SCAT system is designed to measure radar cross section at frequencies of 0.1 to 12 kilomegacycles. Transmitters for frequencies below 0.5 kilomegacycle will incorporate conventional tuned-line pulsed oscillators with 1 kilowatt of peak power output. A TWT transmitting capability is provided from 0.5 to 11.5 kilomegacycles with a peak output power of 1 kilowatt. For these systems, frequency coverage is continuous. Bistatic operation is available at all frequencies. Transmitter and receiver characteristics are shown in Figure 4.

CHARACTERISTICS	
• Pulse Repetition Frequency _____	500 - 5000pps (variable)
• Pulse Width _____	0.1 - 1.0 μ sec (variable)
• Range Gate _____	0.1 - 1.0 μ sec (variable)
• Dynamic Range _____	60 db
• Receiver Bandwidth _____	10 mc or 2 mc (selectable)

Figure 4. Transmitters and Receivers

A large number of transmitters operate on the White Sands Missile Range. It is therefore necessary to schedule operation at certain frequencies to prevent mutual interference. It is desirable that measurement frequencies be known as far in advance of actual use as possible.

Data Recording

The system is designed to record cross section over any 50 db dynamic range. Polar recorders, Scientific-Atlanta APR-31-S36, capable of making 13-inch diameter plots, are provided. Azimuth position of the target is changed by the rotation of the table; the received signal strength causes a radial pen motion. Thus, a polar plot of cross section (σ) vs. azimuth angle is obtained. Rectangular (X-Y) recorders, Scientific-Atlanta APR-21, capable of making 10 by 20-inch plots are also available. Azimuth target position is plotted along the abscissa, and cross section on the ordinate. Equipment for duplicating records is available at the site.

In addition to analog recorders, digital recorders and printer are also available. The digital recording interval is selectable in 0.1, 0.2, 0.4, 1, 2, and 4-degree steps. The recording medium is punched paper tape in 5-level teletype format. A typewriter is provided for tape identification and the insertion of calibration data. Tape duplication equipment is also available. Typical data outputs are shown in Figure 5.

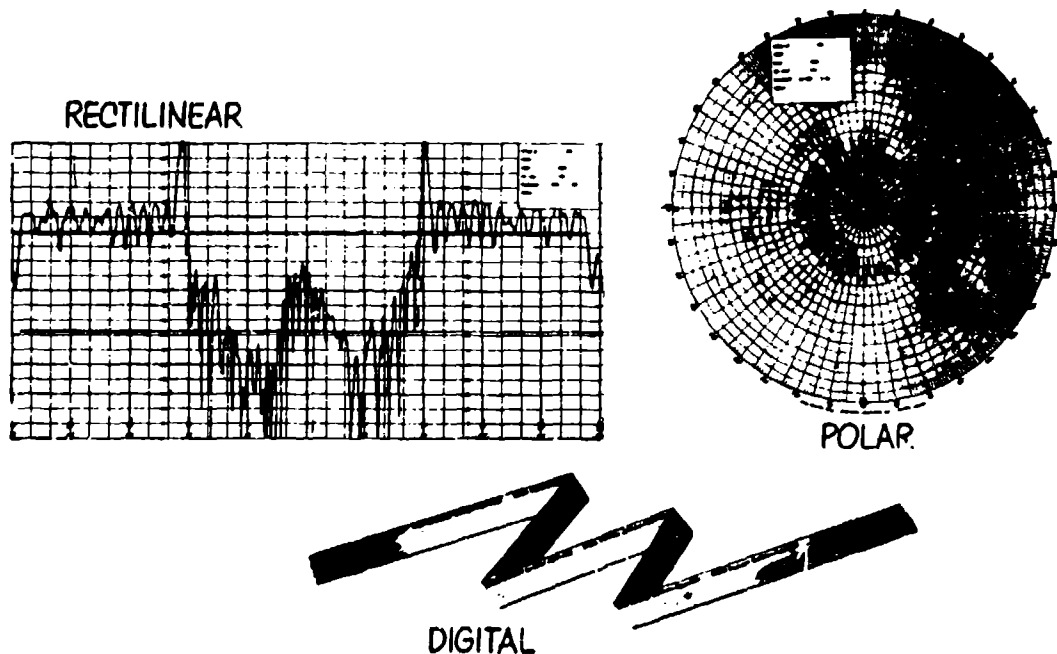


Figure 5. Measured Data Formats

Calibration

Normally, calibration of cross-section measuring equipment is accomplished by the measurement of spheres. Calibration spheres from 36-inch diameter to small ball bearings are available. A retractable corner reflector is positioned at a specific distance in front of the

target and is used as a secondary standard. In typical operation, a sphere will be mounted on the target mount and the equipment calibrated. The range gate is then positioned at the range of the corner reflector, and a calibration is made by using the corner reflector as the secondary standard. The corner reflector is then used as a working standard for each plot. Discrimination between the target and the secondary standard is accomplished by moving the range gate to the appropriate distance. Other calibration methods will be investigated, particularly for bistatic operation.

Target Size

Targets up to 8000 pounds may be measured at RAT SCAT. A primary consideration is the target mount since it must be designed to reflect a substantially smaller cross section than the target to be measured. Usually, the mount must be especially tailored to the target. If the target is designed to reflect a particularly low cross section at certain aspect angles, this information is used in the fabrication of the mount. Frequently, mounts can be fabricated to reflect extremely low cross section over a portion of total azimuth coverage. Therefore, information as to expected cross section will be helpful in designing a mount.

For the initial period, styrofoam mounts will be used. Although styrofoam mounts offer a low cross section, the weight loading capacity is limited. A hydraulic cylinder (used in conjunction with a RAM shield) will also be available for the heaviest targets. Other mounting techniques are being investigated.

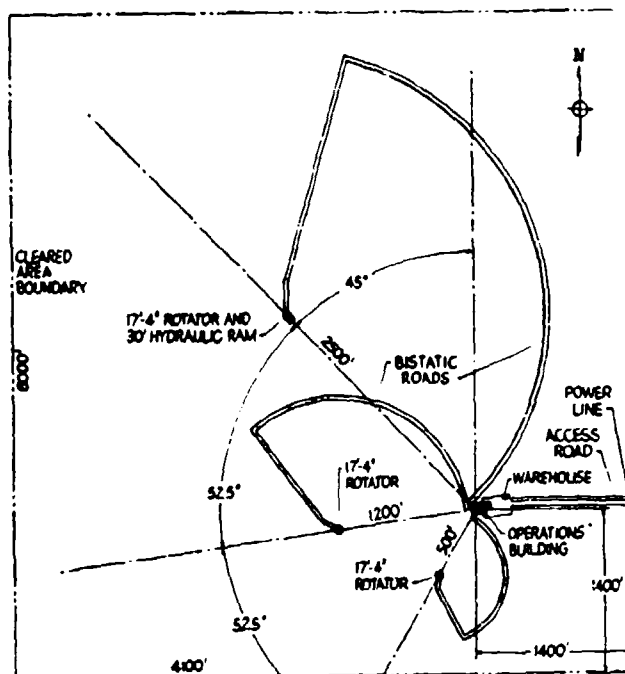
CAPACITY

The range is designed to measure both monostatic and bistatic cross section. Bistatic operation is limited to 0 to 120 degrees. Simultaneous monostatic and bistatic operation and recording are possible on any range. The range at which a target is measured will depend on frequency, target size, and required sensitivity. The RAT SCAT Site has been designed with three target pits at ranges of 500, 1200, and 2500 feet as shown in Figure 6. Any two ranges may be operated simultaneously. Normally, transmitters and receivers are located in the operations building. Where the fixed ranges are not satisfactory, transmitting and receiving equipment can be located in a mobile van which can be positioned at intermediate ranges.

Handling Equipment

Available support equipment is shown in Figure 7. Targets are normally handled by use of a mobile crane. Any special handling equipment, such as jigs slings, etc., must be furnished by the customer. Limited storage is available for targets in a warehouse adjacent to the operations building.

Mobile target shelters are also provided. These shelters are provided



- Target rotators at 3 ranges
- Monostatic van capable of accommodating all bands of equip.
- Bistatic capability on all 3 target stations
- 30 Ft hydraulic ram & rotator for heavy targets
- Mobile equipment for transporting & placing targets on rotators
 - Flat bed trucks & trailers
 - 30 feet - 10 ton crane
- Warehouse for storage of contractors targets

Figure 6. Site Physical Capability

with wheels so that they can be moved over target rotators to protect a target. Two movable hoists (longitudinal and lateral) are provided in the mobile shelter. Additionally, a truck-mounted aerostand is provided to allow personnel to work around the target while it is mounted.

PRIME EQUIPMENT NECESSARY FOR SUPPORT OF SITE

• VEHICLES

- Motor truck crane
- Miscellaneous support vehicles
 - 1 1/2 ton trucks
 - 1/2 ton pick up truck
 - Trailers
 - Tug
 - Fork lift
 - Aerostand

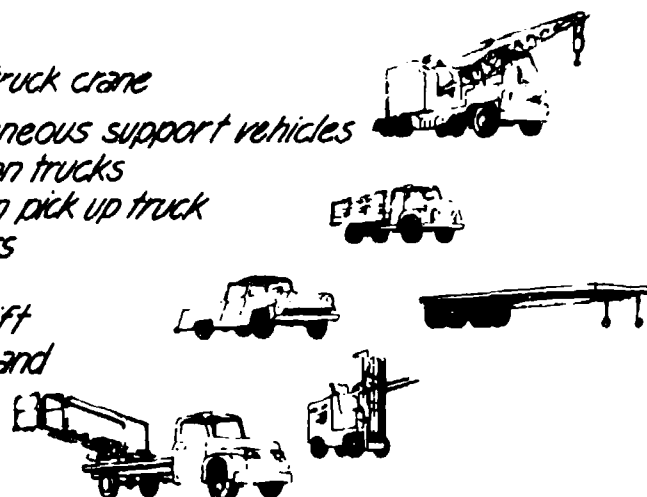


Figure 7. Support Equipment

Measurement Rate

A measurement of radar cross section is defined as the recording in analog (polar and rectangular) and digital form of radar cross section of one target for all aspect angles in a plane for a fixed target elevation angle at one frequency, one polarization, and one bistatic angle. The exact choice of these parameters for a measurement will be made by the PAT SCAT Site customer as coordinated by RADC. The number of measurements which can be made in any time period will depend on the complexity of the instrumentation, target size, bistatic considerations, etc. Other significant factors are the number of personnel assigned to the site, the number of shifts worked, and the use of overtime. For further information concerning measurement rate, refer to General Dynamics Secret Report, "PAT SCAT Measurement Rate Capability" (title unclassified), MRE 375, 14 December 1962.

CAPABILITY BUILD-UP

In terms of frequency coverage and cross-section values, the initial capability and the advanced capability of the site must be considered separately. For the initial capability, available 1 April 1963, the range frequency was 0.5 to 2.0 kilomegacycles. The specially designed styrofoam columns or air bags can accommodate target weights up to 350 pounds. The attitude of the target on the column can be manually adjusted. The amount of adjustment will depend on the shape of the target. The table which supports the column permits tilting the target from 0 to 15 degrees. In order to make a measurement, the target mounted on the table is rotated from 0 to 390 degrees. The radar cross section is recorded as a function of azimuth. Special handling techniques are required on targets over 12 feet in length. Targets with radar cross sections (σ) as low as 10^{-3} square meter can be measured with an accuracy of ± 2 db (1.0 - 2.0 kilomegacycles). For targets with cross sections greater than 10^{-2} square meter, the accuracy is improved to ± 1 db.

The advanced capability will be available on 1 March 1964. Additional frequency coverage, larger target weight capability, and better system accuracy will be provided. The frequency range will then be 0.1 to 12.0 kilomegacycles and weights up to 8000 pounds can be accommodated. The anticipated accuracy for 1.0 to 12.0-kilomegacycle measurements is ± 1 db for a 10^{-4} square meter target. Measurements may be made prior to completion of the initial capability and advanced capability phases. In addition, range improvements will be incorporated after attainment of the advanced capability.

IMPROVEMENT PROGRAM

The range improvement program consists of research and development of improved radar cross section measurement capabilities. The following areas are being considered in the research and development effort: development of advanced target support, background reduction, frequency stepping, range geometry, improved calibration techniques, circular polarization, scattering matrix and cancellation techniques.

The application of the results of the Research and Development Program will facilitate measurements of low cross section targets. In addition, these results will be utilized in the diagnostic investigation of range performance, flare spot location, mount discrimination, and frequency analysis. These results will also be used in meeting current and future measurement requirements and in improving measurement accuracies and techniques.

INVESTIGATION TO DESIGN A METHOD FOR
THE ANALYSIS OF RADAR CROSS-SECTION MEASUREMENT DATA

M. L. Parish
The Martin Company
Denver, Colorado

Early in 1963 Martin-Denver completed an entirely new microwave anechoic chamber to be used for antenna pattern measurement and radar cross section measurement. Because of the radar cross section requirements, it was hoped that the state-of-the-art in chamber performance could at least be equaled and perhaps even be extended. Several companies proposed state-of-the-art chambers equal to the best known facilities in the world. The B. F. Goodrich Company, Shelton, Connecticut, however, proposed a new innovation that upon investigation showed a good probability of extending this performance by 10 to 20 db.

The 20 x 20 x 50 foot structure is located in a new building at the Martin Antenna Range. One end of the chamber is equipped with a draw bridge type mechanism which allows the entire wall to be lowered to ground level to convert the chamber to an outdoor range terminal. The opposite end of the chamber borders on a two-story room which is used for instrumentation of the chamber.

In view of the "beyond the state-of-the-art" performance desired, B. F. Goodrich very high performance material was used in a flat wall design. In addition, a motor driven mechanism was incorporated to vary the tilt angle of the wall behind the object or antenna under measurement. This novel arrangement offers the opportunity to conveniently direct the best null in the wall diffraction pattern back down axis. VHP-26 was used on the tiltable back wall and VHP-18 was used on the remainder of the chamber. The usual walk areas of rigid absorbing material were omitted with the thought that these lower performance materials might adversely affect performance. Ventilation ducts were covered with porous CV-18 absorbing material. All materials (except the floor) were mounted with B. F. Goodrich "Absorba-grip" plastic zipper fasteners.

Ample evidence has been presented by B. F. Goodrich test engineers in conjunction with Martin engineers to show that the new Martin chamber, when used at X Band with a favorable back wall tilt angle, will give the following performance:

(1) Reflection for pattern measurements in excess of 70 db down at worst aspect angles and (2) an equivalent radar cross section of approximately 1×10^{-6} square meters at 25 feet. While the original design goal of a 90 db down chamber was not fully attained, the measured cross section value can be used to calculate that the chamber is down 83 db. This figure is 23 db better than the guaranteed characteristics.

The B. F. Goodrich Company believes that this performance is significantly above that previously attained in any other chamber and is to be attributed to the use of very high performance materials in conjunction with the tiltable back-wall feature.

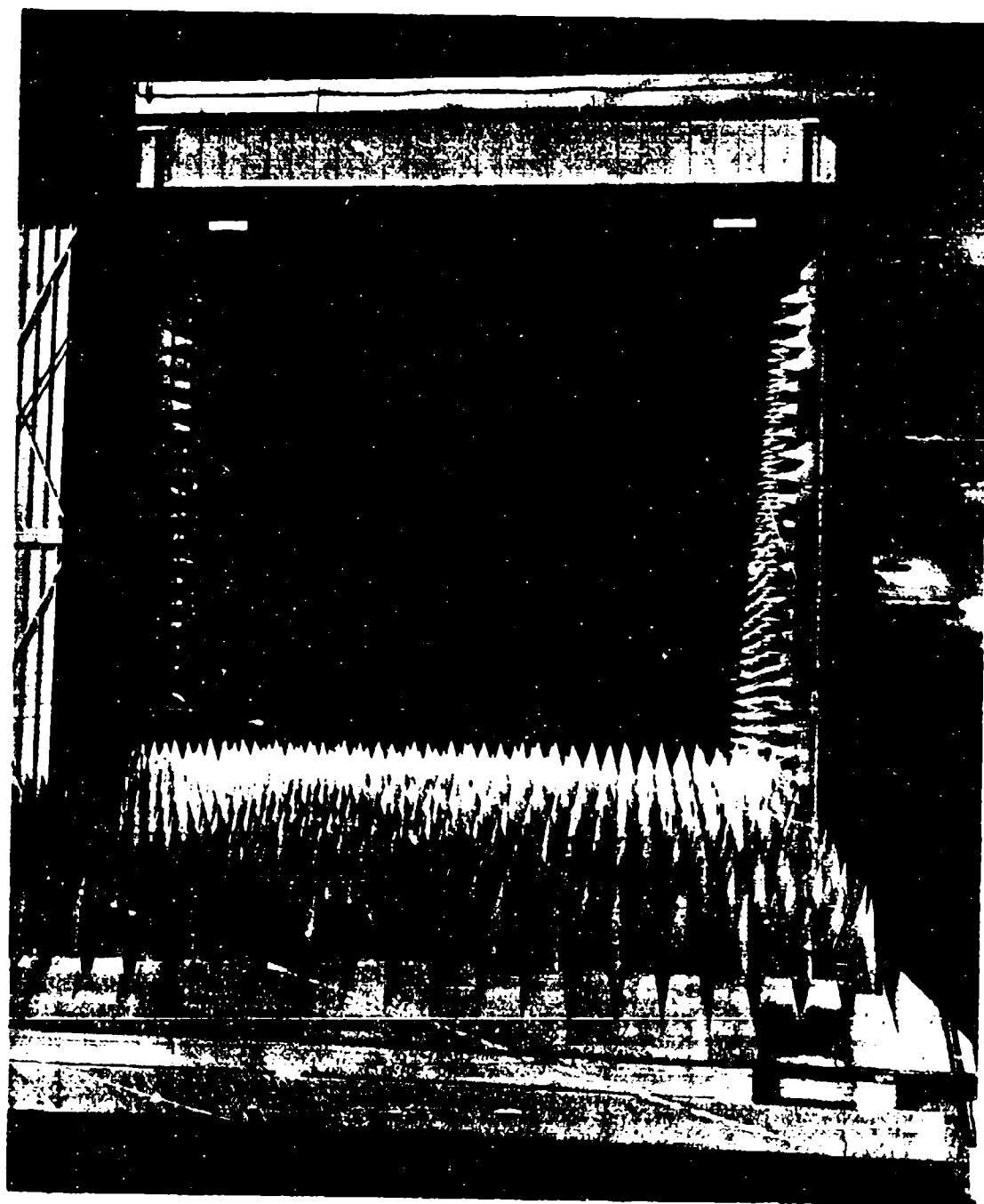


Fig. 1. Microwave Anechoic Chamber.

At present the back-scatter range is fully equipped for both bi-static and mono-static measurements at X-band. Two sources of stable signals are being used. One is a LFE ultra-stable signal generator. The other is a X-13 klystron using the Dymec oscillator-synchronizer. Data is obtained in two ways. A Scientific Atlanta 60 db dynamic range receiver feeds a recorder for a visual presentation. In addition, the returned signal fed through the receiver to a digital voltmeter and then to a punched tape presentation for a permanent record. This punched tape data may then be converted to cards in the Martin-Denver computer facility.

Tests are being run to determine errors involved in various methods of model suspension and rotation. Foam columns, concentric columns and nylon string suspension are being evaluated.

Scale models of proposed re-entry vehicles have been measured to determine the effect of configuration on the radar back-scattering pattern. The re-entry vehicle models have been varied by changing cone half-angles and base configurations. Tests will continue on the effect of shaping and will include the effect of using various absorber materials for reducing the returned signals.

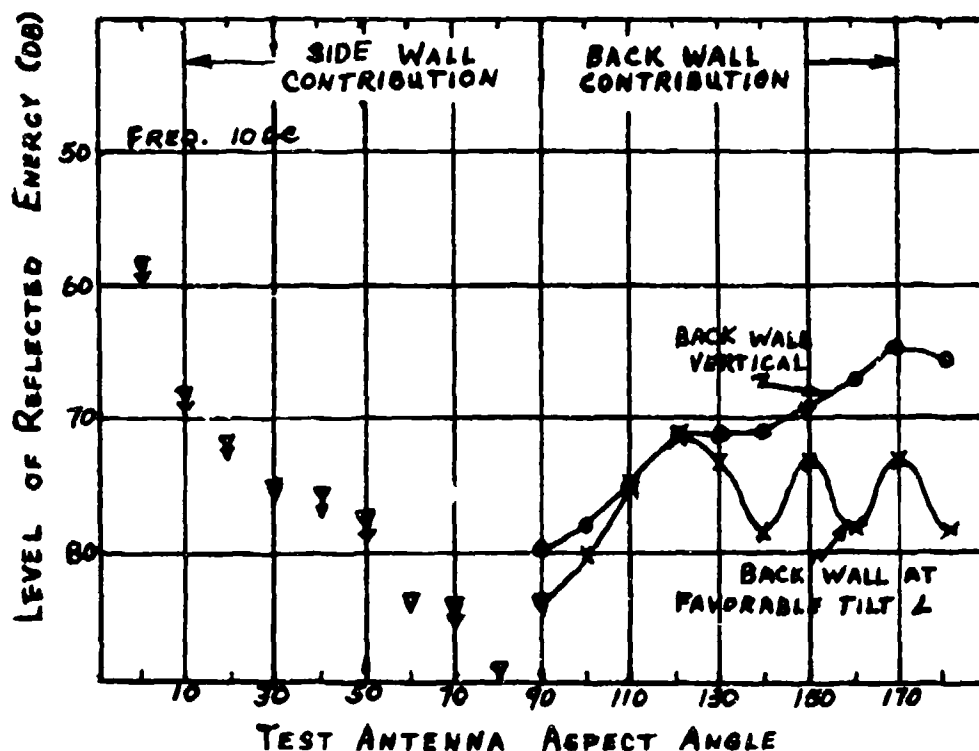


Fig. 2. Level of Reflected Energy vs Aspect Angle

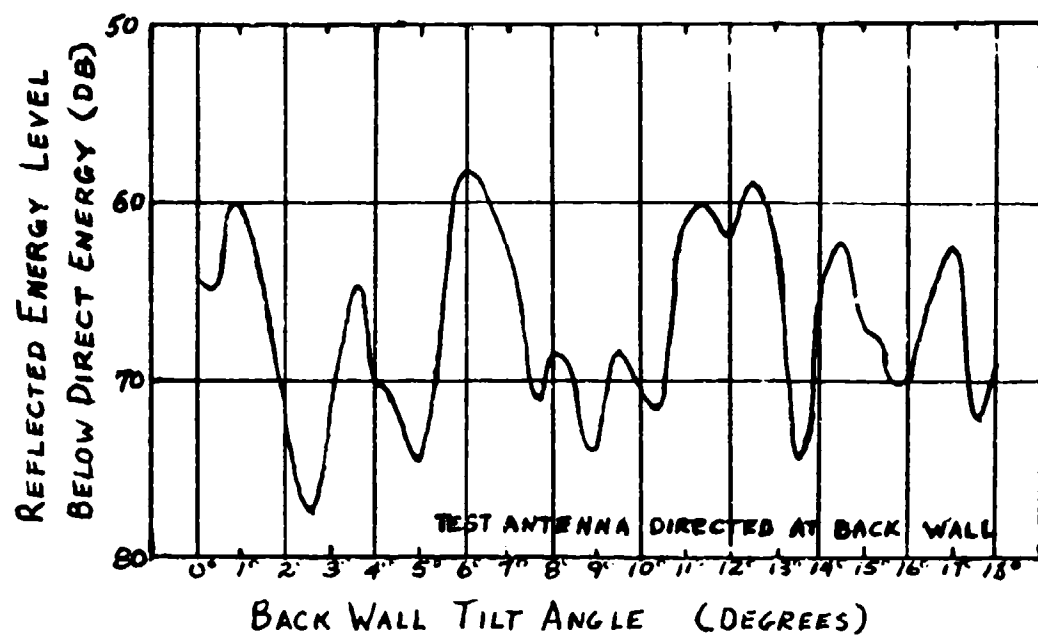


Fig. 3. Reflected Energy Level vs Backwall Tilt

AN ANECHOIC CHAMBER FOR MEASUREMENT OF BACKSCATTER AMPLITUDE AND PHASE AT MULTIPLE POLARIZATIONS

R. W. Roop and S. M. Sherman
Missile and Surface Radar Division
Radio Corporation of America
Moorestown, New Jersey

INTRODUCTION

In making target backscatter measurements, it is sufficient for many applications to measure only backscatter amplitude (or radar cross-section). For other applications the requirements are more sophisticated, and the complete scattering matrix (including amplitudes and phases) must be measured.

As part of a continuing study of the relation between radar signatures and the targets which produce them, the Radio Corporation of America is operating an anechoic chamber at X-band at its Moorestown, New Jersey plant. Models of radar targets are designed by scaling the body dimensions to the wavelength used and are mounted on a pedestal in the chamber. The target is illuminated alternately with orthogonally polarized waves by means of a 400 cps switch which directs the r.f. energy into one of two possible microwave channels.

By means of a synchronized set of switches in the receiving system, the amplitude and phase of two orthogonal polarizations can be measured and recorded during each period of transmission. As a result, the amplitude and phase of each possible combination of polarizations in the scattering matrix of the target can be obtained experimentally as a function of the aspect angle.

The phase measured is not merely of one polarization relative to another, but of each polarization relative to a fixed reference phase.

GEOMETRICAL ARRANGEMENTS

The interior dimensions of the RCA anechoic chamber are 10 ft by 10 ft by 36 ft. As shown in Figure 1, the target is mounted on top of a foam pedestal at a height of about $4\frac{1}{2}$ feet above the absorbing floor. The upper half of the foam pedestal is a cylinder $1\frac{1}{2}$ inches in diameter, with a V notch cut in the top surface, for holding the target. The lower half of the foam pedestal is conical, with a base diameter of 10 inches. The entire pedestal can be rotated about a vertical axis by a geared motor with an external indicator which shows the angular position of the pedestal. The angular position of the target on the pedestal is determined by observing a fiducial mark on the target with a theodolite located outside the chamber and pointing through a window. The accuracy of measurement of the angular position of a target 3 inches long is approximately $\pm 1^\circ$.

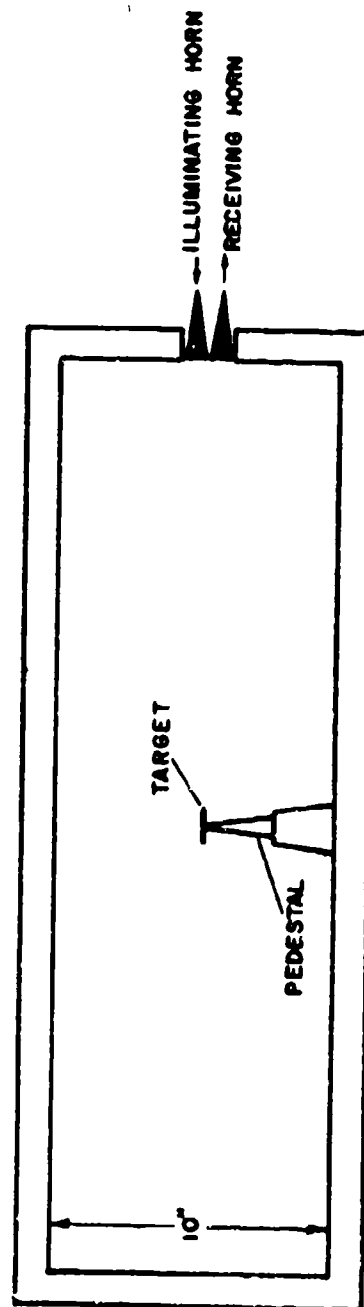
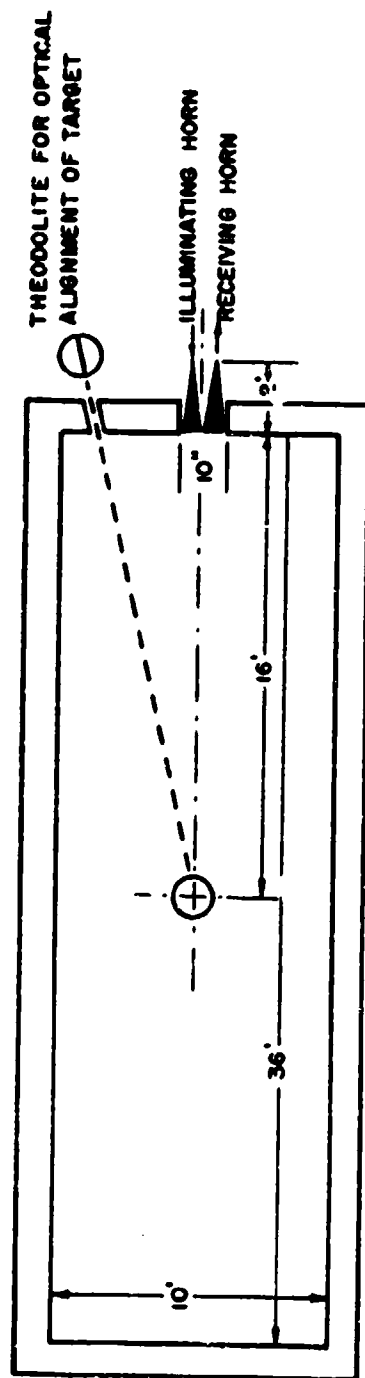


FIG. 1 GENERAL ARRANGEMENT OF RCA ANECHOIC CHAMBER

In one end of the chamber, two square horns are located at the same height as the target. The open end of each horn is 5 inches on a side, and the horn positions are offset both horizontally and vertically. The total bi-static angle between the centers of the two horns for a target on the pedestal is 2.1° . Each horn can be rotated about its longitudinal axis to produce an adjustable angular displacement of the sides of the horn away from the vertical. In normal operation, both the illuminating horn and the receiving horn are aligned with one side vertical. Under these circumstances, the illuminating field can be linearly polarized in either the vertical or the horizontal direction, and the receiving system analyzes the backscattered radiation into vertically and horizontally polarized linear components.

INSTRUMENTATION

A simplified block diagram of the instrumentation for the anechoic chamber is shown in Figure 2. The system operates at 9905 Mc. Diode switches in the r.f. feed are used to direct the illuminating energy first into a waveguide which radiates a horizontally polarized field, and then into a guide which radiates a vertically polarized field from the same horn. The switching rate between these two orthogonal polarizations is 400 cps.

A similar switching arrangement is used in the receiving waveguides, except that the diode switches in the receiving channel operate in quadrature with those in the illuminating channels. This timing is shown in Figure 3. During the first half of the H illumination period, the receiver is connected to the V receiver channel, and during the second half of the H illumination period, the receiver is connected to the H channel. Similarly, during the V illumination period, the receiver is connected first to the V channel, and then to the H channel. In this way, the r.f. signal at the first detector consists of a time shared sampling of four signals, i.e. HV, HH, VV, VH, where the first letter indicates the polarization of the illumination, and the second letter indicates the polarization of the receiver channel.

The local oscillator frequency is generated from the basic r.f. by mixing a 30 Mc oscillator with the X-band signal and using a narrow filter to reject all frequencies except the desired sideband 30 Mc above the illumination frequency. An IF phase reference signal at 30 Mc is generated by mixing the single side band signal with the original r.f.

In the IF stage, the received signal is divided into two channels. The amplitude channel passes through a log amplifier so that the detected IF will have a linear characteristic on a decibel scale. The phase channel is passed through a linear IF amplifier, then limited and passed to a specially designed phase detector. The detected output of the log amplifier and the output of the phase detector are decommutated by a synchronous switch, and passed to a conventional multi-channel oscillograph for low frequency amplification and recording. Four

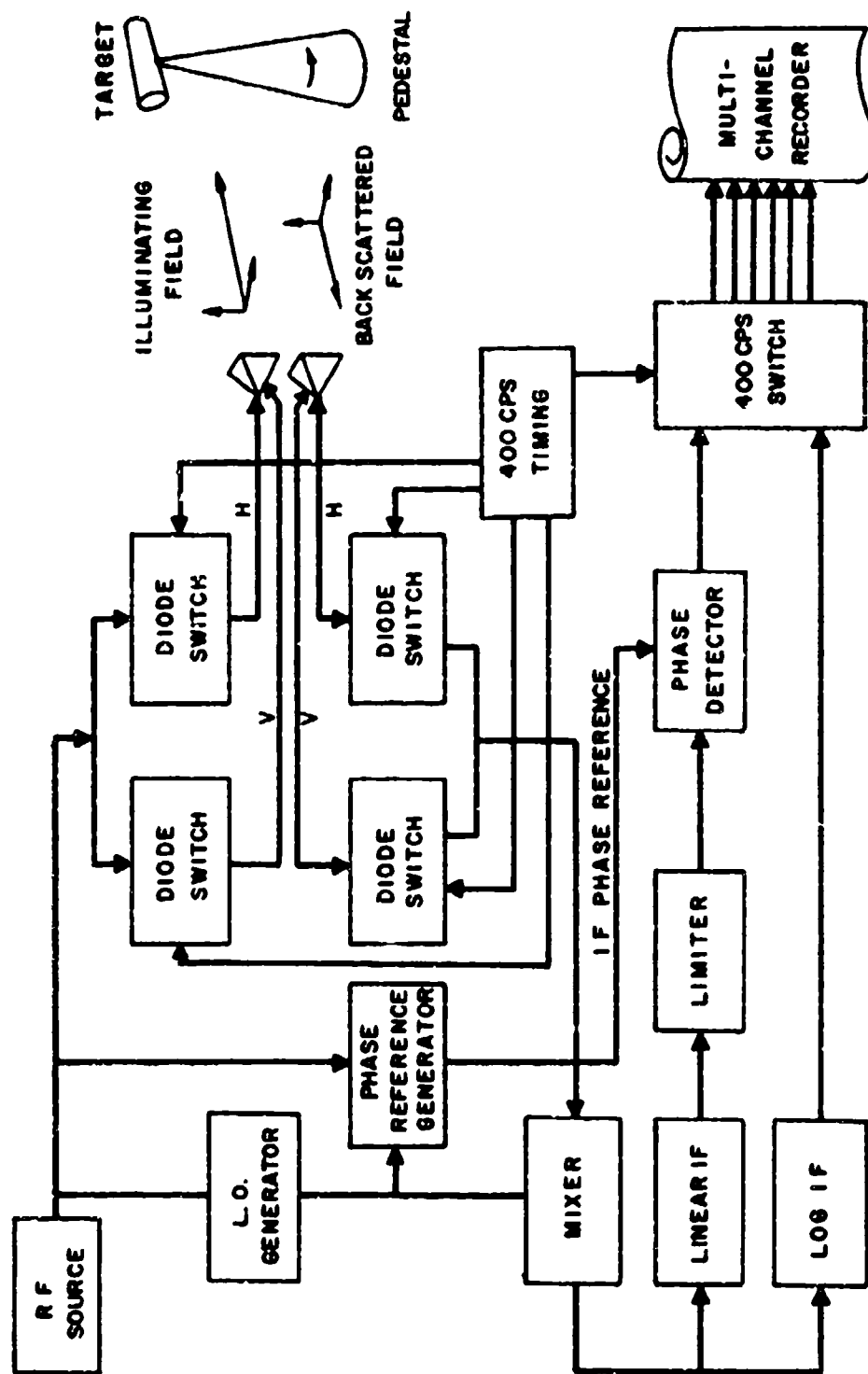


FIG. 2 GENERAL ARRANGEMENT OF RCA ANECHOIC CHAMBER INSTRUMENTATION

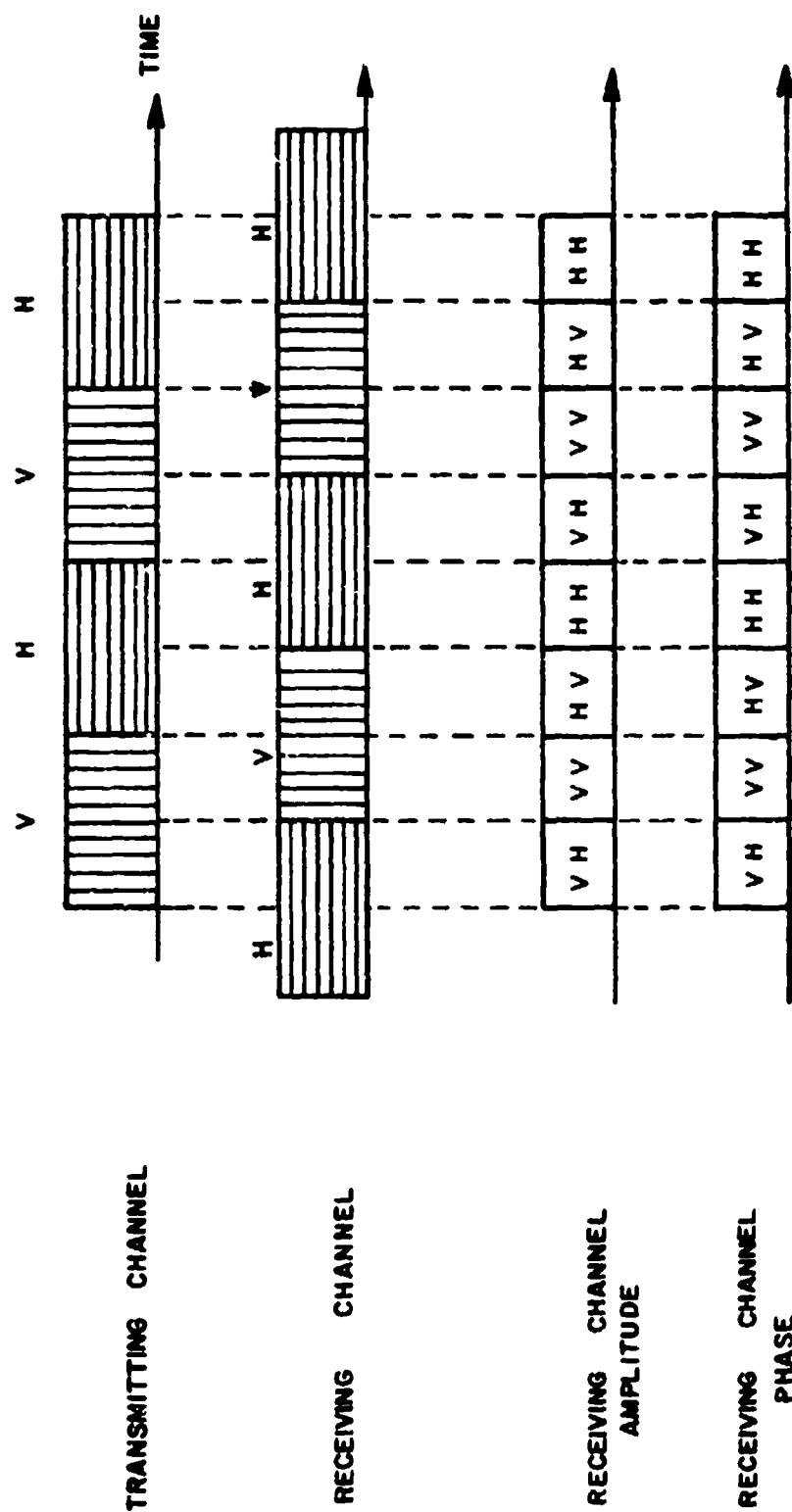


FIG. 3 TIMING DIAGRAM RCA ANECHOIC CHAMBER INSTRUMENTATION

phase signals are available, i.e. ϕ_{HH} , ϕ_{HV} , ϕ_{VH} , ϕ_{VV} , together with the four amplitude signals, \mathcal{T}_{HH} , \mathcal{T}_{HV} , \mathcal{T}_{VH} , \mathcal{T}_{VV} . All the phase detector outputs make use of a single phase reference signal.

TYPICAL OPERATIONS

For the 1 Mc, 50 ohm IF input, thermal noise has a power level of -114 dbm. The operating level of the system is determined by adding the system losses and the desired dynamic range to this figure, as shown in the following table.

Thermal Noise Level	-114 dbm
Path loss for typical target (3 inch diameter sphere)	71 db
Wave guide losses	14 db
Allowance for converter noise figure	17 db
Dynamic range	40 db
Total	142 db = level of transmitter above noise

The absolute level of the r.f. source is +28 dbm.

In normal operation, the stationary return from the empty chamber occurs at a level about 95 db below the source level. This return is cancelled by adjustment of the phase and attenuation of neutralizing channels which feed signals from the illumination channel into selected points in the r.f. receiver channels. Typically, adjustment of the first neutralization channel (between the throats of the horns) can reduce the stationary return from the room to a level about 120 db below the level of the r.f. source. Further adjustments of other neutralization paths, coupled to the receiver channel near the detector, are used to reduce residual spurious signals at the detector to a level only a few db above the thermal noise level at the detector. The actual dynamic range available on a particular run depends on the size of the target and the care with which neutralization is carried out.

Using the system described, it is possible to achieve measurement accuracies of ± 0.5 db in cross section and $\pm 3^\circ$ in phase for each of the elements in the scattering matrix. The absolute accuracy of the alignment of the target relative to the pedestal is better than 2 mils, and the relative accuracy of the measurement of the aspect angle of the target is $\pm 0.1^\circ$.

The performance characteristics of the RCA anechoic chamber are summarized in Table I.

TABLE I
SUMMARY OF ANECHOIC
CHAMBER CHARACTERISTICS

Dimensions	Approx. 36'L, 10'W, 10'H
Frequency (cw)	9.905 gc
Transmitter output power	+28 dbm
Level of spurious room reflections	95 db below radiated level
Neutralization of spurious signal	125 db or more
Polarizations	Transmit H and V or 45° and 135° Receive H and V
(Circular polarizations available with minor modification)	
Cross-polarization isolation	30 db
Amplitude calibration accuracy	± 0.5 db
Amplitude stability	± 0.5 db/hour
Phase measurement accuracy	$\pm 3^\circ$
Recorder	6-channel Sanborn transistorized
Pedestal	Scientific-Atlanta, remote control
0.1° readout on remote indicator	
2.5° electrical pulse output to recorder from photoelectric system.	
Pedestal table turned in place to give max. accuracy of center of rotation.	
Method of target alignment	Theodolite

THE SCALE GROUND PLANE RANGE

R. A. Ross, Associate Engineer
Cornell Aeronautical Laboratory, Inc.

ABSTRACT

This paper reports on a simulation of the full-scale ground plane range (Rat Scat) being built at White Sands Proving Grounds. Prove-in measurements obtained on the simulation range agree with the theory upon which the concept of a ground plane range is based. The effects of environmental variations on the performance of the Rat Scat range constituted one of the studies investigated using the scale range. Some results are presented in this paper.

INTRODUCTION

Quantitative descriptions of the cross sections of relevant operational targets are essential to the radar system designer, and these descriptions must be derived from experimental measurements. A radar cross-section range is normally used as a computer to estimate the cross-section values that would occur in free space.

The radar cross section may be obtained on a full-scale range, in which case the actual target is studied at the frequency of interest. Measurement difficulties attendant upon the physical size of a full-scale range include environmental effects, associated with outdoor operation, and the presence of undesired fields at the target area due to spurious ground reflections. These two factors are controlled by employing a scale facility, providing, of course, that all of the scaling requirements can be satisfied.

In certain instances full-scale measurements are necessary. (This situation arises when the scaling requirements cannot be met or when acceptance measurements are desired.) In order that random reflections from the intervening ground not preclude accurate measurements, it has been suggested that the ground plane concept be applied.¹ The Cornell Aeronautical Laboratory, as a part of its investigation of Rat Scat design possibilities on subcontract P. O. 902568-X to General Dynamics, has constructed a scale-model ground plane range. A description of the scale ground plane range, along with some of the experimental results, is the subject of this paper.

BACKGROUND MATERIAL

A short discussion of the ground plane concept, followed by treatment of the scaling requirements, is presented next.

The Ground Plane Concept

The ground plane range, used successfully for antenna pattern measurements, has been proposed as a technique for radar cross-section measurement. In such a ground plane range the ground is made flat and smooth with respect to λ , the operating wavelength. The antenna and scatterer are located in that region of space where the direct ray and the reflected ray produce reinforcement (Figure 1).

In Figure 1, the height of the radar antenna A above the ground plane is h_a , the height of the target T is h_t . Both h_a and h_t are several wavelengths or more, and r_d , the separation between A and T , is so large that the field at the target falls off as $1/r_d$. The image of the antenna A is at A' , a distance h_a below the reflecting ground plane. The length of the ray from A' to the target T is r . Reflection of the energy transmitted at A occurs at the ground plane position O at the grazing angle ψ . The coefficient of reflection is \mathcal{R} , and the phase shift at reflection is ψ . The electric field strength due to the combined direct and reflected waves at the target may be written

$$\begin{aligned} E &= \frac{E_i}{r_d} e^{j(\omega t + kr_d)} + \frac{\mathcal{R} E_i}{r} e^{j(\omega t + kr + \psi)} \\ &= E_i e^{j(\omega t + kr_d)} \left[\frac{1}{r_d} + \frac{\mathcal{R}}{r} e^{j(kr - kr_d + \psi)} \right] \end{aligned} \quad (1)$$

where the difference $(r - r_d)$ is important in the exponent and $r_d \sim r$ is valid in the denominator. Substituting $\delta = (2\pi/\lambda)(r - r_d)$, we have

$$E = \left[1 + \mathcal{R} e^{j(\psi + \delta)} \right] \frac{E_i}{r} e^{j(\omega t + kr)} \quad (2)$$

Range geometry is chosen so that the target T is located in the maximum of the first lobe. The amplitude pattern implied in equation (2) is of the form

$$\sqrt{1 + \mathcal{R}^2 + 2\mathcal{R} \cos(\psi + \delta)} \quad (3)$$

The polarization dependence of fields above the ground plane is evident in the expression of the reflection coefficient in terms of the ground constants. For horizontal polarization of the transmitting antenna A (E field parallel to the ground plane) we have

$$\mathcal{R}_H e^{j\psi_H} = \frac{\sin \psi - \sqrt{(k/k_0)^2 - \cos^2 \psi}}{\sin \psi + \sqrt{(k/k_0)^2 - \cos^2 \psi}} \quad (4)$$

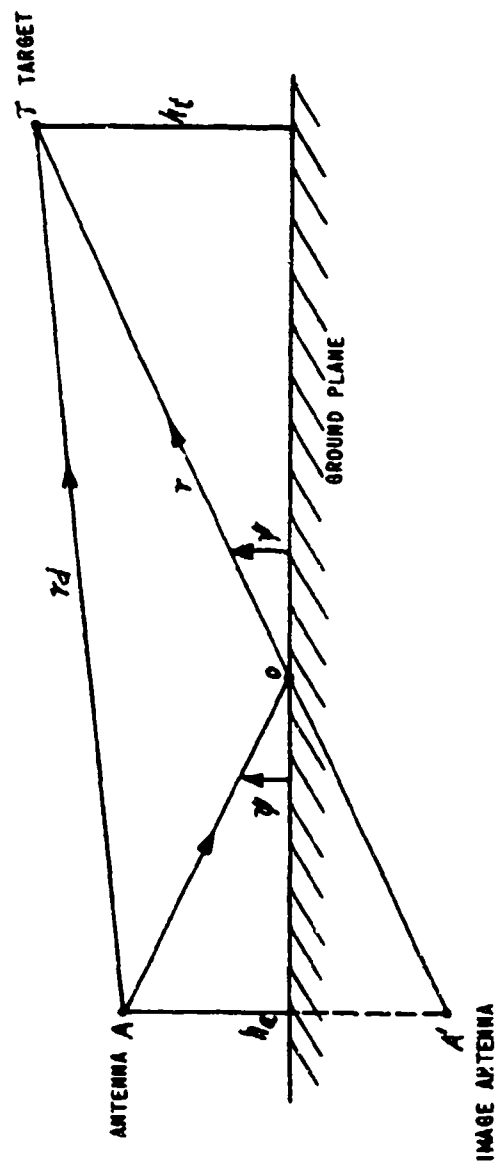


Figure 1 GROUND PLANE INTERACTION

Similarly, for vertical polarization we have

$$R_v e^{j\psi} = \frac{(k_i/k_o)^2 \sin \psi - \sqrt{(k_i/k_o)^2 - \cos^2 \psi}}{(k_i/k_o)^2 \sin \psi + \sqrt{(k_i/k_o)^2 - \cos^2 \psi}} \quad (5)$$

where ψ is the grazing angle and $(k_i/k_o)^2$ is the complex dielectric constant of the ground. In the following analysis it will be convenient to use the notation

$$\begin{aligned} \Gamma_H e^{j\rho} &= [1 + R_H e^{j(\psi_H + \delta)}] \\ \Gamma_V e^{j\rho} &= [1 + R_V e^{j(\psi_V + \delta)}] \end{aligned} \quad (6)$$

In the ideal case $\Gamma e^{j\rho}$ would be independent of polarization and real with magnitude 2. In actual practice Γ approximates the value 2, ρ is some small angle, and the polarization dependence must be retained.

The fundamental requirement for the measurement of cross section is that the phase and amplitude structure of the field encompassing the target approach the uniformity associated with the long range at which an operational target would be observed. While this requirement applies to ranges in general, the ground plane range introduces additional constraints. A ground plane range will be called well behaved if it satisfies the following conditions:

(i) Vertical Coverage Diagram Overlap

There must exist a common volume (the target location) of overlap at the first-lobe maximums for both vertical- and horizontal-polarization field patterns. It is the field in this common volume that should satisfy the uniformity requirement. The resultant amplitude and phase of the field for horizontal polarization need not be equal to those for vertical polarization. (In practice, the horizontal-polarization field strength at the first-lobe maximum is greater than the vertical-polarization field strength.) The overlap condition must be satisfied if cross-section measurements employing polarizations other than the principal polarizations are anticipated.

(ii) Constancy of Ground Parameters

The electrical properties of the ground are influenced by weather and seasonal growth. The physical configuration of the ground plane is subject to winds, etc. It is necessary that ground parameters which affect the range field pattern remain essentially constant over the time interval between range calibrations.

Scaling Requirements

The following two equations relate the dimensions and cross sections of the full-scale range and the scale range.

$$D_M / \lambda_M = D_o / \lambda_o \quad (7)$$

$$\sigma_M / \lambda_M^2 = \sigma_o / \lambda_o^2 \quad (8)$$

where D_o is any dimension of the full-scale range
 D_M is the corresponding dimension of the scale range
 σ_o is the full-scale cross section
 σ_M is the scale-range cross section
 λ_o is the full-scale wavelength
 λ_M is the scale-range wavelength

If the ground plane at the White Sands site were of such high conductivity that there were negligible losses due to surface currents, it would be necessary only that the scale ground plane should have similarly high conductivity. Because the full-scale ground plane has neither extremely high conductivity nor unity permittivity, scaling is exact only if:

(a) The finite conductivity of the full-scale range soil is reproduced in the scale range with a material having this conductivity multiplied by the ratio λ_o / λ_M .

(b) The permittivity or permeability of the full-scale range soil is reproduced in the scale range with material having equivalent electrical properties at the test frequency.

While it proved feasible to implement a scale range which provided valid data when applied to the Rat Scat range, an exact simulation was not possible because the required electrical properties of the Rat Scat soil (at 200 Mc) were not available.

THE SCALE GROUND PLANE RANGE

Description of the Scale Ground Plane Range

In order to provide experimental verification of theoretical results, and to provide data that are best obtained by direct measurement, a scale ground plane range was implemented to simulate the Rat Scat low-frequency complex.² The range uses the CAL K_a CW radar (35 Gc) and was designed to represent operations at 200 Mc.

Although the scale ground plane range must be finite in extent, it was possible to scale a 1400 ft x 700 ft area of the Rat Scat low-frequency range using a 8 ft x 4 ft area in the scale model range. Subsequent experimental

results have verified that the restriction in dimensions should not play a serious role in ground plane performance, since the ground plane area is much greater than a Fresnel zone.

Actual ground plane material was extremely fine-grain bonding sand, held in a 8 x 4 x 1/2 ft. waterproof container lined with radar absorber. Although it is not known whether a complete electrical match was obtained between Rat Scat soil and the sand (200 Mc data on Rat Scat soil was not available), excellent agreement in field strengths was obtained between full-scale and scale-model measurements.

Normal operation involved the scale ground plane range in the smooth sand condition with the target (a 1-inch-square flat plate) placed 34 inches from the antennas (full-scale separation is 500 ft.). Rectangular transmitting and receiving horns, approximately 1 inch square, scale to 15 foot horns, about the size of the Rat Scat low-frequency dishes. These linear-polarization horns were employed to obtain cross sections having the following transmitting-receiving antenna polarization combinations: vertical-vertical, horizontal-horizontal, $\pi/4 - \pi/4$ and vertical-horizontal. A variable-tilt turntable was provided to allow target rotation about an axis perpendicular to the first lobe of the ground plane field pattern. Sand was dammed away from this turntable by means of a plaster of paris cylinder placed flush with the sand surface and extending through the bottom of the table.

A program was carried out to provide field-strength data above the scale ground plane range. A sphere was used to probe field magnitude across the target area in azimuth and elevation; the phase of the field was not obtained. (This technique is identical to that employed on the full-scale Rat Scat range.) Figure 2 illustrates field-strength measurement data in elevation at the control-pit azimuth angle, using dry sand. The magnitudes of the first lobe peaks match to within 1 db for the two principal polarizations, the horizontal polarization peak being larger as expected. Field distributions predicted by theory are observed at the surface of the ground plane; for vertical polarization the surface wave contribution lies about 20 db below the first lobe maximum. The elevation of the first lobe maximum corresponds to a full-scale height of 33 ft. at 200 Mc.

Figure 3 provides gross characteristics of the field above the ground plane, again using dry sand. While contours of constant field strength vary irregularly in the second lobe above the ground plane, the first lobe characteristics are regular for both vertical and horizontal polarizations. An anomaly common to the field-strength patterns for both polarizations is a deep null, symmetrically distributed in azimuth off to the sides of the target area, at the same elevation as the upper null of the first lobe directly above the target location.

Reference measurements on the scale ground plane range were based upon flat plate cross section. Free-space (anechoic chamber) measurements of a reference 1-inch-square flat-plate were compared to ground-plane-range measurements for the principal

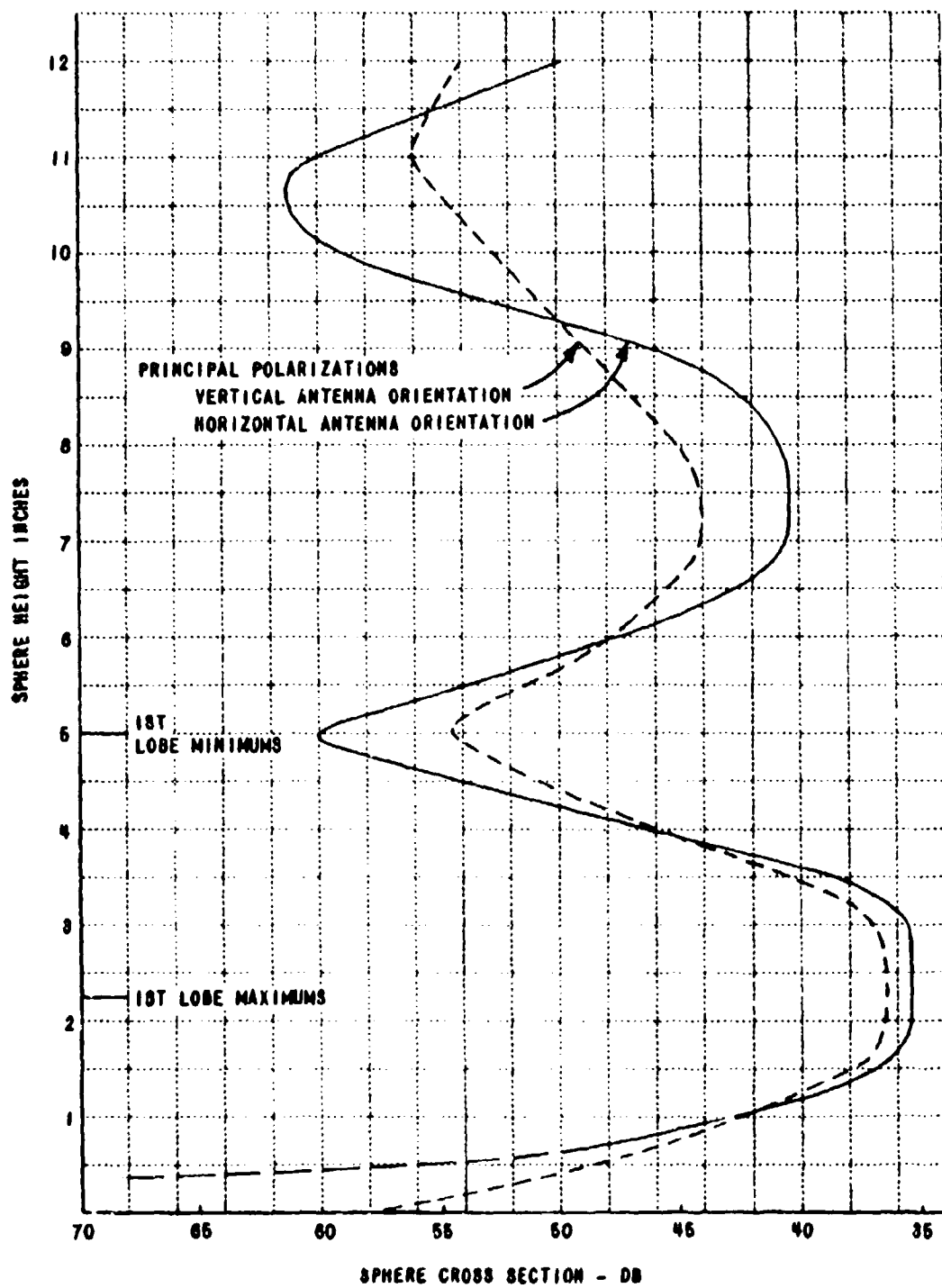


Figure 2 FIELD STRENGTH MEASUREMENTS ABOVE TARGET CONTROL PIT

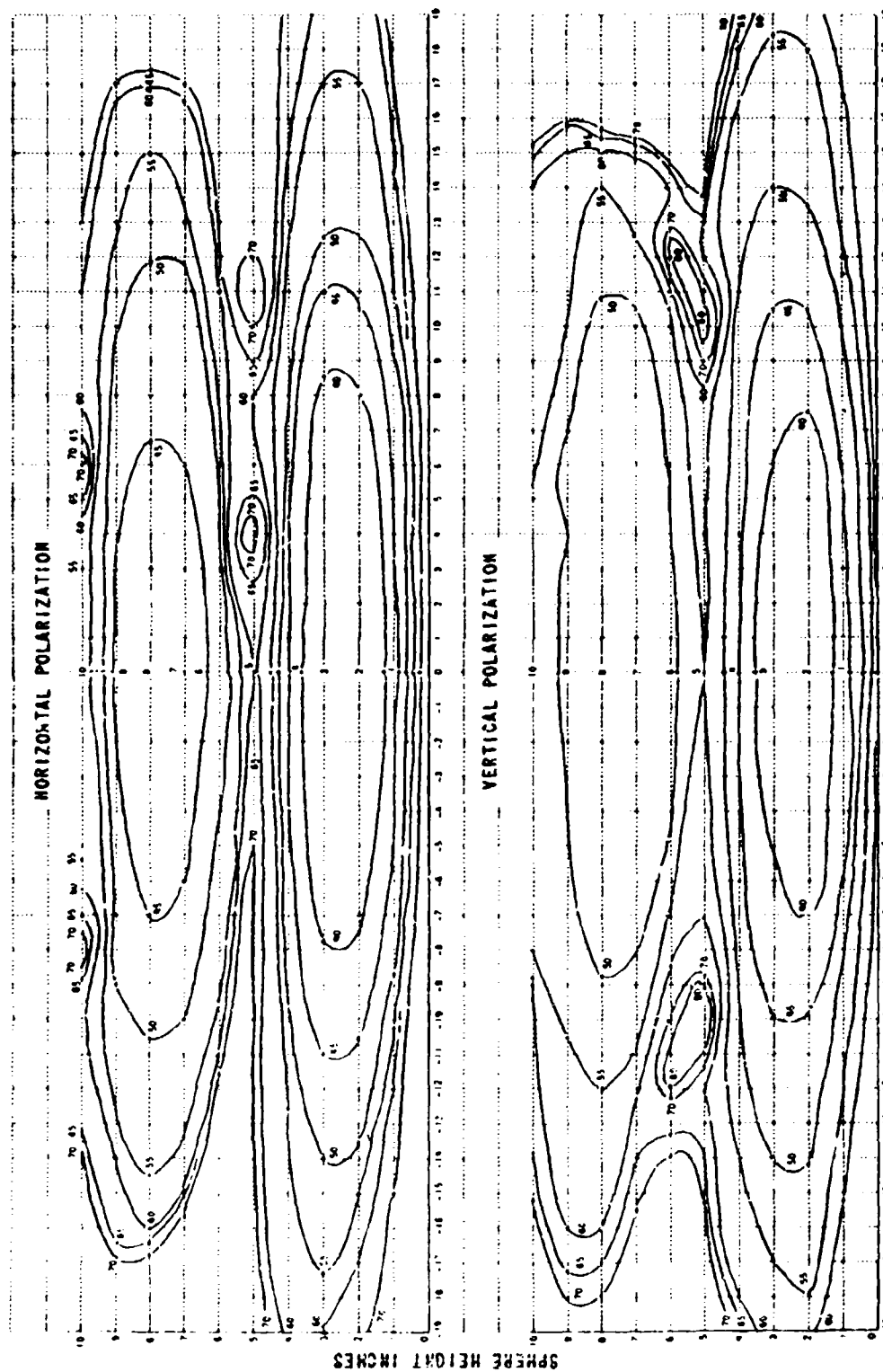


Figure 3 DISTANCE FROM TARGET AREA ACROSS THE GROUND PLANE (INCHES)
FIELD STRENGTH MEASUREMENTS ABOVE THE GROUND PLANE

polarization antenna combinations. (It should be noted that the tilt of the resultant ground plane field requires a target rotation axis slightly inclined towards the antenna position. The proper rotation-axis inclination for the scale ground plane range was about 2 degrees.) Results for vertical and horizontal polarization are shown in Figures 4 and 5, for dry sand. Agreement is excellent. Differences between free space and ground plane cross sections, existing only at the lower cross-section levels, are considered acceptable.

Comparison of measurements indicated that the power returned from a spherical target in the scale ground plane range was only 9 db greater than a free space range, using the same antennas, instead of the 12 db predicted for ideal conditions. The loss in array gain for vertical polarization was directly attributable to a less-than-unity reflection coefficient; the minimum at the ground plane surface corresponded to a reflection coefficient of 0.68 and agreed with the observed 3 db decrease from the ideal case.

Circular Polarization Investigation

The standard configuration of the scale ground plane range has been outlined. A linear polarization configuration employed in preliminary studies involved large three-inch horns capable of circular-polarization operations. Same-sense and opposite-sense circular-polarization cross sections of a three-inch-diameter sphere were measured in those studies. The results stated below illustrate the polarization dependence of the ground plane.

The three-inch horns were aligned such that the antenna center line was 1-1/2 inches above the sand and parallel with the sand surface. Transmission of a right-sense circularly polarized wave produced a first lobe maximum 2-1/2 inches above the sand at a location 70 inches from the antennas. The resultant grazing angle was 3.5 degrees. The measurement program allowed evaluation of the polarization dependence of the scale ground plane for this grazing angle.

The ratio of same-sense to opposite-sense circular-polarization cross sections of a sphere, σ_s/σ_o (sphere), is theoretically zero. Free space (anechoic chamber) measurements on the three-inch diameter sphere gave σ_s/σ_o (sphere) = -32 db. This variance between theoretical and experimental values was largely due to the inability to achieve zero ellipticity in a practical antenna.

Corresponding measurements performed over the scale ground plane produced σ_s/σ_o (sphere) g.p. = -13.5 db. The 18.5 db variation in experimental results can be attributed to the polarization dependence of the ground plane.

$$\frac{\sigma_s}{\sigma_o}(\text{sphere})_{g.p.} = \frac{\left| \left[\frac{r_H e^{j\theta_H}}{r_H e^{-j\theta_H}} \right]^2 - \left[\frac{r_V e^{j\theta_V}}{r_V e^{-j\theta_V}} \right]^2 \right|}{\left| \left[\frac{r_H e^{j\theta_H}}{r_H e^{-j\theta_H}} \right]^2 + \left[\frac{r_V e^{j\theta_V}}{r_V e^{-j\theta_V}} \right]^2 \right|} \quad (9)$$

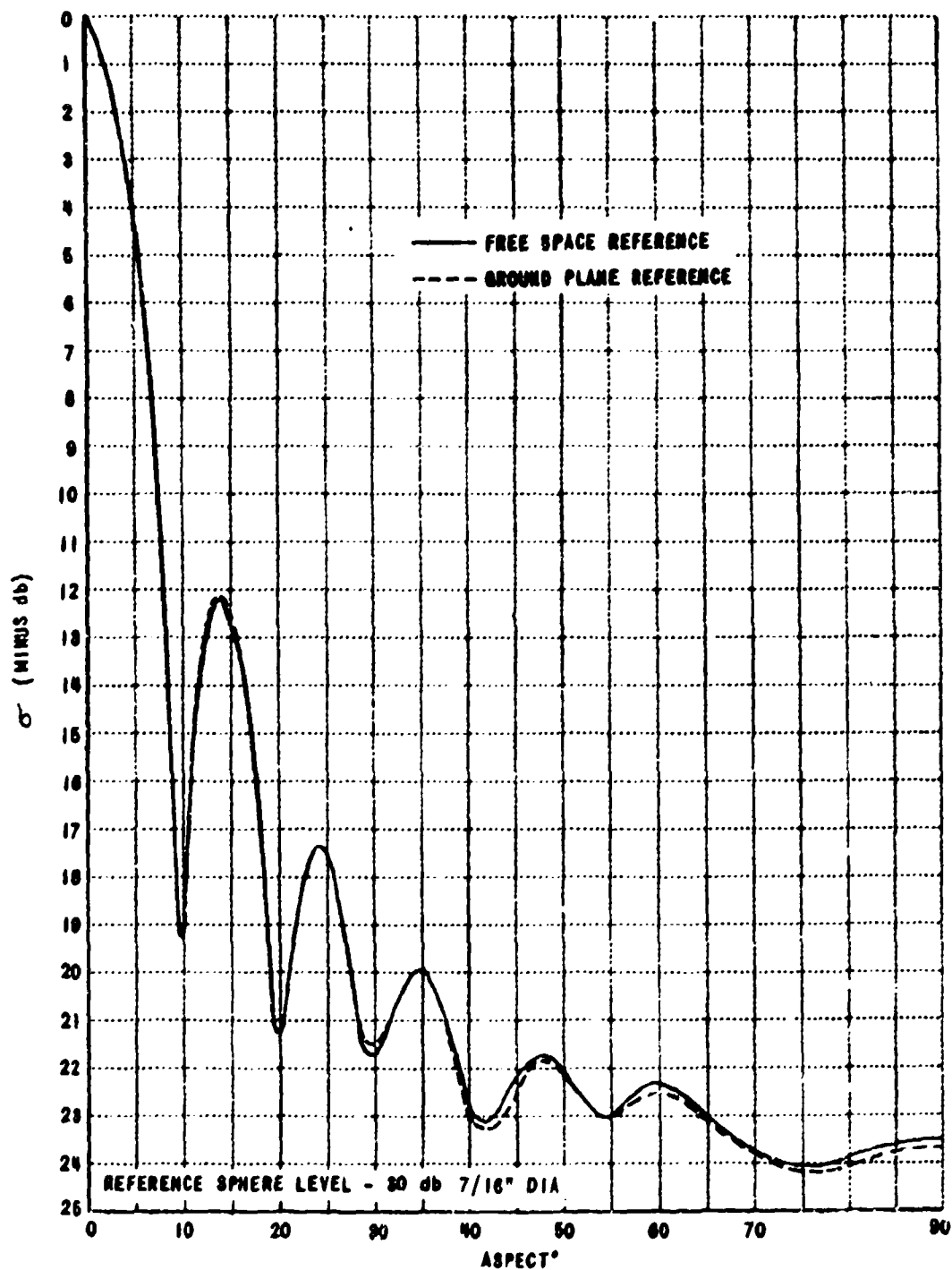


Figure 4 GROUND PLANE REFERENCE RUN, VERTICAL POLARIZATION

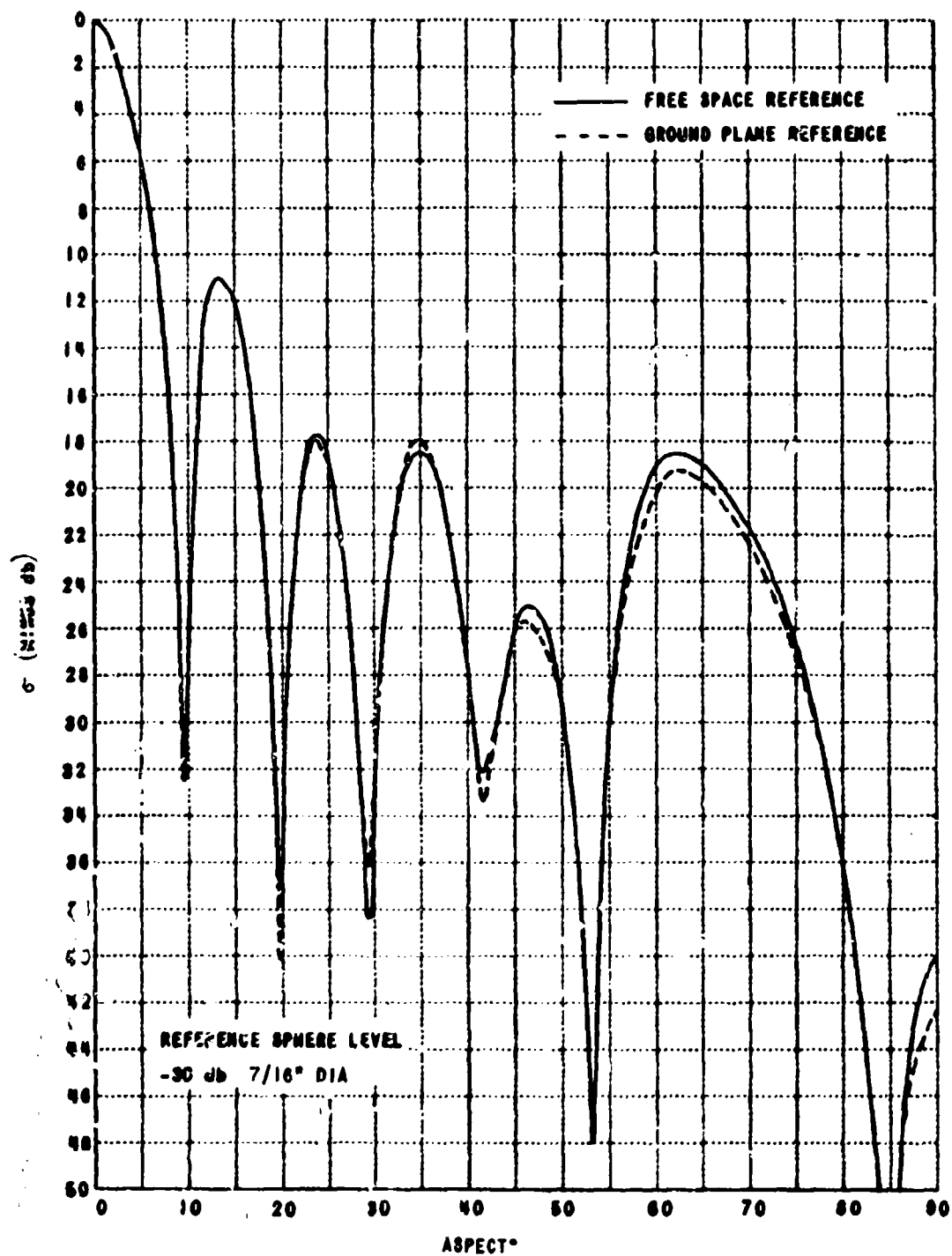


Figure 5 GROUND PLANE REFERENCE RUN, HORIZONTAL POLARIZATION

In the present analysis the righthand side is equated to -18.5 db. Additional linear-polarization cross-section measurements of the sphere were performed on the scale ground plane range. Principal polarization measurements provided the ratio σ_v/σ_h (sphere) g. p. -1 db or $\left[\rho_v/\rho_h\right]^2 = -1$ db. Substitution of this value in equation 9 gives $\rho_v - \rho_h = \pm 8$ degrees. Consideration of the reflection process shows that the minus sign is correct here and that ρ_v and ρ_h are opposite in sign. It is not possible to interpret the above results directly in terms of the primary reflection coefficients $R_h e^{j\phi_h}$ and $R_v e^{j\phi_v}$. However, results of previous measurements at linear polarization gave $R_v = 0.68$, hence $R_h = 0.8$.

Investigation of the Disturbed Ground Plane Range

Operation of the scale ground plane in an anechoic chamber assured measurements on the well-behaved ground plane range defined previously. The following measurement programs were directed toward evaluation of certain disturbances associated with full-scale ground plane range operation.

The Effects of Surface Irregularities

The smooth sand was deliberately disturbed to provide hills and valleys in the region of the first Fresnel zone (between the antenna and target locations). Principal polarization measurements on the reference flat plate were performed. Comparison of rough-sand and smooth-sand cross sections indicated the validity of the Rayleigh criterion for surface irregularities.

$$h_{irreg} < \lambda/16 \psi \quad (10)$$

where h_{irreg} is the allowable height irregularity of the surface.
 λ is the operating wavelength.
 ψ is the grazing angle (in radians).

Even larger irregularities may exist beyond the target location without disturbing measured cross sections.

Variable-Moisture Content Effects

Soil formations at the Rat Scat site result in a natural water basin. The presence of varying depths of water beneath the measurement site could complicate the basic ground plane concept, since the ground plane will exhibit the characteristics of a layered dielectric.

A layered dielectric was simulated on the scale ground plane range by placing a flat base of wet sand beneath a surface of dry sand. Seepage between the wet sand (16% water by weight) and the dry sand (a fraction of one percent) interface was not observed. Dry-sand surface thicknesses of 3, 2, 1 and 0 inches were examined. Using the 3-wavelength-square flat plate as a target for both vertical and horizontal polarizations, layered-dielectric effects became noticeable when the dry

surface thickness was reduced to one inch (corresponding to 15 feet in the full-scale range). Even for the all-wet-sand case, the measured cross sections are within 0.5 db of their free space counterparts.

The all-wet-sand configuration approximates an appreciably conducting ground plane. Investigation of the surface wave for vertical polarization involved raising a sphere through the field to provide a vertical coverage diagram. No increase over the small surface-wave component existing in the dry ground plane case was observed.

SUMMARY

This paper contains the description of a model ground plane range, along with certain prove-in measurements. A study of the effects of surface roughness indicates the validity of the Rayleigh criterion. Cross-section measurements were essentially independent of the moisture content of the scale range ground plane.

REFERENCES

1. Bachman, C. G., et al., "Techniques for Measurement of Reduced Radar Cross Sections," Aerospace Corporation Report No. TDR-930(2119)TN-1, October 1962.
2. Ross, R. A., "Investigation of Scattering Matrix Measurements and Suspension Target Supports," Cornell Aeronautical Laboratory Report No. UB-1806-P-1, January 1964.

U. S. NAVAL MISSILE CENTER
RADAR REFLECTIVITY MEASUREMENT
FACILITIES AND TECHNIQUES

John K. Rozendal
U. S. Naval Missile Center
Point Mugu, California

ABSTRACT

The radar reflectivity measurement facilities utilized at the U. S. Naval Missile Center include a microwave anechoic chamber, an optical simulation facility, and AN/FPS-16 instrumentation radars. A brief description of each of these facilities is included in the paper.

Techniques utilized in the anechoic chamber are presently continuous-wave measurement methods. Optical techniques are utilized in the optical simulation facility to obtain mean radar cross section data. Conventional radar techniques are utilized in the AN/FPS-16 radar installations which are instrumented to obtain radar cross section data.

INTRODUCTION

The radar reflectivity measurement facilities utilized at the U. S. Naval Missile Center (NMC) to determine experimentally the radar cross section characteristics of targets include a microwave anechoic chamber, an optical simulation facility, and AN/FPS-16 instrumentation radars.

MICROWAVE ANECHOIC CHAMBER

The NMC microwave anechoic chamber built by Emerson and Cuming, Inc. provides an electromagnetic environment which approximates that of free space. The outside dimensions of the chamber are 72 feet long, 26 feet wide and 18 feet high. The chamber surfaces are shaped and lined with microwave absorbent material (20 db on the side-walls, ceiling, and floor and 40 db on the end walls) to minimize internal reflections. Targets whose radar cross section is to be measured are mounted (8 feet above the floor) on a styrofoam column on top of an azimuth-over-elevation positioner located near one end of the chamber. An overhead crane located above the ceiling may be used for handling and supporting targets weighing up to 10 tons. Heavy targets are suspended from the crane by nylon ropes through a hole in the ceiling. The transmitting and receiving antennas are located at the opposite end of the chamber. The transmitter, receiver, recording equipment, and positioner control equipment are normally located outside the chamber.

Instrumentation systems for frequencies between 940 mc and 50,000 mc have been used in the chamber. The continuous-wave output of a frequency-stabilized microwave oscillator is connected through a directional coupler to the transmitting antenna which illuminates the target. Energy reflected from the target is received in the other antenna. The received energy and the output of the local oscillator in the Scientific-Atlanta (SA) model 402A receiver are mixed in the crystal mixer to produce the receiver intermediate frequency (IF). The local oscillator frequency is swept several megacycles at a frequency of 1000 cycles per second (cps) thereby producing an IF that is amplitude modulated at 1000 cps. The modulation is detected in the receiver and then amplified in the SA recorder. The pen drive system of the recorder is used to record relative, received signal strength with linear, square-root, or logarithmic (40 db dynamic range) response. The chart paper position is driven in synchronism with the positioner on which the target is mounted. Polar or rectangular recordings of received signal strength versus aspect angle may be recorded.

Because a two-antenna system is used, a signal due to "cross-talk" between the antennas is introduced into the receiver. Another signal due to reflections from the chamber surfaces is also introduced into the receiver. A variable phase shifter and variable attenuator between transmitting and receiving systems are used to eliminate these signals.

The measurement procedures are conventional for this type of reflectivity measurement system. The transmitting and receiving antennas are positioned for the polarization (vertical, horizontal, cross-polarized, or circular) and bistatic angle (0 degree to 18 degrees at the normal operating range of 57 feet) required for the measurements. The antennas used are determined by the size of the target whose radar cross section is to be measured. The beam-width of the antennas used is such that the variation in amplitude across the major dimension of the target is constant within ± 0.75 db. Since a two-antenna system is used, true monostatic measurements are not made. Measurements at bistatic angles less than 1 degree can be treated as monostatic measurements with negligible error for most targets.

Prior to mounting the target on the styrofoam column, the phase shifter and attenuator are adjusted to cancel the signal due to cross-talk and reflections from the chamber. The target is then mounted on the column and aspect angle is varied while the amplitude of the reflected energy is recorded as a function of aspect angle. The target is then removed and the received signal strength noted to ensure that the signals due to cross-talk and reflections remained cancelled during the recording. The target is then mounted at a different roll angle or pitch angle and the procedure is repeated.

After recording the patterns for a particular polarization and bistatic angle, the received signal strength from several standard reflectors (circular flat plates) is recorded in order to obtain a

calibration of received signal strength versus radar cross section. This calibration is used to determine the radar cross section of the target.

For complex targets, the recorded data are reduced to obtain median values of radar cross section within small angular intervals (usually 10 degrees). The data are reduced in this manner for two reasons:

1. The median values of radar cross section can be presented concisely.
2. When radar cross section measurements are conducted in the near zone, an error is introduced into the amplitude of the peaks and nulls. If data obtained by the near-zone measurements are reduced to median values, these values can be treated as far-zone median values with little error.

OPTICAL SIMULATION FACILITY

The NMC optical simulation facility is a room 40 feet long, 20 feet wide, and 12 feet high. The surfaces of the room (except the ceiling) are flat black to minimize internal reflections. Models of targets with mirror-like surfaces are mounted on an elevation-over-azimuth positioner located in the room. A light source, collecting system, recording equipment, and positioner control equipment are also located in the room.

The light source is a standard, white-light projection lamp with an adjustable filament voltage to provide different light intensities. The light beam is amplitude modulated at 540 cps by a mechanical chopper. The light is directed through a lens system (which partially collimates the beam) toward a flat mirror. The mirror is used as a means of effectively increasing the dimensions of the optical facility. A sheet of plate glass is placed at an angle of 45 degrees to the light beam reflected from the flat mirror. The plate glass serves as a beam splitter for monostatic measurements. For bistatic measurements, the beam splitter is not used. The light passing through the plate glass illuminates the model. The light reflected from the model is reflected from the plate glass and directed toward a parabolic mirror with a photomultiplier at the focal point. A mask in front of the photomultiplier determines the resolution angle (normally 4 degrees total) of the collecting system. A camera can replace the collecting system in order to photograph the sources of reflections from the model. The modulation on the light reflected from the model is detected by the photomultiplier and then amplified in the SA recorder. The pen drive system of the recorder is used to record relative, received signal strength with linear, square-root, or logarithmic (40 db dynamic range) response. The chart paper position is driven in synchronism with the positioner on which the target is mounted. Polar or rectangular recording of received signal strength versus aspect angle may be recorded.

Extraneous light is directed away from the model and the receiving system by flat-black baffles. Any stray light (reflection from the baffles, model positioner, and the beam splitter) that is detected by the photomultiplier is eliminated by sampling the source of light with a photo cell and adjusting the phase and amplitude of the signal from the photo cell to eliminate the signal due to stray light.

The measurement procedures are similar to those used in the microwave anechoic chamber. The light source and collecting system are positioned for the bistatic angle (0 to 90 degrees) required for the measurements. Prior to mounting the scale-model of the target (with a mirror-like surface) on the positioner, the azimuth positioner is set to the aspect angle to be used for the measurement. The phase shifter and attenuator are then adjusted to cancel the signal due to reflections from objects in the room. The target is mounted on the positioner and the aspect angle of the elevation positioner is varied while the amplitude of the reflected light is recorded as a function of aspect angle. The model target is then removed from the positioner and the received signal strength is noted to ensure that the signals due to stray reflections remained cancelled during the recording. The procedure is then repeated for a different azimuth positioner aspect angle.

After recording the patterns for a particular bistatic angle, the amplitude of the light reflected from several standard reflectors (sections of spheres with mirror-like surfaces) is recorded in order to obtain a calibration of amplitude of reflected light versus mean radar cross section (after scaling formulas have been applied to the standard reflectors). This calibration is used to determine the mean radar cross section of the target.

No reduction of the recorded data is required because the instrumentation system is designed to record mean radar cross section directly.

AN/FPS-16 INSTRUMENTATION RADARS

The C-band AN/FPS-16 radars at Point Mugu are used primarily to obtain accurate target position data (azimuth angle, elevation angle, and range) by automatically tracking targets during flight testing in the sea test ranges.

The instrumentation of these radars provides permanent records of azimuth angle, elevation angle, range, tracking error voltages (azimuth, elevation, and range), range-gated, automatic gain control (AGC) voltage, and range timing. Boresight towers are used to calibrate the angular tracking error voltages and to determine relative receiver response utilizing a variable-output, signal generator.

Measurement procedures are to track the desired target automatically while recording position information, AGC voltages, and range timing.

The relative, receiver-AGC-voltage response is then determined by locking-on the bore-sight tower and varying the output of the signal generator in discrete steps and recording the AGC voltage. A standard target (a sphere) can then be tracked to obtain AGC voltage for a target of known radar cross section at given ranges.

The recorded data are reduced to obtain radar cross section by using appropriate corrections for range differences and atmospheric absorption.

The radar cross section data obtained from the radars is used to spot-check data obtained by other techniques as qualitative verification of the validity of data obtained by the other techniques.

CONDUCTRON CORPORATION'S RADAR CROSS SECTION RANGE

A. W. Wren, Jr.
Conductron Corporation
Ann Arbor, Michigan

INTRODUCTION

The Conductron Corporation radar cross section range is located on sixty-two acres of flat farm land near Ann Arbor, Michigan. Although the facility was originally developed for the measurement of low cross-section full-scale vehicles, measurement activity now extends from the measurement of small models and decoys in an anechoic chamber to bi-static measurements of the Echo II passive satellite. In all cases, CW measurement systems are used. There are two separate and distinct measurement areas. Measurements are made on full-scale vehicles weighing up to twenty-five hundred pounds on an outdoor range facility. Small models are measured in the indoor anechoic chamber.

OUTDOOR SYSTEM

General Description

Describing the outdoor facility first, we have the frequency coverage as follows: In the UHF region, 200 mc through 600 mc in 50 mc increments; in the L-band region, 1300 and 1350 mc; in the S-band region, continuous tuning between 2.95 and 3.60 gc; in the C-band region, continuous tuning between 5.42 and 5.94 gc; and in the X-band region, continuous tuning between 8.5 and 10.0 gc. Average power on all of these systems is of the order of one watt. The microwave systems are used in conjunction with a Scientific-Atlanta Series 402 wide-range receiving system which operates between 30 mc and 100 gc.

The receiver output is fed into a Scientific-Atlanta Model APR 23 linear, logarithmic rectangular recorder. The overall dynamic range of the system is 40 db. The chart drive of the recorder operates in synchronization with an azimuth positioner capable of 360° azimuth rotation. Recording accuracy is ± 0.25 db in power and 0.05° in angle.

In addition to the above analog output, digital output is available on punched paper tape or cards. The digital output resolution is ± 0.25 db in amplitude with angular resolution of either 0.18° or 0.36° .

For the most part, parabolic reflector antennas are used. To date, measurements have been made using both a true monostatic system and a pseudo monostatic system. Bi-static measurements with a separation of as much as 20° are possible at this time. Antenna polarizations are linear and are arranged so that the electric vector can be oriented at any angle.

Target Support

In general, targets are supported on pellaspan foam or polystyrene columns. These columns are placed on the azimuth positioner and, with the target in place, are rotated 360° while the target return is measured. Present equipment allows the target to be as high as fourteen feet off the ground. Considerable effort has been expended in development of techniques for construction of symmetrical columns capable of supporting twenty-five-hundred-pound vehicles without interfering with the measurement of the vehicles. In general, we strive for and achieve columns with cross sections less than 10^{-5} square meters for use with these heavy vehicles.

Range Criteria

The sensitivity of the CW systems used at Conduction's range is such that complete freedom in selecting range is not possible. A "safe" criteria generally involves selecting a range greater than $2D^2/\lambda$ where D is the largest dimension of the target. Such a selection generally gives a phase flatness criteria that is unnecessarily stringent at some other aspect of the vehicle. It is fortunate that the regions, such as $\pm 45^\circ$ about nose-on for re-entry vehicles, where low signal levels occur present dimensions which allow a substantial reduction in range without a large sacrifice in phase criteria. Conversely, in those regions where the maximum dimension of the vehicle must be considered the return is at a level that permits the use of a greater range. For these reasons a composite range criteria is used in our measurements when 360° coverage is required. In many cases the nose-on region is the only region of interest. It is certainly true in most cases that a physical optics solution is accurate near broad-side aspect.

Field Probe

To determine the exact field distribution, a device constructed at Conduction is used. This device consists of a small cart which travels on small rails attached to a standard TV antenna tower. The cart is driven by remote control and is provided with synchro take-off which permits connection to the SA chart drive. In use, the tower is positioned at discrete increments on a line perpendicular to the direction of propagation and adjusted to lie in a vertical plane. Use of a small pick-up horn or dipole on the cart permits continuous plots of vertical field strength to be made.

System Background

With heavy vehicles or models, the background levels are limited by the column or target support contribution to approximately 10^{-5} square meters. With lighter models (weights less than five hundred pounds) the background levels can be improved. The degree of improvement depends on the model weight and shape. However, system sensitivity limits the achievable background to about 5×10^{-7} square meters.

As an aid in determining background problems Conduction uses a special "nose rock" cart which permits continuous linear motion of the target support and model over several wave lengths in the direction of propagation. This device permits a quantitative measure of the effect of background contributors other than the column.

Calibration

The primary standards used for calibration by Conduction are precision ball bearings. These spheres, which are available in diameters up to twelve inches at moderate prices, are very precise in tolerance on diameter and sphericity. In addition to spheres, flat plates are used in certain tests to eliminate ground and turntable coupling problems. Alignment of antennas is accomplished using the field probe discussed above.

Ground Handling Equipment

To facilitate the measurement of heavy models, special ground handling equipment has been developed by Conduction Corporation. This equipment permits fast, safe, efficient handling of heavy models. Standard run time with full-scale models (where a run consists of transporting the model to the measurement area, setting the model on the column, removal of ground handling equipment, measurement of the model over a 360° interval, and removal of the model from the test area) is five minutes or less.

INDOOR SYSTEM

Conduction's indoor facility is an anechoic chamber approximately twenty feet wide by thirty-eight feet long. The chamber utilizes VHP-18 absorber on the ceiling and walls. The floor utilizes a special vinyl-covered ferrite tile developed by Conduction. The chamber is used primarily at S, C, and X bands. A similar system is used on the indoor range as is used outdoors. The indoor facility again uses the Scientific-Atlanta Series 402 wide-range receiver and the background cancellation technique. The lowest background achieved to date is of the order of 10^{-8} square meters. This figure was obtained in the X-band frequency region with the target positioner at a distance of seven and a half feet from the transmitting antenna.

SPECIAL FEATURES

Although several aspects of Conduction's range mentioned above can be considered special features, the main aspect of our facility which we feel permits accurate and consistent measurements is our data quality control. Each vehicle measured is considered as a separate and distinct measurement problem. Through the use of experienced theoretical and experimental personnel, the vehicle is measured and the data is tested in several ways to determine the validity of the measurements. If theoretical considerations indicate an anomalous response, additional

measurements are made. Errors in measurements are always present. It is therefore necessary that one thoroughly understand the error sources and estimate the error magnitudes for the measurement data to be useful. Through the proper combination of theoretical and experimental talent, we attempt to obtain maximum utility and accuracy in cross section measurements.

SUMMARY OF RANGE CHARACTERISTICS

Freq. Band	Freq. Cov.	Polarization	Back-ground Level	Mono-static	Pseudo Mono-static	Bi-static	Target Weight
UHF	200 mc to 600 mc in 50 mc steps	Linear, 0^0 to 90^0 - 45^0 - 60^0	10^{-5} sqm.	Yes	No	Yes	Up to 2500 lbs.
L	1300 mc to 1350 mc	Linear, 0^0 to 90^0 cont.	$<10^{-5}$ sqm.	Yes	Yes	Yes	Up to 2500 lbs.
S	2.95 to 3.60 gc cont.	Linear, 0^0 to 90^0 cont.	$<10^{-5}$ sqm.	Yes	Yes	Yes	Up to 2500 lbs.
C	5.42 to 5.94 gc cont.	Linear, 0^0 to 90^0 cont.	$<10^{-5}$ sqm.	Yes	Yes	Yes	Up to 2500 lbs.
X	8.5 to 10.0 gc cont.	Linear, 0^0 to 90^0 cont.	$<10^{-5}$ sqm.	Yes	Yes	Yes	Up to 2500 lbs.
S	2.95 to 3.60 gc cont.	Linear, 0^0 to 90^0 cont.	$<10^{-7}$ sqm.	Yes	Yes	No	Up to 50 lbs.
C	5.42 to 5.94 gc cont.	Linear, 0^0 to 90^0 cont.	$<10^{-7}$ sqm.	Yes	Yes	No	Up to 50 lbs.
X	8.5 to 10.0 gc cont.	Linear, 0^0 to 90^0 cont.	$<10^{-7}$ sqm.	Yes	Yes	No	Up to 50 lbs.

Data output: Analog output 0^0 to 360^0 , accuracy ± 0.25 db in power, 0.05^0 in angle. Digital output on punched paper tape, ± 0.25 db in power, 0.15^0 or 0.36^0 in angle.

DESCRIPTION AND OPERATION CHARACTERISTICS OF A SHORT-PULSE,
OBLIQUE RADAR CROSS-SECTION RANGE

Malcolm Yaffe
General Electric Company
Missile and Space Division
Cabot, Cabot and Forbes Bldg. 1
Post Office Box 8661
Philadelphia 1, Pennsylvania

I Physical Design

A. The General Electric Company's Missile and Space Division has designed and built an outdoor radar cross-section measurements facility for taking monostatic (or quasi monostatic) radar cross-section patterns of full scale nose cones and space vehicles. The physical layout of this facility is shown schematically in Figures 1 and 2 and photographically in Figures 3 and 4. A block diagram of the electronics is shown in Figure 5.

B. As depicted in Figures 1 and 2, most substantial sources of reflection lie both out of the beamwidth of the antennas and out of range gate. The turntable, however, for most measurements is in the sidelobes of the antenna but is not outside the range gate. For this reason an absorbing baffle is used in front of it.

C. Since it may be required to support a 2000 pound target 50 feet above the ground, it is sometimes necessary to use a main support rope, between the 65-foot high towers of 2 1/8 inch nylon. A portion of this rope will be in both the range gate and the beamwidths. However, this rope is tilted at a large angle with respect to the wave fronts, so that direct reflections from the rope are negligible and only a slight amount of energy scattered from the forwardmost parts of the target can possibly be again scattered by the rope in the direction of the receiving antenna. The same is essentially true of the mylar tie down ropes which are nearly vertical while the beam direction is at about 11° with respect to the horizontal.

D. The model shown in the photographs weighs several hundred pounds and it is being held in a harness of 1/32 inch thick by 1 inch wide nylon strap sewn together with nylon thread. It has no noticeable effect on the radar cross-section for frequencies at C band and below. Use has also been made of a stocking which fits snugly about a model and is drawn together at the back with a device like a pajama string. Such a stocking, made of nylon no thicker than shirt material, was load tested at 2700 pounds.

E. The tie down cords are usually of pre-stretched mylar, which has almost no elasticity. They may be attached to the turntable, which consists of an azimuth - over - elevation mount, in one of several ways depending on the tradeoff between model characteristics and measurement requirements.

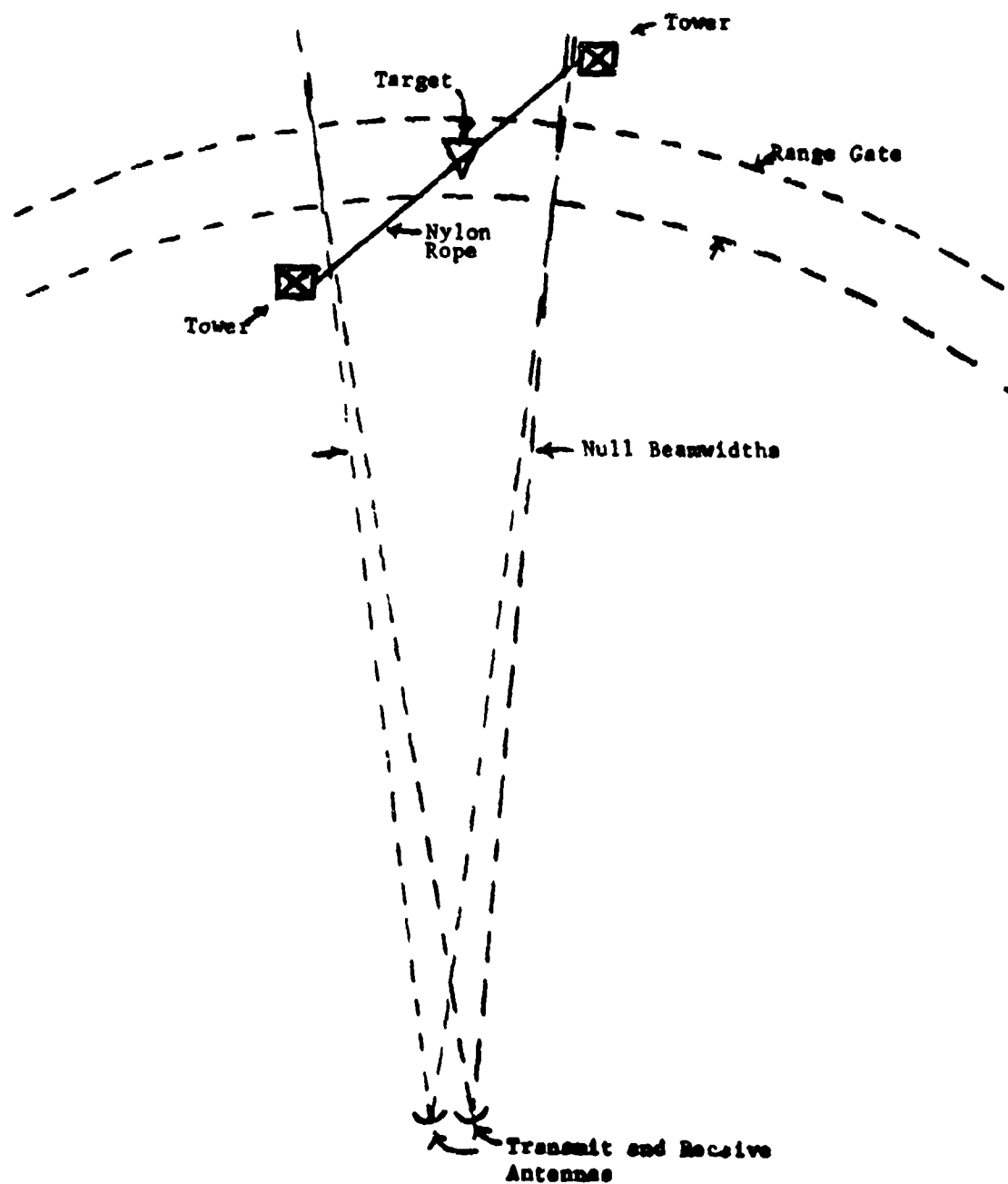


Figure 1. Plan View of Range Layout.

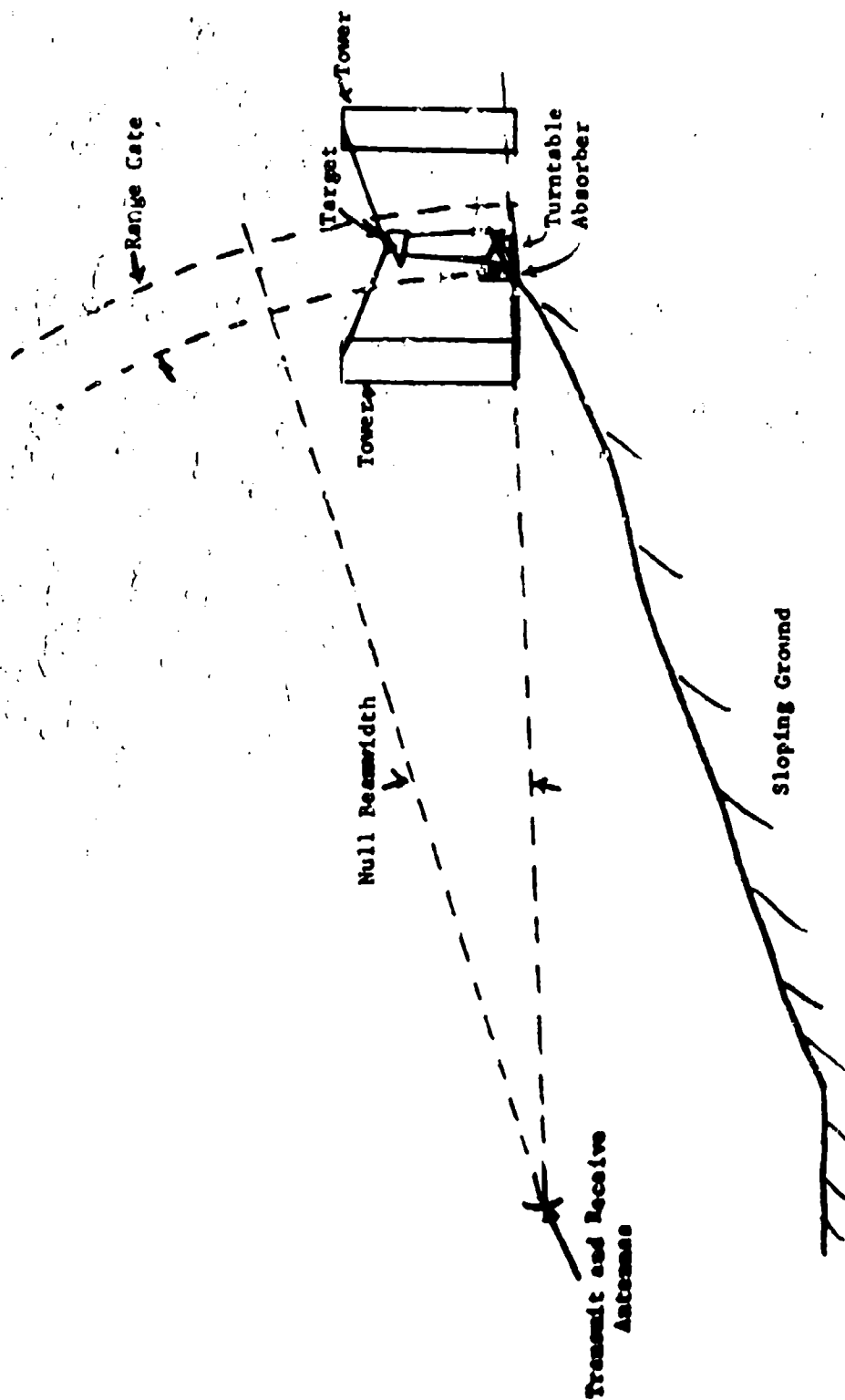


Figure 2. Elevation View of Range Layout.

F. The model characteristics include:

1. Weight
2. Shape. This characteristic is very important, as it involves harnessing requirements and wind effects as well as maximum bistatic scattering.
3. Strength. This determines how "hard" you can hold the model against wind forces etc.
4. Surface hardness. If the model has soft or breakable surface material, a nylon stocking may be required for harnessing.

G. The measurement requirements include:

1. Frequency. The facility has been in operation at $1350 \pm 5\%$ mc, $550 \pm 5\%$ mc, $425 \pm 5\%$ mc, and $5500 \pm 5\%$ mc. Equipment is now on hand for operation at $3000 \pm 5\%$ mc and 36 kmc (fixed frequency).
2. Polarization. Except at 550 mc and 425 mc where there is only one antenna, any linear polarization may be chosen for transmission or reception.
3. Angular accuracy. Angular accuracy can be held to better than $\pm 0.5^\circ$ (depending on the model characteristics vs. the wind velocity).
4. Plane of patterns. Patterns can be taken where any axis of the model remains in the plane of the direction of incidence and a horizontal line perpendicular to the direction of incidence (main plane patterns) by a suitable arrangement of the turntable, harness, and tie downs.
5. Minimum radar cross-section. The minimum radar cross-section that must be measured accurately determines the background level necessary.
6. Maximum radar cross-section.
7. The speed and cost. If speed and cost are unimportant, the other six measurement requirements can all be adjusted to the optimum values. However, any compromise in requirements 3, 4 or 5 can result in great savings in time and cost of measurement.

II Electrical Design

A. A block diagram of the electronic system for the Cross Section Range is shown in Figure 5. The basic timing for the range is set by a 2200 cycle per second tuning fork oscillator which synchronizes a narrow pulse generator. This generator provides both a +20 volt 50 nanosecond synchronizing pulse to trigger the transmitter modulator and a delayed pulse which is used to open the solid state gate. In this discussion the gate is said



Figure 3.

367

651365

to be open when energy is permitted to reach the recording system and closed when it is not.

B. The modulator produces two pulses to operate microwave triode oscillators mounted in re-entrant coaxial cavities. The first pulse is a large positive one with a very fast rise time (about 20 nanoseconds). It is used on the plate of the triode to start it oscillating. The second pulse, which has a variable delay with respect to the first pulse, is negative and also has a very steep leading edge. This pulse is applied to the grid of the triode and turns it off. Thus by varying the delay of the grid pulse with respect to the plate pulse, an R.F. output pulse from the triode can be obtained of any pulse width (measured at the base of the pulse) between 40 and 150 nanoseconds. At 36 mc a conventional narrow pulse magnetron and modulator are used.

C. With exception of UHF the transmitting and receiving antenna are two identical parabolic dishes for each frequency band. At UHF, because the required dish size is 19 feet, it is not feasible to use two dishes, and a hybrid junction separates the transmitted signal from the received signal. A theodolite located at the antenna site is used to set up the model rotation.

D. The signal from the receiving antenna (or hybrid output) is then fed into a calibrated R.F. attenuator designed for the appropriate frequency. At L-band and UHF fixed coaxial pads, variable couplers, "Arra pi lines," and cutoff attenuators are used. At S-band a rotating vane attenuator is used, and at C and K_A bands movable resistance card attenuators are used.

E. From the calibrated attenuator the signal goes into the traveling wave tube amplifier system (TWTA). This system takes one of two forms depending on the operating frequency. At L-band the system is a low noise TWT amplifier followed by an attenuator and a high power (about 4 watts peak power) TWT amplifier. At C-band the system is a low noise TWT amplifier and a C to L-band mixer feeding the high power L-band TWT amplifier. Figure 6 summarizes the low noise TWT system for each frequency band. At other frequencies a low noise TWTA will be used and mixers to L-band will be employed as at C-band. Traveling wave tube amplifiers are used in the receiving system for the following reasons:

1. Low noise figures, (6-11 db) are obtainable which are superior to conventional receivers.
2. The TWT can provide the large bandwidth necessary to amplify the narrow R.F. pulse without distortion so that the gate can be used after R.F. amplification. This is necessary because the switching pulse applied to the gate has harmonics at the R.F. frequency which would be appreciable if amplified through the entire receiving system.
3. The characteristics of a TWTA are such that the higher level signal which comes from the direct coupling between the antenna dishes will oversaturate it so that its output is even less than the input signal. Thus the 60 db of isolation provided by the gate is more than adequate even for the lowest discernible target return.



Figure 4.

6-13-60

4. The linear dynamic range which can be obtained in this application is much greater with conventional receivers.

F. From the high power TWTA the signal passes through a reversed directional coupler (i.e. one which samples the power being reflected back towards the TWTA's) and into an L-band solid state gate (that is, a crystal switch). Signals which are reflected from this gate when it is closed are sampled by means of the directional coupler and detected by an L-band crystal detector. The detected signal sample is fed into the vertical amplifier of a high speed oscilloscope (upper 1 db frequency limit of 40 megacycles with a sweep of 100 nanoseconds per centimeter). This oscilloscope provides a picture (amplitude vs. range) of all the signals which are being received which are not passing through the range gate (i.e. everything except the target when measurements are being made). It enables the range gate to be rapidly and accurately set on the target as well as showing all undesirable "background" at other than the target range which the range gate can be carefully set to avoid.

G. The solid state R.F. range gate is biased to be nominally closed. In the closed position it affords more than 60 db of isolation between the input and the output ports. When the delayed pulse from the pulse generator opens the gate for 50 nanoseconds the R.F. signal which is passing through the gate during that interval is attenuated by less than 2 db.

H. The output from the gate feeds into a bolometer detector which is used to drive a pattern recorder tuned to the 2200 cps pulse repetition rate. The pattern recorder may be operated with either a 4 or a 35 cycle bandwidth. It has a 40 db signal dynamic range and makes a rectilinear plot of signal level in db vs. azimuth angle of the turntable.

III Performance

A. Normally, measurements are made with a background of about -35 to -40 db M^2 . However, with great care and attention to details, backgrounds of 50 db M^2 can be (and have been) obtained, even with the 2 1/8 inch support rope. It should be emphasized that no-phase-cancellation-of-background technique is used and the background with the model present is the same as with it absent, (except for a small possible double scatter contribution from a part of the rope suspension system and the front of the model). All other multiple scatter situations will fall outside the beamwidths and/or the range gate.

IV Conclusion

A. The General Electric short-pulse, oblique radar cross-section range can measure large, heavy, targets with low values of radar cross-section accurately and rapidly (and safely in inclement weather).

B. Measurements can now be made at UHF, L and C bands and soon will be possible through K_A band at all linear polarizations.

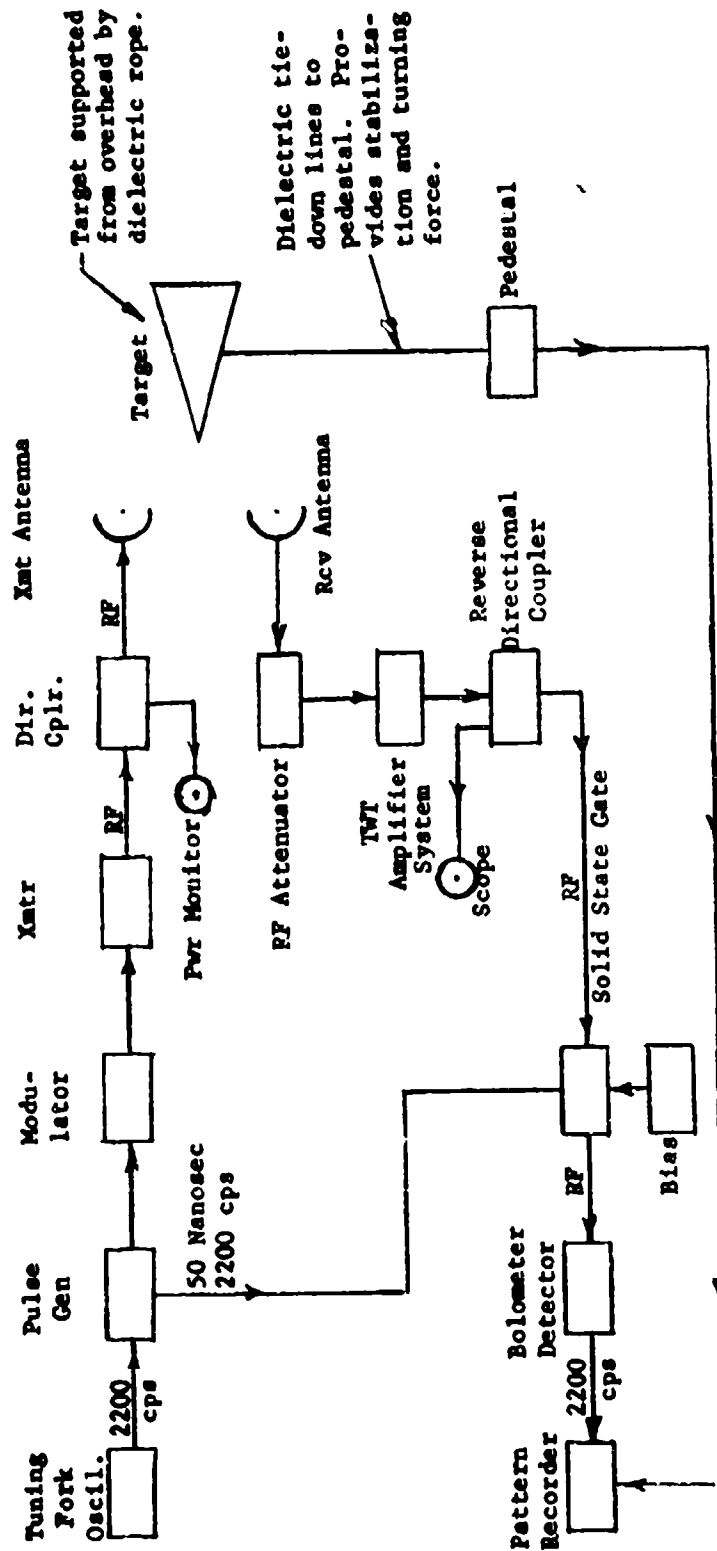


Figure 5 - Block Diagram of Short Pulse Radar

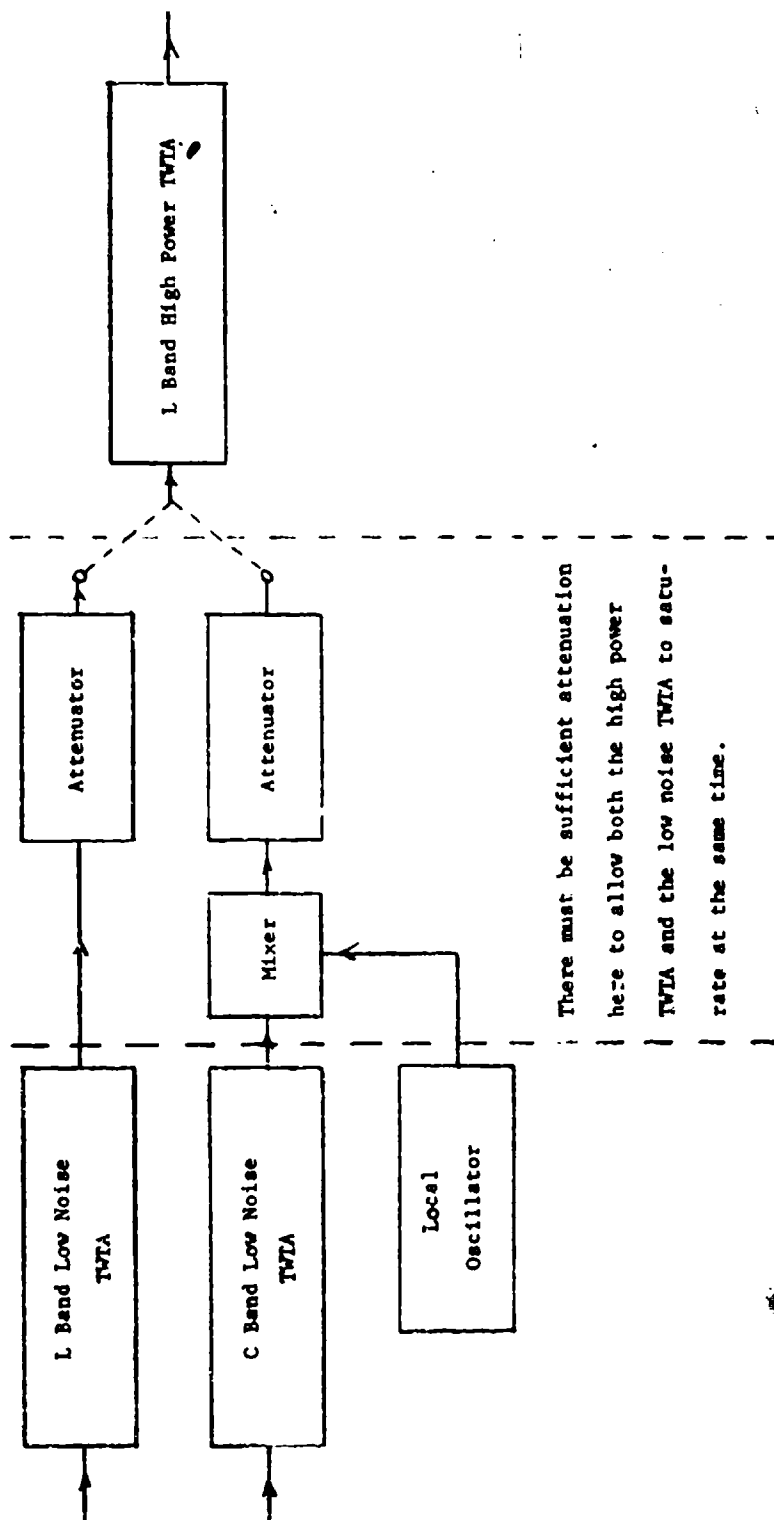


Figure 6. Traveling Wave Tube Amplifier System.